OXFORD SCIENCE PUBLICATIONS

THE PHYSICS OF BLOCK COPOLYMERS

IAN W. HAMLEY

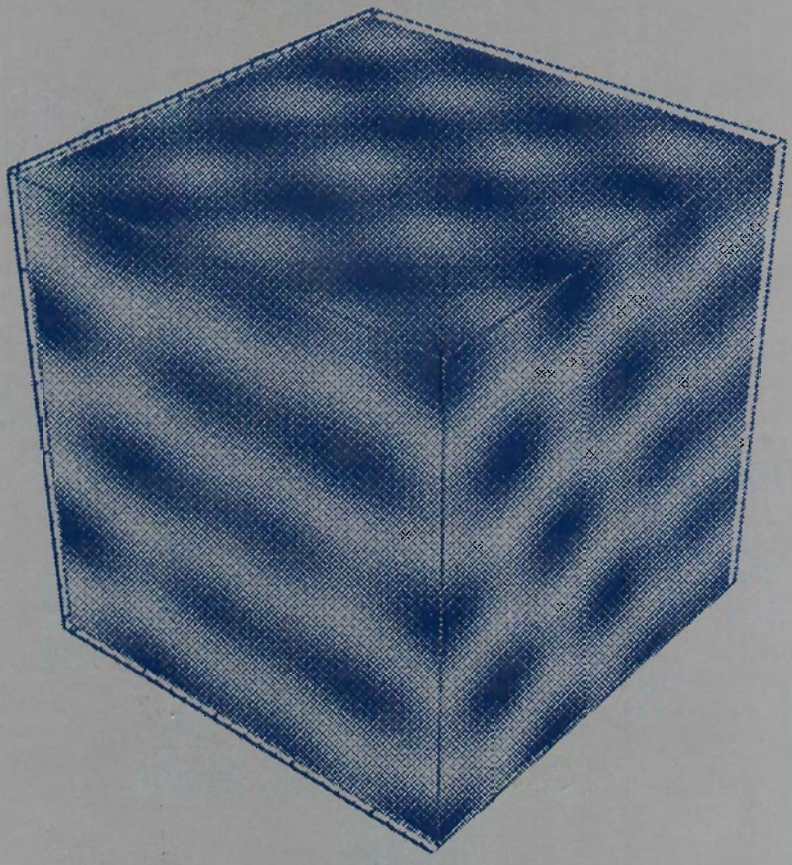

The Physics of Block Copolymers

Ian W. Hamley

School of Chemistry,
University of Leeds

OXFORD • NEW YORK • TOKYO
OXFORD UNIVERSITY PRESS
1998

Oxford University Press, Great Clarendon Street, Oxford OX2 6DP

Oxford New York
Athens Auckland Bangkok Bogota Bombay
Buenos Aires Calcutta Cape Town Dar es Salaam
Delhi Florence Hong Kong Istanbul Karachi
Kuala Lumpur Madras Madrid Melbourne
Mexico City Nairobi Paris Singapore
Taipei Tokyo Toronto Warsaw
and associated companies in
Berlin Ibadan

Oxford is a trade mark of Oxford University Press

Published in the United States
by Oxford University Press, Inc., New York

A catalogue record for this book is available from the British Library

Library of Congress Cataloging in Publication Data
(Data available)

ISBN 0 19 850218 4

Typeset by Best-set Typesetter Ltd., Hong Kong
Printed at Thomson Press (India) Ltd

Preface

Our understanding of the physics of block copolymers is increasing rapidly. It therefore seemed to me to be timely to summarize developments in this burgeoning field. Furthermore, there have been no previous monographs on the subject, and some aspects have not even been reviewed. The present volume is the result of my efforts to 'capture the zeitgeist' of the subject and is concerned with experiments and theory on the thermodynamics and dynamics of block copolymers in melt, solution, and solid states and in polymer blends. The synthesis and applications of these fascinating materials are not considered here.

The book is designed for the reader with some knowledge of polymer science so that familiarity with certain basic concepts is assumed. As the subject is developing so fast, the present monograph can only represent a snapshot of the current state of the art. Nevertheless, it is hoped that it provides a useful reference source and hopefully a discussion of future developments will be incorporated in a subsequent edition.

I would like to acknowledge a number of colleagues for their help and support, both with this book and more generally. I thank Colin Booth for comments on chapters three and four and I am grateful to all those who supplied figure originals. As usual, responsibility for errors and omissions in these and other chapters lies with the author and I shall be grateful to know of any corrigenda, addenda or suggestions for a future edition. It is a pleasure to acknowledge Frank Bates for stimulating my interest in this fascinating subject and Tony Ryan for a particularly fruitful ongoing collaboration. I thank other colleagues for discussions and collaborations over a number of years: Kristoffer Almdal, Patrick Fairclough, Stefan Förster, Ant Gleeson, Corrie Imrie, Ashish Khandpur, Tim Lodge, Tom McLeish, Mark Matsen, Kell Mortensen, Peter Olmsted, Jan Skov Pedersen, Vitaly Podneks, John Pople, Jeff Rosedale, Nick Terrill, Martin Vigild, and Ron Young.

Leeds
May 1998

I. W. H.

Contents

1 Introduction

1.1 Introduction

The nanoscale self-organization of polymers can be achieved simply by joining polymer chains together in a block copolymer. With these remarkable materials, the molecular engineer can combine distinct polymers to give materials with defined physical properties. For example, a composite comprising glassy or crystalline domains in a rubbery matrix can be self-assembled by taking components with these characteristics and combining them in a block copolymer. Because the polymer chains are tethered to each other, macroscopic phase separation cannot occur and structural organization occurs in domains with periodicities $\approx$1–100 nm, whether in the melt, solid or in micellar solution.

Block copolymers are widely used industrially. In the solid and rubbery states they are used as thermoplastic elastomers, with applications such as impact modification, compatibilization and pressure-sensitive adhesion. In solution, their surfactant properties are exploited in foams, oil additives, solubilizers, thickeners and dispersion agents to name a few. Particularly useful reviews of applications of block copolymers in the solid state are contained in the two books edited by Goodman (1982, 1985) and the review article by Riess *et al.* (1985). The applications of block copolymers in solution have been summarized by Schmolka (1991) and Nace (1996). This book is concerned with the physics underlying the practical applications of block copolymers. Both structural and dynamical properties are considered for melts, solids, dilute solutions and concentrated solutions. The book is organized such that each of these states is considered in a separate chapter.

A list of previous books and reviews on block copolymers is given in the bibliography. There have been no authored books in the field since the volume by Noshay and McGrath in 1977, and this was primarily concerned with the chemistry and materials science. Most of the literature consists of outdated edited books, although a number of review articles have appeared recently. The field has advanced rapidly during the last two decades, with major new theoretical developments, discoveries of new morphologies and the initiation of research in new fields such as thin films, crystalline solids and gels in concentrated solutions. It is thus hoped that this book is timely and fulfils the need for an up-to-date summary of the fundamental physics of block copolymers.

In this chapter, the architecture of block copolymers is outlined in Section 1.2, and the types of chemical components from which they are built are listed. The

essential processes that govern the structure of block copolymers in the melt, solid and solution are outlined in Section 1.3. In Section 1.4, the techniques most often used to investigate block copolymers are reviewed.

1.2 Types of block copolymer

Architectures

The architecture of copolymers can be controlled by the synthesis procedure, and it is possible to prepare diblock, triblock, multiblock, starblock and graft copolymers. These are illustrated in Fig. 1.1. Examples of other exotic architectures that have recently been synthesized are shown in Fig. 2.33. The possibilities for molecular design seem to be almost limitless, only being limited by the chemist's imagination. This book is concerned with block copolymers, and graft copolymers

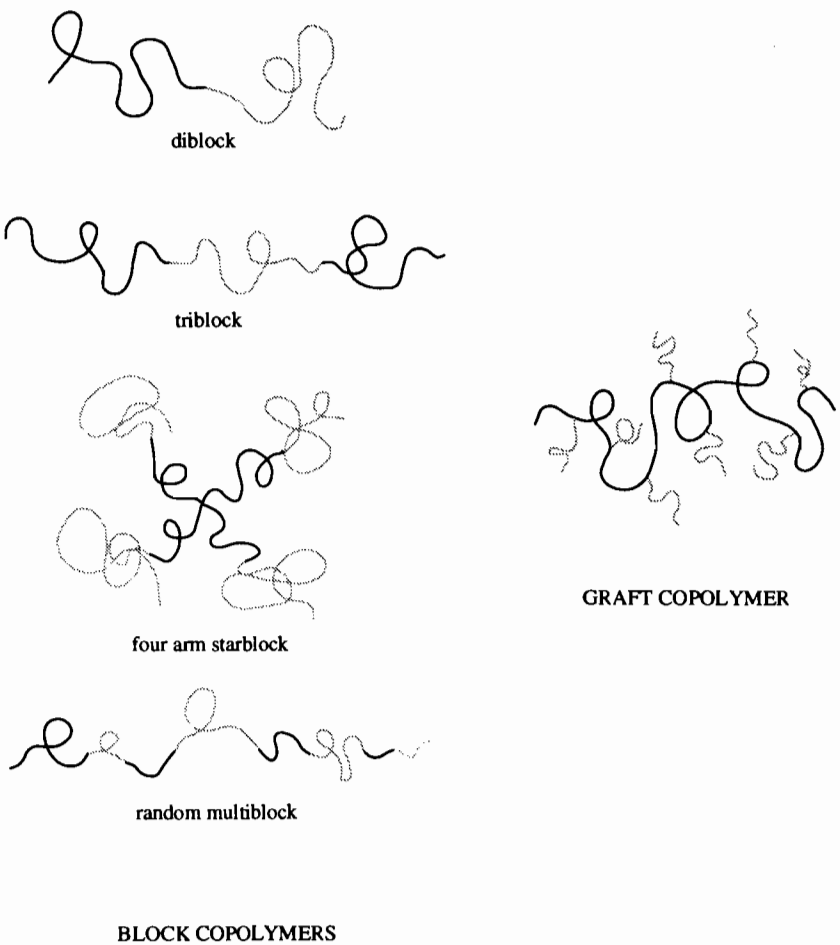

Fig. 1.1 Some block copolymer architectures. Other examples are given in Fig. 2.33.

are not generally considered, although mention is made in Chapter 2 of graft copolymers which have been synthesized in carefully controlled architectures for comparison with star and linear block copolymers. There has been little work on the fundamental thermodynamics and dynamics of multiblock copolymers of controlled sequence distribution and this subject is not considered in the present edition of this book.

Chemistry

The method of choice for synthesis of diblock and triblock copolymers is living polymerization of anionically reactive polymers, which ensures a narrow molecular weight distribution. In anionic polymerization, the polymer grows by addition of monomers to the 'Living' anionic chain. The first anionic block copolymerizations were achieved as early as the 1950s (Scwarc *et al.* 1956). Industrially, block copolymers such as triblock copolymers of poly(styrene)–poly(butadiene)–poly(styrene) (PS–PB–PS, known as SBS), which are used as synthetic rubbers, are prepared by anionic polymerization (Aggarwal 1985). The most common class of copolymer in terms of tonnage produced are the styrenic copolymers, largely PS–PB–PS and PS–PI–PS triblocks, where PI denotes poly(isoprene). Copolymers containing poly(ethylene oxide) and poly(propylene oxide) or poly(butylene oxide) are extensively used as surfactants. The structures corresponding to common components of block copolymers, and those featured most often in this book are shown in Fig. 1.2. The names are often those in common usage, and not the systematic chemical names.

Notation

Consistent notation is adopted throughout this book. Diblock copolymers are written poly(monomer A)–poly(monomer B) or PA–PB, where examples of PA and PB are illustrated in Fig. 1.2. Similarly, triblock copolymers are written poly(monomer A)–poly(monomer B)–poly(monomer C) or PA–PB–PC. Deuterated blocks are denoted *d*poly(monomer A) or *d*PA. The molar mass of a copolymer is denoted by M_w or M_n corresponding to the weight- or number-average respectively, and the composition is specified by the volume fraction of one component, f. In solution, the volume fraction of a copolymer is denoted ϕ, or the concentration as c.

1.3 The structure of block copolymer melts, solids, solutions and blends

1.3.1 Melts

Two competing effects govern the thermodynamics of block copolymer melts. At high temperatures, the chains are mixed homogeneously, as in any polymer melt. As the temperature is reduced, the tendency for the blocks to segregate is enhanced, i.e. the enthalpic process of demixing is favoured. However, this is necessarily accompanied by a reduction in entropy as the chain configuration becomes more constrained. The extent of segregation of the copolymer may then

be expressed using the reduced parameter χN. Here χ is the Flory–Huggins interaction parameter, which contains a significant enthalpic contribution and is governed by the incompatibility of monomers (Flory 1953), and N is the copolymer degree of polymerization, reflecting the N-dependent translational and configurational entropy. The tendency for blocks to segregate on lowering the temperature leads to a process termed microphase separation, where separation of the components occurs into nanoscale domains. Microphase separation is illustrated in Fig. 1.3. Phase separation on a macroscopic level is prevented by the connectivity of the polymer chains that defines block copolymers. The transition from a homogeneous melt of chains to a heterogeneous melt of ordered microphase-separated domains is called the order–disorder transition (ODT). It occurs at a critical value of χN, depending on the composition of the copolymer, which is

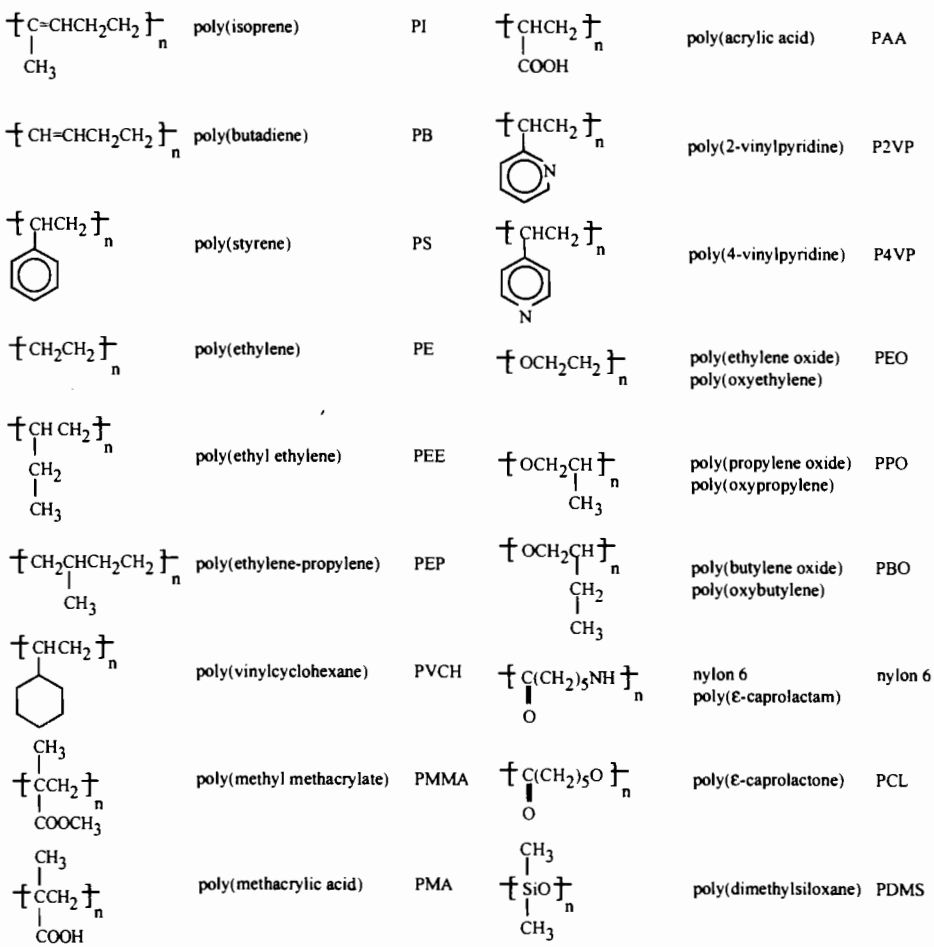

Fig. 1.2 Chemical structures of blocks from which copolymers are commonly constructed.

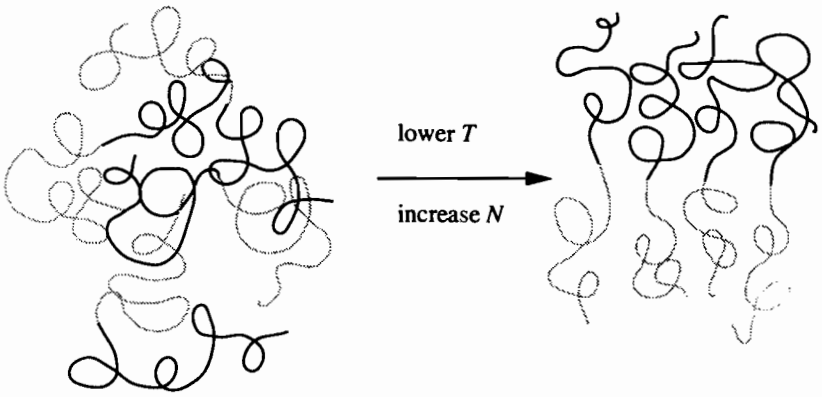

Fig. 1.3 Microphase separation in a block copolymer melt.

parameterized by f. For a symmetric ($f = 0.5$) diblock copolymer, with equal segment sizes, mean field theory predicts a critical $(\chi N)_{ODT} = 10.5$, compared to $\chi N = 2.0$ for phase separation in a symmetric polymer blend. The ordered phase that is formed for $\chi N > (\chi N)_{ODT}$ depends on the composition of the copolymer, which determines the curvature of the interface between blocks and their packing density.

The melt phase behaviour is thus summarized in phase diagrams parameterized by f and χN. Three regimes have been defined depending on the extent of segregation of the blocks: the weak ($\chi N \approx 10$), intermediate ($\chi N \approx 10$–100) and strong segregation ($\chi N \gtrapprox 100$) regimes. In the weak segregation limit, the composition profile is approximately sinusoidal, i.e. the volume fraction of one of the blocks varies sinusoidally about the average value. As χN increases, the profile becomes sharper, with a narrower interphase between blocks and saturation of the composition so that in the strong segregation limit the domains contain essentially pure components. The phase behaviour in the strong segregation limit depends largely on the composition of the copolymer f. However, for weakly segregated copolymers, in addition to f and χN, the degree of polymerization, N, is an independent variable relevant to the phase behaviour. It controls composition fluctuations which are important for block copolymers near the order–disorder transition.

The theory for block copolymer melts in all regimes is now rather advanced, and it is possible to predict the structure of a copolymer of a given χ, N, f and segment length, a. The self-consistent field theory provides a unified mean field picture, with simpler limiting theories for the weak and strong segregation regimes. Consideration of composition fluctuations for weakly segregated copolymers necessitates an approach beyond the mean field level of approximation.

The effect on structure of confining block copolymers in thin films has been examined, largely using neutron reflectivity and atomic force microscopy. A number of features that result from the constraint of reduced dimensionality have been reported, such as the observation of islands and holes at the surface

of a lamellar block copolymer film, when its thickness is not an integral multiple of the bulk layer spacing.

The dynamics of block copolymers melts are as intriguing as their thermodynamics leading to complex linear viscoelastic behaviour and anisotropic diffusion processes. The non-linear viscoelastic behaviour is even richer, and the study of the effect of external fields (shear, electric . . .) on the alignment and orientation of ordered structures in block copolymer melts is still in its infancy. Furthermore, these fields can influence the thermodynamics of block copolymer melts, as recent work has shown that phase transition lines shift depending on the applied shear. The theoretical understanding of dynamic processes in block copolymer melts is much less advanced than that for thermodynamics, and promises to be a particularly active area of research in the coming years.

The fascinating thermodynamics of block copolymers that results from microphase separation are the subject of the parts 2.2, 2.3, and 2.4 of Chapter 2. Part 2.4 is concerned with the complex kinetic processes that accompany phase transitions, and the dynamic processes controlled by the structure of the block copolymer melt.

1.3.2 Solutions

There are two basic processes that characterize the phase behaviour of block copolymers in solution: micellization and gelation. Micellization occurs when block copolymer chains associate into, often spherical, micelles in dilute solution in a selective solvent. The core of the micelle is formed by the insoluble or poorly solvated block, whilst the corona contains the selectively solvated block. Such a micelle is illustrated in Fig. 1.4. At a fixed temperature, micellization occurs on increasing concentration at the critical micelle concentration (cmc). The cmc is usually determined from the sharp decrease in the surface tension as a function of concentration, although other properties such as viscosity also exhibit pronounced changes. The formation of rod-like micelles is commonly favoured at higher concentrations. When copolymer chains become maximally swollen by solvent, spherical micelles can no longer grow, and elongated micelles tend to form. The formation of micelles in dilute block copolymer solutions is the subject of Chapter 3.

There is a substantial body of theoretical work on micellization in block copolymers. The simplest approaches are the scaling theories, which account quite successfully for the scaling of block copolymer dimensions with length of the constituent blocks. Rather detailed mean field theories have also been developed, of which the most advanced at present is the self-consistent field theory, in its lattice and continuum guises. These theories are reviewed in depth in Chapter 3. A limited amount of work has been performed on the kinetics of micellization, although this is largely an unexplored field. Micelle formation at the liquid–air interface has been investigated experimentally, and a number of types of surface micelles have been identified. In addition, adsorption of block copolymers at liquid interfaces has attracted considerable attention. This work is also summarized in Chapter 3.

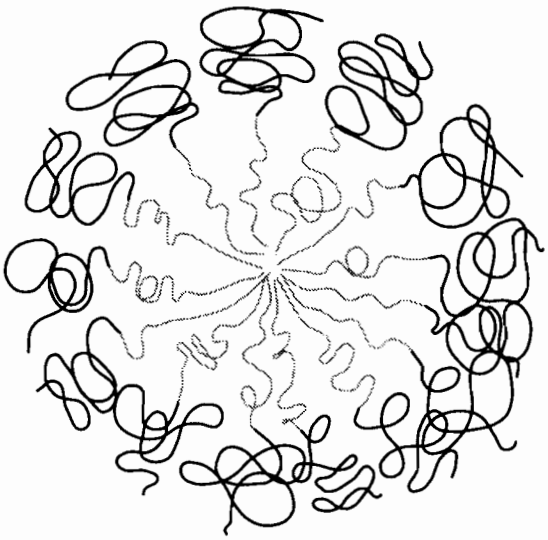

Fig. 1.4 Schematic of a block copolymer micelle.

In concentrated solutions, micelles can order into gels. Soft and hard gels are distinguished from each other and from micellar sols (solutions) by their flow properties, gels being characterized by a finite yield stress. The hard gels seem to be associated with the formation of cubic phases of spherical micelles, whereas soft gels are usually lamellar or hexagonal-packed rod micellar phases. The phase behaviour of these materials has only recently begun to be elucidated using small angle scattering. It promises to be even richer than that of block copolymer melts, at least if results for analogous conventional surfactants are any guide. The flow behaviour of these gels is the basis for many of their applications, and study of the rheology and behaviour under shear of these materials will enhance the fundamental understanding underpinning future developments. The work in this area to date is discussed in Chapter 4. This also includes an account of the limited theoretical work on this subject.

1.3.3 Solids

The structure of block copolymer melts is usually trapped upon vitrification. The mechanisms underlying the glass transition are similar to those of the constituent homopolymers. Thus there is little distinct physics associated with the formation of solid phases by glassy block copolymers.

In contrast, crystallization of one or both components of a block copolymer is accompanied by profound structural and dynamic changes. The fundamental process in crystallization of chains in a crystallizable block copolymer is the change in block conformation, i.e. the adoption of an extended or a folded structure rather than a coiled configuration found in the melt or solution (see Fig. 1.5).

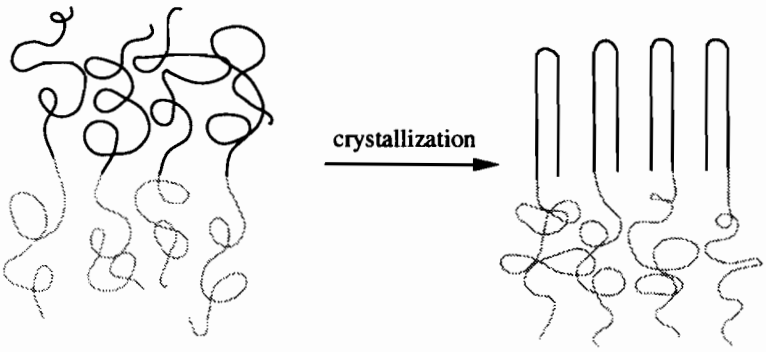

Fig. 1.5 Crystallization from the melt in a block copolymer.

Crystallization from the melt often leads to a distinct (usually lamellar) structure, with a different periodicity from the melt. Crystallization from solution can lead to non-lamellar crystalline structures, although these may often be trapped non-equilibrium morphologies. In addition to the formation of extended or folded chains, crystallization may also lead to gross orientational changes of chains. For example, chain folding with stems parallel to the lamellar interface has been observed for block copolymers containing poly(ethylene), whilst tilted structures may be formed by other crystalline block copolymers. The kinetics of crystallization have been studied in some detail, and appear to be largely similar to the crystallization dynamics of homopolymers.

There is no comprehensive theory for crystallization in block copolymers that can account for the configuration of the polymer chain, i.e. extent of chain folding, whether tilted or oriented parallel or perpendicular to the lamellar interface. The self-consistent field theory that has been applied in a restricted model seems to be the most promising approach, if it is as successful for crystallizable block copolymers as it has been for block copolymer melts. The structure of crystallizable block copolymers and the kinetics of crystallization are the subject of Chapter 5.

1.3.4 Blends

A number of classes of polymer blends containing block copolymers have been studied. Namely, binary blends of a block copolymer with a homopolymer, ternary mixtures of a block copolymer with two homopolymers and blends of two block copolymers. Experimental and theoretical studies of all these mixtures are the subject of Chapter 6.

In binary blends of A homopolymer and AB diblock copolymer, the interplay between microphase separation and macrophase separation is controlled mainly by the relative length of the chains, in addition to the composition of the mixture. Homopolymers shorter than the corresponding block tend to be solubilized within the corresponding domain of a microphase-separated structure. As the homopolymer molecular weight increases to approach that of the corresponding

diblock, the homopolymer tends to be localized more towards the centre of the corresponding domain, as shown by small-angle scattering experiments and transmission electron microscopy in the bulk, and neutron reflectivity in thin films. For high-molecular-weight homopolymers, macrophase separation becomes prevalent.

In a blend of immiscible homopolymers, macrophase separation is favoured on decreasing the temperature in a blend with an upper critical solution temperature (UCST) or on increasing the temperature in a blend with a lower critical solution temperature (LCST). Addition of a block copolymer leads to competition between this macrophase separation and microphase separation of the copolymer. From a practical viewpoint, addition of a block copolymer can be used to suppress phase separation or to compatibilize the homopolymers. Indeed, this is one of the main applications of block copolymers. The compatibilization results from the reduction of interfacial tension that accompanies the segregation of block copolymers to the interface. From a more fundamental viewpoint, the competing effects of macrophase and microphase separation lead to a rich critical phenomenology. In addition to the ordinary critical points of macrophase separation, tricritical points exist where critical lines for the ternary system meet. A Lifshitz point is defined along the line of critical transitions, at the crossover between regimes of macrophase separation and microphase separation. This critical behaviour is discussed in more depth in Chapter 6.

Macrophase separation can also occur in binary blends of diblocks if the molecular weights are sufficiently dissimilar, and the limit for this immiscibility has been investigated. Blends of two AB diblocks with different lengths (but similar compositions) have been used to map the experimental phase diagrams of block copolymers using the 'one component' approximation, where the phase behaviour of the blend is assumed to be the same as that of a pure diblock with the same composition. This limited region of validity of this approximation has been assessed theoretically. Of course, two-phase regions must exist in the two-component blend, which leads to a more complex phase behaviour if the compositions of the copolymers are mismatched. This has been explored using the self-consistent field theory, and in this area the theorereticaI work is somewhat ahead of the experimental effort. In binary blends, segregation of the short diblock to the A–B interface seems to be a general effect.

From the theoretical viewpoint, much of the phase behaviour of blends containing block copolymers has been anticipated or accounted for. The primary approaches consist of theories based on polymer brushes (in this case block copolymer chains segregated to an interface), Flory–Huggins or random phase approximation mean field theories and the self-consistent mean field theory. The latter has an unsurpassed predictive capability but requires intensive numerical computations, and does not lead itself to intuitive relationships such as scaling laws.

1.4 Techniques for studying block copolymers

In this section, a brief outline is given of the major methods used to study block copolymers, whether in the melt, solid or solution state and whether in bulk or

in a thin film. The application of these techniques is discussed in the context of the specific physics in later chapters. The methods are listed alphabetically.

1.4.1 Atomic force microscopy

Atomic force microscopy (AFM) has been demonstrated to be an invaluable technique for characterization of nanoscale structures at the surface of block copolymer films. In this method, the deflection of a cantilever due to repulsive electronic interactions of an attached sharp tip with the surface is measured. The microscopic movement of the tip creates a force which is measured to provide an image of the surface structure. Both contact and tapping mode AFM have been employed for the investigation of surface topography, the latter avoiding contact of the tip with the surface. Uniform thin films of block copolymers can be prepared by spin-casting materials onto a substrate wetted by the polymer and subsequent annealing. The ultimate morphology is a function of copolymer composition, temperature, film thickness and surface tension of the blocks.

Pioneering contact mode AFM studies by Meiners *et al.* (1995) show that chemical sensitivity at the surface of thin polymer films can be achieved by measuring the microscopic friction and stiffness for glassy block copolymers. This provides invaluable information to complement topography on the nature of the block at the surface.

1.4.2 Dilatometry

In dilatometry, the changes in dimensions of a sample are studied. The method is widely used in polymer science to investigate dimensional changes during vitrification, polymerization, crazing, etc., but in this book its use is discussed in the context of crystallization experiments. In this case, volume dilatometry is used to measure changes in specific volume upon crystallization. The sample is immersed in a confining fluid and the combined thermal expansion of the sample and fluid is measured. By subtracting the volume change of the confining fluid, the thermal dilation of the sample itself can be determined. Further details of dilatometry, including instrument designs, can be found in Zoller (1989).

1.4.3 Differential scanning calorimetry

This technique is used to probe thermal properties of polymers such as the melting temperature and enthalpy of fusion, as discussed in Chapter 5. The differential power necessary to maintain a given temperature for two pans containing the polymer and a reference sample is recorded. A phase transition is indicated by a sharp endotherm or exotherm which causes changes in the differential power supplied to the sample. In addition to crystallization, differential scanning calorimetry (DSC) is used to determine glass transition temperatures in polymers, and has also been used to characterize the thermal properties accompanying micellization and gelation in block copolymer solutions, as discussed in

Chapters 3 and 4 respectively. A good review of methods for the examination of thermal properties of polymers is provided by Thompson (1989).

1.4.4 Dynamic light scattering

Dynamic light scattering (DLS) is also known as photon correlation spectroscopy (PCS) or quasi-elastic light scattering (QELS). It involves measuring the temporal fluctuations of the intensity of scattered light. The number of photons entering a detector are recorded and analysed by a digital correlator. The separation in time between photon countings is the correlation time, t. The autocorrelation function of the intensity at an angle θ, I_θ, is computed as

$$g(t) = \lim_{S\to 0}\left[\frac{1}{S}\int_0^S I_\theta(s) I_\theta(s+t)\,\mathrm{d}s\right]. \tag{1.1}$$

Laplace transformation of eqn 1.1 (often using the CONTIN program (Provencher 1982)) yields the distribution of relaxation times, $A(\tau)$. The decay rates of the relaxation modes provide translational diffusion coefficients.

In polymer solutions, DLS is used to determine the hydrodynamic radius of the constituent particles using the Stokes–Einstein equation

$$R_H = k_B T/6\pi\eta D, \tag{1.2}$$

where k_B is the Boltzmann constant, T is the absolute temperature, η is the solvent viscosity and D is the diffusion coefficient.

DLS has largely been exploited to study diffusion in polymer solutions, and details of experimental studies on block copolymer solutions are provided in Chapter 3. Recently, it has been used to investigate relaxation modes in block copolymer melts, and the effects of entanglements on diffusion. The relevant literature is discussed in Chapter 2, and a review article by Stepanek and Lodge (1996) has also recently appeared. The technique is summarized by Berne and Pecora (1976). Because the intensity of scattered light is z-weighted ($z \propto cM_w$ where c = mass concentration and M_w = mass-average molar mass), DLS is sensitive to low levels of high-molar-mass solutes.

1.4.5 Gel permeation chromatography

Gel permeation chromatography (GPC), also known as size exclusion chromatography (SEC), separates particles according to their effective size in solution. The sample solution is introduced into the column, which is filled with a rigid or gel porous packing. The sample is carried by the solvent (mobile phase) through the column and size separation occurs by exchange of solute particles between the bulk solvent and the stationary liquid phase within the pores of the packing material. The method is routinely used to determine the molecular weight distribution of polymers. In this book, its application to the study of micellization in block copolymer solutions is discussed in Chapter 3. It has been used to examine the distribution of molecules and micelles. However, as pointed out in Chapter 3, serious concerns exist with this method due to observations that

the molecule–micelle equilibrium can be dramatically disturbed by adsorption in the GPC gel. Booth and co-workers have developed a technique to circumvent this termed eluent GPC, where the block copolymer solution is used as an eluent instead of a simple solvent (Wang *et al.* 1992). When a solution of different concentration to the eluent is injected into the column, the solution is diluted as it passes through the columns and the concentration approaches that of the eluent. Thus the distribution of molecules and micelles in the solution approaches that in the eluent at equilibrium. In other words, the injected solution probes the equilibrium state of the eluent. A detailed summary of methods for GPC experiments is presented by Johnson (1989).

1.4.6 Light microscopy

Light microscopy has been used in a number of contexts to characterize block copolymer morphology. For crystalline block copolymers, spherulitic structures that result from organization of crystalline lamellae can be examined using microscopy. In solutions, polarized light microscopy can reveal the presence of lamellar and hexagonal-packed cylindrical micellar phases. Cubic micellar phases are optically isotropic, and consequently cannot be distinguished from sols only on the basis of microscopy.

1.4.7 Nuclear magnetic resonance

Nuclear magnetic resonance (NMR) has been used to study segmental motions in block copolymer solutions. The mobility of protons in polymer chains in dilute solutions has been probed using high-resolution ^{1}H NMR. Association of chains into micelles leads to a reduction in mobility in the core, which leads to a broadening of the respective NMR lines that has been studied for a number of systems, as described by Tuzar and Kratochvil (1993). The sol–gel transition in concentrated solutions has been located via ^{1}H transverse relaxation time experiments, as outlined in Chapter 4.

NMR has not been widely employed to study dynamics in block copolymer melts, although field gradient NMR can provide a wealth of information on the diffusion of block copolymer chains (Fleischer *et al.* 1993). The orientation of a deuterated homopolymer in a lamellar diblock copolymer (in a glassy state) was determined using ^{2}H NMR by Valic *et al.* (1994, 1995). Other applications of NMR to probe polymer chain dynamics and details of experimental protocols are described by Bovey and Jelinksi (1989).

1.4.8 Osmometry

In addition to its major use in determining the number-average molecular weight (M_n) of polymers, osmometry has also been used to determine M_n of block copolymer micelles. The method involves determining the osmotic pressure (Π) across a membrane that is permeable to solvent only. Because osmotic pressure is a colligative property, it depends on the number of particles, and hence yields M_n. It also depends on the interactions between particles, and thus

provides the second virial coefficient (A_2) for associated solutes at a concentration C and temperature T such as block copolymer micelles via

$$\Pi/c = RT/M_n + A_2c. \tag{1.3}$$

In a solution containing both unimer and micelles, M_n, which is by definition more sensitive to low molar mass particles, is always less than the weight-average molecular weight, M_w. Further details on osmometry can be found in the review by Adams (1989), whilst examples of its application to micellar block copolymer solutions are given in Chapter 3.

1.4.9 Rheology

The flow properties of block copolymer melts depend on the state of order in the system, and this has been exploited to locate the order–disorder transition (ODT). Ordered phases such as the lamellar and hexagonal-packed cylinder phases are viscoelastic fluids, whereas the disordered melt exhibits viscous flow. Measurements of the dynamic elastic modulus at a fixed frequency on increasing the temperature reveal a sharp decrease in both storage (G') and loss moduli (G'') at the ODT. Rheological measurements have also provided evidence for the effects of composition fluctuations, as discussed in Chapter 2. The frequency dependence of the dynamic elastic moduli depends on the orientation of the microstructure, and the density of defects, for lamellar and hexagonal phases, as discussed in Section 2.4.3. Cubic phases are characterized by a primarily elastic response. Thus, although rheology cannot be used to unambiguously identify ordered phases, it does depend on the symmetry of the structure. However, understanding of block copolymer rheology in terms of microstructure is as yet poorly developed.

Rheology has also been used to locate sol–gel transitions in concentrated block copolymer solutions, as described in Chapter 4. Gels exhibit a finite yield stress (i.e. they are Bingham fluids), which can be measured in steady shear experiments.

Experimentally, the dynamic shear moduli are usually measured by applying sinusoidal oscillatory shear in constant stress or constant strain rheometers. This can be in parallel plate, cone-and-plate or concentric cylinder (Couette) geometries. An excellent monograph on rheology, including its application to polymers, is provided by Macosko (1994).

1.4.10 Small-angle light scattering

In this method, the intensity of elastically scattered light is measured as a function of scattering angle, θ. Because scattering at small angles is probed (using radiation of a wavelength larger than the particle dimensions), small-angle light scattering (SALS) is sensitive to the overall dimensions of polymer chains or associates. It is used to provide the weight-average molecular weight of diblock copolymers, and in solutions yields M_w for micelles, the z-average radius of gyration ($R_{g,z}$), and also the second virial coefficient. In the treatment of light scattering from polymer solutions, only the scattering from polymer molecules is required. The contribution from local solvent concentration fluctuations is

accounted for by defining the excess reduced intensity of scattered light, which is called the excess Rayleigh ratio R_θ.

The usual procedure for obtaining M_w, $R_{g,z}$ and A_2 involves Zimm plots. At small angles, the inverse scattered intensity is given by (Cowie 1991; Gedde 1995; Young and Lovell 1991)

$$\frac{Kc}{R_\theta} = \frac{1}{M_w} + \frac{1}{M_w}\frac{16\pi^2}{3\lambda'^2}\sin^2(\theta/2)R_{g,z}^2 + 2A_2c, \tag{1.4}$$

where c is the concentration of polymer, $\lambda' = \lambda/n_0$ is the wavelength of light in the medium (of refractive index n_0), and K is an optical constant depending on refractive index, wavelength and polarization of the beam (an expression for which is given by Gedde (1995)). A double extrapolation of Kc/R_θ versus $\sin^2(\theta/2) + k'c$, where k' is an arbitrary constant, for a series of concentrations and angles is called a Zimm plot. In the limit $\theta \to 0$,

$$\lim_{\theta\to 0}\frac{Kc}{R_\theta} = \frac{1}{M_w} + 2A_2c, \tag{1.5}$$

which can be used to extract M_w and A_2. $R_{g,z}$ can be obtained by extrapolation to $c \to 0$, knowing M_w.

An alternative, though less satisfactory, method for determining M_w and $R_{g,z}$ is to measure the dissymmetry ratio $Z = R_\theta/R_{\pi-\theta}$. If the dissymmetry is not too large, the intensity at 90° and two angles symmetrical about 90°, usually 45° and 135°, is measured, and extrapolated to $c = 0$. The limiting value of Z is used to obtain the form factor at 90°, $P(90)$ and $R_{g,z}^2$ from published tables which give the variation of $P(90)$ with Z and of Z with $R_{g,z}^2/\lambda$ for scatterers with different geometries (e.g. Gaussian coils, rigid rods, ellipsoids). Light scattering by such particles is the subject of the book by van de Hulst (1957). Light scattering from block copolymers micelles (Tuzar and Kratochvil 1996) and melts (Stepánek and Lodge 1996) has been reviewed recently.

1.4.11 Small-angle neutron and *X*-ray scattering

Both these techniques are ideal for the investigation of morphology of ordered phases in block copolymer melts, solids and gels because length-scales are probed which are typical of those of block copolymer microstructures, i.e. 1–100 nm. In contrast to transmission electron microscopy (TEM), the structure of the sample averaged over the macroscopic size of the beam is probed. Scattering data are presented as a function of the scattering vector $\boldsymbol{q}$ or its magnitude, where

$$q = |\boldsymbol{q}| = \frac{4\pi\sin\theta}{\lambda}. \tag{1.6}$$

The relative positions of a sufficient number of reflections arising from microstructural periodicities enable unambiguous identification of morphology. Further information can be obtained by preparing oriented specimens, and obtaining diffraction patterns for different orientations. For example, in an oriented lamellar phase with the beam incident parallel to the layers, Bragg

reflections at q^*, $2q^*$, $3q^*$, ..., where q^* is the position of the first-order reflection, are observed along a direction parallel to the layer normal.

Small-angle X-ray scattering (SAXS) is appropriate where the electron density contrast between blocks is sufficient for the polymer to diffract X-rays (Balta-Calleja and Vonk 1989). This is often possible with an intense source of X-rays, such as a rotating anode generator or a synchrotron source. Small-angle neutron scattering (SANS) is valuable for studies of polymer structure (Higgins and Benoît 1994) because of the opportunity for contrast variation via isotope labelling. Typically, hydrogen atoms are selectively replaced by deuterium; this changes the scattering contrast and can be used to obtain local information on chain conformation in block copolymer melts or intramicellar structure in block copolymer solutions, for example. Neutron scattering has also been extensively used to enhance the scattering contrast in block copolymers. Further details of this technique can be found in the excellent review of SANS from block copolymers by Richards (1985).

The radius of gyration of block copolymer micelles in dilute solution can be obtained from SAXS and SANS using the Guinier approximation (Guinier 1939, 1963):

$$I(q) = I(0)\exp\left(-q^2 R_g^2/3\right). \tag{1.7}$$

This is valid for small scattering angles, $qR_g \ll 1$. The Guinier approximation has also been used to analyse SANS data from block copolymers in the melt, to extract information on the chain conformation using mixtures with labelled chains. Futhermore, if the intensity is put on an absolute scale, the particle molar mass M can be obtained from $I(0)$ (by extrapolation of the data to $q = 0$) using Kratky's equation (Kratky *et al.* 1951, 1966) if the sample concentration, thickness and density and incident intensity are known. Small-angle X-ray scattering is the subject of the books by Guinier (1963), Guinier and Fournet (1955) and Glatter and Kratky (1982).

Small-angle scattering intensity in the high angle (q) region can be analysed to provide information on interface thickness (e.g. the lamellar interface thickness block in copolymer melts or core–corona interface widths in micelles). For a perfectly sharp interface, the scattered intensity in the Porod regime falls as q^{-4} (Porod 1951). For an interface of finite width this is modified to

$$I(q) \propto (S/V)q^{-4}\exp\left(-\sigma^2 q^2\right), \tag{1.8}$$

where S/V is the interfacial area per unit volume and σ is an interfacial width.

1.4.12 Surface tension

The critical micelle concentration (cmc) in block copolymer solutions can be determined by measurement of the surface tension (γ) as a function of concentration. The method detects complētion of the Gibbs monolayer at the air/water interface, and is a secondary indicator of the onset of micellization. The cmc for solutions of monodisperse polymers is indicated by a fairly sharp decrease in γ versus $\log(c)$.

1.4.13 Transmission electron microscopy

The most direct method for the investigation of block copolymer morphology in the melt and solid phases is transmission electron microscopy (TEM). In this technique a thin section of block copolymer or a solvent-cast film is first microtomed. For soft samples, ultrathin sections are obtained at low temperatures (typically −100 °C), via cryo-ultramicrotomy (i.e. slicing of the sample at low temperature). Contrast between rubbery and glassy components in the section is then achieved by exposing the sample to osmium tetraoxide vapour, which selectively stains the rubbery component (Kato 1965, 1967). In polyolefin diblock copolymers containing poly(ethylene) it has recently been shown that ruthenium tetraoxide can be used as a staining agent, and the amorphous component (e.g. poly(ethylethylene) or poly(ethylene–propylene)) is selectively stained due to reduced diffusivity of RuO_4 in the semicrystalline microdomains (Khandpur *et al.* 1995). The disadvantages of TEM are that misidentification of morphology is possible based on inspection of only a projection of a small region of the sample. For example, the 'ordered bicontinuous double diamond (OBDD)' bicontinuous cubic phase was identified in star block copolymers via TEM images showing a 'wagon wheel' structure (Alward *et al.* 1986; Thomas *et al.* 1986). Subsequent work showed that this projection could also be obtained from the 'gyroid' bicontinuous structure, and this latter morphology was confirmed by SAXS (Förster *et al.* 1994; Hajduk *et al.* 1994). A comprehensive review of electron microscopy from polymers is provided by Thomas (1989).

Transmission electron micrography has, remarkably, been successfully used to image micelles formed by block copolymers in dilute solutions. Price and coworkers used two preparation methods. In the first method (Price and Woods 1973), freeze etching, a drop of solution was rapidly frozen by quenching in liquid nitrogen. Solvent was then allowed to evaporate from a freshly microtomed surface of the droplet. Finally, a replica was made of collapsed micelles raised proud from the frozen surface. In the second method (Booth *et al.* 1978), a drop of micellar solution was allowed to spread and evaporate on a carbon substrate, and OsO_4 was used to selectively stain one of the blocks.

1.4.14 Turbidometry

Turbidometry is simply the quantitative measurement of light transmission in turbid solutions, and is employed to locate the cloud point (i.e. onset of macrophase separation) in block copolymer solutions, as discussed in Chapter 3.

1.4.15 Ultracentrifugation

Sedimentation in a centrifugal field has been demonstrated to be a useful tool in the investigation of micellization in block copolymers, as first demonstrated by Tuzar *et al.* (1974). In this method, the velocity at which a solute species (unimer or micelle) is displaced under the influence of a strong centrifugal force is measured (Brown *et al.* 1995). For a given centrifugal force, the sedimentation velocity of a solute depends on its molecular weight, its buoyancy and friction

factor. It is important to keep in mind when analysing sedimentation velocity data that the molecule–micelle equilibrium in block copolymer solutions is a dynamic process. However, the two peaks in the gradient curves obtained by ultracentrifugation, corresponding to molecules and micelles, are always observed for sufficiently high association numbers, suggesting that the equilibrium is not disturbed too seriously by the transport process. Details of this technique, including experimental apparatus, are summarized by Laue (1989). Examples of its application to block copolymers are listed in Chapter 3.

1.4.16 Viscometry

Viscometry has been used extensively to provide information on the hydrodynamic properties of solutions of block copolymer micelles. The specific viscosity, η_{sp}, divided by the concentration, can be used to determine the intrinsic viscosity, $[\eta]$, by extrapolation via

$$\eta_{sp}/c = [\eta] + k_H[\eta]^2 c. \tag{1.9}$$

Here k_H is the Huggins coefficient. The intrinsic viscosity decreases and the Huggins coefficient increases, as micelles become smaller. On micellization, η_{sp}/c has been observed to increase for some systems but to decrease for others, and unfortunately there are no firm rules governing which case will prevail for a given block copolymer solution. The viscosities of polymer solutions are measured in capillary flow viscometers, which are described in detail by Macosko (1994).

1.4.17 X-ray and neutron reflectivity

These techniques involve measuring the intensity of X-rays or neutrons reflected from a block copolymer film as a function of angle of incidence (or wavevector magnitude q, eqn 1.6) at small angles. The case where the angle of the reflected beam is equal to the incident angle, and the plane of reflection is normal to the surface, is termed specular reflectivity. It provides the scattering density profile normal to the film surface (z direction). Below a critical angle for reflection (which is proportional to the average scattering density in the material), all X-rays or neutrons are reflected. Above (but close to) the critical angle for reflection, the ratio of reflected to incident intensity is given approximately by (Hamley and Pedersen 1994; Russell 1990)

$$R(q) = \frac{(4\pi)^2}{q^4}\left|\int_{-\infty}^{\infty}\frac{d\varrho(z)}{dz}\exp(-iqz)dz\right|^2, \tag{1.10}$$

where $\varrho(z)$ is the scattering density profile. The reflectivity for a film of uniform density falls off as q^{-4} (Fresnel relectivity). Modulations superimposed on this result from the film structure. An exact calculation of reflectivities requires allowance for refraction within the block copolymer film, and can be achieved using methods developed from optics, where the film density profile is considered to be divided up into a finite number of slices (Parratt 1954). As in all scattering techniques, information on the scattering density cannot be obtained

directly; however, in the case of specular reflectivity the information content is further limited by the one-dimensional nature of the profile. Modelling is required to extract quantitative information. An advantage of neutron reflectivity compared to x-ray reflectivity is that the contrast for neutron scattering between polymer components can be enhanced by selective deuteration.

Thin films of block copolymer melts, and block copolymers adsorbed at the liquid–liquid interface, have been investigated using specular reflectivity (largely neutron reflectivity due to the ability to vary the scattering contrast). Off-specular reflection is, in principle, a powerful method for determining in-plane structure in block copolymer films but is not yet widely used.

1.4.18 Other techniques

The following is certainly not a comprehensive list, but a description of some of the less common methods applied to study block copolymers that are encountered in subsequent chapters.

Differential refractometry

Refractometry can be used to determine the composition of a copolymer. In addition, differential refractometry has been used to study micellization in dilute block copolymer solutions (Tuzar and Kratochvíl 1972). The refractive index (n) is obtained in an Abbe refractometer via measurements of the critical angle for external reflection. The refractive index increment $\mathrm{d}n/\mathrm{d}c$, where c is the polymer concentration, can be related to the molecular weight of particles in solution. Further details of the method are provided by Pepper and Samuels (1989).

Low-frequency Raman spectroscopy

Low-frequency Raman spectroscopy (LFRS) has been used to measure the longitudinal acoustic mode (LAM) of semicrystalline diblocks containing poly(ethylene oxide) (Mai *et al.* 1996; Viras *et al.* 1988; Yang *et al.* 1995). The LAM mode frequency is inversely proportional to the crystal stem length, and indicates whether chains are folded or extended.

Rayleigh–Brillouin scattering

In the Rayleigh–Brillouin (R–B) technique, light scattering from phonons in the system is probed (Brown *et al.* 1992). The longitudinal hypersound velocity and spatial attenuation of the hypersonic wave are extracted from the frequency shift and the width of the Brillouin scattering peaks respectively. The method has been applied to investigate the dynamics (α and β relaxation) of polymer chains near the glass transition. Because it is depends on scattering from phonons, the R–B technique is sensitive to the shear modulus in the gigahertz frequency regime, i.e. much higher than that accessible in dynamic mechanical measurements. The method has been applied to study association of micelles into clusters in a Pluronic triblock copolymer in aqueous solution prior to the transition to a cubic gel phase of ordered micelles (Schillén *et al.* 1993). However, it does not provide quantitative information on gelation.

Forced Rayleigh scattering

In the forced Rayleigh scattering (FRS) technique, a transient optical grating (period 1–5μm) is established by exposing a sample containing 1–5% polymer end-labelled with a photochromic dye to crossed beams from a laser (Dalvi *et al.* 1993). The decay of the grating by mass diffusion is then monitored by diffraction of a probe beam from the same laser. A wide range of diffusion times ($10^{-5} \geq D \geq 10^{-16}\text{cm}^2\text{s}^{-1}$) can be probed using this technique.

Ultramicroscopy

In this technique, the movement of particles much smaller than the resolving power of an optical microscope is followed even though their actual size cannot be determined. Use is made of a suspension of small particles (0.02–1μm for organic particles), which perform Brownian motion due to the uneven forces exerted on them by the molecules of the fluid medium. Using an arrangement devised by Siedentopf and Zsigmondy (1903), a strong beam of horizontal light is directed onto the liquid containing the suspended particles and a vertically mounted microscope is focussed on a region just below the surface. The observer sees bright spots of scattered light moving in a dark field, use being made of the fact that the diffraction image around a particle is considerably larger than the particle itself. Price *et al.* (1979) used this technique to determine the diffusion coefficient and hydrodynamic radius of two PS–PI copolymers in solvents selective for the PS and PI block, and a block copolypeptide ionomer in water. The suspension particles were poly(styrene/divinyl benzene) lattices.

Surface forces experiments

This method has been used to obtain force–separation curves for block copolymers adsorbed on planar substrates and subjected to uniaxial compression. Block copolymers are adsorbed from solution onto atomically flat substrates (e.g. mica, quartz) and the force between the plates measured for separations ranging from $\approx$0.1μm to contact. Further details of the experiments are given in Section 3.8.2.

Forward recoil spectrometry

In forward recoil spectrometry (FRES), a beam of ionized helium ions is directed at a surface and the energy spectrum of recoiled protons and deuterons is measured. In a typical configuration, the beam is incident at an angle of 15° to the surface and the energy of recoiled particles is measured in the specular condition (i.e. in the forward scattering direction at 15° to the surface) (Green *et al.* 1986). The distribution of proton and deuteron energies reflects the distribution of the corresponding species as a function of depth in the film, the energy being lower for species nearer the surface. In this way copolymer volume fraction profiles normal to the surface can be constructed.

Nuclear reaction analysis

This method, related to FRES, is used to determine the concentration of deuterium-labelled chains as a function of depth at a surface. The technique

has been described by Klein (1990). Briefly, a beam of accelerated ^{3}He ions is incident on a polymer film. The nuclear reaction

$$^3\text{He} + {}^2\text{H} \rightarrow {}^4\text{He} + Q \quad (Q = 18.3\,\text{MeV})$$

takes place within the sample. From the energy loss of the emitted ^{4}He particles and the known energy losses and reaction cross-section, the concentration of deuterium is obtained as a function of depth.

Bibliography

Aggarwal, S. L. (ed.) (1970). *Block polymers*. Plenum, New York.

Allport, D. C. and Jones, W. H. (ed.) (1973). *Block copolymers*. Wiley, New York.

Bates, F. S. and Fredrickson, G. H. (1990). *Annual Reviews of Physical Chemistry*, **41**, 525.

Burke, J. J. and Weiss, V. (ed.) (1973). *Block and graft copolymers*. Syracuse University Press, New York.

Ceresa, R. J. (1962). *Block and graft copolymers*. Butterworths, London.

Ceresa, R. J. (ed.) (1972). *Block and graft copolymerization*. Wiley, New York.

Folkes, M. J. (ed.) (1985). *Processing, structure and properties of block copolymers*. Elsevier Applied Science, London.

Folkes, M. J. and Keller, A. (1973). The morphology of regular block copolymers. In *The physics of glassy polymers*, (ed. R. N. Haward). Applied Science, London.

Fredrickson, G. H. and Bates, F. S. (1996). *Annual Reviews of Materials Science*, **26**, 501.

Goodman, I. (ed.) (1982). *Developments in block copolymers*, Vol. 1. Applied Science, London.

Goodman, I. (ed.) (1985). *Developments in block copolymers*, Vol. 2. Elsevier Applied Science, London.

Meier, D. J. (ed.) (1983). *Block copolymers. Science and technology*. Harwood Academic Publishers, Chur, Switzerland.

Molau, G. E. (ed.) (1971). *Colloidal and morphological behaviour of block and graft copolymers*. Plenum, New York.

Noshay, A. and McGrath, J. E. (1977). *Block copolymers: overview and critical survey*. Academic, New York.

Riess, G., Hurtrez, G. and Bahadur, P. (1985). Block copolymers. In *Encyclopedia of polymer science and engineering*, Vol. 2, (ed. H. F. Mark and J. I. Kroschwitz). Wiley, New York.

Ryan, A. J. and Hamley, I. W. (1997). Morphology of block copolymers. In *The physics of glassy polymers*, (ed. R. N. Haward and R. J. Young). Chapman and Hall, London.

Tuzar, Z. and Kratochvíl, P. (1976). Block and graft copolymer micelles in solution. *Advances in Colloid and Interface Science*, **6**, 201.

References

Adams, E. T. (1989). Osmometry. In *Encyclopedia of polymer science and engineering*, Vol. 10, (ed. H. F. Mark, N. M. Bikales, C. G. Overberger and G. Menges). Wiley, New York.

Aggarwal, S. L. (1985). Introduction and overview. In *Processing, structure and properties of block copolymers*, (ed. M. J. Folkes). Elsevier, London.

Alward, D. B., Kinning, D. J., Thomas, E. L. and Fetters, L. J. (1986). *Macromolecules*, **19**, 215.

Balta-Calleja, F. J. and Vonk, C. G. (1989). *X-ray scattering of synthetic polymers*. Elsevier, London.

Berne, B. J. and Pecora, R. (1976). *Dynamic Light Scattering*. Wiley-Interscience, New York.

Booth, C., Naylor, T. D., Price, C., Rajab, N. S. and Stubbersfield, R. B. (1978). *Journal of the Chemical Society, Faraday Transactions I*, **74**, 2352.

Bovey, F. A. and Jelinksi, L. W. (1989). Nuclear magnetic resonance. In *Encyclopedia of polymer science and engineering*, Vol. 10, (ed. H. F. Mark, N. M. Bikales, C. G. Overberger and G. Menges). Wiley, New York.

Brown, R. A., Masters, A. J., Price, C. and Yuan, X. F. (1989). Chain segregation in block copolymers. In *Comprehensive polymer science*, Vol. 2, (ed. C. Booth and C. Price). Pergamon, Oxford.

Brown, W., Schillén, K., Johnsen, R. M., Konak, C. and Dvoranek, L. (1992). *Macromolecules*, **25**, 802.

Cowie, J. M. G. (1991). *Polymers: chemistry and physics of modern materials*. Blackie, London.

Dalvi, M. C., Eastman, C. E. and Lodge, T. P. (1993). *Physical Review Letters*, **71**, 2591.

Fleischer, G., Fujara, F. and Stühn, B. (1993). *Macromolecules*, **26**, 2340.

Flory, P. J. (1953). *Principles of polymer chemistry*. Cornell University Press, Ithaca.

Förster, S., Khandpur, A. K., Zhao, J., Bates, F. S., Hamley, I. W., Ryan, A. J. *et al.* (1994). *Macromolecules*, **27**, 6922.

Gedde, U. W. (1995). *Polymer Physics*. Chapman and Hall, London.

Glatter, O. and Kratky, O. (ed.) (1982). *Small angle X-ray scattering*. Academic, London.

Green, P. F., Mills, P. J. and Kramer, E. J. (1986). *Polymer*, **27**, 1063.

Guinier, A. (1939). *Annales de Physique*, **12**, 161.

Guinier, A. (1963). *X-ray diffraction*. W. H. Freeman, San Francisco. Reprinted by Dover, New York.

Guinier, A. and Fournet, G. (1955). *Small angle scattering of X-rays*. Wiley, New York.

Hajduk, D. A., Harper, P. E., Gruner, S. M., Honeker, C. C., Kim, G., Thomas, E. L. *et al.* (1994). *Macromolecules*, **27**, 4063.

Hamley, I. W. and Pedersen, J. S. (1994). *Journal of Applied Crystallography*, **27**, 29.

Higgins, J. S. and Benoît, H. C. (1994). *Polymers and neutron scattering*. Oxford University Press, Oxford.

Johnson, J. F. (1989). Chromatography. In *Encyclopedia of polymer science and engineering*, Vol. 3, (ed. H. F. Mark, N. M. Bikales, C. G. Overberger and G. Menges). Wiley, New York.

Kato, K. (1965). *Journal of Electron Microscopy (Japan)*, **14**, 220.

Kato, K. (1967). *Polymer Engineering Science*, **7**, 38.

Khandpur, A. K., Macosko, C. W. and Bates, F. S. (1995). *Journal of Polymer Science B: Polymer Physics*, **33**, 247.

Klein, J. (1990). *Science*, **250**, 640.

Kratky, O., Pilz, I. and Schmitz, P. J. (1966). *Journal of Colloid and Interface Science*, **21**, 24.

Kratky, O., Porod, G. and Kahovec, L. (1951). *Berichte der Bunsengesellscahft für Physikalische Chemie*, **55**, 53.

Laue, T. M. (1989). Ultracentrifugation. In *Encyclopedia of polymer science and engineering*, Vol. 17, (ed. H. F. Mark, N. M. Bikales, C. G. Overberger and G. Menges). Wiley, New York.

Macosko, C. W. (1994). *Rheology. Principles, measurements and applications*. VCH, New York.

Mai, S. M., Fairclough, J. P. A., Hamley, I. W., Denny, R. C., Liao, B., Booth, C. *et al.* (1996). *Macromolecules*, **29**, 6212.

Meiners, J. C., Ritzi, A., Rafailovich, M. H., Sokolov, J., Mlynek, J. and Krausch, G. (1995). *Applied Physics A*, **61**, 519.

Nace, V. M. (1996). *Nonionic surfactants. Polyoxyalkylene block copolymers*. Surfactant Science Series. Marcel Dekker, New York.

Parratt, L. G. (1954). *Physical Review*, **95**, 359.

Pepper, R. E. and Samuels, R. J. (1989). Refractometry. In *Encyclopedia of polymer science and engineering*, Vol. 14, (ed. H. F. Mark, N. M. Bikales, C. G. Overberger and G. Menges). Wiley, New York.

Porod, G. (1951). *Kolloid Zeitschrift*, **124**, 83.

Price, C. and Woods, D. (1973). *European Polymer Journal*, **9**, 827.

Price, C., Canham, P. A., Duggleby, M. C., Naylor, T. D., Rajab, N. S. and Stubbersfield, R. B. (1979). *Polymer*, **20**, 615.

Provencher, S. W. (1982). *Computational Physics Communications*, **27**, 229.

Richards, R. W. (1985). *Advances in Polymer Science*, **71**, 1.

Russell, T. P. (1990). *Materials Science Reports*, **5**, 171.

Schillén, K., Brown, W. and Konák, C. (1993). *Macromolecules*, **26**, 3611.

Schmolka, I. R. (1991). Polyoxamers in the pharmaceutical industry. In *Polymers for controlled drug delivery*, (ed. P. J. Tarcha). CRC Press, Boston.

Scwarc, M., Levy, M. and Milkovich, R. (1956). *Journal of the American Chemical Society*, **78**, 2656.

Siedentopf, H. and Zsigmondy, R. (1903). *Annalen der Physik*, **10**, 1.

Stepánek, P. and Lodge, T. P. (1996). *Macromolecules*, **29**, 1244.

Stepánek, P. and Lodge, T. P. (1996). Light scattering by block copolymer liquids in the disordered and ordered state. In *Light scattering. Principles and development*, (ed. W. Brown). Oxford University Press, Oxford.

Thomas, E. L. (1989). Electron microscopy. In *Encyclopedia of polymer science and engineering*, Vol. 5, (ed. H. F. Mark, N. M. Bikales, C. G. Overberger and G. Menges). Wiley, New York.

Thomas, E. L., Alward, D. B., Kinning, D. J., Martin, D. C., Handlin, D. L. and Fetters, L. J. (1986). *Macromolecules*, **19**, 2197.

Thompson, E. V. (1989). Thermal properties. In *Encyclopedia of polymer science and engineering*, Vol. 16, (ed. H. F. Mark, N. M. Bikales, C. G. Overberger and G. Menges). Wiley, New York.

Tuzar, Z. and Kratochvíl, P. (1972). *Makromoleculaire Chemie*, **160**, 301.

Tuzar, Z. and Kratochvil, P. (1993). Micelles of block and graft copolymers in solutions. In *Surface and colloid science*, Vol. 15, (ed. E. Matijevic). Plenum, New York.

Tuzar, Z. and Kratochvil, P. (1996). Scattering from block copolymer micellar systems. In *Light scattering. Principles and development*, (ed. W. Brown). Oxford University Press, Oxford.

Tuzar, Z., Petrus, V. and Kratochvíl, P. (1974). *Makromoleculaire Chemie*, **175**, 3181.

Valic, S., Deloche, B., Gallot, Y. and Skoulios, A. (1994). *Comptes Rendus de l'Academie des Sciences de Paris II*, **318**, 1027.

Valic, S., Deloche, B., Gallot, Y. and Skoulios, A. (1995). *Polymer*, **36**, 3041.

van de Hulst, H. C. (1957). *Light scattering by small particles*. Dover, New York.

Viras, F., Luo, Y.-Z., Viras, K., Mobbs, R. H., King, T. A. and Booth, C. (1988). *Makromoleculaire Chemie*, **189**, 459.

Wang, Q., Price, C. and Booth, C. (1992). *Journal of the Chemical Society, Faraday Transactions*, **88**, 1437.

Yang, Y.-W., Tanodekaew, S., Mai, S.-M., Booth, C., Ryan, A. J., Bras, W. *et al.* (1995). *Macromolecules*, **28**, 6029.

Young, R. J. and Lovell, P. A. (1991). *Introduction to polymers*. Chapman and Hall, London.

Zoller, P. (1989). Dilatometry. In *Encyclopedia of polymer science and engineering*, Vol. 5, (ed. H. F. Mark, N. M. Bikales, C. G. Overberger and G. Menges). Wiley, New York.

2 Melt phase behaviour of block copolymers

2.1 Introduction

A remarkable property of block copolymers is their ability to self-assemble in the melt into a variety of ordered structures with nanoscale periodicities. These structures can be controlled by varying the composition of the block copolymer or the segregation between blocks (via temperature or degree of polymerization). In addition to the now well-established lamellar (lam), hexagonal-packed cylinder (hex) and body-centred cubic (BCC) micelle phases, a number of new morphologies have been discovered, which supplement the 'classical' structures. The identification of a bicontinuous cubic phase of $Ia\bar{3}d$ symmetry, sometimes called the gyroid phase, is now established. Other 'perforated layer' structures have been reported, but seem to be metastable structures formed during the transition to the gyroid structure. In this chapter, the disordered phase is abbreviated by dis.

The dynamics of block copolymers are equally intriguing, leading to complex linear viscoelastic behaviour and anisotropic diffusion processes. The non-linear viscoelastic behaviour is similarly rich, although the study of the effect of external fields (shear, electric . . .) on the alignment and orientation of ordered structures in block copolymer melts is still in its infancy. Furthermore, these fields can influence the thermodynamics of block copolymer melts, as recent work has shown that phase transition lines shift depending on the applied shear.

The properties of ordered structures in block copolymer melts have yet to be fully exploited, but the structural and rheological anisotropy is likely to lead to applications not all of which can be envisaged yet. The precision self-assembly of block copolymers into ordered structures for thin film and interfacial applications has enormous potential. Other applications such as nanoscale templates, membranes and filters could exploit the self-assembly of block copolymers into domains with periods $\approx$10–100 nm. The possibilities are limited only by the molecular engineer's imagination.

A review of the thermodynamics of block copolymer melts prior to the discovery of complex phases was presented by Bates and Fredrickson (1990). Ryan and Hamley (1997) have recently reviewed the morphology of block copolymers containing a glassy component, in the melt and glassy states, and a discussion of complex phases is included. Fredrickson and Bates (1996) and Colby (1996) have reviewed the dynamics of block copolymer melts, of which the former is a par-

ticularly thorough survey. Hashimoto has also recently summarized the work of the Kyoto group on the melt phase behaviour of block copolymers (Hasegawa and Hashimoto 1996; Hashimoto 1996). Earlier reviews are discussed in the introductory chapter. Here we do not intend a full historical survey, but rather give a view of the current 'state of the art'.

In this chapter we focus on melts of well-defined block copolymers synthesized anionically, i.e. block copolymers with a narrow molecular weight distribution. These polymers serve as model materials for investigating the rich phase behaviour and dynamics of block copolymers in the bulk and in thin films.

This chapter is organized as follows. In Section 2.2, experimental studies of the phase behaviour of block copolymers are reviewed, with particular emphasis on recent experiments where the full phase diagram has largely been mapped. In Section 2.3, theories for microphase separation and the formation of ordered structures in block copolymer melts are outlined. The early mean field theories corresponding to the strong segregation and weak segregation limits are first sketched, then an outline is given of recent developments of the self-consistent field theory, which covers the entire range of block segregations. Fluctuation effects on the mean field phase behaviour are also discussed. Section 2.4 contains a summary of experiments and theory/computer simulation of dynamic processes in block copolymer melts, such as the kinetics of formation of ordered structures and chain diffusion in microphase-separated structures. Finally, in Section 2.5, research on thin films of block copolymer melts is summarized, with an emphasis on the effect of confinement on the bulk structure.

2.2 Experimental studies of the phase behaviour of block copolymers

2.2.1 Classical phases in diblocks and triblocks

In the melt, block copolymers can self-assemble into a variety of ordered structures via the process of *microphase separation*. Microphase separation is driven by the enthalpy of demixing of the constituent components of the block copolymers, whilst macrophase separation is prevented by the chemical connectivity of the blocks. This enthalpy is proportional to the Flory–Huggins segmental interaction parameter χ, which is found to be inversely proportional to temperature and is usually parameterized as $\chi = A/T + B$. Microphase separation leads to ordered structures with periods of several R_g, where R_g is the copolymer radius of gyration. The enthalpic penalty associated with the chain stretching is proportional to the degree of polymerization N. The product χN that expresses the enthalpic–entropic balance is then used to parameterize block copolymer phase behaviour, along with the composition of the copolymer. For a diblock copolymer, the volume fraction of one component, f, controls which ordered structures are accessed beneath the order–disorder transition (ODT). Depending on the degree of incompatibility χN, several regimes have been identified: the weak segregation limit (WSL) corresponds to χN close to $(\chi N)_{\mathrm{ODT}}$. For a symmetric diblock $(\chi N)_{\mathrm{ODT}} = 10.5$ in the mean field limit, the WSL regime extending to

$\chi N \approx 12$, as estimated by Matsen and Bates (1996*a*). The intermediate segregation regime ranges up to about $\chi N \approx 100$, and the strong segregation limit (SSL) extends to higher incompatibilities. The precise definition of these limits depends on the criterion used, for example the purity of each component, which increases as the SSL is approached. In the WSL regime, the composition profile is essentially sinusoidal whereas in the asymptotic SSL limit the components are essentially pure and the interphase between them is narrow (Fig. 2.1).

Symmetric block copolymers form a lamellar phase, with alternating layers of the constituent blocks. For more asymmetric copolymers (i.e. as f varies further from $\frac{1}{2}$) it becomes energetically more favourable for phases with curved interfaces to form. In particular, on increasing $|f - \frac{1}{2}|$ the following sequence of phases is observed in the WSL: a bicontinuous cubic 'gyroid' phase, a phase of hexagonal-packed cylinders and a body-centred cubic phase, with a step increase in mean interfacial curvature on changing morphology in this sequence. However, the interfacial curvature alone does not govern the structure because there is also an entropic penalty for stretching polymer coils to fill space uniformly, i.e. there is a competing tendency towards formation of domains of uniform thickness (Matsen and Bates 1996*b*). In the strong segregation limit, the following sequence of phases is observed for PS-PI diblocks: $f_{PS} < 0.17$, BCC; $0.17 < f_{PS} < 0.28$, hex; $0.28 < f_{PS} < 0.34$, gyroid; $0.34 < f_{PS} < 0.62$, lam; $0.62 < f_{PS} < 0.66$, gyroid; $0.66 < f_{PS} < 0.77$, hex; $f_{PS} > 0.77$, BCC (Bates and Fredrickson 1990).

A phase diagram constructed from experiments on a series of poly(styrene)–poly(isoprene) (PS–PI) diblocks is presented in Fig. 2.2 (Khandpur *et al.* 1995) and this will be used as a guide for the various microstructures. In order to determine a phase diagram experimentally, a variety of methods are

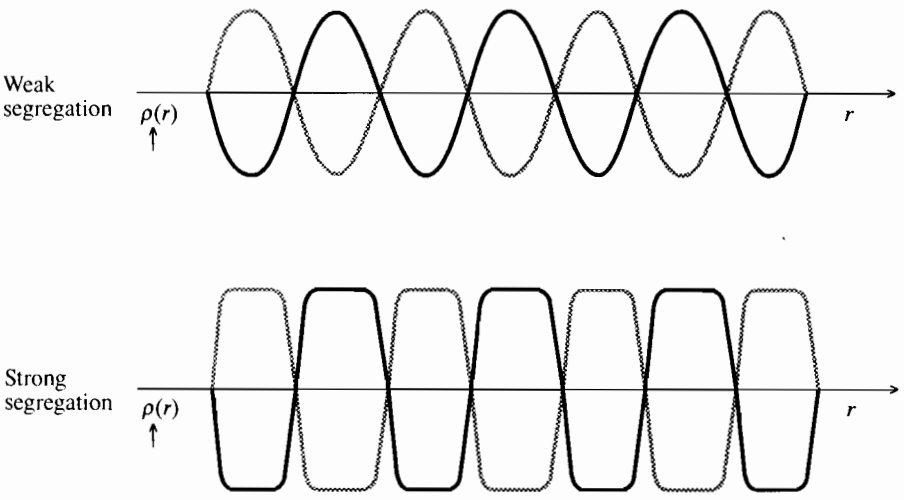

Fig. 2.1 Composition profiles of A and B components in the weak and strong segregation limits, compared to the mean (straight line).

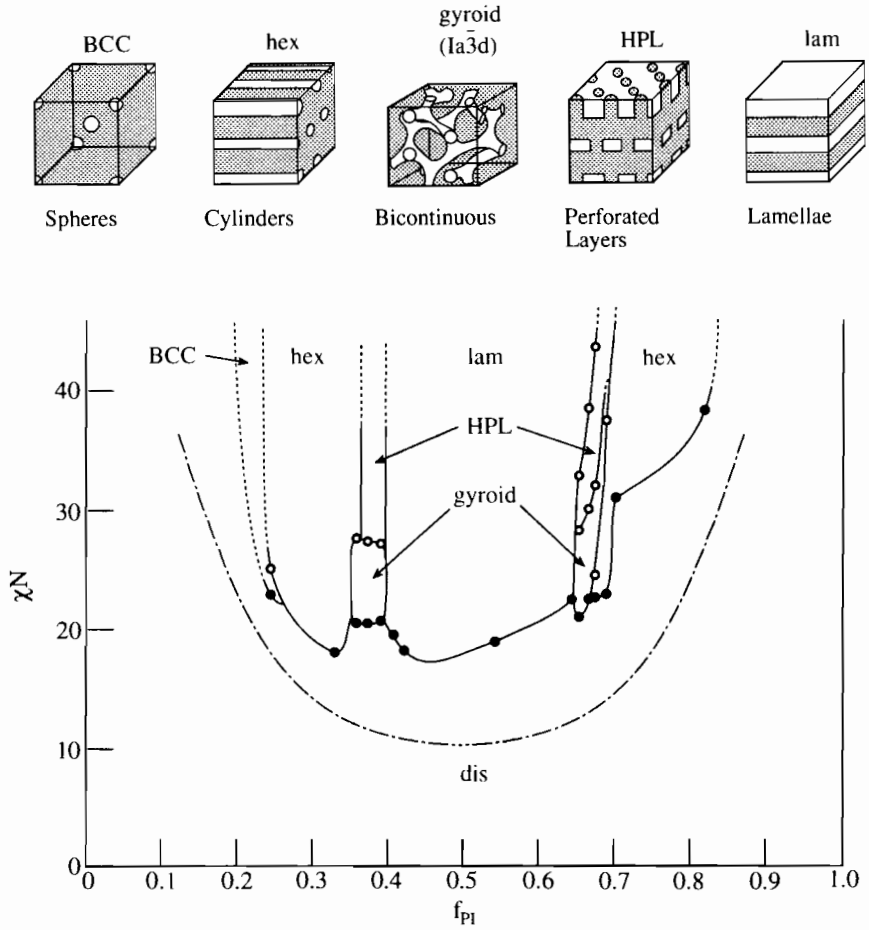

Fig. 2.2 Experimentally-determined phase diagram for PS–PI diblock copolymers (Khandpur *et al.* 1995).

usually employed. First, the temperature dependence of χ is determined, for example by measuring the ODT of a series of polymers by rheology. The microstructure of the copolymers can then be determined by a combination of small-angle X-ray scattering (SAXS), small-angle neutron scattering (SANS) and transmission electron microscopy (TEM). It is possible to assess the block copolymer microstructure from just the SAXS powder pattern if enough reflections are sampled for the pattern to be indexed unambiguously, but this is often the exception rather than the rule. TEM is useful because it provides a direct picture of the morphology, albeit in a small area of the sample. The combination of TEM and scattering from oriented samples makes structure solution relatively simple.

Rheology can be used to locate order–order and order–disorder phase transitions, but not to unambiguously identify a phase. However, the low frequency

scaling of the dynamic shear moduli can provide an indication of the type of structure (disordered liquid, liquid crystal or three-dimensional solid). Representative frequency sweeps for a series of diblocks with different morphologies are shown in Fig. 2.3. The BCC spherical structure and the cubic gyroid phase behave as solids, with the dynamic elastic shear modulus G' independent of frequency in the linear regime at high frequencies. On the other hand, both moduli for the lam and hex phases are strongly frequency dependent for all frequencies.

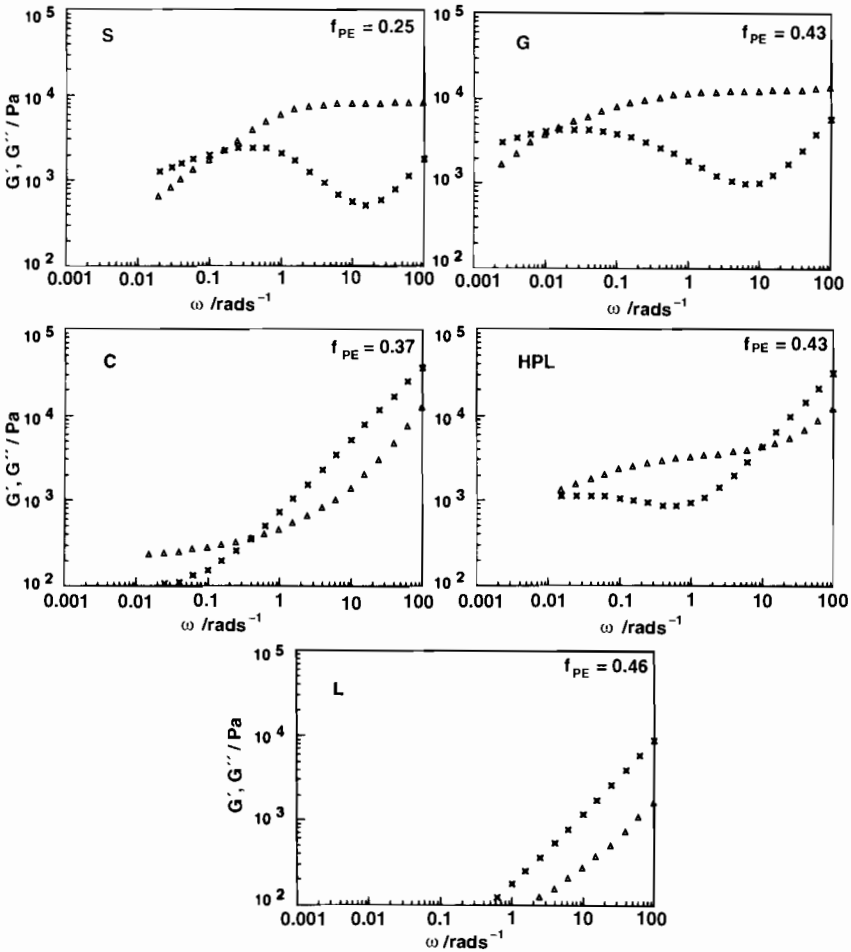

Fig. 2.3 Typical isothermal frequency scans for PE–PEE diblocks with indicated compositions in different ordered phases (Zhao *et al.* 1996). Qualitative differences between the low frequency rheological response for distinct ordered structures similar to these are observed for other diblocks. S = BCC spheres, C = hex cylinders, G = $Ia\bar{3}d$ gyroid, HPL = hexagonal perforated layer, L = lamellae. (△) G', (×) G''. Structural assignments of the ordered phases were made using TEM and SAXS.

The order–disorder transition

The ODT can be located via a number of methods. From rheological measurements, the ODT is identified from a sharp decrease in the low frequency isochronal dynamic elastic moduli obtained during a heating ramp (Bates *et al.* 1990; Rosedale and Bates 1990) (Fig. 2.4(a)); however, this method does not generally provide a well-defined temperature for the ordered BCC–disordered phase

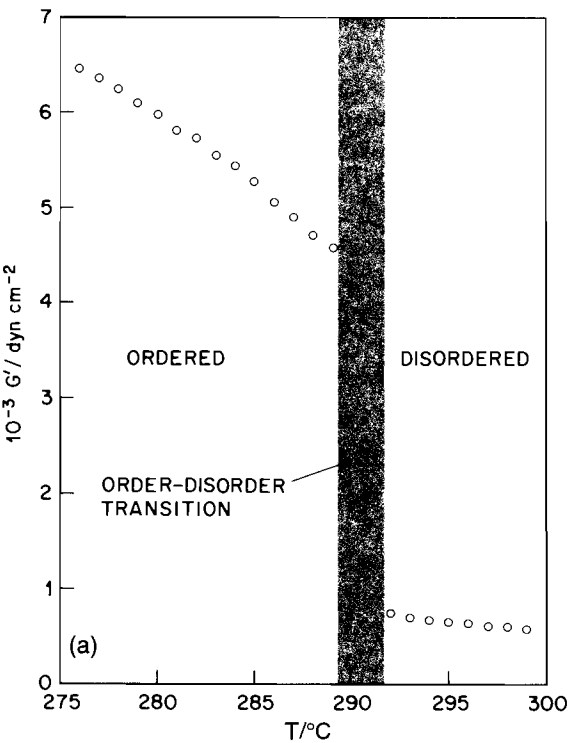

Fig. 2.4 (a) Temperature ramp at a frequency $\omega = 10\,\mathrm{rad\,s^{-1}}$ (strain amplitude $\lambda = 2\%$) for a nearly symmetric PEP–PEE diblock with $M_n = 8.1 \times 10^4\,\mathrm{g\,mol^{-1}}$, heating from the lamellar phase into the disordered phase. The order–disorder transition occurs at $291 \pm 1\,^{\circ}\mathrm{C}$, the grey band indicates the experimental uncertainty on the ODT (Rosedale and Bates 1990). (b) Dynamic elastic shear modulus as a function of reduced frequency (here a_T is the time–temperature superposition shift factor) for a nearly symmetric PEP–PEE diblock with $M_n = 5.0 \times 10^4\,\mathrm{g\,mol^{-1}}$. Shift factors were determined by concurrently superimposing G' and G'' for $\omega > \omega_c'$ and $\omega > \omega_c''$ respectively. The filled and open symbols correspond to the ordered and disordered states respectively. The temperature dependence of G' ($\omega < \omega_c'$) for $96 \leq T/^{\circ}\mathrm{C} \leq 135$ derives from the effects of composition fluctuations in the disordered state (Rosedale and Bates 1990). (c) G' vs. G'' for a PS–PI diblock with $f_{PS} = 0.83$ (forming a BCC phase): (⊙) 110 °C; (△) 115 °C; (□) 120 °C; (▽) 125 °C; (•) 130 °C; (▲) 135 °C; (■) 140 °C (▼) 145 °C. The ODT occurs at about 130 °C (Han *et al.* 1995).

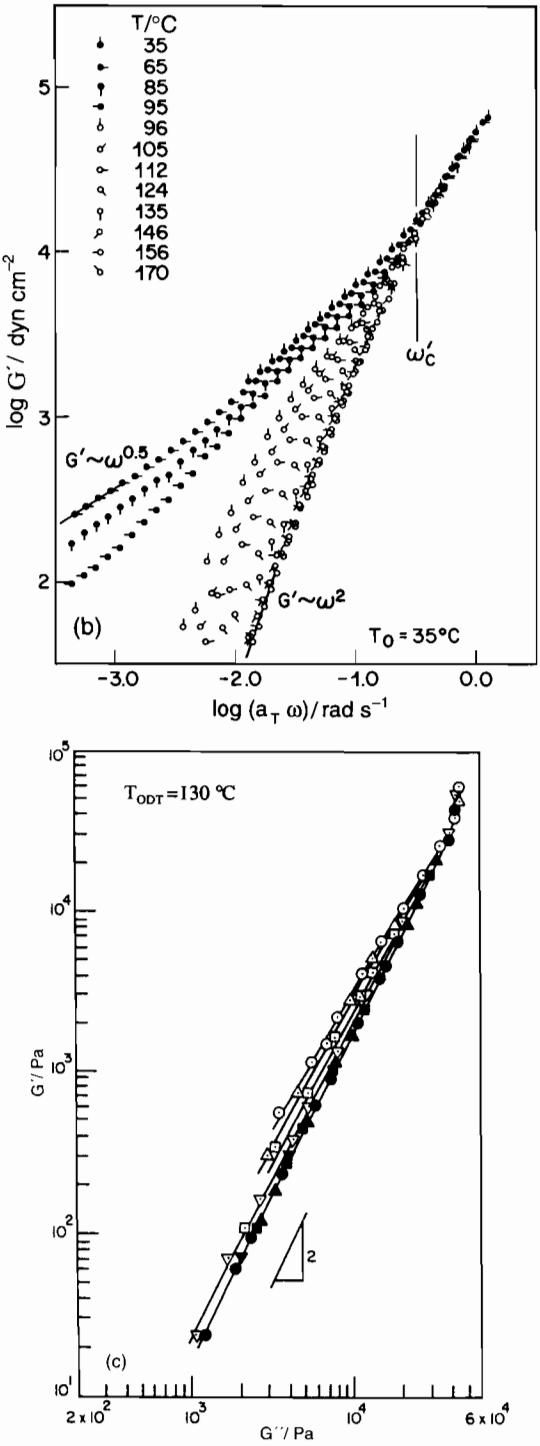

Fig. 2.4 *Continued.*

transition (Han *et al.* 1995; Sakamoto *et al.* 1997). It has been observed by Bates and co-workers that time–temperature superposition can be used to superpose frequency sweeps obtained at different temperatures, and curves of the dynamic elastic modulus as a function of frequency for the ordered lam or hex phase are found to lie on a different branch to those for the disordered phase (Bates *et al.* 1990; Rosedale and Bates 1990) (Fig. 2.4(b)). However, it has been suggested that plots of G' vs. G'' can be used to locate the ODT even for highly asymmetric block copolymers forming a BCC phase, as illustrated in Fig. 2.4(c) (Han *et al.* 1995).

Small-angle scattering techniques are an accurate method of determining the ODT. Both the peak intensity and width show a discontinuity at the transition, although most work indicates that the peak position, q^*, varies continuously (Almdal *et al.* 1990; Mai *et al.* 1996; Sakamoto and Hashimoto 1995). To facilitate comparison with theory, the inverse intensity, I^{-1}, is plotted against the inverse temperature, as shown in Fig. 2.5 (Hasegawa and Hashimoto 1996; Sakamoto and Hashimoto 1995). At high temperatures in the disordered phase the inverse intensity decreases linearly with T^{-1} in agreement with mean field theory (Leibler 1980). As the ODT is approached, composition fluctuations become

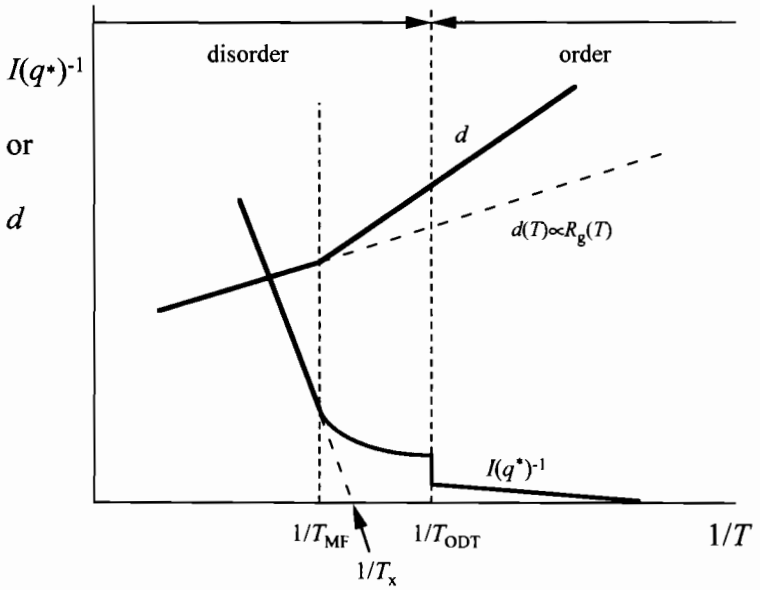

Fig. 2.5 Schematic showing the variation of inverse scattering intensity and domain spacing (as determined from SAXS or SANS) across the order–disorder transition of a block copolymer melt. The mean field transition temperature has been identified operationally as the point where, on heating, the inverse intensity crosses over to a linear dependence on T^{-1} (after Sakamoto and Hashimoto 1995).

more significant and this leads to a non-linear dependence of I^{-1} against T^{-1}. At the ODT, I^{-1} decreases discontinuously. This feature and the non-linear dependence of I^{-1} vs. T^{-1} were first noted by Bates *et al.* (1988, 1990). However, they observed no change in the temperature dependence of $q^* = 2\pi/d$ (where d is the domain spacing) at the ODT, as indicated in Fig. 2.5. More recent work indicates a change in the slope $\mathrm{d}\ln q^*/\mathrm{d}T$ at higher temperatures, which was interpreted as a crossover to mean field behaviour (Rosedale *et al.* 1995). For diblocks composed of pairs of poly(ethylene) (PE), poly(ethyl ethylene) (PEE) or poly(ethylene–propylene) (PEP), it was found that $d\ln q^*/\mathrm{d}T$ is larger than $-\mathrm{d}\ln(R_g)/\mathrm{d}T$ for all three homopolymers for $T > T_x$, where T_x was associated with a mean field–non-mean field transition (Rosedale *et al.* 1995). This was interpreted by Bates and co-workers (Rosedale *et al.* 1995) on the basis of a Gaussian-stretched coil transition (GST) (Almdal *et al.* 1990). Other groups have also reported that the domain spacing starts to vary with temperature faster than the unperturbed radius of gyration at T_x for PS–PI diblocks (Hashimoto *et al.* 1994; Sakamoto and Hashimoto 1994; Stühn *et al.* 1992). Data showing the determination of the ODT via a change in peak width have been presented by Stühn *et al.* (1992), Sakamoto and Hashimoto (1995) and Mai *et al.* (1996) amongst others. The latter parameterized the evolution from a Lorentzian peak in the disordered phase to a Gaussian peak (arising from the instrumental resolution function) in the ordered phase using a Pearson VII function (Mai *et al.* 1996).

Lamellar phase

The most simple ordered morphology is lamellar and an electron micrograph of a polydomain, lamellar, poly(styrene)–poly(isoprene) (PS–PI) ($f_{PS} = 0.64$) block copolymer is shown in Fig. 2.6(a) (Khandpur *et al.* 1995). Long-range order of lamellae within the domains is obvious from the micrograph. The SAXS pattern for the same polymer, which takes an ensemble average over the scattering volume ($\approx 1\ \mathrm{mm}^3$), is isotropic and comprises a series of Debye–Scherrer rings in the position ratio 1:2:3:4. Fig. 2.6(b) shows the powder SAXS pattern, from which the lamellar period is calculated to be $d = 2\pi/q^* = 233$ Å. The individual block lamellar thicknesses can be readily calculated from the corresponding volume fractions.

The first experiments on flow-induced orientation in the lamellar phase of block copolymers were performed by Keller and co-workers (Dlugosz *et al.* 1973; Folkes and Keller 1976). They performed SAXS experiments on an extruded triblock copolymer, and observed circular annuli of lamellae similar to the growth rings of a tree (Dlugosz *et al.* 1973). Later, a modification to the extrusion apparatus enabled sheet-oriented lamellae to be formed (Folkes and Keller 1976). Oriented lamellar microstructures can be seen in Fig. 2.7(a), which shows a TEM micrograph of a local monodomain in a poly(styrene)–poly(2-vinylpyridine) (PS–P2VP) diblock that has been shear oriented in the melt (Schulz *et al.* 1996). Figure 2.7(b) shows SANS patterns of the scattering in three orthogonal orientations defined with respect to the shear direction in Fig. 2.7(c). When the neutron beam is orthogonal to the lamellae (in the parallel orienta-

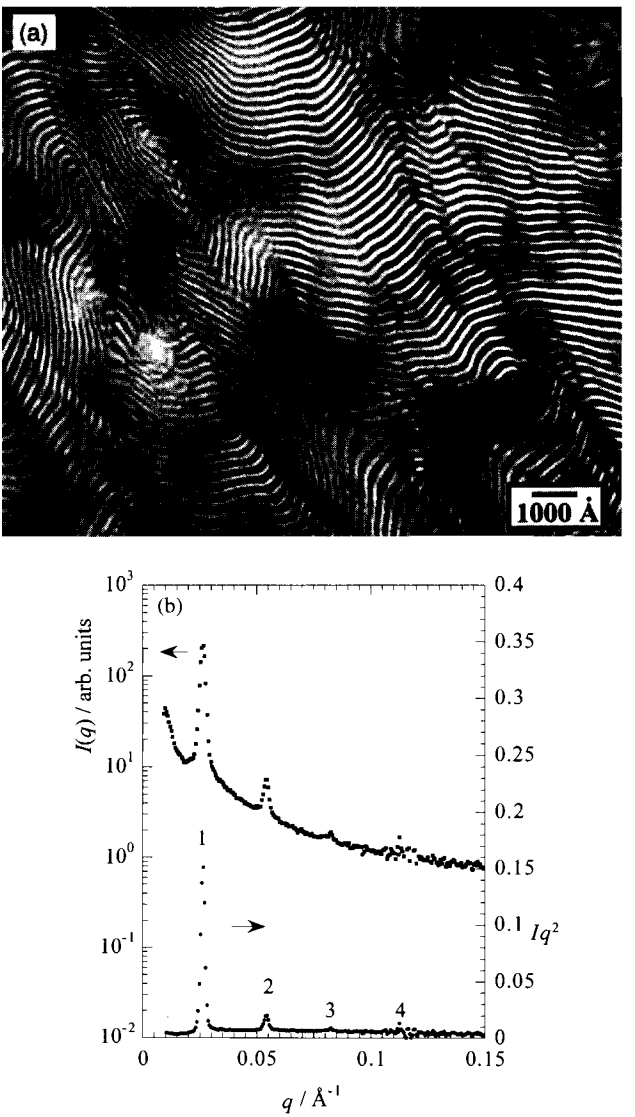

Fig. 2.6 (a) The lamellar microstructure of a PS–PI diblock with $f_{PS} = 0.64$ and $M_n = 39$ kg mol^{-1} shown by TEM where the PI is stained dark (Khandpur *et al.* 1995); (b) SAXS powder pattern from the same material.

tion) there is very little scattering, but when the neutrons are incident parallel to the lamellae there are strongly oriented SANS patterns with relection at q^* and $2q^*$ from the oriented layers in the block copolymer (Schulz *et al.* 1996). These oriented specimens were prepared by shearing in the ordered melt, quenching into liquid nitrogen and then cutting up the vitrified sample (PS is a glass below

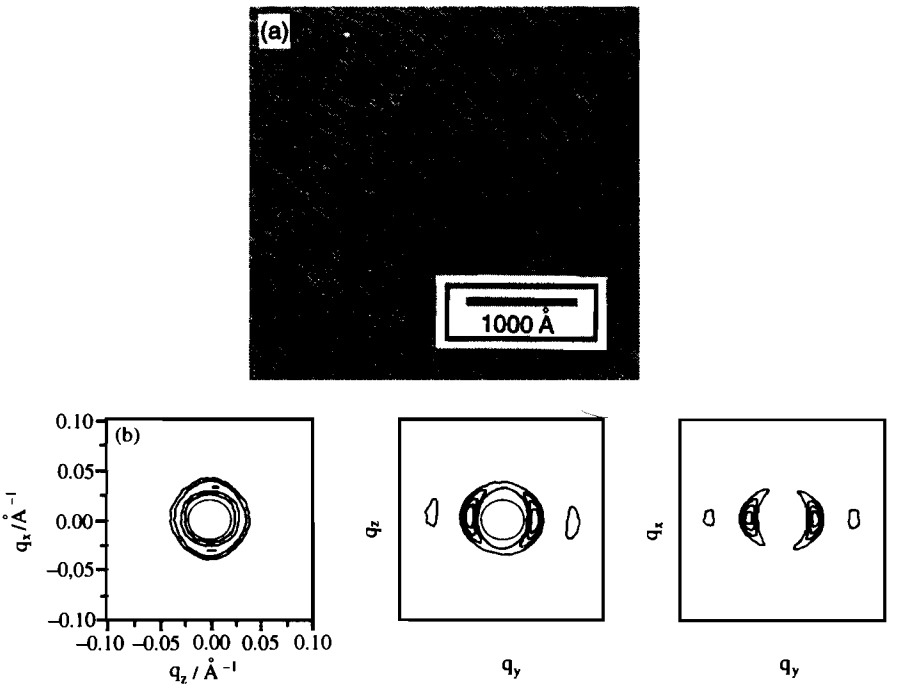

Fig. 2.7 (a) TEM micrograph from an $f_{PS} = 0.40$, $N_n = 209$ PS–P2VP diblock, annealed at 140 °C for 6 h then quenched in liquid nitrogen. Iodine was used to selectively stain the PVP. (b) SANS pattern from the same phase after preshearing at 140 °C (Schulz *et al.* 1996). (c) Possible orientations of the lam phase with respect to the shear coordinates.

about 100 °C). It is also possible to prepare lamellar samples in parallel and perpendicular orientations (where these denote the lamellar normal orientation with respect to the shear plane) by shearing polymers in the non-linear viscoelastic regime (i.e. at large strain amplitudes) and varying the shear–temperature protocol (Koppi *et al.* 1992), as discussed in Section 2.4.3. Figure 2.8 shows SAXS patterns obtained from a symmetric PS–PI diblock sheared at three different reduced frequencies $\omega\tau$ (Zhang *et al.* 1995). Parallel, perpendicular and parallel orientations are observed at high, intermediate and low reduced frequencies respectively. The 'dynamic phase diagram' for sheared lamellar samples is discussed further in Section 2.4.3.

The rheology of lamellar phases has attracted considerable attention. For a quenched lamellar phase it has been observed that where $G' \approx G''$ both scale as $\omega^{1/2}$ for $\omega < \omega_c$, where ω_c is determined operationally as being approximately equal to $0.1\ \tau^{-1}$, where τ is a single-chain relaxation time defined as the frequency where G' and G'' cross (Bates *et al.* 1987; Rosedale and Bates 1990). Similar dynamic moduli scaling was found with PS–PI–PS and PS–PB–PS triblocks (here

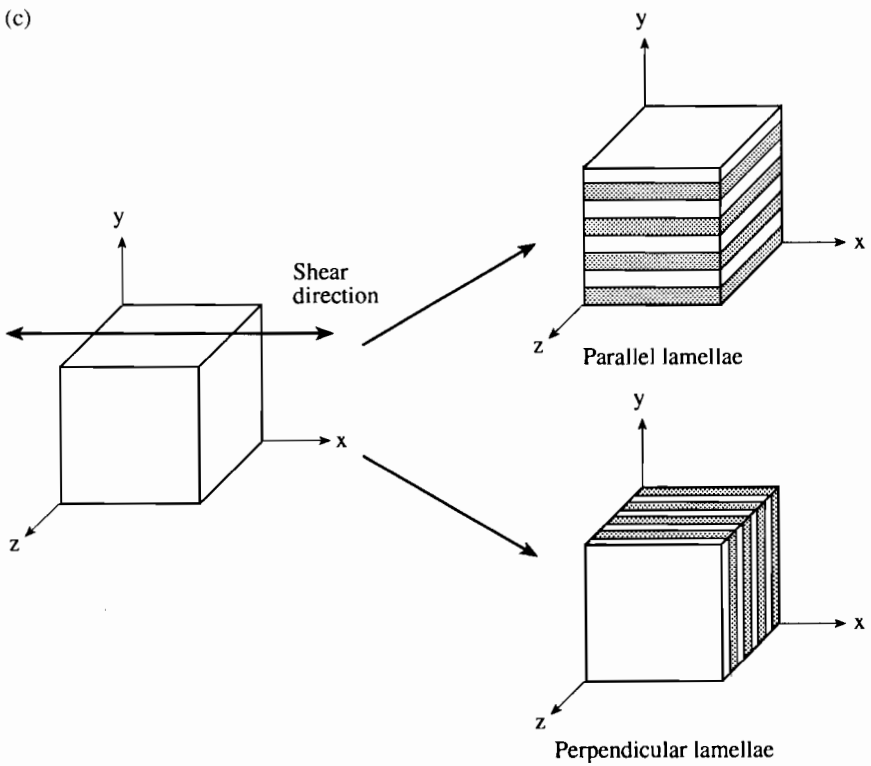

Fig. 2.7 *Continued.*

PB denotes poly(butadiene)) (Chung and Gale 1976; Gouinlock and Porter 1977).

Hexagonal-packed cylinder phase

The first example of the use of scattering from a shear oriented block copolymer was given by Keller and co-workers (Folkes and Keller 1973; Keller *et al.* 1970). Their micrographs from the hexagonal phase of Kraton TR1107 (PS–PB–PS triblock, $f_{PS} = 0.75$) are reproduced here (in Fig. 2.9(a)); when viewed end-on the hexagonal arrangement of the rods is obvious. The powder SAXS pattern from the same grade of polymer (see Fig. 2.9(b)) shows the classical higher order reflections in the ratio $1:\sqrt{3}:\sqrt{7}:\sqrt{9}$. There should also be a reflection at $\sqrt{4}q^*$ but this is coincident with a minimum in the form factor of the cylinders and is systematically absent. The combination of TEM and SAXS is needed to confirm the structure.

The polydomain structure which exists in unoriented hexagonal block copolymers may be seen in Fig. 2.10(a) where the TEM of a PS–P2VP diblock ($f_{PS} = 0.70$) shows two grains which are imaged parallel and perpendicular to the

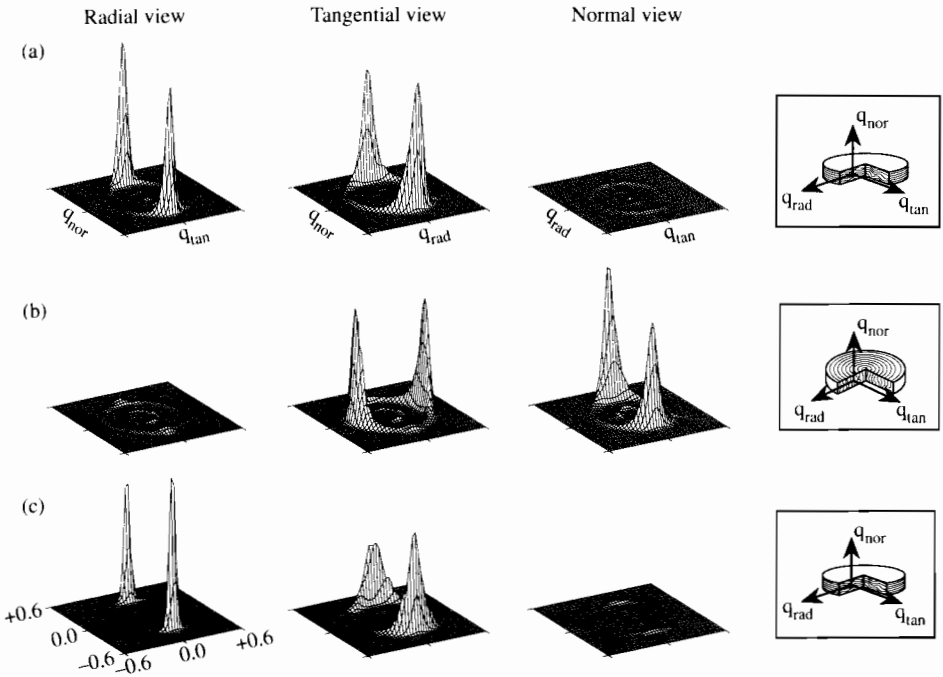

Fig. 2.8 Two-dimensional SAXS patterns for a PS–PI diblock with 43 wt% PS following large-amplitude ($\lambda = 100\%$) oscillatory shearing. Specimens were cut from discs at half the radius, corresponding to 50% strain. (a) $T = 383\,\mathrm{K}$ and $\omega = 10\,\mathrm{rad\,s^{-1}}$ for 5 h; (b) $T = 383\,\mathrm{K}$ and $\omega = 1\,\mathrm{rad\,s^{-1}}$ for 11.5 h; (c) $T = 393\,\mathrm{K}$ and $\omega = 1\,\mathrm{rad\,s^{-1}}$ for 7.5 h. In the insets on the right-hand side, the resulting orientations of the lamellae are depicted (Zhang *et al.* 1995).

rods (Schulz *et al.* 1996). The long-range order that can be induced by shearing is obvious in the SANS patterns in Fig. 2.10(b). The central pattern shows the hexagonal symmetry obtained when the neutron beam is parallel to the rods (and the shear direction), the two outer patterns show only the Bragg peaks arising from planes of rods.

The first studies to show the effect of reciprocating shear on a block copolymer were performed on the hexagonal phase of a PS–PB–PS triblock by Hadzioannou *et al.* 1979*a*,*b*). They demonstrated using SAXS that 'monodomain' specimens could be prepared by reciprocating planar shear. Almdal *et al.* (1992) showed that large-amplitude oscillatory shear can be used to prepare well-oriented domains of the hex phase, by performing SANS on a presheared PEP–PEE diblock. For the PEP–PEE system, it has been found that polymers with $f_{PEP} > 0.5$ exhibit excellent ordering, although samples with $f_{PEP} < 0.5$ are difficult to align. Thus, stiff cylinders (in this case PEP) in a soft matrix are harder to align than the reverse structure (Fredrickson and Bates 1996). Usually, the parallel orientation (of (10) planes with respect to the shear plane) is

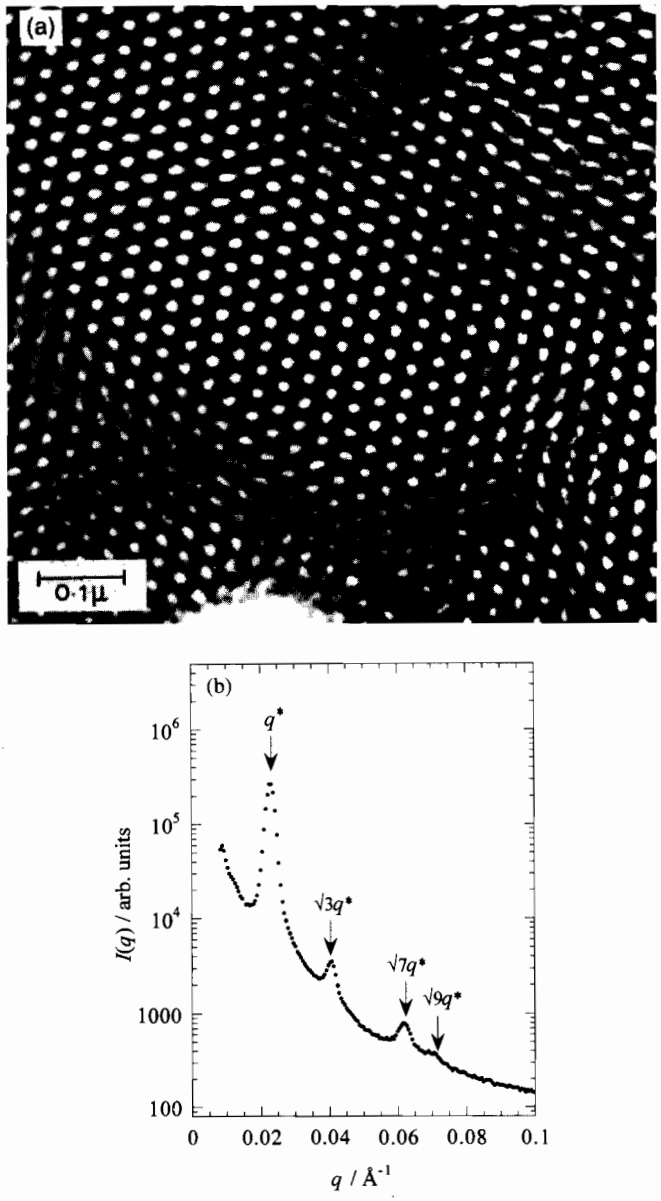

Fig. 2.9 (a) TEM micrographs from the hexagonal morphology in Kraton TR1102, a PS–PB–PS block copolymer with $f_{PS} \approx 0.24$ (Dlugosz *et al.* 1970; Keller and Odell 1985). (b) SAXS powder pattern from Kraton TR1102 (Ryan and Hamley 1997).

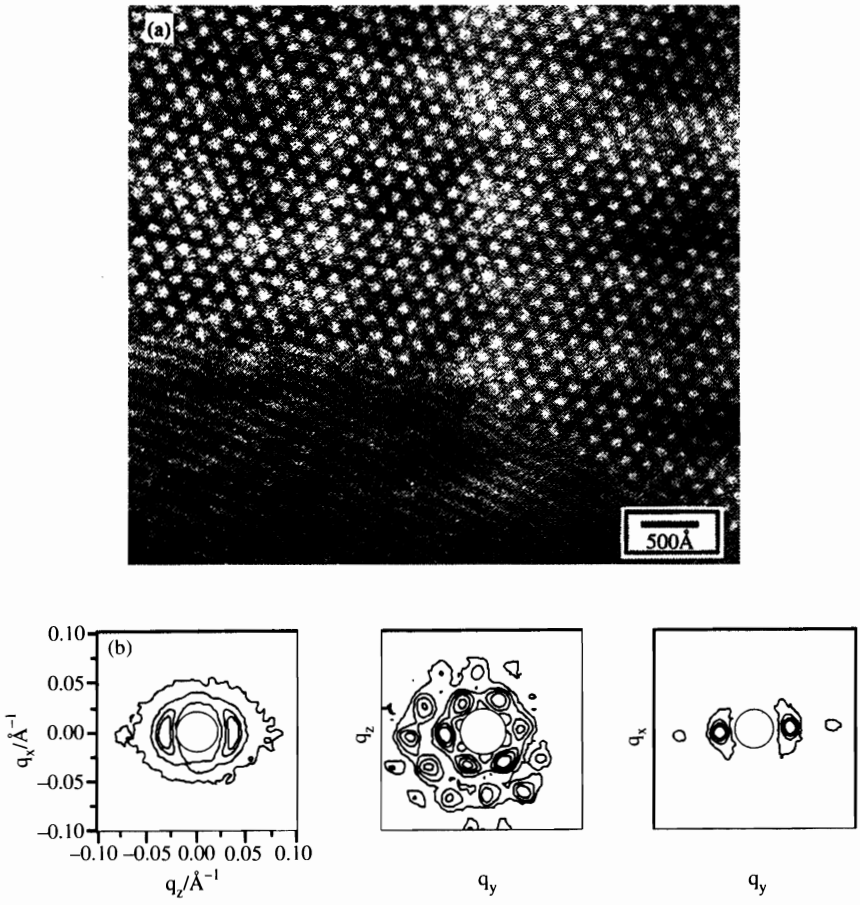

Fig. 2.10 (a) TEM for an $f_{PS} = 0.35$, $N_n = 203$ PS–PVP diblock obtained after annealing at 140 °C for more than 6 h. The PVP-rich region appears dark. (b) SANS patterns from a presheared specimen under the same conditions (Schulz *et al.* 1996).

obtained; however, Tepe *et al.* (1995) showed that the perpendicular orientation could be obtained in a PE–PEP diblock by cooling the disordered melt under high shear. Morrison *et al.* (1993) used SANS to probe the effect of shear on a PS–PB–PS triblock with 23 wt% PS block. The same polymer was used by Nakatani *et al.* (1996) to determine the effect of shear on the order–disorder transition (this work is discussed in Section 2.4.1) and Winter *et al.* (1993) used SAXS to confirm orientation induced by large-amplitude oscillatory Couette shear in a cylinder-forming PS–PI–PS triblock.

Bates *et al.* (1994) suggested that the oriented hex–disorder transition of previously sheared hex phase proceeds via a transient undulating cylinder or BCC spherical state (see Fig. 2.11). This was supported by the observation of the devel-

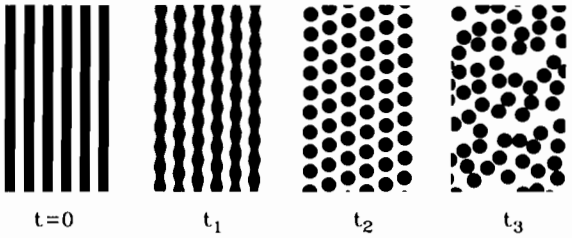

Fig. 2.11 Schematic representation of the transition from hexagonally packed cylinders to disorder following cessation of large-amplitude shear, deduced from SANS experiments on an asymmetric PEP–PEE diblock (Bates *et al.* 1994). Shear was used to stabilize a hex phase above the equilibrium ODT, and the relaxation back to the equilibrium disordered phase was followed after the shear was stopped. Close to the ODT, the transition $\tau_1 \rightarrow \tau_3$ was postulated, while at a higher temperature, $(\tau_1) \rightarrow \tau_2 \rightarrow \tau_3$ was indicated.

opment of azimuthal peaks as a function of time in the SANS pattern at a fixed temperature in the disordered phase, following cessation of shear which stabilized the hex phase above the equilibrium ODT.

BCC phase

A good example of the microstructure observed via TEM for a well-ordered BCC phase is given in Fig. 2.12(a) and (b) which shows the four-fold symmetry due to a [100] projection and the hexagonal symmetry due to a [111] projection of the cubic array respectively. This TEM was obtained for a Y-shaped block copolymer that has two PI arms and a PS arm (Pochan *et al.* 1996*b*) with $f_{PS} = 0.17$. Long-range order may be introduced in this meterial by solvent casting and in Fig. 2.13 the 2D SAXS pattern shows seven orders of reflection, indicative of such long-range order, with the four-fold symmetry of an approximate [100] zone axis. In powder patterns from the BCC phase, reflections are expected with peak positions in the ratio $1:\sqrt{2}:\sqrt{3}:\sqrt{4}:\sqrt{5}:\ldots$.

The first diffraction experiments on shear-oriented block copolymers in the BCC phase were performed by Almdal *et al.* (1993). They sheared a PEP–PEE diblock with $f_{PEP} = 0.83$ using a custom-made shear machine, and then cut up the resulting oriented sheet in three orthogonal planes. SANS patterns were obtained from these three projections of the structure and a twinned BCC structure was found to be consistent with the data. The slip plane was found to be the (110) plane, coincident with the shear plane and the $(\bar{1}11)$ slip direction was coincident with the shear direction. This is one of the principal slip systems for BCC metals, and a similar orientation is also observed for colloidal suspensions under steady shear (Ackerson and Clark 1984), as noted by Koppi *et al.* (1994). The {110} planes are the most widely spaced, and the ⟨111⟩ directions are the closest packed directions. Growth of the BCC phase from the hex phase in the same PEP–PEE sample and additionally one with $f_{PEP} = 0.25$ was subsequently studied by Koppi *et al.* (1994). The low temperature hex phase was oriented by reciprocating shear

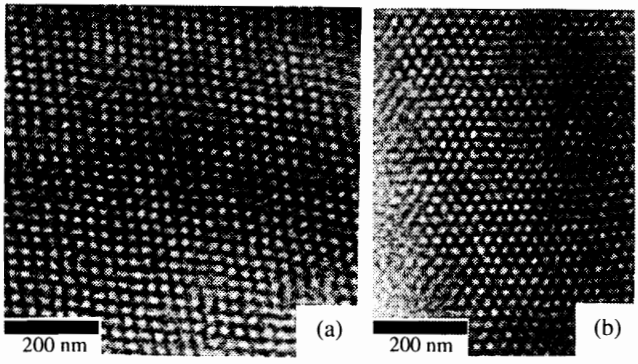

Fig. 2.12 A TEM micrograph from an PI_2PS Y-shaped copolymer with $f_{PS} = 0.17$, $M_W = 100\,kg\,mol^{-1}$ oriented by compression showing (a) four-fold symmetry due to a [100] projection and (b) three-fold hexagonal symmetry due to a (111) projection of the cubic array (Pochan *et al.* 1996*b*).

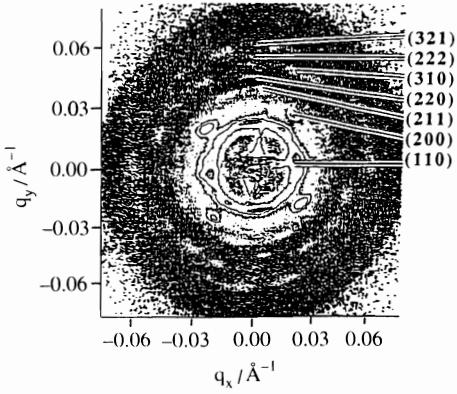

Fig. 2.13 SAXS pattern from an PI_2PS Y-shaped polymer (details as Fig. 2.12) (Pochan *et al.* 1996*b*). The pattern shows four-fold symmetry from an approximate [100] zone axis of a BCC structure.

and then the sample was heated into the BCC phase in the absence of shear. It was observed that twinned BCC structures grow epitaxially from the hex phase, with the [111] direction in the BCC structure coincident with the original cylinder axis (Fig. 2.14). Deformation of the BCC phase under shear resulted in different responses depending on the shear rate relative to the inverse relaxation time of defects in the structure, as illustrated in Fig. 2.15. At low shear rates the crystal orientation is preserved, and BCC spheres slip via creep: {110} planes move along the $(\bar{1}11)$ (shear) direction (Fig. 2.15(a)). At intermediate shear rates, the sample apparently disorders, giving isotropic SANS patterns (Fig. 2.15(b)). However, after cessation of shear the twinned BCC structure reappears. These

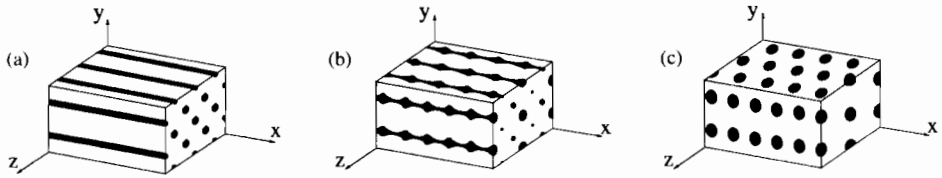

Fig. 2.14 Mechanism of transformation of hex phase to BCC phase, proposed by Koppi *et al.* (1994) on the basis of SANS measurements on asymmetric PEP–PEE diblocks: (a) initial state; (b) intermediate undulating cylinder phase; (c) epitaxially grown BCC spheres. Only one of two possible degenerate BCC orientations is shown in (b) and (c).

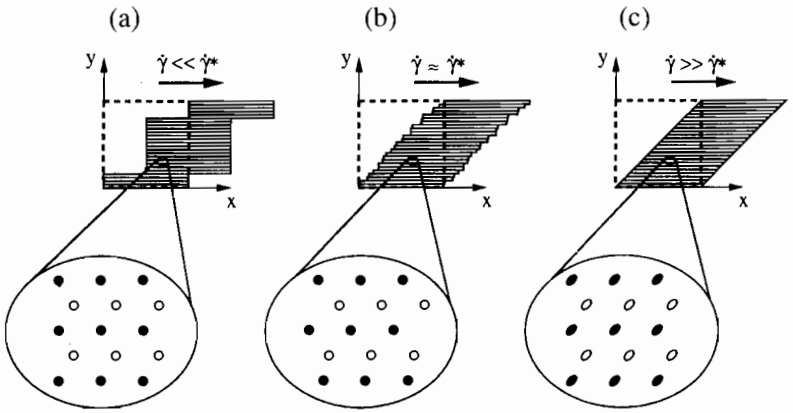

Fig. 2.15 Illustration of three deformation mechanisms proposed for BCC spheres, depending on shear rate (Koppi *et al.* 1994): (a) slow shearing results in creep; (b) at an intermediate shear rate, the generation of numerous defects leads to a loss of translational order; (c) at high shear rates, the spheres, undergo an affine elastic deformation. The layers shown represent {110} planes of a BCC structure. γ^* is the inverse relaxation time of the defects.

results indicate that at intermediate shear rates the {110} planes lose translational order whilst maintaining orientational order. This loss of translational order was ascribed to the generation of defects at a rate faster than they can be annihilated, this occurring above a critical shear rate γ^*. At higher shear rates, the deformation rate exceeds the time required for defect formation. Then large-scale elastic deformation can occur in these soft materials rather than the fracture that would be expected in metals. This is probably achieved as an affine, elastic deformation of spheres within the lattice planes, as illustrated in Fig. 2.15(c). Removal of the shear field then causes the spheres to return to their original shape (Koppi *et al.* 1994).

Simultaneous SAXS/rheology measurements were performed for the BCC phase of a PS–PEP diblock containing PS spheres in the low temperature,

strong segregation regime by Okamoto *et al.* (1994*a*). Large-amplitude oscillatory shear induced preferential orientation of (110) planes in the plane defined by the shear and vorticity directions, i.e. the same as that noted by Almdal *et al.* (1993). The stress amplitude was found to decay with the number of strain cycles and stress recovery was observed after cessation of shear. They also investigated the dynamic response of the BCC lattice during a single cycle of shear (Fig. 2.16) and observed that meridional (110) reflections were fixed in position, whereas the position of $(\bar{1}10)$ reflections varied depending on the strain phase. This was ascribed to the dynamic deformation of the BCC lattice, as sketched in Fig. 2.16. The applied strain and the strain on the lattice were found to be out of phase. In contrast to the results of Almdal *et al.* (1993) the orientation of the {110} planes was found to relax completely upon cessation of shear (Okamoto *et al.* 1994*a*).

Rheologically, the BCC phase behaves as a solid, as expected, i.e. the dynamic elastic modulus is independent of frequency at high frequency in the linear

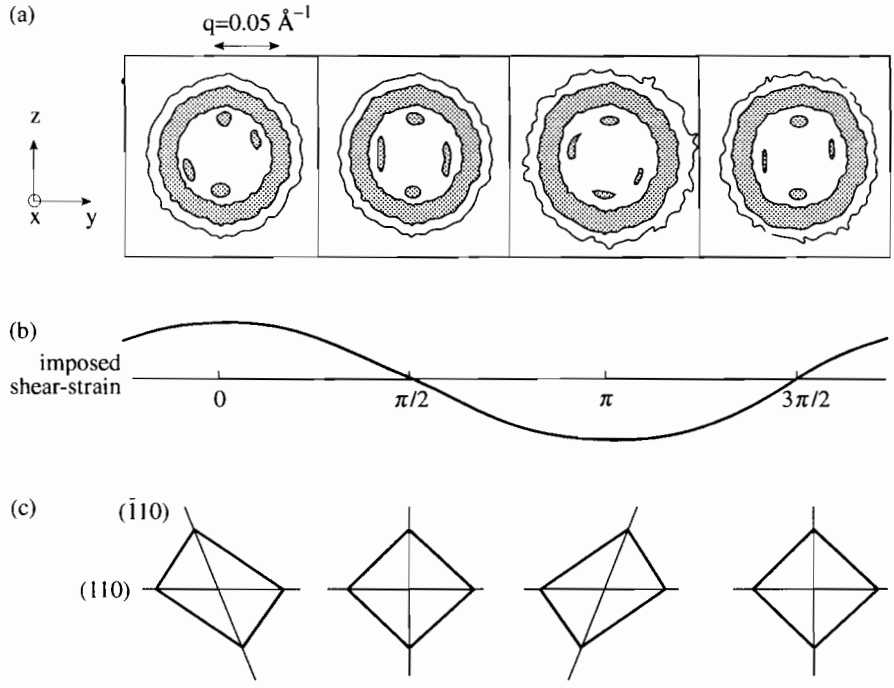

Fig. 2.16 Results obtained from an oscillatory shear experiment on an $f_{PS} = 0.103$ PS–PEP diblock (Okamoto *et al.* 1994*a*). (a) SAXS patterns obtained at four representative strain phases as shown in (b); (c) a model showing (110) and $(\bar{1}10)$ planes that give rise to the four diffraction peaks in (a). The pattern at each phase was obtained by integrating over $[-\Delta + \phi_i, \Delta + \phi_i]$, where $\phi_i = 0$, $\pi/2$, $3\pi/2$ and $\Delta = 0.194\pi$. Each pattern represents an average over 80 strain cycles.

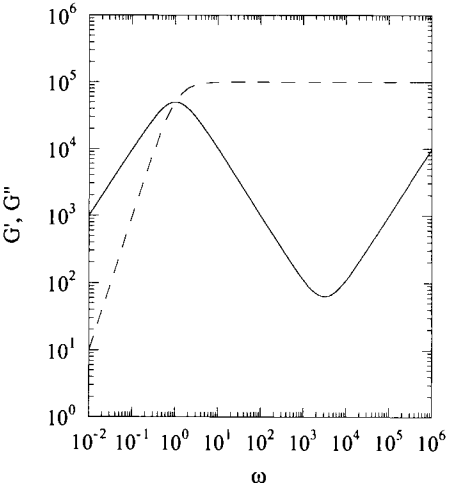

Fig. 2.17 Frequency dependence of dynamic shear moduli computed using a model for the linear viscoelasticity of a cubic phase based on slip planes, introduced by Jones and McLeish (1995). Dashed line: G', solid line: G''. The bulk modulus is chosen to be $G = 10^5$ (arb. units). The calculation is for a slip plane density $N^{-1} = 10^{-5}$ and a viscosity ratio $r_h = \eta/\eta_S = 1$, where η_S is the slip plane viscosity and η is the bulk viscosity. The strain amplitude is 1% (Hamley 1997).

response regime. A representative frequency sweep for a block copolymer in a BCC phase is shown in Fig. 2.3 (Zhao *et al.* 1996). A model for the linear viscoelastic behaviour of surfactant cubic phases presented by Jones and McLeish (1995) can be applied to cubic phases in block copolymers (Hamley 1997). This model for the rheological response to an oscillatory shear strain is based on the development of slip planes above a critical stress. Near the peak in G'' observed experimentally (Fig. 2.3) the behaviour is that of a Maxwell fluid, whereas at high frequencies the system behaves as a Voigt cell, as shown in Fig. 2.17. In this limit, the dynamics are dominated by the bulk viscosity since slippage does not occur. The behaviour is then solid-like, with a small viscous dissipation coming purely from bulk viscosity (Jones and McLeish 1995).

Liquid spherical micelle phase

Recent work has supported early observations (e.g. Aggarwal 1976; Hashimoto *et al.* 1983) of a liquid micellar phase between the BCC micelle phase and the disordered phase. A representative TEM image from a spherical micellar liquid phase is shown in Fig. 2.18. Kinning and Thomas (1984) analysed SANS data obtained by Berney *et al.* (1982) on PS–PB diblocks and PS/PS–PB blends where the minority (PB) component formed spherical micelles with only liquid-like ordering. The Percus–Yevick model for liquids of hard spheres was used to obtain the interparticle contribution to the scattered intensity (Kinning and Thomas 1984). The ordering of an asymmetric PS–PI diblock was observed by Harkless

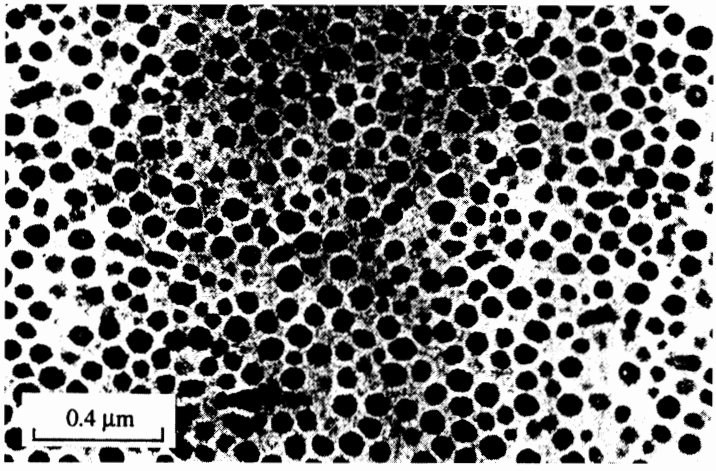

Fig. 2.18 TEM image of a PS–PB diblock with 10 wt% PB (Aggarwal 1976).

et al. (1990) to proceed via a transient liquid phase into a BCC micelle phase using synchrotron SAXS. A liquid-like micellar phase was found using SAXS to be stable in a PS–PI diblock with $f_{PS} = 0.11$ between the disordered and BCC phases by Schwab and Stühn (1996). The structure factor from the micellar liquid was again modelled using the Percus–Yevick analysis for a fluid of hard spheres. The ordering of the spheres onto a lattice is controlled by the volume fraction, Φ, and Schwab and Stühn indeed found that at the ordering transition Φ for their system was close to 0.494, the value expected in a hard sphere liquid.

Rheological measurements also show that PS–PI diblock and PS–PI–PS triblock copolymers with $f < 0.2$ (for either block) exhibit a 'liquid-like' viscoelastic response, even at temperatures below the ODT (Adams *et al.* 1994; Han *et al.* 1995; Sakamoto *et al.* 1997). Han *et al.* (1995) and Sakamoto *et al.* (1997) have observed that the ODT cannot be located for these samples based on a discontinuity in the isochronal shear moduli as a function of temperature but can be obtained from plots of $\log G'$ versus $\log G''$ (Fig. 2.4(c)).

2.2.2 Complex phases in block copolymers

In recent years a number of so-called complex phases, such as the bicontinuous gyroid and perforated layer structures, have been identified. The former has been established as an equilibrium structure, whereas the latter seem to be metastable structures observed during transformations to and from the gyroid structure.

The gyroid phase (of $Ia\bar{3}d$ symmetry) was discovered independently by two groups in 1994. Schulz *et al.* (1994), using SANS, observed this phase on heating a mixture of PS–P2VP diblocks shear-oriented in the hex phase. The gyroid phase developed epitaxially from the hex phase. Hajduk *et al.* (1994*a*) used TEM and SAXS to determine the morphology of a PS–PI diblock with $f_{PS} = 0.33$ and found the SAXS data to be consistent with an $Ia\bar{3}d$ space group. The TEM could be

modelled using a constant-thickness structure related to the gyroid minimal surface. A phase diagram for intermediate molecular weight PS–PI diblocks with $f_{PI} < 0.5$ was constructed using an armoury of techniques (SAXS, SANS, rheology and TEM) by Förster *et al.* (1994). This shows a direct transition between the $Ia\bar{3}d$ phase and the disordered phase for samples with $0.36 < f_{PI} < 0.39$ approximately. A full phase diagram for PS–PI diblocks near the order–disorder transition was obtained using the same combination of techniques and is shown in Fig. 2.1 (Khandpur *et al.* 1995). This phase diagram is asymmetric about $f = 0.5$ which results from 'conformational asymmetry' due to unequal statistical segment lengths of PS and PI. In addition to the $Ia\bar{3}d$ phase, a hexagonal perforated layer (HPL) structure was observed in a region indicated on the phase diagram in Fig. 2.1. Subsequent work by Hajduk *et al.* (1997) indicated that this structure, observed for PS–PI and other diblocks, is metastable. Vigild *et al.* (1997) have reached the same conclusions for PEP–PDMS (PDMS-poly(dimethylsiloxane)) diblocks.

There have been many misassignments of structures as being ordered bicontinuous double diamond (OBDD, space group $Pn\bar{3}m$) which is based on a tetrahedral arrangement of channels when in fact they were Gyroid (Hajduk *et al.* 1995) which has $Ia\bar{3}d$ symmetry and is based on a tripod arrangement of channels (see Fig. 2.19). For example, the OBDD bicontinuous cubic phase was identified in star block copolymers via TEM images showing a 'wagon wheel' structure (Alward *et al.* 1986; Hasegawa *et al.* 1987; Thomas *et al.* 1986). This type of TEM pattern had been previously published by Aggarwal (1976) for a diblock copolymer and was subsequently observed in a whole series of block copolymer/homopolymer blends (Winey *et al.* 1991, 1992*a*,*b*), as discussed in Section 6.2.3.

Fig. 2.20 shows the three-fold (wagon wheel) and four-fold structures observed using TEM (Förster *et al.* 1994) for the two projections of a bicontinuous cubic structure in a PS–PI diblock ($f_{PS} = 0.39$). TEM micrographs like these have been modelled as if they were OBDD (Thomas and Lescanec 1994) and the reason is that the density projections of [111] and [100] for $Ia\bar{3}d$ and $Pn\bar{3}m$ structures are very similar. It was not until 1994 that this structure was correctly identified using small-angle scattering (Hajduk *et al.* 1994*a*; Förster *et al.* 1994).

The SAXS pattern (Fig. 2.21(a)) found for a shear-oriented sample of a PEP–PDMS diblock blend with $f_{PEP} = 0.67$ has 10 spots on the inner ring, consistent with the {211} reflections from the $Ia\bar{3}d$ structure and their angular spread indicates that the [111] direction is coincident with the shear direction. A scheme for indexing this pattern is shown in Fig. 2.21(b). The 10 inner reflections arise from random rotation of single crystal domains rotated by an angle θ around the [111] direction, which is the closest packed direction in BCC structures. A full rotation (360°) of the reciprocal space runs three times through the sequence of eight patterns in Fig. 2.21(b). The angular relationships between the reflections in the experimental data are consistent with this model. The 1D SAXS data for a PS–PI diblock with $f_{PS} = 0.39$ in Fig. 2.22 show multiple reflections which can be indexed to the $Ia\bar{3}d$ space group. Figure 2.22(b) illustrates the indexing of this cubic pattern through a straight line fit of $(h^2 + k^2 + l^2)^{1/2}$ (where h, k, l are Miller indices for allowed reflections) as a function of q.

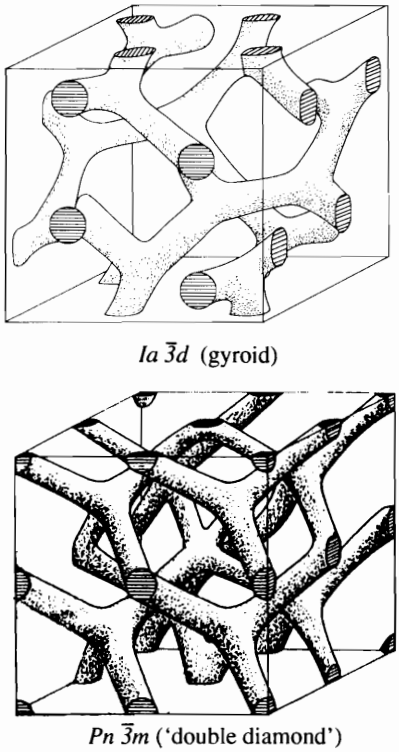

Fig. 2.19 Structures belonging to space group $Ia\bar{3}d$ (gyroid) and space group $Pn\bar{3}m$ ('double diamond') (after Seddon 1990).

Once the space group of the bicontinuous cubic structure has been established using small-angle scattering then TEM images can be used to their best. Figure 2.23 shows TEM images of the [111] projection and the [100] reflections of the $Ia\bar{3}d$ gyroid phase, the insets on the left and in the centre show the optical transform of the image and the indexed diffraction pattern, respectively, simulations of the TEM projections are given on the right. That the gyroid structure is consistent with the 'wagon wheel' patterns (Fig. 2.20(a), Fig. 2.23(a)) in TEM micrographs was supported via such simulations of TEM images from different orientations of the structure (Hajduk *et al.* 1994*a*).

The existence of a second class of complex phases, the modulated and perforated layer structures, has largely been explored by Bates and co-workers (Förster *et al.* 1994; Hamley *et al.* 1993, 1994; Khandpur *et al.* 1995; Schulz *et al.* 1996), who used SANS and TEM to investigate shear oriented structures. The thermally-induced phase transition from the lam to the hex phase in polyolefin diblocks was studied in detail by Hamley *et al.* (1993, 1994) using SANS, TEM and rheology. Intermediate hexagonal modulated lamellar (HML) and hexagonal perforated layer (HPL) structures were observed on heating PEP–PEE, PE–PEP and PE–PEE diblocks, where PEP is poly(ethylene–propylene), PEE is

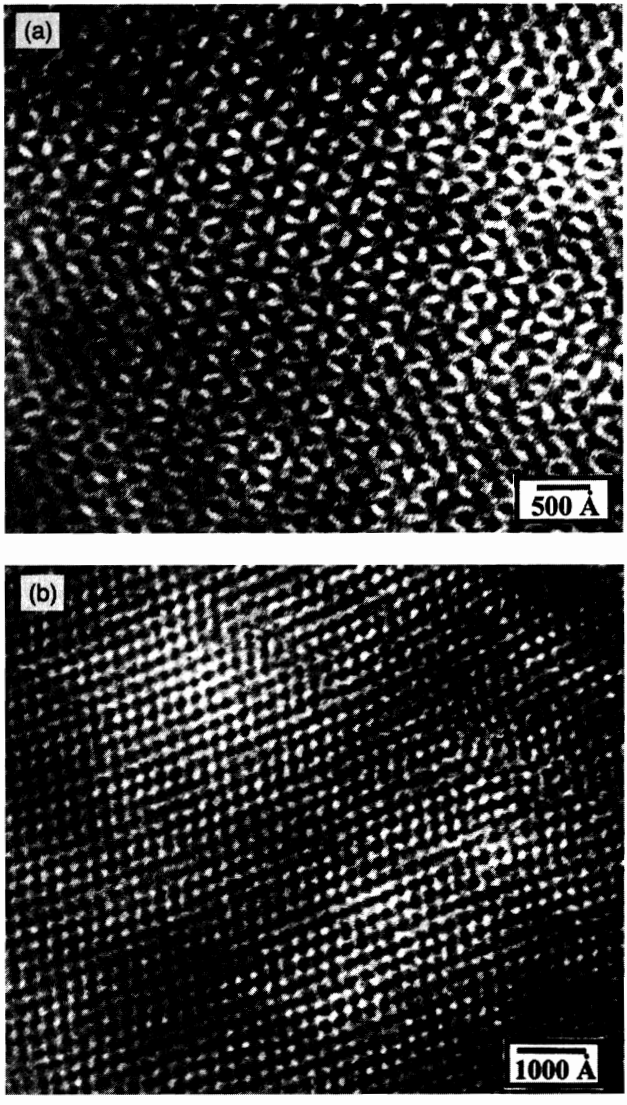

Fig. 2.20 TEM images from a PS–PI diblock with $f_{PS} = 0.39$ and $M_n = 3.2 \times 10^4 \text{g mol}^{-1}$, selectively stained with OsO_4, showing (a) three-fold and (b) four-fold projections of the bicontinuous $Ia\bar{3}d$ structure (Förster *et al.* 1994).

poly(ethyl ethylene) and PE is poly(ethylene). The thermal transition between the lam and hex phases exhibited by a PS–PE diblock was investigated using SAXS and TEM by Hajduk *et al.* (1994*b*), who also observed a modified layer phase between these two structures. The transition was observed to occur in two stages. In the first, fluctuations in the lamellae grew until cylinders formed. The layers of cylinders were initially in poor register, but annealing led to long-range

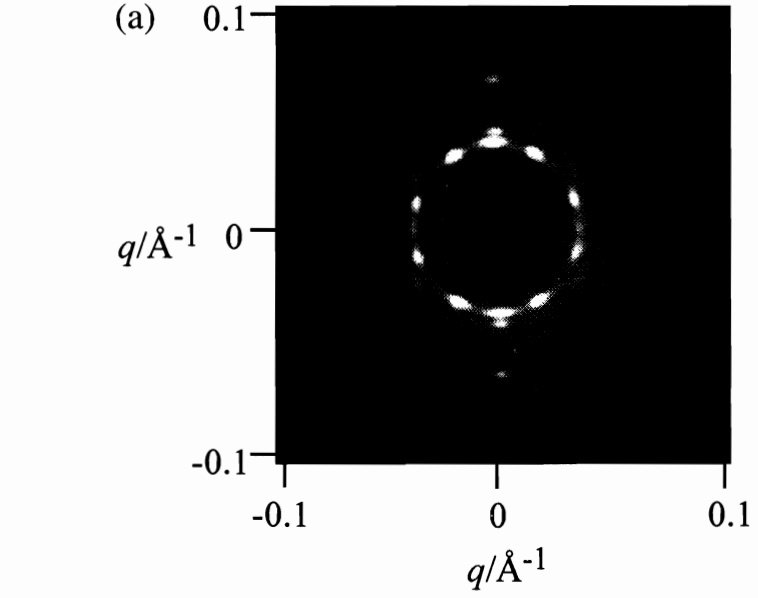

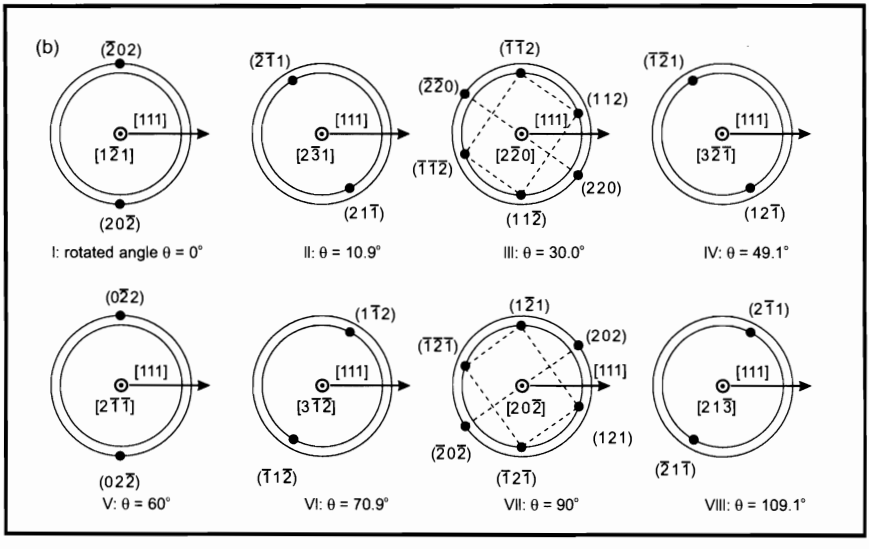

Fig. 2.21 (a) SAXS pattern from the $Ia\bar{3}d$ phase of an $f_{PEP} = 0.67$ PEP–PDMS diblock blend oriented using reciprocating shear. (b) Indexing of the first two rings of reflections in the SAXS pattern on the basis of grains rotated aroung the [111] direction by an angle θ (Vigild *et al.* 1998).

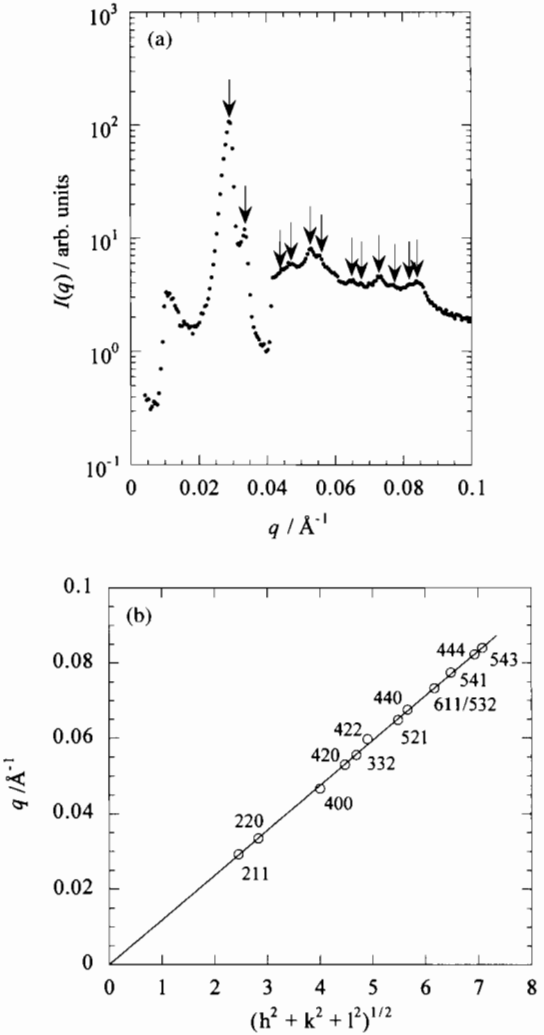

Fig. 2.22 (a) SAXS powder pattern from a PS–PI diblock ($f_{PS} = 0.39$ and $M_n = 3.2 \times 10^4$ g mol^{-1}) in the $Ia\bar{3}d$ phase (Förster *et al.* 1994); the data for $q > 0.04$ Å^{-1} shows the higher order reflections on an expanded vertical scale. (b) Indexation of the peak position (Hamley and Ryan 1994).

hexagonal order in the second stage. Recent experimental work suggests that these structures are not stable equilibrium ones, but the HML may be a transient, and the HPL structure a long-lived metastable phase (Hajduk *et al.* 1997, Vigild *et al.* 1997). The perforated layer structures have been studied theoretically (Fredrickson 1991; Hamley and Bates 1994; Laradji *et al.* 1997*a*,*b*; Matsen and Schick 1994*a*) but have never been found to be the lowest energy morphology. This conclusion is supported by recent theoretical calculations by Qi and

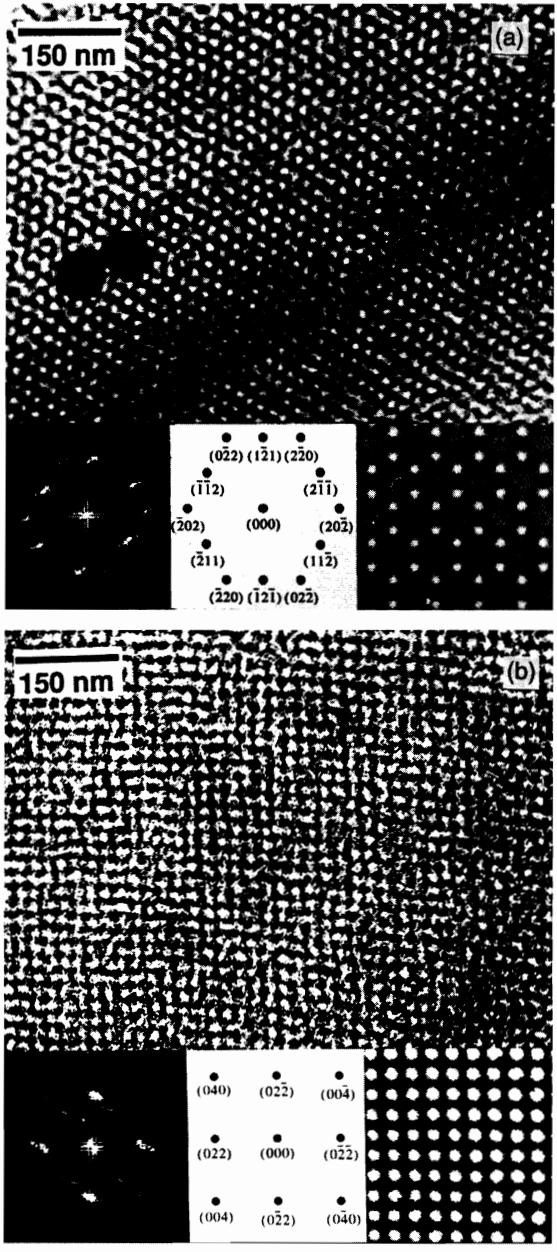

Fig. 2.23 TEM images from an $f_{PS} = 0.33$, $M_n = 2.7 \times 10^4\,g\,mol^{-1}$ PS–PI diblock (Hajduk *et al.* 1994*a*). (a) Approximate three-fold symmetry is evident from the [111] projection of the cubic structure. Inset are the Fourier transform of the image and indexed diffraction pattern. The inset on the right is a simulated [111] projection of the constant-thickness gyroid structure. (b) Another region of the same sample, showing four-fold symmetry, with a diffraction pattern, its indexation and a simulated [100] projection of the gyroid structure inset. The minority component (PS) appears light in the micrographs and simulations.

Wang (1997) using the time-dependent Landau–Ginzburg equation for weakly segregated systems. They find structures similar to the HML and HPL phases by cell-dynamic simulations or solution of single-wavenumber kinetic equations following temperature jumps from the lam phase to the hex phase. A modulated lamellar phase is observed as a transient as the system leaves the stable lam phase. A pseudostable perforated lamellar structure results from saddle points in the free energy surface, and if such a saddle point exists the modulated lamellar phase evolves into the perforated lamellar phase, which eventually decays to the hex phase (Qi and Wang 1997).

SANS patterns from the HPL phase show strong layer peaks, with higher order reflections, and weaker off-meridional reflections from the layer perforations. A typical SANS pattern from an HPL phase is shown in Fig. 2.24(b) for a PS–PVP ($f_{PS} = 0.65$) diblock which has all the typical features of a perforated layer structure (Schulz *et al.* 1996); the perforations in the lamellar structure can be seen in the TEM micrograph in Fig. 2.24(a). In order to obtain unambiguous scattering patterns shear oriented samples must be used, because radially averaging the scattering, either numerically or by using a polydomain sample, removes the spatial information. Typically, the inter-perforation spacing and lamellar length-

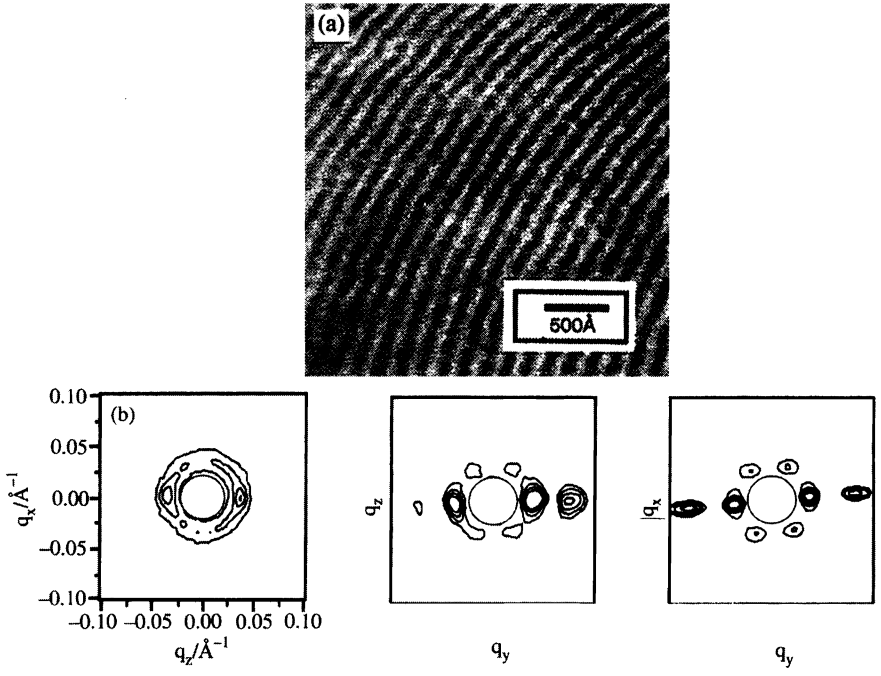

Fig. 2.24 (a) TEM image from a PS–PVP diblock with $f_{PS} = 0.65$ and $N_n = 196$ after disordering, quenching and annealing at 140 °C for 18 h (Schulz *et al.* 1996). The dark-stained region corresponds to PVP. (b) Two-dimensional SANS pattern from a presheared sample of the same diblock in the same phase.

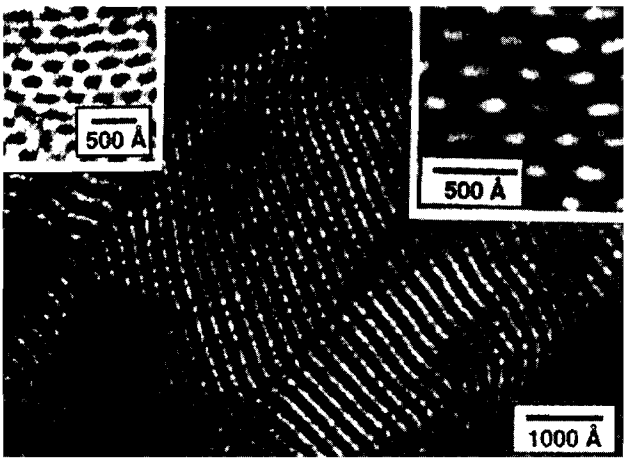

Fig. 2.25 TEM image of the HPL phase in a PS–PI diblock with $f_{PS} = 0.68$ and $M_n = 40\,kg\,mol^{-1}$ after annealing for 6 h at 145 °C followed by quenching in liquid nitrogen (Khandpur *et al.* 1995). The PI appears dark. The inset on the left shows a section with the sample parallel to the microscope stage, the one on the right shows a magnification of the perpendicular orientation shown in the main figure.

scales are similar but not equal (Hamley *et al.* 1994). The orientation and arrangement of the perforations can be imaged directly in PS–PI diblocks (Khandpur *et al.* 1995) and Fig. 2.25 illustrates the hexagonal nature of the PI perforations through PS lamellae in a PS–PI diblock with $f_{PS} = 0.68$.

2.2.3 ABC triblocks

Given the morphological complexity of AB diblock and ABA triblock copolymers, it might be expected that the phase behaviour of ABC triblocks would be even more rich, and indeed this has been confirmed by recent experiments from a number of groups. From a practical viewpoint, ABC triblocks can also act as compatibilizers in blends of A and C homopolymers (Auschra and Stadler 1993). In addition to the composition of the copolymer, an important driving force for structure formation in these polymers is the relative strength of incompatibilities between the components, and this has been explored by synthesis of chemically distinct materials.

In the earliest studies, so-called 'core–shell' morphologies were identified, where the core of the minority end-component is separated from the other endblock by a shell of the midblock (B). Spherical microdomains surrounded by a shell of the midblock have been observed using TEM for a number of polymers (Arai *et al.* 1980; Riess *et al.* 1989). Mogi *et al.* (1992*a*) studied a series of PI–PS–P2VP triblocks where the volume fraction of the PS middle block was varied from 0.3 to 0.8, whilst the volume fractions of the endblocks were kept equal to each other. On increasing the PS volume fraction a core–shell lamellar

structure (composition 1:1:1), a tricontinuous structure (1:2:1), a cylindrical phase with separate PS and P2VP rods (1:4:1) and a spherical morphology (1:8:1) were observed. It was suggested that the most efficient packing of the two types of rods leads to a tetragonal morphology. The tricontinuous structure in this system was analysed in detail in a separate paper (Mogi *et al.* 1992*b*), and assigned an 'ordered tricontinuous double diamond' morphology, by analogy with the 'ordered bicontinuous double diamond' structure that was then thought to exist in AB block copolymers. However, because the OBDD phase in other block copolymers has subsequently been reassigned as gyroid, and because self-consistent field theory indicates that a gyroid phase is stable for ABC triblocks (Matsen 1997), this is likely to be the structure observed by Mogi *et al.* (1992*b*). Because the two continuous lattices in the matrix of the majority phase in the gyroid phase are distinct (i.e. one is composed of component A and the other of component C), it has a lower symmetry than $Ia\bar{3}d$, namely $I4_132$. Matsen (1998) considered triblocks with symmetric end-blocks ($f_A = f_C$ and $\chi = \chi_{AB} = \chi_{BC}$) in the case of relatively short endblocks ($f_A < 0.3$). He discussed the stability of the tetragonal cylinder phase. Although this arrangement is not the most efficient at filling space, it does enable A cylinders to be distributed around C cylinders and vice versa. This is favoured because the A and C cylinders are necessarily bridged by B chains.

Illustrating the importance of the relative strengths of incompatibility between blocks, an ABC triblock made of the same components as the polymers studied by Mogi *et al.* (1992*a*,*b*) but with the sequence changed was investigated by Gido *et al.* (1993). TEM micrographs from a P2VP–PI–PS triblock with equal volume fractions are shown in Fig. 2.26 in two orthogonal planes. They clearly reveal a cylindrical 'core–shell' structure for this sample with composition 1:1:1, with a P2VP core. This structure forms even though a PI–PS–P2VP triblock with the same composition formed a lamellar core–shell morphology (Mogi *et al.* 1992*a*) (the molecular weights of the polymers differ by a factor of two, but this does not change the microstructure if the blocks are strongly segregated). This morphology change was rationalized by Stadler *et al.* (1995) on the basis that a lamellar morphology is expected for a PI–PS–P2VP symmetric triblock ($f_A = f_B = f_C$) because the interfacial tension $\gamma_{PI-PS} \approx \gamma_{PS-P2VP}$. However, for P2VP–PI–PS, $\gamma_{PI-P2VP} \gg \gamma_{PI-PS}$, so that the system will tend to create a large PI–PS interface which allows a reduction in stretching of PS (and PI) chains and a small PI/P2VP contact area to reduce interactions between these highly immiscible polymers. As a result of this imbalance between A/B and B/C interactions, a core–shell morphology with a P2VP core forms.

A number of remarkable new morphologies have recently been discovered by Stadler and co-workers in poly(styrene)–poly(butadiene)–poly(methyl methacrylate) (PS–PB–PMMA) triblocks, and their hydrogenated analogues, poly(styrene)–poly(ethylene-*co*-butylene)–poly(methyl methacrylate) (PS–PEB–PMMA) (Breiner *et al.* 1996, 1997; Krappe *et al.* 1995; Stadler *et al.* 1995). The common features of the polymers exhibiting this complex phase behaviour are that the midblock is the minority component and that the incompatibility between the outer blocks is much weaker than the incompatibility of each of

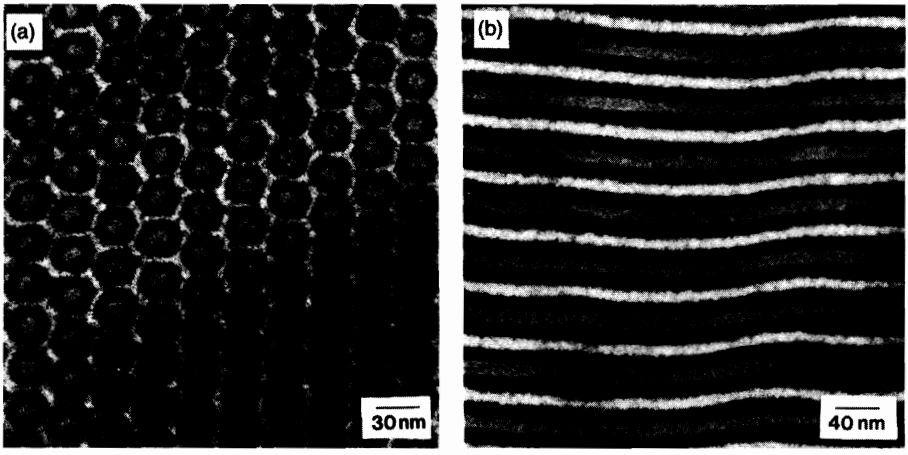

Fig. 2.26 TEM from a poly(2-vinylpyridine)–poly(isoprene)–poly(styrene) ABC triblock copolymer, showing a hexagonal cylinder 'core–shell structure' (Gido *et al.* 1993). The light, grey and black regions correspond to the PS, P2VP and PI respectively in sections (a) perpendicular and (b) parallel to the rod direction.

these blocks with respect to the midblock. The morphologies were investigated using TEM. Selective staining with OsO_4 was used to stain the PB domain in PS–PB–PMMA triblocks, where RuO_4 stains both PS and PB. In contrast, sufficient contrast between blocks was achieved using RuO_4 for PS–PEB–PMMA samples.

A structure consisting of PEB cylinders at the interface between PS and PMMA lamellae was observed for a triblock with volume fractions $f_{PS} = 0.48$, $f_{PEB} = 0.20$ and $f_{PMMA} = 0.32$ (see Fig. 2.27) (Auschra and Stadler 1993; *et al.* 1995). A morphology with PB spheres at the PS–PMMA interface that was observed using TEM (Beckmann *et al.* 1994; *et al.* 1995) is shown in Fig. 2.28. In contrast, when the midblock of the triblock is hydrogenated to give a PS–PEB–PMMA triblock with the same composition, a morphology with PEB rings around PS cylinders in a matrix of PMMA is observed (Auschra and Stadler 1993) (see Fig. 2.29). Incorporation of the PEB block changes the PS–PMMA morphology, as well as the domain structure adopted by the midblock; this is because the AB and BC interaction parameters are changed, as well as the B segment length. Recent work indicates the richness of phase behaviour of this type of triblock. A fascinating variety of structures of PB or PEB domains at the interface between PMMA cylinders and a PS matrix have been observed. Some are illustrated schematically in Fig. 2.30 (Breiner *et al.* 1997). Examples of two of the nicest micrographs corresponding to two of these structures (Fig. 2.30d and e) are included in Fig. 2.31. A new morphology has been reported for a PS–PB–PMMA triblock with nearly equal volume fractions of each block ($f_{PS} = 0.36$, $f_{PMMA} = 0.33$) intermediate between a lamellar phase formed by a sample with a majority of PB and a phase with PB cylinders at the interface of PS–PMMA lamellae,

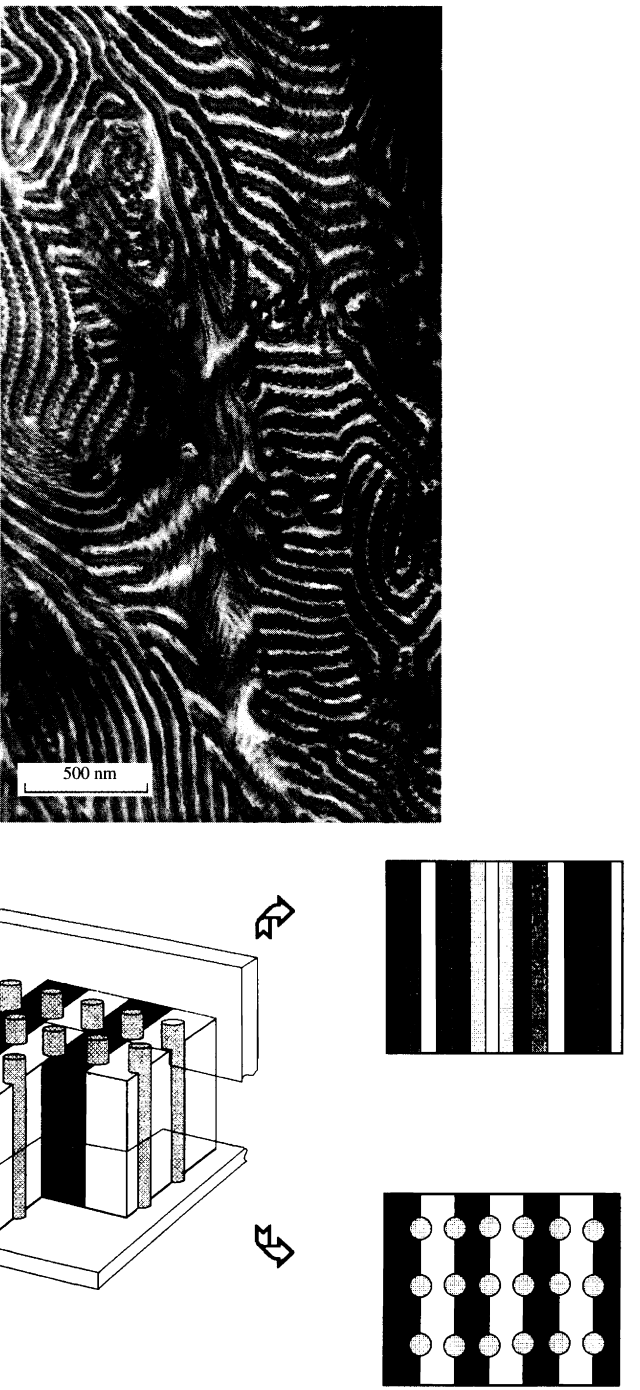

Fig. 2.27 TEM and schematic structure of the 'rods between lamellae' morphology in a PS–PEB–PMMA triblock with $M_n = 240\,kg\,mol^{-1}$, $f_{PS} = 0.48$, $f_{PEB} = 0.20$ and $f_{PMMA} = 0.32$ (Stadler *et al.* 1995).

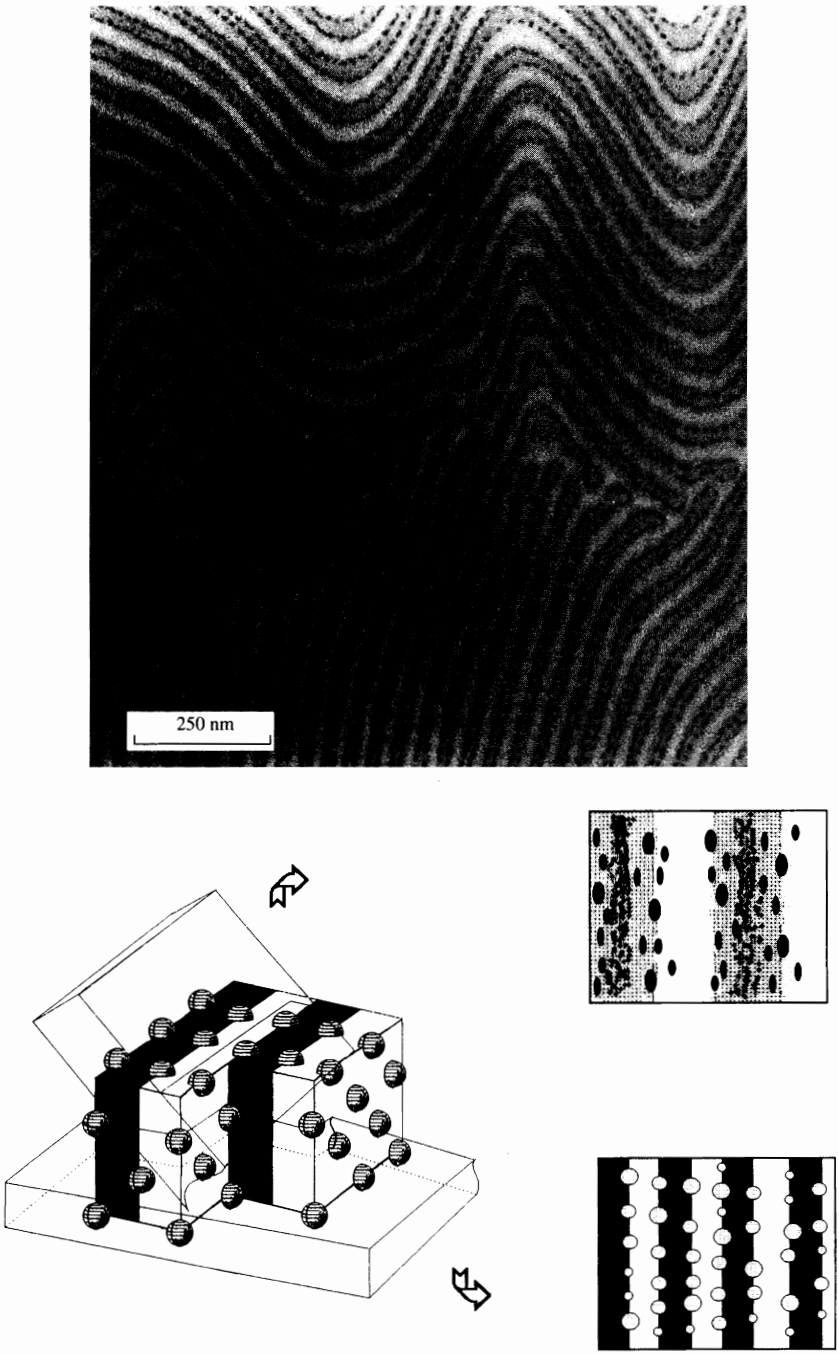

Fig. 2.28 TEM and schematic of the 'spheres between lamellae' morphology in a PS–PB–PMMA triblock with $M_n = 226\,kg\,mol^{-1}$, $f_{PS} = 0.47$, $f_{PB} = 0.075$ and $f_{PMMA} = 0.455$. The PS lamellae appear grey and the PMMA lamellae are light (Stadler *et al.* 1995).

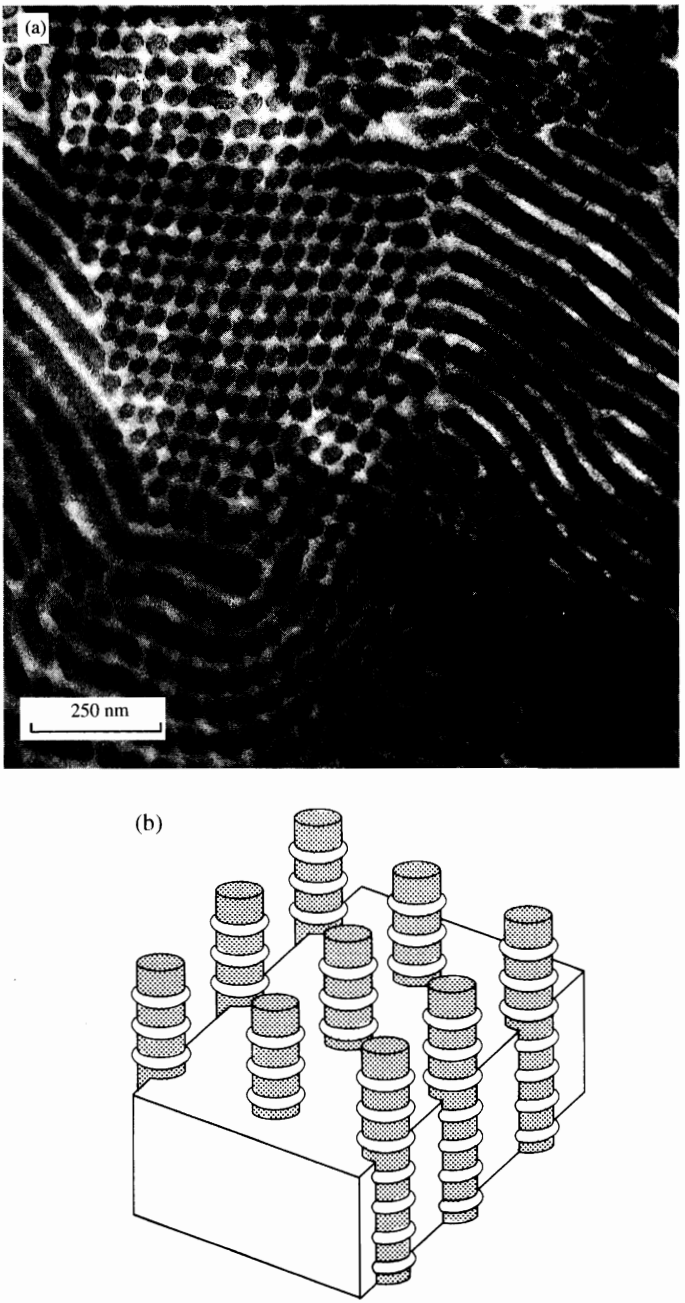

Fig. 2.29 (a) TEM from a PS–PEB–PMMA triblock with $M_n = 238\,\text{kg mol}^{-1}$, $f_{PS} = 0.47$, $f_{PEB} = 0.075$ and $f_{PMMA} = 0.455$. The PS cylinders appear dark and the PMMA matrix is light. The arrow indicates a region where a cross-section of PEB rings (dark) can be seen. (b) Schematic of the morphology (Auschra and Stadler 1993).

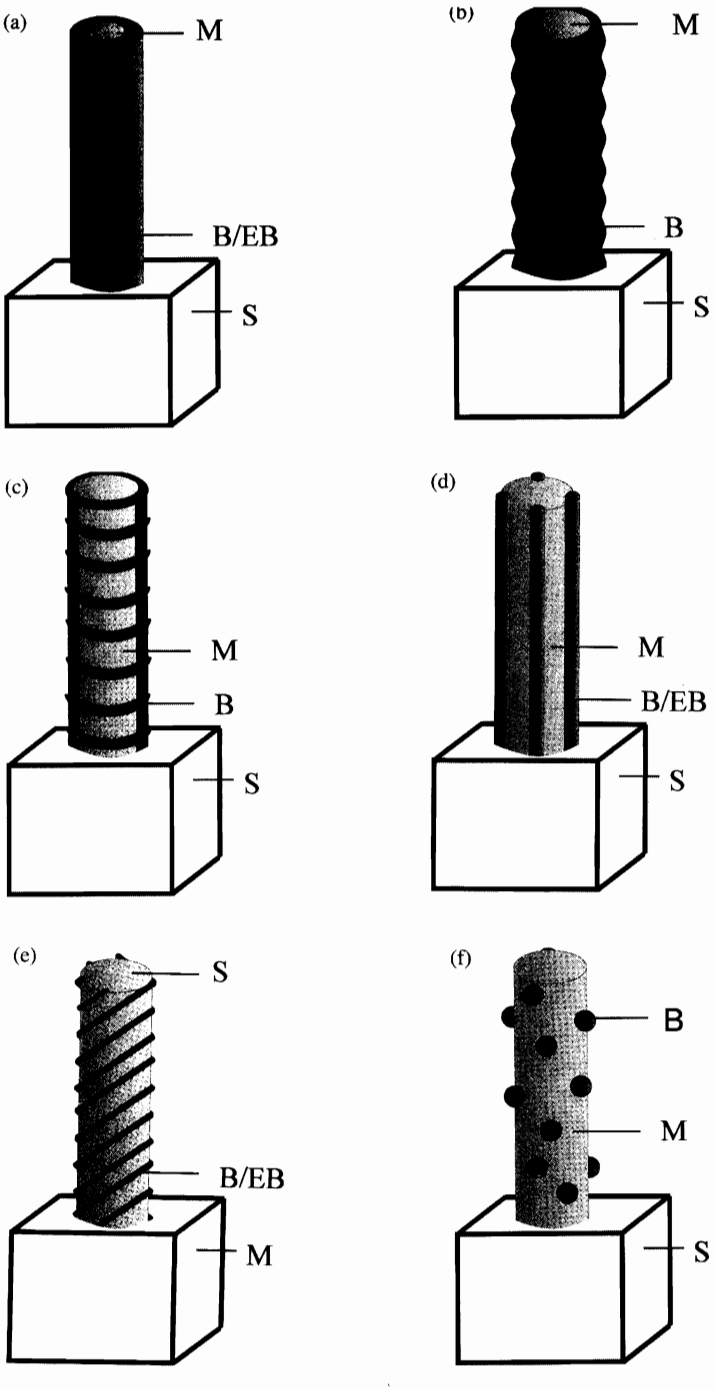

Fig. 2.30 Schematic of morphologies proposed for PS–PB–PMMA or PS–PEB–PMMA triblocks with a PS or PMMA matrix (indicated) and a minority of PB or PEB (Breiner *et al.* 1997). Here B = PB, EB = PEB, M = PMMA, and S = PS.

with formed by samples with a minority of PB. This structure, termed 'knitting pattern', is illustrated in Fig. 2.32. Whether all of these exotic structures are in equilibrium or are trapped non-equilibrium states due to the prior microphase separation of two blocks constraining the other has not been determined. In the absence of a comprehensive theory for the stability of such morphologies caution should be exercised over assigning them as being at equilibrium.

These observations of complex phases formed by midblock segregation at the AC interface have been accounted for by Stadler *et al.* (1995), who extended the Semenov strong-segregation theory (Semenov 1985) to the case of ABC

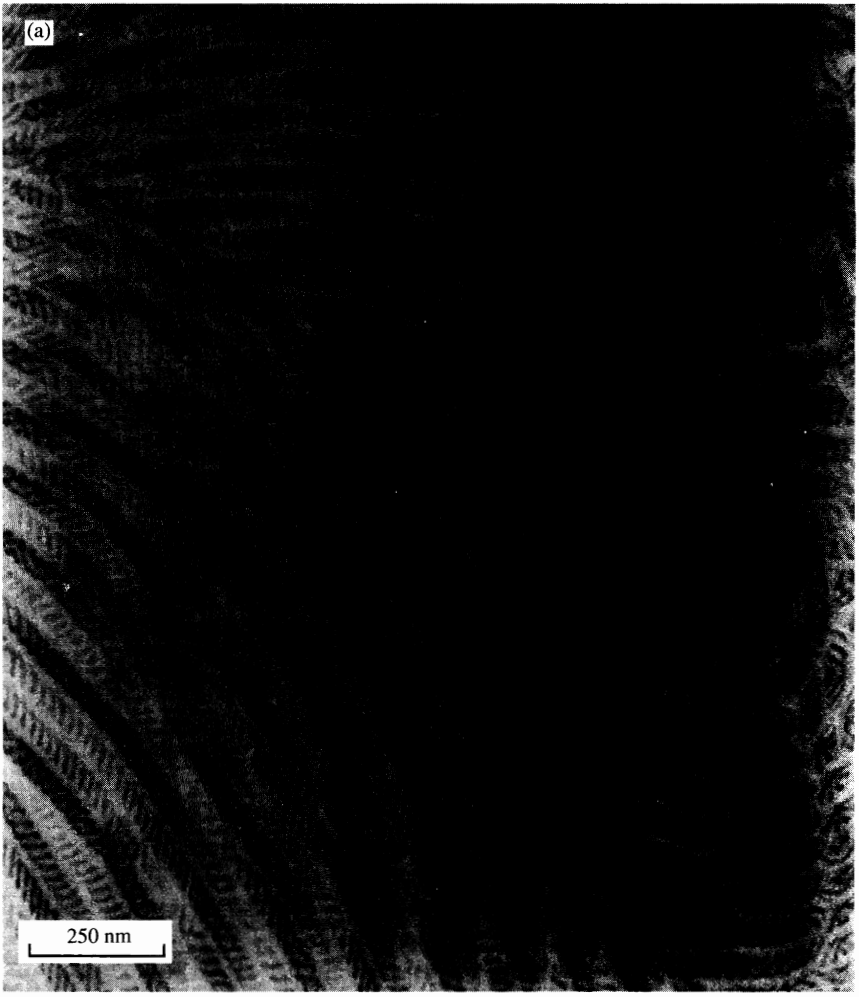

Fig. 2.31 TEM images for triblocks with: (a) $M_n = 218\,\text{kg mol}^{-1}$, $f_{PS} = 0.25$, $f_{PMMA} = 0.62$. This morphology is illustrated schematically in Fig. 2.30(e); (b) $M_n = 129\,\text{kg mol}^{-1}$, $f_{PS} = 0.65$, $f_{PMMA} = 0.19$ (Breiner *et al.* 1997). This structure is schematized in Fig. 2.30(d).

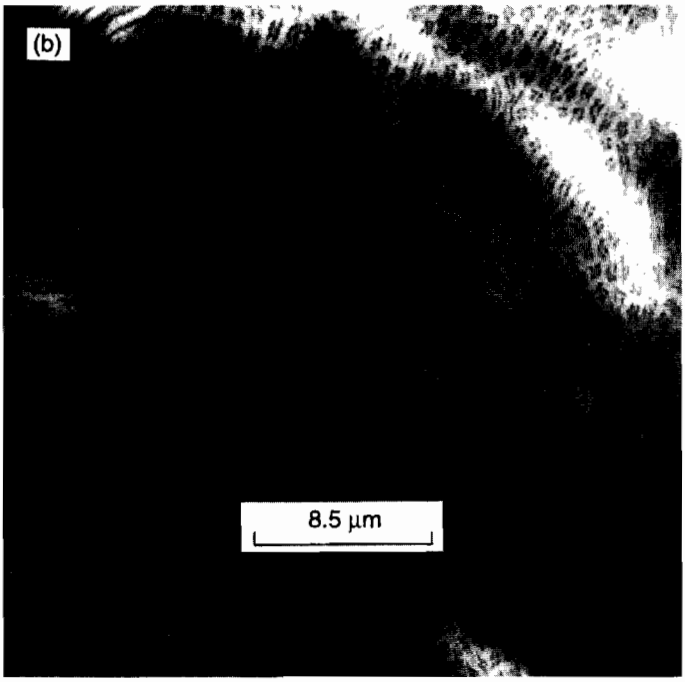

Fig. 2.31 *Continued.*

triblocks. Using this approach, a phase diagram was constructed for the copolymers studied by Stadler and co-workers, which have a midblock composition $f_B < 0.4$, that is in good agreement with the experimental results (Stadler *et al.* 1995), although only a limited number of morphologies were considered.

2.2.4 Starblocks and multiblocks

The first study of the effect of arm number on the morphology exhibited by a block copolymer was performed by Price *et al.* (1972) on a series of diblock, triblock and three- and four-armed block copolymers of styrene and isoprene.

Since the mid-1970s, Fetters and co-workers (see Bi and Fetters 1975, 1976) have synthesized a range of $(AB)_n$ starblock copolymers of PS and PI that have been morphologically characterized by a number of groups. An example of the 'wagon wheel' morphology, later misidentified as a projection of the OBDD phase, but subsequently reassigned to the $Ia\bar{3}d$ phase, was observed using TEM on a 15-arm PS-PI starblock with $f_{PS} = 0.3$ by Aggarwal (1976). The molecular architecture was shown to change the morphology of block copolymers of a given composition via representative TEM images for PS/PB starblocks and linear triblocks of fixed composition by Aggarwal (1976).

Interest in the morphology of PS-PI starblocks was revived in 1986, when Thomas and co-workers investigated the effect of arm number and molecular

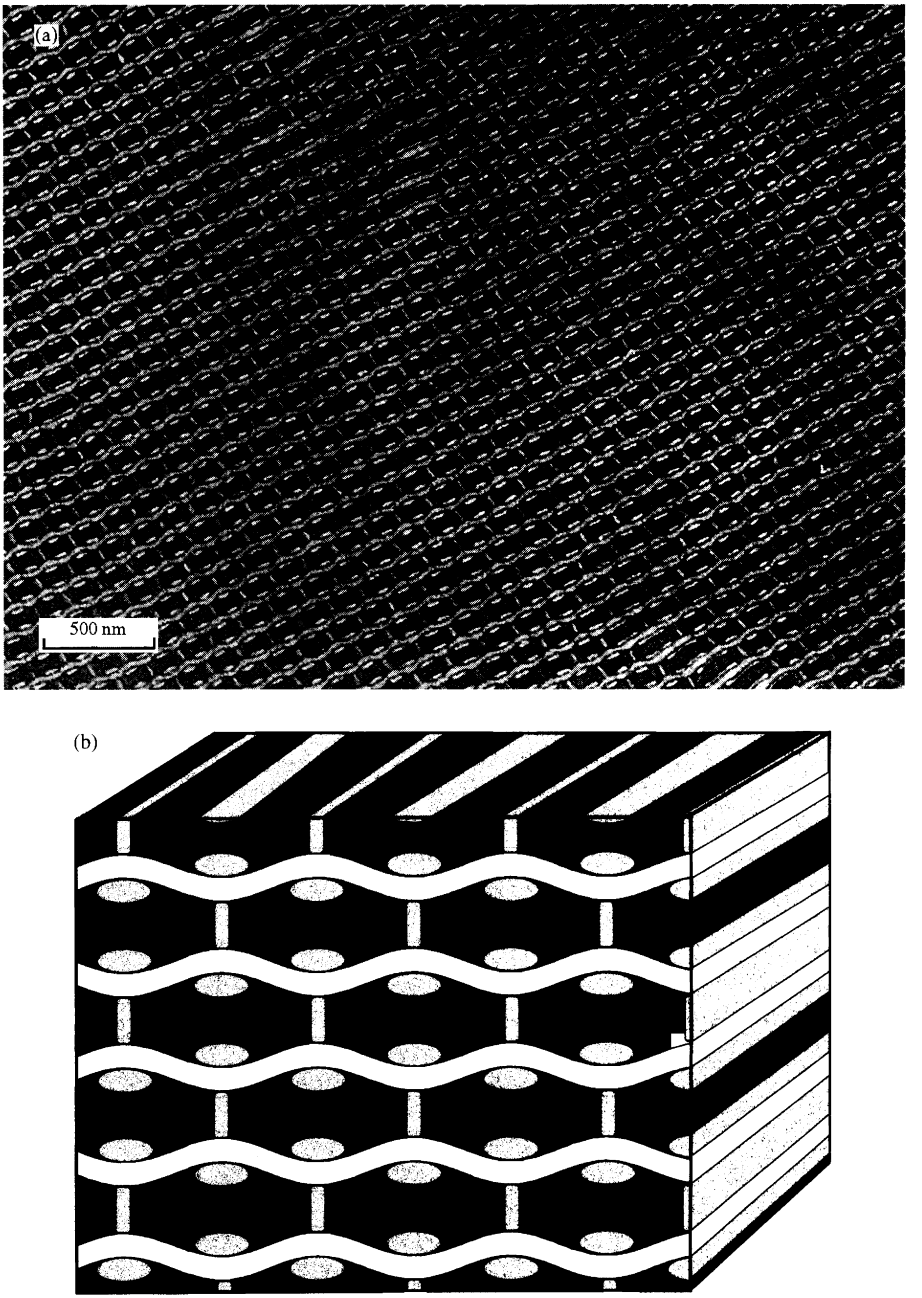

Fig. 2.32 (a) TEM image of a PS–PEB–PMMA triblock with $M_n = 117\,kg\,mol^{-1}$, $f_{PS} = 0.36$, $f_{PMMA} = 0.33$. The PS phase (stained with RuO_4) is dark and the PMMA forms the wavy lamellae. (b) Schematic of the structure.

weight on structure (Alward *et al.* 1986). They perfomed SAXS, TEM and dynamic mechanical thermal analysis on a range of $(AB)_n$ stars with n ranging from 2 to 18 with a constant composition ($f_{PS} = 0.27$, PS at the arm end). They reported that the 'OBDD' phase becomes more favourable with respect to a hex phase as the number of arms increases or the arm molecular weight increases (Alward *et al.* 1986). Detailed modelling of tilt-series TEM images for the 'OBDD' phase for 6- and 8-arm stars was presented by Thomas *et al.* (1986). The bicontinuous morphology in this class of starblock was later reassigned as an $Ia\bar{3}d$ structure by Hajduk *et al.* (1995) on the basis of SAXS on 6- and 18-arm stars from this series. Indeed, Anderson and Thomas (1988) had previously found that the OBDD structure is unstable with respect to the hex phase theoretically. The composition-dependence of morphology in 18-arm stars was investigated by Herman *et al.* (1987) using TEM. On increasing PS composition, the classical sequence of phases observed for linear block copolymers was observed, with the additional bicontinuous phase observed for PS compositions $f_{PS} = 0.27$ and 0.32 between the hex and lam phases with PS the outer block, and in an $f_{PS} = 0.73$ starblock where PI was the outer block.

The order–disorder transition in starblock copolymers of PS and PI was investigated using SAXS by Hashimoto and co-workers (Hashimoto *et al.* 1988; Ijichi *et al.* 1989). They studied a series of polymers having a fixed molecular weight and composition, but with the arm number varying from 1 to 18. They observed that the order–disorder transition temperature and spinodal temperature were almost independent of n for $n > 2$ (Ijichi *et al.* 1989). By fitting the SAXS profiles in the disordered phase to Leibler's structure factor, eqn 2.11 (Leibler 1980), the Flory–Huggins interaction parameter, χ, was determined, and this was observed to be n-dependent using this analysis scheme. The scattering in the disordered state of a concentrated solution of an 18-arm PS–PI starblock was confirmed by Fetters *et al.* (1987) to follow the predictions of the Leibler-like random phase approximation theory for the disordered phase of starblock melts introduced by Olvera de la Cruz and Sanchez (1986). This theory was developed to include order–order phase transition lines for $(AB)_n$ starblock and asymmetric triblock melts by Mayes and Olvera de la Cruz (1989).

Hadjichristidis and co-workers have worked extensively on starblock copolymers of the A_nB_m type, which they term 'miktoarm' block copolymers, from the Greek for mixed arm. This work has been reviewed by Hadjichristidis *et al.* (1996*a*,*b*). Some of the block copolymer architectures they have investigated are illustrated in Fig. 2.33. Copolymers with three different arms have been synthesized (Iatrou and Hadjichristidis 1992; Sioula *et al.* 1997), following earlier work where miktoarm A_2B-type (Huynh *et al.* (1980); Mays 1990) or A_2B_2 (Quirk and Ignatz-Hoover 1987; Tsitsilianis *et al.* 1990) copolymers respectively were prepared. The morphology and miscibility of PS_2PI, PS–PI–PB, and $PSPI_2$ terpolymers were investigated by Hadjichristidis *et al.* (1993), who observed that the PS arms always separate from the polydienes, but the PI and PB arms mix when they occur in the same molecule. Microphase separation in $PSPI_2$ and PS–PI–PB star copolymers was studied using SAXS and rheology by Floudas *et al.* (1994*a*). The ODT was determined for two samples forming a hex phase from SAXS and

rheology data and a discontinuity was reported in q^* at the ODT, as well as larger discontinuities in the inverse intensity and peak width compared to diblocks. The morphology of miktoarm A_2B and A_3B starblocks of PS and PI, determined using SAXS and TEM, was compared by Tselikas *et al.* (1996*a*) to theory. The theory,

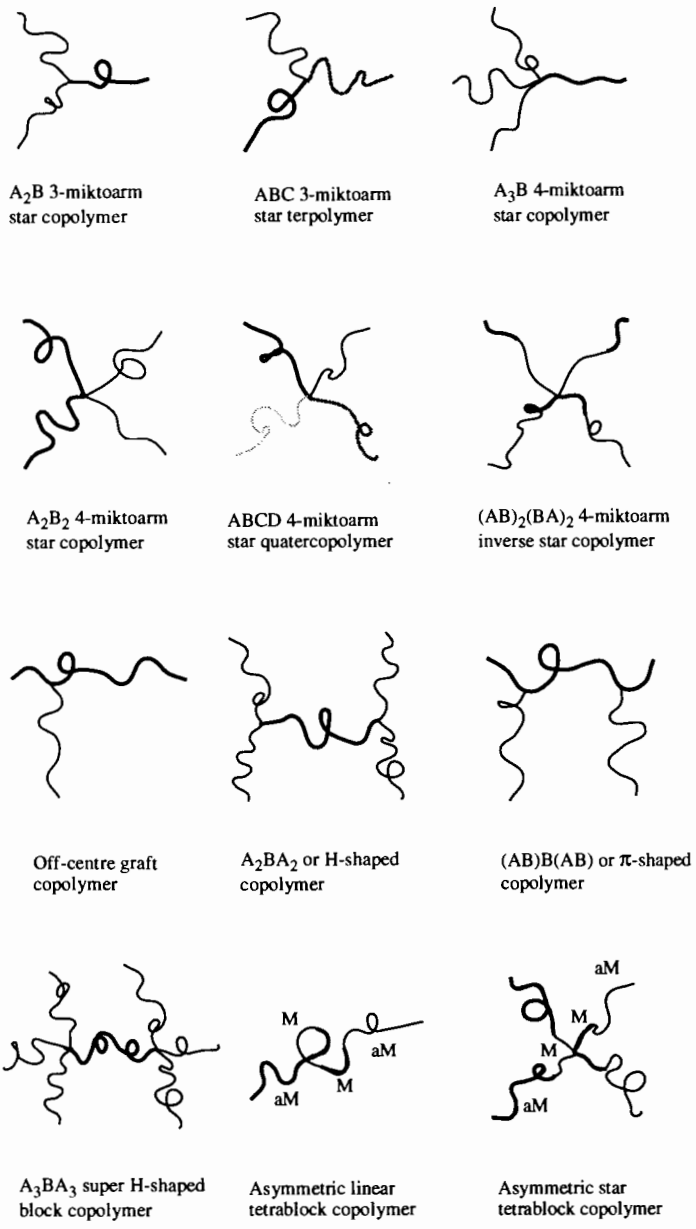

Fig. 2.33 Block copolymer architectures studied by Hadjichristidis *et al.* (1996*a*,*b*).

due to Milner (1994), accounts for the bending energy of the microphase interface and the ability of the chains to stretch away from the interface using methods developed for polymer brushes. The dependence of morphology on arm number and chain stiffness is contained in a single parameter in this theory,

$$\varepsilon = \frac{n_A}{n_B}\left(\frac{l_A}{l_B}\right)^{1/2}, \tag{2.1}$$

where n denotes the number of arms and l is a 'packing length', $l = M/\varrho R_0^2 N_A$, where $V = M/\varrho N_A$ is the volume occupied by a chain and R_0^2 is the mean-square unperturbed end-to-end distance. Milner's theory leads to the phase diagram shown in Fig. 2.34 and it was found to account for the experimental results quite well, the small differences were speculated to be due to the effects of compression of chains in gaps between adjacent domains (Tselikas *et al.* 1996*a*). The synthesis and characterization of PI/PS A_2B_2 stars was described by Young and co-workers (Allgaier *et al.* 1996), and SAXS and rheology provide evidence for the stability of different phases at a given composition in the star compared to the linear polymer (Hamley *et al.* 1997).

Microphase separation in $(AB)_4$ stars of PS (corona) and PI (core) was investigated for an $f_{PS} = 0.25$ sample by Floudas *et al.* (1996*a*) using rheology and SAXS. The morphology was found to be cubic-packed spheres. This phase behaviour was compared to results from weak-segregation limit theory, with allowance for compositional harmonics as well as fluctuations. However, the computed phase diagrams do not appear to be correct, because only unphysically small islands of the hex phase were found to survive between the large regions of lam, disordered and gyroid phases.

The synthesis of 'super-H shaped' (Fig. 2.33) block copolymers of the B_3AB_3 type, has been reported (Iatrou *et al.* 1994). The same authors have detailed the preparation of A_2B_2 and ABCD starblock copolymers (Iatrou and Hadjichristidis 1993). More recently, A_8B_8 block copolymers (termed 'vergina') have been obtained (Avgeropoulos *et al.* 1996). The morphology of all these PS–PI copolymers with $f_{PS} = 0.37$, 0.44 and 0.47 is lamellar (Beyer *et al.* 1997). The scaling of the molecular weight corrected, dimensionless area per molecule with the number of arms, z, for diblocks, three- and four-arm miktoarm starblocks and vergina stars was investigated. A relationship $\sigma N^{2/3}/R_g^2 = z^{1.29}$ (here σ is the interfacial area per molecule) was found, or $\sigma N^{2/3}/R_g^2 = 4.6z^{0.82}$ excluding the vergina stars. This is in good agreement with the predicted scaling from a simple Alexander–de Gennes model of $z^{1.0}$ (Alexander 1977; de Gennes 1976). Physically, this means that the spacing between molecules at the interface increases with graft functionality or arm number, z. This results in more spreading of at least some of the arm trajectories parallel to the interface compared to linear diblocks (Beyer *et al.* 1997). The complex topologies of block copolymers currently being synthesized is evidence for the elegant molecular engineering possible. Tselikas *et al.* (1996*b*) have synthesized and determined the morphology of a series of compositionally symmetric but conformationally asymmetric miktoarm copolymers $(PS_{\alpha M}\text{-}PI_M)_n\text{–}(PS_M\text{-}PI_{\alpha M})_n$, where $n = 1$ or 2 and the arm asymmetry parameter

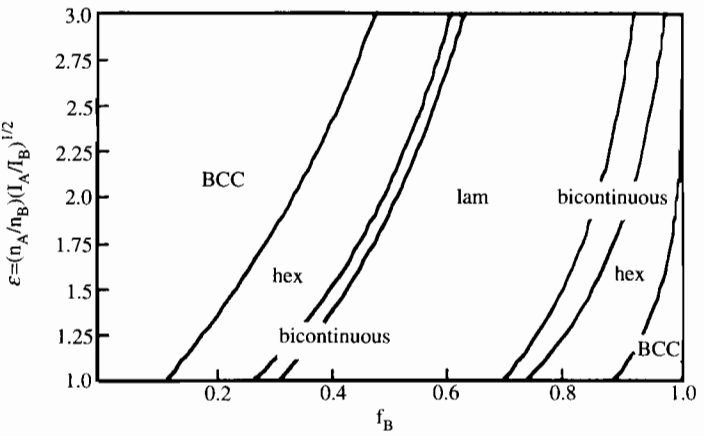

Fig. 2.34 Phase diagram in the strong segregation limit for starblock copolymers with n_A A arms and n_B B arms as a function of the volume fraction of the B monomer (Milner 1994).

takes values $\alpha = 1, 2$ or 4 (α is the ratio of the outer block molecular weight to that of the inner block). For linear tetrablocks ($n = 1$) with $\alpha = 1, 2$ or 4 and for inverse starblocks ($n = 2$) with $\alpha = 1$ or 2, a lamellar morphology was observed using TEM and SAXS. For the inverse star with the highest molecular weight asymmetry between the inner and outer blocks of the arms, however, a tricontinuous morphology was observed. The observation of a tricontinuous cubic structure in a compositionally symmetric system was explained on the basis of packing of PS–PI junctions. A curved interface was believed to relieve the overcrowding of the four PS–PI junctions at the block interface. The cubic space group could not be identified using the limited TEM and SAXS data available.

Gido and co-workers have recently investigated the phase behaviour of a series of graft and starblock copolymers with trifunctional branch points (Pochan *et al.* 1996*b*). The morphology of a series of PI_2PS Y-shaped miktoarm copolymers was probed using SAXS and TEM, and the results compared to the theoretical predictions of Milner (1994). The phase behaviour of most samples differed from that of a linear diblock of the same composition, as anticipated by Milner's theory. In general, the agreement between experiment and theory was good (Pochan *et al.* 1996*b*). However, a new morphology was observed consisting of worm-like micelles not ordered on a lattice in a copolymer with $f_{PS} = 0.81$ (Pochan *et al.* 1996*a*,*b*). This is the composition where the two PI chains are initially forced onto the concave side of the PS/PI interface, and it was suggested that this packing frustration is the driving force for this new structure. The mechanism of the transition from the initial morphology in a solvent-cast specimen of this polymer to the final worm-like micelle structure was studied in detail using TEM on quenched samples (Pochan *et al.* 1996*a*). A kinetically trapped, non-equilibrium folded-lace structure was observed to transform to the equilibrium worm-like micellar phase theough an intermediate folded-lace morphology (see

Fig. 2.35). The synthesis and morphology of more complex trifunctional branched graft copolymers have recently been discussed. Gido *et al.* (1996) prepared PS_2–PI–PS_2 (H-shaped) and (PS–PI)PI(PS–PI) (π-shaped) copolymers (see Fig. 2.33). The observed morphology of these samples was compared to the theory of Milner, the comparison being facilitated by considering the H- and π-shaped molecules to each be composed of two single graft copolymers. This generally produced a satisfactory mapping onto the phase diagram in Fig. 2.34.

There have only been a very limited number of studies on multiblock copolymers with controlled block length (we exclude here the vast literature on random block copolymers such as polyurethanes). Microphase separation in $(PS\text{-}PI)_n$ linear multiblocks with $1 \leq n \leq 4$ with nearly equal block lengths was studied by Spontak and co-workers (Smith *et al.* 1993, 1994). All (symmetric) samples were

Fig. 2.35 Transition from folded lace to 'worm-like micelle' morphology in an $f_{PS} = 0.81$ I_2S copolymer (Pochan *et al.* 1996*a*). (a) TEM image of 'folded-lace' structure, following annealing of the sample at 120 °C for 1 week (OsO_4 was used to selectively stain the PI); (b) 'randomly oriented worm' structure after annealing at 125 °C for 20 days; (c) Schematic of the transition from lamellae via 'folded-lace' to worm-like micelles.

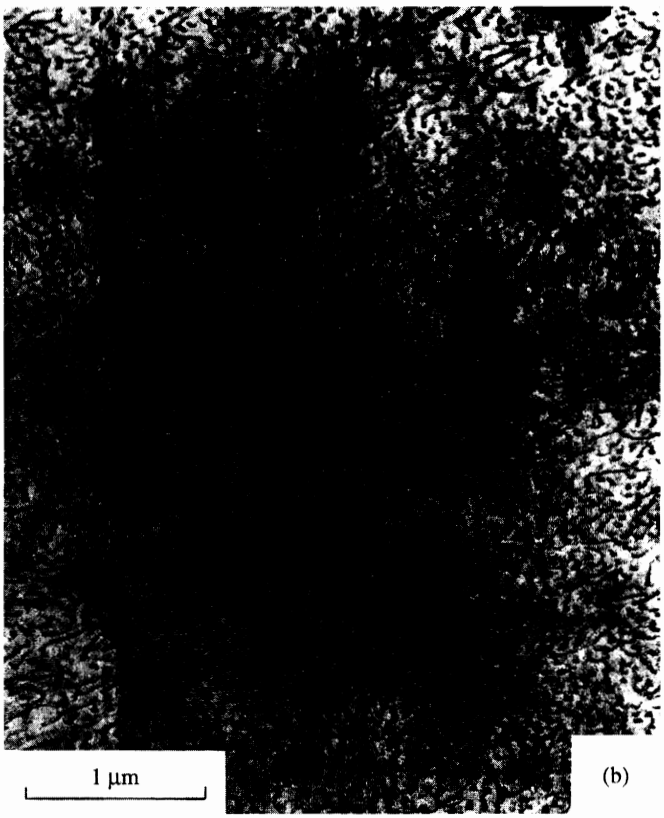

Fig. 2.35 *Continued.*

observed to form a lamellar phase, with a domain period that counter-intuitively decreased with n. This trend is in agreement with the weak segregation limit theory of Kavassalis and Whitmore (1991). A confined chain, mean field model (based on the earlier approaches of Meier (1969) and Leary and Williams (1973, 1974) for $(AB)_n$ copolymers was presented by Zielinski and Spontak (1992). They predicted that at constant copolymer composition and molecular weight, increasing n reduces the segregation between A and B blocks, making microphase separation easier. On the other hand, if the block lengths are held constant and M is allowed to vary with n, microphase separation becomes more energetically favoured as n is increased from unity. The sequential diblock approximation, where an $(AB)_n$ copolymer is modelled as an AB diblock of reduced molecular weight (M/n) was found not to accurately model the microstructural parameters of multiblocks, due to topological constraints (bridging and looping) in the latter that are not present for diblocks. Looping in linear multiblocks was studied in more detail using the same theoretical methods by Spontak *et al.* (1992*a*). It was found that for constant-length copolymers adopting the most probable looped conformations, the domain spacing scales as $d \approx n^{0.86}$ at fixed M and $d(n) \approx M^{b}$,

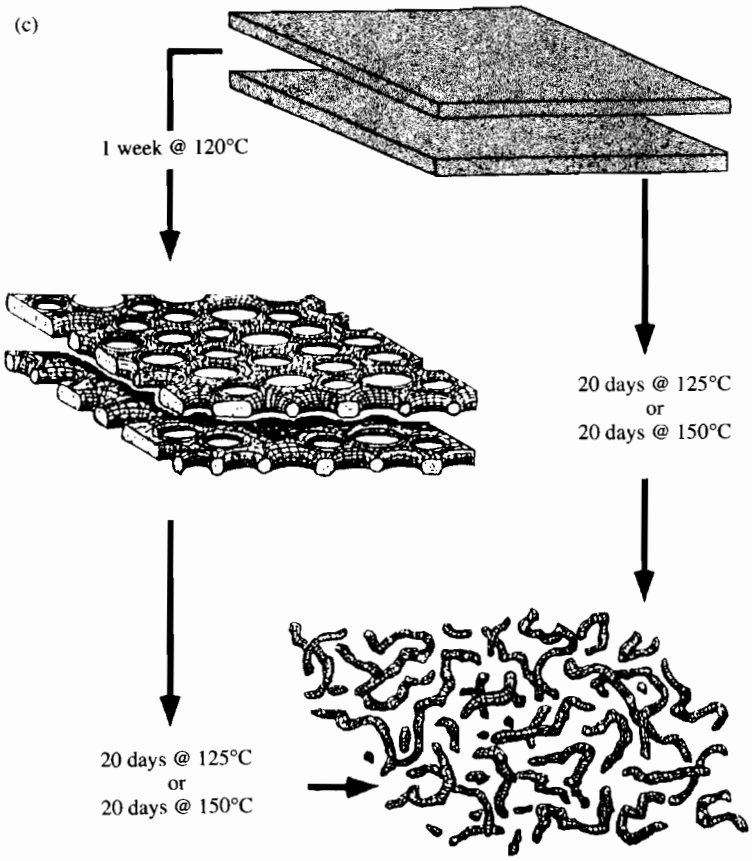

Fig. 2.35 *Continued.*

where $b = b(n)$ increases from about 0.63 ($n = 1$) to 0.79 ($n = 4$). The former prediction was found to be in good agreement with experiments (Spontak *et al.* 1992*b*).

These results serve to illustrate that molecular architecture significantly influences phase behaviour compared to linear block copolymers due to changes in molecular packing, and particularly interfacial area per block. This is most graphically illustrated in the phase diagram in Fig. 2.34.

2.2.5 Rod–coil diblocks

As we have seen, the phase behaviour of block copolymers consisting of flexible polymer coils is remarkably rich. If one of the blocks is rigid, the copolymer would be expected to exhibit even more complex phase behaviour. For example, the rigid block could be mesogenic. This leads to the possibility of self-assembly of structures consisting of domains of liquid crystalline material within a microphase-separated block copolymer superstructure. Diblock copo-

lymers consisting of a rigid block attached to a coiled block are termed rod–coil copolymers.

The first synthesis and characterization of rod–coil block copolymers was reported by Douy and co-workers (Perly *et al.* 1974, 1976). They studied AB diblock copolymers consisting of PB and the poly(peptide) poly(γ-benzyl L-glutamate) (PBLG) or poly(N^5-hydroxypropylglutamine) and found that their copolymers formed a lamellar structure in the melt and in concentrated solution. In this system, the PBLG adopts a stiff helical conformation (rod block) and the PB forms the coil block. PBLG is often used as a model rod-like polymer, and forms liquid crystal phases in solution (Lee and Meyer 1988). Later, Nakajima *et al.* (1979*a*,*b*) investigated the phase behaviour of triblock copolymers consisting of PBLG endblocks and a PB or poly(oxytetramethylene) midblock. They reported lamellar, cylindrical and spherical domain morphologies as a function of copolymer composition; however, the phase boundaries for these structures were observed to be shifted with respect to the phase boundaries of coil–coil block copolymers (Hayashi 1985). Subsequent work on poly(peptide)-containing block copolymers, and their relevance as models for biophysical systems, was reviewed by Hayashi (1985).

Recently, Stupp and co-workers have reported the synthesis and structural characterization via microscopy of rod–coil copolymers with a short (60 Å) mesogenic block end-attached to carboxylated poly(isoprene) of varying molecular weight (Radzilowski and Stupp 1994; Radzilowski *et al.* 1993). A representation of such a rod–coil copolymer is shown in Fig. 2.36. The mesogenic block was shown

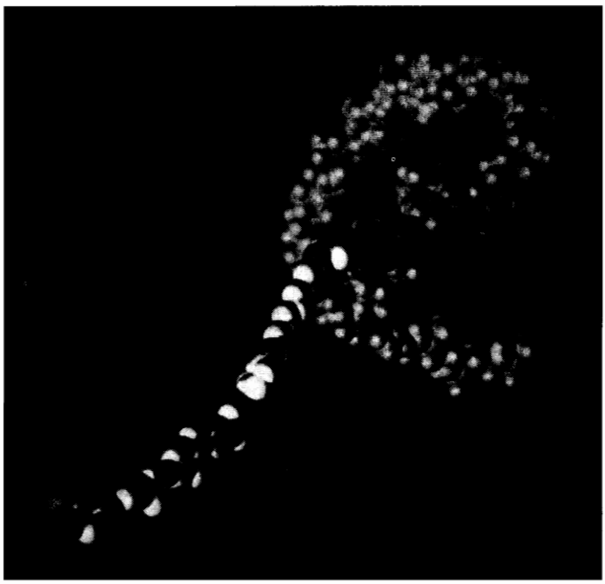

Fig. 2.36 Representation of the energy-minimized conformation of a rod–coil diblock prepared by Radzilowski *et al.* (1993). The rod is a mesogenic moiety 60 Å long, the coil is low molecular weight PI. The volume fraction of rod is about 0.2.

to form a liquid crystal phase using polarized light microscopy and microphase separation in the block copolymers was confirmed using TEM. However, it has not yet been shown whether the mesogenic block exists in a liquid crystalline phase within the microphase-separated block copolymer structure.

The potential for novel phase behaviour in rod–coil block copolymers is illustrated by the recent work of Thomas and co-workers on poly(hexyl isocyanate)(PHIC)–PS rod–coil diblock copolymers (Chen *et al.* 1996). PHIC, which adopts a helical conformation in the solid state, has a long persistence length (50–60 Å) (Bur and Fetters 1976) and can form lyotropic liquid crystal phases in solution (Aharoni 1980). The polymer studied by Thomas and co-workers has a short PS block attached to a long PHIC block. A number of morphologies were reported—wavy lamellar, zigzag and arrowhead structures—where the rod block is tilted with respect to the layers, and there are different alternations of tilt between domains (Chen *et al.* 1996) (Fig. 2.37). These structures are analogous to tilted smectic thermotropic liquid crystalline phases (Chen *et al.* 1996).

2.3 Theories for the melt phase behaviour of block copolymers

2.3.1 Strong segregation limit theory

The first theories for block copolymers were developed for the strong segregation limit (SSL) and the essential physical principles underlying phase behaviour in the SSL were established in the early 1970s (Leary and Williams 1970, 1973, 1974; Meier 1969). Most notably, the self consistent field theory of Helfand and co-workers (Helfand 1975*a*; Helfand and Wasserman 1976, 1982) was developed from a general theory of inhomogeneous polymers (Helfand 1975*b*), and permits calculation of free energies, composition profiles and chain conformations. Self-consistent field theory (SCFT) was used to calculate the configurational statistics of block copolymer chains (Helfand 1975*a*). In the SCFT method, the external mean fields acting on a polymer chain are calculated self-consistently with the composition profile. The theory was simplified by the introduction of the narrow interphase approximation, which assumes that the boundary between A and B domains is narrow compared to the domain width (Helfand and Wasserman 1976). The interfacial layer thickness is predicted to be $a\chi^{-1/2}$, where a is a statistical segment length. Phase boundaries are predicted to depend only on copolymer composition, f (Helfand and Wasserman 1982), as illustrated by the calculated phase diagram in Fig. 2.38. Experimental work on strongly segregated block copolymers supports this prediction (Hasegawa *et al.* 1987). This theory does not extend to the weak segregation limit, therefore phase boundaries are terminated at $\chi N = 100$, which is a rough limit for SSL behaviour. For the same reason, the ODT line in Fig. 2.38 is inaccurate. The most general formulation of SCFT is due to Matsen and co-workers, and enables the phase behaviour, composition profiles and chain conformations to be computed in the strong, intermediate and weak segregation regimes. This theory is discussed in detail in Section 2.3.3.

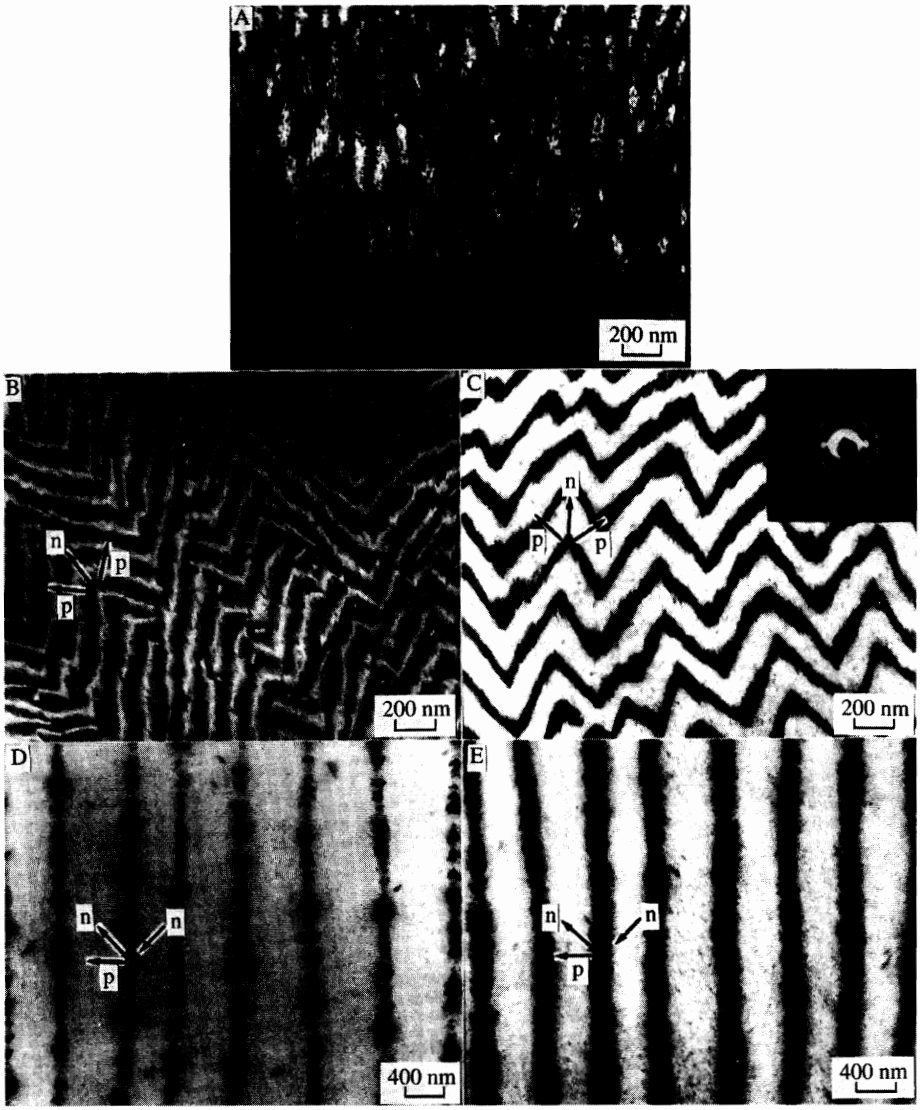

Fig. 2.37 Morphologies of PHIC–PS rod–coil block copolymers studied by Chen *et al.* (1996). *Top*: TEM images from diblocks with different compositions. The dark regions correspond to PS, which have been preferentially stained with RuO_4. (A) $f_{PHIC} = 0.42$; (B) $f_{PHIC} = 0.73$; (C) $f_{PHIC} = 0.89$; (D) $f_{PHIC} = 0.96$; (E) $f_{PHIC} = 0.98$. The PHIC chain axis and lamellar normals are denoted by **n** and **p**. (F, G, H): schematic models showing the packing arrangement of the rod–coil chains. The PHIC block is represented by the white rod, and the PS block by the black ellipsoid. (F) Wavy lamellar morphology; (G) zig-zag morphology; (H) bilayer and interdigitated arrowhead morphologies.

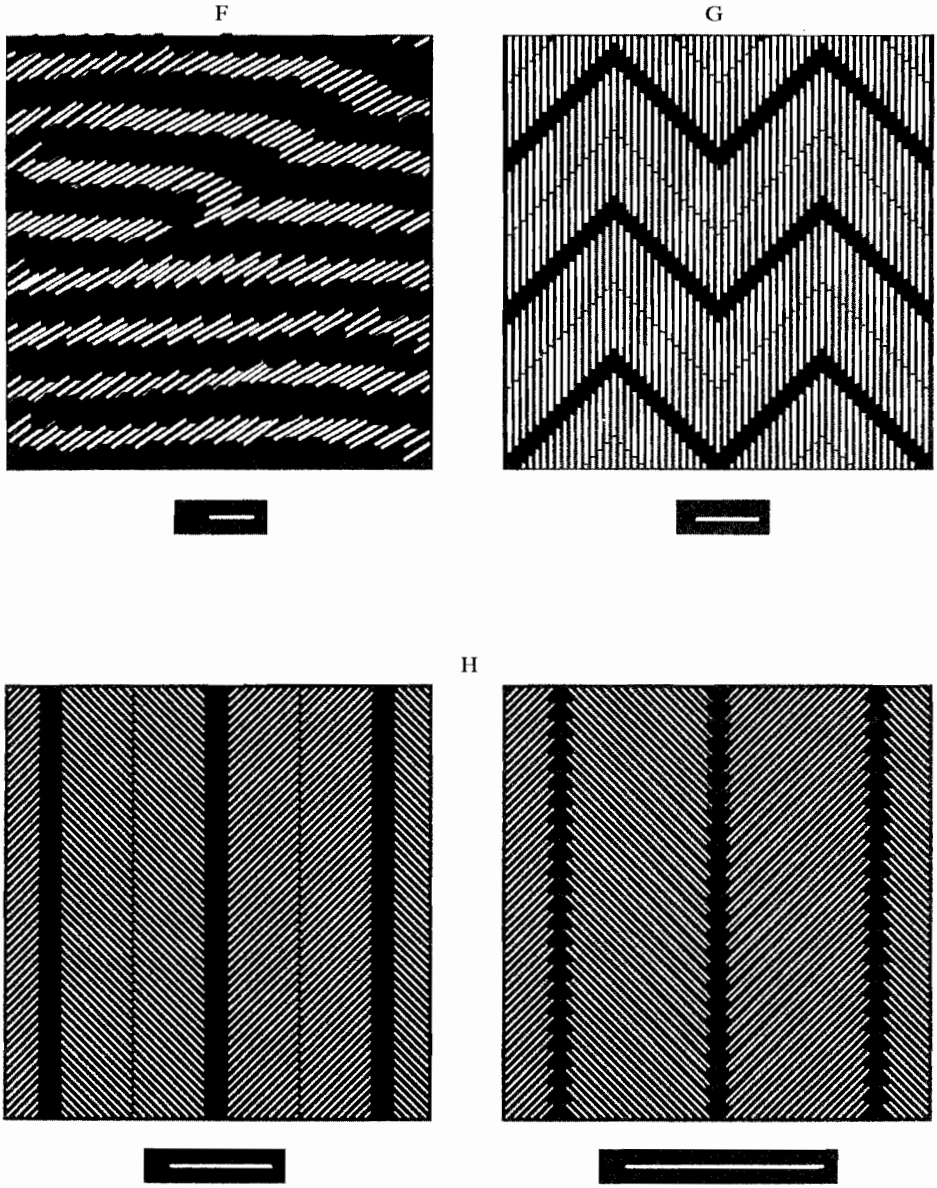

Fig. 2.37 *Continued.*

Application of Helfand's theory has been limited due to the necessity for numerical analysis (although FORTRAN code to facilitate calculations is provided by Helfand and Wasserman (1982)). This problem was circumvented with the introduction of the seminal analytical SSL theory by Semenov (1985).

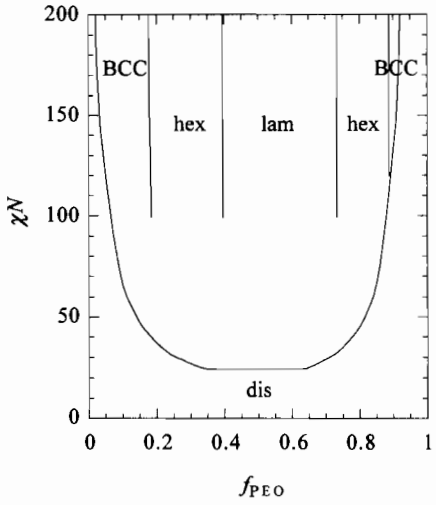

Fig. 2.38 Phase diagram computed using the strong segregation limit theory of Helfand and Wasserman (1982) for the poly(ethylene oxide)-poly(butylene oxide) (PEO–PBO) diblock system. Because the ratio of statistical segment lengths $a_{PBO}/a_{PEO} > 1$, the phase diagram is asymmetric about $f = 0.5$ (Hamley 1997).

Semenov argued that the copolymer chains are highly stretched in this regime, but non-uniform stretching at microdomain boundaries leads to an excess of chain ends in domain interiors. Thus the polymer brushes (i.e. polymer chains with junctions at an interface) are treated at a more sophisticated level than the Alexander–de Gennes scaling theory (Alexander 1977; de Gennes 1976), which assumes that chains are uniformly stretched with chain ends confined to a plane. Semenov computed the chain configurations using a classical elastic analogy, and the interaction between microdomains was analysed using an electrostatic analogy.

Despite the significant chain deformations predicted for the SSL, the domain (stretching) contribution per chain was found by Semenov (1985) to have the same scaling at for a Gaussian chain, namely.

$$F_{\text{domain}}/kT \sim d^2/a^2N, \tag{2.2}$$

where d is the domain period, and a is the statistical segment length. The contribution from the chain-end distribution and non-uniform chain stretching is only reflected in a constant prefactor. In the limit of large incompatibility, the domain free energy is balanced by the interfacial free energy (per chain)

$$F_{\text{interface}}/kT \sim \gamma\sigma \sim Na\chi^{1/2}/d, \tag{2.3}$$

where the results for the interfacial tension, $\gamma \sim \chi^{1/2}a^{-2}$, and for the area per chain, $\sigma \sim Na^3/d$, have been used (Bates and Fredrickson 1990; Halperin *et al.* 1992).

Minimization of the total free energy (sum of eqns 2.2 and 2.3) with respect to d leads to a predicted domain spacing scaling as (Semenov 1985)

$$d \sim aN^{2/3}\chi^{1/6}. \tag{2.4}$$

This result has been shown to be asymptotically correct in the limit $\chi N \to \infty$ (Matsen and Bates 1996*a*; Matsen and Whitmore 1996). These exponents differ from those obtained by Helfand and Wasserman, who found $d \sim aN^{0.643}\chi^{0.143}$ (with a geometry-dependent prefactor) and $F_{\text{domain}}/kT \sim (d/aN^{1/2})^{2.5}$ (Helfand and Wasserman 1976). The difference arises because Helfand's calculations were only carried out numerically to $d/aN^{1/2} \approx 3$, whereas in the limit $d/aN^{1/2} \gg 1$, the scaling (eqn 2.4) is obtained. As in the Helfand–Wasserman theory, phase boundaries can be computed using Semenov's theory, and are also found to be independent of χN (Semenov 1985).

Bicontinuous cubic phases have not, to date, been accounted for using SSL theory. The OBDD phase has been shown to be unstable with respect to lam and hex phases (Likhtman and Semenov 1994; Olmsted and Milner 1994*a*,*b*). As discussed above, it now appears that the OBDD was a misidentified gyroid phase; however, SSL calculations for the gyroid structure have not been performed as yet. A perforated layer structure was found to be unstable by Fredrickson (1991), using SSL theory following Semenov's method.

Ohta and Kawasaki (1986) developed a mean field theory for block copolymer melts that employs the random phase approximation, which is rigorously valid in the weak segregation limit. The results of Leibler were recovered in this limit. However, the theory was also applied in the SSL, where it is not rigorously valid. Nonetheless, predictions for the phase behaviour and domain spacings that are in qualitative accord with the results of Semenov and Helfand–Wasserman were obtained, in particular the scaling behaviour of domain spacing with degree of polymerization, $d \sim N^{2/3}$, was derived phenomenologically. This theory does not allow for a non-uniform distribution of chain ends, and is thus more restricted than the SCFT discussed in section 2.3.3. As noted by Bates and Fredrickson (1990), its primary advantage is the simplification of the calculation of ordered phase boundaries to a purely geometric problem.

2.3.2 Weak segregation limit theory

Mean field theory

Near the ODT, the composition profile of ordered microstructures is approximately sinusoidal (Fig. 2.1). The phase behaviour in this regime, where the blocks are weakly segregated, can then be modelled using Landau–Ginzburg theory, where the mean field free energy is expanded with reference to the average composition profile. The order parameter for A/B block copolymers may be defined as (Leibler 1980)

$$\psi(\boldsymbol{r}) = \langle \varrho_{\text{A}}(\boldsymbol{r}) - f \rangle, \tag{2.5}$$

where $\varrho_{\text{A}}(\boldsymbol{r})$ is the local number density of monomer A and f is the the average composition. The average over the system is denoted by $\langle \ldots \rangle$.

The phase diagram for weakly segregated diblocks was first computed within the Landau mean field approximation by Leibler (1980). Because it has proved to be one of the most influential theories for microphase separation in block copolymers, an outline of its essential features is given here. The reader is referred to the original paper by Leibler (1980) for a complete account of the theory.

Within Landau–Ginzburg theory, the free energy functional near a second-order or weakly first-order phase transition is expanded in terms of an order parameter $\psi(\boldsymbol{q})$:

$$F[\psi(\boldsymbol{q})] = \frac{1}{2!}\int_{q} S^{-1}(\boldsymbol{q})\psi(\boldsymbol{q})\psi(-\boldsymbol{q}) + \frac{1}{3!}\int_{q}\int_{q'} \mu(\boldsymbol{q},\boldsymbol{q}',-\boldsymbol{q}-\boldsymbol{q}')\psi(\boldsymbol{q})\psi(\boldsymbol{q}')\psi(-\boldsymbol{q}-\boldsymbol{q}') + \frac{1}{4!}\int_{q}\int_{q'}\int_{q''} \lambda(\boldsymbol{q},\boldsymbol{q}',\boldsymbol{q}'',-\boldsymbol{q}-\boldsymbol{q}'-\boldsymbol{q}'')\psi(\boldsymbol{q})\psi(\boldsymbol{q}')\psi(\boldsymbol{q}'')\psi(-\boldsymbol{q}-\boldsymbol{q}'-\boldsymbol{q}''). \tag{2.6}$$

Here $\boldsymbol{q}$ is a wavevector (eqn 1.6), $\psi(\boldsymbol{q})$ is the Fourier transform of $\psi(\boldsymbol{r})$, and $S(\boldsymbol{q})$ is the structure factor (Fourier transform of the two-point correlation function). The cubic term, μ, is zero for a symmetric system and otherwise may be chosen to be positive. The quartic term, γ, is then positive to ensure stability. For block copolymers, these coefficients may be expressed in terms of vertex functions calculated in the random phase approximation (RPA) by Leibler (1980). The structure factor is given by

$$S(\boldsymbol{q}) = W(\boldsymbol{q})/[\Sigma(\boldsymbol{q}) - 2\chi W(\boldsymbol{q})], \tag{2.7}$$

where Σ is the sum of all elements and W is the determinant of the matrix of the correlation functions of the ideal independent copolymer chains $[S_{ij}]$. The calculation of the S_{ij} is straightforward within the RPA and the following expressions were obtained by Leibler for a diblock copolymer:

$$S_{11}(\boldsymbol{q}) = Ng(f,x); \tag{2.8a}$$

$$S_{22}(\boldsymbol{q}) = Ng(1-f,x); \tag{2.8b}$$

$$S_{12}(\boldsymbol{q}) = S_{21}(\boldsymbol{q}) = \frac{1}{2}N[g(1,x) - g(f,x) - g(1-f,x)]. \tag{2.8c}$$

Here $g(f,x)$ is the Debye function defined as

$$g(f,x) = 2[fx + \exp(-fx) - 1]/x^2 \tag{2.9}$$

and

$$x = q^2Na^2/6 = q^2R_g^2, \tag{2.10}$$

with R_g denoting the radius of gyration of a Gaussian chain. The final formula for $S(\boldsymbol{q})$ then reads

$$S(\boldsymbol{q}) = N/\left[F(x) - 2\chi N\right], \tag{2.11}$$

where

$$F(x) = g(1,x)\Big/\left\{g(f,x)g(1-f,x) - \frac{1}{4}\left[g(1,x) - g(f,x) - g(1-f,x)\right]^2\right\}. \tag{2.12}$$

The expressions 2.7–2.12 which define the Leibler structure factor have been widely used to interpret scattering data from block copolymers (Bates and Fredrickson 1990; Mori *et al.* 1996; Rosedale *et al.* 1995; Schwahn *et al.* 1996; Stühn *et al.* 1992; Wolff *et al.* 1993). The structure factor calculated for a diblock with $f = 0.25$ is shown in Fig. 2.39 for different degrees of segregation χN. Due to the Gaussian conformation assumed for the chains (Leibler 1980), the domain spacing in the weak segregation limit is expected to scale as $d \sim N^{1/2}$.

The structure factor diverges at a spinodal point defined by $2(\chi N)_s = F(x^*,f)$ where x^* is given by eqn 2.10 with $q = q^*$. The spinodal for block copolymers is close to, but not identical to, the ODT (except for symmetric block copolymers in mean field theory) and defines the stability limit of the disordered phase.

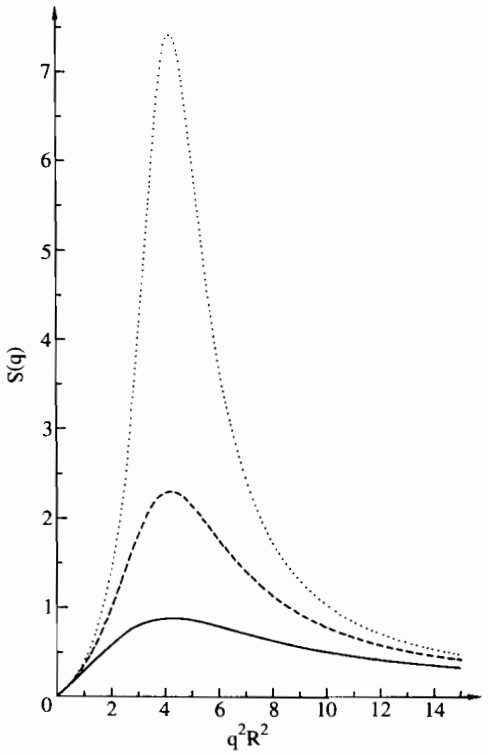

Fig. 2.39 Structure factor computed by Leibler (1980) for an $f = 0.25$ diblock copolymer melt as a function of $x = q^2R_g^2$. (· · ·) $\chi N = 17.5$; (---) $\chi N = 16.0$; (—) $\chi N = 12.5$ (the structure factor diverges at $\chi N = 18.2$ at this composition, this is the spinodal point).

The calculation of the phase diagram within Leibler's theory proceeds by comparing the free energy of different ordered phases, and of ordered phases with respect to the disordered phase. The integrals in eqn 2.6 are replaced by summations over the wavevector sets for given ordered structures. These wavevector sets correspond to the sets of allowed reflections in the scattering pattern for the ordered phase. The resulting expressions for the free energy for lam, hex and BCC phases can be simplified (in the case that the wavevector dependence of the vertex functions μ, λ is neglected, see Kats *et al.* 1993; Podneks and Hamley 1996):

$$F_{\mathrm{MF}}^{\mathrm{lam}} = \frac{\tau}{2} A_1^2 + \frac{\lambda}{4!}\frac{3}{2} A_1^4, \tag{2.13}$$

$$F_{\mathrm{MF}}^{\mathrm{hex}} = \frac{\tau}{2} A_1^2 - \frac{\mu}{3!}\sqrt{\frac{2}{3}} A_1^3 + \frac{\lambda}{4!}\frac{5}{2} A_1^4, \tag{2.14}$$

$$F_{\mathrm{MF}}^{\mathrm{BCC}} = \frac{\tau}{2} A_1^2 - \frac{\mu}{3!}\sqrt{\frac{4}{3}} A_1^3 + \frac{\lambda}{4!}\frac{15}{4} A_1^4. \tag{2.15}$$

Here, the 'effective temperature', $\tau = S^{-1}(\boldsymbol{q})$, and A_1 denotes the amplitude of the first harmonic order parameter. The free energy is minimized with respect to A_1 at a given temperature and compared for the ordered and disordered phases.

The resulting phase diagram for diblock copolymers is shown in Fig. 2.40. The theory predicts that microphase separation occurs to a body-centred cubic structure for all compositions except $f = \frac{1}{2}$, where a direct second-order transition to a lamellar structure is predicted. First-order transitions to hex and lam phases are expected on further lowering the temperature for asymmetric diblocks.

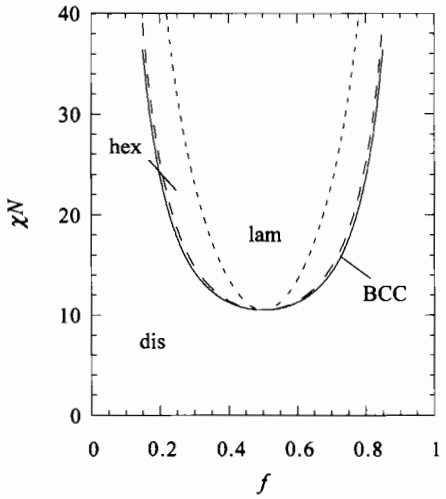

Fig. 2.40 Phase diagram for diblock copolymers in the weak segregation limit (Leibler 1980).

Leibler's theory was extended to triblock and $(A_l\text{–}B_m)_k$ star copolymers by Mayes and Olvera de la Cruz (1989). Dobrynin and Erukhimovich (1993) considered in addition asymmetric triblocks and graft copolymers ($A_lB_mA_n$), miktoarm starblocks $(A_l)_k(B_m)_k$ and linear multiblocks and polygraft copolymers $(A_lB_m)_k$. For all these types of copolymers, regions of phase stability are found to be shifted with respect to the diblock phase diagram. For example, for an ABA triblock the asymmetry parameter $\tau = f_1/f$ was introduced, where f_1 is the fraction of the N total segments in block 1 (Mayes and Olvera de la Cruz 1989). For an asymmetry parameter $\tau = 0.25$ at $f = 0.5$ a transition from the disordered phase to a BCC phase and to hex and then lam phases on further lowering the temperature is predicted. This contrasts with the direct transition to a lam phase for an $f = 0.5$ diblock. In general, asymmetry in the triblock leads to asymmetric phase diagrams. An example is the phase diagram for a triblock with $\tau = 0.5$ shown in Fig. 2.41, where at $\chi N = 19$ and $f = 0.4$ the melt is predicted to be disordered, whereas at the same χN and $f = 0.6$, the hex phase is found to be stable (Mayes and Olvera de la Cruz 1989).

To account theoretically for the stability of 'complex phases' such as the HPL and $Ia\bar{3}d$ phases, it is necessary to allow for the effect of harmonics in the com-

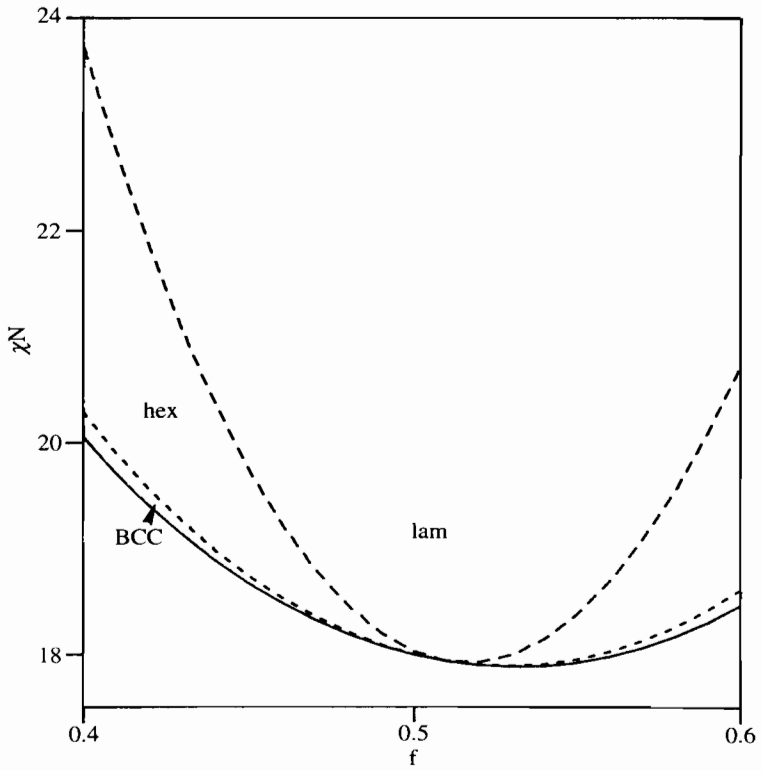

Fig. 2.41 Phase diagram for a symmetric ABA triblock copolymer ($\tau = 0.25$) (Mayes and Olvera de la Cruz 1989).

position profile. This was first done in the weak segregation regime, where the composition profile is still nearly sinusoidal, by Olvera de la Cruz (1991) and Olvera de la Cruz *et al.* (1992). They found, somewhat counter-intuitively, that allowance for harmonics leads to microphase separation to an HPL structure for a symmetric diblock (Olvera de la Cruz *et al.* 1992). This conclusion was found to be incorrect by Hamley and Bates (1994), who found that an HPL phase is not stable with respect to the classical lam or hex phases anywhere in the phase diagram. These authors also found the ordered bicontinuous double diamond phase to be unstable, as confirmed by later experiments. An $Ia\bar{3}d$ phase was found to be stable in Landau mean field theory, allowing for the second harmonic, which is close to the first harmonic for this structure (Milner and Olmsted 1997; Podneks and Hamley 1996). The stability window between lam and hex phases was found to terminate at a triple point just below the order–disorder transition, in accord with the SCFT results of Matsen and Schick (1994*b*) and Matsen and Bates (1996*a*,*b*).

Marko (1993) has considered microphase separation in cyclic block copolymers, and found that the spinodal is shifted to higher χN for a given copolymer composition compared to a diblock. This is due to the suppression of composition fluctuations because of the closed topology of the ring polymer.

Order–disorder transitions and spinodals were computed for linear multiblock copolymers with differing sequence distributions by Fredrickson *et al.* (1992). This type of copolymer includes polyurethanes, styrene–butadiene rubber, high impact polystyrene (HIPS) and acrylonitrile–butadiene–styrene (ABS) block copolymers. Thus the theory is applicable to a broad range of industrial thermoplastic elastomers and polyurethanes. The parameter

$$\lambda = p_{AA} + p_{BB} - 1 \tag{2.16}$$

was used to specify the sequence distribution. Here p_{ii} are elements of the Markovian 2×2 matrix that specify the conditional probability that an i monomer is immediately followed by another i monomer. For an alternating copolymer, $\lambda = -1$, for an ideal random copolymer $\lambda = 0$ and for a mixture of pure A and B homopolymers $\lambda = +1$. A general conclusion for stochastic multiblocks was that the broad distribution of sequence lengths leads to the absence of long-range order in the microphase separated state, as indeed observed, for example, for polyurethanes (Ryan *et al.* 1992). For $\lambda > \lambda_L \approx -0.268$, the first instability on cooling from the homogeneous melt was predicted to be phase separation into two homogeneous liquid phases (Fredrickson *et al.* 1992) as shown in Fig. 2.42. On further lowering the temperature microphase separation occurs. In contrast, for $\lambda < \lambda_L$ a melt first becomes unstable to a microphase separated state at $\chi = \chi_{SM}$. For the critical composition $f = \frac{1}{2}$, the point (λ_L, χ_L) was found to be an isotropic Lifshitz point, being the point where lines corresponding to phase separation with $q^* = 0$ and $q^* \neq 0$ meet.

Composition fluctuation theory

As noted by Leibler (1980), allowance for composition fluctuations changes the mean field prediction of a second-order phase transition for a symmetric diblock

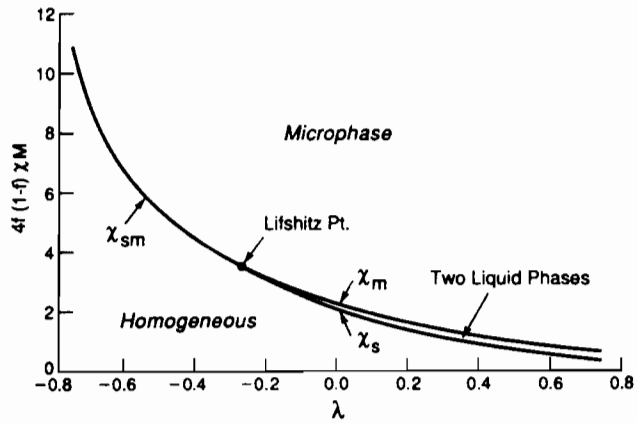

Fig. 2.42 Spinodal lines for a random multiblock copolymer melt of variable λ (Fredrickson *et al.* 1992). On cooling a melt with $\lambda > \lambda_L \approx -0.268$, the first instability is predicted to be phase separation into two homogeneous liquid phases ($\chi = \chi_m$). On further cooling to $\chi = \chi_m$, the two liquid phases become unstable with respect to formation of a microphase. In contrast, a melt with $\lambda < \lambda_L$ first becomes absolutely unstable to the formation of microphases ($\chi = \chi_{sm}$). At the critical composition of $f = \frac{1}{2}$, the point (λ_L, χ_L) is an isotropic Lifshitz point.

to a first-order transition. Fredrickson and Helfand (1987) studied this effect for block copolymers and showed that composition fluctuations, incorporated via the method of Brazovskii, lead to a 'finite size effect', where the phase diagram depends on chain size, i.e. the degree of polymerization.

In Landau–Brazovskii theory, the density modulation (or composition for block copolymers) is written as

$$\psi'(\boldsymbol{r}) = \psi(\boldsymbol{r}) + \eta(\boldsymbol{r}), \tag{2.17}$$

where $\psi(\boldsymbol{r})$ is the component possessing the symmetry of the ordered lattice, and $\eta(\boldsymbol{r})$ is the fluctuating component, with a thermodynamic average equal to zero.

The determination of the stability of different plases starts from the free energy functional (expressed in units of $k_B T$) (Fredrickson and Binder 1989; Podneks and Hamley 1996)

$$H[\psi'(\boldsymbol{r})] = \int d\boldsymbol{r} \left[\frac{\tau}{2} \psi'(\boldsymbol{r})^2 + \frac{\xi_0^2}{8q^{*2}} \left[\left(\nabla^2 + q^{*2} \right) \psi'(\boldsymbol{r}) \right]^2 + \frac{\mu}{3!} \psi'(\boldsymbol{r})^3 + \frac{\lambda}{4!} \psi'(\boldsymbol{r})^4 \right] \tag{2.18}$$

The first, third and fourth terms on the right-hand side of this equation are the real space version of eqn 2.6. The second term accounts for the quadratic free energy penalty for fluctuations with wavevectors close to the sphere $q = q^*$. The

quantity ξ_0 is a correlation length, and the other parameters were defined following eqn 2.6. For the system to be close to a short-wavelength instability it is assumed that $|\tau| \ll \xi_0^2 q^{*2}$. As shown by Brazovskii (1975), the effect of thermal fluctuations can be considered in the lowest non-trivial (Hartree) order of self-consistent perturbation theory. A simple form for the free energy in the Hartree approximation was obtained by Podneks and Hamley (1996):

$$F_{\text{Hartree}} = F_{\text{MF}} + 2\alpha\sqrt{r} - \frac{\lambda}{2}\frac{\alpha^2}{r}. \tag{2.19}$$

Here F_{MF} is the mean field free energy, defined for the lam hex and BCC phases in eqns 2.13–2.15. The term $\alpha = q^{*2}/4\pi\xi_0$ occurs in the expression for the mean square fluctuation

$$\langle \eta^2 \rangle = \frac{2\alpha}{\sqrt{r}}. \tag{2.20}$$

In turn, the renormalized inverse susceptibilities are given for lam, hex and BCC phases by (Brazovskii 1975; Fredrickson and Helfand 1987)

$$r = \tau + \frac{\lambda}{2}\langle \eta^2 \rangle + \frac{\lambda}{2} A_1^2. \tag{2.21}$$

The set of equations 2.19–2.21, together with 2.13–2.15, enables the straightforward construction of a phase diagram within Landau–Brazovskii theory. Examples of such phase diagrams are shown in Fig. 2.43. The Fredrickson–Helfand theory for block copolymers predicts that the spinodal is suppressed to a temperature $T = 0$ K. Furthermore, the order–disorder transition occurs at a larger value of χN than predicted by mean field theory, the correction for a symmetric diblock scaling as $\overline{N}^{-1/3}$. Here $\overline{N} = (6R_g^2)^3 v_0^{-2} = Na^{-3}$, with a a monomer length and v_0 a segmental volume. In contrast to the mean field prediction, direct transitions to the hexagonal-packed cylinder or lamellar phases are possible for asymmetric diblocks. The region of stability of the body-centred cubic phase is moved to compositions away from $f = \frac{1}{2}$.

The principal requirement for validity of the Landau–Brazovskii theory can be expressed for block copolymers as the inequality (Podneks and Hamley 1996)

$$\varkappa \equiv \frac{(a\lambda)^{2/3}}{\xi_0^2 q^{*2}} = \frac{(d\lambda)^{2/3}}{6x^*}\overline{N}^{-1/3} \ll 1, \tag{2.22}$$

where $d = 3x^*/2\pi$. We note that this inequality leads to the $\overline{N}^{-1/3}$ scaling for the ODT in a symmetric diblock in Fredrickson–Helfand theory. Fredrickson and Helfand (1987) estimated that the Hartree approximation is only valid for block copolymers with $\overline{N} > 10^4$.

The effect of harmonics in the composition profile has been considered in Landau–Brazovskii theory, as well as mean field theory. Olvera de la Cruz (1991) found a hexagonal perforated layer (HPL) structure to be stable for symmetric or nearly symmetric diblocks in addition to the classical phases. Recent work has

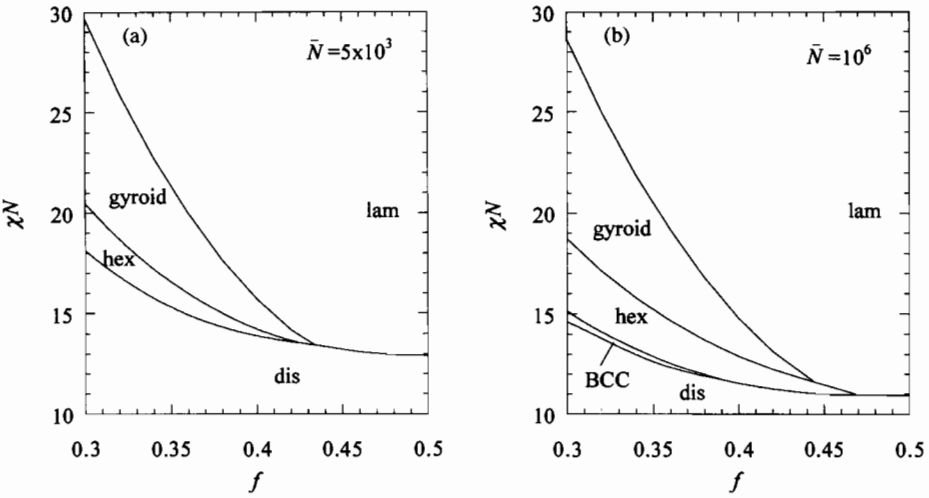

Fig. 2.43 Phase diagrams calculated (Hamley and Podneks 1997) within the Landau–Brazovskii approximation, applied to block copolymers by Fredrickson and Helfand (1987): (a) for a degree of polymerization $\bar{N} = 5 \times 10^3$, a direct transition between gyroid and dis phases occurs near $f = 0.43$; (b) for $\bar{N} = 10^6$, there is no direct transition between these phases (Hamley and Podneks 1997).

shown that, in fact, this structure is not stable and the gyroid phase is the only stable complex phase accounted for theoretically (Podneks and Hamley 1996). It is found that allowance for composition fluctuations for the $Ia\bar{3}d$ phase, with the second harmonic from {220} reflections in addition to the first harmonic from {211} reflections, leads to the possibility of a direct transition between the isotropic and $Ia\bar{3}d$ phases, as observed experimentally (Förster *et al.* 1996; Khandpur *et al.* 1995). This transition is anticipated theoretically in a narrow composition range between lam and hex phases below a critical degree of polymerization, $\bar{N} \approx 1 \times 10^4$ (Hamley and Podneks 1997).

The fluctuation theory for weakly segregated block copolymers was extended by Barrat and Fredrickson (1991*a*) to include a wavevector dependence of the correlation functions. This allowed for a shift in the peak position of the structure factor to be computed as a function of χN, in quantitative agreement with the results of neutron scattering experiments. In addition, by considering tagged chains the effect of concentration fluctuations on single chain statistics in the melt was investigated. By calculating the components of the radius of gyration tensor it was shown that strong deviations from Gaussian statistics exist for chains of finite molecular weight. A local segregation between monomers of the two blocks ('dumb-bell' configuration) results in an enlargement in the radius of gyration of the copolymer that increases with χN.

The first experimental confirmation of the importance of composition fluctuations in a block copolymer melt was reported by Bates *et al.* (1988), and numer-

ous further studies have confirmed many of the theoretical predictions, as discussed in Section 2.2.1.

2.3.3 Self-consistent field theory

The strong and weak and segregation limit theories for block copolymer melts have recently been unified by Matsen and co-workers (Matsen and Bates 1996*a*; Matsen and Schick 1994*a*). This approach involves numerical solution of self-consistent field equations, without approximations such as the narrow interphase approximation. The SCFT reduces the problem of calculating the interactions in an ensemble of polymer chains to that of a single non-interacting polymer in external fields that are obtained self-consistently with the composition profiles. To date, it has been used at the mean field level. Inclusion of fluctuations is a challenging theoretical problem. Although calculation of a complete phase diagram is computationally intensive, calculations are not restricted to any degree of segregation, and detailed information on chain conformation, composition profiles and equilibrium phase behaviour can be obtained. The phase behaviour of pure diblock (Matsen 1995*a*), triblock (Whitmore and Vavasour 1995), star-block (Matsen and Schick 1994*b*) and linear multiblock (Matsen 1995*b*) melts has been considered, as well as blends of homopolymer with diblock and diblock blends, as discussed in Chapter 6. In this section, we focus on the application of the theory to the simplest case of copolymer: diblocks; its application to other systems is straightforward. An outline of the theory, following Matsen and Schick (1994*a*), is presented in the Appendix.

By comparing the free energies for different phases, the phase diagram shown in Fig. 2.44 is obtained. This phase diagram is obtained for conformationally-symmetric diblocks, where the statistical segment lengths of A and B blocks are equal. When the ratio $a_A/a_B > 1$, the phase diagram is skewed so that phase boundaries move to towards larger f_A, and the converse is true if $a_A/a_B < 1$ (Matsen and Bates 1997*a*; Vavasour and Whitmore 1993). Increasing the segment length of the majority block also leads to a reduction of instability of perforated layer phases, although the topology of the stable phases is unaffected (Matsen and Bates 1997*a*).

As shown in Fig. 2.44, SCFT accounts for a stable gyroid phase in the weak segregation regime, between the classical lam and hex phases predicted by Leibler (1980). Matsen and co-workers also considered the stability of mono-continuous and bicontinuous perforated layer structures and the OBDD structure (Matsen and Bates 1996*a*; Matsen and Schick 1994*a*). A bicontinuous perforated layer structure was found to be nearly stable along the lam–hex transition line. The OBDD phase was found to be even less stable. In the wings of the phase diagram close to the ODT there are also regions of stability of a close-packed sphere (CPS) structure (Matsen and Bates 1996*a*). Face-centred cubic and hexagonal close-packed structures (which correspond to ABCABC... or ABAB... stackings of close-packed spheres respectively) were found to be essentially degenerate in free energy in the strong segregation limit, and the spacings between nearest neighbour spheres were indistinguishable (Matsen

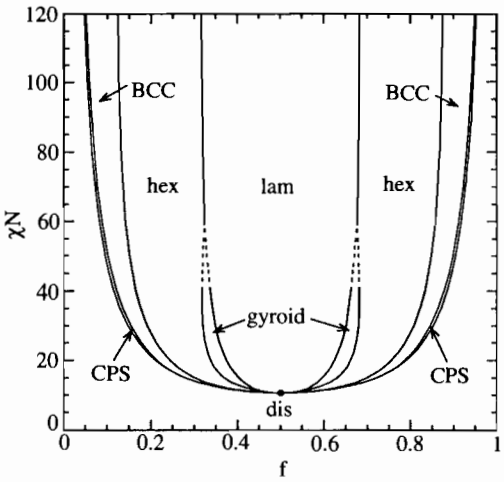

Fig. 2.44 Phase diagram for a conformationally-symmetric diblock copolymer, calculated using self-consistent mean field theory. Regions of stability of disordered, lamellar, gyroid, hexagonal, BCC and close-packed spherical (CPS), phases are indicated (Matsen and Schick 1994*a*). All phase transitions are first order, except for the critical point which is marked by a dot.

and Bates 1996*a*). Similarly, the free energies of hexagonal perforated layer structures with these stacking sequences were found to be nearly equal in the SSL (Matsen and Bates 1996*a*; Matsen and Schick 1994*a*). A physical interpretation of the stability of the gyroid phase was provided by Matsen and Bates (1996*b*), who argued that both minimization of molecular packing frustration and reduction of interfacial tension through the formation of constant mean curvature surfaces are important. Due to the tendency to form uniform thickness domains, the interfaces in block copolymer structures are not constant mean curvature surfaces. The relative influence of these factors on the stability of the gyroid, HPL and OBDD phases was investigated and the gyroid found to be stable for melts of diblocks although perforated layer and OBDD phases can be stabilized by addition of homopolymer to the majority or minority domain respectively (Matsen and Bates 1996*b*).

In contrast to experimental observations of a direct transition between isotropic and $Ia\bar{3}d$ phases, mean field SCFT predicts a triple point for $Ia\bar{3}d$ phase boundaries above the ODT (Matsen and Schick 1994*a*). Allowance for composition fluctuations in the WSL leads to the possibility of a direct transition (Podneks and Hamley 1996), as discussed in the preceding section. It is likely that composition fluctuations will also significantly alter the phase diagram in the region of CPS phase stability, possibly eliminating or reducing the stability window of these structures, which have not been observed experimentally, although liquid micellar phases have been identified, as discussed in Section 2.2.1.

The scaling of domain spacing, d, with N has also been investigated using SCFT. It is found that the scaling in the weak and intermediate segregation regimes cannot be described by a simple power law, in contrast to the predictions of earlier theories. Even in the WSL close to the ODT the approximate scaling $d \sim N^{0.994}$ is found (Matsen and Bates 1996*a*), which is much steeper than the $d \sim N^{1/2}$ scaling from the RPA (Leibler 1980). This scaling is only recovered in SCFT deep in the disordered phase. SCFT shows that the SSL scaling $d \sim N^{2/3}$ predicted by Semenov (1985) is approached asymptotically for large segregations ($\chi N > 100$). A steeper scaling $d \sim N^{0.8}$ has been observed in the weak segregation limit (Almdal *et al.* 1990; Hadziioannou and Skoulios 1982; Papadakis *et al.* 1996*a*). SCFT was found to reproduce well the domain spacing scaling with N of a series of poly(oxyethylene)–poly(oxybutylene) diblocks determined using small-angle X-ray scattering (Mai *et al.* 1996).

2.3.4 Integral equation theories

Liquid state theory has recently been applied to block copolymer melts by David and Schweizer (1994*a*,*b*). In this approach, the polymer molecules are modelled as chains of interaction sites (which usually represent a collection of monomers) using an extension of the liquid state theory used for systems of small molecules or atoms. The off-lattice polymer reference interaction site model (PRISM) theory was applied to block copolymers, using a 'Gaussian thread' model for symmetric copolymers (David and Schweizer 1994*a*). The theory was related to Leibler theory using the 'reference molecular mean spherical approximation' (R-MMSA) closure within the thread idealization. This closure can be viewed as the integral equation theory realization of mean field theory. The dependence of the effective χ and structure factor on temperature, density, composition, molecular weight and spatial range of interactions was investigated (David and Schweizer 1994*a*). The molecular weight dependence of the fluctuation stabilization close to the ODT was found to be the same as in the Fredrickson–Helfand theory (Fredrickson and Helfand 1987). However, in contrast to the latter theory, the phase behaviour of block copolymers in the David–Schweizer model is non-universal, depending via the interaction range on the detailed polymer structure. Thus the David–Schweizer model has great potential for incorporating effects due to the real chemical structure of block copolymers. However, presumably due to its computational complexity, this theory has yet to be applied to analyse or interpret experimental results.

In a sister paper (David and Schweizer 1994*b*), local and long-range properties of diblock copolymer melts were investigated using PRISM theory and two molecular-based closure approximations. The R-MMSA closure and the 'reference-molecular Percus–Yevick' (R-MPY) approximation were investigated numerically for structurally symmetric, flexible and semiflexible copolymers with finite hard-core diameters. The position and intensity of the structure factor peak were computed, along with radial distribution functions. With both types of closure, the theory predicts the elimination of the spinodal for finite degrees of polymerization (David and Schweizer 1994*b*). Adopting the R-MMSA closure, a

spinodal is never reached for finite N, as in composition fluctuation theory in the weak segregation limit (Section 2.3.2). However, the region where fluctuations are significant is smaller for longer chains. Only low-molecular-weight ($N \leq 500$) polymers were considered by David and Schweizer (1994*b*). Within PRISM theory the absence of a spinodal instability may be tied to intrinsic 'molecular' length-scales. This was in accord with the results of computer simulations. Two competing fluctuation effects were suggested: (i) local density fluctuations which decrease the effective χ as N increases, and (ii) long wavelength concentration fluctuations which destabilize the isotropic phase as N increases. These fluctuation contributions were believed to exhibit only a very slow approach to the asymptotic limiting behaviour, which from the Gaussian thread model was a finite size effect similar to that obtained from the Fredrickson–Helfand theory (David and Schweizer 1994*a*,*b*). A temperature regime in which there is an apparent chain-length independent fluctuation stabilization for moderate degrees of polymerization was observed using the R-MPY closure.

2.3.5 Computer simulation

There have been a number of computer simulations of block copolymers by Binder and co-workers (Fried and Binder 1991*a*,*b*), and this work was reviewed in Binder (1994). Although computer simulations are limited due to the restriction on short chain lengths that can be studied, finite size effects and equilibration problems at low temperatures, the advantages are that the models are perfectly well characterized and ideal (monodisperse, etc.) and microscopic details of the system can be computed (Binder 1994). In the simulations by Binder and co-workers, diblocks were modelled as self- and mutually-avoiding chains on a simple cubic lattice, with chain lengths $N = 14$ to 60 for $f = \frac{1}{2}$. A purely repulsive pairwise interaction between A and B segments on adjacent sites was assumed. A finite volume fraction of vacancies was included to speed the thermal equilibration process (Binder 1994).

Because the maximum of the structure factor $S(q^*)$ was found to vary smoothly in the simulation, Fried and Binder (1991*a*) adopted a dynamic criterion to locate the ODT. In particular, they determined the point at which the randomly reorienting structure factor for the isotropic phase evolves into the oriented $S(\boldsymbol{q})$ for the lamellar phase. If the ODT was a second-order phase transition, critical slowing down would be expected at the phase transition, and the spontaneous symmetry breaking in the 'time averaging' done by the Monte Carlo simulation would appear as an 'ergodicity breaking', since the relaxation time for the reorientation of the preferred direction diverges (Fried and Binder 1991*a*,*b*). A major advantage of the simulations is the ability to determine spatially-averaged single-chain properties such as the radius of gyration. A good example is the observation that the mean-square interblock distance R_{AB} increases more rapidly than R_g, showing chain stretching into a 'dumb-bell' conformation (Fig. 2.45) (as also predicted by Barrat and Fredrickson (1991*a*,*b*), see Section 2.3.2). By determining the χN dependence of the collective length-scale $z_0 = q^* R_{AB}/\sqrt{2}$ with respect

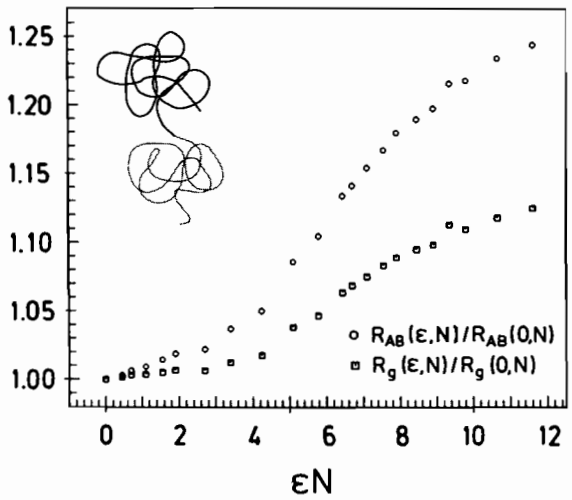

Fig. 2.45 Illustrating the formation of a 'dumb-bell' conformation in an AB diblock copolymer, computer simulation results show that the r.m.s. separation between A and B blocks, R_{AB}, increases faster than the radius of gyration, R_g, with increasing segregation εN (ε is a monomeric interaction energy) (Fried and Binder 1991*a*). The ODT is estimated to occur at $\varepsilon N \approx 7.5$–9.

to $x_0 = q^* R_g$ it was shown that the collective length-scale $\lambda_0 = 2\pi/q^*$ increases faster than any single-chain property (Fried and Binder 1991*a*,*b*). Thus λ_0 reflects a wavelength due to 'clusters' of molecules rather than individual chains. Fried and Binder also observed that there is no sharp transition where coil-stretching sets in, in contrast to results from neutron scattering experiments (Almdal *et al.* 1990; Papadakis *et al.* 1996*b*).

2.3.6 Rod–coil copolymers

There have been fewer theories devoted to ordering in rod–coil block copolymers than to coil–coil systems, reflecting the limited amount of experimental work to date on the former. However, recent developments highlight the predictive power of self-consistent field theory for the phase behaviour of these materials, as well as for the simpler phase behaviour of flexible block copolymers.

Early work predicted smectic (or lamellar) ordering in rod–coil copolymers (Semenov 1991; Semenov and Vasilenko 1986). In liquid crystals, a smectic A phase is a lamellar phase where the molecules are, on average, parallel to the layer normal. In a smectic C phase, the molecules are tilted with respect to this direction. The imbalance in interfacial area per chain for a rod or coil can lead to tilting of chains to maintain uniform density. Semenov (1991) constructed a phase diagram for rod–coil copolymers in which second-order phase transitions

from the nematic to smectic A phase and from the nematic to smectic C phase were predicted as the χ parameter is increased. A number of phase transitions between different smectic A and C phases were also predicted (Semenov 1991). A mean field analysis of the lamellar phase in rod–coil copolymers in a selective solvent of low molecular weight was presented by Halperin (1989). He predicted a first-order transition between smectic A and smectic C phases due to a competition between the deformation free energy of the flexible blocks and the surface free energy of the rod-like segments. Following work by Halperin (1990) on rod–coil solutions, Williams and Fredrickson (1992) argued that a phase consisting of cylindrical 'hockey puck' micelles is more stable in the melt than a monolayer lamellar phase over most of the phase diagram. These cylindrical disc-like micelles consist of pieces of lamellae cut into cylinders. Williams and Fredrickson (1992) point out that the phase behaviour is governed by a balance between the incompatibility of blocks (as for coil–coil copolymers) favouring separation of rod and coil, and the penalty for chain stretching. Because the chains can stretch less at the top and bottom of the 'hockey pucks' relative to flat lamellae (at the cost of creating an extra curved surface), these micelles can form a stable phase. It was also argued that spherical micelles are not stable, due to packing constraints on the rod block in the centre of micelles (Williams and Fredrickson 1992).

Numerical self-consistent field theoretical calculations for rod–coil diblocks by Müller and Schick (1996) show that only morphologies in which the coils are on the convex side of the interface are thermodynamically stable in both the strong and weak segregation limits. A phase diagram in the weak segregation limit contains a large region of stability of the hex phase (including $f_{rod} = 0.5$) and a narrow region of stability of the lam phase at larger f_{rod}, indicating the importance of interfacial curvature introduced by the rod block (Müller and Schick 1996). The value of χN at the ODT in rod–coils is lower than for flexible diblocks, i.e. the rod block acts to stabilize ordered phases (Holyst and Schick 1992; Singh *et al.* 1994).

SCFT has also been applied to semiflexible block copolymers, following early work which indicated the dramatic change in phase behaviour that occurs if the A block in an AB diblock goes through the isotropic–nematic transition (Williams and Halperin 1993). The region of stability of spherical micelles was predicted to be greatly enhanced as the A core block stretches in the nematic phase. As the temperature is lowered, or the volume fraction of the nematic block is increased, a lamellar phase is expected to be stable (Williams and Halperin 1993). SCFT calculations have recently been performed by Netz and Schick (1996) where dipolar and quadrupolar interactions were considered as an external anisotropic field and as interactions between chains giving rise to liquid crystal phases. Depending on the type of interaction, transitions between isotropic and nematic or lamellar phases were predicted (Netz and Schick 1996). Matsen has considered the effect of molecular rigidity in symmetric semiflexible diblocks by adopting the worm-like chain model (Matsen 1996). Here a dimensionless bending modulus parameterizes the chain configuration, in addition to the contour length. Since only diblocks symmetric in composition and flexibility

were considered, the theory is only concerned with the domain spacing scaling and ODT in the lamellar phase (Matsen 1996). In agreement with the calculations for rod–coil diblocks discussed above, $(\chi N)_{ODT}$ was predicted to decrease as the polymer stiffens.

2.4 Dynamic processes in block copolymer melts

2.4.1 Dynamics of structure formation

To date there have only been a limited number of studies of the kinetics of ordering of block copolymers. In part, this may be due to the necessity for measurements of structure development with a high temporal resolution. Experiments on the time evolution of structure in microphase-separated block copolymers can be carried out using synchrotron small-angle X-ray scattering. An early study of the ordering of an asymmetric PS–PB diblock onto a cubic lattice was performed by Harkless *et al.* (1990). Following a quench from the disordered phase, the development of the ordered structure was monitored using SAXS with a time resolution of 1–3 s. The development of a structure factor peak from an ordered liquid of PS spheres was observed initially. At later times, the liquid peak decayed as the first-order Bragg peak from a BCC lattice developed. The measured intensity of the Bragg peak is proportional to the fraction of ordered material in the sample. Harkless *et al.* (1990) interpreted the development of ordered structure using an Avrami model where the fraction of ordered material grows as

$$\zeta = \left(1 - e^{-kt^n}\right), \tag{2.23}$$

where k is a constant, and for thermal growth of spherical domains $n = 4$. They found this scaling in the early stage of growth, but in the late stage the data could be fitted with $n = 1$. The apparent slowing of growth at late times was suggested to be due to impingement of grains and site saturation (Harkless *et al.* 1990). This is accounted for in the theory of Cahn (1956) for nucleation on two-dimensional defects, and application of this theory yielded a good fit for all times. The ordering kinetics were studied as a function of quench depth and a minimum in the associated time constant was found for intermediate quenches. The larger time constants for deep quenches are due to a reduced thermal activation whilst those for shallow quenches reflect 'critical slowing down' due to the smaller free energy difference between the phases (Harkless *et al.* 1990).

In contrast to these results, Floudas *et al.* (1994*b*) found that for a symmetric PS–PI diblock, the kinetics of development of the lamellar phase (determined from the dynamic shear moduli) following a shallow quench from the disordered phase can be described by nucleation and growth of three-dimensional objects with a lamellar microstructure. However, for deeper qunches the Avrami equation could only describe the initial stages of ordering (Floudas *et al.* 1994*b*). Hashimoto *et al.* (1986*a*,*b*) performed time-resolved SAXS experiments on the order–disorder transition induced by a T-jump in PS–PB diblocks in

n-tetradecane. The apparent diffusivity, D_{app}, was obtained from the decay rate of the time-dependent scattered intensity,

$$I(q,t) = I(q,t=0)\exp\{-2R(q)t\}, \tag{2.24}$$

where $R(q) = q^2 D_{app}$. Values of $D_{app} \approx 10^{-14}$ to $10^{-13}\,cm^2\,s^{-1}$ were obtained. The time required for disordering was found to be short ($\approx$10 s) despite the small D_{app} because the distances ($d = 2\pi/q^*$) for diffusion were small. The concentration and temperature dependence of D_{app} were described in detail in Hashimoto *et al.* (1986*a*). Similar results were also reported for a 55 wt% solution of a PS–PB–PS triblock in dipentene (Hashimoto 1985). The kinetics of the disorder–lamellar phase transition were also investigated for this solution following a fast quench (Hashimoto 1987). In the initial stage of the transition, the peak position q^* was essentially constant, and the intensity at a given q value was found to increase exponentially with time. This reflects the first stage of microphase separation. At later times, the scattering peak became sharper reflecting a 'shaping up' process of microdomains.

These conclusions were later supported by time-resolved SAXS experiments by Stühn *et al.* (1994) who studied the ordering of a PS–PI diblock with $f_{PS} = 0.44$ following quenches from the disordered phase into the lamellar phase. They found that the relaxation times of the structure factor were wavevector dependent, and consistent with the Cahn–Hilliard from (Cahn and Hilliard 1958)

$$\frac{1}{\tau_q} = \frac{\Lambda(q)q^2}{S(q)}, \tag{2.25}$$

where τ_q is the relaxation time at wavevector q and $\Lambda(q)$ is a kinetic Onsager coefficient. The formation of the lamellar structure was found to proceed via a two-step process. Initially, the disordered liquid relaxes into a metastable structure with an associated time-scale of several seconds. Subsequently, the ordered domains order into a lattice. This latter process was modelled as the sharpening of a Gaussian peak (which develops from a Lorentzian at high temperatures) as the lamellar order improved (Stühn *et al.* 1994). The decrease in width of the Gaussian was found to follow Avrami kinetics (eqn 2.23) with $n = 2$, in contrast to $n = 4$ expected for the development of spherical domains in three dimensions (Gedde 1995), and observed by Harkless *et al.* (1990).

The ordering kinetics of a PS–PI diblock, a $PSPI_2$ graft copolymer and a PSPIPB miktoarm terpolymer, all forming a hex phase, were studied using SAXS and rheology by Floudas and co-workers. For shallow quenches, the ordering was found to proceed via heterogeneous nucleation and growth of three-dimensional grains ($n = 3$), as determined from an analysis using the Avrami equation. For deeper quenches, the Avrami exponent, n, changed from 3 to 4, indicating a different growth mechanism (Floudas *et al.* 1994*a*). The ordering kinetics of an $(AB)_4$ starblock with PS corona and PI core ($f_{PS} = 0.25$) were studied using rheology via the time dependence of the dynamic elastic moduli following a quench. A dramatic slowing down of the ordering process compared to linear

diblocks was observed due to the constraints on chain mobility imposed by the molecular topology. In particular, the characteristic times obtained from fits of the Avrami equation to the growth of G' and G'' following a quench from the disordered phase were found to be three orders of magnitude larger than for the corresponding linear diblock (Floudas *et al.* 1996*a*).

The nucleation and growth of grains of the lamellar phase in a PS–PI diblock was studied using depolarized light scattering by Balsara and co-workers (Dai *et al.* 1996). They found that in the early stage following a quench from the disordered phase, the grains have an elongated shape with an aspect ratio of about four. In the late stage, where grains grow by defect annihilation, grain growth occurred only along the minor axes (Dai *et al.* 1996). The growth of the lamellae with respect to the grain axes in a PS–PI diblock was determined using TEM in the early stages following a quench into the lam phase by Hashimoto *et al.* (1996). They observed isolated anisotropic grains of lamellae in the disordered matrix, with a size along the lamellar normal larger than that parallel to the lamellae as also noted by Dai *et al.* (1996). This anisotropic growth was reproduced using a cell-dynamic simulation (CDS) of a time-dependent Ginzburg–Landau (TDGL) model (*vide infra*) (Hashimoto *et al.* 1996). The anisotropic growth of lamellar domains has been predicted using Landau–Brazovskii theory in a phenomenological droplet theory of nucleation by Hohenberg and Swift (1995).

The kinetics of ordering in block copolymer melts have been studied using cell dynamics simulations of the TDGL equation (Bahiana and Oono 1990; Chakrabarti *et al.* 1991; Puri and Oono 1988; Qi and Wang 1996, 1997; Shiwa *et al.* 1996). Here, the time evolution of the order parameter ψ is followed:

$$\frac{\partial \psi(\boldsymbol{r},t)}{\partial t} = M\nabla^2\left(\frac{\partial F}{\partial \psi}\right) + \eta(\boldsymbol{r},t). \tag{2.26}$$

Here M is a mobility coefficient, which is assumed to be constant and $\eta(r,t)$ is the random thermal noise term, which for a system in equilibrium at temperature T satisfies the fluctuation–dissipation theorem. The free energy functional is taken to be of a Ginzburg–Landau form. In the notation of Qi and Wang (1996, 1997) it is given by

$$F[\psi(\boldsymbol{r})] = \int \mathrm{d}\boldsymbol{r}\left\{\psi(\boldsymbol{r})\left[-\frac{\tau}{2} + \frac{a}{2}(1-2f)^2 - \frac{b}{2}\nabla^2\right]\psi(\boldsymbol{r}) + \frac{\nu}{3}(1-2f)\psi(\boldsymbol{r})^3 + \frac{u}{4}\psi(\boldsymbol{r})^4\right\}$$
$$+ \frac{c}{2}\int \mathrm{d}\boldsymbol{r}_1 \int \mathrm{d}\boldsymbol{r}_2\, G(\boldsymbol{r}_1 - \boldsymbol{r}_2)\psi(\boldsymbol{r}_1)\psi(\boldsymbol{r}_2) \tag{2.27}$$

where τ is related to the ordering temperature and the coefficients a, b, c, u and ν can be computed by evaluating the vertex functions calculated by Leibler (1980). The long-range interaction arises from the connectivity between blocks

and satisfies $\nabla^2 G(\boldsymbol{r}_1 - \boldsymbol{r}_2) = -\delta(\boldsymbol{r}_1 - \boldsymbol{r}_2)$. A large class of physical systems with competing short-range and long-range interactions can be described by eqns 2.26 and 2.27. Equation 2.26 is not limited to systems with conserved order parameters such as block copolymer melts. For block copolymers, it is applicable in the weak segregation limit because a single wavenumber dominates during structure formation in this regime.

The evolution of a system described by an equation related to eqn 2.26 was studied using cell dynamics simulations by Oono and co-workers (Bahiana and Oono 1990; Puri and Oono 1988). In the CDS method the continuous order parameter is discretized on a lattice and at time t is denoted $\psi(t,n)$, where n labels the lattice site. Kinetic equations for the time-evolution were obtained by Puri and Oono (1988). They are governed by underlying physical forces arising from the local driving force for phase separation due to the chemical potential and the diffusive effect due to the difference of the order parameter value in neighbouring cells. This method was first applied to block copolymer melts by Bahiana and Oono (1990), who investigated the development of microphase-separated structures for asymmetric and symmetric block copolymers in two dimensions, starting from an initially disordered configuration. A representative example of the structure obtained is shown in Fig. 2.46, for a symmetric system. It is evident that strongly segregated, but randomly oriented, lamellae have formed from an initially homogeneous configuration. The effects of boundary conditions and hydrodynamics in obtaining highly oriented lamellae were also studied by

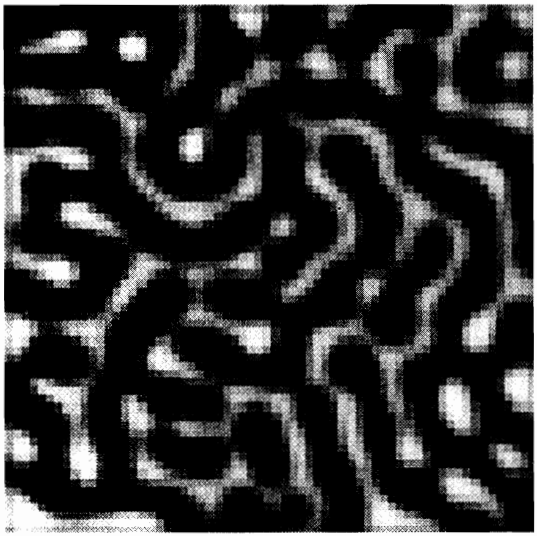

Fig. 2.46 Cell-dynamical simulation of a symmetric block copolymer in two dimensions (64×64 lattice) (Hamley 1997). This structure forms from an initially homogeneous state via time-dependent Ginzburg–Landau kinetics at a temperature below the ODT.

Bahiana and Oono (1990). Shiwa *et al.* (1996) have recently investigated the kinetics of structure factor development for microphase separation of two-dimensional lamellae. Qi and Wang (1996, 1997) have developed cell dynamics simulations of the TDGL equation to consider the evolution of structure following a temperature jump from one phase to another. They considered temperature jumps between all classical ordered phases, i.e. lam, hex and BCC and the disordered phase (Qi and Wang 1997). The TDGL equations were simulated in three dimensions using the CDS method, and additionally mode analyses were performed in the single-wavenumber approximation, which reduces the problem to a series of coupled equations describing the steepest descent of the order parameters on the free energy surface. Of particular note in relation to experiments was their observation that a quench from the lam to the hex phase can proceed via metastable perforated lamellar or transient modulated lamellar structures (see Fig. 2.47), depending on the topology of the free energy surface (Qi and Wang 1997). These results were compared to the experimental observations by Hamley *et al.* (1993, 1994) of such structures on heating from the lam to the hex phase in a series of asymmetric polyolefin diblock copolymers. For a T-jump from the hex to the BCC phase, a modulated hexagonal cylinder structure was found to exist as an intermediate before the BCC micelles 'pinched off' (Qi and Wang 1996) (see Fig. 2.14). These results were related to experiments on asymmetric PEP–PEE diblocks, where such a mechanism was proposed (Koppi *et al.* 1994), as discussed in Section 2.2.1. Analysis of the TDGL equation, including cell dynamics simulations, is one of the most promising approaches to the study of dynamics in block copolymer melts.

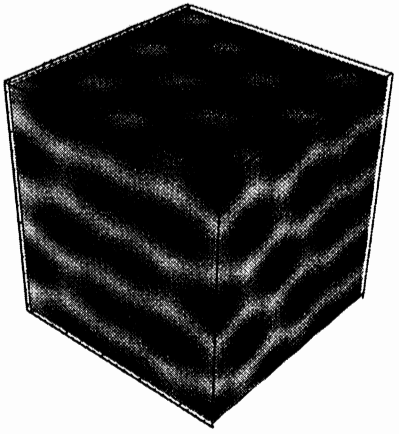

Fig. 2.47 Pseudostable perforated layer structure, observed following a quench from the lam to hex phase using a multimode analysis of the time-dependent Ginzburg–Landau equation, within the single-wavenumber approximation (Qi and Wang 1997). This structure results from the superposition of six BCC-type wavevectors.

2.4.2 Diffusion

Experiments

Self-diffusion of block copolymer chains has been investigated using a number of techniques including dynamic light scattering (DLS), forced Rayleigh scattering (FRS), field gradient nuclear magnetic resonance (NMR) and forward recoil spectroscopy (FRES). DLS has also been used to probe collective relaxation modes in block copolymers.

One of the most powerful methods for studying chain diffusion is FRS, and this has been applied to study diffusion in lamellar and disordered diblocks by Ehlich *et al.* 1993*a*,*b*) and Lodge and co-workers (Dalvi *et al.* 1993; Dalvi and Lodge 1993, 1994; Eastman and Lodge 1994; Lodge and Dalvi 1995). Dalvi *et al.* (1993) investigated the effect of entanglements on diffusion in unoriented samples by comparing the behaviour of two well-entangled PEP–PEE diblocks with that of two PS–PVP samples that were essentially unentangled. For the PS–PVP samples, the lower molecular weight (M) sample was in the disordered phase, and the higher M one was in the lam phase. Data for the diffusion coefficient, D, as a function of temperature for both samples were found to reduce to a single master curve, when the data for the lower molecular weight sample were scaled down using the Rouse scaling $D \sim M^{-1}$ (Fig. 2.48) (in the lamellar phase D corresponds to a combination of diffusivities parallel and perpendicular to the lamellar interface). This observation indicated that lamellar

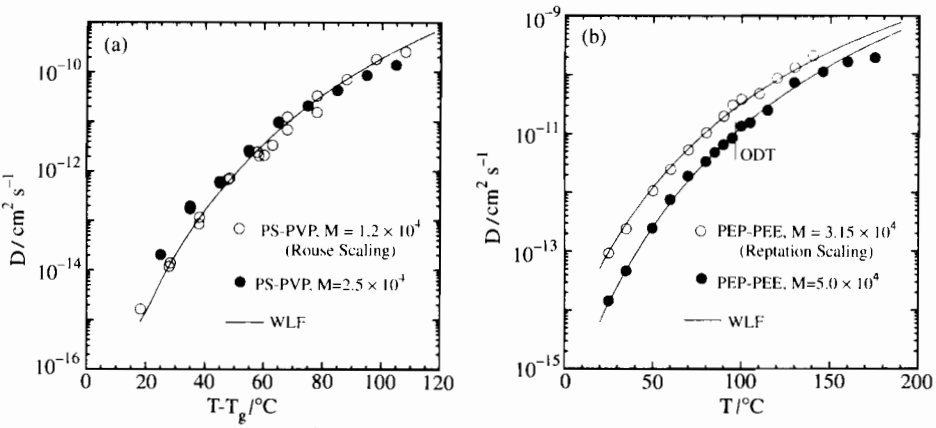

Fig. 2.48 Self-diffusion of nearly symmetric diblock copolymers measured using forced Rayleigh scattering (Dalvi *et al.* 1993). (a) Diffusivities, D, for the lower molecular weight PS–PVP sample, which is disordered at these temperatures, have been scaled down by a factor of 0.48, assumming Rouse dynamics; (b) D for the lower molecular weight symmetric PEP–PEE diblock copolymer have been scaled down by a factor of 0.40, assuming reptation dynamics. The solid line indicates a fit of the standard Williams–Landel–Ferry (WLF) temperature dependence to the data for the lower molecular weight sample. Values of M are in g mol^{-1}.

order had no effect on the measured chain diffusivity. Of the two PEP–PEE samples, the lower molecular weight one was disordered in the temperature range over which diffusivities were measured, whereas the higher molecular weight sample passed through an ODT. The temperature-dependent diffusivities for the lower molecular weight sample were reduced using the reptation scaling for entangled chains $D \sim M^{-2}$ and were found not to reduce onto the curve for the higher molecular weight sample (Fig. 2.48). The latter had a much lower mobility, both in the ordered phase and even at higher temperatures in the disordered phase. The difference between the two data sets was observed to increase as T decreased. Thus, it was concluded that reptating chains are significantly retarded. This was ascribed to the thermodynamic penalty for diffusion in the reptating tube, due to the localization of chains caused by the presence of interfaces in the lamellar structure. The fact that retardation was observed even above the ODT for the higher molecular weight PEP–PEE sample was ascribed to the effect of composition fluctuations, which persist well above the ODT in this system (Bates *et al.* 1990; Rosedale and Bates 1990). These composition fluctuations are apparently sufficient to retard the overall mobility of the individual chains (Dalvi *et al.* 1993). The fact that the FRS signals from unoriented lamellar samples of PS–PVP could be described by single exponential decays was interpreted by Eastman and Lodge (1994) as evidence that diffusion through the lamellae is not greatly retarded relative to diffusion in the lamellar planes and/or that the orientational correlation length of the lamellae is small. However, this is in conflict with the results of Fleischer *et al.* (1993) on PS–PI diblocks using field gradient NMR measurements, which showed a fast diffusion process ascribed to molecular motion along lamellae within a grain and a slower process resulting from 'crossing the enthalpic barrier' between PS and PI. It is worth pointing out here that part of this discrepancy may be because field gradient NMR and FRS probe structures at different length-scales. FRS depends on structural features in the 1–10 μm length-scale, whereas NMR probes dynamics on a length-scale about an order of magnitude smaller. The observation by Dalvi *et al.* (1993) that there are no significant changes in diffusivities across the ODT was, however, supported by Fleischer *et al.* (1993), who also noted that local order remains above the ODT, consistent with the presence of composition fluctuations.

The observation that D does not change across the ODT was first made by Shull *et al.* (1991) using FRES on a PEP–PEE diblock. A film of thickness 0.1 μm of partially deuterated polymer was spun cast onto a film (>2 μm) of the hydrogenous analogue. After annealing for different times, the deuterium depth profile of the diffused polymer was determined using FRES. Two diffusion coefficients were needed to model non-Fickian diffusion behaviour and these were tentatively associated with diffusion parallel and perpendicular to the lamellar planes. However, in a polycrystalline sample, Dalvi *et al.* (1993) showed using FRS that these diffusivities are not resolved. The observation of two diffusion processes in the annealed film studied using FRES was assumed to be associated with the preferential orientation of lamellar domains parallel to the film surface, whereas in the unannealed sample the average diffusion coefficient, $\langle D \rangle = \frac{1}{3}D_{\perp} + \frac{2}{3}D_{\parallel}$,

is measured (Shull *et al.* 1991), where the diffusivity perpendicular to the lamellar plane is denoted $D_\perp$ and $D_\parallel$ is the parallel diffusivity.

The effect of sample orientation on chain diffusion was also explored using FRS on a nearly symmetric PEP–PEE diblock by Dalvi and Lodge (1993). They prepared samples of the lamellar phase sheared in parallel or perpendicular orientations. The anisotropy in measured diffusivities was small but they were able to conclude that the inequalities $(D_\perp/D_\parallel)_{\text{Rouse}} \leq (D_\perp/D_\parallel)_{\text{measd}} \leq 1$ were valid. Here $D_\perp \leq D_\parallel$ because the PEP block must move through the PEE domain and vice versa. The diffusivities within the Rouse model were calculated using the theory of Barrat and Fredrickson (1991*b*) for weakly segregated symmetric diblocks. The observation of a lower anisotropy than predicted using the Rouse model was probably due to the fact that the PEP–PEE diblock was expected to be entangled, and therefore Rouse dynamics do not apply. Lodge and Dalvi (1995) probed self- and tracer-diffusion in a series of macroscopically oriented, well-entangled PEP–PEE diblocks. Diffusivities both parallel and perpendicular to the lamellar interface were measured. As pointed out by them, reptation of an AB block copolymer necessitates pulling of the A block into the B-rich domain and vice versa. There is thus a thermodynamic penalty for motion in any direction within the microstructure. For the parallel diffusivity, they found that data for PEP–PEE samples could be described as an activated process, with an exponential dependence $(D_\parallel/D_0) = \exp\{-0.237(\chi N - 7.6)\}$, where D_0 is the diffusivity in the disordered phase, having the reptation scaling $D_0 \sim N^{-2}$. The point where $\chi N = 7.6$ is an estimate of where monomer motion first becomes sufficient to impede diffusion; as noted by Fredrickson and Bates (1996) this may correspond to the crossover between weak- and intermediate-segregation regimes. Lodge and Dalvi (1995) also studied the tracer diffusion of two PEP–PEE diblocks in a higher molecular weight PEP–PEE matrix and the self-diffusion of the high molecular weight polymer. They found that in this case $D_\parallel/D_0$ was independent of temperature. The barrier to diffusion was thus entropic in origin and a possible interpretation of this is that slow arm retraction occurs at the lamellar interface. Tracer-diffusion measurements of $D_\perp$ were also made for these molecules, and were found to be described by an activated process with an exponential dependence on χN, as for the self-diffusion measurements of $D_\parallel$. Anisotropy of FRS intensity was observed for the lamellar phase of a PS–PI diblock oriented biaxially by hot pressing by Ehlich *et al.* (1993*b*). In a companion paper, Ehlich *et al.* (1993*a*) reported a double-exponential relaxation of FRS signals for a PS–PI diblock. The fast and slow processes were suggested to be due respectively to diffusion parallel to the lamellar interface and diffusion parallel to lamellar interfaces tilted with respect to the measuring direction (Ehlich *et al.* 1993*a*).

Dynamic light scattering has traditionally been applied to polymer solutions, and DLS results for block copolymer solutions are discussed in Chapters 3 and 4. A number of recent papers have described the application of the technique to disordered block copolymer melts (Anastasiadis *et al.* 1993*a*,*b*; Boudenne *et al.* 1996; Floudas *et al.* 1995; Fytas *et al.* 1993; Jian *et al.* 1994*a*; Stepanek and Lodge 1996; Vogt *et al.* 1994). Due to the limited range of dynamic time-scales that can

be accessed (10^{-6}–10^{3} s), only relatively fast relaxations in the disordered phase of low molecular weight samples have been investigated to date. Nevertheless, a multiplicity of relaxation modes has been found. The interpretation, or even reproducibility, of some of these observations is still controversial, and a comprehensive picture has not yet emerged. The following is thus a 'snapshot' of ongoing research.

The dynamic structure factor of block copolymer liquids (melts and solutions) has been accounted for using dynamical mean-field theory by Benmouna *et al.* (1987*a*,*b*). For a block copolymer melt, the dynamic structure factor can be written (Stepanek and Lodge 1996)

$$\frac{S(q,t)}{S(q,0)} = A_{\mathrm{I}} \exp(-\Gamma_{\mathrm{I}} t) + A_{\mathrm{H}} \exp(-\Gamma_{\mathrm{H}} t), \tag{2.28}$$

where the subscripts I and H denote the internal and heterogeneity mode respectively. The former arises from the relative motion of blocks and the latter from compositional variations for different chains. For $qR_{\mathrm{g}} << 1$, the decay rate Γ_{I} is independent of q and equal to τ_{I}^{-1}, where τ_{I} is the longest viscoelastic relaxation time of the chain. The heterogeneity mode has a decay rate $\Gamma_{\mathrm{H}} = q^2 D_{\mathrm{H}}$, where D_{H} is an effective diffusion coefficient (Jian *et al.* 1994*a*). Expressions for the amplitudes, A, of the two modes are given by Jian *et al.* (1994*b*, 1995).

An additional relaxation mode in block copolymer melts was first identified by Anastasiadis *et al.* (1993*b*). They performed DLS in the polarized (VV, V = vertical) geometry on a PS–poly(methyl phenyl siloxane) diblock and identified a slow diffusive mode, with a typical decay time of 1 s or longer, that modified the scattered intensity significantly as the temperature was decreased. This mode was termed the 'cluster' mode, in analogy to molecular and macromolecular glass-forming materials (Anastasiadis *et al.* 1993*b*). It has been attributed to long-range density correlations, and is unrelated to the fact that the chains are block copolymers (Stepanek and Lodge 1996). A correlation length, ξ, can be assigned to this slow diffusive process via the Stokes–Einstein equation (eqn 1.2)

$$\xi = kT/6\pi\eta D_{\mathrm{cl}}, \tag{2.29}$$

where η is the zero shear viscosity and D_{cl} is the 'cluster' diffusion coefficient. This yields a correlation length or hydrodynamic size ~1000 Å (Anastasiadis *et al.* 1993*a*,*b*; Stepanek and Lodge 1996). Figure 2.49 shows DLS evidence of cluster, heterogeneity and internal modes observed by Anastasiadis *et al.* (1993*a*).

In depolarized (VH, H = horizontal) light scattering, a mode arising from segmental reorientational dynamics has been observed for PS-containing copolymers (Hoffmann *et al.* 1993; Jian *et al.* 1994*a*; Papadakis *et al.* 1996*a*; Vogt *et al.* 1992), which have sufficient optical anisotropy and slow enough dynamics for this mode to be observed using DLS. A slower VH mode has also been reported for PS–PB and PS–PI diblocks (Hoffmann *et al.* 1993; Papadakis *et al.* 1996*a*), and attributed to chain stretching and orientation. A similar mode in disordered PS-poly(methyl phenyl siloxane) and PS–PI melts (with $\Gamma \sim q^0$) was ascribed to a coupling between orientational and compositional fluctuations, due to the growth of

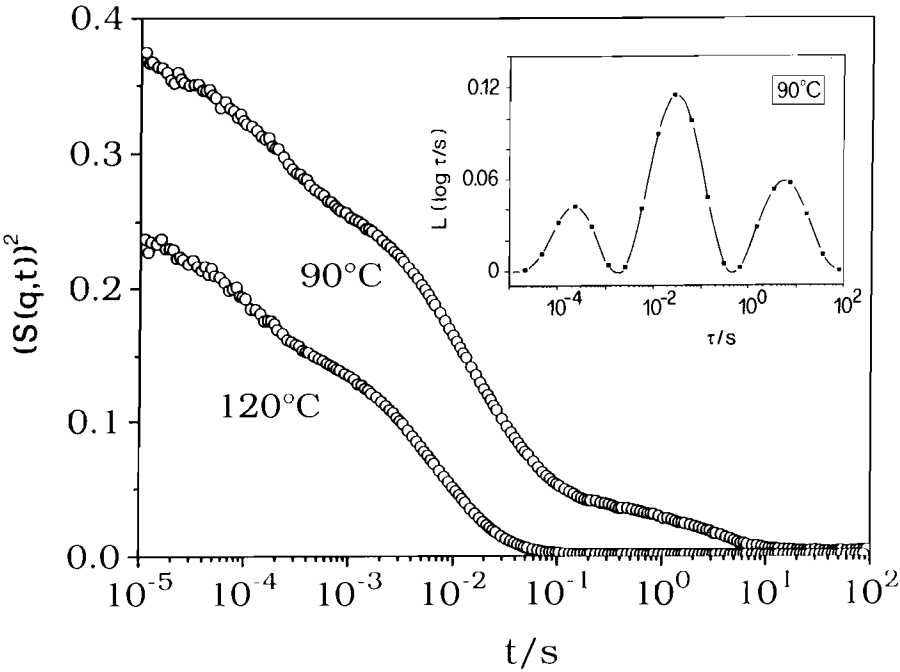

Fig. 2.49 Dynamic structure factor at two temperatures for a nearly symmetric PEP–PDMS diblock (N = 1110) determined using dynamic light scattering in the VV geometry at a fixed wavevector $q = 2.5 \times 10^5 \text{cm}^{-1}$ (Anastasiadis *et al.* 1993*a*). The inverse Laplace transform of the correlation function for the 90 °C data is shown in the inset. Three dynamic modes (cluster, heterogeneity and internal) are evident with increasing relaxation times.

large-amplitude composition fluctuations as the ODT is approached (Jian *et al.* 1994*a*). Papadakis *et al.* (1996*a*) reported a VV mode with Γ independent of q, which could be the same as the internal mode for PS–PB melts. However, they also found a VH mode with a similar Γ, and the internal mode is not VH active. Thus, they attributed both VV and VH modes to a combination of chain stretching and orientation, following the interpretation of Hoffmann *et al.* (1993) for the VH mode in PS–PI diblocks. Stepanek *et al.* (1997) suggest that all modes for block copolymer melts well above T_g can be accounted for as combinations of four VV modes and only one VH mode. It was suggested that other modes in the VH spectrum are due to the depolarizing nature of the block copolymer that leads to the detection of modes that are not actually depolarized (Stepanek *et al.* 1997).

The use of time-resolved depolarized light scattering to study the ordering kinetics of a PS–PI diblock melt was demonstrated by Floudas *et al.* (1995). By following the depolarized scattered intensity as a function of time following a quench from the disordered phase to the lamellar phase, they were able to estimate a size for lamellar grains. Adopting a model of grain relaxation via a rotational diffusion mechanism, they were able to obtain a grain size in agreement with that deter-

mined from the SAXS peak width, by assuming that grains rotate slowly in a medium with the effective viscosity of a liquid (Floudas *et al.* 1995).

Theory

Collective diffusion processes in block copolymers have been modelled using time-dependent Ginzburg–Landau theory. The equation of motion is of the form of eqn 2.26. This equation assumes that the Onsager coefficient (M) is frequency independent, which effectively restricts its application to dynamical processes that are slow compared with the internal modes of a block copolymer chain, i.e. slow compared to the Rouse or reptation time of a chain (Fredrickson and Bates 1996). This is not of concern in the vicinity of the ODT, where collective dynamics are critically slowed (Fredrickson 1986; Fredrickson and Larson 1987; Larson and Fredrickson 1987), but might be important in developing theories for more strongly segregated block copolymers. The free energy functional in eqn 2.26 is generally taken to be the Landau form for block copolymers (Leibler 1980). More sophisticated functionals have been proposed that attempt to account for the effect of critical composition fluctuations that become important close to the ODT (Fredrickson and Binder 1989).

A general formalism for deriving Langevin equations of the form (2.26) has been developed by Kawasaki and Sekimoto (1987, 1988), starting with a microscopic dynamical description of a copolymer melt. A simpler approach based on the dynamical random phase approximation (Kumaran and Fredrickson 1994) can be applied for ordered phases in the weak segregation limit or in the disordered phase. Explicit expressions for M that depend on microscopic kinetic coefficients (e.g. monomeric friction coefficients, copolymer composition and molecular weight) can be derived from both these approaches. These expressions are difficult to evaluate in the general case, although expressions for the Fourier transform of the Onsager coefficient in the disordered phase have been developed for reptating diblock chains (Kawasaki and Sekimoto 1989) and for unentangled diblock melts (Leibig and Fredrickson 1996). Unlike binary fluid mixtures or homopolymer melts, 'mode coupings' of momentum density fluctuations to composition fluctuations are very weak for block copolymer melts (Fredrickson and Helfand 1988; Onuki 1987).

Theory for the self- and tracer-diffusion of a diblock copolymer in a weakly ordered lamellar phase was developed by Fredrickson and Milner (1990). They modelled the interactions between the matrix chains and a labelled tracer molecule as a static, sinusoidal, chemical potential field and considered the Brownian dynamics of the tracer for small-amplitude fields. For a macroscopically-oriented lamellar phase, they were able to account for the anisotropy of the tracer diffusion observed experimentally. The diffusion parallel and perpendicular to the lamellae was found to be sensitive to the mechanism assumed for the Brownian dynamics of the tracer. If the tracer has sufficiently low molecular weight to be unentangled with the matrix, then its motion can be described by a Rouse model, with an added term representing the periodic potential (Fredrickson and Bates 1996) (see Fig. 2.50). In this case, motion parallel to the lamellae does not change the potential on the chains, and $D_{\|}$ is unaffected by

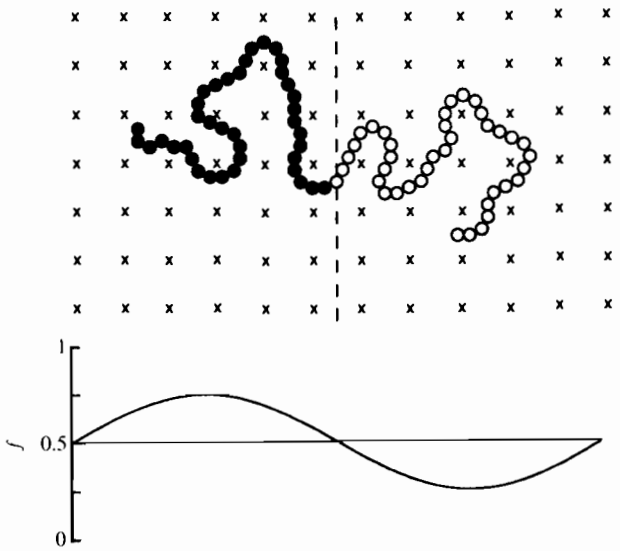

Fig. 2.50 An entangled diblock copolymer chain in a lamellar morphology with a sinusoidal composition profile (Lodge and Dalvi 1995). Entanglement constraints are indicated by x. Coupling between the thermodynamic forces produced by the composition gradients and reptation dynamics leads to an anisotropic diffusion coefficient.

the potential. Perpendicular diffusion is, however, hindered, and Fredrickson and Milner presented a perturbative calculation of $D_\perp$ for small potential amplitudes. These Rouse calculations for unentangled diblock tracers were extended by Barrat and Fredrickson (1991*b*) to arbitrary potential amplitudes and to include higher harmonics in the shape of the potential. They observed a strong suppresion of $D_\perp$ for large potential amplitude, consistent with an activated transport mechanism, $D_\perp \approx \exp(-F^\ddagger)$, $F^\ddagger \sim \chi N$, whereas $D_\perp$ was insensitive to the potential shape (square wave vs. cosine). Self-diffusion of diblock copolymers in the disordered phase near the ODT has been considered (Genz and Vilgis 1994; Leibig and Fredrickson 1996; Tang and Schweizer 1995). In this regime, the chemical potential field experienced by the tracer chain results from long-lived dynamic composition fluctuations. The fluctuation-induced reduction in the diffusion coefficient obtained theoretically is nevertheless small and consistent with experiment (Leibig and Fredrickson 1996; Tang and Schweizer 1995).

In strongly segregated block copolmers, other physical factors are important. Perpendicular diffusion is expected to be strongly suppressed due to the enthalpic penalty for incursion of a block into the nearly pure domain of the other component. This diffusion is thermally activated, i.e. $D_\perp \sim \exp(-F^\ddagger)$, and a number of postulates have been made for the transition state, resulting in different estimates for the free energy barrier $F^\ddagger$. Helfand (1992) has suggested a 'hyperstretched' state in which an A block traversing a B domain avoids exposing all fN of its monomers to the B environment. An alternative picture of the transition state is

a collapsed A coil in the B domain (Rubinstein and Obukhov 1993). The 'hyper-stretched' mechanism is expected to be favoured for large copolymers with a small block incompatibility. However, a universal SSL transition state may not exist due to differences in χ and segment length and volume for different polymers. Parallel diffusion in the SSL is also expected to obey an activated diffusion law, with an associated free energy that is predominantly entropic in origin (Fredrickson and Bates 1996). When excursions of A segments into the B phase are strongly suppressed by enthalpic interactions and the blocks are large enough to be entangled, parallel diffusion probably occurs through a transition state similar to that suggested for star polymer melts (Pearson and Helfand 1984; Rubinstein and Obukhov 1993). In this state, a block retracts along the primitive path from the junction point to its free end to release entanglements and permit motion of the centre-of-mass of the block in the plane parallel to the lamellae. Based on results for star polymers, where diffusion occurs in the absence of osmotic pressure gradients, a diffusion law, $D_{\parallel} \sim \exp(-F^{\ddagger})$, is anticipated, where $F^{\ddagger} \sim N/N_e$ where N_e is the entanglement degree of polymerization. Because the retraction in a block copolymer is done against a pressure gradient, an additional enthalpic contribution to the energy barrier exists, $F^{\ddagger} \sim N/N_e + (\chi N)^{2/3}$, where numerical prefactors are omitted. For large enough diblocks, the entropic term is expected to dominate the free energy barrier (Fredrickson and Bates 1996).

2.4.3 The effect of shear

Experiment

Shearing of block copolymers can influence the associated thermodynamic behaviour, as illustrated by the experiments of Koppi *et al.* (1993) on a PEP–PEE diblock. Large-amplitude reciprocating shear applied to a disordered sample at high shear rates $\dot{\gamma}$ was found to induce spontaneous ordering of perpendicular lamellae (Fig. 2.7(c)), whereas reduction of $\dot{\gamma}$ led to disorder. Similar results were obtained by heating and cooling the sample at fixed $\dot{\gamma}$. The upper branch of the data shown in Fig. 2.51 confirms that the ODT increases with shear rate, and that this increase is consistent with the theoretical prediction $T_{ODT} \sim \dot{\gamma}^2$ (note, however, there are insufficient data points in the plot by Koppi *et al.* (1993) to distinguish this from a linear dependence (Nakatani *et al.* 1996)). These results have been interpreted on the basis that if the shear rate is high enough compared to the fluctuation relaxation time, composition fluctuations parallel to the shear direction are suppressed and the system becomes more mean-field like (Koppi *et al.* 1993). The lower branch in Fig. 2.51 was interpreted as the limit of stability (spinodal) of the disordered phase (Koppi *et al.* 1993).

Experiments on asymmetric diblocks reveal similar behaviour. An initially disordered $f_{PEP} = 0.77$ PEP–PEE polymer forming a hex phase was observed to order on application of reciprocating shear (Almdal *et al.* 1996). The ODT was found to increase, with the same scaling as for lamellae, as anticipated by theory. The limit of stability of the disordered phase obtained by Almdal *et al.* (1996) was fitted with a functional form, $A/(B|\dot{\gamma}|^{-1/3} + 1)$, that is in agreement with the theory of Marques and Cates (1990) together with the assumption that

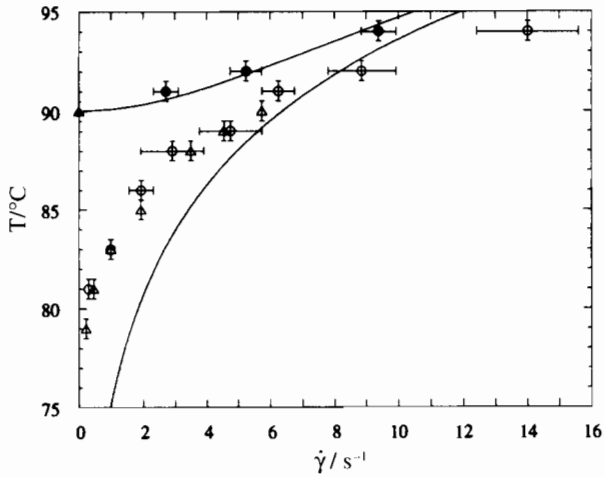

Fig. 2.51 Effect of reciprocating shear (strain amplitude, $\lambda = 200\%$) on the ODT of an $f_{PEP} = 0.55$ PEP–PEE diblock (Koppi *et al.* 1993). Here $\dot{\gamma}$ denotes the shear rate. The equilibrium order–disorder transition (●,▲) and disordered state stability limit (△,○) are shown. The upper curve is a fit to the scaling relation $T_{ODT} \sim \dot{\gamma}^2$. The lower curve represents the scaling $\tau_s(\Delta) \sim \Delta^{-1/3}\tau_{ODT}$, where $\Delta = \dot{\gamma}/\dot{\gamma}^*$, with $\dot{\gamma}^*$ an adjustable parameter. Points given by ● and ○ were obtained at fixed temperature by varying $\dot{\gamma}$, while those represented by ▲ and △ were determined by varying the temperature at fixed $\dot{\gamma}$.

$\chi = A/T + B$ (where A and B are constants); however, the parameters from the fit cannot straightforwardly be interpreted on a molecular basis (Almdal *et al.* 1996). A transition from shear-induced order to shear-induced disorder on increasing the shear rate has recently been reported in an asymmetric PS–PI diblock in concentrated solution (Balsara and Dai 1996). The low-shear rate ordering was consistent with the suppression of fluctuations, and the high-shear rate disordering was interpreted as arising from fluctuations of the ordered (cylindrical) microstructure (Balsara and Dai 1996).

For a quenched lamellar phase it has been observed that $G' \approx G''$ scales as $\omega^{1/2}$ for $\omega < \omega_c$, where ω_c is defined operationally as being approximately equal to $0.1\tau^{-1}$, and τ is a single-chain relaxation time defined as the frequency where G' and G'' cross (Bates *et al.* 1990; Rosedale and Bates 1990). This behaviour has been accounted for theoretically by Kawasaki and Onuki (1990). For a PEP–PEE diblock that was presheared to create two distinct orientations (see Fig. 2.7(c)), Koppi *et al.* (1992) observed a substantial difference in G' for quenched samples and parallel and perpendicular lamellae. In particular, $G'_\perp$ and the viscosity $\eta'_\perp$ for a perpendicular lamellar phase sheared in the plane of the lamellae were observed to exhibit near-terminal behaviour ($G' \sim \omega^2$, $\eta' \sim \omega^0$), which is consistent with the behaviour of an oriented lamellar phase which flows in two dimensions. These results highlight the fact that the linear viscoelastic behaviour of the lamellar phase is sensitive to the state of sample orientation.

Large-amplitude shear can be used to change the orientation of a structure in

a block copolymer melt. The first such observation was made by Koppi *et al.* (1992) who found that two orientations could be accessed in a PEP–PEE diblock subjected to $\lambda = 100\%$ dynamic shear (where λ is the strain amplitude) depending on the shear rate and temperature. A perpendicular orientation was obtained at high frequencies and high temperatures, the parallel orientation being obtained otherwise (Fig. 2.52(a)). The perpendicular orientation could be obtained by shearing a sample in the parallel orientation at a higher shear rate. However, the reverse process (perpendicular–parallel) was not observed. The high frequency behaviour near the ODT was interpreted as the result of shear-induced disordering, followed by reordering in the perpendicular orientation. The parallel orientation was believed to result from defect-mediated growth (Koppi *et al.* 1992).

The transverse orientation, where the lamellar normal is parallel to the shear direction, that is not found for low molecular weight diblocks was observed for

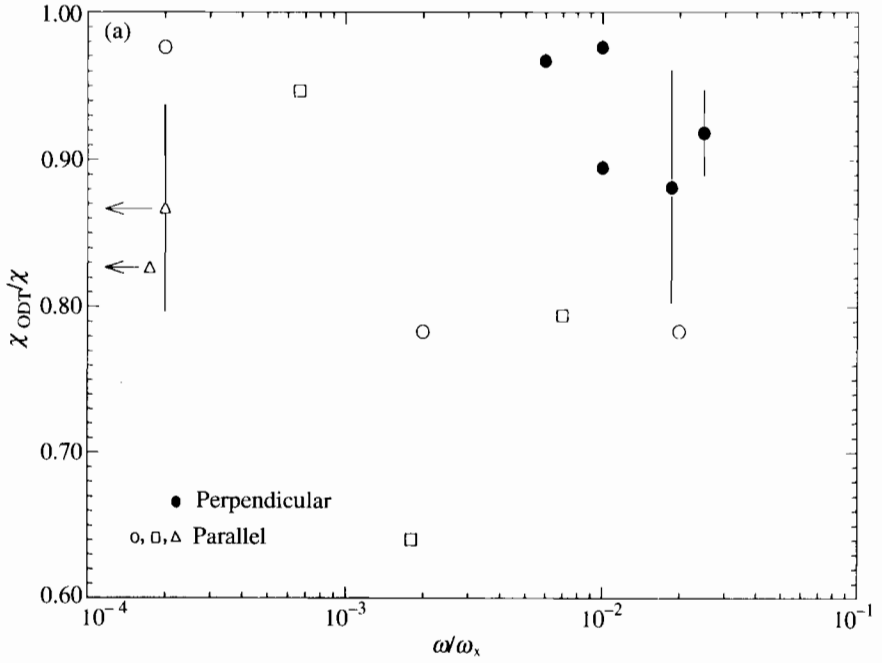

Fig. 2.52 (a) Lamellar orientation as a function of reduced frequency (ω_x is the frequency where G' and G'' cross) and reduced χ-parameter for polyolefin diblocks subjected to 100% strain amplitude dynamic shearing (Koppi *et al.* 1992). (b) Orientation diagram for PS–PI diblock copolymers under large-amplitude oscillatory shear in the vicinity of T_{ODT} (Maring and Wiesner 1997). Positions of transitions from parallel to perpendicular lamellae for a symmetric PS–PI diblock at 409 K are shown as filled symbols. The open symbol indicates an estimate of the flipping transition point from perpendicular lamellar to parallel at higher strain values observed by Gupta *et al.* (1996), mapped onto the region around ω_c.

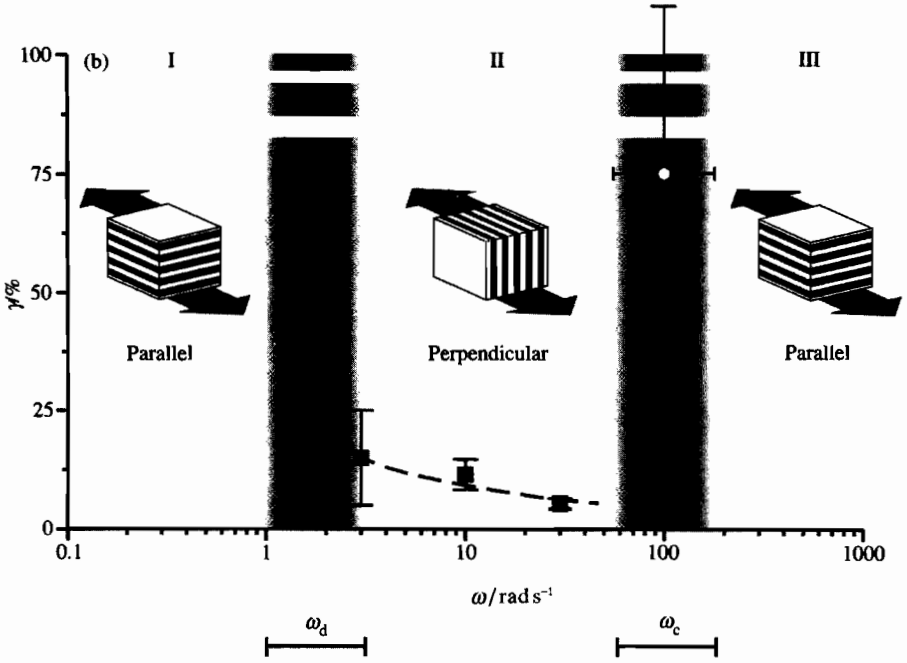

Fig. 2.52 *Continued.*

PS–PI samples of intermediate molecular weight by Zhang and Wiesner (1995). They deduced this orientation using SAXS on samples presheared at high frequency and interpreted it in terms of topological constraints due to entanglements of PI. This was also noted by Fredrickson and Bates (1996) who pointed out that the mechanical constrast of PS–PI (PS unentangled, PI entangled) is distinct from that for a mechanically balanced system such as PE–PEP. The proximity to the glass transition of PS to the ODT in PS–PI samples also means that the mechanical constrast in systems containing PS can be highly temperature sensitive. Patel *et al.* (1995) and Riise *et al.* (1995), studying PS–PI diblocks, observed the parallel orientation at high frequency and/or low temperature and the perpendicular orientation at low frequency and/or low temperature. Maring and Wiesner (1997) provide a unified picture for low-molecular-weight PS–PI polymers, with changes in lamellar orientation as a function of reduced frequency (Fig. 2.52(b)). At high frequencies, they suggest that the observed parallel orientation arises from mechanical contrast between PS and PI blocks. At intermediate frequencies, lamellar interface destruction and reorganization occurs leading to a perpendicular orientation whilst at low frequencies the interface reorients as a whole leading to a parallel orientation again (Zhang *et al.* 1995).

The evolution of microstructural orientation in block copolymers was studied in real time by Kornfield and co-workers using birefringence measurements on diblocks sheared *in situ* (Gupta *et al.* 1995; Kannan and Kornfield 1994). The birefringence of the polymer in two orthogonal planes was measured using laser light

incident along the vorticity direction or velocity gradient direction in a planar shear geometry, and this could be directly correlated to changes in the dynamic mechanical properties. There are two contributions to the birefringence of an ordered block copolymer. The intrinsic birefringence is due to the tendency of chains to segregate away from microdomain interfaces. The form birefringence results from the anisotropy of the microphase-separated structure. Both contributions are coaxial under weak flow conditions so that the principal axes of the refractive index tensor correspond to those of the ordered structure (e.g. the lamellar normal). The birefringence observed in PEP–PEE is primarily intrinsic, whereas PS–PI possesses predominantly form birefringence (Fredrickson and Bates 1996). For the PEP–PEE diblock studied by Koppi *et al.* (1992), Kornfield and co-workers observed that the flow process leading to the parallel alignment was associated with inhomogeneous deformation, such that ordered domains in the polymer were rocked irreversibly into the aligned structure. In contrast, the process that produces perpendicular orientation occurs under conditions in which the deformation was nearly homogeneous (Kannan and Kornfield 1994). More recently, the evolution of orientation in a nearly symmetric PS–PI diblock was studied using the same technique (Gupta *et al.* 1995). It was found that at high frequencies a parallel alignment was obtained, whereas at lower frequencies the perpendicular orientation resulted, in contrast to the results of Koppi *et al.* (1992) on the PEP–PEE diblock, In either case, the alignment process was observed to proceed via an initial fast process, followed by a slow one ($\approx$1 h) (Gupta *et al.* 1995). The fast process was dominated by depletion of lamellae in the transverse ('forbidden') orientation when forming the ultimate perpendicular orientation and depletion of perpendicular lamellae when developing the ultimate parallel lamellar structure. In both cases, enhancement of the orientation distribution towards the ultimate alignment was noted. The resulting biaxial distributions were transformed into a uniaxial one during the slow process. During the slow process, the visoelastic properties were not observed to change significantly (Gupta *et al.* 1995). A biaxial lamellar structure was observed using SAXS on a sheared PS–PEP diblock by Okamoto *et al.* (1994*b*), and in a PS–PI diblock by Zhang and Wiesner (1995). Polis and Winey (1996) used TEM to investigate a biaxial morphology in a sheared PS–PEP sample, where kink bands were observed between parallel and transverse lamellae. The formation of kink bands suggested that the transverse lamellae could be the result of buckling of perpendicular lamellae. Relaxation of the kink band structure during quiescent annealing occurred through lamellar tilting rather than twisting, leading to a variety of defect structures (Polis and Winey 1996).

Theory

Theory for block copolymer rheology is still in its infancy. There are no models that can predict the rheological behaviour of a block copolymer from microscopic parameters. Fredrickson and Helfand (1988) considered fluctuation effects on the low frequency linear viscoelastic properties of block copolymers in the disordered melt near the ODT. They found that long-wavelength transverse momentum fluctuations couple only to compositional order parameter fluctua-

tions, which are predominantly on the scale of the radius of gyration. Crossover expressions were obtained for the renormalized transport and viscosity coefficients.

Kawasaki and Onuki (1990) developed a theory applicable to quenched lamellar phases of block copolymers using a local constitutive equation to derive a formal expression for the ensemble-averaged frequency dependent viscosity. They obtained $G' \approx G'' \sim (B\eta\omega)^{1/2}$, where η is an average local viscosity and B is the compressional elastic modulus. As noted by Fredrickson and Bates (1996), this scaling cannot persist to arbitrarily low frequencies due to the Kramers–Kronig relationship. However, the scaling is in agreement with the experiments of Bates *et al.* (1990) and Rosedale and Bates (1990) (see Fig. 2.4(b)). Rubinstein and Obukhov (1993) considered stress relaxation in a strongly segregated lamellar phase, using a model of copolymer brushes. Well-entangled polymers were considered, and the number of entanglements of a particular chain with an opposite brush was found to vary from chain to chain even in a monodisperse system. This dispersion of the number of entanglement leads to a power-law-like stress relaxation function $\log G \approx (\log t)^{\alpha}$ with $\alpha = \frac{1}{2}$ in the strong segregation limit. Oriented diblocks with block lengths below the entanglement threshold are expected to show conventional Rouse-like rheological behaviour. The experimental observation that Rouse-like behaviour is not observed in low molecular weight (unentangled) PS–PI diblocks is consistent with the presence of defects. Rubinstein and Obukhov (1993) also considered stress relaxation in quenched (randomly oriented) lam and hex phases. They argued that for strongly segregated samples, the relaxation of stress is controlled by processes of equilibration of excess chain density along the layers. Localized regions of lower or higher than the average areal chain density must annihilate each other by diffusion along the lamellar interface, facilitated by retraction of copolymer chains. This mechanism leads to the scaling $G(t) \approx t^{-1/2}$ for quenched lamellae and $G(t) \approx t^{-1/4}$ for quenched cylinders. Fredrickson and Bates (1996) suggest that, except for extremely high molecular weight polymers, stress relaxation for quenched lamellae is dominated by the mechanism proposed by Kawasaki and Onuki (1990), rather than the Rubinstein–Obukhov mechanism. This is supported by the observation that experiments on quenched smectic liquid crystals, unentangled block copolymers and entangled block copolymers all show the same linear visocelasticity, despite the obvious molecular-scale differences. To date, the linear visocelastic properties of other ordered phases in block copolymers have not been considered. However, Kawasaki and Ohta (1986) have derived microscopic expressions for the static elastic constants of the hexagonal and BCC phases in mean field theory. Amundson and Helfand (1993) and Wang (1994) derived expressions for the static elastic constants of the lam phase in weak segregation theory, allowing for composition fluctuations and an analogous calculation was carried out for the hex phase by Hamley (1994). For both phases, a buckling instability is predicted to set in above a critical extensional strain. Wang (1994) also analysed the free energy of deformed lamellae in the strong segregation limit and obtained expressions for the elastic constants and calculated stress–strain curves.

Fredrickson (1994) was able to account qualitatively for the effect of shear on

the ODT for the PEP–PEE diblock studied by Koppi *et al.* (1992) by developing the theory due to Cates and Milner (1989) to the case of the dis–lam transition in diblock melts under shear. Fredrickson (1986) and Onuki (1987) had showed earlier that steady flows suppress composition fluctuations in disordered block copolymers and lead to an anisotropic fluctuation spectrum. They employed the Langevin equation (2.26), with an additional convective term. This equation was then used by Cates and Milner (1989) who investigated the effect of steady shear on the disorder–order transition. In a later paper by Fredrickson (1994), mechanical contrast between blocks was allowed for and an energetic coupling between composition fluctuations and the preferred lamellar normal in the ordered phase was introduced. Perpendicular lamellae were predicted to be stable at the ODT under strong shear conditions, while lowering the temperature (and thereby increasing the degree of segregation and frictional difference between A and B components) led to a transition to parallel lamellae. In the parallel alignment, the less viscous layers permit sliding more readily, which favours this orientation. At low shear rates, the parallel orientation is stable even at the ODT because composition fluctuations with wavevectors directed near the average lamellar normal are preferred (Fredrickson 1994). The frictional contrast between blocks preserves this orientation on lowering the temperature under weak shear. These results can be compared to the experiments of Wiesner and coworkers (see Fig. 2.52(b)). However, because this theory assumes slow flow in modelling the fluid mechanics and collective diffusion, it cannot describe shear orientation at high frequencies in the plateau region. Thus, it does not predict the transition from perpendicular to parallel lamellae at high frequencies in PS–PI diblocks observed by Zhang *et al.* (1995) and Patel *et al.* (1995).

Computer simulation

Sophisticated simulation methods have been used to investigated the effect of shear on the hexagonal phase in block copolymers. A two-dimensional cell-dynamical simulation of oscillatory shear flow was performed by Ohta *et al.* (1993). They found two relaxation processes under shear flow. A fast shape relaxation occurred within each domain, and on longer time-scales a lattice relaxation via slippage of lattice planes was observed. This is evident in Fig. 2.53, which shows structure within the simulation box during relaxation following step shear. The shape relaxation occurs for any applied strain, whereas the latter only takes place when the applied strain is large. A third relaxation mechanism due to chain entanglement is not included in this model as the associated time-scale is much shorter than those for the domain relaxations studied in the simulation. The slippage of lattice planes leads to a double stress relaxation in the case of step–strain deformations or Lissajous patterns in the stress–strain relationship in the case of oscillatory shear strains of sufficient amplitude. It was noted (Ohta *et al.* 1993) that lattice slippage in block copolymers occurs via lattice planes moving in concert, a distinct mechanism from the creation and propagation of defects which leads to plasticity in metals. An unrealistic aspect of the simulations is that the coupled fluid mechanics–elasticity problem is neglected by assuming a uniform shear rate. In other words, non-affine deformation behaviour results

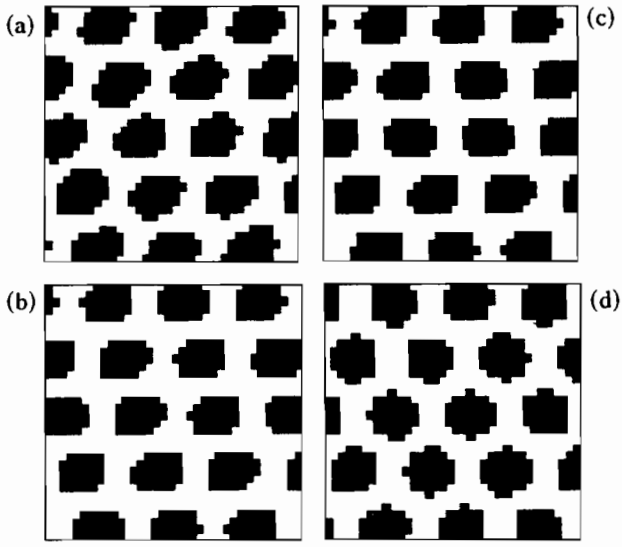

Fig. 2.53 Computer simulation results, using time-dependent Ginzburg–Landau dynamics, of a lattice model of an asymmetric copolymer forming a hex phase subject to a step-shear along the horizontal axis (Ohta *et al.* 1993). The evolution of the domain pattern after the application of the step-shear is shown. (a) $t = 1$ (the pattern immediately after the shear is applied); (b) $t = 5000$; (c) $t = 10000$; (d) $t = 15000$. The time-scale corresponds to the characteristic time for motion of an individual chain, $t = R_g^2/M$.

from interfacial stresses and differing viscoelastic properties of A and B domains (Fredrickson and Bates 1996). In a companion paper, Doi *et al.* (1993) employed a statistical theory for the rheology of the hex phase using a coupled multilayer model. This theory was able to reproduce the behaviour found in the computer simulations. In particular, non-linear rheological responses associated with the slippage of lattice planes and viscoplastic flow behaviour with a true yield stress were reproduced.

2.5 Structure of thin films of block copolymers

2.5.1 Lamellar phase

Films confined at one surface

The morphology of thin films of block copolymers forming a lamellar phase has been primarily studied using neutron reflectivity, atomic force microscopy (AFM) and phase interference microscopy. The former provides the scattering length density profile normal to the surface to a resolution of 1 Å, whereas AFM is a powerful technique for determining morphology and topology at the surface also to near-atomic resolution. Interference microscopy provides a picture of variations in sample thickness to sub-micron resolution. Due to the weak electron density contrast between blocks in many copolymeric materials, X-ray reflectivity

has yet to be widely applied to study structure in thin films. The neutron and X-ray reflectivity methods are currently being extended so that off-specular reflectivity can be performed, which should yield a wealth of information on the in-plane structure of block copolymer films. An excellent review of the application of X-ray scattering (specular reflectivity and grazing incidence diffraction) techniques to the study of polymer interfaces is provided by Foster (1993).

Thin films of PS–PMMA diblocks forming a lamellar phase were extensively studied by Russell and co-workers using neutron reflectivity. Early results following the application of the technique to symmetric block copolymers were reviewed by Russell (1990). These studies showed that layers form parallel to the silicon substrate, and the PMMA is always preferentially located at the substrate interface, whereas PS segregates to the air interface due to its lower surface energy. A representative reflectivity profile for a symmetric PS–*d*PMMA (the prefix *d* denotes a deuterated block) diblock is shown in Fig. 2.54, together with a scattering length density profile that produces the reflectivity curve shown as a line. Preferential block segregation necessarily leads to a film thickness quantized as $(n + \frac{1}{2})d$, where d is the lamellar period and n is an integer (Coulon *et al.* 1989, 1990; Russell *et al.* 1989). If the initial thickness differs from these quantized values, then islands form at the surface. For example, if the initial film thickness is $(n + 1)d$, then upon annealing islands form on the surface with a height

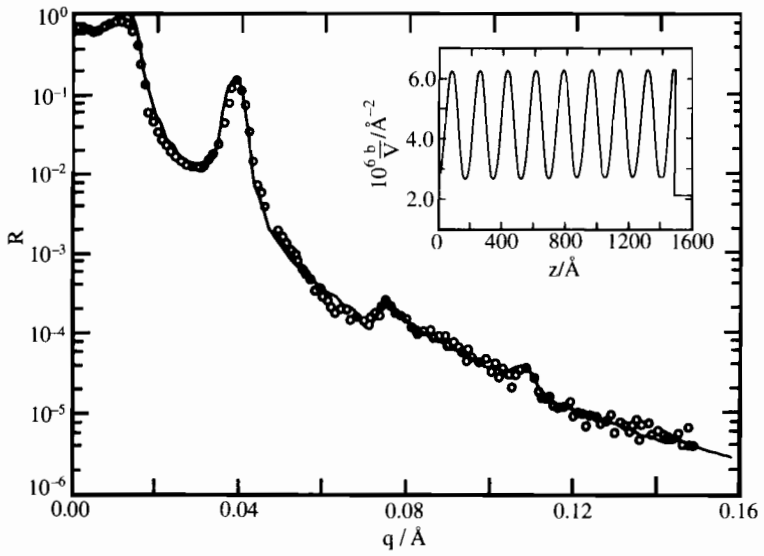

Fig. 2.54 Neutron reflectivity profile for a symmetric PS–*d*PMMA diblock (M_w = 30 kg mol^{-1}) as a function of incident wavevector (Russell 1990). The inset shows the scattering length density (b/V, the neutron scattering length per unit volume) profile normal to the film surface that was used to calculate the reflectivity profile shown as the solid line. This is typical of a block copolymer film containing a multilayer stack, with lamellae parallel to the surface.

$(n + \frac{3}{2})d$ with respect to the substrate. With time, the islands coalesce, minimizing the surface area of the specimen. The presence of these islands can be observed directly using phase interference microscopy and is also manifested in X-ray reflectivity profiles. An AFM image of islands at the surface of a film of a poly(styrene)–poly(butyl methacrylate) diblock is shown in Fig. 2.55. In general,

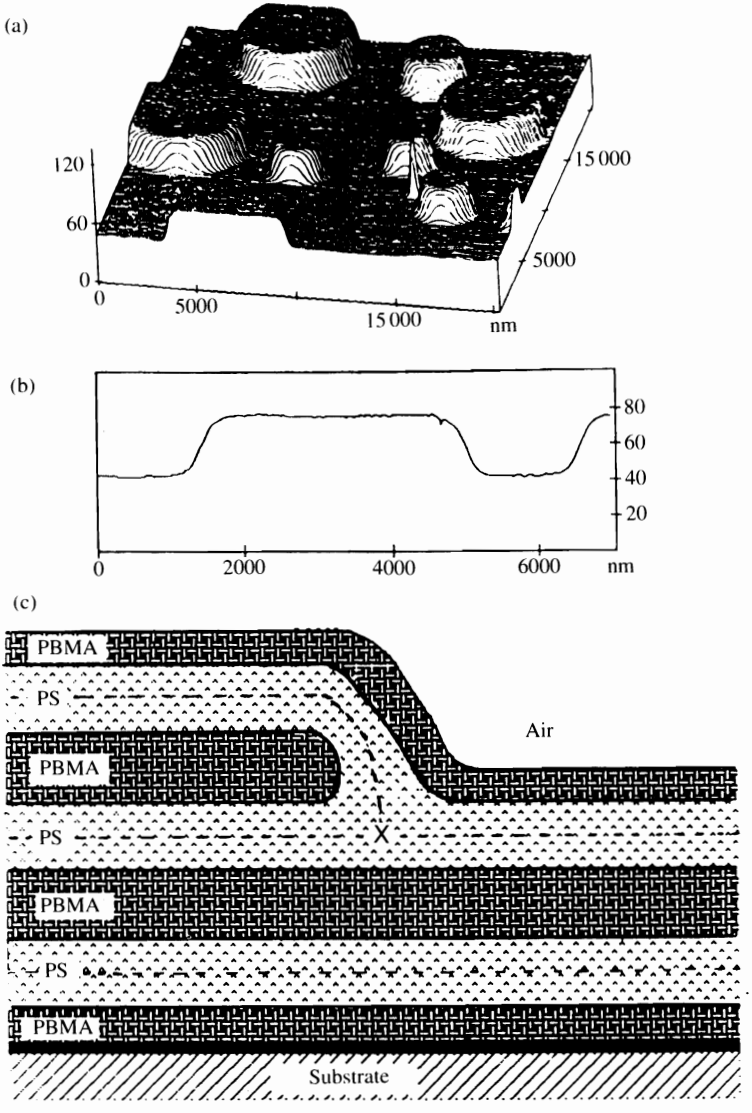

Fig. 2.55 (a) Atomic force microscopy image (constant force mode) of islands at the surface of a PS–PBMA diblock (M = 82 kg mol^{-1}) copolymer film (Maaloum *et al.* 1992). The height of the islands is 310 Å. (b) Section of one domain with a diameter of 4 μm. (c) Assumed structure at the domain edge.

the electron density difference between the component blocks of a block copolymer is smaller than the respective electron density differences with respect to air or the substrate. Therefore, the X-ray reflectivity profile is dominated by the air–polymer and polymer–air interfaces. In the case of island formation, discrete sample thicknesses lead to a beating of the interference fringes in the X-ray reflectivity profile, where the beat period results from the island height (generally d) and the high frequency Kiessig fringes are reciprocally related to the film thickness. An example of an X-ray reflectivity profile from a P2VP–PS–P2VP triblock copolymer film is shown in Fig. 2.56 (de Jeu *et al.* 1993). The beating results from coexisting film thicknesses of 1935 and 2229 Å. The difference is equal to the lamellar period, determined independently from neutron reflectivity. The observation of beating in the reflectivity profile requires the lateral size of the islands to be larger than the coherence length of the X-rays (Russell 1990). Islanding in a symmetric PS–PMMA diblock was studied using optical microscopy and X-ray reflectivity by Coulon *et al.* (1993). They reported that a film of thickness $d/2$ forms a stable monolayer, whereas films of thickness $d/2 < t < d$ were found to be unstable, forming either a stretched monolayer or islands.

X-ray reflectivity, AFM and optical microscopy have been used to probe lateral structure in a thin film of a symmetric PS–PMMA diblock that formed islands at the surface (Cai *et al.* 1993). The step height obtained from beating of fringes in the X-ray reflectivity profile was found to be in good agreement with a direct

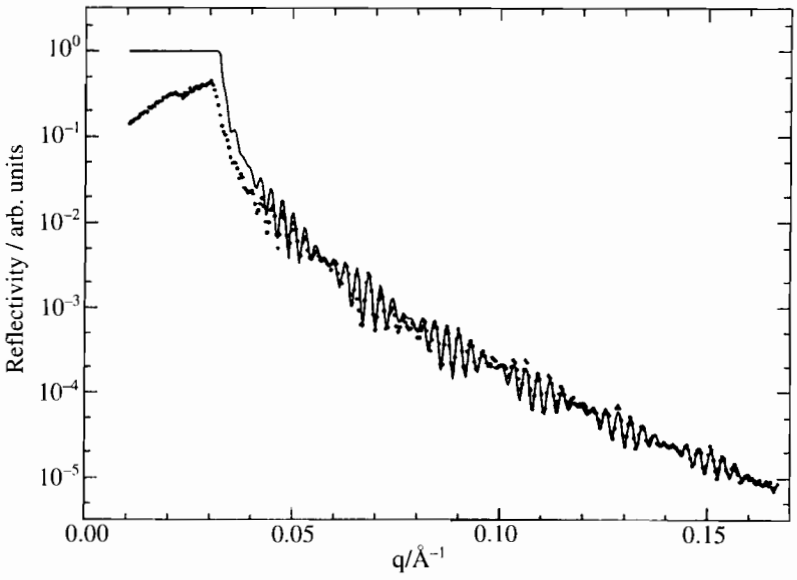

Fig. 2.56 Beating of Kiessig fringes observed using X-ray reflectivity from a PVP–PS–PVP triblock copolymer film ($f_{PS} = 0.48$, $M_w = 120\,kg\,mol^{-1}$) with two discrete thicknesses of 1935 and 2229 Å (de Jeu *et al.* 1993). The difference in height results from island and hole formation at the free surface, and is equal to the bulk domain spacing.

measurement from AFM. In addition, the lateral size of the islands was determined using the various techniques and compared. In the X-ray reflectivity experiment, transverse rocking scans were performed (where the angle θ of reflection in the specular plane is scanned). For films which are islanded, this leads to off-specular peaks. The periods associated with these peaks (5 and 11 μm) were found to be in agreement with peaks in the real space domain–domain correlation function from AFM, which measures the average separation between islands (Cai *et al.* 1993). X-ray speckle patterns resulting from coherent scattering at grazing incidence resulting from islands with length-scales up to 100 μm were observed by Cai *et al.* (1994). The speckle pattern results from interference between waves which undergo optical path differences or phase shifts after being scattered by different parts of the sample. The utility of phase interference (or Nomarski) microscopy for the determination of step heights in block copolymers was demonstrated for PS–PMMA diblock copolymers (PS has a refractive index $n = 1.6$, and for PMMA $n = 1.5$) by Coulon *et al.* (1990). A representative micrograph for a nearly symmetric *d*PS–PMMA diblock is shown in Fig. 2.57. Different colours result from different optical paths (as in Newton's rings, familiar from optics), which can be interpreted in terms of integral lamellar steps.

The formation of islands at the surface of lamellar block copolymer films has been studied in some detail using AFM by Coulon and co-workers (Ausserré *et al.* 1993; Coulon *et al.* 1993; Maaloum *et al.* 1992). The edge profile was investi-

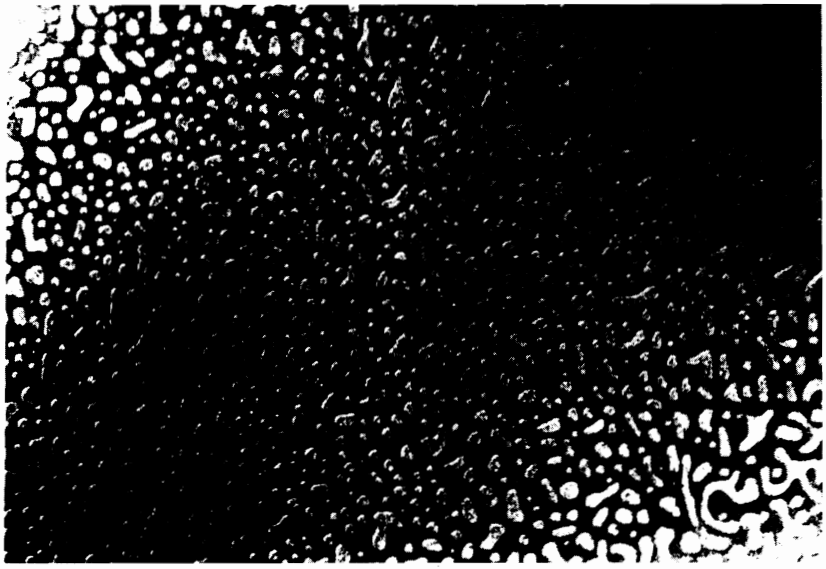

Fig. 2.57 Phase interference micrograph of a nearly symmetric *d*PS–PMMA diblock, initially 860 Å thick, after annealing at 170 °C, showing surface domains resulting from the formation of islands (Coulon *et al.* 1990). The step height, determined from the optical path for successive interference colours is 390 Å and the long dimension of the micrograph is 140 μm.

gated in detail, and its shape accounted for using continuum mechanics for the free surface of a smectic liquid crystal above an edge dislocation (Maaloum *et al.* 1992), indicated by x in Fig. 2.55. However, the profile width was found to be much larger than the theoretical estimate, which was ascribed to the effect of polymer/air surface tension. The kinetics of growth of islands were investigated using a model for the polymeric flow by Ausserré *et al.* (1990). The flows involved in the domain growth were shown to be confined to a bilayer which is disrupted at dislocation lines. The growth of islands was found to be thermally activated, whereas holes were found to shrink, with the radius decaying as the $\frac{1}{3}$ power of time (Ausserré *et al.* 1990). The growth of islands in a PS–PMMA diblock was suggested on the basis of AFM experiments to follow a process resembling two-dimensional spinodal decomposition (the process was effectively two-dimensional because the film thickness was much less than the lateral extent of the domains, $\approx 1\,\mu$m) (Maaloum *et al.* 1993). A film of initial thickness $t = 2d$ was found to decompose ultimately into a film of coexisting domains of $3d/2$ and $5d/2$. However, at intermediate times a metastable state of thickness $2d$ was observed that demixed into the two stable thicknesses. Terracing of block copolymer droplets has been observed using AFM (Ausserré *et al.* 1993; Carvalho and Thomas 1994) (see Fig. 2.58). Carvalho and Thomas (1994) observed terraces at the edge of droplets of a PS–PMMA diblock. The step height corresponded to

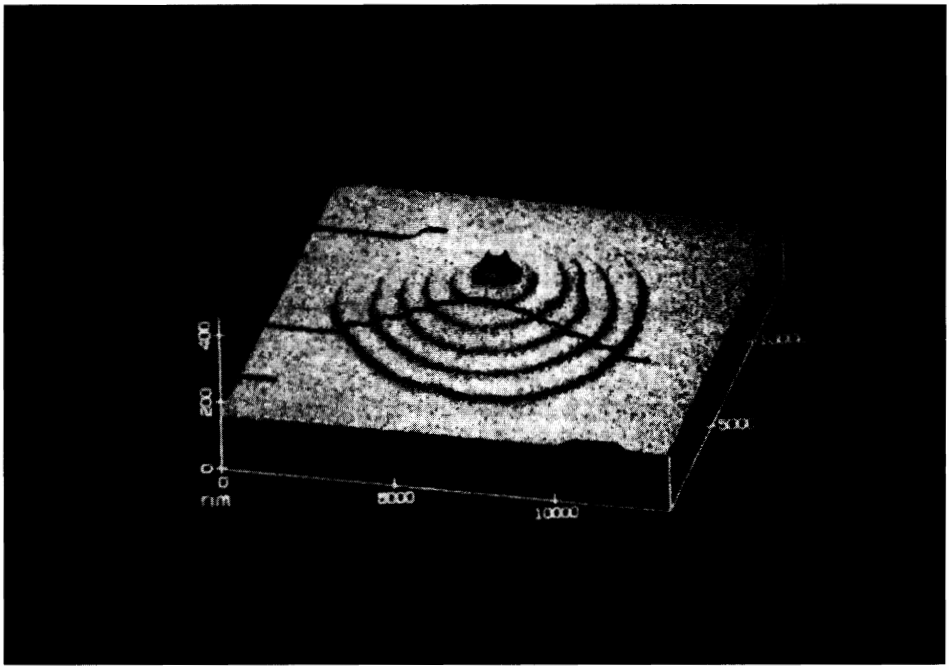

Fig. 2.58 Terracing in a thin film of a symmetric PS–PMMA diblock observed using atomic force microscopy ($M = 57\,\text{kg mol}^{-1}$) (Ausserré *et al.* 1993).

either a copolymer monolayer or bilayer. TEM on a section of terraced droplet revealed that the lamellae were homogeneously oriented in the steps, perpendicular to the step edge, whereas the usual parallel orientation was observed in the terraces. This orientation was also found at the holes of depressions at the surface of a film.

The surface of bulk block copolymer samples has been studied using TEM by Turturro *et al.* (1995). They report that non-equilibrium structures with lamellar and cylindrical microdomains oriented normal to the free surface can result from solvent casting, with a high evaporation rate. However, slower evaporation of solvent from their PS–PB diblocks resulted in the equilibrium conformation with domains parallel to the free surface. Perpendicular orientation of PS–PB lamellae at the free surface was observed earlier by Henkee *et al.* (1988) who studied thin films prepared by solvent casting. They observed that a reduction of this orientation occurs in favour of the parallel one on annealing the sample.

To give an idea of a typical interfacial thickness, for a series of PS–PMMA diblocks studied by Anastasiadis *et al.* (1990), the interfacial width between PS and PMMA domains was determined to be 50 ± 3 Å, independent of the copolymer molecular weight (M_w ranging from 30 to 300 kg mol^{-1}). This width was found to be identical to that for a *d*PMMA/PS homopolymer bilayer studied by Fernandez *et al.* (1988). In the latter work, a layer of *d*PMMA was deposited on PS and for both as-cast and annealed specimens an interfacial width of 50 Å (expressed as the width of a hyperbolic tangent function, which is the theoretical profile for strongly segregated block copolymers (Helfand and Wasserman 1976) and homopolymers (Helfand and Sapse 1975; Helfand and Tagami 1972)) was found using neutron reflectivity.

Surface-induced ordering

The contraints imposed by the finite film thickness lead to a number of other effects that have been elucidated using neutron reflectivity. Russell and co-workers (Anastasiadis *et al.* 1989; Menelle *et al.* 1992) reported that surface fields (propagating from both air and substrate interfaces) induce lamellar ordering at the surface, even when the bulk copolymer is above its order–disorder transition (see Fig. 2.59). The scattering length density profiles in this situation were modelled using an exponentially damped sinusoidal function, a form anticipated by Fredrickson (1987). Because induced lamellar order exists even in the disordered phase, it was found to be impossible to define an order–disorder transition in thin lamellar films, only a transition from partially ordered to fully ordered which occurs on lowering the temperature (Menelle *et al.* 1992). This effect was found to become less significant as the film thickness increased, as anticipated as the bulk phase behaviour becomes dominant. An increase in lamellar order in the centre of thin films of PEP–PEE diblocks of different M_w was observed by Foster *et al.* (1992) at a fixed temperature and approximately constant film thickness by increasing the degree of polymerization, N. For a particular PEP–PEE diblock, the same authors reported that q^* in a thin film was lower than the bulk value, the reduction becoming greater above the bulk ODT. This was rationalized using arguments similar to those of Russell and co-workers, i.e. layer melting in the

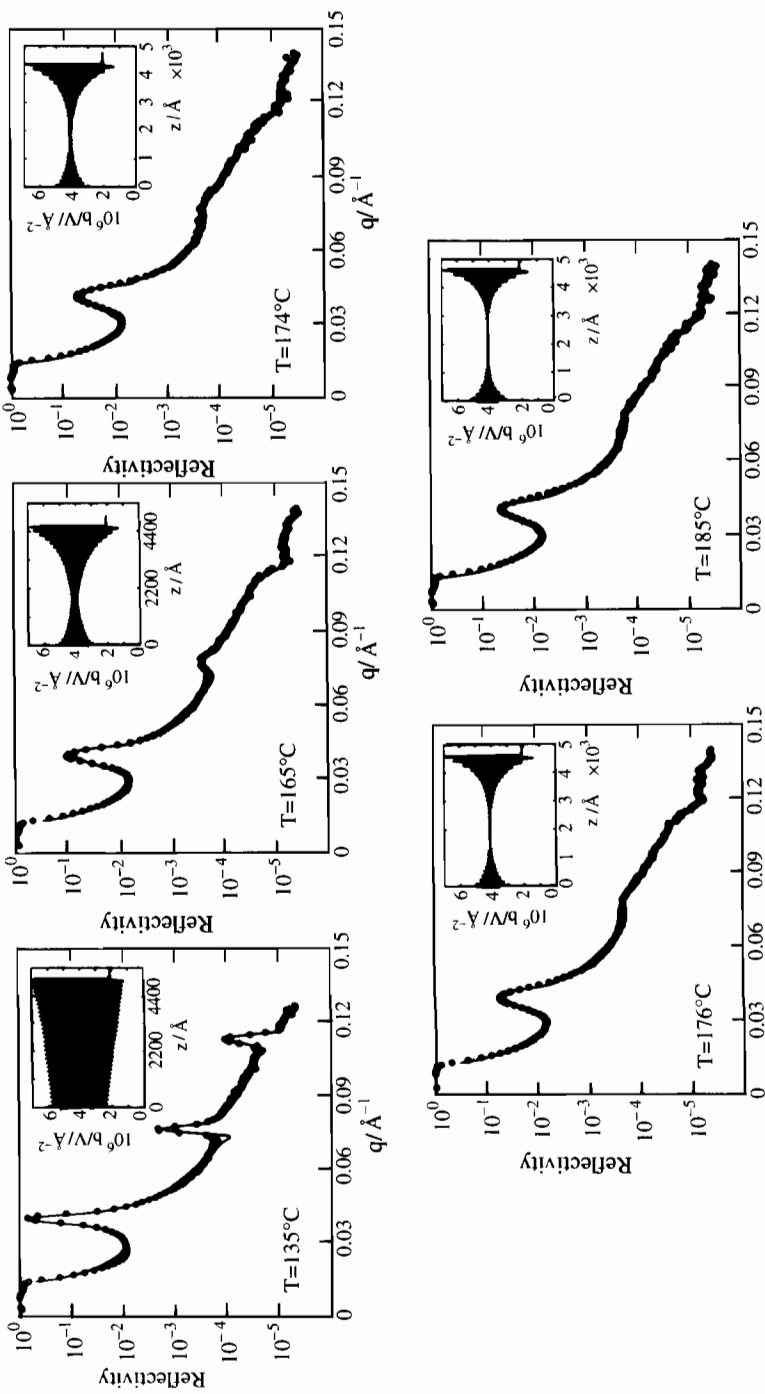

Fig. 2.59 Neutron reflectivity profiles for a PS–*d*PMMA symmetric diblock copolymer ($M_w = 29.7\,\mathrm{kg\,mol^{-1}}$) film of total thickness 5232 Å (Menelle *et al.* 1992). Experiments were performed on samples annealed at the temperatures shown. The solid lines were computed using the scattering length density profiles shown in the insets, which show that the surface induces lamellar order even above the bulk ODT 157 ± 8 °C (the air–polymer interface is located at $z = 0$).

centre of the film, with lamellar ordering retained at the air–polymer and polymer–substrate interfaces. However, the scaling of q^* with N was found to be similar to that of bulk ordered samples below (but close to) the order–disorder transition, i.e. $q^* \sim N^{-0.8}$ (Foster *et al.* 1992).

Films constrained at both surfaces

The effect of constraints introduced by confining diblock copolymers between two solid surfaces was examined by Lambooy *et al.* (1994) and Russell *et al.* (1995). They studied a symmetric PS–PMMA diblock sandwiched between a silicon substrate, and silicon oxide evaporated onto the top (homopolymer PMMA) surface. Neutron reflectivity showed that lamellae formed parallel to the solid interfaces with PMMA at both surfaces. The period of the confined multilayers deviated from the bulk period in a cyclic manner as a function of the confined film thickness, as illustrated in Fig. 2.60. First-order transitions were observed at $t/d_0 = (n + \frac{1}{2})d_0$, where t is the film thickness and d_0 is the bulk lamellar period, between expanded states with n layers and states with $(n + 1)$ layers where d was contracted. Finally, the deviation from the bulk lamellar spacing was found to decrease with increasing film thickness (Lambooy *et al.* 1994; Russell *et al.* 1995). These experimental results are complemented by the phenomenologi-

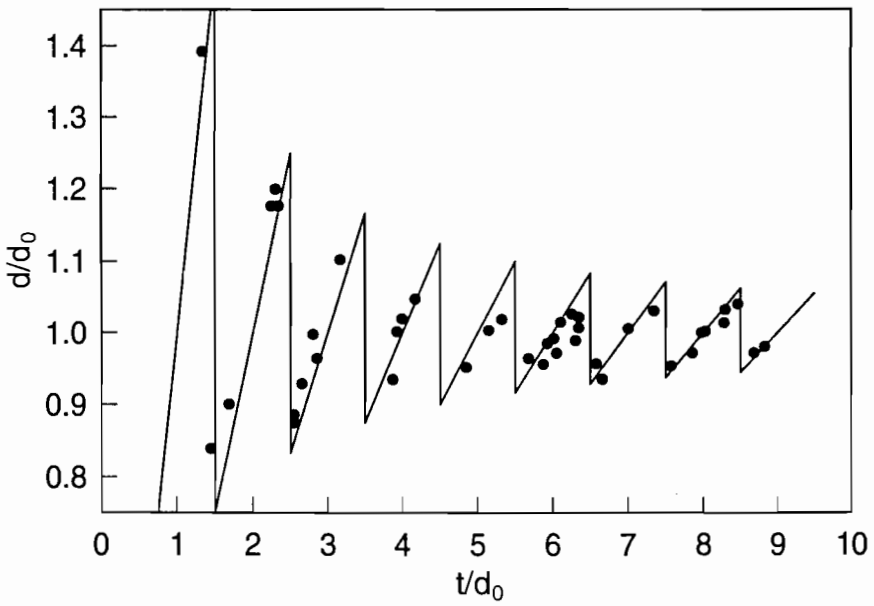

Fig. 2.60 The period, d, of lamellae formed in symmetric dPS–PMMA diblock copolymer films (determined using neutron reflectivity) relative to the bulk period, d_0, as a function of t/d_0, where t is the initial film thickness (Russell *et al.* 1995). The vertical lines indicate when $t/d_0 = (n + \frac{1}{2})d_0$, and the remaining solid lines, having slopes of $\frac{1}{2}n$, indicate the values of d/d_0 expected if the deviation is distributed uniformly throughout the layers.

cal theory of Turner (1992), which accounts for changes from n to $(n + \frac{1}{2})$ layers with increasing film thickness. Similar results were reported for PEP–PEE diblocks (where both blocks were amorphous, in contrast to the PS–PMMA diblock studied by Russell and co-workers) confined between similar walls (both PS) and dissimilar walls (PS and silicon) by Koneripalli *et al.* (1995). By varying wall–block interactions, Kellogg *et al.* (1996) studied the effect of changes in surface energy on the ordering of a symmetric *d*PS–PMMA diblock confined between parallel solid walls. For highly specific interactions (bare walls) the PMMA was found to segregate to both interfaces. In contrast, by coating the walls with a random PS–PMMA copolymer, specific interactions were reduced and perpendicular ordering of the diblock was observed such that both block components were present at the walls (Kellogg *et al.* 1996).

Lattice Model Carlo simulations of a block copolymer confined between parallel hard walls by Kikuchi and Binder (1993, 1994) revealed a complex interplay between film thickness and lamellar period. In the case of commensurate length-scales (t an integral multiple of d), parallel ordering of lamellae was observed. On the other hand, tilted or deformed lamellar structures, or even coexistence of lamellae in different orientations, were found in the case of large incommensurability. Even at temperatures above the bulk ODT, weak order was observed parallel to the surface and the transition from surface-induced order to bulk ordering was found to be gradual. The latter observations are in agreement with the experimental work of Russell and co-workers (Anastasiadis *et al.* 1989; Menelle *et al.* 1992) and Foster *et al.* (1992).

Surface segregation

Sikka *et al.* (1993, 1994) proposed that entropy-driven surface segregation leads to segregation of the block with the smallest statistical segment length to the surface in block copolymer films. Neutron reflectivity experiments on three PEP–*d*PEE, *d*PE–PEE and *d*PE–PEP diblocks revealed that the smaller *d*PEE block segregates to the air–polymer interface in the former two diblocks, whereas in the latter, the smaller PEP block was found at the surface (Sikka *et al.* 1993, 1994). These results were explained using arguments developed by Fredrickson and co-workers (Donley and Fredrickson 1995; Wu *et al.* 1996). These follow from the observation for a binary blend of homopolymers that an entropic penalty arises from unequal conformational perturbations experienced in the presence of an impenetrable wall, this leading to surface wetting by the more flexible component. Carignano and Szleifer (1995) also reported that for flexible–stiff diblocks, the flexible block segregates to the surface in most cases, based on a molecular theory. However, Yethiraj and co-workers (Kumar *et al.* 1995; Yethiraj 1995; Yethiraj *et al.* 1994) have emphasized the importance of enthalpic interactions, and suggest that these, rather than purely entropic effects, provide the mechanism for the surface segregation observed by Sikka *et al.* (1993). Yethiraj (1995) performed Monte Carlo computer simulations on blends of branched and linear polymers and found that in the athermal system, an entropic segregation is possible which favours the linear polymers at the surface. When attractive interactions between polymers are introduced, the branched polymers (with smaller

statistical segment length) are found preferentially at the surface. He suggests that the conflicting effects of entropic and enthalpic interactions leads to non-universal segregation behaviour at the surface of polymer blends or block copolymers (Yethiraj 1995).

2.5.2 Non-lamellar phases

An AFM study of thin films of a triblock copolymer forming a hexagonal-packed cylinder phase has been reported (van Dijk and van den Berg 1995). A change in orientation of hexagonal-packed cylinders from parallel to perpendicular with respect to the substrate was observed in a PS–PB–PS triblock using tapping mode AFM. The low resolution AFM image in Fig. 2.61(a) shows an array of holes in a thin film. A higher resolution image (Fig. 2.61(b)) shows that the sample comprises regions where the PS rods are parallel to the film surface and thinner areas where the PS rods are orthogonal to the film surface. Unlike the behaviour observed in lamellar block copolymers (Ausserré *et al.* 1993; Carvalho and Thomas 1994) there appears to be no terracing at the polymer–air interface.

The morphology and surface topology of thin films of nearly symmetric and asymmetric PEP–PEE diblocks was studied using neutron reflectivity and phase interference microscopy by Karim *et al.* (1994). As-cast samples of the asymmetric diblock ($f_{PEP} = 0.77$) were found to be characterized by the lack of long-range order of the cylinders. Neutron reflectivity profiles revealed that following annealing, the PEE cylinders formed into a hexagonal array as in the bulk material. However, the cylinders were observed to be distorted, which was believed to result from non-integral layering. These distortions were amplified at the surfaces where PEE formed lamellae. In terms of surface topology, the asymmetric sample was found to be macroscopically smooth, unlike symmetric PEP–PEE thin films, which were islanded. The surface topography of symmetric and asymmetric polyolefin block copolymer films was studied in greater detail by Singh *et al.* (1995) using phase interference microscopy. Two distinct mechanisms of evolution and coarsening of islands and holes were observed by them. In the first, islands nucleated and grew slowly, whereas in the second, a spontaneous evolution of the surface structure (resembling two-dimensional spinodal decomposition) was followed by a rapid coarsening. The long-term stability of the surface topography with respect to block copolymer composition was studied for films containing a non-integral number of layers. It was found that copolymers containing a majority of the wetting component form islands and holes more readily, while those having a minor fraction remain flat for long times (up to months) after annealing. In particular, for the PEP–PEE system, diblocks with $f_{PEE} \geq 0.5$ (including samples forming a hex phase) were found to form islands.

TEM was used by Henkee *et al.* (1988) to study thin films of PS–PB diblocks forming cylindrical (hex) and spherical structures. Cylinders were observed to form parallel to the substrate and to each other, and stacking of layers of cylinders was observed. Mansky *et al.* (1995) were able to obtain the metastable per-

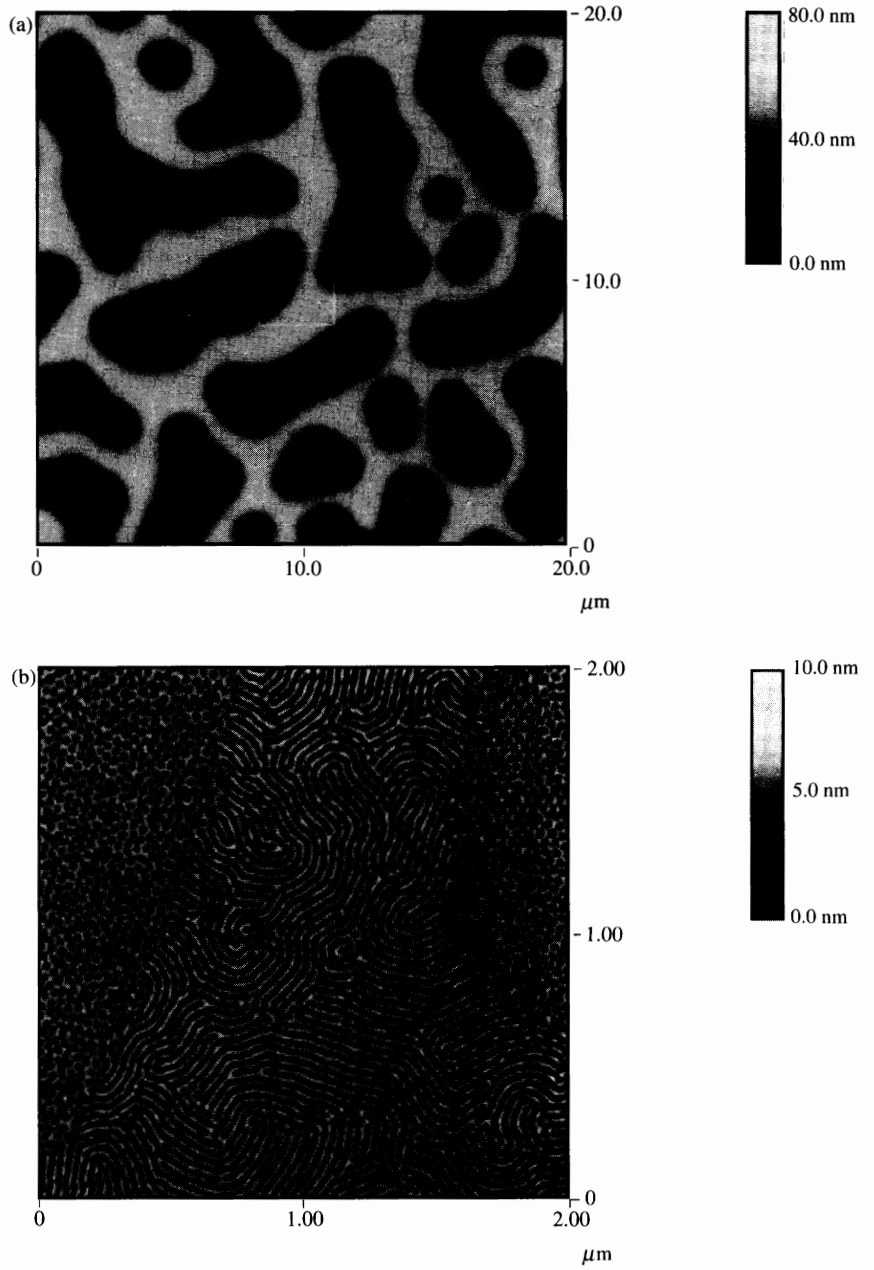

Fig. 2.61 AFM micrographs of thin films of a Kraton PS–PB–PS triblock copolymer with $f_{PS} \approx 0.24$. Part (b) is an enlargement of the square region in part (a), showing the coexistence of regions with parallel and perpendicular cylinders of PS (van Dijk and van den Berg 1995).

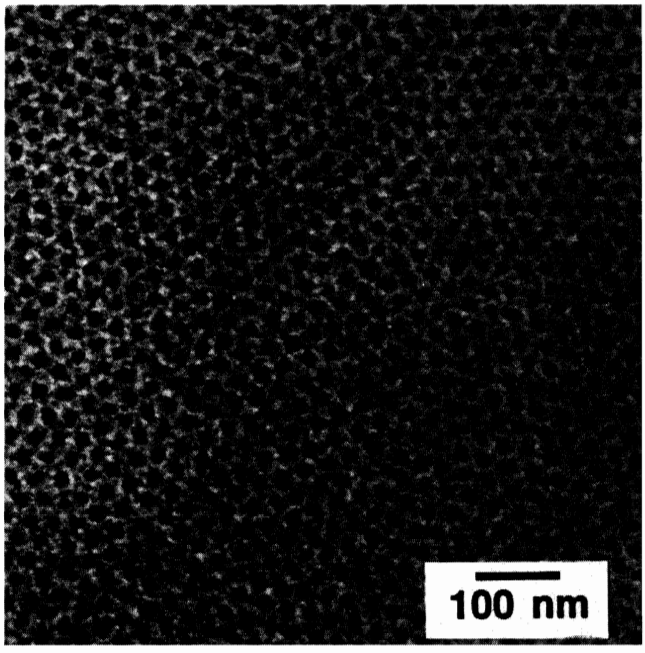

Fig. 2.62 TEM image of spheres in a than film of a PS–PB diblock, with molecular weights M_w(PS) = 65 kg mol^{-1}, M_w(PB) = 10 kg mol^{-1} (Mansky *et al.* 1995). Dark regions are OsO_4-stained PB micelles.

pendicular orientation of cylinders by placing a drop of a dilute solution of a PS–PB diblock in toluene onto water. Due to the rapidity of the solvent evaporation process, the cylinders aligned perpendicular to the plane of the film. Annealing preserved the perpendicular orientation, whilst improving the lateral ordering of rods. The perpendicular orientation can also be obtained by sectioning an oriented bulk sample normal to the cylinder axis, as also demonstrated by Mansky *et al.* (1995) using TEM. Well-oriented domains of spheres were also observed using TEM in this study, as shown in Fig. 2.62. In samples forming a spherical morphology, the spheres were found to be stacked in layers consisting of hexagonally-packed arrays of micelles. Unlike the earlier work of Henkee *et al.* (1988), terracing of sphere-containing layers was not observed by Mansky *et al.* (1995), who obtained monolayers. The potential application of hexagonal arrays of pores as polymer membranes has been discussed by Widawski *et al.* (1994). They observed a honeycomb morphology upon evaporating solutions of PS–poly(paraphenylene) block copolymers in carbon disulphide under a flow of moist gas. Rather monodisperse pores about 10–20 μm in diameter and open to the air were found to form spontaneously, as observed using electron microscopy (see Fig. 2.63).

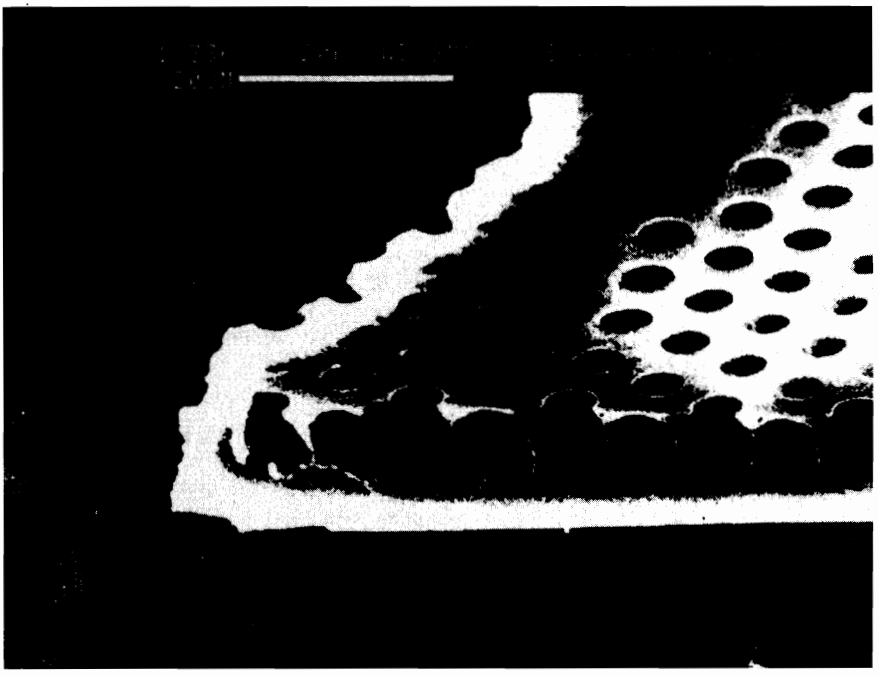

Fig. 2.63 Scanning electron micrograph showing a monolayer of pores in a PS–poly(para-phenylene) diblock copolymer film (Widawski *et al.* 1994). The scale bar represents 20 μm.

References

Ackerson, B. J. and Clark, N. A. (1984). *Physical Review A*, **30**, 906.

Adams, J. L., Graessley, W. W. and Register, R. A. (1994). *Macromolecules*, **27**, 6026.

Aggarwal, S. L. (1976). *Polymer*, **17**, 938.

Aharoni, S. M. (1980). *Journal of Polymer Science: Polymer Physics*, **18**, 1439.

Alexander, S. (1977). *Journal de Physique*, **38**, 977.

Allgaier, J., Young, R. N., Efstratiadis, V. and Hadjichristidis, N. (1996). *Macromolecules*, **29**, 1794.

Almdal, K., Rosedale, J. H., Bates, F. S., Wignall, G. D. and Fredrickson, G. H. (1990). *Physical Review Letters*, **65**, 1112.

Almdal, K., Bates, F. S. and Mortensen, K. (1992). *Journal of Chemical Physics*, **96**, 9122.

Almdal, K., Koppi, K. and Bates, F. S. (1993). *Macromolecules*, **26**, 4058.

Almdal, K., Mortensen, K., Koppi, K. A., Tirrell, M. and Bates, F. S. (1996). *Journal de Physique II*, **6**, 617.

Alward, D. B., Kinning, D. J., Thomas, E. L. and Fetters, L. J. (1986). *Macromolecules*, **19**, 215.

Amundson, K. and Helfand, E. (1993). *Macromolecules*, **26**, 1324.

Anastasiadis, S. H., Russell, T. P., Satija, S. K. and Majkrzak, C. F. (1989). *Physical Review Letters*, **62**, 1852.

Anastasiadis, S. H., Russell, T. P., Satija, S. K. and Majkrzak, C. F. (1990). *Journal of Chemical Physics*, **92**, 5677.

Anastasiadis, S. H., Fytas, G., Vogt, S. and Fischer, E. W. (1993*a*). *Physical Review Letters*, **70**, 2415.
Anastasiadis, S. H., Fytas, G., Vogt, S., Gerharz, B. and Fischer, E. W. (1993*b*). *Europhysics Letters*, **22**, 619.
Anderson, D. M. and Thomas, E. L. (1988). *Macromolecules*, **21**, 3221.
Arai, K., Kotaka, T., Kitano, Y. and Yoshimura, K. (1980). *Macromolecules*, **13**, 1670.
Auschra, C. and Stadler, R. (1993). *Macromolecules*, **26**, 2171.
Ausserré, D., Chatenay, D., Coulon, G. and Collin, R. (1990). *Journal de Physique*, **51**, 2571.
Ausserré, D., Raghunathan, V. A. and Maaloum, M. (1993). *Journal de Physique II*, **3**, 1485.
Avgeropoulos, A., Poulos, Y. and Hadjichristidis, N. (1996). *Macromolecules*, **29**, 6076.
Bahiana, M. and Oono, Y. (1990). *Physical Review A*, **41**, 6763.
Balsara, N. P. and Dai, H. J. (1996). *Journal of Chemical Physics*, **105**, 2942.
Barrat, J.-L. and Fredrickson, G. H. (1991*a*). *Journal of Chemical Physics*, **95**, 1281.
Barrat, J.-L. and Fredrickson, G. H. (1991*b*). *Macromolecules*, **24**, 6378.
Bates, F. S., Bair, H. E. and Hartney, M. A. (1987). *Macromolecules*, **17**, 1987.
Bates, F. S. and Fredrickson, G. H. (1990). *Annual Reviews of Physical Chemistry*, **41**, 525.
Bates, F. S., Rosedale, J. H., Fredrickson, G. H. and Glinka, C. J. (1988). *Physical Review Letters*, **61**, 2229.
Bates, F. S., Rosedale, J. H. and Fredrickson, G. H. (1990). *Journal of Chemical Physics*, **92**, 6255.
Bates, F. S., Koppi, K. A., Tirrell, M., Almdal, K. and Mortensen, K. (1994). *Macromolecules*, **27**, 5934.
Beckmann, J., Auschra, C. and Stadler, R. (1994). *Macromolecular Rapid Communications*, **15**, 67.
Benmouna, M., Benoit, H., Borsali, R. and Duval, M. (1987*a*). *Macromolecules*, **20**, 2620.
Benmouna, M., Duval, M. and Borsali, R. (1987*b*). *Journal of Polymer Science B: Polymer Physics*, **25**, 1839.
Berney, C. V., Cohen, R. E. and Bates, F. S. (1982). *Polymer*, **23**, 1222.
Beyer, F. L., Gido, S. P., Poulos, Y., Avgeropoulos, A. and Hadjichristidis, N. (1997). *Macromolecules*, **30**, 2373.
Bi, L. K. and Fetters, L. J. (1975). *Macromolecules*, **8**, 90.
Bi, L. K. and Fetters, L. J. (1976). *Macromolecules*, **9**, 732.
Binder, K. (1994). *Advances in Polymer Science*, **112**, 181.
Boudenne, N., Anastasiadis, S. H., Fytas, G., Xenidou, M., Hadjichristidis, N., Semenov, A. N. *et al.* (1996). *Physical Review Letters*, **77**, 506.
Brazovskii, S. A. (1975). *Soviet Physics JETP*, **41**, 85.
Breiner, U., Krappe, U. and Stadler, R. (1996). *Macromolecular Rapid Communications*, **17**, 567.
Breiner, U., Krappe, U., Abetz, V. and Stadler, R. (1997). *Macromolecular Chemistry and Physics*, **198**, 1051.
Bur, A. J. and Fetters, L. J. (1976). *Chemical Reviews*, **76**, 727.
Cahn, J. W. (1956). *Acta Metallurgica*, **4**, 449.
Cahn, J. W. and Hilliard, J. (1958). *Journal of Chemical Physics*, **28**, 258.
Cai, Z.-H., Huang, K., Montano, P. A., Russell, T. P., Bai, J. M. and Zajac, G. W. (1993). *Journal of Chemical Physics*, **98**, 2376.
Cai, Z.-H., Lai, B., Yun, W. B., McNulty, I., Huang, K. G. and Russell, T. P. (1994). *Physical Review Letters*, **73**, 82.

Carignano, M. A. and Szleifer, I. (1995). *Europhysics Letters*, **30**, 525.
Carvalho, B. L. and Thomas, E. L. (1994). *Physical Review Letters*, **73**, 3321.
Cates, M. E. and Milner, S. T. (1989). *Physical Review Letters*, **62**, 1856.
Chakrabarti, A., Toral, R. and Gunton, J. D. (1991). *Physical Review A*, **44**, 6503.
Chen, J. T., Thomas, E. L., Ober, C. K. and Mao, G.-P. (1996). *Science*, **273**, 343.
Chung, C. I. and Gale, J. C. (1976). *Journal of Polymer Science: Polymer Physics*, **14**, 1149.
Colby, R. H. (1996). *Current Opinion in Colloid and Interface Science*, **1**, 454.
Coulon, G., Russell, T. P., Deline, V. R. and Green, P. F. (1989). *Macromolecules*, **22**, 2581.
Coulon, G., Ausserré, D. and Russell, T. P. (1990). *Journal de Physique*, **51**, 777.
Coulon, G., Daillant, J., Collin, B., Benattar, J. J. and Gallot, Y. (1993). *Macromolecules*, **26**, 1582.
Dai, H. J., Balsara, N. P., Garetz, B. A. and Newstein, M. C. (1996). *Physical Review Letters*, **77**, 3677.
Dalvi, M. C. and Lodge, T. P. (1993). *Macromolecules*, **26**, 859.
Dalvi, M. C. and Lodge, T. P. (1994). *Macromolecules*, **27**, 3487.
Dalvi, M. C., Eastman, C. E. and Lodge, T. P. (1993). *Physical Review Letters*, **71**, 2591.
David, E. F. and Schweizer, K. S. (1994*a*). *Journal of Chemical Physics*, **100**, 7767.
David, E. F. and Schweizer, K. S. (1994*b*). *Journal of Chemical Physics*, **100**, 7784.
de Gennes, P. G. (1976). *Journal de Physique*, **37**, 1443.
de Jeu, W. H. Lambooy, P., Hamley, I. W., Vaknin, D., Pedersen, J. S., Kjaer, K. *et al.* (1993). *Journal de Physique II*, **3**, 139.
Dlugosz, J., Keller, A. and Pedemonte, E. (1970). *Kolloid Z.u.Z. Polymere*, **242**, 1125.
Dlugosz, J., Folkes, M. J. and Keller, A. (1973). *Journal of Polymer Science B: Polymer Physics*, **11**, 929.
Dobrynin, A. V. and Erukhimovich, I. Y. (1993). *Macromolecules*, **26**, 276.
Doi, M., Harden, J. L. and Ohta, T. (1993). *Macromolecules*, **26**, 4935.
Donley, J. P. and Fredrickson, G. H. (1995). *Journal of Polymer Science B: Polymer Physics*, **33**, 1343.
Eastman, C. E. and Lodge, T. P. (1994). *Macromolecules*, **27**, 5591.
Ehlich, D., Takenaka, M. and Hashimoto, T. (1993*a*). *Macromolecules*, **26**, 492.
Ehlich, D., Takenaka, M., Okamoto, S. and Hashimoto, T. (1993*b*). *Macromolecules*, **26**, 189.
Fernandez, M. L., Higgins, J. S., Penfold, J., Ward, R. C., Shackleton, C. and Walsh, D. J. (1988). *Polymer*, **29**, 1923.
Fetters, L. J., Richards, R. W. and Thomas, E. L. (1987). *Polymer*, **28**, 2252.
Fleischer, G., Fujara, F. and Stühn, B. (1993). *Macromolecules*, **26**, 2340.
Floudas, G., Hadjichristidis, N., Iatrou, H., Pakula, T. and Fischer, E. W. (1994*a*). *Macromolecules*, **27**, 7735.
Floudas, G., Pakula, T., Fischer, E. W., Hadjichristidis, N. and Pispas, S. (1994*b*). *Acta Polymerica*, **45**, 176.
Floudas, G., Fytas, G., Hadjichristidis, N. and Pitsikalis, M. (1995). *Macromolecules*, **28**, 2359.
Floudas, G., Pispas, S., Hadjichristidis, N., Pakula, T. and Erukhimovich, I. (1996*a*). *Macromolecules*, **29**, 4142.
Floudas, G., Hadjichristidis, N., Iatrou, H. and Pakula, T. (1996*b*). *Macromolecules*, **29**, 3139.
Folkes, M. J. and Keller, A. (1973). Morphology of block copolymers and its consequences. In *Block and graft copolymers*, (ed. J. J. Burke and V. Weiss), p. 87. Syracuse University Press, Syracuse.

Folkes, M. J. and Keller, A. (1976). *Journal of Polymer Science B: Polymer Physics*, **13**, 833.
Förster, S., Khandpur, A. K., Zhao, J., Bates, F. S., Hamley, I. W., Ryan, A. J. *et al.* (1994). *Macromolecules*, **27**, 6922.
Förster, S., Wenz, E. and Lindner, P. (1996). *Physical Review Letters*, **77**, 95.
Foster, M. D. (1993). *Critical Reviews in Analytical Chemistry*, **24**, 179.
Foster, M. D., Sikka, M., Singh, N., Bates, F. S., Satija, S. K. and Majkrzak, C. F. (1992). *Journal of Chemical Physics*, **96**, 8605.
Fredrickson, G. H. (1986). *Journal of Chemical Physics*, **85**, 5306.
Fredrickson, G. H. (1987). *Macromolecules*, **20**, 2535.
Fredrickson, G. H. (1991). *Macromolecules*, **24**, 3456.
Fredrickson, G. H. (1994). *Journal of Rheology*, **38**, 1045.
Fredrickson, G. H. and Bates, F. S. (1996). *Annual Reviews of Materials Science*, **26**, 501.
Fredrickson, G. H. and Binder, K. (1989). *Journal of Chemical Physics*, **91**, 7265.
Fredrickson, G. H. and Helfand, E. (1987). *Journal of Chemical Physics*, **87**, 697.
Fredrickson, G. H. and Helfand, E. (1988). *Journal of Chemical Physics*, **89**, 5890.
Fredrickson, G. H. and Larson, R. G. (1987). *Journal of Chemical Physics*, **86**, 1553.
Fredrickson, G. H. and Milner, G. H. (1990). *Materials Research Society Symposium Proceedings*, **177**, 169.
Fredrickson, G. H., Milner, S. T. and Leibler, L. (1992). *Macromolecules*, **25**, 6341.
Fried, H. and Binder, K. (1991*a*). *Journal of Chemical Physics*, **94**, 8349.
Fried, H. and Binder, K. (1991*b*). *Europhysics Letters*, **16**, 237.
Fytas, G., Anastasiadis, S. H., Karatasos, K. and Hadjichristidis, N. (1993). *Physica Scripta T*, **49**, 237.
Gedde, U. W. (1995). *Polymer physics.* Chapman and Hall, London.
Genz, U. and Vilgis, T. A. (1994). *Journal of Chemical Physics*, **101**, 7111.
Gido, S. P., Schwark, D. W., Thomas, E. L. and Gonçalves, M. C. (1993). *Macromolecules*, **26**, 2636.
Gido, S. P., Lee, C., Pochan, D. J., Pispas, S., Mays, J. W. and Hadjichristidis, N. (1996). *Macromolecules*, **29**, 7022.
Gouinlock, E. V. and Porter, R. S. (1977). *Polymer Engineering and Science*, **17**, 535.
Gupta, V. K., Krishnamoorti, R., Kornfield, J. A. and Smith, S. D. (1995). *Macromolecules*, **28**, 4464.
Gupta, V. K., Krishnamoorti, R., Kornfield, J. A. and Smith, S. D. (1996). *Macromolecules*, **29**, 1359.
Hadjichristidis, N., Iatrou, H., Behal, S. K., Chludsinski, J. J., Disko, M. M., Garner, R. T. *et al.* (1993). *Macromolecules*, **26**, 5812.
Hadjichristidis, N., Iatrou, H., Tselikas, Y. and Efstratiadis, V. (1996*a*). *Chimika Chronika*, **24**, 189.
Hadjichristidis, N., Tselikas, Y., Iatrou, H., Efstratiadis, V. and Avgeropoulos, A. (1996*b*). *Journal of Macromolecular Science, Pure and Applied Chemistry A*, **33**, 1447.
Hadziioannou, G. and Skoulios, A. (1982). *Macromolecules*, **15**, 258.
Hadziioannou, G., Mathis, A. and Skoulios, A. (1979*a*). *Colloid and Polymer Science*, **257**, 15.
Hadziioannou, G., Mathis, A. and Skoulios, A. (1979*b*). *Colloid and Polymer Science*, **257**, 136.
Hajduk, D. A., Harper, P. E., Gruner, S. M., Honeker, C. C., Kim, G., Thomas, E. L. *et al.* (1994*a*). *Macromolecules*, **27**, 4063.
Hajduk, D. A., Gruner, S. M., Rangarajan, P., Register, R. A., Fetters, L. J., Honeker, C., Albalak, R. J. *et al.* (1994*b*). *Macromolecules*, **27**, 490.

Hajduk, D. A., Harper, P. E., Gruner, S. M., Honeker, C. C., Thomas, E. L. and Fetters, L. J. (1995). *Macromolecules*, **28**, 2570.
Hajduk, D. A., Takenouchi, H., Hillmyer, M. A., Bates, F. S., Vigild, M. E. and Almdal, K. (1997). *Macromolecules*, **30**, 3788.
Halperin, A. (1989). *Europhysics Letters*, **10**, 549.
Halperin, A. (1990). *Macromolecules*, **23**, 2724.
Halperin, A., Tirrell, M. and Lodge, T. P. (1992). *Advances in Polymer Science*, **100**, 31.
Hamley, I. W. (1994). *Physical Review E*, **50**, 2872.
Hamley, I. W. (1997). Unpublished results.
Hamley, I. W. and Bates, F. S. (1994). *Journal of Chemical Physics*, **100**, 6813.
Hamley, I. W. and Podneks, V. E. (1997). *Macromolecules*, **30**, 3701.
Hamley, I. W. and Ryan, A. J. (1994). Unpublished work.
Hamley, I. W., Koppi, K. A., Rosedale, J. H., Bates, F. S., Almdal, K. and Mortensen, K. (1993). *Macromolecules*, **26**, 5959.
Hamley, I. W., Gehlsen, M. D., Khandpur, A. K., Koppi, K. A., Rosedale, J. H., Schulz, M. F. *et al.* (1994). *Journal de Physique II*, **4**, 2161.
Hamley, I. W., Buzza, D. M. A., McLeish, T. C. B., Fzea, A. and Young, R. N. (1997). Unpublished results.
Han, C. D., Baek, D. M., Kim, J. K., Ogawa, T., Sakamoto, N. and Hashimoto, T. (1995). *Macromolecules*, **28**, 5043.
Harkless, C. R., Singh, M. A., Nagler, S. E., Stephenson, G. B. and Jordan-Sweet, J. L. (1990). *Physical Review Letters*, **64**, 2285.
Hasegawa, H. and Hashimoto, T. (1996). Self-assembly and morphology of block copolymer systems. In *Comprehensive polymer science. Second supplement*, (ed. S. L. Aggarwal and S. Russo), p. 497. Pergamon, London.
Hasegawa, H., Tanaka, H., Yamasaki, K. and Hashimoto, T. (1987). *Macromolecules*, **20**, 1651.
Hashimoto, T. (1985). Time resolved small-angle X-ray scattering studies on kinetics and molecular dynamics of order–disorder transition of block polymers. In *Physical optics of dynamic phenomena and processes in macromolecular systems*, (ed. B. Sedlácek), p. 106. Walter de Gruyter, Berlin.
Hashimoto, T. (1987). *Macromolecules*, **20**, 465.
Hashimoto, T. (1996). Order–disorder transition in block polymers. In *Thermoplastic elastomers*, (ed. G. Holden, N. R. Legge, R. P. Qurik and H. E. Schroeder), p. 430. Hanser, Munich.
Hashimoto, T., Shibayama, M., Fujimara, M. and Kawai, H. (1983). Microphase separation and the polymer–polymer interphase in block polymers. In *Block copolymers. Science and technology*, (ed. D. J. Meier). Harwood Academic Publishers, Chur, Switzerland.
Hashimoto, T., Kowsaka, K., Shibayama, M. and Kawai, H. (1986*a*). *Macromolecules*, **19**, 754.
Hashimoto, T., Kowsaka, K., Shibayama, M. and Suehiro, S. (1986*b*). *Macromolecules*, **19**, 750.
Hashimoto, T., Ijichi, Y. and Fetters, L. J. (1988). *Journal of Chemical Physics*, **89**, 2463.
Hashimoto, T., Ogawa, T. and Han, C. D. (1994). *Journal of the Physical Society of Japan*, **63**, 2206.
Hashimoto, T., Sakamoto, N. and Koga, T. (1996). *Physical Review E*, **54**, 5832.
Hayashi, T. (1985). Block copolymers as models of biophysical systems. In *Developments in block copolymers*, Vol. 2, (ed. I. Goodman), p. 109. Elsevier, London.
Helfand, E. (1975*a*). *Macromolecules*, **8**, 552.

Helfand, E. (1975*b*). *Journal of Chemical Physics*, **62**, 999.
Helfand, E. (1992). *Macromolecules*, **25**, 492.
Helfand, E. and Sapse, A. M. (1975). *Journal of Chemical Physics*, **62**, 1327.
Helfand, E. and Tagami, Y. (1972). *Journal of Chemical Physics*, **56**, 3592.
Helfand, E. and Wasserman, Z. R. (1976). *Macromolecules*, **9**, 879.
Helfand, E. and Wasserman, Z. R. (1982). Microdomain structure and the interface in block copolymers. In *Developments in block copolymers*, Vol. 1, (ed. I. Goodman), p. 99. Applied Science, London.
Henkee, C. S., Thomas, E. L. and Fetters, L. J. (1988). *Journal of Materials Science*, **23**, 1685.
Herman, D. S., Kinning, D. J., Thomas, E. L. and Fetters, L. J. (1987). *Macromolecules*, **20**, 2940.
Hoffmann, A., Koch, T. and Stühn, B. (1993). *Macromolecules*, **26**, 7288.
Hohenberg, P. C. and Swift, J. B. (1995). *Physical Review E*, **52**, 1828.
Holyst, R. and Schick, M. (1992). *Journal of Chemical Physics*, **96**, 721.
Huynh, B.-G., Jérome, R. and Teyssié, P. (1980). *Journal of Polymer Science, Polymer Chemistry*, **18**, 3483.
Iatrou, H. and Hadjichristidis, N. (1992). *Macromolecules*, **25**, 4649.
Iatrou, H. and Hadjichristidis, N. (1993). *Macromolecules*, **26**, 2479.
Iatrou, H., Avgeropoulos, A. and Hadjichristidis, N. (1994). *Macromolecules*, **27**, 6232.
Ijichi, Y., Hashimoto, T. and Fetters, L. J. (1989). *Macromolecules*, **22**, 2817.
Jian, T., Semenov, A. N., Anastasiadis, S. H., Fytas, G., Yeh, F.-J., Chu, B. *et al.* (1994*a*). *Journal of Chemical Physics*, **100**, 3286.
Jian, T., Anastasiadis, S. H., Semenov, A. N., Fytas, G., Adachi, K. and Kotaka, T. (1994*b*). *Macromolecules*, **27**, 4762.
Jian, T., Anastasiadis, S. H., Semenov, A. N., Fytas, G., Fleischer, G. and Vilesov, A. D. (1995). *Macromolecules*, **28**, 2439.
Jones, J. L. and McLeish, T. C. B. (1995). *Langmuir*, **11**, 785.
Kannan, R. M. and Kornfield, J. A. (1994). *Macromolecules*, **27**, 1177.
Karim, A., Singh, N., Sikka, M., Bates, F. S., Dozier, W. D. and Felcher, G. P. (1994). *Journal of Chemical Physics*, **100**, 1620.
Kats, E. I., Lebedev, V. V. and Muratov, A. R. (1993). *Physics Reports*, **228**, 1.
Kavassalis, T. A. and Whitmore, M. D. (1991). *Macromolecules*, **24**, 5340.
Kawasaki, K. and Ohta, T. (1986). *Physica A*, **139**, 223.
Kawasaki, K. and Onuki, A. (1990). *Physical Review A*, **42**, 3664.
Kawasaki, K. and Sekimoto, K. (1987). *Physica A*, **143**, 349.
Kawasaki, K. and Sekimoto, K. (1988). *Physica A*, **148**, 361.
Kawasaki, K. and Sekimoto, K. (1989). *Macromolecules*, **22**, 3063.
Keller, A. and Odell, J. A. (1985). The interrelation between microstructure and properties of block copolymers. In *Processing, structure and properties of block copolymers*, (ed. M. J. Folkes), p. 29. Elsevier, London.
Keller, A., Pedemonte, E. and Willmouth, F. M. (1970). *Nature*, **225**, 538.
Kellogg, G. J., Walton, D. G., Mayes, A. M., Lambooy, P., Russell, T. P., Gallagher, P. D. *et al.* (1996). *Physical Review Letters*, **76**, 2503.
Khandpur, A. K., Förster, S., Bates, F. S., Hamley, I. W., Ryan, A. J., Bras, W. *et al.* (1995). *Macromolecules*, **28**, 8796.
Kikuchi, K. and Binder, K. (1993). *Europhysics Letters*, **21**, 427.
Kikuchi, K. and Binder, K. (1994). *Journal of Chemical Physics*, **101**, 3367.
Kinning, D. J. and Thomas, E. L. (1984). *Macromolecules*, **17**, 1712.

Koneripalli, N., Singh, N., Levicky, R., Bates, F. S., Gallagher, P. D. and Satija, S. K. (1995). *Macromolecules*, **28**, 2897.
Koppi, K. A., Tirrell, M., Bates, F. S., Almdal, K. and Colby, R. H. (1992). *Journal de Physique II*, **2**, 1941.
Koppi, K. A., Tirrell, M. and Bates, F. S. (1993). *Physical Review Letters*, **70**, 1449.
Koppi, K. A., Tirrell, M., Bates, F. S., Almdal, K. and Mortensen, K. (1994). *Journal of Rheology*, **38**, 999.
Krappe, U., Stadler, R. and Voigt-Martin, I. (1995). *Macromolecules*, **28**, 4558.
Kumar, S. K., Yethiraj, A., Schweizer, A. and Leermakers, F. A. M. (1995). *Journal of Chemical Physics*, **103**, 10332.
Kumaran, V. and Fredrickson, G. H. (1994). *Physica A*, **204**, 378.
Lambooy, P., Russell, T. P., Kellogg, G. J., Mayes, A. M., Gallagher, P. D. and Satija, S. K. (1994). *Physical Review Letters*, **72**, 2899.
Laradji, M., Shi, A.-C., Desai, R. C. and Noolandi, J. (1997*a*). *Macromolecules*, **30**, 3242.
Laradji, M., Shi, A.-C., Noolandi, J. and Desai, R. C. (1997*b*). *Physical Review Letters*, **78**, 2577,
Larson, R. G. and Fredrickson, G. H. (1987). *Macromolecules*, **20**, 1897.
Leary, D. and Williams, M. (1970). *Journal of Polymer Science B*, **8**, 335.
Leary, D. and Williams, M. (1973). *Journal of Polymer Science: Polymer Physics*, **11**, 345.
Leary, D. and Williams, M. (1974). *Journal of Polymer Science: Polymer Physics*, **12**, 265.
Lee, S.-D. and Meyer, R. B. (1988). *Physical Review Letters*, **61**, 2217.
Leibig, C. M. and Fredrickson, G. H. (1996). *Journal of Polymer Science B: Polymer Physics*, **34**, 163.
Leibler, L. (1980). *Macromolecules*, **13**, 1602.
Likhtman, A. E. and Semenov, A. N. (1994). *Macromolecules*, **27**, 3103.
Lodge, T. P. and Dalvi, M. C. (1995). *Physical Review Letters*, **75**, 657.
Maaloum, M., Ausserré, D., Chatenay, D., Coulon, G. and Gallot, Y. (1992). *Physical Review Letters*, **68**, 1575.
Maaloum, M., Ausserré, D., Chatenay, D. and Gallot, Y. (1993). *Physical Review Letters*, **70**, 2577.
Mai, S. M., Fairclough, J. P. A., Hamley, I. W., Denny, R. C., Liao, B., Booth, C. and Ryan, A. J. (1996). *Macromolecules*, **29**, 6212.
Mansky, P., Chaikin, P. and Thomas, E. L. (1995). *Journal of Materials Science*, **30**, 1987.
Maring, D. and Wiesner, U. (1997). *Macromolecules*, **30**, 660.
Marko, J. F. 1993. *Macromolecules*, **26**, 1442.
Marques, C. M. and Cates, M. E. (1990). *Journal de Physique*, **51**, 1733.
Matsen, M. W. (1995*a*). *Macromolecules*, **28**, 5765.
Matsen, M. W. (1995*b*). *Journal of Chemical Physics*, **102**, 3884.
Matsen, M. W. (1996). *Journal of Chemical Physics*, **104**, 7758.
Matsen, M. W. (1998). *Journal of Chemical Physics*, **108**, 785.
Matsen, M. W. and Bates, F. S. (1996*a*). *Macromolecules*, **29**, 1091.
Matsen, M. W. and Bates, F. S. (1996*b*). *Macromolecules*, **29**, 7641.
Matsen, M. W. and Bates, F. S. (1997*a*). *Journal of Polymer Science B: Polymer Physics*, **35**, 945.
Matsen, M. W. and Bates, F. S. (1997*b*). *Journal of Chemical Physics*, **106**, 2436.
Matsen, M. W. and Schick, M. (1994*a*). *Physical Review Letters*, **72**, 2660.
Matsen, M. W. and Schick, M. (1994*b*). *Macromolecules*, **27**, 6761.
Matsen, M. W. and Whitmore, M. D. (1996). *Journal of Chemical Physics*, **105**, 9698.
Mayes, A. M. and Olvera de la Cruz, M. (1989). *Journal of Chemical Physics*, **91**, 7228.

Mays, J. W. (1990). *Polymer Bulletin*, **23**, 247.
Meier, D. J. (1969). *Journal of Polymer Science C*, **26**, 81.
Menelle, A., Russell, T. P., Anastasiadis, S. H., Satija, S. K. and Majkrzak, C. F. (1992). *Physical Review Letters*, **68**, 67.
Milner, S. T. (1994). *Macromolecules*, **27**, 2333.
Milner, S. T. and Olmsted, P. D. (1997). *Journal de Physique II*, **7**, 249.
Mogi, Y., Kotsuji, H., Kaneko, Y., Mori, K., Matsushita, Y. and Noda. I. (1992*a*). *Macromolecules*, **25**, 5408.
Mogi, Y., Mori, K., Matsushita, Y. and Noda, I. (1992*b*). *Macromolecules*, **25**, 5412.
Mori, K., Okawara, A. and Hashimoto, T. (1996). *Journal of Chemical Physics*, **104**, 7765.
Morrison, F. A., Mays, J. W., Muthukumar, M., Nakatani, A. I. and Han, C. C. (1993). *Macromolecules*, **26**, 5271.
Müller, M. and Schick, M. (1996). *Macromolecules*, **29**, 8900.
Nakajima, A., Hayashi, T., Kugo, K. and Shinoda, K. (1979*a*). *Macromolecules*, **12**, 840.
Nakajima, A., Kugo, K. and Hayashi, T. (1979*b*). *Macromolecules*, **12**, 844.
Nakatani, A. I., Morrison, F. A., Douglas, J. F., Mays, J. W., Jackson, C. L., Muthukumar, M. *et al.* (1996). *Journal of Chemical Physics*, **104**, 1589.
Netz, R. R. and Schick, M. (1996). *Physical Review Letters*, **77**, 302.
Ohta, T. and Kawasaki, K. (1986). *Macromolecules*, **19**, 2621.
Ohta, T., Enomoto, Y., Harden, J. L. and Doi, M. (1993). *Macromolecules*, **26**, 4928.
Okamoto, S., Saijo, K. and Hashimoto, T. (1994*a*). *Macromolecules*, **27**, 3753.
Okamoto, S., Saijo, K. and Hashimoto, T. (1994*b*). *Macromolecules*, **27**, 5547.
Olmsted, P. D. and Milner, S. T. (1994*a*). *Physical Review Letters*, **72**, 936.
Olmsted, P. D. and Milner, S. T. (1994*b*). *Physical Review Letters*, **74**, 829.
Olvera de la Cruz, M. (1991). *Physical Review Letters*, **67**, 85.
Olvera de la Cruz, M. and Sanchez, I. (1986). *Macromolecules*, **19**, 2501.
Olvera de la Cruz, M., Mayes, A. M. and Swift, B. W. (1992). *Macromolecules*, **25**, 944.
Onuki, A. (1987). *Journal of Chemical Physics*, **87**, 3692.
Papadakis, C. M., Brown, W., Johnsen, R. M., Posselt, D. and Almdal, K. (1996*a*). *Journal of Chemical Physics*, **104**, 1611.
Papadakis, C. M., Almdal, K., Mortensen, K. and Posselt, D. (1996*b*). *Europhysics Letters*, **36**, 283.
Patel, S. S., Larson, R. G., Winey, K. I. and Watanabe, H. (1995). *Macromolecules*, **28**, 4313.
Pearson, D. S. and Helfand, H. (1984). *Macromolecules*, **17**, 888.
Perly, B., Douy, A. and Gallot, B. (1974). *Comptes Rendus de l'Academie des Sciences de Paris*, **C279**, 1109.
Perly, B., Douy, A. and Gallot, B. (1976). *Makromoleculaire Chemie*, **177**, 2569.
Pochan, D. J., Gido, S. P., Pispas, S. and Mays, J. W. (1996*a*). *Macromolecules*, **29**, 5099.
Pochan, D. J., Gido, S. P., Pispas, S., Mays, J. W., Ryan, A. J., Fairclough, J. P. A. *et al.* (1996*b*). *Macromolecules*, **29**, 5091.
Podneks, V. E. and Hamley, I. W. (1996). *JETP Letters*, **64**, 617.
Polis, D. L. and Winey, K. I. (1996). *Macromolecules*, **29**, 8180.
Price, C., Watson, A. G. and Chow, M. T. (1972). *Polymer*, **13**, 333.
Puri, S. and Oono, Y. (1988). *Physical Review A*, **38**, 1542.
Qi, S. and Wang, Z. G. (1996). *Physical Review Letters*, **76**, 1679.
Qi, S. and Wang, Z. G. (1997). *Physical Review E*, **55**, 1682.
Quirk, R. and Ignatz-Hoover, F. (1987). In *Recent advances in anionic polymerization*, (ed. T. E. Hogen-Esch and J. Smid). Elsevier, New York.
Radzilowski, L. H. and Stupp, S. I. (1994). *Macromolecules*, **27**, 7747.

Radzilowski, L. H., Wu, J. L. and Stupp, S. I. (1993). *Macromolecules*, **26**, 879.
Riess, G., Schlienger, M. and Marti, S. (1989). *Journal of Macromolecular Science, Physics B*, **17**, 355.
Riise, B. L., Fredrickson, G. H., Larson, R. G. and Pearson, D. S. (1995). *Macromolecules*, **28**, 7653.
Rosedale, J. H. and Bates, F. S. (1990). *Macromolecules*, **23**, 2329.
Rosedale, J. H., Bates, F. S., Almdal, K., Mortensen, K. and Wignall, G. D. (1995). *Macromolecules*, **28**, 1429.
Rubinstein, M. and Obukhov, S. P. (1993). *Macromolecules*, **26**, 1740.
Russell, T. P. (1990). *Materials Science Reports*, **5**, 171.
Russell, T. P., Coulon, G., Deline, V. R. and Miller, D. C. (1989). *Macromolecules*, **22**, 4600.
Russell, T. P., Lambooy, P., Kellogg, G. J. and Mayes, A. M. (1995). *Physica B*, **213/214**, 22.
Ryan, A. J. and Hamley, I. W. (1997). Morphology of block copolymers. In *The physics of glassy polymers*, (ed. R. N. Haward and R. J. Young). Chapman and Hall, London.
Ryan, A. J., Macosko, C. W. and Bras, W. (1992). *Macromolecules*, **25**, 6277.
Sakamoto, N. and Hashimoto, T. (1995). *Macromolecules*, **28**, 6825.
Sakamoto, N., Hashimoto, T., Han, C. D., Kim, D. and Vaidya, N. Y. (1997). *Macromolecules*, **30**, 1621.
Schulz, M. F., Bates, F. S., Almdal, K. and Mortensen, K. (1994). *Physical Review Letters*, **73**, 86.
Schulz, M. F., Khandpur, A. K., Bates, F. S., Almdal, K., Mortensen, K., Hajduk, D. A. *et al.* (1996). *Macromolecules*, **29**, 2857.
Schwab, M. and Stühn, B. (1996). *Physical Review Letters*, **76**, 924.
Schwahn, D., Frielinghaus, H., Mortensen, K. and Almdal, K. (1996). *Physical Review Letters*, **77**, 3153.
Seddon, J. M. (1990). *Biochimica et Biophysica Acta*, **1031**, 1.
Semenov, A. N. (1985). *Soviet Physics JETP*, **61**, 733.
Semenov, A. N. (1991). *Molecular Crystals and Liquid Crystals*, **209**, 191.
Semenov, A. N. and Vasilenko, S. V. (1986). *Soviet Physics JETP*, **63**, 70.
Shiwa, Y., Taneike, T. and Yokojima, Y. (1996). *Physical Review Letters*, **77**, 4378.
Shull, K. R., Kramer, E. J., Bates, F. S. and Rosedale, J. H. (1991). *Macromolecules*, **24**, 1383.
Sikka, M., Singh, N., Karim, A., Bates, F. S., Satija, S. K. and Majkrzak, C. F. (1993). *Physical Review Letters*, **70**, 307.
Sikka, M., Singh, N., Bates, F. S., Karim, A., Satija, S. and Majkrzak, C. F. (1994). *Journal de Physique II*, **4**, 2231.
Singh, C., Goulian, M., Liu, A. J. and Fredrickson, G. H. (1994). *Macromolecules*, **27**, 2974.
Singh, N., Kudrle, A., Sikka, M. and Bates, F. S. (1995). *Journal de Physique II*, **5**, 377.
Sioula, S., Tselikas, Y. and Hadjichristidis, N. (1997). *Macromolecules*, **30**, 1518.
Smith, S. D., Spontak, R. J., Satkowski, M. M., Ashraf, A. and Lin, J. S. (1993). *Physical Review B*, **47**, 14555.
Smith, S. D., Spontak, R. J., Satkowski, M. M., Ashraf, A., Heape, A. K. and Lin, J. S. (1994). *Polymer*, **35**, 4527.
Spontak, R. J., Zielinski, J. M. and Lipscomb, G. G. (1992*a*). *Macromolecules*, **25**, 6270.
Spontak, R. J., Smith, S. D., Satkowski, M. M., Ashraf, A. and Zielinski, J. M. (1992*b*). In *Polymer solutions, blends and interfaces*, (ed. I. Noda and D. N. Rubingh), p. 65. Elsevier, Amsterdam.

Stadler, R., Auschra, C., Beckmann, J., Krappe, U., Voigt-Martin, I. and Leibler, L. (1995). *Macromolecules*, **28**, 3080.
Stepanek, P. and Lodge, T. P. (1996). *Macromolecules*, **29**, 1244.
Stepanek, P., Almdal, K. and Lodge, T. P. (1997). *Journal of Polymer Science B: Polymer Physics*, **35**, 1643.
Stühn, B., Mutter, R. and Albrecht, T. (1992). *Europhysics Letters*, **18**, 427.
Stühn, B., Vilesov, A. and Zachmann, H. G. (1994). *Macromolecules*, **27**, 3560.
Tang, H. and Schweizer, K. S. (1995). *Journal of Chemical Physics*, **103**, 6296.
Tepe, T., Schulz, M. F., Zhao, J., Tirrell, M., Bates, F. S., Mortensen, K. *et al.* (1995). *Macromolecules*, **28**, 3008.
Thomas, E. L. and Lescanec, R. L. (1994). *Philosophical Transactions of the Royal Society of London*, **348**, 149.
Thomas, E. L., Alward, D. B., Kinning, D. J., Martin, D. C., Handlin, D. L. and Fetters, L. J. (1986). *Macromolecules*, **19**, 2197.
Tselikas, Y., Iatrou, H., Hadjichristidis, N., Liang, K. S., Mohanty, K. and Lohse, D. J. (1996*a*). *Journal of Chemical Physics*, **105**, 2456.
Tselikas, Y., Hadjichristidis, N., Lescanec, R. L., Honeker, C. C., Wohlgemuth, M. and Thomas, E. L. (1996*b*). *Macromolecules*, **29**, 3390.
Tsitsilianis, C., Ghaumont, P. and Rempp. P. (1990). *Makromoleculaire Chemie*, **191**, 2319.
Turner, M. S. (1992). *Physical Review Letters*, **69**, 1788.
Turturro, A., Gattiglia, E. and Vacca, P. (1995). *Polymer*, **36**, 3987.
van Dijk, M. A. and van den Berg, R. (1995). *Macromolecules*, **28**, 6773.
Vavasour, J. D. and Whitmore, M. D. (1993). *Macromolecules*, **26**, 7070.
Vigild, M. E., Almdal, K., Mortensen, K., Hamley, I. W., Fairclough, J. P. A. and Ryan, A. J. (1997). *Macromolecules*, submitted.
Vogt, S., Gerharz, B., Fischer, E. W. and Fytas, G. (1992). *Macromolecules*, **25**, 5986.
Vogt, S., Anastasiadis, S. H., Fytas, G. and Fischer, E. W. (1994). *Macromolecules*, **27**, 4335.
Wang, Z. G. (1994). *Journal of Chemical Physics*, **100**, 2298.
Whitmore, M. W. and Vavasour, J. D. (1995). *Acta Polymerica*, **46**, 341.
Widawski, G., Rawiso, M. and François, B. (1994). *Nature*, **369**, 387.
Williams, D. R. M. and Fredrickson, G. H. (1992). *Macromolecules*, **25**, 3561.
Williams, D. R. M. and Halperin, A. (1993). *Physical Review Letters*, **71**, 1557.
Winey, K. I., Thomas, E. L. and Fetters, L. J. (1991). *Journal of Chemical Physics*, **95**, 9367.
Winey, K. I., Thomas, E. L. and Fetters, E. L. (1992*a*). *Macromolecules*, **25**, 2645.
Winey, K. I., Thomas, E. L. and Fetters, L. J. (1992*b*). *Macromolecules*, **25**, 422.
Winter, H. H., Scott, D. B., Gronski, W., Okamoto, S. and Hashimoto, T. (1993). *Macromolecules*, **26**, 7236.
Wolff, T., Burger, C. and Ruland, W. (1993). *Macromolecules*, **26**, 1707.
Wu, D. T., Fredrickson, G. H. and Carton, J. P. (1996). *Journal of Chemical Physics*, **104**, 6387.
Yethiraj, A. (1995). *Physical Review Letters*, **74**, 2018.
Yethiraj, A., Kumar, S., Hariharan, A. and Schweizer, K. S. (1994). *Journal of Chemical Physics*, **100**, 4691.
Zhang, U. and Wiesner, U. (1995). *Journal of Chemical Physics*, **103**, 4784.
Zhang, Y., Wiesner, U. and Spiess, H. (1995). *Macromolecules*, **28**, 778.
Zhao, J., Majumdar, B., Schulz, M. F., Bates, F. S., Almdal, K., Mortensen, K. *et al.* (1996). *Macromolecules*, **29**, 1204.
Zielinski, J. M. and Spontak, R. J. (1992). *Macromolecules*, **25**, 653.

3 Block copolymers in dilute solution

3.1 Introduction

The formation of micelles in a solvent that is selective for one of the blocks is one of the most important and useful properties of block copolymers. For example, micelles formed by block copolymers can solubilize otherwise insoluble substances, they can be used to microscopically 'mix' incompatible substances and they can stabilize colloidal particles or form microemulsions.

Since this chapter is concerned with block copolymers in dilute solution, it is useful to include a definition of the dilute regime for polymer solutions in the Introduction. This regime extends up to a volume fraction above which swollen coils overlap (de Gennes 1979):

$$\phi^* \cong a^3 N / R_F^3 = N^{1-3\nu}, \tag{3.1}$$

where N is the degree of polymerization, R_F is the end-to-end distance of the chain, a is the polymer segment length and ν is the Flory exponent ($\nu = 0.588$ in a good solvent or $\nu = 0.5$ in a theta solvent). Then the dilute region is defined by $\phi < \phi^*$. With increasing ϕ the copolymer solution is successively in the semidilute and concentrated regimes. Above the overlap concentration, the chains in solution become increasingly densely packed and in the case of block copolymers this can lead to micellization.

Micellization occurs in dilute solutions of block copolymers in a selective solvent at a fixed temperature above a concentration called the critical micelle concentration (cmc). At higher concentrations, the micelles can order onto a lattice above a critical gel concentration (cgc). These regimes are illustrated in Fig. 3.1. This chapter is concerned with block copolymer solutions and micelles, and not gels formed at high concentrations which are the subject of chapter 4. At a fixed concentration, micellization can occur on changing the temperature above or below the critical micelle temperature (cmt), depending on whether the self-assembly process is endothermic or exothermic. The micellization of block copolymers often occurs via a closed association process, leading to a dynamic equilibrium between micelles with a narrow molar mass and size distribution and dispersed copolymer molecules. The micelle structure depends on the length of the block forming the micellar core with respect to the block forming the corona, and can be classified into a number of types, discussed in Section 3.4.1.

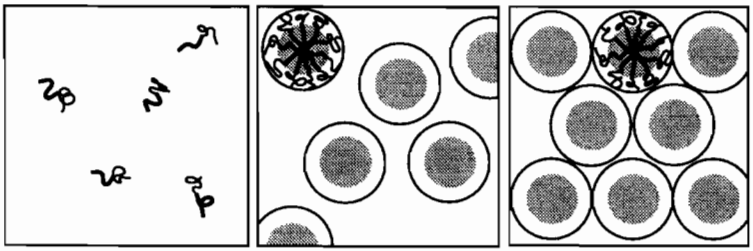

Fig. 3.1 Illustration of the critical micelle concentration (cmc) and critical gel concentration (cgc) in a block copolymer solution.

An early review of micellization in block copolymers was presented by Tuzar and Kratochvíl (1976), and these authors have recently provided an excellent review of the literature up to 1992 (Tuzar and Kratochvíl 1993). Micellar properties of block copolymers were also reviewed by Price (1982). A discussion of micellization was included in the general reviews on block copolymers by Riess *et al.* (1985) and Brown *et al.* (1989). Excellent reviews focussed on the solution properties of a particular class of copolymer, i.e. copolymers of poly(oxyethylene) with poly(oxypropylene) have been presented by Alexandridis and Hatton (1995) and by Chu (1995) and Chu and Zhou (1996). Micellization and micellar association in related poly(oxyethylene)/poly(oxybutylene) copolymers have been summarized by Booth *et al.* (1997).

In this chapter, the focus is largely on experimental and theoretical studies of micellization in a range of solutions of model block copolymers prepared by anionic polymerization. A discussion of both neutral and ionic block copolymers is included, and features specific to the latter type are detailed. The adsorption of block copolymers at the liquid interface is also considered in this chapter. Recent experiments on copolymer monolayers absorbed at liquid–air and liquid–liquid interfaces are summarized, and recent observations of surface micelles outlined. Thus this chapter is concerned both with bulk micellization and the surface properties of dilute copolymer solutions.

This chapter is organized as follows. The thermodynamics of the critical micelle concentration are considered in Section 3.2. Section 3.3 is concerned with a summary of experiments characterizing micellization in block copolymers, and tables are used to provide a summary of some of the studies from the vast literature. Theories for dilute block copolymer solutions are described in Section 3.4, including both scaling models and mean field theories. Computer simulations of block copolymer micelles are discussed in Section 3.5. Micellization of ionic block copolymers is described in Section 3.6. Several methods for the study of dynamics in block copolymer solutions are sketched in Section 3.7. Finally, Section 3.8 is concerned with adsorption of block copolymers at the liquid interface.

3.2 The critical micelle concentration

Micelles are formed by association of molecules in a selective solvent above a critical micelle concentration (cmc). Since micelles are a thermodynamically stable system at equilibrium, it has been suggested (Chu and Zhou 1996) that association is a more appropriate term than aggregation, which usually refers to the non-equilibrium growth of colloidal particles into clusters. There are two possible models for the association of molecules into micelles (Elias 1972, 1973; Tuzar and Kratochvíl 1976). In the first, termed open association, there is a continuous distribution of micelles containing 1,2,3, . . . , n molecules, with an associated continuous series of equilibrium constants. However, the model of open association does not lead to a cmc. Since a cmc is observed for block copolymer micelles, the model of closed association is applicable. However, as pointed out by Elias (1973), the cmc does not correspond to a thermodynamic property of the system, it can simply be defined phenomenologically as the concentration at which a sufficient number of micelles is formed to be detected by a given method. Thermodynamically, closed association corresponds to an equilibrium between molecules (unimers), A, and micelles, A_p, containing p molecules:

$$A \rightleftharpoons (1/p)A_p, \tag{3.2}$$

with an associated equilibrium constant

$$K = [A_p]^{1/p} / [A]. \tag{3.3}$$

For an advancement of the equilibrium from left to right by a fractional extent α, K is given by (Yang *et al.* 1995)

$$K = [\beta/(1-\alpha)](\alpha/p\beta)^{1/p}[A]^{(-1+1/p)}, \tag{3.4}$$

where $\beta = 1 - \alpha + \alpha/p$. If the association number is large ($1/p \to 0$) and independent of temperature (Hall 1987; Holtzer and Holtzer 1974) then $K \approx [A]^{-1}$ and the standard Gibbs energy of association is

$$\Delta_{\text{mic}} G^0 = -RT \ln K \approx RT \ln[A]. \tag{3.5}$$

Under this condition, for molecules and micelles in equilibrium just above the critical concentration (Attwood and Florence 1983)

$$\Delta_{\text{mic}} G^0 \approx RT \ln(\text{cmc}), \tag{3.6}$$

Otherwise eqn 3.4 must be used to obtain K. For a small association number, say $p = 10$, the error in approximating K by 1/cmc is large; calculation of $\Delta_{\text{mic}}G^\circ$ via eqn 3.6 requires $p \gtrsim 50$ (Hall 1987). For example, for $\alpha = 0.1$ and cmcs of 10^{-1} and 10^{-6} mol dm^{-3}, the error in $\Delta_{\text{mic}}G^0$ is 30 and 15% respectively. For a large association number, the standard enthalpy of micelle formation is then

$$\Delta_{\text{mic}} H^\circ = R \frac{\mathrm{d} \ln(\text{cmc})}{\mathrm{d}(1/T)}. \tag{3.7}$$

However, $\Delta_{mic}H^0$ and $T\Delta_{mic}S^0$, determined from the temperature dependence of the Gibbs energy, are less sensitive to the association number than is $\Delta_{mic}G^0$ itself (Yang *et al.* 1995). Assuming that $\Delta_{mic}H^0$ is approximately constant within a certain temperature range, eqn 3.7 can be integrated to yield

$$\ln(\text{cmc}) = \frac{\Delta H^0}{RT} + \text{const.} \tag{3.8}$$

Thus the logarithm of the cmc can be plotted against inverse temperature to extract information on the micellization enthalpy. Equivalently, the logarithmic concentration can be plotted against the inverse critical micelle temperature (Alexandridis *et al.* 1994*a*; Yang *et al.* 1994).

Experiments by Tsunashima *et al.* (1990) on a PS–PB diblock in dilute solutions in a range of solvents provide information on the processes associated with the cmc. These authors determined translational diffusion coefficients and hydrodynamic radii using dynamic light scattering (DLS). By using solvents isorefractive to either block, the dimensions of individual blocks could be determined. It was found that in three good solvents, the PS–PB dilock was molecularly dispersed and adopted a highly stretched conformation due to much stronger repulsive interactions between like segments than S–B segmental interactions. Intramolecular segregation of S and B subchains was never observed for the solutions in good solvents. However, in *n*-decane (selective for PB), conformational transitions were observed depending on the copolymer concentration, *c*. At low concentration, the PS–PB chains were molecularly dispersed and unimolecular micelles containing collapsed PS chains were formed. At a higher concentration, the copolymers coagulated intermolecularly to form spherical micelles with a PS core, thus defining the cmc.

The cmc is often determined from plots of the surface tension versus logarithmic concentration. The surface tension decreases rapidly with increasing concentration up to the cmc, above which there is a plateau. Examples are discussed in more detail in Section 3.3.2.

3.3 Experimental studies of block copolymer micelles

3.3.1 Introduction

The size and structure of block copolymer micelles can be obtained from a number of methods. Scattering techniques such as static light scattering (SLS) and small angle X-ray and small-angle neutron scattering (SAXS and SANS) are among the most powerful. The structural detail that can be resolved is inversely proportional to the magnitude of the scattering vector $q = 4\pi \sin\theta/\lambda$, where 2θ is the scattering angle and λ is the wavelength. Because it covers small q values, in the range $\approx 5 \times 10^{-3}$–$5 \times 10^{-2}\,\text{nm}^{-1}$, SLS only provides information on the radius of gyration of micelles, and not their internal structure. Furthermore, this is often an apparent value due to a different contrast between the core and the corona in a given solvent. On the other hand, SAXS and SANS cover wavenumbers $q \approx 3 \times 10^{-3}$ to $5\,\text{nm}^{-1}$ and can provide information on intramicellar

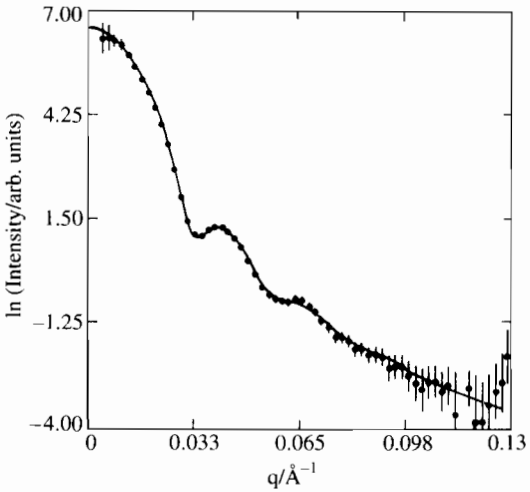

Fig. 3.2 Small-angle neutron scattering intensity as a function of wavevector magnitude for a *d*PS–PB diblock forming micelles in PB, $c = 5 \times 10^{-2}\,\mathrm{g\,cm^{-3}}$. *Symbols*, experimental results; *line*, theoretical scattering profile for a uniform sphere (Selb *et al.* 1983).

structure, for example by use of contrast variation via isotope labelling in SANS experiments to isolate scattering from the core or corona. Both techniques can also yield information on intermicellar ordering. The form factor of block copolymer micelles may be obtained from SAXS or SANS experiments. An example is illustrated in Fig. 3.2 which shows SANS data for a *d*PS–PB diblock micellar solution, together with a form factor calculated using a model of uniform spheres. SANS offers the advantage compared to SAXS that the scattering contrast within the system can be readily changed by mixing isotopically labelled and unlabelled solvent (and/or selective labelling of the block copolymer). A model for the form factor of micelles of block copolymers was developed by Pedersen and Gerstenberg (1996). They considered Gaussian chains attached to a uniform spherical core. Because coronal chains are excluded from the core, it was necessary to move the starting point of the Gaussian chains to a virtual position outside the core radius, which was found to mimic well the effect of non-penetration of the core. This model was applied successfully to SANS data from a dilute solution (2%) of a *d*PS–PI diblock in decane (Farago *et al.* 1993), and also to SAXS data from a PS–PI diblock and matched PS–PI–PS triblock in dibutyl phthalate (DBP) in the semidilute regime ($\phi = 0.14$ (Hamley *et al.* 1998) and $\phi = 0.20$ (Hamley *et al.* 1998; Lodge *et al.* 1996)).

The mass-average molar mass of the block copolymer solute, M_w, and the second virial coefficient, A_2, can be obtained from SLS. These quantities can be determined from the concentration dependence of the scattered light intensity using the relationship (cf. Section 1.4.10)

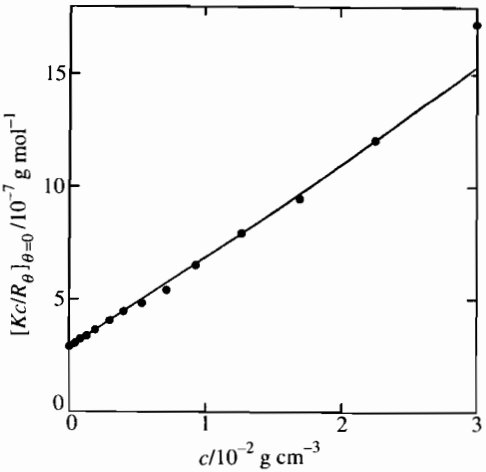

Fig. 3.3 Example of plot of Kc/R_θ, where K is an optical constant and R_θ is difference between the Rayleigh ratio of the solution and that of the pure solvent, vs. concentration. From an SLS experiment on a PS–PI diblock (M_w = 43 kg mol^{-1}, 81% PS) in dimethylacetamide at 26.5 °C (Booth *et al.* 1978).

$$Kc/R_{\theta=0} = 1/M_w + 2A_2c + \ldots, \tag{3.9}$$

where K is an optical coefficient and the Rayleigh ratio, $R_{\theta=0}$, is the excess intensity (relative to the molecular solution) of scattered radiation extrapolated to $\theta = 0$. Figure 3.3 shows a plot using eqn 3.9 to determine a micellar M_w and A_2 for a PS–PI solution. The second virial coefficient can also be obtained via membrane osmometry, which in addition provides the number-average molar mass M_n. Because this is, by definition, more sensitive to lower molar mass particles it is always lower than M_w.

In dynamic light scattering (DLS), or photon correlation spectroscopy, temporal fluctuations of the intensity of scattered light are measured and this is related to the dynamics of the solution. In dilute micellar solutions, DLS provides the z-average of the translational diffusion coefficient. The hydrodynamic radius, R_H, of the scattering particles can then be obtained from the Stokes–Einstein equation (eqn 1.2). The intensity fraction as a function of apparent hydrodynamic radius is shown for a triblock solution in Fig. 3.4. The peak with the smaller value of apparent hydrodynamic radius, $R_{H,app}$ corresponds to molecules and that at large $R_{H,app}$ to micelles.

Transmission electron microscopy (TEM) has been used to provide a direct image of block copolymer micelles that complements the indirect information obtained from scattering experiments. Because of the technical difficulties of obtaining electron micrographs from solutions it is not employed routinely. Price and co-workers (Booth *et al.* 1978; Price and Woods 1973) obtained specimens for TEM investigation by two methods. In the first (Price and Woods 1973),

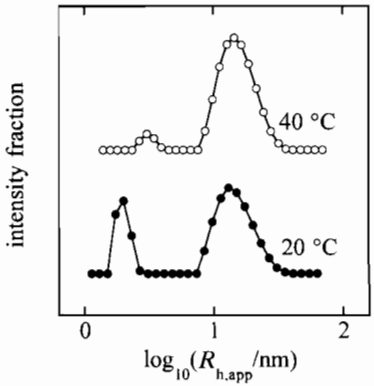

Fig. 3.4 Showing the coexistence of molecules and micelles via dynamic light scattering. Intensity fraction versus the apparent hydrodynamic radius for solutions of $PBO_5PEO_{39}PBO_5$ (120 g cm^{-3}, 20 and 40 °C) (Booth *et al.* 1997; Yang *et al.* 1996*a*). Here PBO denotes poly(oxybutylene) and PEO poly(oxyethylene). The peaks correspond to molecules (or molecular clusters) at small values of $R_{h,app}$ and to micelles at large values of $R_{h,app}$.

freeze-etching, a drop of solution was rapidly frozen by shock-cooling with liquid nitrogen. Solvent was then allowed to evaporate off from a freshly microtomed surface and a replica was made of any collapsed micelles on the frozen surface. In the second method (Booth *et al.* 1978), a drop of micellar solution was allowed to spread and evaporate on a carbon TEM substrate. The micelles were stained with osmium tetroxide prior to isolation to enhance contrast for TEM (see Fig. 3.5).

The distribution of micelles and unimers in a solution can be determined via gel permeation chromatography (GPC), also known as size exclusion chromatography (SEC). In this technique, a porous rigid gel is used in a separation process and fractionation occurs as particles of different hydrodynamic radius are eluted through the gel. The main disadvantage of this method is that it requires separate calibration because it is not an absolute method. In addition, serious concerns exist with this method because it has been observed that the unimer $\rightleftharpoons$ micelle equilibrium can be perturbed, and copolymer 'lost', possibly by adsorption within the GPC gel (Booth *et al.* 1978; Price *et al.* 1982; Teo *et al.* 1986). Booth and co-workers have developed a technique to circumvent this termed eluent GPC, where the block copolymer solution is used as an eluent instead of a simple solvent (Wang *et al.* 1992*a*, 1993*a*). When a solution of different concentration to the eluent is injected into the column, the solution is diluted as it passes through the column and the concentration approaches that of the eluent. Thus the mass distribution of molecules and micelles in the solution approaches that in the eluent at equilibrium. In other words, the injected solution probes the equilibrium state of the eluent.

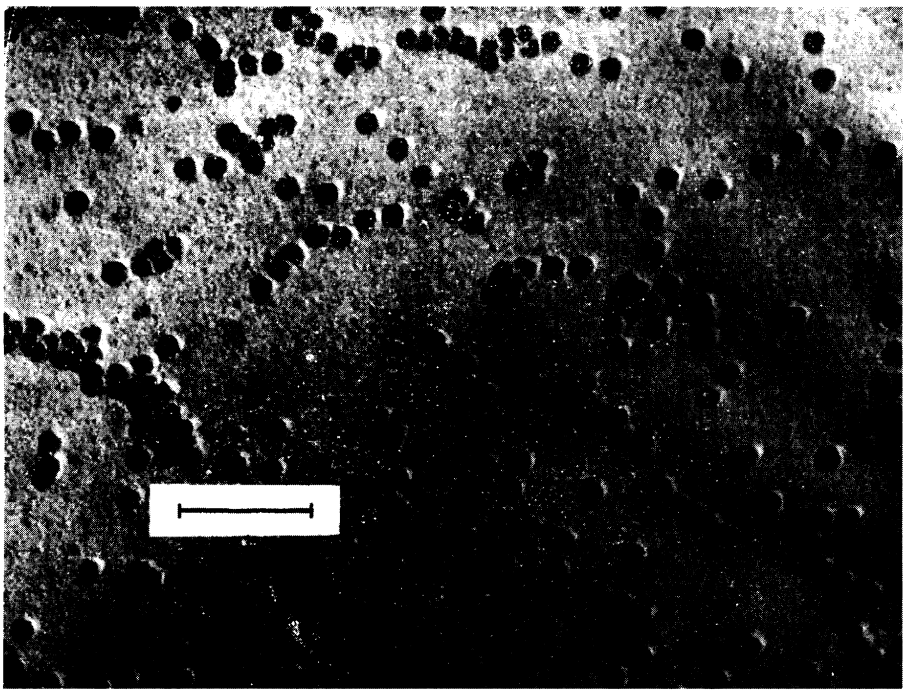

Fig. 3.5 A transmission electron micrograph of collapsed miclles isolated from a solution of a PS–PI diblock in dimethylacetamide (Booth *et al.* 1978). The micelles were stained with OsO_4 and lightly shadowed in the dry state with C/Pt. The scale bar indicates 200 nm.

Ultracentrifugation can be used to determine the weight fraction of micelles present in a solution via sedimentation velocity measurements. In this technique, the velocity at which a solute species is displaced under the influence of a strong centrifugal force is measured. The sedimentation velocity of a solute depends on its molecular weight, its buoyancy and friction coefficient and on the centrifugal force applied. Although this method depends on the continuously disturbed and re-established unimer $\rightleftharpoons$ micelle equilibrium during transport, it has been applied successfully to analyse micellization in block copolymer solutions. An example of a gradient curve showing sedimentation in diblock solutions is shown in Fig. 3.6.

Viscometry can provide information on the hydrodynamic properties of micellar systems. The intrinsic viscosity and Huggins coefficient, determined from the concentration dependence of the specific viscosity (eqn 1.9) are dependent on the micellar dimensions. The intrinsic viscosity gives the number-average hydrodynamic volume and the more compact the micelles, the lower the intrinsic viscosity and the higher the Huggins coefficient, k_H. It has frequently been reported that a decrease of intrinsic viscosity occurs on passing from a good to a selective solvent, indicative of micellization (Climie and White 1960; Demin *et al.* 1974*a*,*b*;

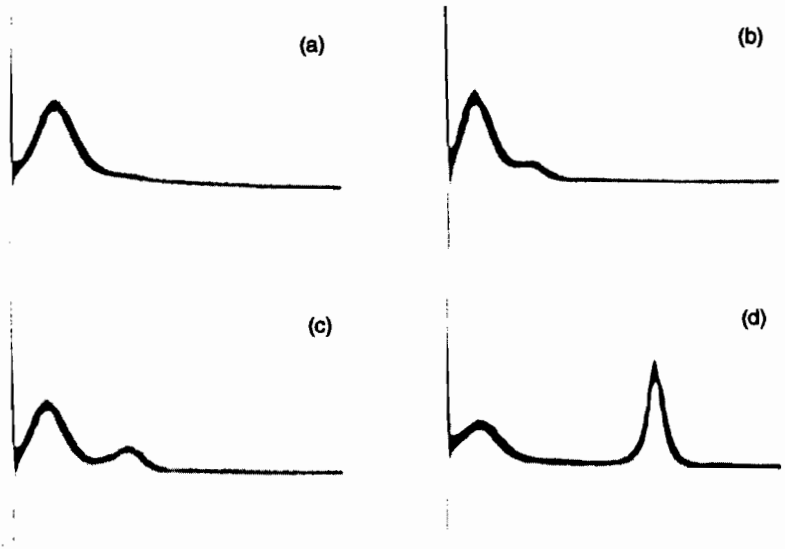

Fig. 3.6 Sedimentation velocity profiles for PS–poly(4-vinyl-*N*-ethylpyridinium bromide) (M_w = 33 kg mol^{-1}, 8% PS) in methanol/34% water/LiBr mixtures at different LiBr concentrations: (a) 0.01 M; (b) 0.015 M; (c) 0.02 M; (d) 0.1 M. From Selb and Gallot (1981b).

Gallot *et al.* 1963; Merrett 1957; Price *et al.* 1974; Tuzar and Kratochvíl 1972). The changes in quality of the solvent have been achieved either by varying the temperature in a one-component system or by adding a selective precipitant for one copolymer component, or by a combination of both procedures.

Other more 'exotic' techniques have been employed to study block copolymer micelles. For example, Price and co-workers used ultramicroscopy (Chapter 1) to determine diffusion coefficients and hydrodynamic radii of diblocks in selective solvents (Price *et al.* 1979).

3.3.2 Micellization in poly(oxyalkylene) block copolymers

Much recent work on micellization in block copolymers has been focussed on this industrially important type of polymer. We therefore describe experiments on micellization in aqueous solutions of poly(oxyalkylene) diblocks and triblocks in some detail. This serves to illustrate many of the important features of micellization of block copolymers, also observed in other systems such as the styrenic block copolymers covered in the following section.

Poly(oxyethylene)/poly(oxypropylene) copolymers

The micellization of water-soluble poly(oxyethylene)–poly(oxypropylene)–poly(oxyethylene), also known as poly(ethylene oxide)–poly(propylene oxide)–poly(ethylene oxide) (PEO–PPO–PEO) triblock copolymers, has been extensively studied due to the industrial applications of these materials arising from

their surfactant properties. Commercially, PEO–PPO–PEO copolymers are marketed as Pluracare (BASF) or Synperonic (ICI) polyols. The Pluracare series were formerly known as Pluronics and we adopt the old name, because this is the one used in the literature. Schmolka (1991) reports over 1000 articles on applications of these materials in the medical and pharmaceutical industries alone. The phase behaviour of PEO–PPO–PEO triblocks has recently been reviewed by Almgren *et al.* (1995) and Chu and Zhou (1996), who summarize recent results from a number of groups, and we do not repeat all the details here. Instead, the essential features of micellization in PEO–PPO–PEO triblocks are summarized, following Chu and Zhou (1996).

Micelle formation in PEO–PPO–PEO block copolymers in water is believed to be due to dehydration of the PPO block with increasing temperature, water being a selective solvent for PEO. This explains why the solution properties of Pluronic surfactants are strongly temperature dependent. For most commercially available PEO–PPO-PEO surfactants, the critical micelle temperature (cmt), at which micelles begin to form, is between 20 and 50 °C. The cmt increases with decreasing copolymer concentration (Chu and Zhou 1996). The number of oxypropylene repeats has a strong effect on micellization, copolymers with a larger hydrophobic PPO block forming micelles at much lower concentrations. Indeed, the critical micelle concentration (cmc) is found to decrease exponentially with the PPO block length (Alexandridis *et al.* 1994*a*; Chu and Zhou 1996; Wanka *et al.* 1994) (See Fig. 3.7). On the other hand, the PEO block has a smaller influence on the micellization (Chu and Zhou 1996; Mortensen and Brown 1993).

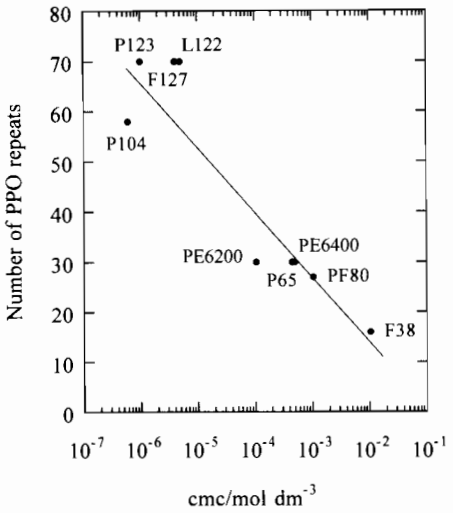

Fig. 3.7 Logarithm of the cmc value for aqueous solutions of $PEO_nPPO_mPEO_n$ blocks with different n values at 40 °C (Wanka *et al.* 1994). F38, $n = 42, m = 16$; PF80, $n = 73, m = 27$; PE6200, $n = 11$, $m = 30$; PE6400, $n = 13$, $m = 30$; P65, $n = 20$, $m = 30$; P104, $n = 17$, $m = 56$; L122, $n = 11, m = 70$; P123, $n = 20, m = 70$; F127, $n = 106, m = 70$.

An increase in the number of PEO units leads to a small increase in the cmc and cmt (Chu and Zhou 1996). The cmt and cmc decrease with increasing total molecular weight of the copolymer, if comparisons are made for a constant PPO/PEO ratio. The lower the relative PEO content, the larger is the influence of the total molar mass. By plotting the logarithmic cmc versus the reciprocal temperature (see eqn 3.8) a large positive enthalpy of micellization is derived of about 200–400 $kJ\,mol^{-1}$ (Chu and Zhou 1996, and references therein), whereas the standard free energy ($\Delta_{mic}G^{o}$) of micellization is about -24 to $-28\,kJ\,mol^{-1}$ (Alexandridis *et al.* 1994*a*). This demonstrates that in PEO–PPO–PEO solutions, the association process is entropy driven. Association numbers for micelles formed by Pluronic copolymers in the temperature range 20 to 50 °C vary between about 10 and 400 (Chu and Zhou 1996). Chain architecture has a great influence on the formation of micelles. For example, the tendency for micellization of a PPO–PEO–PPO copolymer is reduced compared to a PEO–PPO–PEO copolymer of the same composition (Zhou and Chou 1994), as discussed in the next section in the context of copolymers containing poly(oxybutylene) instead of poly(oxypropylene).

An intriguing phenomenon, known as anomalous micellization, has been reported by several groups on a variety of block copolymer systems (Chu and Zhou 1996; Tuzar and Kratochvíl 1993). In most cases, this anomaly is clearly observed during temperature-induced micellization and in some cases can be detected via the concentration dependence of micellization. The anomalous behaviour manifests itself as the presence of large particles before the onset of micellization, thus exhibiting a strong opalescent appearance. Several mechanisms have been proposed to explain the origin of this effect, such as the formation of elongated chains of associated monomolecular micelles, the coexistence of metastable worm-like structures with regular spherical micelles and the transient formation of emulsion droplets. For poly(oxyethylene) block copolymers, anomalous micellization has been most clearly observed for $PEO_{13}PPO_{30}PEO_{13}$ (Pluronic L64) (Peng and Zhou 1986; Zhou and Chu 1987, 1988). An analysis of dynamic light scattering data reveals the existence of large particles coexisting with either unimers or unimers and micelles. The large particles are estimated to constitute at most a few per cent of the total mass, but nevertheless dominate the solution properties. Chu and Zhou (Chu and Zhou 1996; Zhou and Chu 1987, 1988) provide evidence that anomalous micellization actually results from composition polydispersity of the copolymers. This could be large even for a copolymer with a narrow molar mass distribution. It is known that PEO–PPO–PEO triblocks are usually contaminated with small quantities of more hydrophobic block copolymers that appear as by-products in the preparation process (Ding *et al.* 1991). These minor components then become insoluble on varying temperature or concentration before the onset of micellization of the major component. To confirm that anomalous micellization is not a property of the block copolymer solution such as correlated concentration fluctuations (Price *et al.* 1986), Zhou and Chu (1987, 1988) performed filtration experiments to remove minor insoluble components. If anomalous behaviour was due to either local concentration fluctuations in the transition region or large elongated particles in

equilibrium with normal, spherical micelles, filtration would not remove it. However, experiments on L64 demonstrated that after filtration the anomalous region vanished and a normal transition was observed, thus confirming that composition heterogeneity is the origin of anomalous micellization (Reddy 1990*a*).

The surface activity and surface adsorption of PEO–PPO–PEO triblocks are also summarized by Chu and Zhou (1996). The physical characteristics of poly(oxyalkylene) block copolymers in solution, including wetting and foaming properties, have been reviewed by Nace (1996*a*), and Edens (1996) has summarized applications of these materials. Nace (1996*b*) has compared the surface activity and surfactant effectiveness of poly(oxyethylene)–poly(oxybutylene) diblocks and analogous PEO–PPO diblocks, the former being found to lower the surface tension more than the latter due to a lower cmc for the PEO–PBO analogues. The surface activity reflects the ability of the copolymer to reduce the surface tension of water, and surface adsorption relates to the tendency for solute to concentrate at the air–water interface. The absorbed amount and surface area per surfactant molecule at the air–water interface are provided via surface tension measurements as a function of the bulk concentration. This technique yields (i) the surface tension at the cmc, γ_{cmc}, (ii) the cmc/c_{20} ratio (where c_{20} is the copolymer concentration at which the water surface tension is lowered by $20\,mN\,m^{-1}$) which reflects the competition between micellization and adsorption, and (iii) the surface concentration at complete coverage or the surface area per copolymer molecule, A, at the cmc. The surface tension profile of Pluronic copolymers in aqueous solution is complex, particularly when a wide range of concentrations and a broad temperature range are covered. Prasad *et al.* (1979) made extensive surface tension measurements on seven Pluronic copolymers at 20 °C and observed two breaks in the surface tension curves. Hoffman and co-workers (Wanka *et al.* 1994) performed surface tension measurements also at different temperatures. They found that the temperature has a significant influence on the cmc and the area, A, at the cmc, whereas the surface tension value at the cmc shows little temperature dependence, as shown in Fig. 3.8. Alexandridis *et al.* (1994*b*) also observed two breaks in the concentration curve of the surface tension (Fig. 3.9), the lower concentration one being ascribed to collapse of the copolymer molecules at the air–water interface and the second to the formation of micelles. Chu and Zhou (1996) summarize the surface-active behaviour and surface absorption of PEO–PPO–PEO triblocks as follow. (i) At complete surface coverage, the area occupied by a copolymer molecule increases with increasing temperature. (ii) The area per molecule increases with the number of EO units in the chain, showing a scaling relationship $A \propto N_{EO}^{\nu}$, with $\nu = 0.43$ (Alexandridis *et al.* 1994*b*). (iii) An increase in the PPO block length at fixed PEO block length leads to a decrease in the area occupied by each copolymer molecule. (iv) An increase in the cmc/c_{20} ratio indicates that micellization is inhibited more than adsorption, or that adsorption is facilitated more than micellization. This ratio ranges between 100 and 40000 for Pluronic surfactants at 25 °C, increasing with increasing PEO length, but decreasing with increasing PPO block length and increasing temperature. (v) For Pluronics with two breaks in the γ–log$c$ curve, the separation between them decreases with

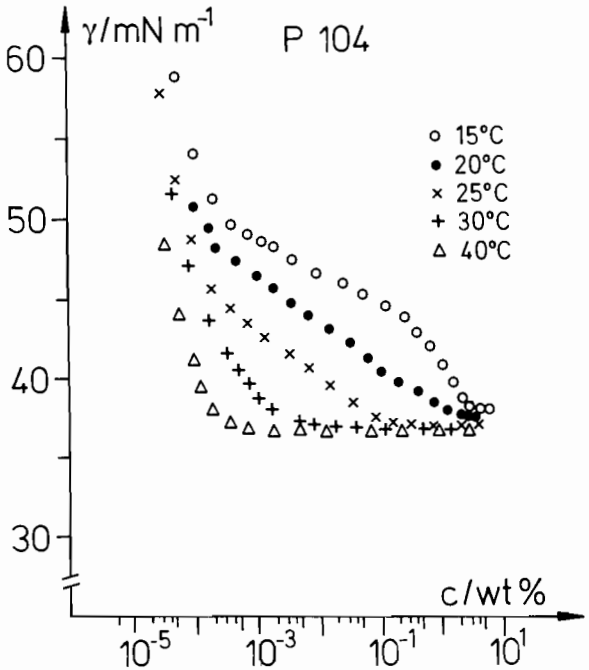

Fig. 3.8 Surface tension, γ, as a function of concentration for Pluronic P104 ($PEO_{17}PPO_{56}PEO_{17}$) at various temperatures (Wanka *et al.* 1994).

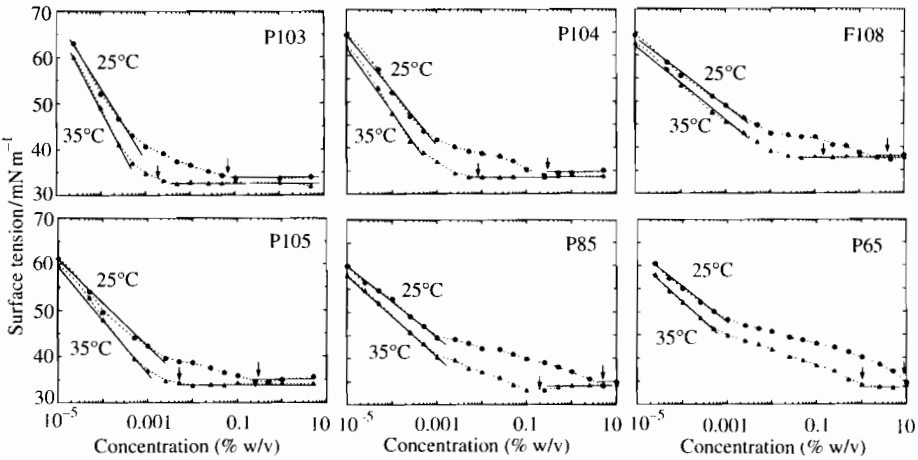

Fig. 3.9 Surface tension data for Pluronic solutions as a function of concentration at two temperatures (25 and 35 °C) (Alexandridis *et al.* 1994*b*). P103, $PEO_{17}PPO_{56}PEO_{17}$; P104, $PEO_{27}PPO_{56}PEO_{27}$; F108, $PEO_{132}PPO_{56}PEO_{132}$; P105, $PEO_{37}PPO_{56}PEO_{37}$; P85, $PEO_{26}PPO_{39}PEO_{26}$; P65, $PEO_{19}PPO_{30}PEO_{19}$. The arrows mark the cmc obtained using dye solubilization experiments.

increasing temperature and finally vanishes at about 40 °C. this appears to be associated with the enhanced micellization tendency at high temperature.

The solubilization behaviour of PEO–PPO–PEO triblocks has been investigated for a number of solubilizates. Solubilization is defined as the enhanced solubility of a substance (called solubilizate) that is normally insoluble in the solvent, by reversible interaction with the micelles of a surfactant (called solubilizer) (Zhou and Chu 1987, 1988). Solubilization is relevant in many areas such as detergency, emulsion polymerization and separation processes. In general, aromatic hydrocarbons are selectively solubilized over aliphatic hydrocarbons by Pluronics (Nagarajan *et al.* 1986). The presence of the solubilizate increases the association tendency of the copolymer surfactant. The influence of copolymer composition and structure on the solubilization has been studied using polycyclic aromatic hydrocarbons (Hurter and Hatton 1992). It was found that the solubilized amount increases with increasing PPO content and increasing total copolymer molecular weight.

Poly(oxyethylene)/poly(oxybutylene) copolymers

Micellization and gelation in aqueous solutions of poly(oxyethylene)–poly(oxybutylene) copolymers have been investigated by Booth and co-workers in Manchester since the late 1980s. Denoting the poly(oxyethylene) or poly(ethylene oxide) block by PEO and the poly(oxybutylene) (or poly(butylene oxide)) block by PBO, they have performed systematic studies on PEO–PBO diblocks, PEO–PBO–PEO and PBO–PEO–PBO triblocks, and cyclic copolymers using light scattering (static and dynamic), NMR, GPC, rheology, polarized light microscopy, surface tension and DSC. Much of this work is summarized in a recent review aricle (Booth *et al.* 1997). The Dow Chemical Company has produced a range of water-soluble PEO–PBO–PEO triblock and PEO–PBO diblock copolymers for surfactant applications. Two copolymers with higher M_n that have low water solubilities are useful as emulsifiers. Compared to the poly(oxypropylene) in PEO–PPO–PEO Pluronic triblocks, poly(oxybutylene) is less polar and consequently more soluble in oil phases. This polarity difference partly explains why surface and interfacial tension lowering is more effective for PEO–PBO copolymers compared to PEO–PPO copolymers. A minimum of four poly(oxybutylene) units is required to ensure micellization at accessible concentrations, compared to 10–13 PPO units in a PEO–PPO–PEO triblock. The association of commercial PEO–PBO copolymers has been investigated by Booth and coworkers (Yu *et al.* 1996*a*). They used static and dynamic light scattering to determine the cmc and the micellar hydrodynamic radius, molar mass, association number and expansion (swelling) factors for $PEO_{18}PBO_9$, $PEO_{43}PBO_{14}PEO_{43}$, $PEO_{13}PBO_{10}PEO_{13}$ and $PEO_{33}PBO_{10}PEO_{33}$.

Critical micelle concentrations for a range of PEO–PBO, PBO–PEO (here the block order reflects the synthesis sequence), PEO–PBO–PEO, PBO–PEO–PBO and cyclo-PBO–PEO ring copolymers are listed by Booth *et al.* (1997). Polymerization of PEO second (PBO–PEO diblock) leads to a broader PEO block length distribution, which in turn leads to a difference, for example, in surface tension (this is illustrated for $PEO_{41}PBO_8$ and PBO_8PEO_{41} by Booth *et al.*

(1997)). For all copolymer architectures, the cmc is found to decrease with increasing temperature, as expected. Micellar association numbers and radii are also tabulated in Booth *et al.* (1997). This reveals that the cmc and association number p are primarily determined by the length of the PBO block. Although marked trends are not evident, a small increase in the cmc and decrease in p with increase in PEO block length at fixed PBO block would be consistent with the behaviour of PEO–PPO (Chu and Zhou 1996) and PEO–PM (Reddy *et al.* 1990*b*) copolymers in aqueous solution (here PM denotes a methylene block). As for PEO–PPO copolymers, the association number increases with increasing temperature as the solvent becomes poorer. Hydrodynamic radii are found not to be very temperature dependent, which results from a balance between an increase in p and a decrease in swelling of the PEO-block fringe (Attwood *et al.* 1985), as also observed for PEO/PPO copolymers. The thermodynamics of micellization have also been investigated by the Manchester group (Booth *et al.* 1997). The enthalpy of micellization was determined for a number of solutions, via plots of log(c) vs. 1/cmt (which is equivalent to log(cmc) vs. $1/T$ following eqn 3.8), as shown in Fig. 3.10. This yields enthalpies in the range $\Delta_{mic}H^{o} = 24$–$125\,kJ\,mol^{-1}$ (Booth *et al.* 1997), which are lower than those obtained for PEO–PPO copolymers. However, standard Gibbs energies in the range $\Delta_{mic}G^{o} \approx -10$–$-30\,kJ\,mol^{-1}$ (between 20 and 40 °C) (Booth *et al.* 1997) are comparable to those for PEO/PPO copolymers. These results indicate that micellization of PEO–PBO copolymers in water is entropy driven, consistent with the hydrophobicity of the PBO block. Booth *et al.* (1997) noted that $\Delta_{mic}H^{o}$ per mole of BO units is significantly lower for long blocks (1–$3\,kJ\,mol^{-1}$) than for shorter blocks (7–$16\,kJ\,mol^{-1}$). This has been attributed to the long blocks (especially in the PEO/PBO and PBO–PEO–PBO architectures) being in a tightly coiled conformation, so that the interaction with water via hydrophobic interactions is reduced compared to that for the shorter blocks (Bedells *et al.* 1993; Tanodekaew *et al.* 1993), i.e. the copolymer may exist as a monomolecular micelle. This argument

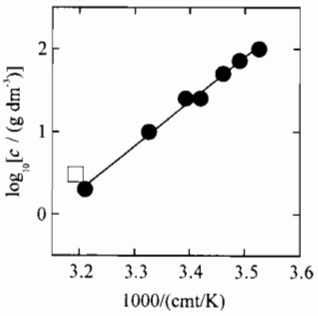

Fig. 3.10 Logarithm of concentration vs. reciprocal of the critical micelle temperature for aqueous solutions of triblock copolymer $PEO_{21}PBO_8PEO_{21}$ (Booth *et al.* 1997; Yang *et al.* 1994). The unfilled data point is log(cmc) from surface tension plotted against reciprocal temperature.

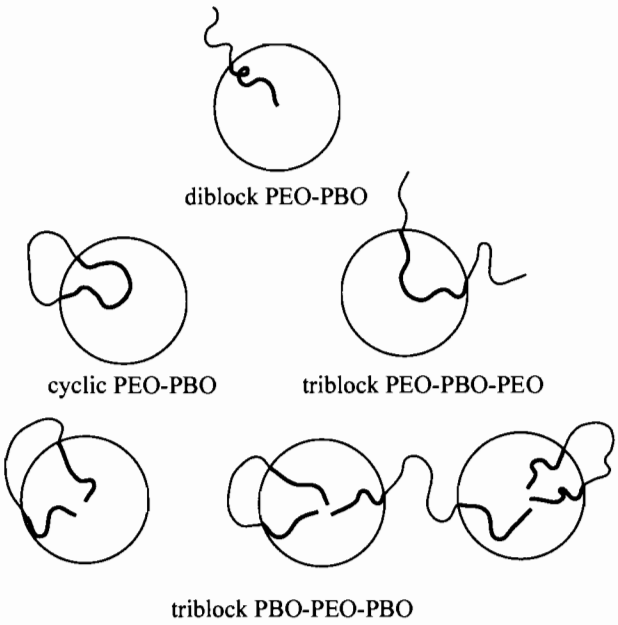

Fig. 3.11 Schematic representation of chain conformation in micelles formed from linear diblock copolymers, cyclic diblock copolymers and linear triblock copolymers (Booth *et al.* 1997).

has also been used (Bedells *et al.* 1993) to explain the smaller enthalpies of micellization of BO-containing copolymers compared to PO-containing copolymers. In other words, the more hydrophobic PBO blocks lead to a tightly coiled conformation so that interaction with water molecules via hydrogen bonding is much reduced compared to the less hydrophobic PPO block.

The influence of chain architecture has been investigated more extensively for PEO/PBO copolymers than for related systems such as PEO/PPO copolymers due to the wider range of polymers synthesized by the Manchester group (Booth *et al.* 1997). A schematic illustration of micelles formed from copolymers with different architectures is shown in Fig. 3.11 (Booth *et al.* 1997). Compared to diblock copolymers, the triblock and cyclic copolymers are entropically disfavoured in the micellar state, the restriction being that two block junctions per molecule must reside in the core–fringe interface. Making comparisons at constant composition and chain length, this means that the cmc of a linear diblock must be significantly lower than those of other architectures. In addition, the maximum possible radius of spherical micelles formed from a linear diblock will be twice (or more) that of micelles formed from copolymers of the other architectures, i.e. the association number and radius of the diblock will be large. Compared to triblocks p is larger by a factor of $2^3 = 8$ and R_H (or the thermodynamic radius, R_t) by a factor of 2. These trends are confirmed by experimental results

for PEO–PBO (Deng *et al.* 1995; Li *et al.* 1997; Yang *et al.* 1994, 1995), PEO–PBO–PEO (Luo *et al.* 1992; Yang *et al.* 1995; Yu *et al.* 1996*a*) and PBO–PEO–PBO (Yang *et al.* 1994, 1996*a*) copolymers. A cyclic copolymer in a micelle experiences the greatest conformational restriction, since both of its blocks must loop, whereas only one block of the linear triblock copolymers must loop, either in the core (PEO–PBO–PEO–) or the fringe (PBO–PEO–PBO–). However, because a cyclic copolymer is restricted in both unassociated (solution) and micellar states, the additional contribution to the Gibbs free energy from this effect is likely to be small (Booth *et al.* 1997). Comparisons of experimental results for cyclic PBO–PEO and PEO–PBO–PEO copolymers showed that the cyclic copolymers formed larger micelles than their linear triblock counterparts, and had lower cmcs (Yu *et al.* 1996*b*,*c*).

The effect of copolymer architecture is also manifested in the bridging of chains between micelles that is possible for PBO–PEO–PBO copolymers, as shown, for example, by dynamic light scattering (Booth *et al.* 1997; Yang *et al.* 1996*a*,*b*; Zhou *et al.* 1996*a*,*b*,*c*). Zhou *et al.* (1996*c*) performed light scattering experiments on $PBO_{12}PEO_{260}PBO_{12}$ in aqueous solution and observed that closed association of micelles occurs in dilute solution, with the cmc decreasing with increasing temperature. However, even in relatively dilute solutions (1–2% w/v), secondary associates were formed, as shown by DLS which revealed a mode corresponding to associates with a size up to 100 nm at a concentration 20 mg cm^{-3}, as shown in Fig. 3.12. The secondary associates increase in both number and size with increasing concentration and temperature and were ascribed to the formation of open, branched structures due to bridging of micelles by the long PEO blocks. This leads to highly viscous solution at concentrations as low as 4%, and a marked increase of viscosity with temperature (Zhou *et al.* 1996*c*).

Critical micelle concentration data for PEO_mPBO_n and $PBO_{n/2}PEO_mPBO_{n/2}$ copolymers are plotted as a function of n in Fig. 3.13 (Booth *et al.* 1997). Comparison of data for the copolymers indicates that the cmc at a given value of n is approximately two orders of magnitude lower for the diblocks due to the conformational entropy arguments discussed above. The slopes, however are similar and correspond to an increment in $\Delta_{mic}G^{\circ}$ of approximately 2.7 kJ (mol B units)$^{-1}$. The cmc for $PEO_{m/2}PBO_nPEO_{m/2}$ diblocks is intermediate between values for the other two architectures, although the situation is complicated by the broader PEO-block length distribution for these molecules. That p directly reflects the core volume, which is expected to be in the ratio 8:1 for a diblock versus triblock copolymer, is illustrated by Fig. 3.14, although p values for $PEO_{m/2}PBO_nPEO_{m/2}$ copolymers with $n \leq 10$ are higher than expected, which reflects the wide PEO block length distribution. The hydrodynamic radius depends largely on the PEO fringe block length in PEO/PBO micelles because the core is very small. Comparing cyclic copolymers with linear triblock analogues, Booth *et al.* (1997) conclude that micellization is favoured in the cyclic copolymer compared to the triblock.

The effect of adding salt to aqueous solutions of a PEO/PBO copolymer has been investigated (Deng *et al.* 1995), as it has for PEO/PPO Pluronics. Static and

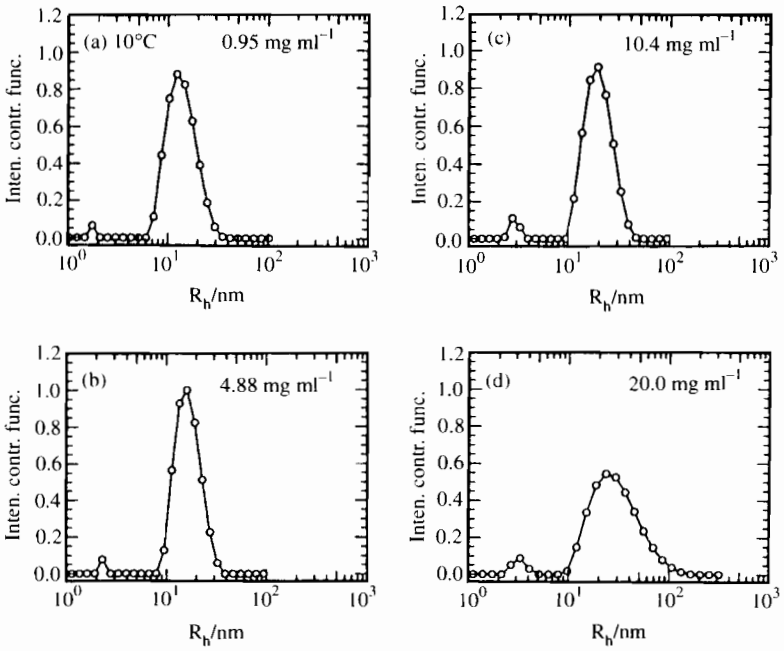

Fig. 3.12 Intensity contribution function, extracted from dynamic light scattering intensities, versus apparent hydrodynamic radius for $PBO_{12}PEO_{260}PBO_{12}$ in aqueous solution at 10 °C and different concentrations (indicated) (Zhou *et al.* 1996*c*).

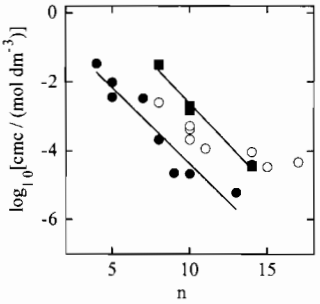

Fig. 3.13 Log(cmc) versus number of PBO units (n) in copolymer for aqueous solutions of PEO–PBO block copolymers at 30 °C: (●) PEO_mPBO_n; (■) $PBO_{n/2}PEO_mPBO_{n/2}$; (○) $PEO_{m/2}PBO_nPEO_{m/2}$ (Booth *et al.* 1997).

dynamic light scattering data for $PEO_{40}PBO_{10}$ indicate that adding salt reduces the excluded volume of the micelles. The concentration dependences of micellar dimensions obtained by Deng *et al.* (1995) are consistent with the PEO block fringe approaching the theta condition as the concentration of salt is increased.

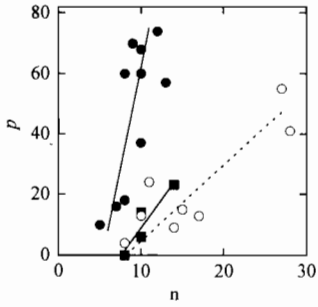

Fig. 3.14 Association number (p) as a function of number of PBO units (n) in the copolymer for aqueous solutions of E/B block copolymers at 30 °C: (●) PEO_mPBO_n; (■) $PBO_{n/2}$ $PEO_mPEO_{n/2}$; (○) $PEO_{m/2}PEO_nPEO_{m/2}$ (Booth *et al.* 1997).

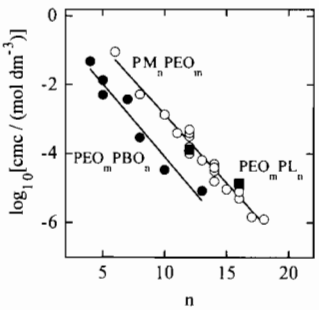

Fig. 3.15 Log(cmc) versus hydrophobic block length for aqueous solutions at 25 °C of: (●) PEO_mPBO_n; (○) PM_nPEO_m; (■) PEO_mPL_n copolymers (Booth *et al.* 1997).

The Manchester group (Booth *et al.* 1997; Yang *et al.* 1995) has also compared the cmc and association number of PEO–PBO diblocks with PEO–PL diblocks and PM–PEO diblocks, where PM denotes poly(methylene) and PL = poly(DL-lactide). Poly(oxyethylene)–polyester block copolymers such as PEO–PL diblocks are of interest because the polyester block is potentially biodegradable through hydrolysis of the ester link (Tanodekaew *et al.* 1997). Plots of the cmc versus n have similar slopes for all three types of copolymer, indicating that PBO, PM and PL groups make similar incremental contributions to the Gibbs energy of micellization (Fig. 3.15). For the association number, the major determinant is the length of the hydrophobic block, giving similar slopes for the PBO and PL blocks where each unit contributes three backbone atoms, and a lower slope for the PEO_mPM_n copolymers where each unit contributes one backbone atom. For $PEO_mPPO_nPEO_m$ triblocks (Alexandridis *et al.* 1994*b*; Wanka *et al.* 1994; Yu *et al.* 1992), the cmc data versus n can be brought into coincidence with that for $E_nB_mE_n$ triblocks by plotting the latter data versus $4n$ (Yang *et al.* 1995), i.e. one BO unit is equivalent to four PO units. The same adjustment also brings the data for p

into approximate agreement. The relative hydrophobicities of the four types of unit studied have been placed in the ratios BO:M:L:PO 4:3:3:1 (Booth *et al.* 1997).

3.3.3 Micellization of styrenic block copolymers

Because the essentials of micellization have been discussed in depth for poly(oxyethylene)-containing block copolymers, we do not describe experimental studies on styrenic block copolymers in solution in great detail. Instead, the features are summarized in tabular form (see Tables 3.1–3.4). Experiments on ionic block copolymers containing polystyrene are discussed in Section 3.6.2.

3.3.4 Other block copolymers in solution

Only a limited number of studies of micellization have been performed using non-ionic block copolymers that do not contain PS or belong to the PEO–containing class. Notable examples include the early observation of micellization via viscosity and turbidity measurements in solutions of PMMA–poly(acrylonitrile) diblocks in dimethylformamide (DMF) and DMF/benzene mixtures, which are selective solvents for PMMA (Climie and White 1960). The micellar structure of a PEO–poly(2-hydroxyethyl methacrylate) diblock (M_n = 9.5 kg mol^{-1}, 10.4% PHEMA) was investigated in water, a selective solvent for PEO, by Ikemi *et al.* (1981). They used SAXS and fluorimetric measurements to determine the detailed micellar structure, including the core radius, the core–shell interfacial width and the radius of gyration.

The solution properties of some ionic block copolymers that do not contain PS are discussed in Section 3.6.3.

3.3.5 Mixed micelles

Hybridization can occur in solutions of block copolymer micelles of different sizes, when small micelles grow at the extent of large ones (Tian *et al.* 1993). Thermodynamic considerations predict that for two similar copolymers, the lowest Gibbs energy is obtained for the system with fully hybridized, uniform micelles. However, as the dissimilarity between the copolymer sizes increases, it becomes increasingly difficult to accommodate the chains in the same micelles. The situation is similar for liquid mixtures. As the interaction between components becomes increasingly unfavourable, demixing occurs into two phases with composition depending on the change in Gibbs energy. By analogy, a mixture of two dissimilar block copolymers in a selective solvent will produce two types of hybridized micelles. This was investigated for micelles formed by PS–poly(methacrylic acid) diblock and triblock copolyelectrolytes in water–dioxane mixtures, this combination being a selective solvent for PS (Tian *et al.* 1993). Sedimentation velocity measurements were made by ultracentrifugation following the mixing of micellar solutions with micelles of different size and sedimentation coefficient. Using static and dynamic light scattering and surface tension measurements, Yang *et al.* (1996*b*) provided evidence for the formation

Table 3.1 Studies of PS–PB block copolymers in solution

M (kg mol^{-1}) and composition of polymer(s)[a]	Solvent (quality)[b]	Nature of study[c]	Techniques[d]	Reference
PS–PB–PS M_w = 135–165, 9–70%	Dioxane + ethanol (selective for PS)	Measurement of viscosity and k_H. Determination of micellar M_w and cmc	Viscometry, DR, SLS	Tuzar and Kratochvíl (1972)
PS–PB–PS M = 140, 26% M = 140, 52%	Dioxane + ethanol PB solubilizate	Solubilization of PB. Determination of micellar R_g and M	Viscometry, SLS	Tuzar and Kratochvíl (1973)
PS–PB–PS M_w = 140, 51%	MEK (selective for PS)	Determination of micellar R_g and M	SAXS	Plěstil and Baldrian (1973)
PS–PB M_n = 64.7, 24%	Heptane (selective for PB)	Determination of micellar R_B, R_g and M	SAXS	Plěstil and Baldrian (1975)
PS–PB–PS M_w = 56.1, 50% M_w = 66.5, 29% M_w = 97.9, 29%	Butanone (selective for PS)	Determination of micellar M_w	SLS	Krause and Reismuller (1975)
PS–PB–PS M = 120–160, 9–90%	Isopropyl acetate (selective for PS)	Anomalous micellization (large particles observed at onset of micellization)	SLS, sed. vel.	Tuzar *et al.* (1977)
PS–PB–PS M = 89, 17%	$CDCl_3$, toluene (non-selective) Dimethoxyethane (selective for PB) Ethyl acetate (selective for PS)	Chain dynamics of PB block via ^{13}C NMR	NMR	Heatley and Begum (1977)
PS–PB–PS M_n = 141, 27% M_n = 84, 26%	MEK	Determination of micellar M, p and R_g	SLS	Enyiegbulam and Hourston (1978)
PS–PB–PS M_w = 220, 50%	THF + 2-methoxy ethanol (selective for PS)	Cross-linking of micelles via photochemical stabilization. Characterization of micellar M_w	SLS, sed. vel.	Procházka *et al.* (1979)

Table 3.1 *Continued*

M (kg mol^{-1}) and composition of polymer(s)[a]	Solvent (quality)[b]	Nature of study[c]	Techniques[d]	Reference
PS–PB–PS M_w = 70, 10% M_w = 101, 14%	Ethyl acetate	Formation of worm-like micelles from spherical micelles, associated with cloud point	Turbidometry, TEM, SLS	Canham *et al.* (1980)
PS–PB–PS 33–80%	Dioxane + ethanol THF + allyl alcohol (selective for PS) Solubilization of PB and PS–PB–PS triblock	Micellar structure with solubilizate	SLS	Tuzar *et al.* (1982)
PS–PB M_n = 56, 24%	Heptane	Monomeric mobilites via high-resolution proton NMR	NMR	Spěváček (1982)
PS–PB–PS M_n = 100, 42%	1,4-Dioxane with few vol% D_2O (selective for PS)			
PS–PB M_n = 52–294, 11–88%	*n*-Tetradecane (selective for PB) DBP (selective for PS)	Investigation of onset of micellar ordering	Rheometry, SAXS	Reviewed in Watanabe and Kotaka (1984)
PS–PB M_w = 77, 29% M_w = 83, 14% M_w = 105.5, 12%	Heptane	Micellar R_g	SAXS	Bluhm and Whitmore (1985)
PS–PB M = 185, 50 mol%	DMA (selective for PS)	cmc, $\Delta_{mic}H^o$ and $\Delta_{mic}G^o$. Micellar R_H and M_w	DLS, SLS	Zhou *et al.* (1993)
PS–PB M_w = 204, 50 mol%	DMA	cmc, $\Delta_{mic}H^o$ and $\Delta_{mic}G^o$. Micellar diffusion coefficients, R_H, R_g, M_w, p and A_2	DLS, SLS	Zhou *et al.* (1994, 1995)

[a] Composition in wt% PS unless otherwise specified.

[b] Abbreviations: MEK, methyl ethyl ketone; THF, tetrahydrofuran; DBP, dibutyl phthalate; DMA, dimethylacetamide.

[c] Abbreviations: K_H Huggins coefficient; M, molar mass; R_g radius of gyration; R_B, core radius; p, association number; $\Delta_{mic}H^o$, standard enthalpy of micellization, $\Delta_{mic}G^o$, standard Gibbs energy of micellization; A_2, second virial coefficient; R_H, hydrodynamic radius.

[d] Abbreviations: DR, differential refractometry; SLS, static light scattering; DLS, dynamic light scattering; SAXS, small-angle X-ray scattering; TEM, transmission electron microscopy.

Table 3.2 Studies of PS–PI block copolymers in solution

M (kg mol^{-1}) and composition of polymer(s)[a]	Solvent (quality)[b]	Nature of study[c]	Techniques[d]	Reference
PS–PI M = 57, 25% $(PS–PI)_4$ M = 208, 25%	White oil (selective for PB)	Technique for imaging micelles	TEM	Price and Woods (1973)
PS–PI M_n = 21–50, 25–81%	Hexane (selective for PI) DMF (selective for PS)	Viscosity measurements. Determination of micellar p and M_n	Viscometry, osmometry, sed. vel.	Periard *et al.* (1973)
PS–PI M = 64, 25%	Decane (selective for PI)	Viscosity measurements. Determination of micellar M_w, R_H and D	SLS, DLS, Viscometry	Price *et al.* (1974)
PS–PI M_w = 43, 81%	DMA (selective for PS)	Determination of micellar polydispersity, M_w and R_g.	GPC, TEM, DLS	Booth *et al.* (1978)
PS–PI M_w = 170, 52%	DMA	Measurement of diffusion coefficient and R_H	Ultramicroscopy, DLS	Price *et al.* (1979)
PS–PI M_w = 54, 24%	Decane			

Table 3.2 *Continued*

M (kg mol^{-1}) and composition of polymer(s)[a]	Solvent (quality)[b]	Nature of study[c]	Techniques[d]	Reference
PS–PI Range: M_n = 29–53, 31–62%	DMF, DMA, MEK (selective for PS) Heptane, octane, decane and dodecane (selective for PI)	Viscosity measurements. Determination of micellar R_H, p, R_B and R_A	DLS, viscometry, NMR	Bahadur *et al.* (1985)
PS–PI Range: M_w = 4.5–70, 31–55%	Heptane	Determination of micellar R_g	SAXS	Bluhm and Malhotra (1986)
PS–PI–PS M_w = 165, 27%	Heptane	Observation of loose 'branched' structures rather than micelles	SLS, DLS, SANS, viscometry	Raspaud *et al.* (1994)
PS–PI M_w = 11, 36%	methylcyclohexane (selective for PI)	Determination of cmt, R_g and R_H	SLS, DLS	Adam *et al.* (1996)
PS–PI M_w = 60, 20%	DBP	Study of ODT and structure of elongated micelles	Rheometry, SAXS	Hamley *et al.* (1998)
PS–PI–PS M_w = 120, 20%				

[a] Composition in wt% PS unless otherwise specified.
[b] Abbreviations as Table 3.1 + DMF, dimethylformamide.
[c] Abbreviations as Table 3.1 + D, diffusion coefficient; R_A, corona radius.
[d] Abbreviations as Table 3.1 + GPC, gel permeation chromatography; SANS, small-angle neutron scattering.

Table 3.3 Studies of PS–PMMA block copolymers in solution

M (kg mol^{-1}) and composition of polymer(s)[a]	Solvent (quality)[b]	Nature of study[c]	Techniques[c]	Reference
PMMA–PS–PMMA M_w = 440, 59% M_w = 17, 40% M_w = 14, 60% M_w = 35, 71%	Cyclohexane, dioxane and mixtures (selective for PS)	Measurement of viscosity. Determination of micellar M_w, k_H and R_g.	Viscometry, SLS	Gallot *et al.* (1963)
PMMA–PS–PMMA M_n = 316	Butanone, toluene (neutral) Acetone (selective for PMMA) Triethyl benzene (selective for PS)	Viscosity measurements. Micellization in acetone, triethyl benzene (not butanone or toluene): micellar R_g and A_2	SLS, viscometry	Krause (1964)
PS–PMMA M = 30, 45%	*p*-Xylene (selective for PS)	Determination of micellar M_w, R_g and A_2	SLS	Tanaka *et al.* (1972)
PMMA–PS–PMMA M = 147.4, 41%				
PS–PMMA PMMA–PS–PMMA M_n = 55–390, 36–85%	Range of selective solvents	Viscosity measurements. Determination of micellar M_w	Viscometry, sed. vel.	Kotaka *et al.* (1972)

Table 3.3 *Continued*

M (kg mol^{-1}) and composition of polymer(s)[a]	Solvent (quality)[b]	Nature of study[c]	Techniques[c]	Reference
PS–PMMA 40–60 mol%	Ethanol + dioxane (dioxane selective for PS, ethanol selective for PMMA)	Observation of micellization	Viscometry	Demin *et al.* (1974)
PS–PMMA–PS M = 98, 29%	Ethyl acetate	Observation of clouding	SLS	Lally and Price (1974)
PS-PMMA M_w = 640–1500, 24–69% PMMA–PS–PMMA M_w = 110, 50%	Toluene + *p*-cymene (selective for PS)	Micellar shape transition as a function of toluene/*p*-cymene mixture composition.	SLS	Kotaka *et al.* (1978)
PS–PMMA M_n = 46–375, 18–88%	*n*-Alkanes (selective for PB) DMF, DMA, MEK (selective for PS)	Viscosity measurements. Determination of R_H and *p*. Study of solutilization of PS and PB homopolymers	DLS, viscometry, ^{1}H NMR	Oranli *et al.* (1985)
PS–PMMA M = 160, 49% M = 196, 43%	*p*-Xylene (selective for PS)	Determination of micellar structure (R_B)	SANS, osmometry, viscometry	Edwards *et al.* (1986)

[a] Composition in wt% PS unless otherwise specified.
[b] Abbreviations as Table 3.2.
[c] Abbreviations as Table 3.1.
[d] Abbreviations as Table 3.2.

Table 3.4 Studies of other styrenic block copolymers in solution

Polymer	M (kg mol^{-1}) and composition of polymer(s)[a]	Solvent (quality)[b]	Nature of study[c]	Techniques[d]	Reference
PS–PEO	M_w = 17–74, 26–91%	Ethyl benzene (selective for PS)	Observation of micelles	SLS, birefringence, dielectric constant (Kerr effect) measurements	Franta (1966)
PS–PEO PEO–PS–PEO	M_n = 14–91, 30–35% M_n = 13–109, 37–31%	Water (selective for PEO)	Determination of micellar M_w and p	SLS	Riess and Rogez (1982)
PS–PEO	Range: M_n = 17–109, 5–56 mol%	Toluene + propan-2-ol + water mixtures	Turbidity and R_H measurements	Turbidometry, DLS	Barker and Vincent (1984)
PS–PEO	M = 187.5, 96% M = 11, 74%	Cyclopentane, *d*-cyclohexane (selective for PS) with trace amounts of water	Detailed study of micellar structure (R, R_B, R_g and screening length). Comparison to scaling theories	SAXS, SANS	Cogan *et al.* (1991); Gast (1996)
PS–PEO	M_n = 25, 18% M_n = 28, 20%	methanol + water (selective for PEO)	Exchange of labelled chains between micelles	Fluorescence, DLS	Wang *et al.* (1995)
PS–PEO	M = 26–33, 76–97%	Water	Observation of multiple associated structures (vesicles, rods, large compound micelles)	TEM	Yu and Eisenberg (1996)
PS–PDMS	M_n = 23.2–154.2, 3–17% PS	*n*-Alkanes (selective for PDMS)	Determination of micellar p and size	TEM	Dawkins and Taylor (1979)
PS–PDMS	M_n = 57.3, 76%	Dodecane (selective for PDMS)	Determination of R_B.	SAXS	Brown *et al.* (1987)
PS–PDMS	M_n = 57.3, 76%	Dodecane Octamethylcyclotetrasiloxane (selective for PDMS)	Determination of R_g.	SAXS	Broadbent *et al.* (1987)
PS–P(E/B)–PS	M_w = 60, 28% M_w = 74, 29%	Dioxane (selective for PS)	Determination of micellar M, R_g, R_H, D and R_B	SLS, DLS, SAXS, osmometry, viscometry	Tuzar *et al.* (1983)

Table 3.4 *Continued*

Polymer	M (kg mol^{-1}) and composition of polymer(s)[a]	Solvent (quality)[b]	Nature of study[c]	Techniques[d]	Reference
PS–P(E/P)	M = 48 and 80, 38%	Decane (selective for P(E/P)) *trans*-Decalin (neutral) and mixtures with decane	Micellar D, R_H and viscosity. Evidence for micellar association	Viscometry, SLS, DLS	Mandema *et al.* (1979*a*,*b*)
PS–P(E/P)	M_w = 106, 40%	Base lubricating oil (selective for P(E/P))	Micellar p, D and R_H	TEM, DLS	Price *et al.* (1980)
PS–P(E/P)	M_w = 106, 39% M_w = 168, 34%	Base lubricating oil	Micellar M_w, R_g and size distribution. Evidence for copolymer adsorption by GPC gel	SLS, GPC	Price *et al.* (1982)
PS–P(E/P)	M_w = 160, 34%	Lubricating oil	Measurement of D and monomeric mobilities	TEM, DLS, NMR	Candau *et al.* (1984)
PS–P(E/P)	M_w = 700, 28%	Heptane (selective for P(E/P)) 1,4-Dioxane/25% heptane (selective for PS)	Micellar R_B, M and cgc	SAXS, viscometry	Plěstil *et al.* (1990)
PS–P4VP		Toluene (selective for PS)	Determination of scattering density profile and comparison to scaling theory	SANS	Förster *et al.* (1996)
Polycaprolactam–PS–polycaprolactam	M_w = 31–53, 41–70%	Toluene/2,2,3,4-tetrafluoropropanol	Determination of R_H and M. Observation of large micellar associates	SLS, DLS, DR	Tuzar *et al.* (1988)
PS–poly(arylates)	Range	MEK (selective for PS) Trichloroethanol (selective for poly(arylates)) Benzene (selective for PS) THF, dioxane, chloroform, cyclohexane (neutral)	Measurement of viscosity. Determination of micellar M, A_2 and k_H.	SLS, viscometry, TEM	Pavlova *et al.* (1981)

[a] Composition in wt% PS unless otherwise specified.
[b] Abbreviations as Table 3.2.
[c] Abbreviations as Table 3.1 + cgc, critical gel concentration.
[d] Abbreviations as Table 3.3.

of mixed micelles in solutions of PBO_8PEO_{41} and $PBO_{12}PEO_{76}PBO_{12}$ (50:50 mixture) in water. The triblock copolymer in the mixed micelles was predominantly in a looped conformation. However, at higher concentrations bridging of triblock copolymers led to the association of mixed micelles into clusters.

3.4 Theories for dilute block copolymer solutions

3.4.1 Scaling theories for block copolymer micelles

A simple scaling model of block copolymer micelles was derived by de Gennes (1978). He obtained scaling relations assuming uniformly stretched chains for the core radius, R_B, of micelles with association number p. This model can be viewed as a development of the Alexander–de Gennes theory (Alexander 1977; de Gennes 1976, 1980) for polymer brushes at a planar interface, where the density profile normal to the interface is a step function. In the limit of short coronal (A) chains (crew-cut micelles) de Gennes (1978) predicted

$$R_B \sim a N_B^{2/3} \left(\gamma a^2 / T\right)^{1/3}, \tag{3.10}$$

where γ is the A–B interfacial tension and a is a segment length. The number of chains per micelle was found to be linear in N_B (the degree of polymerization of the core block):

$$p \sim N_B \gamma a^2 / T. \tag{3.11}$$

The Daoud–Cotton model (Daoud and Cotton 1982) for star-like polymers in a good solvent is based on a simple geometric picture of polymer 'blobs', with chain ends confined on a spherical surface (Fig. 3.16), an extension of the original Alexander–de Gennes theory. It has been applied to analyse experimental results for the scaling of micellar dimensions in block copolymer solutions. For block copolymer micelles the number of arms f is replaced by the association number p. Daoud and Cotton (1982) identified three regions with characteristic density profiles: (i) an inner melt-like core, (ii) an intermediate concentration region (dense brush) and (iii) a swollen brush in the outer semidilute region. In this model, the density profile of a star with f arms and Flory exponent ν (ν = 0.588 for a good solvent or $\nu = 0.5$ for a theta solvent) and a fixed monomer excluded volume parameter decays as

$$\phi(r) \sim f^{(3\nu-1)/2\nu} r^{(1-3\nu)/\nu}, \tag{3.12}$$

which yields (i) $\phi(r) \sim r^0$ for the core, (ii) $\phi(r) \sim f^{1/2} r^{-1}$ for the unswollen brush, and (iii) $\phi(r) \sim f^{2/3} r^{-4/3}$ for the outer swollen brush (Fig. 3.17). Thus, for a fixed number of arms, in a good solvent the profile should decay as $1/r$. The average brush height referenced to the end-to-end distance of the chains (R_o) should scale as $l/R_o \sim f^{(1-\nu)/2}$, which gives a scaling (i) $f^{1/3}$ in the core, (ii) $f^{1/4}$ in the unswollen brush, and (iii) $f^{1/5}$ in the swollen brush. The Daoud–Cotton model predicts that in a good solvent the star polymer radius in the limit of very long chains scales as

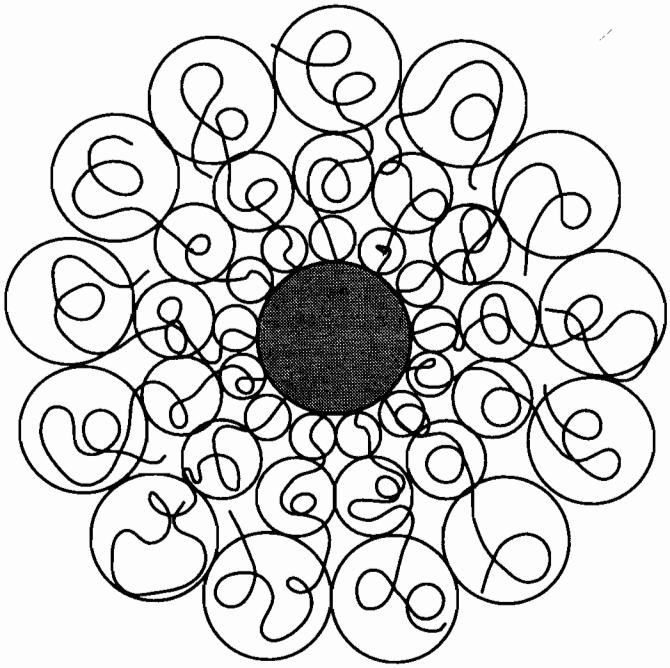

Fig. 3.16 Star polymer model for chains tethered to a curved surface. Chains are represented as a string of blobs extending radially from the core of the star.

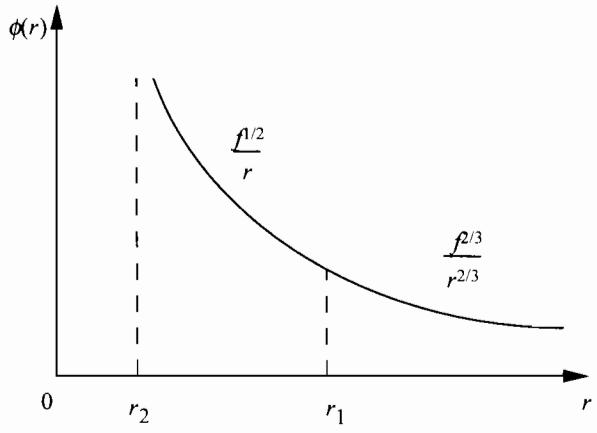

Fig. 3.17 The density profile predicted for a star polymer with f arms (after Daoud and Cotton 1982).

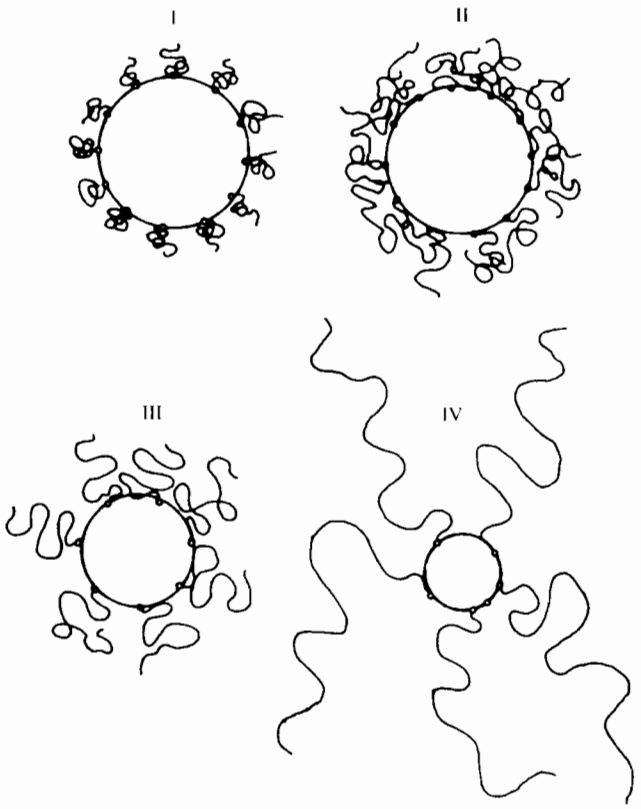

Fig. 3.18 Schematic of micellar structure in regimens I–IV defined by Zhulina and Birshtein (1985).

$$R \sim N_A^{3/5} f^{1/5}, \tag{3.13}$$

for a given statistical segment length and monomeric volume (Daoud and Cotton 1982).

Scaling theory was used by Zhulina and Birshtein (1985) for the specific case of a micelle formed by an AB diblock in a solvent selective for the A block. Four regions were identified depending on the copolymer composition (Fig. 3.18). In region I, A blocks behave like isolated chains, attached at one end to the core. The core–shell interfacial area per monomer (σ), R_B and p depend only on N_B. This situation prevails in region II, where there is some overlapping of the A blocks. In region III, the micellar parameters depend on N_A: σ increases, while R_B and p decrease with increasing R_A. With further increase in N_A (region IV), the curvature of the core enables each A block to occupy a larger area of the interface. Consequently, the dependence of the micellar parameters R_B, p and σ on N_A disappears. Zhulina and Birshtein (1985) also found that the core chains

Table 3.5 Predictions of Zhulina and Birshtein (1985) for micellar characteristics in an AB diblock in a solvent selective for the A block[a]

Region	Copolymer composition	R_B	R_A	p	σ
I	$N_A < N_B^{\nu/6}$	$N_B^{2/3}$	N_A^{ν}	N_B	$N_B^{1/3}$
II	$N_B^{\nu/6} < N_A < N_B^{(1+2\nu)/6\nu}$		$N_A\, N_B^{(\nu-1)/6\nu}$		
III	$N_B^{(1+2\nu)/6\nu} < N_A < N_B^{(1+2\nu)/5\nu}$	$N_B N_A^{-2\nu/(1+2\nu)}$	$N_A^{3\nu/(3\nu+1)}$	$N_B^2 N_A^{-6\nu/(1+2\nu)}$	$N_A^{2\nu/(1+2\nu)}$
IV	$N_A > N_B^{(1+2\nu)/5\nu}$	$N_B^{3/5}$	$N_A^{\nu} N_B^{2(1-\nu)/5}$	$N_B^{4/5}$	$N_B^{2/5}$

[a]Here ν is the scaling exponent for the radius of gyration of linear polymers, $R_g \sim M^{\nu}$ ($\nu = 1/2$ for θ solvent and $\nu = 0.588$ for good solvent).

are stretched in block copolymer micelles compared to the unperturbed value, the stretching relaxing from region I towards IV. The scaling of micellar parameters in the four regimes is summarized in Table 3.5.

Halperin (1987) also developed a model for regime IV, and derived the same scaling relationships for p and R_B as Zhulina and Birshtein (1985). For a large core micelle (regime I), it was pointed out that the tendency for the system to lower its interfacial free energy is countered by the stretching of the core-forming blocks which increases the free energy. For a small-core micelle (regime IV), micellar growth was found to be limited by the confinement free energy associated with the corona. Halperin also obtained a scaling relationship for the total micellar radius in the small core limit ($N_B \ll N_A$):

$$R/a \sim N_B^{4/25} N_A^{3/5}. \tag{3.14}$$

It is worth emphasizing that all scaling theories (due to de Gennes, Daoud and Cotton, Zhulina and Birshtein, and Halperin) for block copolymer micelles with a small core and large corona predict that the association number and core radius are independent of the coronal chain length.

A scaling analysis based on the starblock copolymer model of Daoud and Cotton for the solubilization of a low molecular weight solute in spherical micelles formed by an AB diblock in a selective solvent was presented by Nagarajan and Ganesh (1993). Scaling relations for the association number, the core radius, the coronal layer thickness, R_A, and the volume fraction of copolymer in the core, ϕ_B, were derived for a number of situations, including the case where the solvent is a good or theta solvent for the shell block A, and the solute is a good or theta solvent for the core block.

It may be noted that, denoting the fraction of A monomers in the corona belonging to the copolymer by η, and the micellar association number by p, incompressibility conditions give simple relations between R, R_B, p and η (de Gennes 1978; Leibler *et al.* 1983):

$$4\pi R_B^3/3 = pN_B a^3, \tag{3.15}$$

$$4\pi\left(R^3 - R_B^3\right)\eta/3 = pN_A a^3. \tag{3.16}$$

3.4.2 Mean field theories for block copolymer micelles

The self-consistent field theory of Noolandi and co-workers

A self-consistent field theory for the emulsifying effects of block copolymers in immiscible polymer blends was developed by Noolandi and Hong (1982). They considered micelle formation, and obtained an estimate of the diblock copolymer cmc in the homopolymer matrix. They found that the cmc falls rapidly with increasing molecular weight of the copolymer. This result was rationalized by observing that one block of a copolymer chain in a random configuration has a large enthalpy of mixing in the incompatible homopolymer, and for long chains the contribution to the free energy is much smaller in the spherical micellar configuration, easily outweighing the associated loss of entropy. Comparison was made with the experimental results of Riess and co-workers (Gaillard *et al.* 1980) on a quaternary system containing PS, PB homopolymer, PS–PB diblock and styrene monomer (Noolandi and Hong 1982). In a later paper (Noolandi and Hong 1983), the simpler system of AB diblock copolymer micelles in solution was considered, with the insoluble B block forming a uniform core and a uniform corona of A blocks in a spherical micelle. A mean field theory was employed and using a simple approximation for the interfacial tension, together with the known block copolymer composition, molecular weight and concentration in solution, the equilibrium size of micelles could be obtained. The theory was found to be in excellent agreement with results from SAXS experiments by Plestil and Baldrian (1975) on PS–PB micelles in heptane. The scaling of micelle size, association number and radius with copolymer degree of polymerization was found to be in general agreement with the earlier results of de Gennes (1978). The core radius was found to scale as $R_B \sim N_B^{0.64}$, independent of the coronal chain length and the association number was found to scale as $p \sim N_B^{0.9}$ (Noolandi and Hong 1983). Whitmore and Noolandi (1985) developed the approach of Noolandi and Hong (1983), and obtained the following scaling relations:

$$R_B \sim N_B^{\beta} N_A^{\mu}, \qquad R_A \sim N_A^{\omega}, \tag{3.17}$$

where $0.67 \leq \beta \leq 0.76$, $-0.1 \leq \mu \leq 0$, and $0.5 \leq \omega \leq 0.86$. These authors also found that the cmc is dominated by an exponential dependence on the product $\chi_{AB}N_B$, and that the fraction of copolymer in a micelle increases exponentially with decreasing temperature. The scaling of micellar dimensions was compared to SANS results (Selb *et al.* 1983) on PS–PB diblocks in PB homopolymers, where PS forms the core. Selb *et al.* (1983) obtained $-0.19 \leq \mu < -0.14$ and $0.75 \leq \beta < 0.81$ for a number of copolymers of different molecular weights in blends with homopolymers of varying M_w. The theoretical exponents are in reasonable agreement with these experimental values. Bluhm and Whitmore (1985) applied the Noolandi–Hong model in detail to micelles with a PS core and a PB shell in heptane. They obtained

$$R_B \sim N_B^{0.67} N_A^{-0.01}, \qquad R_A \sim N_B^{0.12} N_A^{0.54}. \tag{3.18}$$

It is notable that R_B scales with N_B with a power close to two-thirds, as obtained in the simple de Gennes (1978) model. This scaling is also obtained for strongly

segregated block copolymer melts (Section 2.3.1), illustrating that the core chains are effectively in a melt-like state. The power law scaling of R_A with N_A has an exponent slightly greater than a half, the exponent for the scaling of the radius of gyration with N for a θ solvent. Both these scalings were found to be consistent with the scaling dependence of the micellar radius of gyration, R_g, on the number-average molar mass of the copolymer, M_n (Bluhm and Whitmore 1985):

$$R_g \sim M_n^{0.44}. \tag{3.19}$$

Results from SAXS experiments for PS–PB in heptane (Bluhm and Whitmore 1985) were consistent with this scaling. An exponent 0.5, close to the theoretical prediction (eqn 3.19), was observed using SAXS on PS–PI diblocks in heptane, using copolymers with a wider range of M_n (Bluhm and Malhotra 1986).

Other self-consistent field theories

A self-consistent field theory (SCFT) for micelle formation of block copolymers in selective solvents was developed by Yuan *et al.* (1992). They emphasized the importance of treating the isolated chain at the same level of theoretical approximation at the micelle, in contrast to earlier approaches. This was achieved by modifying the Edwards diffusion equation for the excluded volume of polymers in solution to the case of block copolymers, with one block in a poor solvent. The results of the continuum model were compared to experimental results for PS–PI diblocks in hexadecane, which is a selective solvent for PI and satisfactory agreement was obtained.

A number of publications have dealt with SCFT applied to polymer brushes tethered to spherical interfaces, and this work forms a basis for SCF theories for the related system of block copolymer micelles. The Edwards diffusion equation approach (Dolan and Edwards 1974) was applied to polymer brushes densely tethered to a curved interface in a good solvent by Dan and Tirrell (1992). They found that the chain dimensions only obey limiting power laws in the limit of high interface curvature or chain molecular weight. Wijmans and Zhulina (1993) considered polymer brushes in athermal solvents at curved surfaces (cylindrical and spherical) using the lattice version of SCFT developed by Scheutjens and Fleer (1979). In agreement with Dan and Tirrell, these authors found an exclusion (dead) zone for chains at the impenetrable interface, which will not exist for block copolymers where the core is not completely impenetrable. Lin and Gast (1996) used the continuum version of SCFT to investigate the structure of, and interactions between, layers of polymer chains tethered to a spherical interface. Results for the chain configuration in a curved geometry were used to calculate interaction potentials between curved surfaces. On varying the core radius, degree of polymerization and the tethering density in an athermal polymer, the tethered layer was found to adopt structures ranging from those in star polymers to planar polymer brushes.

The formation of micelles of a diblock copolymer in a selective solvent was considered by van Lent and Scheutjens (1989), who extended Scheutjens–Fleer lattice SCFT for homopolymers (Scheutjens and Fleer 1979, 1980). van Lent and

Scheutjens were able to calculate the cmc for diblock copolymer solutions, and this was shown to depend most strongly on the length of the block forming the micellar core and the solvent quality. A strong repulsion between A and B segments (large χ_{AB}) was found to slightly disfavour association. The micelles were usually found to be spherical, but when the A blocks are much longer than the B blocks, a lamellar bilayer was predicted to be the preferred structure. They also obtained isotherms for adsorption at a solid–liquid interface. Block copolymer micellization in a mixture with two immiscible solvents was considered by Cogan *et al.* (1992), also employing modified Scheutjens–Fleer theory. They considered the case where each of the solvents is selective for one of the blocks and found that for highly incompatible solvents, one segregates in the centre of the micelle whilst the other selectively solvates the corona. The capacity of the micelle to disperse a second solvent was found to be controlled by the size of the core block. It was reported that the number of dispersed molecules and copolymer chains assembled in a micelle change most rapidly as the background solvent concentration approaches saturation levels. The theory was applied to interpret earlier experimental results (Cogan and Gast 1990; Vagberg *et al.* 1991) on PS–PEO diblock copolymers in cyclopentane with trace amounts of water, which is a selective solvent for the PEO block that forms the micellar core. The addition of water was found to lower the cmc. Futhermore, swelling of the core with water led to an increase in p by up to a factor of five, as shown by light scattering experiments.

The lattice SCFT of Scheutjens and Fleer has been applied specifically to PEO–PBO diblock and triblock copolymers (Pluronics) in aqueous solution by Linse (1993*a*,*b*, 1994*a*,*b*) and Linse and Malmsten (1992). The cmc, association number and hydrodynamic radius were determined for a number of copolymers (Linse 1993*a*,*b*), and a semiquantitative description of the temperature dependence of these quantities was compared to experimental results for Pluronic F127 ($PEO_{106}PPO_{69}PEO_{106}$) (Linse 1993*a*; Linse and Malmsten 1992). An increase in molecular mass or a decrease in the PEO/PBO ratio was found to reduce the cmt at a given polymer concentration, and to decrease the cmc at a given temperature. A similar trend was found on going from a triblock to a diblock. At high temperatures, a transition from spherical to rod-like micelles was observed, in agreement with the experimental phase diagram for several Pluronics (Linse 1993*b*). Linse also considered the effect of polymer impurities (Linse 1994*a*) and copolymer polydispersity (Linse 1994*b*). For a PEO–PPO–PEO triblock solution, a PEO–PPO diblock copolymer and PEO and PPO homopolymers were considered as impurities (Linse 1994*a*). The presence of a diblock impurity was found to reduce the cmc and increase the aggregation number. Because the diblock associates more readily than the triblock, an enhancement of diblock copolymer association was observed at the cmc. Homopolymer PPO was also observed to reduce the cmc, but to a lesser extent. Solubilization of PPO in the hydrophobic micellar core was observed, leading to an enhancement of solubility by several orders of magnitude. This solubilization was found to increase with temperature, and with the volume fraction of free PPO. PEO was found to have a negligible effect on micellization. The effect of molecular mass polydispersity was modelled

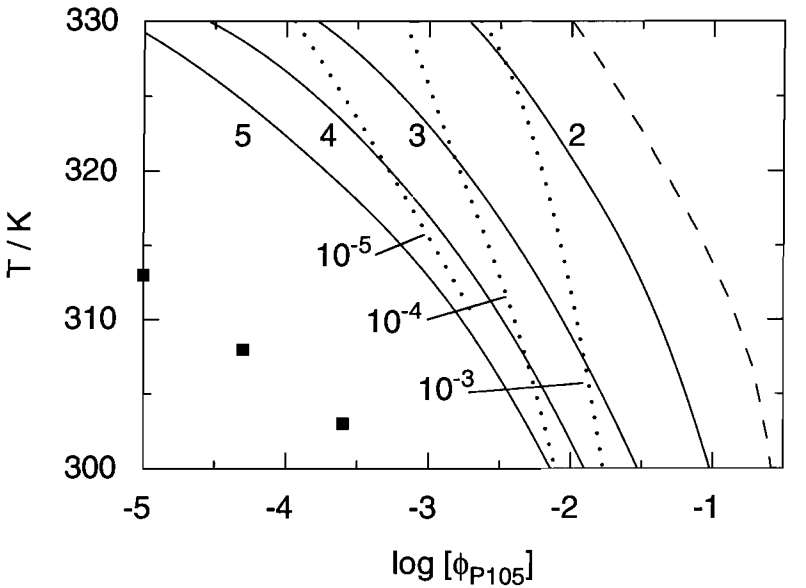

Fig. 3.19 Critical micelle temperature versus the polymer concentration calculated for an aqueous solution of Pluronic P105 ($PEO_{37}PPO_{56}PEO_{37}$) (Linse 1994*b*). Results from a polydisperse model ($M_w/M_n = 1.2$) are shown as solid lines and for the monodisperse polymer as a dashed line. The curves for the polydisperse system are labelled in terms of the number of components representing the polydisperse polymer. Points with constant micellar volume fractions (criterion of the cmc) are represented by dotted curves, the volume fraction being indicated. Experimental data from Alexandridis *et al.* (1994*a*) are also included as filled squares.

by Linse (1994*b*) using a Schulz–Zimm distribution. It was found that polydispersity leads to a reduction of the cmc by several orders of magnitude, bringing the theory into closer agreement with experiment. The cmt is also reduced, as illustrated in Fig. 3.19. The precise value of the cmc was found to depend strongly on the criterion used to define it. Polydispersity also leads to an increase in micellar size, a greater separation of the EO and PO segments, and a marked decrease in micellar size with increasing polymer concentration. Close to the cmc the micelles are predominantly formed by the longest components, whereas at high polymer concentrations, the solution becomes strongly depleted of the long polymers. The strong temeperature dependence of the cmc and association number was not significantly changed by polydispersity. Predictions of the polydisperse model were compared to experimental results for L64 ($PEO_{13}PPO_{30}PEO_{13}$) (Alexandridis *et al.* 1994*a*; Pandya *et al.* 1993; Reddy *et al.* 1990*a*; Wanka *et al.* 1994), P105 ($PEO_{37}PPO_{56}PEO_{37}$) (Alexandridis *et al.* 1994*a*) and F127 (Alexandridis *et al.* 1994*a*; Attwood *et al.* 1985; Linse and Malmsten 1992; Rassing and Attwood 1983; Wanka *et al.* 1994). Limited studies of chemical polydispersity were also performed by Linse (1994*b*), and this was found to have

a similar effect to mass polydispersity. The Scheutjens–Fleer lattice SCF theory has been applied to model micelle formation and solubilization in PEO–PPO block copolymer solutions by Hurter *et al.* (1993*a*,*b*). They performed detailed calculations of the cmc, volume fraction profiles, association numbers and partitition coefficients for Pluronic $(PEO–PPO–PEO)_4$ triblocks and tetronic $(PEO–PPO)_4$ starblocks in aqueous solution.

The model of Leibler and co-workers

A simple mean field theory for micelle formation by a diblock copolymer in a homopolymeric solvent was developed by Leibler *et al.* (1983). This model enables the calculation of the size and number of chains in a micelle and its free energy of formation. The fraction of copolymer chains aggregating into micelles can also be obtained. A cmc was found for low copolymer contents even for weak incompatibilities between components. Leibler *et al.* (1983) emphasize that for a finite aggregation number p, the cmc is a region rather than a well-defined concentration and some arbitrariness is involved in its definition.

In the model, spherical micelles of radius R comprising a core of B monomers (radius R_B) and a corona of A monomers (radius $R_A = R - R_B$) are considered (Leibler *et al.* 1983). Only a fraction η of A monomers in the corona belongs to the copolymer, the rest belonging to the homopolymer chains penetrating the corona. The homopolymer chains are shorter than the copolymer, the parameter $\alpha = N/N_H$ (where N is the total degree of polymerization of the copolymer and N_H is that of the homopolymer) being greater than two. The case of relatively incompatible components was considered, and in this case the A–B interfacial region is fairly narrow. Thus, the interface was taken to have the same properties as that between two incompatible homopolymers. The free energy of a micelle containing p copolymer chains and $\alpha p(1 - \eta)/2\eta$ homopolymer chains can than be written as

$$F_{\text{micelle}} = F_{\text{core}} + F_{\text{corona}} + F_{\text{int}}. \tag{3.20}$$

Here F_{core} is the free energy due to deformation of chains in the micelle core

$$F_{\text{core}} = p\frac{3}{2}k_BT\left(\frac{R_B^2}{N_Ba^2} + \frac{N_Ba^2}{R_B^2} - 2\right). \tag{3.21}$$

This equation assumes that the blocks have an end-to-end distance R_B that is undeformed with respect to the unperturbed dimension $(N_B)^{1/2}a$.

The free energy of the corona contains contributions from the deformation energy (cf. eqn 3.21) and from the entropy of mixing of homopolymer chains and A blocks in the micellar corona (de Gennes 1978; Meier 1969; Noolandi and Hong 1982). Summing these two terms gives (Leibler *et al.* 1983)

$$F_{\text{corona}} = p\frac{3}{2}k_BT\left(\frac{R_A^2}{N_Aa^2} + \frac{N_Aa^2}{R_A^2} - 2\right) + \frac{pk_BTN_A(1-\eta)}{\eta N_H}\ln(1-\eta). \tag{3.22}$$

The interfacial free energy is

$$F_{\text{int}} = 4\pi R_{\text{B}}^2 \left[\frac{k_{\text{B}}T}{a^2} \left(\frac{\chi_{\text{AB}}}{6} \right)^{1/2} \right], \tag{3.23}$$

where the term in brackets is the Helfand–Tagami (Helfand and Sapse 1975; Helfand and Tagami 1972) expression for the interfacial free energy between A and B homopolymers. Figure 3.20 shows representative results from this theory for the fraction of copolymer chains aggregated in micelles, ζ, as a function of copolymer volume fraction.

The total free energy of the micellar phase contains contributions from the translational entropy of the micelles, the entropy of mixing of homopolymers and copolymers and their interaction outside the micelles. It can be written as (Leibler *et al.* 1983)

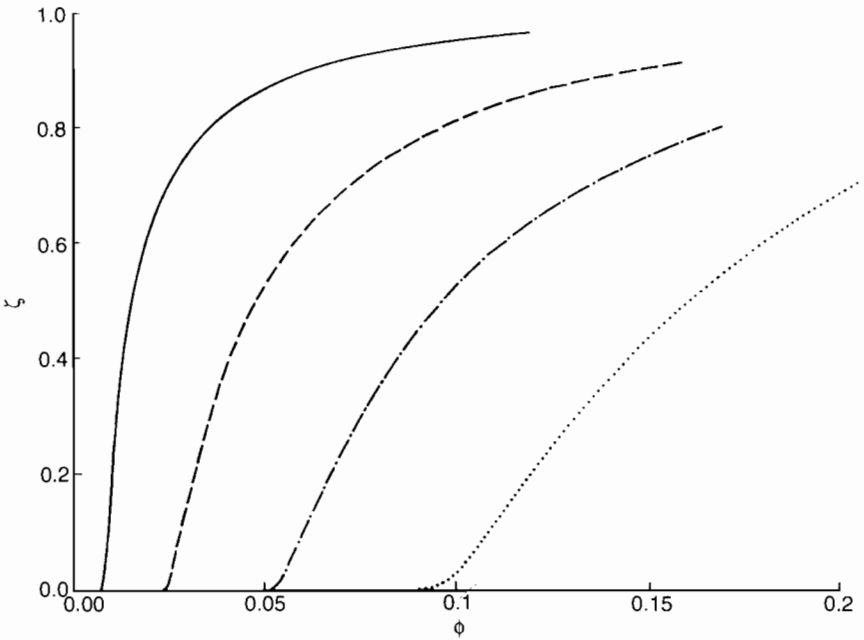

Fig. 3.20 Fraction, ζ, of copolymer chains aggregated in micelles as a function of the overall copolymer volume fraction, ϕ, for different values of the incompatibility parameter χN ($\alpha = 5, N = 200$) (Leibler *et al.* 1983). The number of copolymer chains in a micelle, p, and the volume fraction of copolymer monomers in the micelle corona, η, depend weakly on ϕ. Full line, $\chi N = 20$, for $\phi = 0.1$, $p \approx 79.9$, $\eta = 0.194$; for $\phi = 0.009$, $p \approx 77.0$, $\eta = 0.19$. Dashed line, $\chi N = 17.5$, for $\phi = 0.16$, $p \approx 78.3$, $\eta = 0.194$; for $\phi = 0.026$, $p \approx 75.0$, $\eta = 0.189$. Dotted–dashed line, $\chi N = 16$, for $\phi = 0.18$, $p \approx 77.8$, $\eta = 0.196$; for $\phi = 0.054$, $p \approx 74.5$, $\eta = 0.191$. Dotted line, $\chi N = 15$, for $\phi = 0.19$, $p \approx 78.6$, $\eta = 0.201$; for $\phi = 0.1$, $p \approx 76.0$, $\eta = 0.197$. Here $\chi = \chi_{\text{AB}}$.

$$\frac{F_{\text{total}}}{k_B T} = \frac{\phi\zeta F_{\text{micelle}}}{N} + (1-\xi\phi\zeta)\left[\frac{\phi_1}{N}\ln\phi_1 + \frac{1-\phi_2}{N/\alpha}\ln(1-\phi_2) + \frac{\chi\phi_1}{1+r}\left(1-\frac{\phi_1}{1+r}\right)\right] - \left[\frac{\phi\zeta}{pN}\ln(\zeta\xi\phi) + \frac{1-\zeta\xi\phi}{\xi pN}\ln(1-\zeta\xi\phi)\right] \tag{3.24}$$

where $r = N_A/2N_B$. The first term on the right-hand side is equal to the free energy of the micelles in solution, the second represents the free energy of mixing copolymer and solvent outside the micelles, and the last term accounts for the translational entropy of the micelles. ϕ_1 is the volume fraction of copolymer chains outside the micelles and is given by

$$\phi_1 = \frac{\phi(1-\zeta)}{1-\zeta\xi\phi}, \tag{3.25}$$

and

$$\xi = \frac{r+\eta}{\eta(1+r)}. \tag{3.26}$$

F_{total} can be expressed in terms of three independent variables p, ζ, and η and requires the specification of model parameters N_A, N_B, N_H, χ_{AB} and r. Calculations by Leibler *et al.* (1983) showed that for small incompatibility, p scales as $N^{0.6}$, and $R_B \sim N^{0.53}$. Under conditions of strong segregation, for the case of symmetric diblocks considered by them, Leibler *et al.* (1983) found that the cmc depends exponentially on $\chi N_A = \chi N_B$, for a fixed homopolymer degree of polymerization.

Analogous equations to (3.20–3.26) can be written for triblock copolymer micelles in a homopolymeric solvent (Balsara *et al.* 1991; ten Brinke and Hadziioannou 1987). However, in a BAB triblock copolymer where the solvent is selective for the A block, for a single micelle the A block must be looped. Then each chain enters the core twice, and eqn 3.21 must be multiplied by two, with a similar multiplier of the analogous term in eqn 3.22. An additional contribution must be added to the free energy of the corona due to looping. Balsara *et al.* (1991) estimated this to be

$$F_{\text{loop}} = -pk_B T \ln q, \tag{3.27}$$

where q is the fraction of chains that end up in the A–B interfacial shell. This estimate is significantly lower than the one obtained earlier by ten Brinke and Hadziioannou (1987), $F_{\text{loop}} = \beta\frac{3}{2}pk_B T \ln N_A$, where β is a correction factor introduced in the cyclization approximation introduced to account for the entropy loss due to looping. This difference has a substantial effect on the predictions of the theory such as the fraction of copolymer that forms micelles, as shown in Fig. 3.21 which shows the fraction of associated copolymer chains as a function of the overall volume fraction occupied by the copolymer in the system.

Mayes and Olvera de la Cruz (1988) applied the model of Leibler *et al.* to the

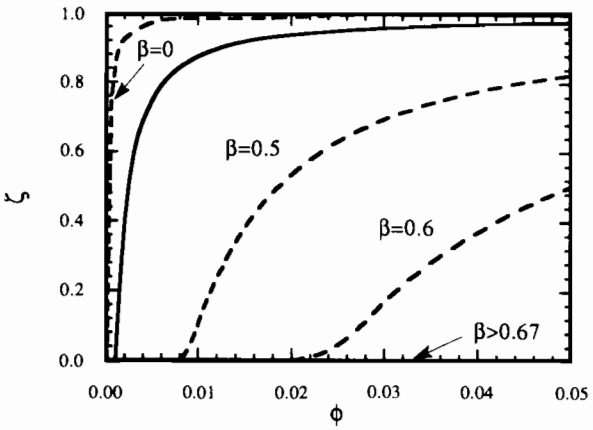

Fig. 3.21 Theoretical predictions for the dependence of ζ on ϕ. Dashed lines show the calculations of ten Brinke and Hadziioannou (1987) for various values of β. The solid line represents the results of Balsara *et al.* (1991). $N_A = 200$, $N_B = 100$, $N_H = 40$, $x = 0.1$. (The number of copolymer chains per micelle, p, and the coronal concentration, η, depend weakly on ϕ. For $\phi = 2.0 \times 10^{-3}$, $\zeta = 0.394$, $p = 38.3$ and $\eta = 0.189$. For $\phi = 2.0 \times 10^{-2}$, $\zeta = 0.938$, $p = 39.2$ and $\eta = 0.191$.)

case of dilute solutions where intermicellar interactions can be neglected. The cmc was determined for cylindrical and spherical micelles. A trend towards the formation of cylinders was observed with increasing core-block fraction and increasing homopolymer molecular weight. Extension of the theory to consider the formation of polydisperse micelles in binary diblock/homopolymer blends was reported by Kao and Olvera de la Cruz (1990).

The model of Nagarajan and Ganesh

A theory for the self-assembly of block copolymers into micelles in a selective solvent was developed by Nagarajan and Ganesh (1989*a*), following their earlier treatment of micellization in low molecular weight surfactants. In the theory, the copolymer–solvent system is treated as a multicomponent system consisting of solvent molecules, singly dispersed copolymer molecules and micelles of all possible sizes, each treated as a distinct chemical component. An expression for the difference in the reference state free energy between a copolymer in its micellized state and that its singly dispersed state was derived. An expression for the equilibrium size distribution of micelles was also obtained. Illustrative calculations of micellar properties were carried out for a range of block copolymer–solvent systems studied experimentally. In contrast to earlier theories (de Gennes 1978; Leibler *et al.* 1983; Noolandi and Hong 1983), Nagarajan and Ganesh (1989*a*) found that the solvent-compatible coronal A block can have a strong influence on the micellar properties, especially when the solvent is very good for the A block. As an example of their comparisons with systems studied experimentally, they obtained scaling relations for PEO–PPO block copolymers

in water (i.e. a system of a diblock in a good solvent), using interaction parameters estimated from activity data in the literature:

$$R_B \propto N_A^{-0.17} N_B^{0.73}, \qquad p \propto N_A^{-0.51} N_B^{1.19}, \qquad R_A \propto N_A^{0.74} N_B^{0.06}. \tag{3.28}$$

For PS–PB diblocks in the near-theta solvent *n*-heptane, the scalings

$$R_B \propto N_A^{-0.08} N_B^{0.70}, \qquad p \propto N_A^{-0.24} N_B^{1.10}, \qquad R_A \propto N_A^{0.68} N_B^{0.07} \tag{3.29}$$

were obtained (Nagarajan and Ganesh 1989*a*).

Clearly, this model predicts a strong dependence of R_B and p on the size of the coronal block N_A, in contrast to the earlier theoretical work (de Gennes 1978; Leibler *et al.* 1983; Noolandi and Hong 1983). By combining numerical results for the systems PS–PB/heptane, PS–PI/heptane, PPO–PEO/water and two model systems, Nagarajan and Ganesh obtained 'universal' scaling relations:

$$R_B = \frac{\left[3N_B^2\left(\gamma_{BS}a^2/k_BT\right) + N_B^{3/2} + N_B N_A^{1/2}\left(R_B/R_A\right)^{1/3}\right.}{\left[1 + N_B^{-1/3} + \left(N_B/N_A\right)\left(R_A/R_B\right)^2\right]^{1/3}} a, \tag{3.30}$$

$$p = \frac{\left[4\pi N_B\left(\gamma_{BS}a^2/k_BT\right) + \left(4\pi/3\right)N_B^{1/2} + \left(4\pi/3\right)N_A^{1/2}\left(R_B/R_A\right)\right.}{\left[1 + N_B^{-1/3} + \left(N_B/N_A\right)\left(R_A/R_B\right)^2\right]}, \tag{3.31}$$

$$\frac{R_A}{R_B} = 0.867\left[\frac{1}{2} + \frac{N_A N_B^2}{\left(N_A + N_B\right)^3} - \chi_{AS}\right]^{1/5} N_A^{6/7} N_B^{-8/11}. \tag{3.32}$$

Here γ_{BS} is the core–solvent interfacial tension and χ_{AS} is the coronal block–solvent interaction parameter.

Other theories

Among other approaches, a theory for intermolecular interactions in dilute block copolymer solutions was presented by Kimura and Kurata (1981). They considered the association of diblock and triblock copolymers in solvents of varying quality. The second and third virial coefficients were determined using a mean field potential based on the segmental distribution function for a polymer chain in solution. A model for micellization of block copolymers in solution, based on the thermodynamics of associating multicomponent mixtures, was presented by Gao and Eisenberg (1993). The polydispersity of the block copolymer and its influence on micellization was a particular focus of this work. For block copolymers below the cmc, a collapsed spherical conformation was assumed. Interactions of the collapsed spheres were then described by the Hamaker equation, with an interaction energy proportional to the radius of the spheres.

The dependence of the cmc on the length of the insoluble block and its polydispersity was calculated, and reasonable agreement with experimental results for the PS–PI/hexadecane (Price *et al.* 1987) and PS–poly(sodium acrylate)/water systems (Astafieva *et al.* 1993) were obtained. The cmc was found to decrease as the polydispersity increased, in agreement with the calculations of Linse discussed above. The fraction of dispersed chains and molecular weight distributions of the dispersed chain and the micelles were found to be influenced by the dependence of the cmc of each component in the polydisperse mixture on the insoluble block length (Gao and Eisenberg 1993).

The adsorption of block copolymers from a selective solvent was considered by Ligoure (1991). He predicted the existence of surface micelles (see Fig. 3.22) in the case when the block interacting unfavourably with the solvent only partially wets the surface. The model predicts a critical surface micellar concentration (csmc) that differs from the bulk cmc. When the contact angle, which characterizes the interfacial interactions between the copolymer, adsorbing surface, and solvent is lower than some universal value, surface micelles were predicted to appear at a lower copolymer concentration than bulk ones. Experimental results on surfaces are discussed in Section 3.8.4.

3.4.3 Comparison with experiments

The scaling theory for spherical polymer brushes due to Daoud and Cotton (1982) (Section 3.4.1) has been applied to analyse the coronal density profile of block copolymer micelles by Förster *et al.* (1996). If the density profile is of the hyperbolic form $r^{-\alpha}$, as found by Förster *et al.* (1996) for the coronal layer of block copolymer micelles, the brush height scales as

$$l/R_0 \sim f^{(2-\alpha)/2(3-\alpha)}. \tag{3.33}$$

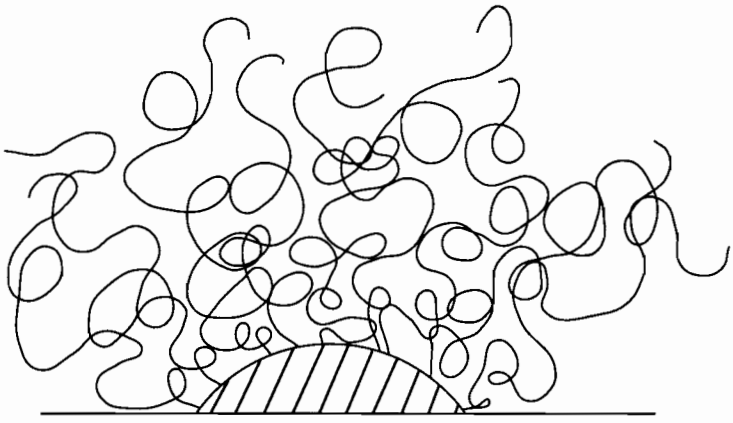

Fig. 3.22 Schematic illustration of a surface micelle with swollen A coronal blocks attached to a core formed by B blocks.

For the PS–P4VP micelles studied by them, Förster *et al.* (1996) determined that the P4VP coronal density profile can be modelled as a hyperbolic function with an exponent α between 1.05 and 1.35.

Results from TEM experiments on solutions of a series of poly(styrene)–poly(cinnamoylethyl methacrylate) (PS–PCEMA) diblocks with short PS blocks and long PCEMA blocks have been compared (Tao *et al.* 1997) to the theories for block copolymer micelles described above. Micelles of type IV in the Zhulina–Birshtein classification (Fig. 3.18) formed in cyclopentane, which is a selective solvent for PCEMA (coronal A block), when the ratio of N_A/N_B was greater than nine (Tao *et al.* 1997). Assuming that the association number is independent of N_A (as predicted by scaling theories and the theory of Noolandi and co-workers), it was found to scale as $p \sim N_B^{0.92}$, the exponent being in good agreement with the Zhulina-Birshtein theory. The scaling of the core radius, $R_B \sim N_B^{0.63}$, was also in good agreement with the theories of de Gennes, Zhulina and Birshtein, Halperin, Noolandi and Hong, and Nagarajan and Ganesh. Tao *et al.* (1997) also compared the scaling of the coronal thickness with the predictions of the Daoud and Cotton (1982) model for star polymers in a good solvent. Excellent agreement with the scaling (eqn 3.13) was obtained (see Fig. 3.23), assuming that the core dimension was much smaller than the coronal thickness.

Xu *et al.* (1992) used light scattering to characterize micelles formed by a wide range of PS–PEO di- and tri-block copolymers in dilute solution in water. Although full analysis of the data was complicated by the tendency of the micelles to undergo secondary association, they did find that the micellar radius scaled as eqn 3.14, in agreement with the predictions of Halperin (1987). With values of p and R_B from the star-like micelle model, Xu *et al.* (1992) were able to compute χ parameters for the interactions of PEO with water and with PS, in

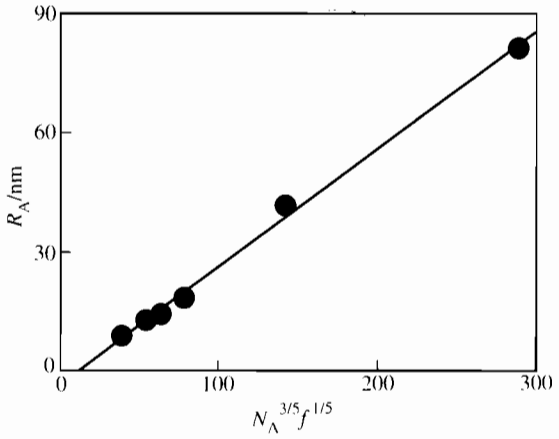

Fig. 3.23 Coronal thickness, R_A, plotted as a function of $N_A^{3/5} f^{1/5}$ for micelles formed by PS–poly(2-cinnamoylethyl metharylate) diblocks in cyclopentane (Tao *et al.* 1997). This yields a straight line in accord with the predictions of scaling theory for the micellar radius (the core radius for these micelles was small enough to be neglected, then $R_A = R$).

good agreement with values obtained from independent measurements. Antonietti *et al.* (1994) determined association numbers for micelles formed by asymmetric PS–P4VP diblocks in solvents selective for PS. The association number was found to scale with N_B^{β}, with β between 1.5 and 2 in agreement with the predictions of the Zhulina–Birshtein (1985) theory for type III micelles, i.e. $\beta = 2$. Evidently, the block copolymers studies by Antonietti *et al.* (1994) were not sufficiently asymmetric to lead to micelles in regime IV of Zhulina and Birshtein (1985), i.e. the type of micelle also considered by Halperin (1987). An exponent $\beta = 1.62$ or 1.89 was obtained by Qin *et al.* (1994) for micelles of poly(styrene)–poly(methacrylic acid) (PS–PMA) diblock and triblock copolymers in a dioxane–water mixture containing 20% water. The dilute solutions were characterized using static and quasi-elastic light scattering (Qin *et al.* 1994). However, it was also found that the association number (and hydrodynamic radius) depended on N_A with an exponent $\mu = -0.86$ or -0.41 for diblocks and triblocks respectively. Since the core radius was not much smaller than the micellar radius, the micelles can be classified in regime III of Zhulina and Birshtein (1985), in which case a dependence of p and micellar radius on N_A is expected. However, the exponents β and μ were not in agreement with the scaling theory predictions (Table 3.5). A complication in the case of the copolymers studies by Qin *et al.* (1994), however, is the ionic nature of the PMA block. Other work (Zhang *et al.* 1995) on the ionic diblock poly(styrene)–poly(acrylic acid) in aqueous solution also provided scaling relationships for R_B not in agreement with theoretical predictions for non-ionic block copolymer micelles. In addition to the ionic nature of the solutions studied by Eisenberg and co-workers (Zhang *et al.* 1995), thermodynamic equilibrium may not have been reached in the solutions, as shown by the slow exchange kinetics of PS–PAA micelles in water such that they remained intact after elution from a GPC column (Zhong *et al.* 1992). Experiments and theories for ionic block copolymer solutions are discussed further in Section 3.6.

Micelles formed by PS–poly(caesium acrylate) and PS–poly(caesium methacrylate) in toluene, a selective solvent for the PS block, have been characterized using SAXS (Nguyen *et al.* 1994). Since the scattering was dominated by the cores, which were much smaller than the distance between them, the structure factor and form factor were well separated in the SAXS pattern, enabling detailed information to be extracted on the core dimensions. It was found that the core radius scales as $N_B^{3/5}$, as shown in Fig. 3.24, in agreement with the prediction of the Zhulina–Birshtein (1985) and Halperin (1987) models for type IV polymeric micelles. Also in agreement with these theories, the association number scaled as $N_B^{4/5}$ and the surface area per chain as $N_B^{2/5}$. Thus, these ionic block copolymer micelles obeyed the same scaling laws with core block length as micelles formed by neutral block copolymers.

3.4.4 Theories for solubilization in block copolymer micelles

The solubilization of low-molecular-weight solute J in micelles of AB diblocks formed in a selective solvent S was considered theoretically by Nagarajan and

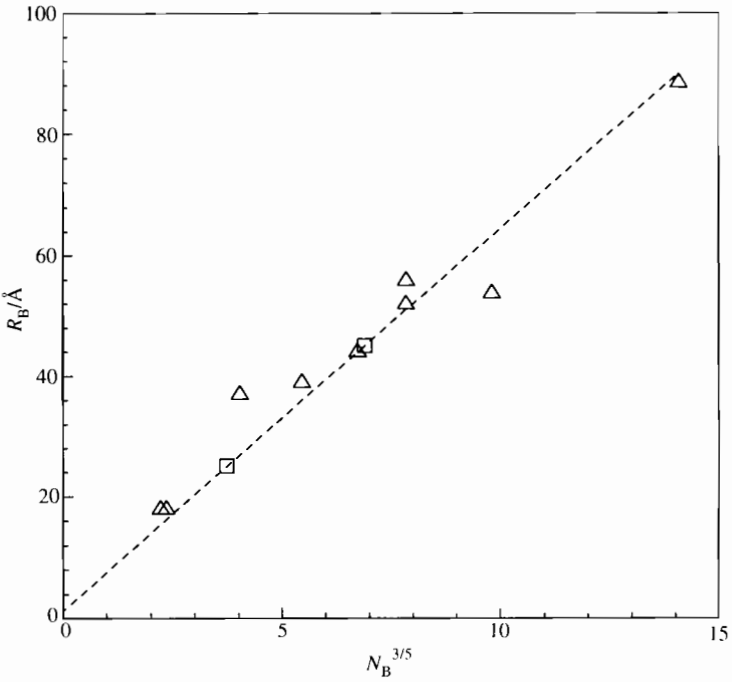

Fig. 3.24 Micellar core radius, R_B, as a function of $N_B^{3/5}$ for PS–poly(caesium acrylate) (△) and PS–poly(caesium methacrylate) (□) in toluene (Nguyen *et al.* 1994). A linear relationship is anticipated by the scaling theories of Zhulina and Birshtein (1985) and Halperin (1987, 1990) for type IV micelles.

Ganesh (1989*b*). Predictions were made for the cmc, the size and composition distribution of the micelles containing J, the association number of the micelles, the maximum extent of solubilization, and the core radius and shell thickness of the micelles. Calculations indicated that micelles containing solubilizate tend to be essentially monodisperse in size and extent of solubilization. The solubilization behaviour of the micelles and their geometrical characteristics were found to be significantly influenced by the interactions between the solute and the solvent-incompatible B block of the copolymer as well as the J–S interfacial tension. The micellar structure was also found to be affected by the interactions between S and the coronal A block, though to a somewhat lesser degree when compared to the corresponding solute-free systems. The predictions of the theory (Nagarajan and Ganesh 1989*b*) were compared to experimental data for water-soluble PEO–PPO diblocks with hydrocarbon solutes, the solubilization being measured by contacting of aqueous micellar solutions with the hydrocarbons (Nagarajan *et al.* 1986). The presence of solubilizate was shown to lower the cmc, as illustrated in Fig. 3.25. Theory and experiments on the solubilization of hydrophobic substances by block copolymer solvents have been reviewed by Nagarajan (1997).

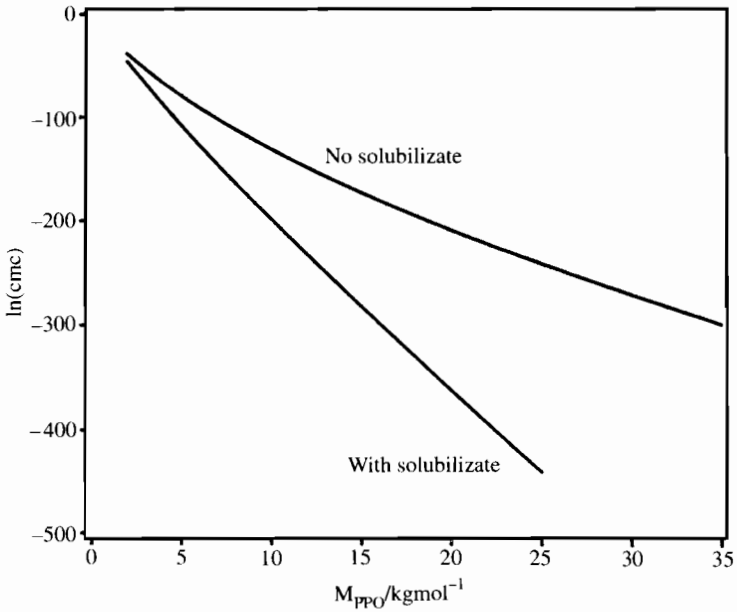

Fig. 3.25 Calculated critical micelle concentration in water of PEO–PPO diblocks with a constant PEO molecular weight, and varying PPO molecular weight, M_{PPO} (Nagarajan and Ganesh 1989*b*). The cmc with and without (benzene) solubilizates is shown.

A simple thermodynamic model to describe solubilization in block copolymer micelles was developed by Munk and co-workers (Tian *et al.* 1995). The theory assumed that the association number of copolymer molecules within the micelle is not affected by the process of solubilization. The extent of solubilization represents an equilibrium between the favourable interaction of the core component with the solubilizate (with both enthalpic and entropic contributions) and the surface tension at the core boundary that acts against solubilization. The theoretical predictions were found to agree reasonably well with experimental results for PS–PMA diblocks in solution in 80:20 dioxane:water mixtures, a selective solvent for PMA, with a variety of organic solubilizates. In the experiments, static light scattering was used to determine the extent of solubilization and dynamic light scattering was used to obtain the micellar hydrodynamic radius (Tian *et al.* 1995). Solubilization of benzene in solutions of the same copolymer type in the same selective solvent was investigated earlier (Kiserow *et al.* 1992) using quasi-elastic light scattering and fluorimetric measurements on tagged chains. Further details are provided in Section 3.6.2. Gadelle *et al.* (1995) investigated the solubilization of aromatic solvents in micelles formed by PEO–PPO (Pluronic type) triblocks in water using gas chromatography and determined solubilization isotherms and solute partition coefficients. They found that the addition of apolar solubilizates promotes association of the copolymer, and that

solubilization is initially a replacement process in which water molecules in the core are displaced from the micellar core by the solubilizate.

Dan and Tirrell (1993) presented a model for the phase diagram of a diblock copolymer in a mixture of incompatible and highly selective solvents using a mean field scaling theory approach. The properties of the diblock copolymer as an emulsifier were investigated, and the microdomain geometry and size were determined by an analysis of the interfacial layer. They found that solvent selectivity leads to copolymer association at the liquid–liquid interface and the formation of stable microdomains. Symmetric copolymers were found to form lamellae at all copolymer concentrations, whereas asymmetric copolymers were shown to associate in spherical microdomains in equilibrium with the two bulk solvent phases. The interfacial curvature and surface density were found to increase, and the volume of the emulsion phase to decrease, with the copolymer degree of asymmetry. The critical association number, above which chains assemble at the liquid–liquid interface and microdomains form, was found to be significantly lower than the critical micelle concentration. The emulsion phase volume was found to increase linearly with copolymer concentration until, when one of the solvents is exhausted, cylindrical domains appear. At high copolymer concentrations lamellae replace the cylindrical domains. As noted by Dan and Tirrell (1993), this sequence of phase transitions is similar to that predicted for block copolymer–homopolymer blends (Leibler 1988; Wang and Safran 1990). Earlier work by Cantor (1981) addressed diblock copolymers as emulsifiers in mixtures of immiscible solvents using mean field Flory-type theory for semidilute solutions. However, only a lamellar phase was considered.

3.4.5 Theories for ionic block copolymers

To date, there has been a very limited effort devoted to developing theory for ionic block copolymers. González-Mozuelos and Olvera da la Cruz (1994) studied diblock copolymers with oppositely charged chains in the melt state and in concentrated solutions using the random phase approximation (RPA) (de Gennes 1970). However, this work has not been extended to dilute solutions.

Theory for the critical micelle concentration in block copolymers with one polyelectrolyte block and one neutral block in a selective solvent has been developed by Shusharina *et al.* (1996*a*,*b*). It was shown that application of scaling arguments of the Alexander–de Gennes (Alexander 1977; de Gennes 1979) type leads to the open association of molecules into micelles in this system. The distribution function for micelles in the vicinity of the cmc was found to be rather broad and does not have the pronounced bimodal character typical of closed association, although such a distribution is found for concentrations above the cmc (see Fig. 3.26). The cmc was manifested by the occurrence of an inflection point on the micelle size distribution function (Fig. 3.26). These conclusions were supported by molecular dynamics simulations of flexible linear chains interacting via a repulsive Lennard-Jones interaction, with additional screened Coulombic interactions between head and tail end units. These results conflict with most experimental work (Astafieva *et al.* 1993; Khougaz *et al.* 1994) which shows that

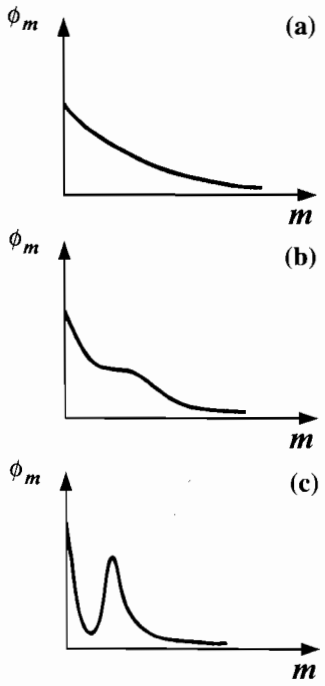

Fig. 3.26 Qualitative form of the dependence of volume fraction occupied by the core of complexes of m molecules (m-mers), ϕ_m, on m for: (a) $c <$ cmc; (b) $c =$ cmc; (c) $c >$ cmc (Shusharina *et al.* 1996*b*).

molecules associate via a closed micellization process. A phase diagram corresponding to different micellar structural regimes was constructed by Shusharina *et al.* (1996*a*), with different density profiles for the coronal block depending on the strength of electrostatic interactions.

3.5 Computer simulations of block copolymer micelles

Computer simulations of a range of properties of block copolymer micelles have been performed by Mattice and co-workers. These simulations have been based on bead models for copolymer chains on a cubic lattice. Types of allowed moves for bead chains are illustrated in Fig. 3.27. The formation of micelles by diblock copolymers under weak segregation conditions was simulated with pairwise interactions between A and B beads and between the A bead and vacant sites occupied by solvent, S (Wang *et al.* 1993*b*). This leads to the formation of micelles with a B core. The cmc was found to depend strongly on N_B and $\chi = \chi_{AB} = \chi_{AS}$. In the range $3 < (\chi/z)N_B < 6$, where z is the lattice constant, the cmc was found to be exponentially dependent on χN_B. It was found than in the micelles the insoluble block is slightly collapsed, and that the soluble block becomes stretched as N_A increases, with N_B and p held constant. The size of the micelles was found to

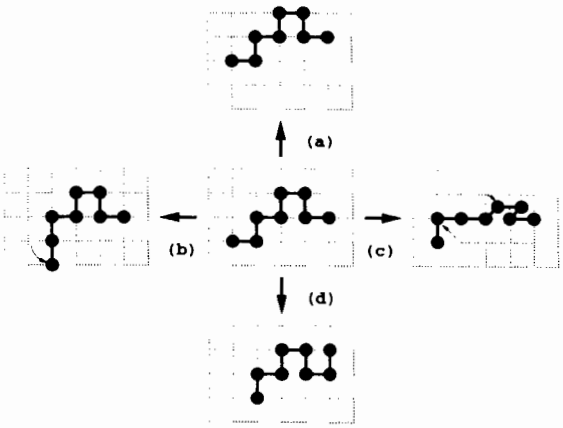

Fig. 3.27 Schematic of the Monte Carlo moves in the lattice simulations of micellization and adsorption of block copolymers by Mattice and co-workers. (a) Brownian moton of a chain; (b) end flip of an end bead; (c) two types of kink jump; (d) reptation of a chain (Zhan *et al.* 1993*a*).

be close to that estimated by a model based on the packing of the constituent beads. The exponential dependence of the cmc on χN_B is in agreement with the predictions of Leibler *et al.* (1983) for symmetric diblocks with a degree of polymerization much less than N_B, under conditions of strong segregation in a homopolymer solvent (Wang *et al.* 1993*b*) (see Section 3.4.2). The theory was subsequently generalized to the case of diblocks with different block stiffnesses (Adriani *et al.* 1994). It was found that when the stiffness of the insoluble block increases, the cmc decreases and the average micelle size increases. On the other hand, an increase in stiffness of the soluble block did not affect the micellization process to any appreciable extent. The decrease in the cmc with increasing stiffness of the insoluble block was interpreted as arising from the conformation contribution to the effective χ parameter, due to increased contacts between the insoluble block and the solvent molecules (Adriani *et al.* 1994).

These simulations have been extended to consider dynamical processes, for example the exchange dynamics of chains between micelles formed by diblocks in dilute solution in a selective solvent (Haliloglu *et al.* 1996). Two types of exchange mechanisms were identified: chain insertion/expulsion and micellar merging/splitting. From an analysis of the kinetics, it was found that the high frequency relaxation modes result from the chain insertion/expulsion mechanism, the micellar merger/splitting transitions leading to lower frequency eigenmodes of the relaxation. The latter become more important at higher concentrations and less important (relative to the exchange via free chains) at higher interaction energies. These results were correlated to fluorescence decay measurements of the dynamics of exchange of labelled chains (Procházka *et al.* 1992; Wang *et al.* 1992*b*, 1995). These experiments involved measuring the time dependence of the efficiency of non-radiative singlet energy transfer between micelles which originally contain copolymers labelled with a donor or an acceptor exclusively, at the

insoluble block or at the junction between two blocks. Exchange produces a population of micelles that contains both donor and acceptor. Simulations suggest that if the solvent is very poor for the insoluble block, no exchange is observed. However, if the solvent quality (with respect to the insoluble block) is improved, both insertion/expulsion and merger/splitting are generally important. These mechanisms operate on time-scales differing by more than an order of magnitude, and this was correlated to the experimental observations of two such processes (Haliloglu *et al.* 1996).

The micellization of triblock copolymers has also been investigating using Monte Carlo simulations by Mattice and co-workers. The same simulation scheme and interactions were employed as for the diblock simulations. The formation of a micelle was observed for a symmetric $B_5A_{10}B_5$ triblock, which had a dense-packed core of B beads, a diffuse interface and a corona that was less expanded than for the corresponding diblock (Rodrigues and Mattice 1992). By determining intraparticle distribution functions, both solvent and A beads were found to penetrate further into the triblock micellar core than into the core of the corresponding diblock micelle, In addition to micelles, gel phases have been observed using Monte Carlo simulations of symmetric BAB triblock copolymers in selective solvents (Nguyen-Misra and Mattice 1995*a*). A solvent that was athermal for the middle block and poor for the end-blocks was chosen. In this system, the triblock can form bridges between micelles, in addition to loops, leading to the formation of a micellar network. The effect of block size and solubility of the end-blocks on the system properties, particularly the cmc and cgc, were investigated. The weight-average association number and number density of micelles and functionality of the micellar network were determined. Populations of elastically active (bridging) chains and elastically inactive chains (loops, free and dangling ends) were also calculated. The phase diagram was found to contain regions of homogeneous solution, micellar solution, gel and possibly precipitation on increasing the copolymer volume fraction at a fixed degree of incompatibility (above a critical value), as illustrated in Fig. 3.28. Both the cmc and cgc were found to depend strongly on the degree of incompatibility between B segments and either A segments or solvent. However, the cmc and cgc were only weakly dependent on the middle block size. As the incompatibility increased, the cmc was found to exhibit a slower dependence than the exponential decrease predicted by Leibler *et al.* (1983) for diblocks in low-molecular-weight-homopolymer solution. Instead, the cmc and cgc were found to depend in a power-law manner on the incompatibility parameter (Nguyen-Misra and Mattice 1995*a*).

In a companion paper (Nguyen-Misra and Mattice 1995*b*), the relaxation dynamics of the transient networks formed by BAB triblock copolymers were investigated. The stress relaxation moduli were determined from the distributions of bridging block lifetimes, and their dependence on solvent quality, concentration, middle-block size and end-block size was investigated. In general it was found that application of a step strain led to stress decay as stress-supporting bridges converted to dangling ends (via an end-breaking mechanism) and loops (via a fusion mechanism). The transition rates of bridges to other states was

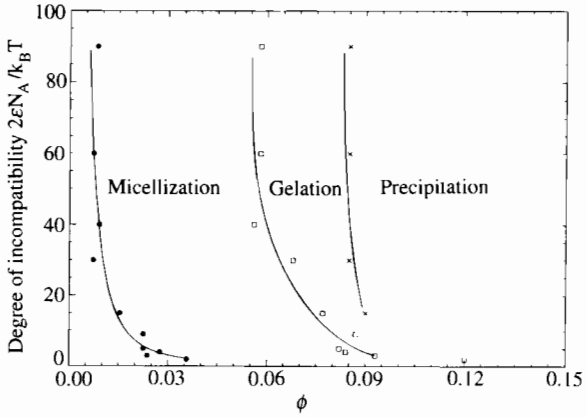

Fig. 3.28 Phase diagram determined from computer simulations of an ABA triblock copolymer with $N_B = 10$ in a selective solvent for the B block and insoluble end blocks (Nguyen-Misra and Mattice 1995*a*).

observed to depend strongly on the interaction energy ($k_BT\varepsilon$) between end-block segments and the solvent molecules, and on the end-block size, but weakly on the middle-block size and concentration. The bridge lifetime did not fit a simple exponential function, leading to a non-exponential stress relaxation, probably due to polydispersity of micelles as well as the existence of more than one relaxation pathway. In fact, the stress relaxation appeared to be described by a stretched exponential. As $k_BT\varepsilon$ increased, the lifetime distribution became increasingly more non-exponential, with a tail extending to longer lifetimes. The contributions from slower modes were found to become more significant as $k_BT\varepsilon$ increased, leading to longer average bridging lifetimes. On the other hand, as the end-block size increased, the bridges had shorter lifetimes on average. As $k_BT\varepsilon$ increased, the rubbery plateau region was observed to broaden and its height increased. With increasing B block length, both the width and height of the plateau region decreased while the transition to flow occurred at a faster rate (Nguyen-Misra and Mattice 1995*b*).

Solubilization of small molecules in micelles formed by BAB triblocks in selective solvents for the midblock has recently been investigated using Monte Carlo simulations by Xing and Mattice (1997). The presence of solubilizates was found to greatly enhance the micellization of the block copolymer. This is in agreement with the conclusions of Gadelle *et al.* (1995) on the basis of gas chromatography measurements of the solubilization isotherms and solute partition coefficients of Pluronic PEO/PPO triblocks in aqueous solutions, with aromatic solubilizates. In the simulations, the amount of solubilizate absorbed by the micelles, the micelle–solvent partition coefficient, and the solubilization capacity were found to be augmented by increasing the amount of solubilizate, in agreement with the experiments of Gadelle *et al.* (1995) and Hurter and Hatton (1992) (also on Pluronic triblocks). The polymer concentration was also found to play a role in

determining micellar properties. The higher the concentration, the bigger the micelles and the larger the partition coefficient and the solubilization capacity, also in accord with experimental observations (Gadelle *et al.* 1995; Hurter and Hatton 1992). It was also noted that the higher the immiscibility between the incompatible components (i.e. between block components or between the B block and solvent or B block and solubilizate or between solvent and solubilizate) the larger the micelles and the stronger the solubilization. Finally, longer insoluble blocks enforce the solubilization by increasing the partition coefficient, but the solubilization capacity is lowered. The soluble block size has no significant effect if its length is only changed slightly (Xing and Mattice 1997).

3.6 Ionic block copolymers

3.6.1 Early work

An excellent review of micellization in ionic block copolymers was presented by Selb and Gallot (1985), and the following section owes much to this for a summary of the literature prior to 1985. However, aspects of the applications of ionic block copolymers discussed in detail by Selb and Gallot are not considered here.

In ionic block copolymers, micellization occurs in a solvent that is selective for one of the blocks, as for non-ionic block copolymers. However, the ionic character of the copolymer introduces a new parameter governing the structure and properties of micellar structures. In particular, the ionic strength plays an important role in the conformation of the copolymer, and the presence of a high charge density leads to some specific properties unique to ionic block copolymers. Many of the studies on ionic block copolymers have been undertaken with solvents selective for the ionic polyelectrolyte block, generally water or related solvents, such as water–methanol mixtures. However, it has been observed that it is often difficult to dissolve ionic hydrophilic–hydrophobic block copolymers in water. These dissolution problems are far more pronounced than for block copolymers in non-aqueous selective solvents, although they do not always reflect real insolubility. In many cases, dissolution can be achieved if a better solvent is used first and examples of the use of cosolvents are listed by Selb and Gallot (1985).

Evidence for micellization in ionic block copolymers has been obtained from a variety of techniques. The viscosity of the solution is one of the simplest methods and it was observed early that some ionic block copolymers have a considerable viscosity in solution in water. Indeed for PS–poly(4-vinyl-*N*-ethylpyridinium bromide) copolymers, Selb and Gallot (1980*a*) observed that dilute aqueous solutions can behave almost like a gel and that the viscosity remains noticeable even at very low copolymer concentrations (below 0.01%). This behaviour cannot be ascribed solely to the observation that polyelectrolyte chains are highly extended in a salt-free medium. Indeed, such high viscosities can only be achieved with polyelectrolytes of very high molecular weight, which is not the case for the ionic blocks of these copolymers. These findings may indi-

cate the presence of particles with a molecular weight higher than that of the single chains, likely due to the aggregation of copolymers into supramolecular structures. As for neutral block copolymers, light scattering is a powerful technique for characterization of micelles in ionic block copolymers. Static light scattering can provide an apparent molecular weight, and dynamic light scattering is used to determine a hydrodynamic radius. Selb and Gallot (1975, 1980*b*,*c*, 1981*a*,*b*) performed extensive elastic light scattering experiments on diblocks containing quaternized poly(4-vinylpyridine) (QP4VP) (e.g. poly(4-vinyl-*N*-ethylpyridinium bromide)) in water–methanol–LiBr solutions. Sedimentation velocity measurements via ultracentrifugation experiments have also been performed on ionic block copolymers, and together with light scattering data a good description of micellization was obtained (Selb and Gallot 1980*b*). Fluorescence experiments using copolymers containing the fluorophore poly(9-vinylphenanthrene) provide evidence for the formation of hydrophobic domains when the block copolymer is dissolved in water, in agreement with a micellar structure with the hydrophobic block in the core segregated from the ionic block in the corona (Morishima *et al.* 1981, 1982*a*,*b*).

The influence of the solvent on micellization in PS–QP4VP block copolymers in methanol–water–LiBr mixtures was explored by Selb and Gallot (1975, 1980*b*,*c*, 1981*a*). Both water and methanol are selective for QP4VP, but to different extents. As for neutral copolymers, formation of micelles was observed above a certain water content (cmc), separating regions 1 and 2 in Fig. 3.29. The proportion and molecular weight of the micelles increase simultaneously as the concentration is increased. The cmc was accompanied by a sharp increase of the intrinsic viscosity, which was explained on the basis that the compact PS block with a lower molecular weight contributes less to the viscosity than the QP4VP block. The change in viscosity is then due to the hydrophilic parts of the micelles that from above the cmc. However, in contrast to neutral copolymers where addition of a selective solvent leads to an increasingly associated state, the degree of association in the system studied by Selb and Gallot passed through a maximum, as evident in the concentration dependence of the Huggins coefficient in Fig. 3.29. This phenomenon was attributed to two opposite effects governing the solubility of the polymer chains: water is a better solvent than methanol for QP4VP, but is a stronger non-solvent for PS. Therefore, as the water content is increased, the solvent power with respect to the whole molecule passes through a minimum which leads to a maximum of association. At still higher concentrations (region 3 in Fig. 3.29), where the association number decreases, the solubility of the copolymer is mainly controlled by the preference of the solvent for QP4VP. Although the apparent micellar mass and sedimentation coefficient decrease at high concentrations, the intrinsic viscosity increases. This was rationalized on the basis that the micellar volume increases due to the expansion of the polyelectrolyte corona, despite the decrease in association number.

The influence of block molecular weight on micelle formation was studied by Selb and Gallot (1980*c*; 1981*a*) using PS–QP4VP diblocks. It was found that the degree of association (p = 10–60) increases with insoluble PS block molecular weight, and decreases with increasing length of the QP4VP block.

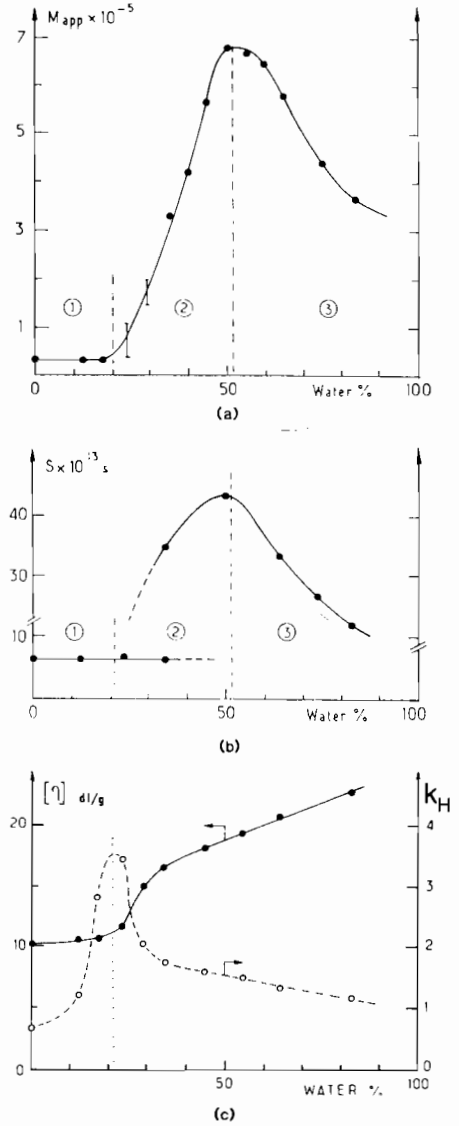

Fig. 3.29 Dependence of (a) apparent molecular weight, (b) sedimentation coefficient and (c) intrinsic viscosity $[\eta]$, and Huggins coefficient, k_H, on solvent composition (methanol–water–0.1 M LiBr mixtures) for solutions of a PS–poly(4-vinyl-*N*-ethylpyridinium bromide) ($M_w = 32.7\,\text{kg mol}^{-1}$, 8% PS) diblock (Selb and Gallot 1981*a*).

The micellization process was found to be much more strongly dependent on the insoluble block molecular weight than the soluble block molecular weight, as for non-ionic block copolymers. These conclusions were supported by fluorescence measurements by Morishima *et al.* (1981, 1982*a*,*b*).

As for neutral copolymers, BAB ionic triblock copolymers are found to be more soluble than AB diblocks in a selective solvent for the B block. Experimental results in support of this conclusion for diblocks with A = PS and B = QP4VP were presented by Ishizu *et al.* (1982), and similar findings were reported by Selb and Gallot (1981*a*) for the same type of copolymer. The effects of changing copolymer architecture have also been explored by using different homologous reactions to introduce ionic sites. For example, Schwab and Heilweil (1983) used different quaternizing agents to modify PS–P2VP. The viscosity of aqueous solutions of copolymers quaternized with long-chain alkyl halides (e.g. $C_8H_{12}Br$) is much lower than that obtained with shorter derivatives (e.g. C_2H_5Br). The hydrophobicity of long alkyl chains is responsible for this behaviour; the quaternized poly(vinylpyridine) blocks behave as polysoaps, which have amphiphilic properties in addition to those resulting from the block nature of the copolymer.

The effect of ionic strength on the micellization of ionic block copolymers has also been investigated. The most striking effect of the addition of salt to micellar solutions of ionic block copolymers is the large decrease in the viscosity, consistent with the behaviour of polyelectrolytes in salt solutions. The effect can be dramatic, for example Schwab and Heilweil (1983) reported a drop in the viscosity of a PS–poly(*N*-methyl-2-vinylpyridinium iodide) diblock solution from 0.182 Pa s in pure water to 2.8×10^{-3} Pa s in the presence of 3% NaCl. The presence of salt changes the quality of the solvent, in addition to altering the conformation of the polyelectrolyte. Consequently, the salt concentration is another important parameter governing the micellization of ionic block copolymers. This is shown by an increase in turbidity which has been observed in some cases when salt is added to a clear copolymer solution, reflecting a higher degree of association. In contrast to variations in copolymer concentration, solvent composition or temperature, a change in ionic strength only modifies the solubility of the polyelectrolyte chain. This is supported by evidence from fluorescence experiments, which show that the conformation of the insoluble block is almost unaffected whereas the ionic block contracts when the salt concentration is increased (Schwab and Heilweil 1983). The effect of salt on micellization in PS–QP4VP/water–methanol mixtures at different LiBr contents has been explored by Selb and Gallot (1980*c*, 1981*b*). They found that the cmc is shifted to lower concentrations as more salt is added. Above the cmc, the weight fraction of micelles and the micellar weight simultaneously increase with increasing salt concentration unit a plateau sets in above a particular salt concentration. It was noted that the salt concentration only has an important effect for short PS blocks ($M_w < 3$ kg mol^{-1}) whereas the molecule–micelle equilibrium is affected much less or not at all for higher PS molecular weights.

For block copolymers with a polyacid or polybase block, the structure and properties of micellar solutions depend on the pH. For example, Morishima *et al.* (1982*b*) found that for a poly(9-vinylphenanthrene)–poly(methacrylic acid) (PVPT–PMA) diblock in water, the rate constant for the fluorescence quenching of phenanthrene groups by oxidative non-ionic quencher is pH dependent. These authors suggested that at low pH the polyacid units are not fully ionized and may participate in the formation of hydrophobic domains, cooperatively with PVPT. An alternative explanation is that the PMA chains are less solvated when

their ionization level decreases, which favours association and thus larger hydrophobic domains. The same authors also demonstrated that interactions between the fluorescent chromophores of the micelle core and the quenching agent depend strongly on electrostatic effects. Thus, depending on pH, the effective charge of the micellar core can generate a potential which may hinder access of an ionic quencher into the core.

As for neutral block copolymers, increasing temperature shifts the equilibrium from molecules to micelles in solutions of ionic block copolymers. However, for ionic block copolymers the effect of temperature is also influenced by salt concentration. For example, for a PS–PQVP diblock in a water–methanol mixture at low LiBr contents, complete dissociation of micelles into molecules occurs above a given temperature (Selb and Gallot 1981*b*). However, for higher salt contents, both micelles and molecules are present, in proportions determined by the polymer concentration. When the molecular weight of the hydrophobic block exceeds 3 kg mol^{-1}, the role of temperature becomes less important, since the hydrophobic PS interactions then primarily govern the micellization process. An unexpected effect of temperature on the conformation of polyelectrolyte chains in micelles formed by an ionic block copolymer has been noted by Schwab and Heilweil (1983). They observed that the polar portion of the micelle appeared to contract as the temperature was increased, which was explained on the basis of dehydration. Another possible explanation (Selb and Gallot 1981*a*) is that in the micelle there is a high polymeric segment density and thus a high charge density in the shell. The polyelectrolyte blocks must therefore be strongly stretched due to strong electrostatic repulsions. By increasing the temperature, the micellar association number is decreased leading to a reduction of charge density and consequently to a smaller extension of the ionic blocks.

The literature prior to 1985 on the solution properties of copolymers with two oppositely charged blocks was also summarized by Selb and Gallot (1985). Polymers containing both anionic and cationic charged blocks are a type of macromolecular polyampholyte. The first studies of such copolymers were carried out by Stille and co-workers (Kamachi *et al.* 1972; Stille *et al.* 1971) using polybase–polyacid diblocks with a poly(2-vinylpyridine) base and a poly(methacrylic acid) or poly(acrylic acid) acid block. The ampholytic character of these copolymers was shown by the fact that they dissolved only in strongly acid or alkaline aqueous media, and that they were insoluble at intermediate pH values. As with classical polyampholytes, potentiometric titration showed an isoelectric point, i.e. a value of the pH at which complete neutralization occurs between the opposite charges. When the pH was varied from the isoelectric point, the turbidity decreased and the viscosity of the solution increased. These results emphasize that the conformation of the copolymer depends on pH due to the interactions between the different ionic blocks. Obviously, the pH value at the isoelectric point of a copolyelectrolyte depends linearly on the relative lengths of the two blocks. A more detailed investigation of the conformation of this type of polyampholyte has been reported by Varoqui *et al.* (1979) for poly(styrene sulphonate)–poly(2-vinylpyridine) (PSS–P2VP) diblocks in water. Ultraviolet spectroscopy measurements showed that the behaviour of the P2VP chain in the copolymer is quite

different to that of the P2VP homopolymer. In particular, curves of the degree of ionization of the P2VP units versus pH show a shift towards higher pH values for the block copolymer compared to the homopolymer. The increase in basicity of the pyridine rings in the copolymer has been ascribed to the strong electric field generated by the neighbouring PSS block. This interpretation was confirmed by the observation that both the reduced viscosity and conductivity of the solution drop steadily with pH as the isoelectric point is approached. This implies that the copolymer becomes more compact whilst simultaneously the effective charge on the polymer diminishes. From these observations, the authors proposed that at high pH values, the P2VP chain is not charged and the block copolymer exhibits a segregated conformation, with a relatively compact P2VP block and an extended PSS block (however, the presence of micelles could not be ruled out). When the pH is decreased, the pyridine groups become ionized and ion-pairing leads to a kind of 'cross-linked' structure and finally at the isoelectric point to an internal polysalt complex with an extremely compact structure.

3.6.2 Polystyrene–poly(acrylic acid) and related ionic block copolymers

Eisenberg and co-workers have investigated micellization of block copolyelectrolytes based on PS and poly(sodium acrylate) in water over a number of years (Astafieva *et al.* 1993). The PS block length ranged from 6 to 100, while that of the polyelectrolyte varied from about 300 to about 1400. Fluorescence measurements with a pyrene probe were used to determine the cmc. At a constant polyelectrolyte block length, changing the insoluble block length from 6 to 100 lowered the cmc from 1.6×10^{-5} to 5×10^{-8} M. In contrast, changing the soluble block length from 300 to 1400 typically changed the cmc values by less than a factor of two, in agreement with trends for neutral block copolymers. For very short PS blocks, the cmc decreased very rapidly with increasing length of the insoluble block, whereas for more than 12 repeat units, the drop in the cmc was more gradual (Astafieva *et al.* 1993). Micelles formed by PS–poly(caesium acrylate) and PS–poly(caesium methacrylate) in toluene, a selective solvent for the PS block, have been characterized using SAXS (Nguyen *et al.* 1994). Comparisons of the micelle core dimensions were made with the Zhulina–Birshtein (1985) and Halperin (1987) models for type IV polymeric micelles, as discussed in Section 3.4.3. The cmc of a family of PS–poly(sodium acrylate) diblocks with fixed PS block length (660 repeat units) and 2.6 to 14 ionic block units in tetrahydrofuran has been investigated using light scattering (Khougaz *et al.* 1994). The cmcs and micellar dimensions of the same type of copolymer in aqueous and NaCl salt solutions have been the subject of studies using fluorescence measurements (Astafieva *et al.* 1995) and static light scattering experiments (Khougaz *et al.* 1995). A complex dependence of the cmc on block lengths was observed in the fluorescence experiments, with a maximum in the cmc as a function of the soluble poly(sodium acrylate) (PNaA) block length (Astafieva *et al.* 1995). Micelles formed by PS–PNaA and PS–PAA dissolved in organic solvents have been characterized by the same group using a variety of techniques including size exclu-

sion chromatography and static and dynamic light scattering (Khougaz *et al.* 1996).

The effect of salt concentration on the association numbers, radii of gyration and second virial coefficients of micelles was investigated using static light scattering (Khougaz *et al.* 1995). It was found that p increased as a function of salt concentration at low salt contents, but remained constant above about 0.10 M NaCl. The data were compared to the predictions of the star polymer scaling theories (Halperin 1987; Zhulina and Birshtein 1985), and several of the mean field models for block copolymer micelles (Leibler *et al.* 1983; Nagarajan and Ganesh 1989*a*; Whitmore and Noolandi 1985). Good agreement was found with several of the models, although it was not possible to discriminate between the quality of the theories with the data available (Khougaz *et al.* 1995).

'Crew-cut' micelles with a short coronal block attached to a long core block, i.e. type IV in Fig. 3.18, have been the focus of recent work by the Eisenberg group (Gao *et al.* 1994*a*; Yu and Eisenberg 1996; Zhang and Eisenberg 1995, 1996; Zhang *et al.* 1996). They first reported the formation of such micelles in aqueous solutions of PS–P4VP diblocks quaternized with methyl iodide (Gao *et al.* 1994*a*). In subsequent work, crew-cut micelles of highly asymmetric PS–PAA (Zhang and Eisenberg 1995) and non-ionic PS–PEO (Yu and Eisenberg 1996) diblocks in water were studied using TEM. Multiple micellar morphologies for the former were observed using TEM (Zhang and Eisenberg 1995, 1996) on copolymers with 80–98% PS. Micellization occurred in the range 3–6 wt% polymer, depending on its composition (Zhang and Eisenberg 1996). For a series of diblocks with a fixed number of PS repeats (200), transitions from spheres to rods to vesicles to compound micelles were observed on decreasing the PAA block length, as illustrated in Fig. 3.30. The micrometre-size compound micelles were observed to have an internal structure made up of a core containing reverse micelles with PS in the corona (Fig. 3.30(e) and (f)). Such compound structures have been predicted theoretically for ABC triblock copolymer melts in the 'superstrong segregation' limit (Dormidontova and Khokhlov 1997). In this limit, segregation between, say, B and C blocks can occur within micelles in the A matrix. A similar effect is likely to underlie the observation of compound micelles in block copolymer solutions. Zhang and Eisenberg (1995, 1996) occasionally observed lamellar structures for compositions where vesicles were otherwise seen (i.e. an alternative bilayer structure), and simple reverse micelle-like aggregates were also noted. The addition of homopolystyrene was observed to drive transitions from the bilayer or cylindrical morphologies into the spherical micelle structure (Zhang and Eisenberg 1996). A transition between morphologies of crew-cut micelles was also observed for non-ionic PS–PEO diblocks, in particular a transition between spherical to rod-like or vesicular structures was induced by increasing the length of the hydrophilic PEO blocks (Yu and Eisenberg 1996). The effect of salt on inducing transitions between micellar structures was also explored for PS–PAA and PS–PEO diblocks in water (Zhang *et al.* 1996). It was found that addition of ions in micromolar ($CaCl_2$ or HCl) or millimolar (NaCl) quantities can change the morphology of PS–PAA micelles in dilute aqueous solutions. In particular, on increasing the acid or salt concentration, the morphology changed from spheres to rods to vesicles and then to large compound vesicles. Gelation could also be

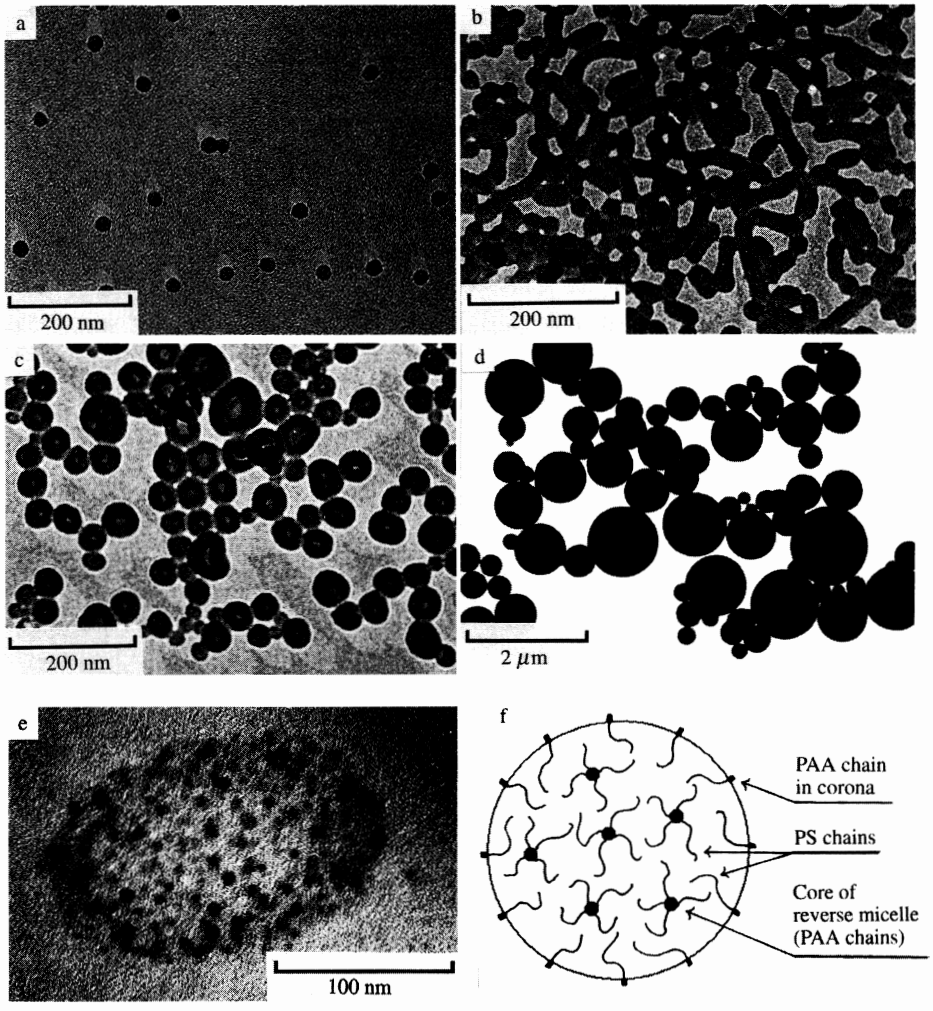

Fig. 3.30 Morphologies formed by PS–PAA diblocks in aqueous solution: (a) PS_{200}–PAA_{21}; (b) PS_{200}–PAA_{15}; (c) PS_{200}–PAA_8; (d) PS_{200}–PAA_4: (e) enlargement of one of the large complex micelles in (d) showing the internal structure. The elongation in one direction was probably caused by the strong shear forces during microtoming. (f) A schematic of the structure of the large complex micelle filled with bulk reverse micelles (Zhang and Eisenberg 1995).

induced with the addition of ions to the solution, and the formation of a 'pearl necklace morphology' (shown in Fig. 3.31) was observed when HCl at a particular concentration was added to a solution containing spherical micelles formed by a PS–PAA copolymer (Zhang *et al.* 1996).

Micellization of PS–PMA diblock and triblock copolymers in 80:20 dioxane:water mixtures was investigated by Qin *et al.* (1994) using static and quasi-elastic light scattering, differential refractometry, viscometry, sedimentation

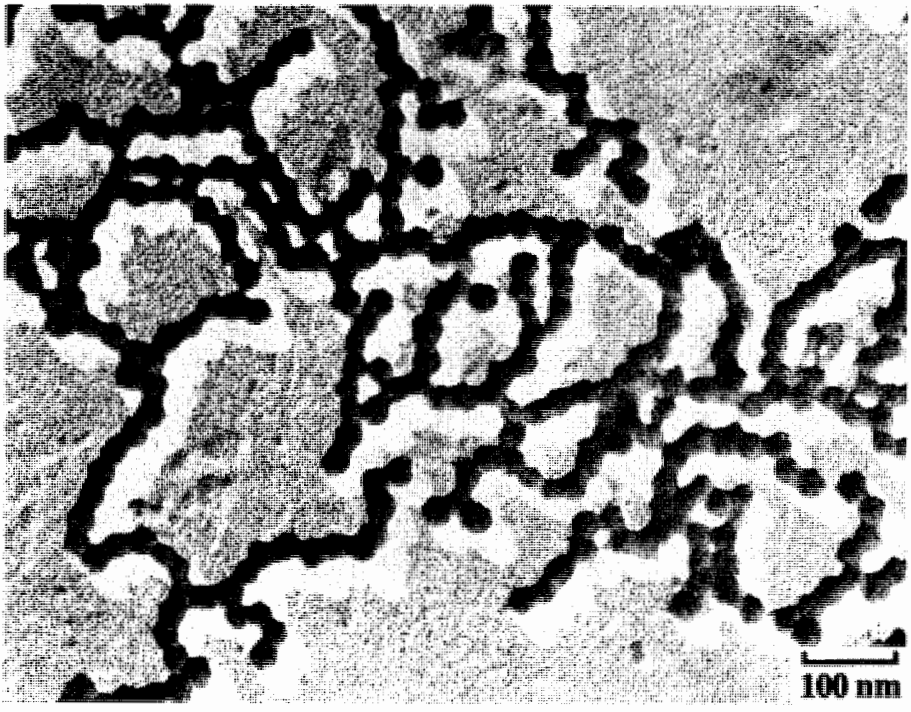

Fig. 3.31 'Pearl necklace' morphology formed by micelles of PS_{500}–PAA_{60} in gelled aqueous solution (Zhang *et al.* 1996). The structure was induced by the addition of 20 mM HCl.

velocity measurements and densitometry. Sedimentation velocity measurements yielded information on the polydispersity of micellar solutions, which were shown to consist almost exclusively of single micelles. Scaling relationships for the micellar association number and hydrodynamic radius were compared to scaling theories, as discussed in Section 3.4.3. Tian *et al.* (1995) subsequently investigated the solubilization of a range of organic compounds in the same system. The extent of solubilization obtained from static light scattering data was compared to the predictions of a simple thermodynamic model (Tian *et al.* 1995). Solubilization of benzene in micelles formed in the same system was studied earlier (Kiserow *et al.* 1992; Procházka *et al.* 1992) using static and dynamic light scattering and fluorimetric measurements on tagged chains. Fluorescent probe mobility was monitored by following excimer formation and time-dependent fluorescent anisotropy, which yielded detailed information on the core swelling during solubilization.

3.6.3 Other ionic block copolymers

A block ionomer of poly(L-glutamic acid)–poly(L-leucine) was studied in aqueous solution using ultramicroscopy (Section 1.4.18) and DLS by Price *et al.*

(1979). Poly(L-glutamic acid) is ionic and poly(L-leucine)is hydrophobic. The diffusion coefficient and hydrodynamic radius obtained from the two techniques were compared, and found to be in reasonable agreement.

Armes and co-workers have described the characterization of micellization in a range of hydrophilic–hydrophobic block copolymers (Baines *et al.* 1996; Tuzar *et al.* 1997). The micellization of poly[(2-dimethylamino)-ethyl methacrylate]–PMMA (PDMAEMA–PMMA) diblocks in aqueous solution was studied using static and dynamic light scattering, ultracentrifugation and surface tension measurements (Baines *et al.* 1996). For these copolymers, the cmc was found to increase (Baines *et al.* 1996) with the length of the hydrophobic block if the hydrophilic block length was fixed, in contrast to the trend for most neutral and ionic block copolymers. Increasing the overall molar mass of the copolymer also increased the cmc for a given composition. Increasing the overall molar mass of the copolymer for a given composition produced larger micelles with a lower association number. Both micelle size and association number decreased with the length of the hydrophobic block if the hydrophilic block length was fixed. For these ionic block copolymers, the size and association number of the micelles can be systematically controlled by changing the temperature, pH or ionic strength of the solution (Baines *et al.* 1996). Tuzar *et al.* (1997) performed static and dynamic light scattering and small-angle neutron scattering experiments on two poly(3-[*N*-(2-methacroyloylethyl)-*N*,*N*-dimethylammonio]-propane sulphonate)–PMMA diblocks. Micellization in a series of block copolymers based on tertiary amine methacrylates has recently been investigated using dynamic light scattering and surface tension measurements (Bütün *et al.* 1997). Copolymers of PDMAEMA–PDEAEMA, where the latter block has a 2-diethylamino group in place of the 2-dimethylamino block in the former were studied. It was found that PDMAEMA-rich copolymers in water formed micelles with a PDEAEMA core. However, copolymers with more than 50 mol% PDEAEMA were insoluble under these conditions (Bütün *et al.* 1997). Micellization in aqueous solutions of diblocks of poly(methyl triethylene glycol vinyl ether) (PMTEGVE, hydrophilic) and poly(isobutyl vinyl ether) (PIBVE, hydrophobic) has been characterized using dynamic light scattering, aqueous GPC and dye solubilization (Patrickios *et al.* 1996). Dihydrophilic block copolymers of poly(methyl vinyl ether) (PMVE) and PMTEGVE have been shown to form micelles at elevated temperatures (Forder *et al.* 1996), due to the increasingly hydrophobic nature of PVME above 50 °C. Proton NMR spectroscopy confirmed that the PVME block formed the micellar core, and that micellization was reversible.

3.7 Dynamics in block copolymer solutions

3.7.1 Chain dynamics

Dynamic light scattering

The concentration dependence of the mutual diffusion coefficient, D, in binary solution can be expressed as

$$D(c) = D_0(1 + k_d c + \ldots). \tag{3.34}$$

Here D_0 is the infinite dilution diffusion coefficient, k_d is the concentration coefficient and c is the concentration. A plot illustrating this behaviour is shown in Fig. 3.32. The concentration coefficient is given by (Vink 1985).

$$k_d = \left.\frac{\partial(D/D_0)}{\partial c}\right|_{c\to 0} = 2A_2M - k_f - 2V, \tag{3.35}$$

where A_2 is the second virial coefficient and V is the partial specific volume, which is generally small compared to the other two terms on the right-hand side of eqn 3.35. The parameter k_f that describes the initial concentration dependence of the frictional interaction between solute and solvent is given by Yamakawa (1971) as

$$k_f = 1.2A_2M + 0.2[\eta]. \tag{3.36}$$

The value of k_d is large and positive for high molecular weight polymers in good solvents, where the term involving A_2 dominates, while in theta solvents ($A_2 = 0$), k_d has a small negative value which reflects k_f (Kent *et al.* 1994).

There is a substantial body of work using dynamic light scattering to probe the hydrodynamic properties of poly(oxyethylene)-based block copolymers in aqueous solution. The work of Brown and co-workers has been reviewed by

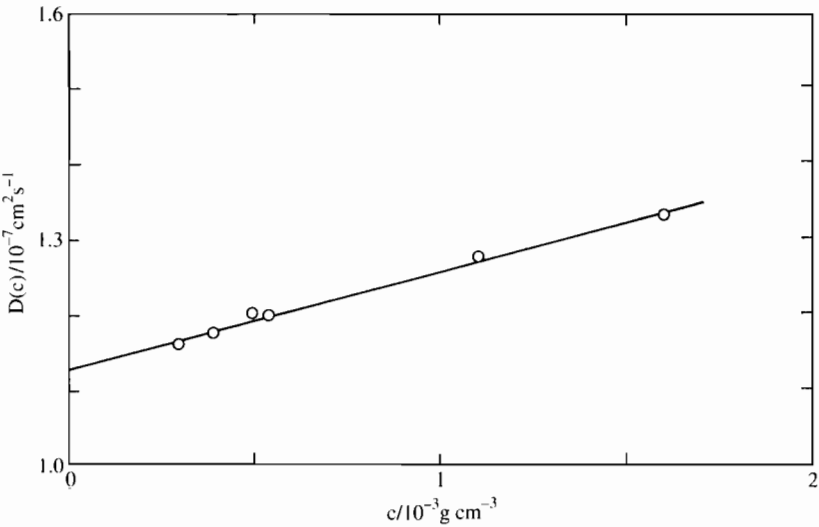

Fig. 3.32 Concentration dependence of the translational diffusion coefficient $D(c)$ for a PS–PMMA diblock (M_w = 153 kg mol^{-1}, 39% PS) in benzene at 30 °C (Tsunashima and Kawamata 1993).

Almgren *et al.* (1995), and also by Chu and Zhou (1996). DLS on aqueous solutions of a Pluronic triblock was employed to determine the fraction of unimers, micelles and micellar aggregates as a function of temperature, and thus to locate the cmc (Brown *et al.* 1991). The hydrodynamic radii of the particles were extracted from the concentration-dependent diffusion coefficients. A micellar sphere-to-rod transition was identified at high temperature in the same system using DLS by Schillén *et al.* (1994). Increasing depolarized scattering at high temperature was due to a transition to anisotropic micelles. Two relaxation modes were observed from aqueous solutions of this triblock; the slow mode, diffusive in nature, provided the translational diffusion coefficient, whereas the fast mode yielded the rotational diffusion coefficient, and this could be interpreted to given an estimate of the length of the rod-like micelles. A comparison of the micellization of $PEO_mPPO_nPEO_m$ Pluronics with n fixed equal to 39, and m = 6, 67 or 96 involved extensive dynamic and static light scattering measurements (Brown *et al.* 1992). The formation of gels at high concentrations was also observed, but discussion of this is reserved for Chapter 4. Other examples include the experiments by Bahadur *et al.* (1992) which showed that addition of salt does not much affect the diffusion coefficient in Pluronic F68 ($PEO_{76}PPO_{30}PEO_{76}$). Anomalous micellization in L64 (discussed in Section 3.3.2) was examined using DLS by Almgren *et al.* (1992) and modes corresponding to large clusters were ascribed to the presence of diblock impurities in the sample.

Chu and co-workers have also made extensive use of dynamic light scattering to study micellization in PEO/PPO triblocks. This work is discussed in Section 3.3.2 and reviewed by Chu and Zhou (1996), and we do not repeat details here. In addition, temperature-dependent micellization in solutions of a PS–poly (*tert*-butylstyrene) (PtBS) diblock and PtBS–PS–PtBS triblock in dimethylacetamide has been probed using this technique by Chu and co-workers (Zhou *et al.* 1993, 1995). Booth and co-workers use DLS routinely in their studies of PEO–PBO copolymers, as also discussed in Section 3.3.2 and reviewed by Booth *et al.* (1997).

The dynamics of PS blocks in a PS–PMMA diblock in dilute solution in benzene, which is a good solvent for PS and PMMA, have been investigated using DLS (Tsunashima and Kawamata 1993). The translational diffusion coefficient of the copolymer chain was obtained from the slow mode in the DLS spectrum. However, it was observed that diffusion was retarded due to strong intrachain hydrodynamic interactions. The diffusive motion coupled very strongly with the internal modes of motion and led to a deformation of the block copolymer chain during diffusion. The fast DLS mode provided information on the internal copolymer motions, providing evidence for chains with non-draining hydrodynamic interactions. Kent *et al.* (1994) compared the diffusive behaviour of solutions of PS–PMMA random or diblock copolymers with the corresponding homopolymers. Dynamic and static light scattering were used to determine whether interactions between unlike monomers in dilute solution of copolymers alter the solution properties from those of the corresponding homopolymers (Kent *et al.* 1994). Solvents of different quality were used for this work. For dilute solutions of a random copolymer in a solvent slightly better than theta,

DLS measurements showed that intramolecular interactions between unlike monomers caused the coil to be expanded compared to the corresponding homopolymers. This was consistent with cloud point and viscosity data. There was no evidence for repulsive interactions increasing the repulsive potential between coils in a good solvent. For diblock copolymers, intramolecular interactions were found not to lead to an additional expansion of the molecule, as measured by the hydrodynamic radius, nor to expansion of individual blocks as probed by light scattering with one block contrast-matched to the solvent. This was speculated to be due to the fact that most intramolecular interactions occur between monomers separated by a relatively short distance along the chain. Properties of dilute diblock copolymers, such as the diffusion coefficient, viscosity, and radius of gyration, in the limit of infinite dilution gave little indication of behaviour different from homopolymers. In contrast, at low but finite concentration, values of virial coefficients extracted from DLS experiments suggested that intermolecular interactions between block copolymers may induce behaviour which is quite different than for homopolymers, such that weak ordering may exist far from the conditions where ordered micellar phases are observed (Kent *et al.* 1994).

The dynamic structure factor of block copolymer liquids (melts and solutions) has been accounted for using dynamical mean-field theory by Benmouna *et al.* (1987*a*,*b*). For block copolymers in non-selective good solvents, two modes are predicted: a cooperative diffusion mode, due to fluctuations in the total polymer concentration, and an internal mode arising from the relative motions of the two blocks. The former has a decay rate proportional to q^2, and the latter mode has a decay rate independent of wavevector q when $qR_g \ll 1$, where R_g is the radius of gyration. Later, a theory was developed that allows for the compositional heterogeneity of all real copolymers, i.e. fluctuations in composition from chain to chain (Jian *et al.* 1995). This permits fluctuations in relative block concentration of arbitrarily long wavelength and generates an additional diffusive DLS mode, with decay rate governed by the translational diffusion of the whole chain. This mode is termed the 'heterogeneity' mode by Stepanek and Lodge (1996), to emphasize that fluctuations in chemical composition rather than molecular weight are relevant, although 'polydispersity' mode has also been employed (Jian *et al.* 1995).

Nuclear magnetic resonance

The dynamics of PS–P(E/P) chains in micelles formed in paraffinic solvents were studied by ^{1}H and ^{13}C NMR by Candau *et al.* (1984), in tandem with DLS and TEM which provided direct evidence for spherical micelles. In dilute solutions in octane below 50 °C, the PS core was found to have two components, a 'rigid' component with the same NMR linewidth as bulk glassy PS and a 'mobile' component attributed to a plasticized surface layer. The 'rigid' component underwent a sharp linewidth transition at 50 °C attributed to segmental motions. In octane, the micelles were found to dissociate above 80 °C. In higher alkanes, the dissociation occurred at increasing temperature with increasing solvent molecular weight. High-resolution NMR spectroscopy was used by Spěváček (1982) to investigate

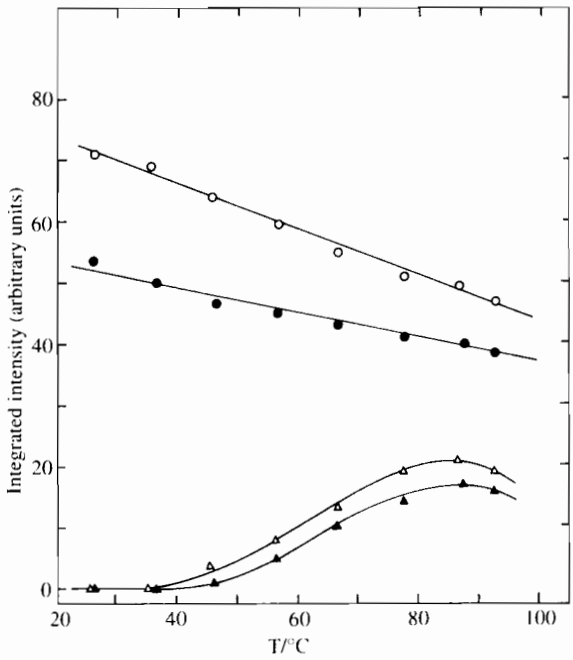

Fig. 3.33 Temperature dependence of the integrated intensity of –CH=CH– protons (○,●) and of aromatic protons (△,▲) from ^{1}H NMR experiments on a PS–PB diblock (M_n = 64 kg mol^{-1}, 24% PS) in heptane (Spěváček 1982). $c_1 = 5 \times 10^{-2}$ g cm^{-3} (○,△) $c_2 = 2 \times 10^{-3}$ g cm^{-3} (●,▲).

chain dynamics in micellar solutions of a PS–PB diblock in heptane (selective for PB) and a PS–PB–PS triblock in 1,4-dioxane and 1,4-dioxane/D_2O mixtures (precipitant for PB). An increase in mobility of PS units above about 40 °C was observed in the PS–PB solution, as shown in Fig. 3.33, caused by a gradual swelling of the PS core, both in polymolecular micelles and in unimolecular micelles. For the PS–PB–PS solution, considerable mobility of the PB was noted and entanglements between PB in the core could not be detected, which was ascribed to the effect of isotropic Brownian motion averaging the dipolar interactions. The order of magnitude difference in segmental mobilites of PS and PB (Fig. 3.33) explained why this effect was not relevant for the system with PS-core micelles (Spěváček 1982).

Field gradient NMR has been employed to determine the self-diffusion coefficient of a Pluronic triblock, and the hydrodynamic radius has been compared to DLS measurements on the same system (Almgren *et al.* 1992). NMR was found to give a somewhat lower value for the hydrodynamic radius than DLS. However, at infinite dilution the values obtained from the two techniques are the same. A similar observation has been made for cyclo-$PBO_{27}PEO_{144}$ in aqueous solution (Yu *et al.* 1996*c*). This effect has been attributed (Almgren *et al.* 1995) to the difference in dynamic averaging for the DLS and NMR experiments. In DLS,

monomers and micelles are distinguished from their relaxation times, which depend on their z-average dimensions. In contrast, the NMR diffusion coefficients are close to a number average value. Thus, the NMR measurement reflects averaging of both monomeric and micellar motion and hence provides lower values for diffusion coefficients.

Proton NMR longitudinal and transverse relaxation time measurements have been used to determine changes in segmental dynamics upon micellization of $PEO_{93}PPO_{44}PEO_{93}$ (Godward *et al.* 1995). At the critical micelle temperature, there was a marked transition in the relaxation times of the hydrophobic PPO block attributed to a change from well-solvated mobile chains below the cmt to a more restricted, concentrated micelle–core environment above the cmt. However, the dynamics of PEO segments were not changed at the cmt, indicating the persistence of a solvated, mobile chain structure. Considerable interpenetration of PEO and PPO blocks at the interface was indicated and relaxation times analysed using a two-mode correlation function supported the conclusions from relaxation time measurements regarding segmental mobilities.

Chain dynamics at the segmental level in the corona of micelles formed by ionic block copolymers or in the area surrounding the ionic cores have been investigated using ^2H NMR experiments (Gao *et al.* 1994*b*). Segmental dynamics were probed in micelles formed by PS–PNaA (and also sodium carboxylate terminated polystyrene), where part of the PS block was deuterium labelled (about three units), in CCl_4. The distance between the ^2H-labelled segments and the ionic cores was controlled by the number of styrene units separating the labelled segment from the non-ionic–ionic block junction. NMR linewidths, signal intensity, and relaxation times of the block ionomers and their non-ionic precursors (PS–poly(*tert*-butyl acrylate)) indicated that the mobility of the soluble segments near the ionic cores was dramatically reduced. At a distance of 25 repeat units from the non-ionic–ionic block junctions, the mobility was still significantly lower than in single chains, while at a distance of 50 repeat units from the junction, the mobility was essentially the same as that in the single chains. Even for sodium carboxylate-terminated PS, where there is only a single ionic group, the ^2H-labelled styrene segments 14 repeat units away from the block junction experienced restricted mobility due to the ionic association. Deuterium-labelled ionomers with the same PS block but different lengths of ionic blocks were also examined, and it was found that the longer the ionic block, the slower the motion in the corona, but the effect was diminished for ionic blocks with more than six repeat units (Gao *et al.* 1994*b*). High-resolution proton NMR was used to investigate molecular motions in PS–PEO diblock copolymers in D_2O/sodium lauryl sulphate mixtures, with 5% D_2O and 2.5–10% SLS (Nakamura *et al.* 1977). It was reported that the molecular motions of the PS block of the copolymer in aqueous solution were activated by interactions between the PS block and the added sodium lauryl sulphate.

Neutron spin echo

In the neutron spin echo technique, the normalized intermediate dynamic structure factor $I(q,t)/I(q,0)$ is measured directly. This method has been used to probe

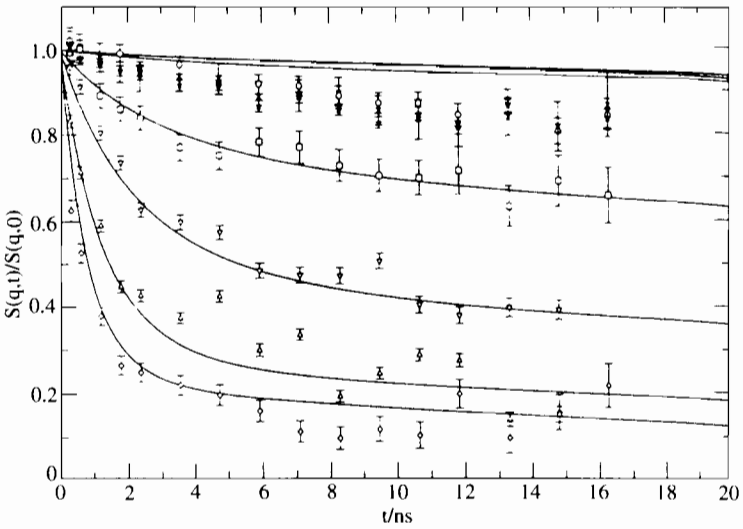

Fig. 3.34 Normalized intermediate dynamic structure factor for the corona of a PS–PI diblock ($M_w = 8.5\,kg\,mol^{-1}$, 12% PS) in deuterated decane (2% polymer). Different symbols correspond to measurements at $q/10^{-3}\,Å^{-1}$ = (□) 26, (▽) 32, (∗) 38, (×) 51, (◇) 64, (△) 89, (○) 115. Solid lines correspond to a model described by Farago *et al.* (1993).

the dynamics of the micellar corona of PS–PI diblocks in dilute solution in decane (selective for PI) (Farago *et al.* 1993). The thermal density fluctuations of the PI corona were probed in the neutron spin experiment, using solutions contrast-matched with respect to PS. The relaxation behaviour observed, with an initial fast decay followed by a relaxation with a long time tail, was described remarkably well by a generalization of the model of de Gennes (1986) for the dynamics of an adsorbed polymer layer in solution to the case of spherical micelles. In the theory by de Gennes, the dynamics of the adsorbed polymer layer is determined by the balance of a restoring force due to the osmotic pressure gradient and a viscous force exerted on the polymer due to its motion with respect to the solvent background (de Gennes 1986). The model for spherical micelles allowed for the 'breathing modes' of radial shells in the micelles and a comparison of the calculated $I(q,t)$ with the experimental results revealed good agreement, as shown in Fig. 3.34 (Farago *et al.* 1993).

3.7.2 Kinetics of micellization

There have been very few studies on the kinetics of micellization in block copolymer solutions. Micellization in aqueous surfactant systems close to equilibrium occurs on a time-scale far below one second. Experimental results obtained by fast reaction techniques, such as temperature jumps or pressure jumps or steady-state methods such as ultrasonic absorption, NMR and ESR, show that at least

two relaxation processes are involved with the re-establishment of equilibrium: (i) a faster process with a relaxation time of 10^{-6} to 10^{-3}s that is attributed to unimer $\rightleftharpoons$ micelle equilibration at a constant concentration of micelles, (ii) a slow process (about 100 times slower than the fast one) is then assigned to an association $\rightleftharpoons$ dissociation equilibration, accompanied by changes in micellar concentration (Tuzar and Kratochvil 1993). In the case of block copolymers, the dynamics are likely to be complicated by entanglements of the blocks that are absent for low molecular weight surfactants. It has been pointed out that a promising technique for investigation of the dynamic molecule $\rightleftharpoons$ micelle equilibrium without perturbation of the system is to follow the kinetics of mixing of fluorescence-labelled molecules (Tuzar and Kratochvil 1993).

Indirect methods for obtaining information on the kinetics of the association/dissociation equilibrium include sedimentation velocity and GPC experiments. The application of these techniques is based on comparison of sedimentation or GPC elution curves with model curves based on theories for separation of unimers and micelles during a sedimentation velocity (Gilbert 1955) or GPC (Ackers and Thompson 1965; Coll 1971; Procházka *et al.* 1988, 1989) experiment. Experiments have been performed that demonstrate several of the qualitative model predictions (Procházka *et al.* 1989). The main conclusions were that GPC curves with two well-separated peaks can only result from a slow dynamic molecule $\rightleftharpoons$ micelle equilibrium, and that no simple interpretation of elution curves in terms of relative concentrations of unimer and micelles is possible (Procházka *et al.* 1989). Thus no quantitative information on the kinetics of the molecule $\rightleftharpoons$ micelle equilibrium can be obtained from sedimentation velocity or GPC data.

Direct methods, such as the stopped-flow technique, appear to be more promising than GPC. A stopped-flow study, with light scattering detection, has been performed of association and dissociation in solutions of a PS–PB diblock or a PS–PB–PS triblock (Bednár *et al.* 1988). Both copolymers formed micelles with aliphatic cores and polystyrene shells in 1,4-dioxane and its mixtures with up to 30% heptane. The process of micelle formation was induced by mixing a 1% copolymer solution in a good solvent mixture of 1,4-dioxane/40 vol% heptane with the same amount of 1,4-dioxane to give a final solution with composition 1,4-dioxane/20 vol% heptane. Decomposition of micelles was achieved by mixing a 1% micellar solution in 1,4-dioxane with the same amount of heptane. In the stopped-flow experiment, two syringes containing the liquids to be mixed were used to inject the components into a light scattering cell and fill a stopping syringe. When the plunger of the stopping syringe hits a stop block, the flow is stopped and just before this the detection system is activated. The time dependence of the scattered light from these systems indicated exponential-type behaviour (see Fig. 3.35). The decay curves could be best fitted by a double-exponential function, and the mean value of the associated relaxation times was used to characterize the rate of micelle formation or dissociation. For the association process, relaxation times of 43 and 69 ms for the diblock and triblock respectively were obtained. A two-step process of micelle formation has been

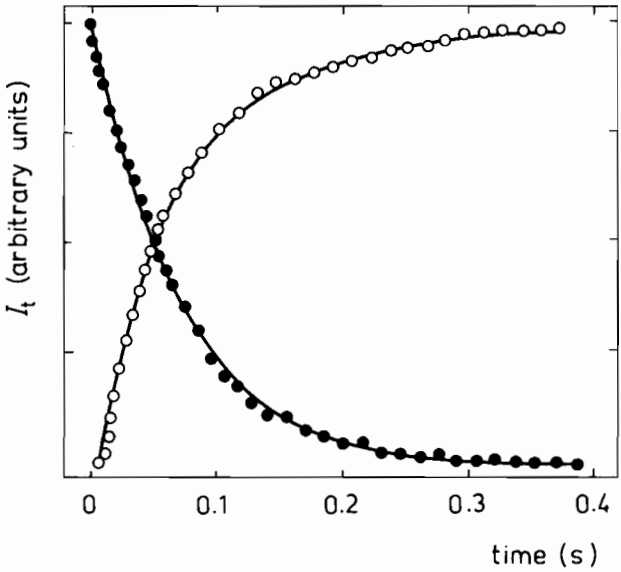

Fig. 3.35 Time dependence of the intensity of scattered light, I_t, after mixing 1% micellar solutions of a PS–PB–PS triblock (M_w = 105 kg mol^{-1}, 40% PS) in 1,4-dioxane with an equal amount of heptane (●); 1% unimer solution of the same copolymer in 1,4-dioxane/40 vol% heptane with an equal amount of 1,4-dioxane (○) (Bednár *et al.* 1988).

proposed: first, the association of unimers and second the rearrangement of core blocks to adopt their equilibrium conformation. It was proposed that the results of the stopped-flow experiment only correspond to the first of these processes, which was thus not a simple, one-step process. In the decomposition process, the first step would be a rapid influx of solvent molecules into the micellar core, followed by a solvent-assisted separation of copolymer molecules. The low value of the relaxation time for dissociation of a diblock (τ = 1 ms) compared to a triblock (τ = 137 ms) was explained on the basis that the dissociation is faster for diblocks, because they cross the micellar core–shell interface once (Bednár *et al.* 1988).

The observation by Price and co-workers (Booth *et al.* 1978; Price *et al.* 1982; Teo *et al.* 1986) of a 'loss' of copolymer during elution through a GPC column was ascribed to adsorption of copolymer by the gel in the column. Spacek (1986) proposed the alternative explanation that some of the micelles, formed inside the gel particles, cannot leave narrow pores permeable only for the unimer. A simplified diffusion model was used to estimate the time needed for the formation of micelles under the conditions of the GPC experiment. The value obtained was in reasonable agreement with results from a stopped-flow experiment (Bednár *et al.* 1988). On the other hand, the experimental fact that the major part of the

micelles remained intact during elution (over a time-scale up to hours) was interpreted as a result of a very slow unimer ⇌ micelle equilibration.

The dynamics of formation of mixed micelles of PS–PMA diblock and triblock copolyelectrolytes in water–dioxane mixtures have been studied by sedimentation velocity measurements following extraction of aliquots of the solution during the relaxation from the initial non-equilibrium state (Tian *et al.* 1993). The rate of hybridization was found to be a very sensitive function of the architecture of both copolymers and of the thermodynamics of the solvent mixture. It was found that the transfer of unimers from the large micelles to the small ones was dominant in all cases, contrary to the expectation that transport from small micelles to large ones would dominate. It was suggested that this was because small unimers cannot enter the large micelles appreciably, as this would destabilize both large and small micelles. The rate-determing step is then the movement of large unimers and their escape from the large micelles (Tian *et al.* 1993).

3.8 Adsorption from block copolymer solutions

3.8.1 Computer simulation of adsorbed block copolymers

The adsorption of block copolymers from solution has been investigated experimentally, theoretically and by computer simulation. The adsorption of diblock copolymers from a *non-selective* solvent was studied using Monte Carlo simulations by Zhan *et al.* (1993*a*,*b*). Adsorption isotherms and kinetics of adsorption were discussed in this case where no micellization occurs (Zhan *et al.* 1993*a*). Where micellization occurred, the kinetics were described by a two-stage process. The first process with a high rate of adsorption was found to be a diffusion-controlled process, with small interactions between the adsorbed chains. The second process with a low rate of adsorption is a rearrangement of the conformation of adsorbed chains into a more brush-like structure. The adsorption kinetics were observed to be strongly dependent on the block lengths of the copolymer and the solution concentration (Zhan *et al.* 1993*a*). These results were compared to experimental studies of adsorption kinetics of diblock copolymers (Huguenard *et al.* 1991; Motschmann *et al.* 1991; Munch and Gast 1990; Tassin *et al.* 1989). The structure of the adsorbed layer was also determined in detail (Zhan *et al.* 1993*b*). The bound fraction of the anchoring block B was found to increase as the surface affinity increased, to decrease as the length of the B block increased, and to decrease with increase in copolymer volume fraction. The probability of adsorption of the middle beads in the B block was found to be larger than that for the end beads. The surface coverage of the B block in the first layer increased as the concentration of copolymer increased, and as the surface affinity increased. The height and position of the adsorption peak for the non-anchoring blocks were found to be determined by the length of the non-anchoring block and the surface affinity. The non-anchoring block was found to be stretched. Only a limited number of experimental studies (Guzonas *et al.* 1992; Wu *et al.* 1991) were available for comparison with the theoretical pre-

dictions for thermodynamic aspects of adsorption. However, a more detailed comparison was made (Zhan *et al.* 1993*b*) with the self-consistent field theory of Evers *et al.* (1990, 1991*a*,*b*).

The self-assembly and adsorption of a diblock copolymer from a *selective* solvent were analysed in detail by Zhan and Mattice (1994*a*,*b*). The B block was in a poor solvent and the A block in a good solvent, thus adsorption of the former onto a surface occurred, with the latter extending into the solution to form an external layer. Copolymer self-assembly was found to have a large effect on adsorption (Zhan and Mattice 1994*b*). According to the adsorption behaviour of the copolymer, the overall concentration was divided into three regions. Below the cmc, the adsorption of the copolymer occurs from the free chains. The equilibrium is mainly between the free chains and the adsorbed chains. Just above the cmc, the micelles do not contribute significantly to the adsorption, and the adsorption also occurs from the free chains. There are then two equilibria, between free chains and micelles and between free chains and adsorbed chains. The lower adsorbed amount observed just above the cmc was ascribed to the lower concentration of free chains. At higher concentrations, adsorption may occur from either free chains or micelles. There are then three equilibria in the system, and the absorbed amount is largely controlled by the adsorption of micelles. Close to the cmc the structure of the adsorbed layer in a selective solvent was found to be similar to that in a non-selective solvent, but well above the cmc the segment density profiles had a different shape because of the self-assembly of adsorbed chains (Zhan and Mattice 1994*b*). These results were compared to the experimental results of Tassin *et al.* (1989) and Munch and Gast (1990). The former measured the angular variation of reflected intensity from surface plasmons to study the adsorption of PS–P2VP diblocks on a silver surface, and observed that the first stages of adsorption corresponded to the adsorption of micelles, and that adsorption of single chains is a slower process. Munch and Gast (1990) investigated the kinetics of adsorption of PS–PEO diblocks from cyclopentane, which is a selective solvent for PS, via ellipsometry. The adsorption of the copolymers onto a dielectric substrate from gently flowing solutions was measured. It was observed that the initial rate of adsorption above the cmc is faster than just below the cmc, whereas the final adsorbed amount is greater for adsorption from solutions just below the cmc. This was explained on the basis of two adsorption mechanisms. Above the cmc, the rapid initial rate of adsorption indicated that micelles adsorbed. Below the cmc, the adsorption of single chains results in a more homogeneous, and thus enhanced, coverage (Munch and Gast 1990).

Balazs and Lewandowski (1990) have performed simulations of the adsorption of triblock copolymers onto a planar surface, and examined the conformations of the adsorbed chains. Monte Carlo simulations were performed of the motion of hydrophilic–hydrophobic chains on a cubic lattice. These simulations revealed a complex structure in the interfacial region due to the self-assembly of chains, driven by the solvent-incompatible block, reducing adsorption onto the surface. The influence on the surface coverage of length of the hydrophilic segement, polymer concentration, interaction energy between hydrophilic block and the

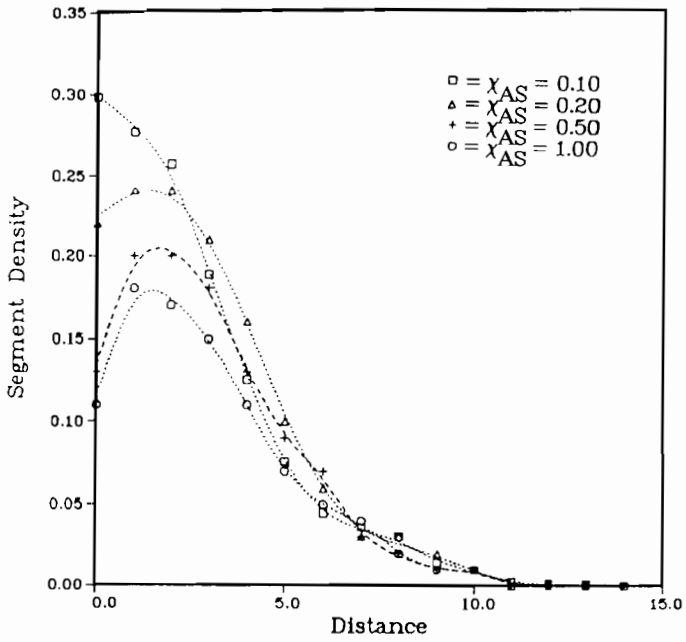

Fig. 3.36 Segment density profiles from a Monte Carlo computer simulation of adsorption of a BAB triblock at a planar interface, where the hydrophobic B block is preferentially adsorbed (Balazs and Lewandowski 1990). Profiles are plotted for different A segment–surface interaction parameters, χ_{AS}, with $\chi_{AS} = 0$ and a chain length = 30 units.

surface, polydispersity and reversible adsorption were examined in detail. As an example of their calculations, segment density profiles for adsorbed triblocks with different segment–surface interaction parameters are shown in Fig. 3.36. In a companion paper, the adsorption of BAB triblocks from a selective solvent for the B block onto a rough, corrugated surface was investigated (Balazs *et al.* 1990). It was found that the B blocks can bind to the ridges of the bumpy surface and the A segments span the troughs, if the end-to-end distance of the chain is comparable to the well width, if the copolymer has short, sticky B blocks at each end and if the B–surface interaction is highly attractive while the A–surface interaction is repulsive. Consequently, the adsorption of triblocks acts to smooth a rough surface (Balazs *et al.* 1990).

Monte Carlo simulations have also been performed of the adsorption of triblock copolymers on an impenetrable surface from a non-selective solvent (Haliloglu *et al.* 1997), the results being compared to Langmuir adsorption studies using ellipsometry by Dorgan *et al.* (1993) of adsorption via end-blocks of a PEO–PS–PEO triblock copolymer from a non-selective solvent (toluene). Haliloglu *et al.* (1997) additionally calculated Langmuir adsorption isotherms and analysed adsorption kinetics. Comparison was also made with simulations for diblocks, and it was found that the adsorbed amount is lower for the diblock than for the triblock (corresponding to two joined diblocks) at low concentration.

However, the surface coverage is the same for both copolymers when weakly adsorbed to the surface. Surface density profiles were also compared. Finally, scaling relationships for triblock copolymer adsorption under weak adsorption conditions were derived (Haliloglu *et al.* 1997). In a related paper (Nguyen-Misra *et al.* 1996), adsorption and bridging of triblock copolymers in an athermal solvent and confined between two parallel flat surfaces were studied, and the dynamic response of the system to sinusoidal and step shear was examined.

3.8.2 Surface force experiments on adsorbed block copolymers

The first report of the use of the surface force apparatus for measuring forces between adsorbed layers of block copolymers was by Hadziioannou *et al.* (1986). They attached symmetric PS–PVP diblock copolymers via adsorption of the PVP block, the PS block being non-adsorbing, to mica surfaces in the good solvent toluene. It was demonstrated that the PS chains were strongly stretched normal to the adsorbing surface forming a polymer brush at the liquid–solid interface. A force–distance profile for a P2VP–PS diblock absorbed on mica from a cyclohexane solution is illustrated in Fig. 3.37. This shows that well below the theta temperature for PS in cyclohexane ($T_\theta = 34\,^\circ\mathrm{C}$), there is pronounced attraction at large plate separations, whereas at higher temperatures the force is purely repulsive (Hadziioannou *et al.* 1986). To mimic a layer of end-grafted polymer chains more closely, Taunton *et al.* (1988, 1990) investigated highly asymmetric diblock copolymers and demonstrated that PS–PEO diblock copolymer chains with a short PEO block can be terminally anchored on mica through the adsorption of EO segments on the mica surface with the PS blocks dangling freely into the solvent (e.g. toluene). At high surface coverage, the PS chains were found to be strongly stretched, and the monotonically repulsive interaction profiles of two such polymer brushes were in good agreement with theoretical predictions (Taunton *et al.* 1988, 1990).

The interaction of end-adsorbed diblock and triblock copolymers in toluene against a bare mica surface was investigated by surface force measurements by Dai and Toprakcioglu (1992). Only monotonically repulsive forces were observed when a bare mica sheet interacted with a single layer of PS–PEO diblock, end-adsorbed at a toluene–mica interface. In contrast, clearly detectable attractive forces were found for PEO–PS–PEO triblock copolymers under similar conditions. The attraction was attributed to polymer bridges in which the two PEO endblocks of a single triblock chain simultaneously adsorbed onto opposing mica surfaces. The experimentally detected evolution of the force profiles from attractive to repulsive with successive compression–decompression cycles was proposed to result from the dynamics of conformational rearrangments and the subsequent migration of chains between the surfaces. The results further indicated that the relative populations of chains adsorbed in a loop or tail conformation depend on the adsorption energy of the anchoring blocks, as does the degree of stretching of the bridging chains before rupture upon separation of the mica surfaces (Dai and Toprakcioglu 1992). Cosgrove *et al.* (1994) combined surface force experiments with simultaneous neutron reflectivity experiments on

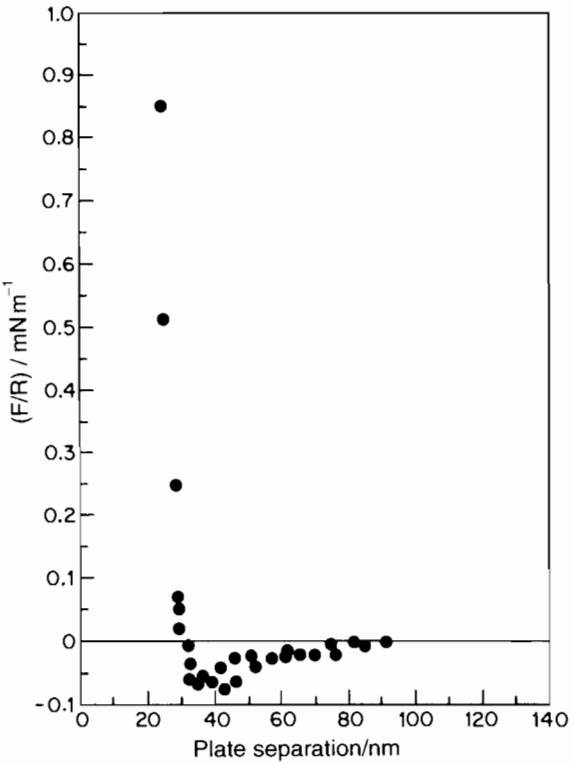

Fig. 3.37 Force–distance profile for layers of a $P2VP_{60}$–PS_{60} diblock adsorbed on mica in cyclohexane at 21 °C (Hadziioannou *et al.* 1986).

PS–PEO diblocks adsorbed on glass plates. Adsorption from toluene led to preferential adsorption of PEO; however, due to the very high asymmetry of the copolymers studied, and the favourable adsorption energy, PS was also adsorbed. On the approach of a second coated plate, the PS volume fraction increased near the interface, indicative of strong interlayer repulsion (Cosgrove *et al.* 1994).

Surface force measurements on a PEO–PBO diblock in aqueous solution have revealed purely monotonic repulsive forces between the PBO_8PEO_{41} layers adsorbed onto hydrophobically-modified mica (to which PBO is adsorbed) (Schillén *et al.* 1997). Ellipsometry was used to determine adsoprtion isotherms (adsorbed amount as a function of concentration), and the adsorbed amount as a function of time. The range of the steric repulsion was found to increase with increasing bulk copolymer concentration, whereas the concentration of an inert salt (up to 0.1 M KBr) did not influence the surface force profiles. The adsorption kinetics were found to be described by two adsorption regimes. Initially, diffusion of polymer to the interface at the solid surface dominated; thus this was a diffusion-controlled regime. When the surface was fully covered, a crossover into a second regime occurred and the increase in surface coverage was less rapid due

to interactions between block copolymer molecules at the surface. These features were reproduced by lattice self-consistent field calculations, which were also used to calculate volume fractions of adsorbed segments.

3.8.3 Neutron and X-ray reflectivity studies of adsorbed block copolymers

The density profile of end-adsorbed diblock copolymers was studied by Field *et al.* (1992*a*) using specular neutron reflectivity. It was found that for PS–PEO diblocks adsorbed from *d*-toluene onto quartz, the PEO block strongly adsorbs onto the quartz substrate while the PS remains in solution. Thus, the chains formed a terminally attached polymer brush. The reflectivity profiles were found to be well described by a parabolic or error function polymer density profile, in agreement with the analytical theory for polymer brushes (Milner *et al.* 1988*a*; Zhulina *et al.* 1989). A representative reflectivity profile is shown in Fig. 3.38, together with models used to fit the data. A parabolic density profile was found to fit the data better than an error function form. The interlayer thickness values were found to be in good agreement with the results of the interlayer force measurements on the same system (Dai and Toprakcioglu 1992). The molecular weight dependence of the layer thickness and adsorbance obtained from the data were shown to obey scaling laws in accord with the brush theory (Alexander 1977; Milner *et al.* 1988*a*; Zhulina *et al.* 1989, 1990).

The structure of a monolayer of a PS–PDMS diblock spread on the surface of ethyl benzoate, a selective solvent for PS, was probed using neutron reflectivity by Kent and co-workers (Factor *et al.* 1993; Kent *et al.* 1992, 1995; Lee *et al.* 1994). They found that the insoluble block remains on the surface of the solvent and acts as an anchor for the soluble block which extends into the solution. The concentration profile was found to be best described by a parabolic profile; however, the maximum extension of the polymer layer was found to depend on the surface density much more weakly than the 1/3 power law predicted for strongly stretched polymer brushes (Milner *et al.* 1988*a*,*b*). Thus the energy required to stretch the chains was much larger than predicted theoretically. Addition of mobile PS homopolymer chains in semidilute solutions was found to lead to contraction of the polymeric brush (Lee *et al.* 1994). This was interpreted as evidence of penetration of the mobile chains into the tethered layer. However, for low mobile chain concentrations, the mobile chains appeared to be squeezed out of the tethered layer as the surface density increased (Lee *et al.* 1994). These results were compared (Lee *et al.* 1994) to the scaling and SCF theories for planar grafted chains in contact with a solution of mobile chains. Field *et al.* (1992*b*) investigated the conformation of PS–PVP diblocks adsorbed onto quartz in toluene using neutron reflectivity. By varying the PS grafting density, they observed a change in the polymer density, and upon increasing PVP molecular weight, a transition from a 'brush' to a 'mushroom' conformation was observed. The polymer density profiles were compared to the predictions of the Alexander–de Gennes (Alexander 1977; de Gennes 1980) scaling theory for polymeric brushes and mushrooms. The structure of three different copolymers at the liquid–liquid

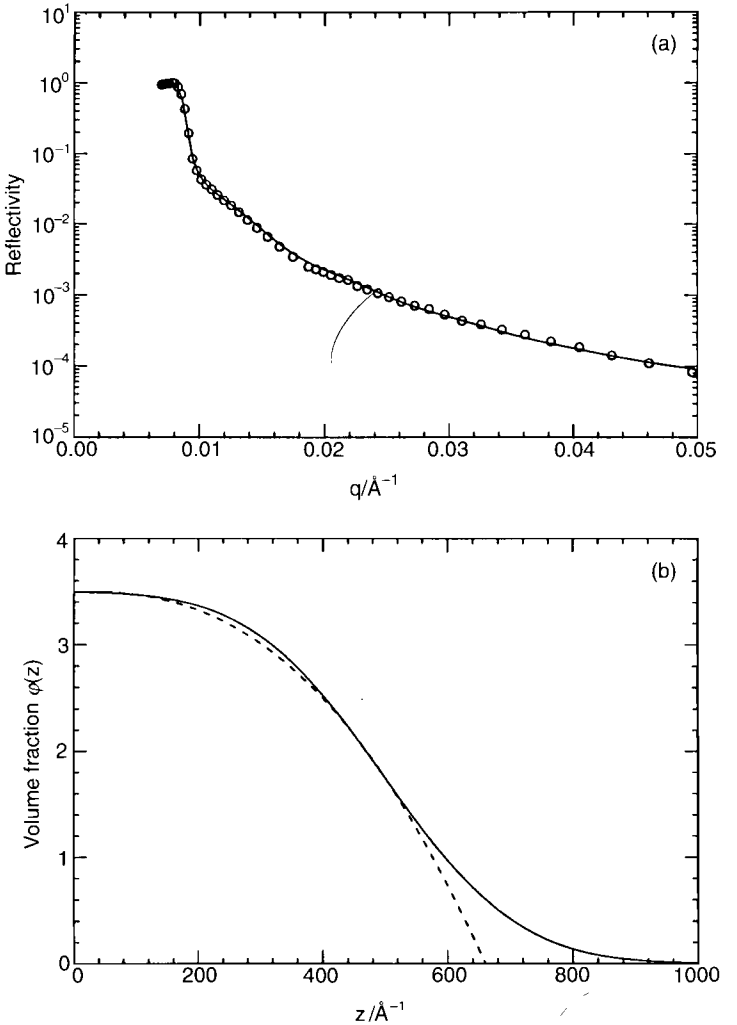

Fig. 3.38 (a) Neutron reflectivity profile for a PS–PEO diblock (M_w = 15 kg mol^{-1}, 1.5% PEO) end-adsorbed from *d*-toluene onto quartz (Field *et al.* 1992*a*). The symbols indicate measured values, whilst the full line is a fit to a parabolic volume fraction profile. (b) Models for the density profile. The parabolic function was found to give the best fit to the data.

interface was investigated using neutron reflectivity by Phipps *et al.* (1993). They studied a PEO–PPO–PEO (Pluronic) triblock, a random poly(vinyl alcohol-*co*-acetate) copolymer and a PDMS–poly(2-vinylpyridine *N*-oxide) diblock at the hexane–water interface. Both of the former copolymers have hydrophobic blocks, for which hexane is also a poor solvent. The Pluronic triblock copolymer was found to adopt a stretched conformation, with a diffuse

layer thicker than the bulk micellar radius. The shape of the volume fraction profile was in qualitative agreement with calculations based on the Scheutjens–Fleer model (Scheutjens and Fleer 1979, 1980). In contrast to the first two polymers, PDMS is very soluble in hexane, and this appeared to have a much greater influence on the polymer structure, with a substantial proportion of the copolymer dissolved on the hexane side of the interface (Phipps *et al.* 1993).

Richards *et al.* (1994, 1997) used the same technique to study a spread layer of an amphiphilic PEO–PMMA block copolymer at the air–water interface. A two-layer structure was deduced with the PMMA block at the air interface. Layer thickness and density and the distribution of water in the PEO-rich layer (which appeared to be entirely in the aqueous subphase) were obtained by detailed modelling of the reflectivity profiles. Surface quasi-elastic light scattering has been used by the same group to determine the surface viscoelastic properties of a diblock copolymer at the air–water interface (Richards *et al.* 1996). In this technique, light scattering from thermally-excited capillary waves (with amplitude $\approx$ 2 Å) at the fluid interface is probed. The surface tension, transverse surface shear viscosity, dilatational modulus and viscosity were determined for a symmetric PEO–PMMA diblock as a function of copolymer concentration. From the surface tension and transverse shear viscosity and using a simple Maxwell fluid model of the spread polymer, a relaxation time was obtained which, from its concentration dependence at a fixed angle of incidence, suggested a single relaxation process. The frequency dependence of the surface viscoelastic parameters was explored for capillary wave frequencies in the range 1×10^4–$2 \times 10^5 s^{-1}$. These data could also be interpreted using a Maxwell model, but there was additional evidence for a distribution of relaxation times (Richards *et al.* 1996).

Thomas and co-workers (Su *et al.* 1996) have reported neutron and X-ray reflectivity studies of water-soluble block and statistical copolymers absorbed at the air–water interface. The diblock copolymer of poly(2-(dimethylamino)ethyl methacrylate)–poly(*n*-butyl methacrylate) (PDMAEMA–PBMA) used is a weak polyelectrolyte. The surface properties of the adsorbed layer were studied as a function of pH and ionic strength. The main influencing factor was found to be the adsorption (or depletion) of ions associated with copolymer molecules. Neutron and X-ray reflectivity revealed a thin copolymer layer, protruding out of the aqueous surface, and a thicker one immersed in the water. Under all conditions of pH and ionic strength the surface layer remained fairly concentrated, but when the DMAEMA segments were fully charged and the ionic strength was high, this layer was more extended into the solution (Su *et al.* 1996). The same group (An *et al.* 1997) reported neutron reflectivity measurements on a PDMAEMA–PMMA diblock adsorbed at the air–water interface. A surface phase transition, with a doubling of layer thickness, was observed for a copolymer concentration close to that at which micellar association occurred in bulk. By contrast variation using isotope labelling, the structure of the layer below and above this transition was determined in detail. At low surface concentrations, the two blocks were approximately uniformly distributed in the direction normal to the interface and the layer was partially immersed in water.

Above the bulk cmc, the adsorbed layer cross-section had a structure resembling surface micelles, with a majority of the more hydrophobic PMMA forming the core. The outer layers, comprising predominantly PDMAEMA were not equivalent, being much more highly extended on the aqueous side of the interface (An *et al.* 1997).

3.8.4 Surface micelles

Surface micelles have been observed for a number of ionic block copolymers by Eisenberg and co-workers (Zhu *et al.* 1991*a*,*b*, 1992*a*). Direct evidence was first obtained using transmission electron microscopy (Zhu *et al.* 1991*a*) and atomic force microscopy (Zhu *et al.* 1992*a*) for PS–P4VP diblocks, quaternized with decyl iodide (denoted QP4VP), spread as a monolayer at the air–water interface. Langmuir–Blodgett films were deposited on carbon-coated copper grids, and this enabled TEM images to be obtained, which revealed self-assembled circular surface micelles at low surface pressures ($<2\,mN\,m^{-1}$). The distance between micelles (at low surface pressures) was found to be consistent with fully extended quaternized P4VP chains extending from a central core of PS coils. An apparent first-order phase transition was detected at high pressures from a plateau in surface pressure/area isotherms, as shown in Fig. 3.39. This was correlated to TEM images which suggested that the polyelectrolyte block changed from a surface-adsorbed 2D state to a submerged aqueous state with less order (quasi-2D) at this transition (Zhu *et al.* 1991*a*). This transition was more graphically termed as being between 'starfish' micelles and 'jellyfish' micelles (Zhu *et al.* 1992*a*,*b*), sketched in Fig. 3.40.

In subsequent work, Langmuir films of more asymmetric copolymers of the same type at the air–water interface were investigated (Zhu *et al.* 1992*b*,*c*). Cicular or starfish micelles were observed for copolymers with less than 86% PS,

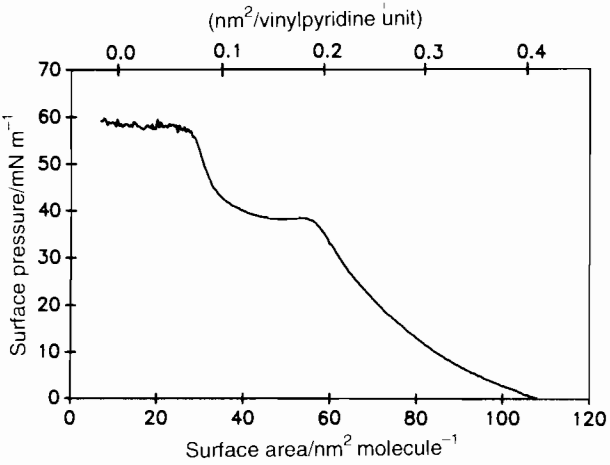

Fig. 3.39 Surface pressure vs. area per molecule for a PS_{260}–$PQ4VP_{240}$ diblock adsorbed as a Langmuir monolayer at the air–water interface (Zhu *et al.* 1991*a*).

rod- or ribbon-shaped surface micelles were observed for copolymers with between 86 and 94% PS, and planar micelles were observed for PS contents between 94 and 97%. These structures are shown in Fig. 3.41. This sequence of phase transitions is distinct from phase transitions in the bulk, where the sequence lamellae–hexagonal-packed cylinders–BCC-packed spherical micelles is observed on increasing the asymmetry of strongly segregated block copolymers. The rod micelles were found to be made up of two layers of the diblocks, whilst the planar aggregates appeared to be one PS block thick, although they extend up to several microns in width (Zhu *et al.* 1992*b*). In parallel with bulk observations, addition of PS homopolymer was found to induce changes in the morphology of the surface micelles (circle, ribbon or plane) (Meszaros *et al.* 1994). For example, addition of homopolymer PS was observed to induce a transition from ribbon surface micelles to planar micelles in a PS_{260}–$QP4VP_{240}$

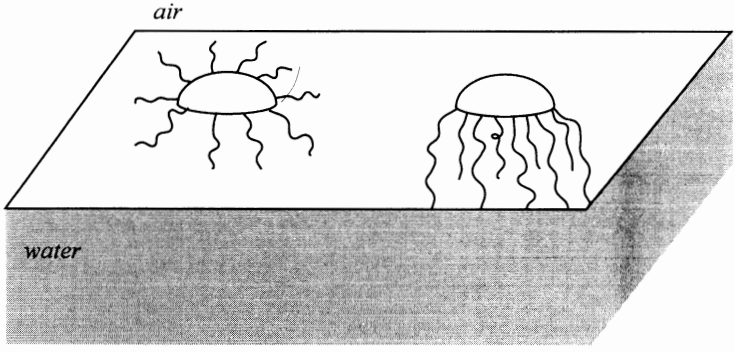

Fig. 3.40 Schematic of 'starfish' and 'jellyfish' micelles. Typical association numbers are actually $p \approx 100$.

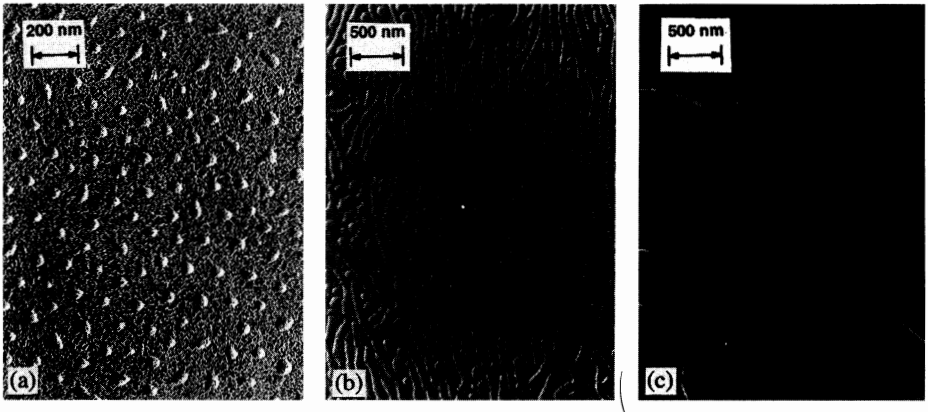

Fig. 3.41 Transmission electron micrographs of thin films of PS_m–$QP4VP_n$ (Meszaros *et al.* 1994). (a) Circular surface micelles, $m = 480$, $n = 200$; (b) ribbon surface micelles, $m = 480$, $n = 34$; (c) planar surface micelles, $m = 480$, $n = 13$.

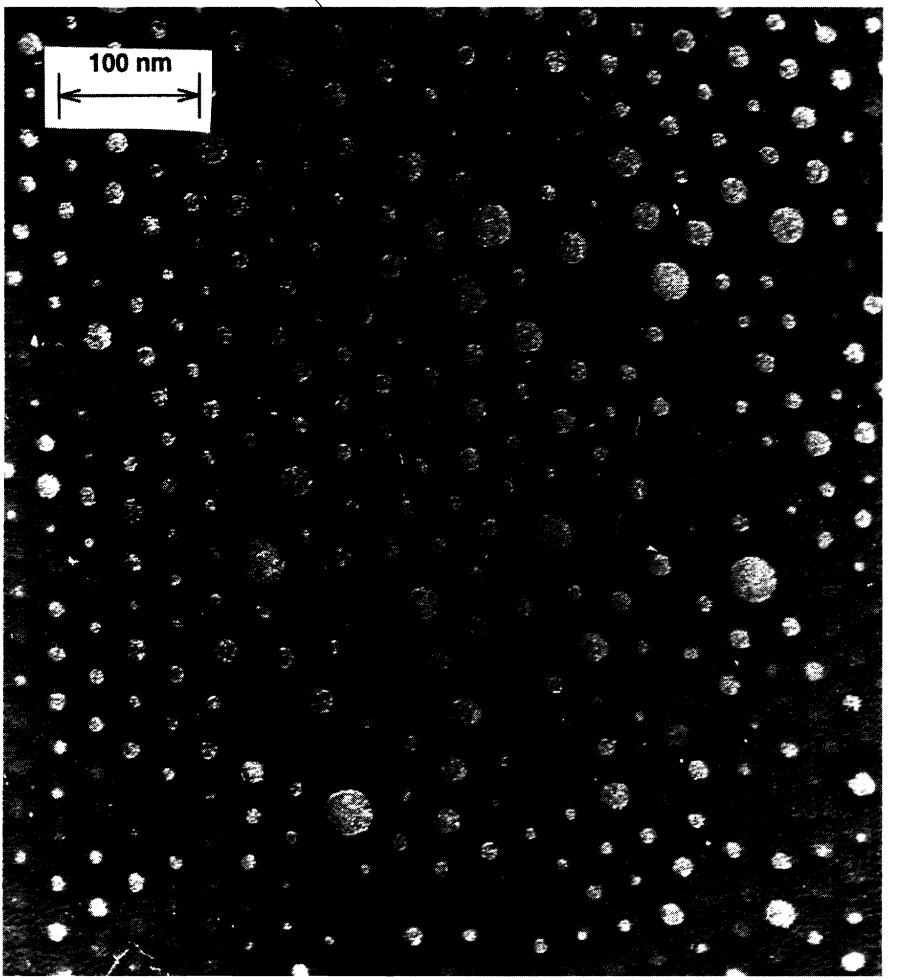

Fig. 3.42 Region of two-dimensional foam formed by a PS_{135}–$PNaA_{26}$ Langmuir–Blodgett film within the confines of a planar surface micelle domain (Meszaros *et al.* 1994).

diblock. A cellular or foam morphology (i.e. the inverse of the circular surface micelle phase) was observed in some areas (up to 10%) of Langmuir–Blodgett films formed by PS-poly(sodium acrylate) and PS–poly (sodium methacrylate) block copolymers, as shown in Fig. 3.42. The cell areas of these nanofoams ranged from 100 to 5000 nm^2 (Meszaros *et al.* 1994).

The effect of variation of the length of the pyridinium alkylating agent was also investigated by Zhu *et al.* (1992*d*). It was found that both the counterion and the hydrophobicity of the quaternization agent (alkyl iodide or bromide) determined whether the surface micelles were surface-adsorbed (starfish conformation) or were submerged (jellyfish conformation). In one extreme, the C_{10} and C_{18} alkyl chain derivatives formed starfish micelles at low surface pressures. In

the other limit, the chains quaternized with a C_1 alkyl halide formed jellyfish micelles. The surface micellization is driven by PS–PS interactions, but the aggregate size was found to be influenced by the hydrophobicity of the quaternizing agent. The balance between surface-adsorbed and solubilized QP4VP chains could be altered by changing the counterion from Cl^- to Br^- to I^- or by changing the concentration of the counterion. It was found that the size, association number and shape of surface micelles can be tuned by a judicious choice of quaternizing agent, counterion, temperature and polymer concentration (Zhu *et al.* 1992*d*).

Circular surface micelles have also been observed for non-ionic block copolymers. Li *et al.* (1993) reported TEM and AFM of starfish micelles formed by PS–poly(*n*-butyl methacrylate), PS–poly(*tert*-butyl methacrylate) and poly(*tert*-butyl acrylate) diblock copolymers. Plateaus observed in surface/area isotherms of the Langmuir–Blodgett films at the air–water interface were consistent with the formation of surface micelles.

References

Ackers, G. K. and Thompson, T. E. (1965). *Proceedings of the National Academy of Sciences of the United States of America*, **53**, 342.

Adam, M., Carton, J.-P., Corona-Vallet, S. and Lairez, D. (1996). *Journal de Physique II*, **6**, 1781.

Adriani, P., Wang, Y. and Mattice, W. L. (1994). *Journal of Chemical Physics*, **100**, 7718.

Alexander, S. (1977). *Journal de Physique*, **38**, 977.

Alexandridis, P. and Hatton, T. A. (1995). *Colloids and Surfaces A*, **96**, 1.

Alexandridis, P., Holzwarth, J. F. and Hatton, T. A. (1994*a*). *Macromolecules*, **27**, 2414.

Alexandridis, P., Athanassiou, V., Fukuda, S. and Hatton, T. A. (1994*b*). *Langmuir*, **10**, 2604.

Almgren, M., Bahadur, P., Jansson, M., Li, P., Brown, W. and Bahadur, A. (1992). *Journal of Colloid and Interface Science*, **151**, 157.

Almgren, M., Brown, W. and Hvidt, S. (1995). *Colloid and Polymer Science*, **273**, 2.

An, S. W., Su, T. J., Thomas, R. K., Baines, F. L., Billingham, N. C., Armes, S. P. *et al.* (1997). *Journal of Physical Chemistry B*, **102**, 387.

Antonietti, M., Heinz, S., Schmidt, M. and Rosenauer, C. (1994). *Macromolecules*, **27**, 3276.

Astafieva, I., Zhong, X. F. and Eisenberg, A. (1993). *Macromolecules*, **26**, 7339.

Astafieva, I., Khogaz, K. and Eisenberg, A. (1995). *Macromolecules*, **28**, 7127.

Attwood, D. and Florence, A. T. (1983). *Surfactant systems: their chemistry, pharmacy and biology*. Chapman and Hall, London.

Attwood, D., Collett, J. H. and Tait, C. J. (1985). *International Journal of Pharmaceutics*, **26**, 25.

Bahadur, P., Sastry, N. V., Marti, S. and Riess, G. (1985). *Colloids and Surfaces*, **16**, 337.

Bahadur, P., Li, P., Almgren, M. and Brown, W. (1992). *Langmuir*, **8**, 1903.

Baines, F. L., Armes, S. P., Billingham, N. C. and Tuzar, Z. (1996). *Macromolecules*, **29**, 8151.

Balazs, A. C. and Lewandowski, S. (1990). *Macromolecules*, **23**, 839.

Balazs, A. C., Huang, K. and Lantman, C. W. (1990). *Macromolecules*, **23**, 4641.

Balsara, N. P., Tirrell, M. and Lodge, T. P. (1991). *Macromolecules*, **24**, 1975.
Barker, M. C. and Vincent, B. (1984). *Colloids and Surfaces*, **8**, 297.
Bedells, A. D., Arafeh, R. M., Yang, Z., Attwood, D., Heatley, F., Padget, J. C. *et al.* (1993). *Journal of the Chemical Society, Faraday Transactions*, **89**, 1235.
Bednár, B., Edwards, K., Almgren, M., Tormod, S. and Tuzar, Z. (1988). *Makromoleculaire Chemie, Rapid Communications*, **9**, 785.
Benmouna, M., Benoit, H., Borsali, R. and Duval, M. (1987*a*). *Macromolecules*, **20**, 2620.
Benmouna, M., Duval, M. and Borsali, R. (1987*b*). *Journal of Polymer Science B: Polymer Physics*, **25**, 1839.
Bluhm, T. L. and Malhotra, S. L. (1986). *European Polymer Journal*, **22**, 249.
Bluhm, T. L. and Whitmore, M. D. (1985). *Canadian Journal of Chemistry*, **63**, 249.
Booth, C., Naylor, T. D., Price, C., Rajab, N. S. and Stubbersfield, R. B. (1978). *Journal of the Chemical Society, Faraday Transactions I*, **74**, 2352.
Booth, C., Yu, G.-E. and Nace, V. M. (1997). Block copolymers of ethylene oxide and 1,2-butylene oxide. In *Amphiphilic block copolymers: self-assembly and applications*, (ed. P. Alexandridis and B. Lindman). Elsevier, Amsterdam.
Broadbent, G., Brown, D. S. and Dawkins, J. V. (1987). *Polymer Communications*, **28**, 282.
Brown, D. S., Dawkins, J. V., Farnell, A. S. and Taylor, G. (1987). *European Polymer Journal*, **23**, 463.
Brown, R. A.., Masters, A. J., Price, C. and Yuan, X. F. (1989). Chain segregation in block copolymers. In *Comprehensive polymer science*, Vol. 2, (ed. C. Booth and C. Price), p. 155. Pergamon, Oxford.
Brown, W., Schillén, K., Almgren, M., Hvidt, S. and Bahadur, P. (1991). *Journal of Physical Chemistry*, **95**, 1850.
Brown, W., Schillén, K. and Hvidt, S. (1992). *Journal of Physical Chemistry*, **96**, 6038.
Bütün, V., Billingham, N. C. and Armes, S. P. (1997). *Journal of Materials Chemistry*, **7**, 1963.
Candau, F., Heatley, F., Price, C. and Stubbersfield, R. B. (1984). *European Polymer Journal*, **20**, 685.
Canham, P. A., Lally, T. P., Price, C. and Stubbersfield, R. B. (1980). *Journal of the Chemical Society, Faraday Transactions I*, **76**, 1857.
Cantor, R. (1981). *Macromolecules*, **14**, 1186.
Chu, B. (1995). *Langmuir*, **11**, 414.
Chu, B. and Zhou, Z. (1996). Physical chemistry of polyoxyalkylene block copolymer surfactants. In *Nonionic surfactants. Polyoxyalkylene block copolymers*, Vol. 60, (ed. V. N. Nace). Marcel Dekker, New York.
Climie, I. E. and White, E. F. T. (1960). *Journal of Polymer Science*, **47**, 149.
Cogan, K. A. and Gast, A. P. (1990). *Macromolecules*, **23**, 745.
Cogan, K. A., Gast, A. P. and Capel, M. (1991). *Macromolecules*, **24**, 6512.
Cogan, K. A., Leermakers, F. A. M. and Gast, A. P. (1992). *Langmuir*, **8**, 429.
Coll, H. (1971). *Separation Science*, **6**, 207.
Cosgrove, T., Zarbakhsh, A., Luckham, P. F., Hair, M. L. and Webster, J. R. P. W. (1994). *Faraday Discussions of the Chemical Society*, **98**, 189.
Dai, L. and Toprakcioglu, C. (1992). *Macromolecules*, **25**, 6000.
Dan, N. and Tirrell, M. (1992). *Macromolecules*, **25**, 2890.
Dan, N. and Tirrell, M. (1993). *Macromolecules*, **26**, 637.
Daoud, M. and Cotton, J. P. (1982). *Journal de Physique*, **43**, 531.
Dawkins, J. V. and Taylor, G. (1979). *Makromoleculaire Chemie*, **180**, 1737.
de Gennes, P. G. (1970). *Journal de Physique*, **31**, 325.

de Gennes, P. G. (1976). *Journal de Physique*, **37**, 1443.
de Gennes, P. G. (1978). Macromolecules and liquid crystals: reflections on certain lines of research. In *Solid state physics*, Vol. 14 (ed. L. Liebert), p. 1. Academic, New York.
de Gennes, P. G. (1979). *Scaling concepts in polymer physics*. Cornell University Press, Ithaca.
de Gennes, P. G. (1980). *Macromolecules*, **13**, 1069.
de Gennes, P. G. (1986). *Comptes Rendus de l'Academie des Sciences de Paris II*, **302**, 765.
Demin, A. A., Rudkovskii, G. D., Dmitrenko, L. V., Ovsyannikova, L. A., Sokolova, T. A., Samsonov, G. *et al.* (1974). *Vysokomolekulyarnye Soedineniya A*, **16**, 2706. English translation: *Polymer Science USSR*, **16**, 3151.
Deng, N.-J., Luo, Y.-Z., Tanodekaew, S., Bingham, N., Attwood, D. and Booth, C. (1995). *Journal of Polymer Science B: Polymer Physics*, **33**, 1085.
Ding, J.-F., Heatley, F., Price, C. and Booth, C. (1991). *European Polymer Journal*, **27**, 895.
Dolan, A. K. and Edwards, S. F. (1974). *Proceedings of the Royal Society of London, Series A*, **337**, 509.
Dorgan, J. R., Stamm, M., Toprakcioglu, C., Jérôme, R. and Fetters, L. J. (1993). *Macromolecules*, **26**, 5321.
Dormidontova, E. E. and Khokhlov, A. R. (1997). *Macromolecules*, **30**, 1980.
Edens, M. W. (1996). Applications of polyoxyethylene block copolymer surfactants. In *Nonionic surfactants. Polyoxyalkylene block copolymers*, Vol. 60, (ed. V. N. Nace), p. 185. Marcel Dekker, New York.
Edwards, C. J. C., Richards, R. W. and Stepto, R. F. T. (1986). *Polymer*, **27**, 643.
Elias, H.-G. (1972). The study of association and aggregation via light scattering. In *Light scattering from polymer solutions*, (ed. M. B. Huglin), p. 397. Academic, London.
Elias, H.-G. (1973). *Journal of Macromolecular Science, Chemistry*, **7**, 601.
Enyiegbulam, M. and Hourston, D. J. (1978), *Polymer*, **19**, 727.
Evers, O. A., Scheutjens, J. M. H. M. and Fleer, G. J. (1990). *Macromolecules*, **23**, 5221.
Evers, O. A., Scheutjens, J. M. H. M. and Fleer, G. J. (1991*a*). *Macromolecules*, **24**, 5558.
Evers, O. A., Scheutjens, J. M. H. M. and Fleer, G. J. (1991*b*). *Journal of the Chemical Society, Faraday Transactions*, **86**, 1333.
Factor, B. J., Lee, L. T., Kent, M. S. and Rondelez, F. (1993). *Physical Review E*, **48**, 2354.
Farago, B., Monkenbusch, M., Richter, D., Huang, J. S., Fetters, L. J. and Gast, A. P. (1993). *Physical Review Letters*, **71**, 1015.
Field, J. B., Toprakcioglu, C., Ball, R. C., Stanley, H. B., Dai, L., Barford, W. *et al.* (1992*a*). *Macromolecules*, **25**, 434.
Field, J. B., Toprakcioglu, C., Dai, L., Hadziioannou, G., Smith, G. and Hamilton, W. (1992*b*). *Journal de Physique II*, **2**, 2221.
Forder, C., Patrickios, C. S., Armes, S. P. and Billingham, N. C. (1996). *Macromolecules*, **29**, 8160.
Förster, S., Wenz, E. and Lindner, P. (1996). *Physical Review Letters*, **77**, 95.
Franta, E. (1966). *Journal de Chimie Physique*, **63**, 593.
Gadelle, F., Koros, W. J. and Schechter, R. S. (1995). *Macromolecules*, **28**, 4883.
Gaillard, P., Ossenbach-Suater, M. and Riess, G. (1980). *Makromoleculaire Chemie, Rapid Communications*, **1**, 771.
Gallot, Y., Franta, E., Rempp, P. and Benoit, H. (1963). *Journal of Polymer Science C*, **4**, 473.
Gao, Z. and Eisenberg, A. (1993). *Macromolecules*, **26**, 7353.

Gao, Z., Varshney, S. K., Wong, S. and Eisenberg, A. (1994*a*). *Macromolecules*, **27**, 7923.
Gao, Z., Zhong, X.-F. and Eisenberg, A. (1994*b*). *Macromolecules*, **27**, 794.
Gast, A. P. (1996). *Langmuir*, **12**, 4060.
Gilbert, G. A. (1955). *Discussions of the Faraday Society*, **20**, 68.
Godward, J., Heatley, F. and Booth, C. (1995). *Journal of the Chemical Society, Faraday Transactions*, **91**, 1491.
González-Mozuelos, P. and Olvera de la Cruz, M. (1994). *Journal of Chemical Physics*, **100**, 507.
Guzonas, D. A., Boils, D., Tripp, C. P. and Hair, M. L. (1992). *Macromolecules*, **25**, 2434.
Hadziioannou, G., Patel, S., Granick, S. and Tirrell, M. (1986). *Journal of the American Chemical Society*, **108**, 2869.
Haliloglu, T., Bahar, I., Erman, B. and Mattice, W. L. (1996). *Macromolecules*, **29**, 4764.
Haliloglu, T., Stevenson, D. C. and Mattice, W. L. (1997). *Journal of Chemical Physics*, **106**, 3365.
Hall, D. G. (1987). In *Nonionic surfactants: physical chemistry.* Surfactant Science Series, Vol. 23, (ed. M. J. Schick), p. 233. Marcel Dekker, New York.
Halperin, A. (1987). *Macromolecules*, **20**, 2943.
Halperin, A. (1990). *Macromolecules*, **23**, 2724.
Hamley, I. W., Fairclough, J. P. A., Ryan, A. J., Ryu, C. Y., Lodge, T. P., Gleeson, A. J. *et al.* (1998). *Macromolecules*, **31**, 1188.
Heatley, F. and Begum, A. (1977). *Makromoleculaire Chemie*, **178**, 1205.
Helfand, E. and Sapse, A. M. (1975). *Journal of Chemical Physics*, **62**, 1327.
Helfand, E. and Tagami, Y. (1972). *Journal of Chemical Physics*, **56**, 3592.
Holtzer, A. and Holtzer, M. F. (1974). *Journal of Physical Chemistry*, **78**, 1443.
Huguenard, C., Varoqui, R. and Pefferkorn, E. (1991). *Macromolecules*, **24**, 2226.
Hurter, P. N. and Hatton, T. A. (1992). *Langmuir*, **8**, 1291.
Hurter, P. N., Scheutjens, J. M. H. M. and Hatton, T. A. (1993*a*). *Macromolecules*, **26**, 5030.
Hurter, P. N., Scheutjens, J. M. H. M. and Hatton, T. A. (1993*b*). *Macromolecules*, **26**, 5592.
Ikemi, M., Odagiri, N., Tanaka, S., Shinohara, I. and Chiba, A. (1981). *Macromolecules*, **14**, 34.
Ishizu, K., Kashi, Y., Fukotomi, T. and Kakurai, T. (1982). *Makromoleculaire Chemie*, **183**, 3099.
Jian, T., Anastasiadis, S. H., Semenov, A. N., Fytas, G., Fleischer, G. and Vilesov, A. D. (1995). *Macromolecules*, **28**, 2439.
Kamachi, M., Kurihara, M. and Stille, J. K. (1972). *Macromolecules*, **5**, 161.
Kao, C. R. and Olvera de la Cruz, M. (1990). *Journal of Chemical Physics*, **93**, 8284.
Kent, M. S., Lee, L. T., Farnoux, B. and Rondelez, F. (1992). *Macromolecules*, **25**, 6240.
Kent, M. S., Tirrell, M. and Lodge, T. P. (1994). *Journal of Polymer Science B: Polymer Physics*, **32**, 1927.
Kent, M. S., Lee, L. T., Factor, B. J., Rondelez, F. and Smith, G. S. (1995). *Journal of Chemical Physics*, **103**, 2320.
Khougaz, K., Gao, Z. and Eisenberg, A. (1994). *Macromolecules*, **27**, 6341.
Khougaz, K., Astafieva, I. and Eisenberg, A. (1995). *Macromolecules*, **28**, 7135.
Khougaz, K., Zhong, X. F. and Eisenberg, A. (1996). *Macromolecules*, **29**, 3937.
Kimura, T. and Kurata, M. (1981). *Macromolecules*, **14**, 1104.
Kiserow, D., Procházka, K., Ramireddy, C., Tuzar, Z., Munk, P. and Webber, S. E. (1992). *Macromolecules*, **25**, 461.

Kotaka, T., Tanaka, T. and Inagaki, H. (1972). *Polymer Journal*, **3**, 327.
Kotaka, T., Tanaka, T., Hattori, M. and Inagaki, H. (1978). *Macromolecules*, **11**, 138.
Krause, S. (1964). *Journal of Physical Chemistry*, **68**, 1948.
Krause, S. and Reismuller, P. A. (1975). *Journal of Polymer Science, Polymer Physics*, **13**, 663.
Lally, T. P. and Price, C. (1974). *Polymer*, **15**, 325.
Lee, L.-T., Factor, B. J., Rondelez, F. and Kent, M. S. (1994). *Faraday Discussions of the Chemical Society*, **98**, 139.
Leibler, L. (1988). *Makromoleculaire Chemie, Macromolecular Symposia*, **16**, 1.
Leibler, L., Orland, H. and Wheeler, J. C. (1983). *Journal of Chemical Physics*, **79**, 3550.
Li, S., Hanley, S., Khan, I., Varshney, S. K., Eisenberg, A. and Lennox, R. B. (1993). *Langmuir*, **9**, 2243.
Li, H., Yu, G.-E., Price, C., Booth, C., Hecht, E. and Hoffmann, H. (1997). *Macromolecules*, **30**, 1347.
Ligoure, C. (1991). *Macromolecules*, **24**, 2968.
Lin, E. K. and Gast, A. P. (1996). *Macromolecules*, **29**, 390.
Linse, P. (1993*a*). *Macromolecules*, **26**, 4437.
Linse, P. (1993*b*). *Journal of Physical Chemistry*, **97**, 13896.
Linse, P. (1994*a*). *Macromolecules*, **27**, 2685.
Linse, P. (1994*b*). *Macromolecules*, **27**, 6404.
Linse, P. and Malmsten, M. (1992). *Macromolecules*, **25**, 5434.
Lodge, T. P., Xu, X., Ryu, C. Y., Hamley, I. W., Fairclough, J. P. A., Ryan, A. J. *et al.* (1996). *Macromolecules*, **29**, 5955.
Luo, Y. Z., Nicholas, C. V., Attwood, D., Collett, J. H., Price, C. and Booth, C. (1992). *Colloid and Polymer Science*, **270**, 1094.
Mandema, W., Emeis, C. A. and Zeldenrust, H. (1979*a*). *Makromoleculaire Chemie*, **180**, 2163.
Mandema, W., Zeldenrust, H. and Emeis, C. A. (1979*b*). *Makromoleculaire Chemie*, **180**, 1521.
Mayes, A. M. and Olvera de la Cruz, M. (1988). *Macromolecules*, **21**, 2543.
Meier, D. J. (1969). *Journal of Polymer Science C*, **26**, 81.
Merrett, F. M. (1957). *Journal of Polymer Science*, **24**, 467.
Meszaros, M., Eisenberg, A. and Lennox, R. B. (1994). *Faraday Discussions of the Chemical Society*, **98**, 283.
Milner, S. T., Witten, T. A. and Cates, M. E. (1988*a*). *Macromolecules*, **21**, 2610.
Milner, S. T., Witten, T. and Cates, M. E. (1988*b*). *Europhysics Letters*, **5**, 413.
Morishima, Y., Hashimoto, T., Itoh, Y., Kamachi, M. and Nozakura, S. I. (1981). *Makromoleculaire Chemie, Rapid Communications*, **2**, 507.
Morishima, Y., Hashimoto, T., Itoh, Y., Kamachi, M. and Nozakura, S. I. (1982*a*). *Journal of Polymer Science A: Polymer Chemistry*, **20**, 299.
Morishima, Y., Itoh, Y., Hashimoto, T. and Nozakura, S.-I. (1982*b*). *Journal of Polymer Science A: Polymer Chemistry*, **20**, 2007.
Mortensen, K. and Brown, W. (1993). *Macromolecules*, **26**, 4128.
Motschmann, H., Stamm, M. and Toprakcioglu, C. (1991). *Macromolecules*, **24**, 3681.
Munch, M. R. and Gast, A. P. (1990). *Macromolecules*, **23**, 2313.
Nace, V. M. (1996*a*). Properties of polyoxyalkylene block copolymers. In *Nonionic surfactants. Polyoxyalkylene block copolymers*, Vol. 60, (ed. V. N. Nace). Marcel Dekker, New York.
Nace, V. M. (1996*b*). *Journal of the American Oil Chemists Society*, **73**, 1.
Nagarajan, R. (1997). Solubilization of hydrophobic substances by block copolymer

micelles in aqueous solutions. In *Solvents and self-organization of polymers*, NATO ASI Series, Vol. E 327, (ed. S. Webber, P. Munk and Z. Tuzar). Kluwer, Dordrecht.
Nagarajan, R. and Ganesh, K. (1989*a*). *Journal of Chemical Physics*, **90**, 5843.
Nagarajan, R. and Ganesh, K. (1989*b*). *Macromolecules*, **22**, 4312.
Nagarajan, R. and Ganesh, K. (1993). *Journal of Chemical Physics*, **98**, 7440.
Nagarajan, R., Barry, M. and Ruckinstein, E. (1986). *Langmuir*, **1**, 337.
Nakamura, K., Endo, R. and Takeda, M. (1977). *Journal of Polymer Science: Polymer Physics*, **15**, 2087.
Nguyen, D., Williams, C. E. and Eisenberg, A. (1994). *Macromolecules*, **27**, 5090.
Nguyen-Misra, M. and Mattice, W. L. (1995*a*). *Macromolecules*, **28**, 1444.
Nguyen-Misra, M. and Mattice, W. L. (1995*b*). *Macromolecules*, **28**, 6976.
Nguyen-Misra, M., Misra, S. and Mattice, W. L. (1996). *Macromolecules*, **29**, 1407.
Noolandi, J. and Hong, K. M. (1982). *Macromolecules*, **15**, 482.
Noolandi, J. and Hong, K. M. (1983). *Macromolecules*, **16**, 1443.
Oranli, L., Bahadur, P. and Riess, G. (1985). *Canadian Journal of Chemistry*, **63**, 2691.
Pandya, K., Bahadur, P., Nagar, T. N. and Bahadur, A. (1993). *Colloids and Surfaces A*, **70**, 219.
Patrickios, C. S., Forder, C., Armes, S. P. and Billingham, N. C. (1996). *Journal of Polymer Science A: Polymer Chemistry*, **34**, 1529.
Pavlova, S.-S. A., Dubovina, L. V., Belavtseva, Y. M., Ponomareva, M. A. and Senkevich, S. I. (1981). *Vysokomolekulyarnye Soedineniya A*, **23**, 359. English translation: *Polymer Science USSR*, **23**, 401.
Pedersen, J. S. and Gerstenberg, M. C. (1996). *Macromolecules*, **29**, 1363.
Peng, X. and Zhou, Z. (1986). *Acta Chemica Sinica*, **44**, 613.
Periard, J., Riess, G. and Neyer-Gomez, M. J. (1973). *European Polymer Journal*, **9**, 687.
Phipps, J. S., Richardson, R. M., Cosgrove, T. and Eaglesham, A. (1993). *Langmuir*, **9**, 3530.
Pleštil, J. and Baldrian, J. (1973). *Makromoleculaire Chemie*, **174**, 183.
Pleštil, J. and Baldrian, J. (1975). *Makromoleculaire Chemie*, **176**, 1009.
Pleštil, J., Hlavata, D., Hrouz, J. and Tuzar, Z. (1990). *Polymer*, **31**, 2112.
Prasad, K. N., Luong, T. T., Florence, A. T., Paris, J., Vution, C., Seiller, M. *et al.* (1979). *Journal of Colloid and Interface Science*, **69**, 225.
Price, C. (1982). Colloidal properties of block copolymers. In *Developments in block copolymers*, Vol. 1, (ed. I. Goodman), p. 39. Applied Science, London.
Price, C. and Woods, D. (1973). *European Polymer Journal*, **9**, 827.
Price, C., McAdam, J. D. G., Lally, T. P. and Woods, D. (1974). *Polymer*, **15**, 228.
Price, C., Canham, P. A., Duggleby, M. C., Naylor, T. D., Rajab, N. S. and Stubbersfield, R. B. (1979). *Polymer*, **20**, 615.
Price, C., Hudd, A. L., Stubbersfield, R. B. and Wright, B. (1980). *Polymer*, **21**, 9.
Price, C., Hudd, A. L., Booth, C. and Wright, B. (1982). *Polymer*, **23**, 650.
Price, C., Briggs, N., Quintana, J. R., Stubbersfield, R. B. and Robb, I. (1986). *Polymer Communications*, **27**, 292.
Price, C., Chan, E. K. M. and Stubbersfield, R. B. (1987). *European Polymer Journal*, **23**, 649.
Procházka, K., Baloch, M. K. and Tuzar, Z. (1979). *Makromoleculaire Chemie*, **180**, 2521.
Procházka, K., Bednár, B., Tuzar, Z. and Kocirík, M. (1988). *Journal of Liquid Chromatography*, **11**, 2221.
Procházka, K., Bednár, B., Tuzar, Z. and Kocirík, M. (1989). *Journal of Liquid Chromatography*, **12**, 1023.

Procházka, K., Kiserow, D., Ramireddy, C., Webber, S. E., Munk, P. and Tuzar, Z. (1992). *Makromoleculaire Chemie, Macromolecular Symposia*, **58**, 201.
Qin, A., Tian, M., Ramireddy, C., Webber, S. E., Munk, P. and Tuzar, Z. (1994). *Macromolecules*, **27**, 120.
Raspaud, E., Lairez, D., Adam, M. and Carton, J.-P. (1994). *Macromolecules*, **27**, 2956.
Rassing, J. and Attwood, D. (1983). *International Journal of Pharmaceutics*, **13**, 47.
Reddy, N. K., Fordham, P. J., Attwood, D. and Booth, C. (1990*a*). *Journal of the Chemical Society, Faraday Transactions*, **86**, 1569.
Reddy, N. K., Foster, A., Styring, M. G. and Booth, C. (1990*b*). *Journal of Colloid and Interface Science*, **136**, 588.
Richards, R. W., Rochford, B. R. and Webster, J. R. P. (1994). *Faraday Discussions of the Chemical Society*, **98**, 263.
Richards, R. W., Rochford, B. R. and Taylor, M. R. (1996). *Macromolecules*, **29**, 1980.
Richards, R. W., Rochford, B. R. and Webster, J. R. P. (1997). *Polymer*, **38**, 1169.
Riess, G. and Rogez, D. (1982). *Polymer Preprints, American Chemical Society Division of Polymer Chemistry*, **23**, 19.
Riess, G., Hurtrez, G. and Bahadur, P. (1985). Block copolymers. In *Encyclopedia of polymer science and engineering*, Vol. 2, (ed. H. F. Mark and J. I. Kroschwitz), p. 324. Wiley, New York.
Rodrigues, K. and Mattice, W. L. (1992). *Langmuir*, **8**, 456.
Scheutjens, J. M. H. M. and Fleer, G. J. (1979). *Journal of Physical Chemistry*, **83**, 1619.
Scheutjens, J. M. H. M. and Fleer, G. J. (1980). *Journal of Physical Chemistry*, **84**, 178.
Schillén, K., Brown, W. and Johnsen, R. M. (1994). *Macromolecules*, **27**, 4825.
Schillén K., Claesson, P. M., Malmsten, M., Linse, P. and Booth, C. (1997). *Journal of Physical Chemistry B*, **101**, 4238.
Schmolka, I. R. (1991). In *Polymers for controlled drug delivery*, (ed. P. J. Tarcha). CRC Press, Boston.
Schwab, F. C. and Heilweil, I. J. (1983). *Polymer Preprints, American Chemical Society, Division of Polymer Chemistry*, **24**, 65.
Selb, J. and Gallot, Y. (1975). *Journal of Polymer Science, Polymer Letters*, **13**, 615.
Selb, J. and Gallot, Y. (1980*a*). *Makromoleculaire Chemie*, **181**, 809.
Selb J. and Gallot, Y. (1980*b*). *Makromoleculaire Chemie*, **181**, 2605.
Selb, J. and Gallot, Y. (1980*c*). Copolymers with polyvinylpyridinium blocks or grafts: synthesis and properties in solution. In *Polymeric amines and ammonium salts*, (ed. E. J. Goethals), p. 205. Pergamon, Oxford.
Selb, J. and Gallot, Y. (1981*a*). *Makromoleculaire Chemie*, **182**, 1491.
Selb, J. and Gallot, Y. (1981*b*). *Makromoleculaire Chemie*, **182**, 1513.
Selb, J. and Gallot, Y. (1985). Ionic block copolymers. In *Developments in block copolymers*, Vol. 2, (ed. I. Goodman), p. 27. Elsevier, London.
Selb, J., Marie, P., Rameau, A., Duplessix, R. and Gallot, Y. (1983). *Polymer Bulletin*, **10**, 444.
Shusharina, N. P., Nyrkova, I. A. and Khokhlov, A. R. (1996*a*). *Macromolecules*, **29**, 3167.
Shusharina, N. P., Saphonov, M. V., Nyrkova, I. A., Khalatur, P. G. and Khokhlov, A. R. (1996*b*). *Berichte der Bunsengesellschaft fur Physikalische Chemie*, **100**, 857.
Spacek, P. (1986). *Journal of Applied Polymer Science*, **32**, 4281.
Spěváček, J. (1982). *Makromoleculaire Chemie, Rapid Communications*, **3**, 697.
Stepanek, P. and Lodge, T. P. (1996). *Macromolecules*, **29**, 1244.
Stille, J. K., Kamachi, M. and Kurihara, M. (1971). *Polymer Preprints, American Chemical Society Division of Polymer Chemistry*, **12**, 223.

Su, T. J., Styrkas, D. A., Thomas, R. K., Baines, F. L., Billingham, N. C. and Armes, S. P. (1996). *Macromolecules*, **29**, 6892.
Tanaka, T., Kotaka, T. and Inagaki, H. (1972). *Polymer Journal*, **3**, 338.
Tanodekaew, S., Deng, N.-J., Smith, S., Yang, Y.-W., Attwood, D. and Booth, C. (1993). *Journal of Physical Chemistry*, **97**, 11847.
Tanodekaew, S., Godward, J., Heatley, F. and Booth, C. (1997). *Macromolecular Chemistry and Physics*, **198**, 927.
Tao, J., Stewart, S., Liu, G. and Yang, M. (1997). *Macromolecules*, **30**, 2738.
Tassin, J. F., Siemens, R. L., Tang, W. T., Hadziioannou, G., Swalen, J. D. and Smith, B. A. (1989). *Journal of Physical Chemistry*, **93**, 2106.
Taunton, H. J., Toprakcioglu, C., Fetters, L. J. and Klein, J. (1988). *Nature*, **332**, 712.
Taunton, H. J., Toprakcioglu, C., Fetters, L. J. and Klein, J. (1990). *Macromolecules*, **23**, 571.
ten Brinke, G. and Hadziioannou, G. (1987). *Macromolecules*, **20**, 486.
Teo, H. H., Styring, M. G., Yeates, S. G., Price, C. and Booth, C. (1986). *Journal of Colloid and Interface Science*, **114**, 416.
Tian, M., Qin, A., Ramireddy, C., Webber, S. E., Munk, P., Tuzar, Z. *et al.* (1993). *Langmuir*, **9**, 1741.
Tian, M., Arca, E., Tuzar, Z., Webber, S. E. and Munk, P. (1995). *Journal of Polymer Science B: Polymer Physics*, **33**, 1713.
Tsunashima, Y. and Kawamata, Y. (1993). *Macromolecules*, **26**, 4899.
Tsunashima, Y., Hirata, M. and Kawamata, Y. (1990). *Macromolecules*, **23**, 1089.
Tuzar, Z. and Kratochvíl, P. (1972). *Makromoleculaire Chemie*, **160**, 301.
Tuzar, Z. and Kratochvíl, P. (1973). *Makromoleculaire Chemie*, **170**, 177.
Tuzar, Z. and Kratochvíl, P. (1976). *Advances in Colloid and Interface Science*, **6**, 201.
Tuzar, Z. and Kratochvíl, P. (1993). Micelles of block and graft copolymers in solutions. In *Surface and colloid science*, Vol. 15, (ed. E. Matijevic), p. 1. Plenum, New York.
Tuzar, Z., Sikora, A., Petrus, V. and Kratochvíl, P. (1977). *Makromoleculaire Chemie*, **178**, 2743.
Tuzar, Z., Bahadur, P. and Kratochvíl, P. (1982). *Makromoleculaire Chemie*, **182**, 1751.
Tuzar, Z., Plestil, J., Konák, C., Hlavatá, D. and Sikora, A. (1983). *Makromoleculaire Chemie*, **184**, 2111.
Tuzar, Z., Stehlícek, J., Konák, C. and Lednicky, F. (1988). *Makromoleculaire Chemie*, **189**, 221.
Tuzar, Z., Pospisil, H., Plestil, J., Lowe, A. B., Baines, F. L., Billingham, N. C. *et al.* (1997). *Macromolecules*, **30**, 2509.
Vagberg, L. J. M., Cogan, K. A. and Gast, A. P. (1991). *Macromolecules*, **24**, 1670.
van Lent, B. and Scheutjens, J. H. M. (1989). *Macromolecules*, **22**, 1931.
Varoqui, R., Tran, Q. and Pefferkorn, E. (1979). *Macromolecules*, **12**, 831.
Vink, H. (1985). *Journal of the Chemical Society, Faraday Transactions I*, **81**, 1725.
Wang, Z.-G. and Safran, S. A. (1990). *Journal de Physique*, **51**, 185.
Wang, Q., Price, C. and Booth, C. (1992*a*). *Journal of the Chemical Society, Faraday Transactions*, **88**, 1437.
Wang, Y., Balaji, R., Quirk, R. P. and Mattice, W. L. (1992*b*). *Polymer Bulletin*, **28**, 333.
Wang, Q., Yu, G.-E., Deng, Y., Price, C. and Booth, C. (1993*a*). *European Polymer Journal*, **29**, 665.
Wang, Y., Mattice, W. L. and Napper, D. H. (1993*b*). *Langmuir*, **9**, 66.
Wang, Y., Kausch, C. M., Chun, M., Quirk, R. P. and Mattice, W. L. (1995). *Macromolecules*, **28**, 904.

Wanka, G., Hoffmann, H. and Ulbricht, W. (1994). *Macromolecules*, **27**, 4145.
Watanabe, H. and Kotaka, T. (1984). *Polymer Engineering Reviews*, **4**, 73.
Whitmore, M. D. and Noolandi, J. (1985). *Macromolecules*, **18**, 657.
Wijmans, C. M. and Zhulina, E. B. (1993). *Macromolecules*, **26**, 7214.
Wu, D. T., Yokoyama, A. and Setterquist, R. L. (1991). *Polymer Journal*, **23**, 709.
Xing, L. and Mattice, W. L. (1997). *Macromolecules*, **30**, 1711.
Xu, R., Winnik, M. A., Riess, G., Chu, B. and Croucher, M. D. (1992). *Macromolecules*, **25**, 644.
Yamakawa, H. (1971). *Modern theory of polymer solutions*. Harper and Row, New York.
Yang, Z., Packard, S., Deng, N.-J., Barlow, R. J., Attwood, D. and Booth, C. (1994). *Macromolecules*, **27**, 2371.
Yang, Y.-W., Deng, N.-J., Yu, G.-E., Zhou, Z.-K., Attwood, D. and Booth, C. (1995). *Langmuir*, **11**, 4703.
Yang, Y.-W., Yang, Z., Zhou, Z.-K., Attwood, D. and Booth, C. (1996*a*). *Macromolecules*, **29**, 670.
Yang, Z., Yang, Y.-W., Zhou, Z.-K., Attwood, D. and Booth, C. (1996*b*). *Journal of the Chemical Society, Faraday Transactions*, **92**, 257.
Yu, K. and Eisenberg, A. (1996). *Macromolecules*, **29**, 6359.
Yu, G.-E., Deng, Y.-L., Dalton, S., Wang, Q.-G., Attwood, D., Price, C. *et al.* (1992). *Journal of the Chemical Society, Faraday Transactions*, **88**, 2537.
Yu, G.-E., Yang, Y.-W., Yang, Z., Attwood, D., Booth, C. and Nace, V. M. (1996*a*). *Langmuir*, **12**, 3404.
Yu, G.-E., Yang, Z., Attwood, D., Price, C. and Booth, C. (1996*b*). *Macromolecules*, **29**, 8479.
Yu, G.-E., Zhou, Z.-K., Attwood, D., Price, C., Booth, C., Griffiths, P. C. *et al.* (1996*c*). *Journal of the Chemical Society, Faraday Transactions*, **92**, 5021.
Yuan, X.-F., Masters, A. J. and Price, C. (1992). *Macromolecules*, **25**, 6876.
Zhan, Y. and Mattice, W. L. (1994*a*). *Macromolecules*, **27**, 677.
Zhan, Y. and Mattice, W. L. (1994*b*). *Macromolecules*, **27**, 683.
Zhan, Y., Mattice, W. L. and Napper, D. H. (1993*a*). *Journal of Chemical Physics*, **98**, 7502.
Zhan, Y., Mattice, W. L. and Napper, D. H. (1993*b*). *Journal of Chemical Physics*, **98**, 7508.
Zhang, L. and Eisenberg, A. (1995). *Science*, **268**, 1728.
Zhang, L. and Eisenberg, A. (1996). *Journal of the American Chemical Society*, **118**, 3168.
Zhang, L., Barlow, R. J. and Eisenberg, A. (1995). *Macromolecules*, **28**, 6055.
Zhang, L., Yu, K. and Eisenberg, A. (1996). *Science*, **272**, 1777.
Zhong, X. F., Varshney, S. K. and Eisenberg, A. (1992). *Macromolecules*, **25**, 6170.
Zhou, Z. and Chu, B. (1987). *Macromolecules*, **20**, 3089.
Zhou, Z. and Chu, B. (1988). *Macromolecules*, **21**, 2548.
Zhou, Z. and Chu, B. (1994). *Macromolecules*, **27**, 2025.
Zhou, Z., Chu, B. and Peiffer, D. G. (1993). *Macromolecules*, **26**, 1876.
Zhou, Z., Chu, B. and Peiffer, D. G. (1994). *Journal of Polymer Science B: Polymer Physics*, **32**, 2135.
Zhou, Z., Chu, B. and Peiffer, D. G. (1995). *Langmuir*, **11**, 1956.
Zhou, Z., Chu, B. and Nace, V. M. (1996*a*). *Langmuir*, **12**, 5016.
Zhou, Z., Chu, B. Nace, V. M., Yang, Y.-W. and Booth, C. (1996*b*). *Macromolecules*, **29**, 3663.
Zhou, Z., Yang, Y.-W., Booth, C. and Chu, B. (1996*c*). *Macromolecules*, **29**, 8357.

Zhu, J., Eisenberg, A. and Lennox, R. B. (1991*a*). *Journal of the American Chemical Society*, **113**, 5583.

Zhu, J., Lennox, R. B. and Eisenberg, A. (1991*b*). *Langmuir*, **7**, 1579.

Zhu, J., Hanley, S., Eisenberg, A. and Lennox, R. B. (1992*a*). *Makromoleculaire Chemie, Macromolecular Symposia*, **53**, 211.

Zhu, J., Eisenberg, A. and Lennox, R. B. (1992*b*). *Macromolecules*, **25**, 6547.

Zhu, J., Lennox, R. B. and Eisenberg, A. (1992*c*). *Journal of Physical Chemistry*, **96**, 4727.

Zhu, J., Eisenberg, A. and Lennox, R. B. (1992*d*). *Macromolecules*, **25**, 6556.

Zhulina, E. B. and Birshtein, T. M. (1985). *Vysokomolekulyarnye Soedineniya* **27**, 511. English translation: (1986). *Polymer Science USSR*, **27**, 570.

Zhulina, E. B., Borisov, O. V. and Pryamitsin, V. A. (1989). *Vysokomolekulyarnye Soedineniya*, **31A**, 185.

Zhulina, E. B., Borisov, O. V. and Pryamitsin, V. A. (1990). *Journal of Colloid and Interface Science*, **137**, 495.

4 Block copolymers in semidilute and concentrated solutions

4.1. Introduction

The association of block copolymers in a selective solvent into micelles was the subject of the previous chapter. In this chapter, ordered phases in semidilute and concentrated block copolymer solutions, which often consist of ordered arrays of micelles, are considered. In a semidilute or concentrated block copolymer solution, as the concentration is increased, chains begin to overlap, and this can lead to the formation of a liquid crystalline phase such as a cubic phase of spherical micelles, a hexagonal phase of rod-like micelles or a lamellar phase. These ordered structures are associated with gel phases. Gels do not flow under their own weight, i.e. they have a finite yield stress. This contrasts with micellar solutions (sols) (discussed in Chapter 3) which flow readily due to a liquid-like organization of micelles. The ordered phases in block copolymer solutions are lyotropic liquid crystal phases that are analogous to those formed by low-molecular-weight surfactants.

This chapter is concerned with these phases, where a substantial amount of the experimental work has been on poly(oxyethylene)-containing block copolymers in aqueous solution. From another viewpoint, the phase behaviour in concentrated block copolymer solutions has been interpreted using the dilution approximation, which considers concentrated solution phases to be simply uniformly swollen melt phases. Work on styrenic block copolymers in concentrated solution has been interpreted in this framework. There is as yet no unifying theory that treats ordered micellar phases and diluted melt phases coherently.

The ordered phases in semidilute and concentrated solutions have largely been characterized using small-angle X-ray and neutron scattering, which is often complemented by rheological studies of the viscoelastic properties. Polarized light microscopy may be used to locate gel phases, because cubic gels are optically isotropic, whereas lamellar or hexagonal phases exhibit birefringence. Since gelation is a thermal event, DSC has been used to detect the gelation point. The analysis of dynamic light scattering data from liquid crystal phases is complex, and only a limited number of studies have been performed.

Studying this phase behaviour has been the subject of intense effort since the early 1990s. The literature reflects the relatively recent interest in this aspect of block copolymers and much work continues in this area, and will no doubt lead to an expanded version of this chapter in future editions of this book.

The semidilute region is defined by $\phi^* < \phi \leq 1$, where ϕ^* is the overlap volume fraction (eqn 3.1). Two length-scales then become important, relative to the correlation length ξ for segment concentration fluctuations. This correlation length is equal to the 'blob' size, where each blob contains $g = \phi(\xi/a)^3$ monomers, where ϕ is the volume fraction of polymer. For $r < \xi$, the chains appear as self-avoiding walks where excluded volume interactions are important. On the other hand, for $r > \xi$, the copolymer chain can be viewed as a random walk of $Z = N/g$ steps of length ξ. A crossover to concentrated solution behaviour occurs for $\phi \approx 0.1$–0.2. In the concentrated regime, polymer coils in a good solvent achieve their theta dimensions, and there is no further contraction of blobs. The mean field 'dilution approximation' for block copolymers treats concentrated solutions as uniformly swollen melt phases. The phase behaviour maps onto those of melts by replacing χN by $\phi\chi N$. However, there is evidence that the dilution approximation is not universally valid, as discussed in Section 4.5.1.

Several recent reviews have included a discussion of the ordered micellar phase phase behaviour of poly(oxyethylene)/poly(oxypropylene) copolymers (Alexandridis and Hatton 1995; Chu and Zhou 1996) and poly(oxyethylene)/poly(oxybutylene) copolymers (Booth *et al.* 1997).

This chapter is concerned with experiments and theory for semidilute and concentrated block copolymer solutions. The focus is on the thermodynamics, i.e. the phase behaviour of both micellar solutions and non-micellar (e.g. swollen lamellar) phases. The chapter is organized very simply: Section 4.2 contains a general account of gelation in block copolymer solutions. Section 4.3 is concerned with the solution phase behaviour of poly(oxyethylene)-containing diblocks and triblocks. The phase behaviour of styrenic block copolymers in selective solvents is discussed in Section 4.4. Section 4.5 is then concerned with theories for ordered block copolymer solutions, including both non-micellar phases in semidilute solutions and micellar gels. There has been little work on the dynamics of semidilute and concentrated block copolymer solutions, and this is reflected by the limited discussion of this subject in this chapter.

4.2 Gelation in block copolymer solutions

Structure of micellar cubic phases

It is now well established that formation of 'hard' or 'stiff' gels is the result of association of micelles into cubic phases. The notation 'hard gel' follows Hvidt and co-workers (Almgren *et al.* 1995; Hvidt *et al.* 1994) and refers to a micellar solution with a dynamic elastic shear modulus $G' \gtrsim 10^3$ Pa. The correlation between the formation of a cubic phase and the onset of plastic flow (i.e. formation of a gel with a finite yield stress) was first made for PS–PI solutions in

tetradecane above a critical gel concentration (cgc) (Shibayama *et al.* 1983*a*; Watanabe and Kotaka 1982), as discussed further in Section 4.4. Gel formation in poly(oxyethylene)–poly(oxypropylene)–poly(oxyethylene) (PEO–PPO–PEO) copolymers in aqueous solution has also been correlated with the association of micelles into a cubic phase (Wanka *et al.* 1994) and is discussed further in Section 4.3. Mortensen and co-workers (Mortensen 1992; Mortensen and Pedersen 1993; Mortensen *et al.* 1992) used SANS on copolymers under shear to provide evidence that, for concentrated solutions, PEO–PPO–PEO micelles crystallize in a body-centred cubic (BCC) lattice. This is illustrated in Fig. 4.1 which shows SANS patterns from a 25 wt% solution of Pluronic P85 ($PEO_{26}PPO_{39}PEO_{26}$) at different temperatures. The six-fold pattern results from [110] reflections from the BCC structure. A liquid micellar phase is stable at low temperatures, which transforms into the cubic structure at higher temperatures. At even higher temperatures, a phase of hexagonal-packed cylinders is formed (Fig. 4.1), as discussed in more detail below.

Face-centred cubic (FCC) structures have also been observed in Pluronic copolymers, using SAXS (Berret *et al.* 1996). In an aqueous poly(oxyethylene)–poly(oxybutylene) (PEO–PBO) diblock solution, both BCC and FCC phases

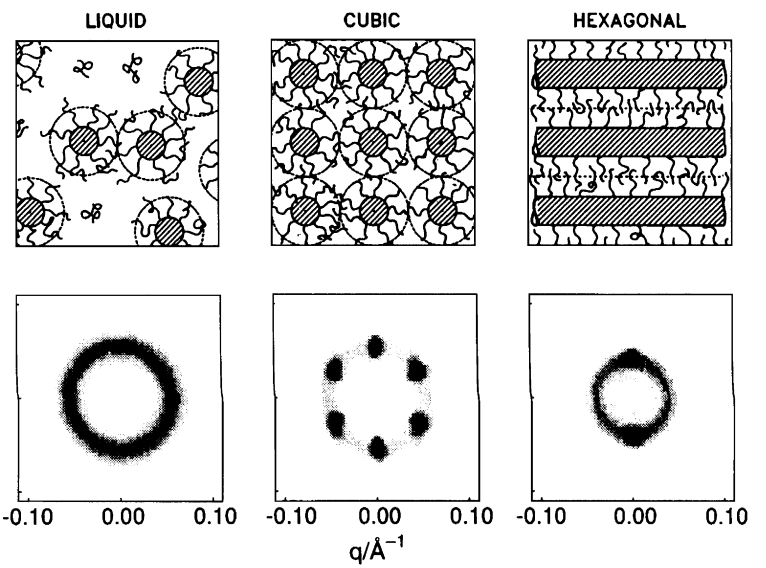

Fig. 4.1 *Top*: schematic illustration of micellar phases formed by the Pluronic copolymer P85 ($PEO_{26}PPO_{39}PEO_{26}$) with increasing temperature. *Bottom*: small-angle neutron scattering patterns from sheared solutions in D_2O of this copolymer (25 wt%). The three columns (*left–right*) correspond to a liquid spherical micelle phase at 25 °C, a cubic phase of spherical micelles at 27 °C and a hexagonal phase of rod-like micelles at 68 °C (Mortensen 1993*a*).

have been observed depending on the concentration of copolymer and on the temperature, and the behaviour of the gels under large-amplitude shear has been examined (Pople *et al.* 1997). These phases were first observed in solutions of poly(styrene)–poly(isoprene) (PS–PI) diblocks in decane (McConnell *et al.* 1993). One or other of the two structures was formed below the order–disorder transition depending on the thickness of the micellar corona compared to the core. Thinner coronas lead to more short-range inter-micellar repulsions and so favour the FCC structure, whereas the BCC phase is favoured for 'softer spheres' with larger coronas (McConnell *et al.* 1993). In Kraton copolymers (PS/hydrogenated PI diblocks and triblocks) Higgins and co-workers have used SANS to investigate cubic micellar phases (Higgins *et al.* 1986, 1988; Phoon *et al.* 1993), and the transition to a gel was shown to be accompanied by a change in rheological response from that of a liquid to that of a solid.

The structure of hard gels is best elucidated using SAXS or SANS because the periods of the ordered structures are on the scale 10–100 nm. In addition to tube inversion and rolling ball viscometry, which are sensitive to yield stress, the formation of a hard gel can be identified by other techniques. These include DSC (gelation is an endothermic process), NMR (via transverse relaxation time, T_2, measurements), polarized light microscopy and rheometry.

Hard sphere crystallization in cubic micellar phases

There is general agreement that gelation in solutions of block copolymers results from the increase in volume fraction of micelles with increasing temperature. The transition to hard gel occurs when the volume fraction of spheres in the system (Φ) reaches a critical value. This is $\Phi_c = 0.74$ for FCC or hexagonal-close packed (HCP) structures (Scordari 1992), $\Phi_c = 0.68$ for a BCC structure (Scordari 1992) or $\Phi_c = 0.494$ for a primitive cubic structure, the latter corresponding to the freezing transition of hard spheres (the melting transition occurs at $\Phi_c = 0.545$) (Hoover and Ree 1968). With an expansion factor, δ, defined as $\delta = v_s/v_a$, where v_s is the hard sphere volume and v_a is the 'dry volume', the critical concentration for gelation, the cgc, in g dm^{-3} is given by (Booth *et al.* 1997; Deng *et al.* 1995)

$$\text{cgc} = \frac{10^3 \Phi \varrho_a}{\delta}, \tag{4.1}$$

where ϱ_a is the density of 'dry' polymer. If the hard sphere volume is equated with the thermodynamic volume v_t (related to the excluded volume, *vide infra*) then $\delta = \delta_t$, the thermodynamic expansion factor. For a given structure (given Φ_c), the determining factor for gelation is δ_t, which in turn is largely determined by the solvation of the coronal block (Booth *et al.* 1997). This depends sensitively on the structure of the micelle (including the association number) and the solvent quality. For large spherical micelles, δ_t becomes smaller as the solvent is made poorer, for example by increasing the temperature or adding salt (Deng *et al.* 1995). Thus, gel phase boundaries depend primarily on the solvent quality and more weakly on the copolymer composition, chain length and architecture. If the

hard gel boundary is to be predicted, knowledge of the micellar association number p and the thermodynamic radius R_t is required (Booth *et al.* 1997). The preferred quantity for obtaining the hard sphere volume of a swollen micelle is the thermodynamic volume (rather than the hydrodynamic volume) (Deng *et al.* 1995) and this is related to the excluded volume of polymer in solution. The excluded volume (u) can be measured using static light scattering via the second virial coefficient. In the simplest theory of dilute polymer solutions, $A_2 = N_A u/2M^2$, where N_A is Avogadro's number and M is the molar mass (Yamakawa 1971). For particles treated as hard spheres $u = 8v_t$. The excluded volume of a polymer in solution depends sensitively on the quality of the solvent. It is small in a poor solvent, and zero in a theta solvent. This reflects the balance of entropic and enthalpic contributions to the Gibbs energy when polymer coils overlap and particularly the relative contributions from solvent–solvent, segment–segment and solvent–segment interactions. In the case of micelles, the contribution of the corona to their thermodynamic volume would be expected to depend on solvent quality in a parallel though not in an identical way. For example, the corona in PEO-containing block copolymer micelles would be expected to make a small contribution to the thermodynamic volume when the solvent is a theta solvent for PEO.

Often, at high temperature, a transition from a hard gel to a soft gel or sol is observed. This results from a number of processes that occur as the temperature increases: (i) the molecule–micelle equilibrium shifts more towards the micellar state; (ii) the association number increases; (iii) the excluded volume of the micelle eventually decreases as the theta temperature for poly(oxyethylene) is approached. The last process provides a mechanism for the release of packing constraints, and enables the formation of a fluid at high temperature. In some PEO-containing diblocks and triblocks a second mechanism for the formation of a fluid at the high temperature has been identified, i.e. a transition from spherical to cylindrical micelles. Rheometry provides a method of detecting 'soft' gels, which cannot be identified on the basis of tube inversion tests. For example, measurements of the dynamic elastic shear modulus illustrated in Fig. 4.2 indicate that a 44 wt% solution of $PEO_{41}PBO_8$ only forms a hard gel whereas the 15 wt% solution exhibits only a soft gel. The 27% solution forms both a hard gel and a soft gel on increasing the temperature.

Thermodynamics of gelation

The enthalpy of gelation may be obtained from the temperature dependence of the cgc, in much the same way as the cmc is derived from the temperature dependence of the cmc (Booth *et al.* 1997; Li *et al.* 1997), as discussed in Section 3.2. The equilibrium

$$\text{micelles in mobile phase} \rightleftharpoons \text{associated micelles (hard gel)},$$

where the mobile phase means micellar sol, can be written more formally as (Li *et al.* 1997)

$$M\text{B} \rightleftharpoons \text{B}_M. \tag{4.2}$$

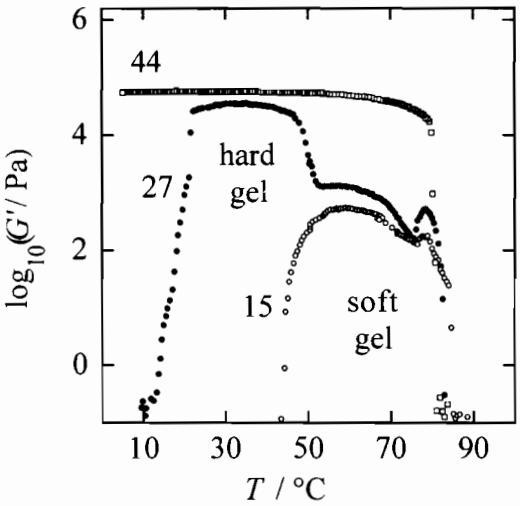

Fig. 4.2 Illustrating regions of 'hard' and 'soft' gel for aqueous solutions of $PEO_{41}PBO_8$ with indicated copolymer concentrations (in wt%). The dynamic elastic shear modulus is plotted as a function of temperature at a frequency of 1 Hz (Booth *et al.* 1997; Li *et al.* 1997).

Here M is a large number. Writing the equilibrium constant for 1 mol of micelles gives (Li *et al.* 1997)

$$K_{\text{gel}} = \frac{\left[B_{\text{M}}\right]_{\text{eq}}^{1/M}}{\left[B\right]_{\text{eq}}} \approx \frac{1}{\left[B\right]_{\text{eq}}} \left(\text{for large } M\right), \tag{4.3}$$

where $[B]_{\text{eq}}$ is the molar concentration of micelles in equilibrium with the hard gel. For micelles of association number p,

$$\left[B\right]_{\text{eq}} = \left[A\right]_{\text{eq}} / p, \tag{4.4}$$

where $[A]_{\text{eq}}$ is the molar concentration of copolymer in the system at the hard-gel boundary at a given temperature. Consequently, the standard Gibbs energy of gelation is given by (Li *et al.* 1997)

$$\Delta_{\text{gel}} G^0 = -RT \ln K = RT \ln\left(\left[A\right]_{\text{eq}} / p\right), \tag{4.5}$$

and the standard enthalpy of gelation is given by (Li *et al.* 1997)

$$\Delta_{\text{gel}} H^0 = R \frac{\text{d} \ln\left[A\right]_{\text{eq}}}{\text{d}\left(1/T\right)} = R \frac{\text{d} \ln c_{\text{eq}}}{\text{d}\left(1/T\right)}, \tag{4.6}$$

where c_{eq} is the mass concentration (g dm^{-3}) of copolymer in the system at equilibrium. The standard states refer to micelles in an ideally dilute solution of concentration 1 mol dm^{-3}, and micelles in the packed gel.

4.3 Poly(oxyethylene)-containing block copolymers in solution

4.3.1 Ordered phases in poly(oxyethylene)/poly(oxypropylene) block copolymer solutions

General

There has been substantial interest in the phase behaviour of poly(oxyethylene)/poly(oxypropylene) (PEO/PPO) copolymers in aqueous solution, in particular focussed on the Pluronic class of PEO–PPO–PEO triblocks because of their commercial production. Extensive experiments leading to phase diagrams of 12 Pluronic copolymers have been performed by Wanka *et al.* (1994) and the Lund group has reported on the phase behaviour of seven members of the Pluronic series (Zhang 1994). Phase diagrams for $PEO_mPPO_nPEO_m$ copolymers with the same PPO block length ($n = 69$) but with m ranging from 5 to 106 are shown in Fig. 4.3. Also for comparison, similar diagrams for copolymers with constant but smaller PPO block lengths and varying PEO content are shown in Figs 4.4 and 4.5 ($n = 30$ and $n = 27$ respectively). The essential features of these phase behaviour studies on Pluronic copolymer solutions can be summarized as follows (Chu and Zhou 1996):

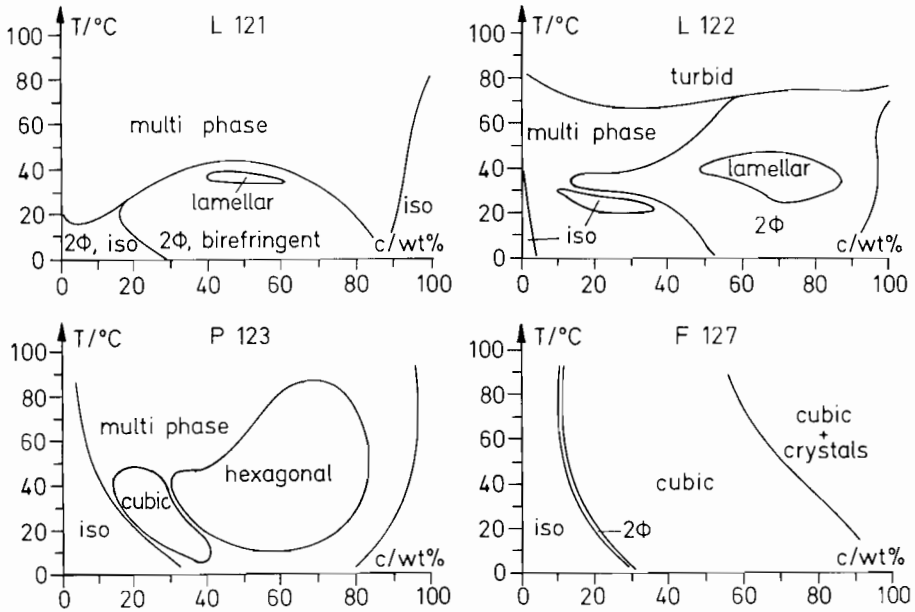

Fig. 4.3 Phase diagrams in water of $PEO_mPPO_nPEO_m$ Pluronics with $n = 69$ and $m = 4$ (L121), $m = 11$ (L122), $m = 20$ (P123) and $m = 99$ (F127) (Wanka *et al.* 1994).

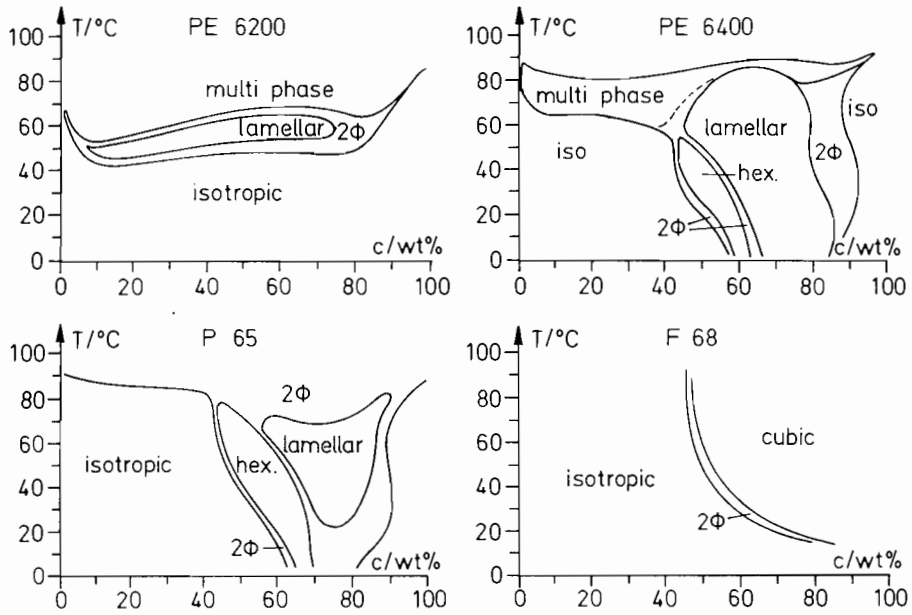

Fig. 4.4 Phase diagrams in water of $PEO_mPPO_nPEO_m$ Pluronics with $n = 30$ and $m = 11$ (PE6200), $m = 13$ (PE6400), $m = 19$ (P65) and $m = 76$ (F68) (Wanka *et al.* 1994).

(i) It appears that below a threshold value of molecular weight ($\approx 2\,kg\,mol^{-1}$) no ordered phase forms up to the cloud point (Zhang 1994).

(ii) The composition of the copolymer and its total molecular weight has a large influence on its phase behaviour. Wanka *et al.* (1994) concluded that the sequence of mesophases observed in the phase diagram depends largely on the PEO/PPO molar ratio (i.e. the m/n ratio). The greater the m/n value, the larger the number of possible mesophases formed. When $m/n \geq 0.5$, spherical micelles are formed for $c >$ cmc. A disorder-to-order transition occurs at higher concentrations, leading to the formation of cubic phases. When m/n is reduced to about 0.25, the hexagonal phase becomes the first ordered mesophase, whereas the lamellar phase appears as the first ordered phase for $m/n \approx 0.15$. In general, the larger the PPO block and the greater the PEO content, the greater is the gelling ability of the Pluronic copolymer. As the molar mass of the PPO block increases, the minimum copolymer concentration required for forming a gel decreases from 60% to about 20%.

(iii) The phase sequence is determined by the copolymer composition, which changes the micellar curvature. A geometrical interpretation of phase behaviour is usually employed for low-molecular-weight surfactants (Mitchell *et al.* 1983). Here the packing of molecules and the associated interfacial curvature govern the phase behaviour. However, low-molecular-weight surfactants are beyond the scope of this chapter and this approach is not detailed here.

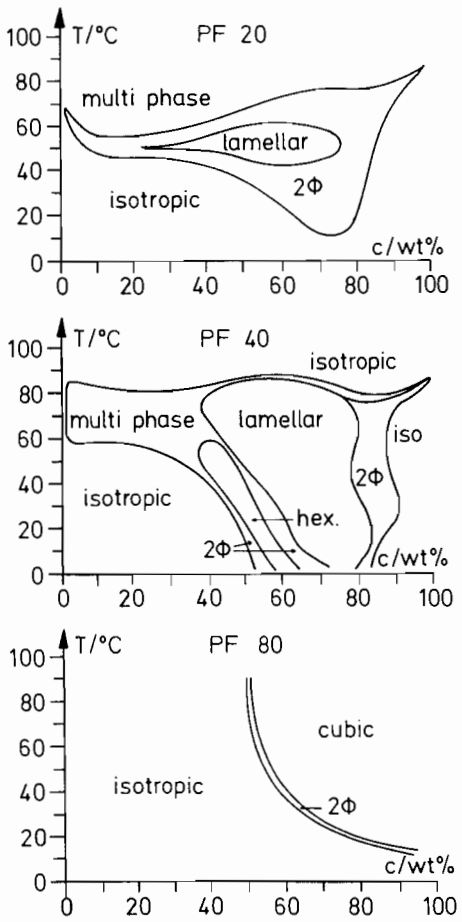

Fig. 4.5 Phase diagrams in water of $PEO_mPPO_nPEO_m$ Pluronics with $n = 27$ and $m = 5$ (PF20), $m = 12$ (PF40) and $m = 73$ (PF80) (Wanka *et al.* 1994).

(iv) The phase boundaries in Figs 4.3–4.5 reveal that thermoreversible transitions are possible in Pluronic surfactants at a fixed concentration. Thermally-induced gelation of Pluronics at high concentrations is one of the characteristic properties of these systems, in addition to strongly temperature-dependent micellization.

A phase diagram for aqueous solutions of Pluronic P85 is shown in Fig. 4.6. The decrease in critical micelle temperature with increasing copolymer concentration can readily be seen. In the temperature range 70–90 °C, a phase of ellipsoidal micelles (length/diameter ratio $L/D \approx 7$) (Schillén *et al.* 1994) is observed at low concentrations, this being a sol because the micelles have liquid-like order. At higher concentrations the rods order onto a hexagonal lattice, and this phase is characterized rheologically as a gel. The cloud point, soft gel and transition

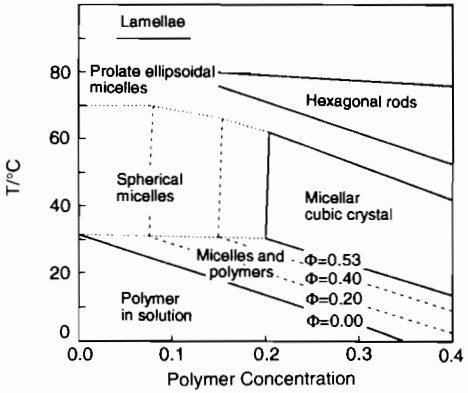

Fig. 4.6 Phase diagram for solutions of P85 ($PEO_{26}PPO_{39}PEO_{26}$) in D_2O. Lines of constant micellar volume fractions (Φ) are indicated, $\Phi = 0$ corresponding to the cmc (Mortensen and Pedersen 1993).

from spherical to rod-like micelles at high temperature in a solution of a PEO-containing block copolymer such as P85 are usually attributed to changes in the PEO-block solvation only (Kjellander and Florin 1981; Linse 1993; Linse and Björling 1991). PEO coils become less extended as water progressively becomes a poorer solvent with increasing temperature (Hvidt *et al.* 1994). As the PEO blocks contract with increasing temperature, the solvation capacity of the micelles decreases. To compensate for this, the PEO coverage at the surface of a micelle increases, and the association number increases leading to an increase in micelle size (thermodynamic radius). The upper size limit for the micelle is controlled by the PPO blocks (Mortensen and Brown 1993) which extend from one side of the micelle to the other. Thus the contraction of PEO blocks forces the micelles to change from a spherical to a rod-like shape (Linse 1993; Mortensen and Pedersen 1993). With increasing temperature the rod-like micelles grow and interact to form a hexagonal gel phase at high concentrations. Finally, at the cloud point, water has become a sufficiently poor solvent for the PEO blocks, such that attractive interactions between the PEO blocks cause phase separation (Karlström 1985). Phase separation can occur into two micellar phases or a polymer-rich phase containing micelles and a phase containing dilute block copolymer. Hard gel formation, on the other hand, is controlled by solvation of both the PPO and PEO blocks. To form a hard gel, the hard sphere volume fraction of spherical micelles must exceed the critical value $\Phi_c = 0.494$. The equilibrium between unimers and micelles shifts towards micelles at higher temperatures due to hydrophobic interactions between the PPO blocks and water. This increases the volume fraction of the micelles whereas their volume fraction is reduced by contraction of the PEO blocks as the temperature rises. The temperature dependencies of these opposing effects determines the critical temperature for hard gel formation. A similar phase diagram to that shown in

Fig. 4.6 was obtained by Glatter *et al.* (1994) using SAXS, ultrasound measurements, DSC, low shear viscometry and light transmission experiments.

Small-angle scattering experiments

Neutron scattering experiments by Mortensen and co-workers (Mortensen 1992, 1993*b*, 1996, 1997; Mortensen and Brown 1993; Mortensen and Pedersen 1993; Mortensen *et al.* 1992) have provided invaluable information on the structure of Pluronic solutions. Initially, they focussed on $PEO_{26}PPO_{39}PEO_{26}$ (Pluronic P85) and $PEO_{103}PPO_{39}PEO_{103}$ (Pluronic F88). Considering P85, at low temperatures, the neutron scattering profiles for a solution with 25 wt% polymer show comparatively weak q dependence, and a small absolute scattered intensity (Fig. 4.7). These features are consistent with fully dissolved Gaussian polymer chains (Mortensen and Pedersen 1993), and the radius of gyration obtained from these data is in agreement with the hydrodynamic radius obtained from dynamic light scattering. As the temperature is increased close to ambient, the PPO becomes almost insoluble leading to the formation of spherical micelles. The equilibrium

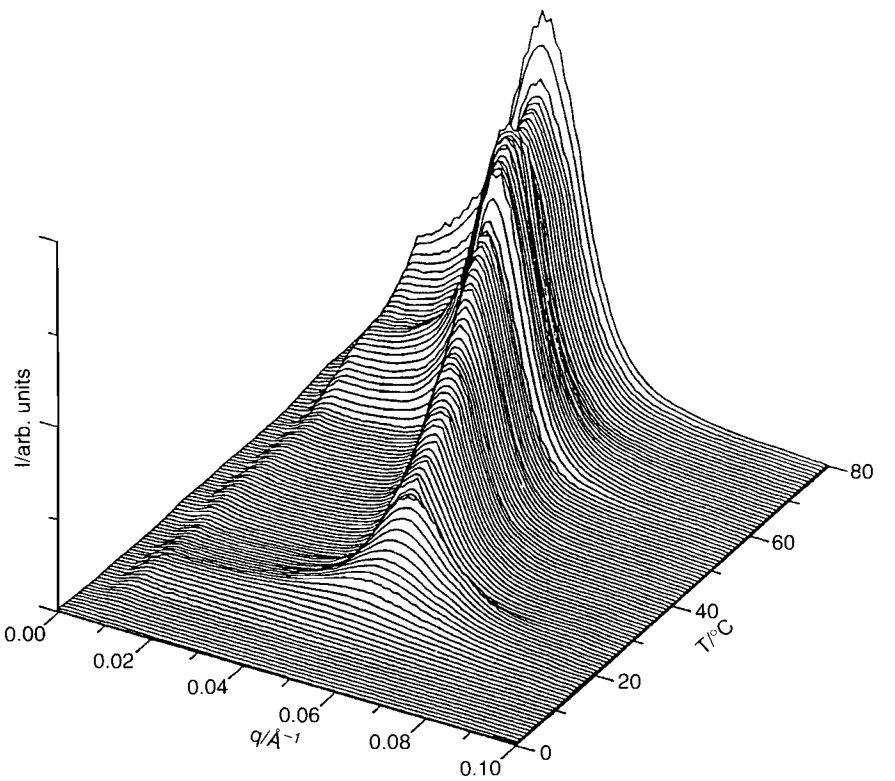

Fig. 4.7 Small-angle neutron scattering intensity versus q for a 25 wt% solution of ($PEO_{26}PPO_{39}PEO_{26}$) in D_2O (Mortensen and Pedersen 1993).

between unimers and micelles shifts in favour of micelles with increasing temperature. This is reflected in a marked increase in the scattered intensity of neutrons, as evident in Fig. 4.7. As the copolymer concentration or temperature is increased further, interactions between micelles become more important and a more pronounced correlation peak develops in the SANS pattern. At the same time, the high q portion of the SANS data remains unchanged, showing that the individual micellar structure is unaffected although the number of micelles is increasing. Mortensen and Pedersen (1993) developed an approach to model these data based on a monodisperse hard sphere model with the Percus–Yevick approximation for the structure factor and a form factor dominated by a dense spherical core. The micelle radius, R, the hard-sphere interaction radius, R_{HS}, and the hard-sphere volume fraction, Φ, could be obtained from this model. Values of Φ extracted from such fits to data for P85 are shown in Fig. 4.8, whilst representative fits are presented in Fig. 4.9. The R and R_{HS} values obtained were found to be essentially independent of copolymer concentration, but increase with temperature as required by the temperature-induced increase in association number. Representative results showing Φ as a function of temperature for a 28% F88 solution at a fixed concentration (28%) are shown in Fig. 4.10. Above the cmt, the volume fraction of micelles increases linearly with temperature until a plateau value $\Phi = 0.53$ is reached where the micelles crystallize onto a cubic lattice (at this volume fraction, the lattice must be primitive). Such an 'inverse melting transition' (Mortensen *et al.* 1992) is, in essence, hard sphere crystallization.

Mortensen and Brown (1993) investigated the conditions for formation of gels formed by spherical or rod-like micelles in a series of Pluronic $PEO_mPPO_nPEO_m$

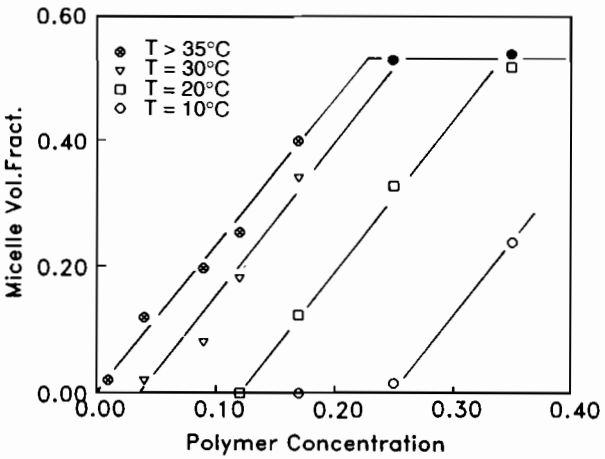

Fig. 4.8 Micelle volume fraction (Φ) versus polymer concentration at different temperatures for solutions of $PEO_{26}PPO_{39}PEO_{26}$ in D_2O (Mortensen 1993*a*). Φ was obtained from fits of the hard sphere Percus–Yevick model to neutron scattering profiles (see Fig. 3.9). At high concentration the asymptote $\Phi = \Phi_c$ for hard sphere crystallization is reached.

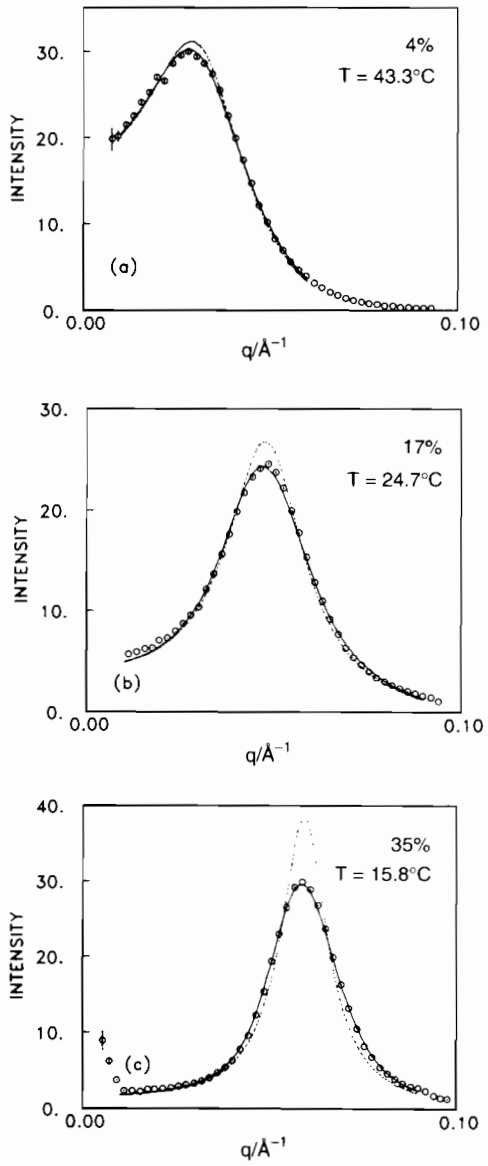

Fig. 4.9 Representative fits of SANS data for $PEO_{26}PPO_{39}PEO_{26}$ at different temperatures and concentrations. The solid lines are the best fits using a hard sphere Percus–Yevick approach and including instrumental smearing. The dotted lines represent the same scattering curves with no instrumental smearing (Mortensen and Pedersen 1993).

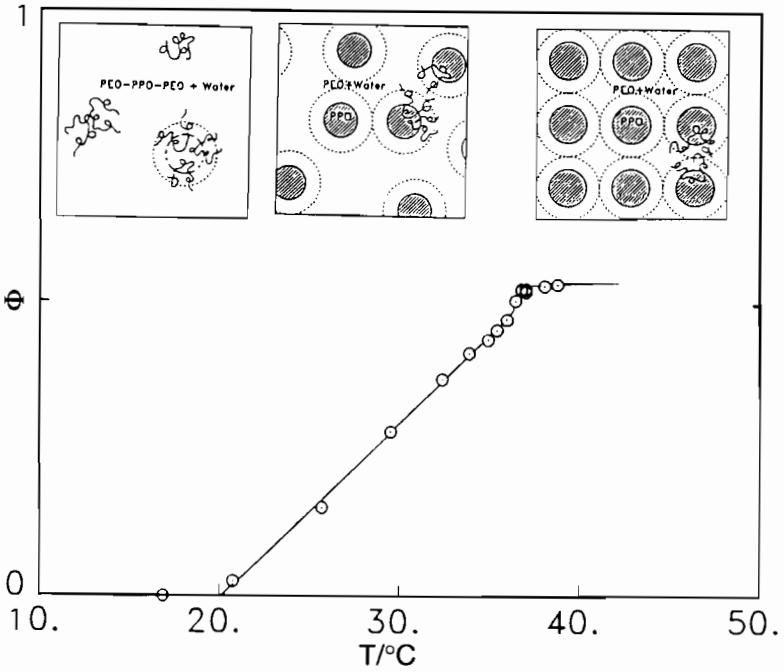

Fig. 4.10 Temperature dependence of the micellar volume fraction for a 28 wt% solution of F88 ($PEO_{103}PPO_{39}PEO_{103}$) in D_2O, as obtained by Percus–Yevick fits to SANS data (Mortensen 1993*b*). The insets show models for the solution structure in the three regimes: unimers in solution at low temperature, micellar liquid above the cmt, and at high temperatures a cubic micellar crystal.

copolymers using small-angle neutron scattering and dynamic light scattering. The copolymers studied had a fixed PPO block length $n = 39$, but varying PEO block length $m = 6$ (L81), 26 (P85), 61 (F87) and 103 (F88), where the bracketed term is the abbreviation for the Pluronic copolymer. The core radius and hard sphere interaction radius were determined using a model for interacting hard sphere micelles. Across the entire temperature range, F88 (the polymer with the largest m) aggregated into micelles with a core diameter smaller than the fully extended PPO block length. On the other hand, the intermediate-m copolymers had a core diameter which approached the size of a fully stretched PPO chain, causing an abrupt departure from a spherical to a rod-like shape. Extrapolating the data to $m = 6$ led to a core size exceeding the length of the fully stretched PPO block, thus explaining the absence of micellization for this polymer (Mortensen and Brown 1993).

Berret *et al.* (1996) have investigated the effect of steady shear, applied using a Couette cell, on the orientation of a face-centred cubic structure in $PEO_{127}PPO_{48}PEO_{127}$ (Pluronic F108) using SAXS, and transitions between shear-

ing flows were elucidated. A twinned FCC structure with a high density of stacking faults due to flow of sliding layers was observed to transform into large homogenous single crystals of either twin, separated on a millimetre scale, on application of large-amplitude oscillatory shear (Diat *et al.* 1996). In a Couette cell it is possible to access both the (q_v, q_e) and (q_∇, q_e) planes, where **v** denotes the shear direction, ∇ the shear gradient direction, and **e** the vorticity direction, by passing the beam radially or tangentially through the cell respectively. Figure 4.11 shows SAXS patterns for a 35 wt% aqueous solution of F108 in these two orientations. A diffraction pattern from a twinned structure in the (q_∇, q_e) plane is shown in Fig. 4.11(b); however, by translating the Couette cell slightly so that the beam was incident closer to the outer rotor it was possible to isolate a diffraction pattern from only one of the twinned single crystals (Fig. 4.11(c)), which were thus shown to be separated radially on a millimetre length-scale. The indexation of the patterns in Fig. 4.11(a) and (c) to a single crystal FCC structure is shown in Fig. 4.12.

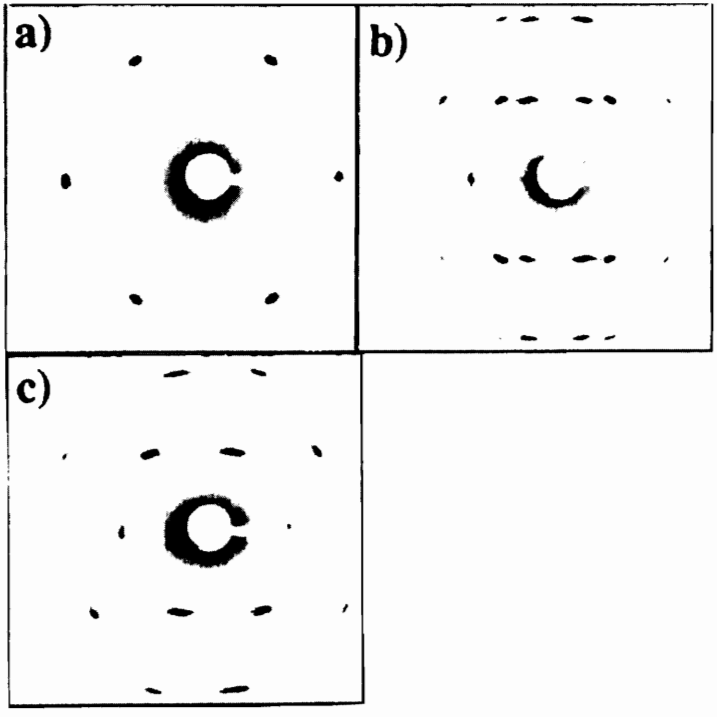

Fig. 4.11 Small-angle X-ray scattering patterns from a face-centred cubic phase formed by a $PEO_{127}PPO_{48}PEO_{127}$ (F108) Pluronic solution (35 wt% in water) at 30 °C during oscillatory shear at 10 rad s^{-1} with a strain amplitude of 40% (Diat *et al.* 1996). The patterns correspond to (a) the (q_v,q_e) plane and (b) the (q_∇,q_e) plane. In (c) the pattern was recorded in the (q_∇,q_e) plane but with the beam incident close to the outer rotor. It corresponds to one of the FCC twins giving the diffraction pattern in Fig. 4.12(b).

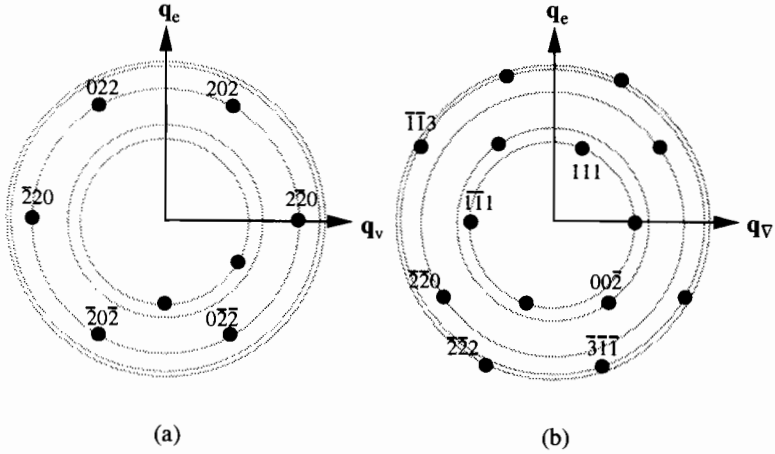

Fig. 4.12 Indexation for a single crystal FCC structure for Fig. 4.11(a) and (c) (Diat *et al.* 1996). The grey circles correspond to powder rings.

Effect of chain architecture

Chain architecture has a large effect on micellar association in block copolymer solutions. Although a large number of studies have been performed on PEO–PPO–PEO polymers, there is only very limited work on PPO–PEO–PPO copolymers. Part of the phase diagram (Mortensen 1997; Mortensen *et al.* 1994) of $PPO_{15}PEO_{156}PPO_{15}$ (Pluronic 25R8) obtained by SANS, static and dynamic light scattering and rheological measurements is shown in Fig. 4.13(a) (Mortensen 1997). At low temperatures and in the dilute region (at lower concentrations than shown in Fig. 4.13(a)), the copolymer exists in the form of Gaussian unimers. Upon increasing the concentration or raising the temperature, intermolecular association of the PPO blocks leads to small clusters which are interconnected by long PEO blocks to form temporary branched structures (Mortensen *et al.* 1994). The tendency for molecular association ahead of micellar association for this copolymer is largely due to the weak hydrophobicity of the short PPO end-blocks (and is enhanced by the long PEO block). At higher concentrations or higher temperatures, spherical micelles containing a PPO core are formed, with PEO blocks acting as bridges between micelles to form an isotropic network (phases I and V), as shown in Fig. 4.13(b). Above 50 wt% copolymer, this kind of structure may constitute the whole sample, making it appear liquid-like. Region II corresponds to a cubic micellar phase, of probable FCC structure. Phase III could not be sheared into a well-ordered monodomain and thus could not clearly be identified. Region IV corresponds to a two-phase system with an elastic rheological response, possibly formed from coexistence of a semicrystalline lamellar structure with the micellar network. The PPO–PEO–PPO class of copolymers exhibit a much lower cloud point in water than their PEO–PPO–PEO equivalents. For example, a 10 wt% aqueous Pluronic

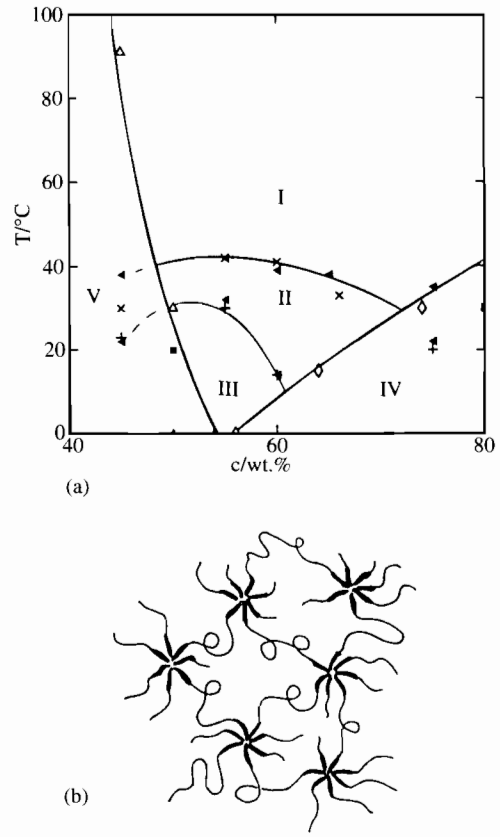

Fig. 4.13 (a) Phase diagram for aqueous solutions of Pluronic 25R8 ($PPO_{15}PEO_{156}PPO_{15}$) determined using SANS, SLS, DLS and rheometry (Mortensen 1997; Mortensen *et al.* 1994). Phases I and V are disordered micellar networks, V with excess water. Phases II and III are cubic micellar phases. Phase IV is a coexistence regime of micelles and crystalline layered PEO. (b) Schematic of the micellar network.

25R8 solution shows a cloud temperature of 16 °C (Chu and Zhou 1996), compared to about 90 °C for P85.

Effect of addition of homopolymer, salt or conventional surfactants

The effect of addition of PEO and PPO homopolymers on the gel formation of Pluronic F127 (defined in Fig. 4.3) in aqueous solution has been studied by Malmsten and Lindman (1993). The structure, studied via SANS, and rheology of neat F127 solutions in the concentration range 10–20% has been probed by Prud'homme *et al.* (1996). Addition of PEO can reduce the gel region and/or eliminate it at sufficiently high PEO concentration. The amount of PEO required to 'melt' the gel depends on the copolymer concentration and decreases with

increasing PEO molecular weight. Whilst PEO of low molecular weight hardly affects the gelation process and high-molecular-weight PEO leads to phase separation, an intermediate M_w (e.g. $M_w = 6\,kg\,mol^{-1}$) homopolymer increases the gelation concentration and decreases the gel–sol temperature. In contrast, low-molecular-weight PPO increases the stability region of the Pluronic F127 gel. However, higher-molecular-weight ($M_w = 4\,kg\,mol^{-1}$) PPO is too large to be solubilized (Malmsten and Lindman 1993).

The effect of salt on the micellization and gelation processes of Pluronic copolymers has been studied by a number of groups (Almgren *et al.* 1995; Jørgensen *et al.* 1997; Malmsten and Lindman 1992; Vadnere *et al.* 1984). Salts such as NaCl, KCl and KF act as structure makers, leading to an increase in the self-hydration of water through hydrogen bonding and therefore a reduction in polymer solubility (Almgren *et al.* 1995; Chu and Zhou 1996; Malmsten and Lindman 1992). On the other hand, salts such as KI and KSCN (and their sodium analogues), as well as urea and ethyl alcohol, act as structure breakers, reducing self-hydration and increasing the hydration of the polymer (Almgren *et al.* 1995; Chu and Zhou 1996; Malmsten and Lindman 1992). Adding a 'salting out' agent such as KCl shifts the gel region and cloud point to lower temperatures, whereas adding a 'salting in' agent moves the gel region and cloud point to higher temperatures (Jørgensen *et al.* 1997; Malmsten and Lindman 1992). Jørgensen *et al.* (1997) have investigated the effects of salt on the phase behaviour of P85. In this system, a hard gel is formed at low temperatures depending on the concentration. On heating, concentrated solutions (e.g. 28.5% polymer in 1 M KF) melt from a spherical micellar hard gel into a sol, then at higher temperatures the soft gel hexagonal phase is formed. The temperature shifts for the spherical–cylindrical micelle phase boundary and the soft gel boundary on addition of salt are found to be equal to the temperature shifts in the cloud points for the different systems. However, this is not the case for the hard gel. The cloud point and soft gel transitions at high temperature in Pluronic triblocks are usually attributed to changes in the PEO-block solvation only (Kjellander and Florin 1981; Linse 1993; Linse and Björling 1991). The onset of micellization is also shifted by the addition of salt in the same direction as the cloud point but by a much smaller amount (Bahadur *et al.* 1993). This shows a weaker effect of salts on the dimensions of the PPO block compared to the PEO block, which explains the reduced influence on the hard gel transition temperature because hard gel formation is controlled by the volume fraction of effective hard spheres, which depends on the swelling of both blocks (Jørgensen *et al.* 1997).

The interaction of Pluronic copolymers with ionic surfactants has been studied by a number of groups, in particular for sodium dodecyl sulphate (SDS) (Almgren *et al.* 1991; Hecht and Hoffmann 1994, 1995; Hecht *et al.* 1995; Vadnere *et al.* 1984; Zhang *et al.* 1995). Almgren *et al.* (1991) studied the micellization of two Pluronics with SDS in the dilute regime using ^{13}C NMR and fluorescence quenching techniques. They found that the copolymers form mixed micelles with SDS at concentrations well below the cmc of SDS and that SDS reduces the size of Pluronic micelles. The influence of SDS on the association of Pluronic F127 was investigated by Hecht and co-workers (Hecht and Hoffmann 1994, 1995;

Hecht *et al.* 1995) using a variety of experimental methods. They found that SDS binds strongly to F127 and can suppress micelle formation by F127 completely. The ordered hexagonal and lamellar phases formed in the Pluronic L64 ($PEO_{13}PPO_{30}PEO_{13}$)/water phase diagram at high copolymer concentrations were found to be replaced upon addition of SDS by an isotropic solution (Zhang *et al.* 1995). At moderate copolymer concentrations, a bicontinuous isotropic solution was transformed into a solution of discrete micelles (Zhang *et al.* 1995). This addition of conventional ionic surfactants to non-ionic polymer surfactants (e.g. Pluronics) can have a dramatic effect on phase behaviour. Because the ionic surfactant often acts as a cosurfactant it can change the packing density at the surfactant–water interface and hence induce transitions to phases with different interfacial curvature, or even lead to the breakup of micellar structures.

4.3.2 Ordered phases in poly(oxyethylene)/poly(oxybutylene) block copolymer solutions

The phase behaviour established for concentrated aqueous solutions of PEO–PPO–PEO copolymers has its counterpart in PEO/PBO copolymer solutions. A phase diagram for $PEO_{58}PBO_{17}PEO_{58}$ based on tube inversion experiments is shown in Fig. 4.14 (Luo *et al.* 1992). The hard gel is isotropic under the polarizing microscope and can be characterized as a cubic phase formed from spherical micelles of a similar size to those in the dilute micellar solution.

The phase behaviour of $PEO_{40}PBO_{10}$ has recently been determined in detail, including the effect of addition of the salt K_2SO_4 (Deng *et al.* 1995). Increasing the concentration of aqueous K_2SO_4 reduces the upper sol–gel transition as shown in Fig. 4.15; however, it has a much weaker effect on the lower gel boundary. This is because the effect of salt in reducing the micellar expansion factor (δ_t) is compensated at the lower boundary by more favourable conditions for formation of micelles in the poorer solvent (i.e. a lower cmc) whereas no such compensation is possible at the upper boundary. Regions of clear and cloudy,

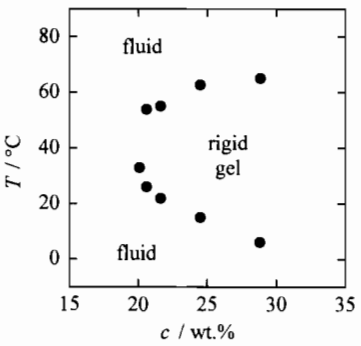

Fig. 4.14 Phase diagram for $PEO_{58}PBO_{17}PEO_{58}$ determined on the basis of tube inversion measurements, which detect the finite yield stress of immobile gel phases or the flow behaviour of fluid sols (Booth *et al.* 1997; Luo *et al.* 1992).

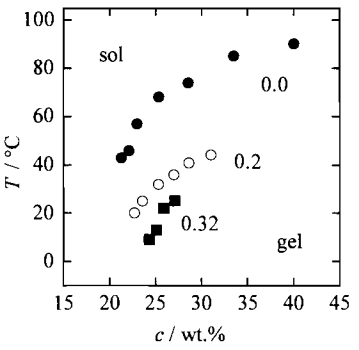

Fig. 4.15 Effect of salt on the upper sol–gel boundary for aqueous solutions of $PEO_{40}PBO_{10}$. Concentrations of K_2SO_4 (mol dm^{-3}) are indicated (Booth *et al.* 1997; Deng *et al.* 1995).

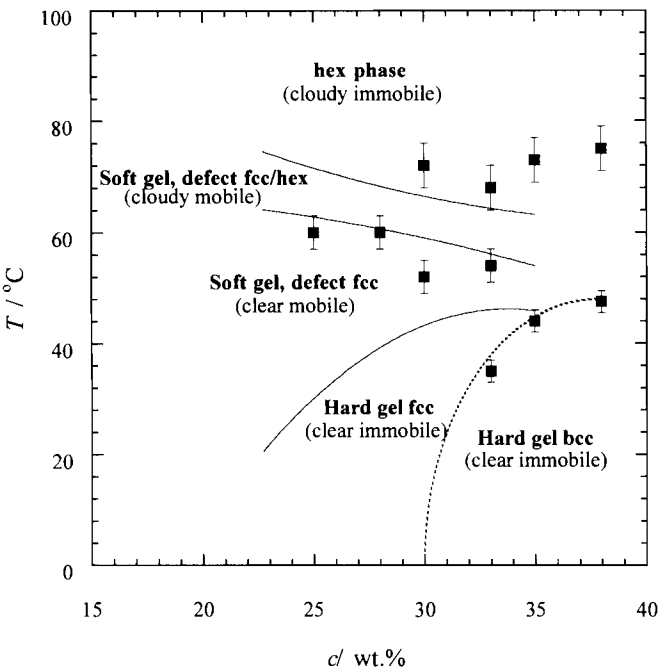

Fig. 4.16 Phase diagram for aqueous solution of $PEO_{40}B_{10}$ determined using SAXS and rheometry (Pople *et al.* 1997). The filled symbols mark the phase boundaries determined by SAXS, with the broken line as a guide to the eye, and the solid lines mark transitions determined using rheology (Deng *et al.* 1995; Pople *et al.* 1997). The error bars indicate uncertainties associated with the phase transitions determined from repeated heating and cooling ramps.

immobile and mobile solutions are illustrated in Fig. 4.16 for $PEO_{40}PBO_{10}$ in 0.2 M K_2SO_4. This solution has phase transitions in a particularly amenable temperature range, for example mobile–immobile gel transitions near room temperature. Hamley and co-workers have used SAXS and rheology to determine the phase behaviour of this system in detail (Pople *et al.* 1997). Representative SAXS patterns for a 38% solution that identify BCC, FCC and hexagonal phases on increasing temperature are shown in Fig. 4.17. The phase diagram in Fig. 4.16

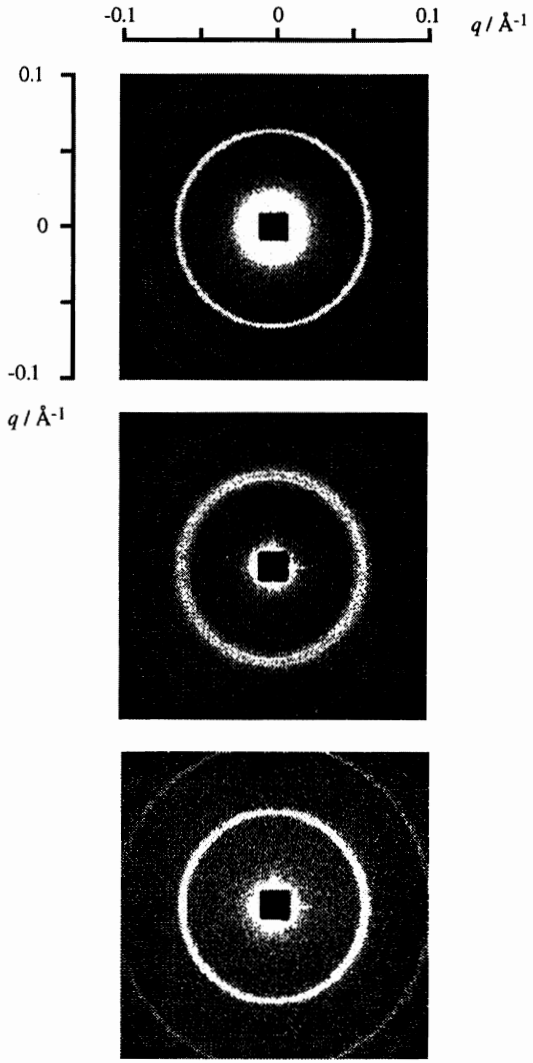

Fig. 4.17 Small-angle X-ray scattering patterns for 38 wt% aqueous solutions of $PEO_{40}PBO_{10}$: (a) BCC phase observed between 5 and 50 °C; (b) FCC structure between 50 and 75 °C; (c) hexagonally-packed cylinder phase above 75 °C (Pople *et al.* 1997).

shows a hard gel BCC cubic phase of spherical micelles at low temperatures at the high concentration end of the phase diagram. On heating, a reversible transition to an FCC cubic structure is observed (Pople *et al.* 1997). Interestingly, the structure appears to remain FCC across the gel–sol transition boundary. A complete explanation for this observation has not yet been provided. The gel FCC phase can be oriented using large-amplitude shear, but the sol FCC phase cannot (Hamley *et al.* 1998*b*). The BCC phase is only observed for concentrations greater than about 30%, the hard gel phase for lower concentrations being FCC only. Finally, above a biphasic region, a hexagonal phase was observed for temperatures higher than about 70 °C. This immobile gel phase is turbid due to light scattering by elongated rod-like micelles (this illustrates that cuation is required when associating turbidity with phase separation). The explanation for the thermally-induced BCC–FCC transition and subsequent formation of a hexagonal phase for the more concentrated solutions (Pople *et al.* 1997). is similar to the explanation provided for the observation of a soft gel, cloud point and sphere-to-rod transition described in Section 4.3.1 for Pluronic copolymers. This is that as the temperature increases, the solvent becomes poorer for PEO which leads to a reduction in the PEO corona thickness. This effect is counterbalanced by the increasing tendency for molecules to associate in micelles, which leads to an increase in micelle size up to a limit imposed by the maximum extension of the PBO block. When this limit is reached the micelles can only grow by transforming from spheres to rods.

The critical gelation concentration (cgc) depends on the thermodynamic expansion factor, δ_t, via eqn 4.1. The critical gelation concentrations found for a series of PEO/PBO diblock copolymers are plotted in Fig. 4.18 against $1/\delta_t$, where δ_t is obtained for micelles in dilute solution via light scattering (Booth *et al.* 1997). The data refer to the upper gel–sol transition, for which the micelle concentration can be equated with the total copolymer concentration. The line shown in Fig. 4.18 corresponds to eqn 4.1 with $\Phi_c = 0.70$, showing that the data are consistent with cubic close-packing (Booth *et al.* 1997; Deng *et al.* 1995).

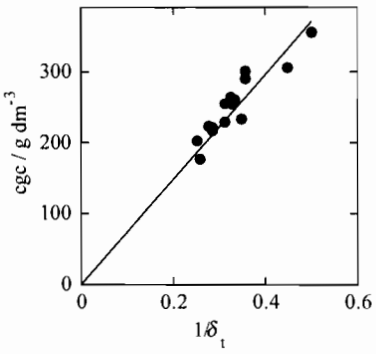

Fig. 4.18 Critical gel concentration versus $1/\delta_t$, where δ_t is the thermodynamic expansion factor, for PEO–PBO diblocks (Booth *et al.* 1997).

Phase diagrams for other PEO/PBO copolymers have been determined by the Manchester group using tube inversion, polarized light microscopy, DSC and rheology. Hard gel boundaries for three triblocks with the same central block length (PBO_{10}) but differing PEO block lengths are shown in Fig. 4.19. Copolymers $PEO_{35}PBO_{10}PEO_{35}$ and $PEO_{21}PBO_{10}PEO_{21}$ form an isotropic cubic phase at low concentrations in the hard gel region (consistent with spherical micelles in the sol), then, as the concentration is increased, a birefringent hexagonal phase. Copolymer $PEO_{16}PBO_{10}PEO_{16}$ forms a hexagonal gel phase (cylindrical micelles in the sol) and a lamellar phase at higher concentration. The phase behaviour of these solutions has been investigated by a range of techniques, including small-angle X-ray and neutron scattering (Fairclough *et al.* 1997). Phase diagrams for PBO–PEO–PBO-type copolymers have also been obtained (see Fig. 4.20) (Booth *et al.* 1997; Yang *et al.* 1997). Tube inversion and polarized light microscopy were used to locate the hard gel boundaries and ordered phases respectively. The phase diagram for $PBO_7PEO_{40}PBO_7$ is complicated by the cloud point curve (dashed line), which passes through both micellar sol and gel phases (Yang *et al.* 1997). Clouding of a micellar PBO–PEO–PBO copolymer is consistent with an attractive micellar interaction through bridging of PEO blocks between micelles (Yang *et al.* 1996*a*,*b*; Zhou *et al.* 1996), which cannot occur for the PEO–PBO–PEO analogue.

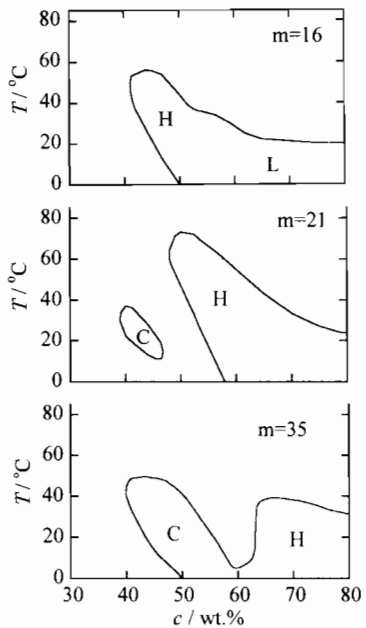

Fig. 4.19 Phase diagrams obtained by the tube inversion method for $PEO_mPBO_{10}PEO_m$ copolymers in aqueous solutions (Booth *et al.* 1997). Ordered phases are indicated: C, cubic; H, hexagonal; L, lamellar.

The thermodynamics of gelation in a PEO–PBO copolymer have been studied by Booth and co-workers (Booth *et al.* 1997; Li *et al.* 1997). Gel formation at the lower boundary (cold gelation) is endothermic, whilst that at the upper boundary (hot gelation) is exothermic. DSC has been used to show that the enthalpy changes associated with cubic gel formation are small, e.g. $\Delta_{gel}H^0 \approx -140\,J\,(mol\,copolymer)^{-1}$ for gelation on cooling (high T boundary, 67 °C) of an aqueous solution containing 30% $PEO_{41}PBO_8$. A plot of log(cgc) against $1/T$ for the hot gelation of $PEO_{41}PBO_8$ gives a straight line (Fig. 4.21), following eqn 4.6, yielding $\Delta_{gel}H^0 \approx -200\,J\,(mol\,copolymer)^{-1}$ (Li *et al.* 1997). Values of similar magnitude, but positive, are found for gelation on heating (low temperature boundary) (Li *et al.* 1997). All are very much smaller than values of $\Delta_{mic}H^0$, which are in the range 30–80 kJ (mol copolymer)$^{-1}$. Compared with micellization, gelation is almost athermal (Booth *et al.* 1997).

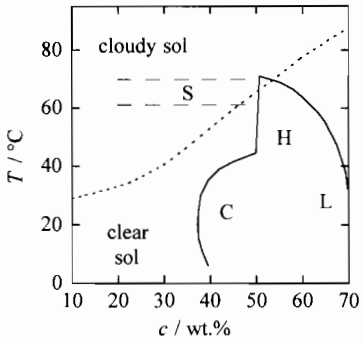

Fig. 4.20 Phase diagram for aqueous solutions of $PBO_7PEO_{40}PBO_7$ (Booth *et al.* 1997; Yang 1996). The dashed line separates clear solutions and gels from cloudy ones. The boundary enclosing the cubic (C), hexagonal (H), and lamellar (L) phases is indicated. An approximate region of gel extending to low concentrations is denoted S.

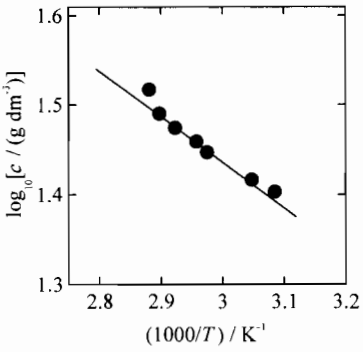

Fig. 4.21 Critical gel concentration versus inverse temperature for aqueous solutions of $PEO_{41}PBO_8$ (Booth *et al.* 1997; Li *et al.* 1997).

4.4 Styrenic block copolymers in solution

4.4.1 Poly(styrene)–poly(isoprene) and polystyrene–poly(butadiene) block copolymers

Gelation

Some of the earliest studies on ordered structures in semidilute and concentrated block copolymer solutions were performed by Hashimoto and co-workers (Shibayama *et al.* 1983*a*). Using SAXS, they studied a poly(styrene)–poly(butadiene) (PS–PB) diblock in tetradecane, a selective solvent for PB. At a fixed concentration, increasing the temperature was found to lead to the loss of long-range lattice order, i.e. melting of a gel phase to a liquid-like micellar solution. At higher temperatures a transition to a homogeneous solution was observed, following the breakup of micelles.

Watanabe and Kotaka examined the structure and viscoelastic properties of the same PS–PB diblock in tetradecane over a wide range of concentration and molecular weight. This work is reviewed by Watanabe and Kotaka (1984). They observed ordered structures at sufficiently high concentrations using SAXS, and a corresponding regime of non-linear, plastic flow was noted in the rheology. The concentration for the onset of plastic flow, i.e. the critical concentration for gelation, was determined for a number of PS–PB diblocks in tetradecane at 25 °C and found to be in the range 1–7 wt%. The flow behaviour was Newtonian at lower concentrations. Rheological data for solutions of different concentrations at a fixed temperature are shown in Fig. 4.22, and it is evident that the apparent yield stress increases with concentration. The observation of a yield stress is consistent with gelation in the ordered micellar phase. For a 20% solution of a PS–PB diblock in tetradecane, they observed plastic flow at low temperatures, then a transition to a phase with linear viscoelasticity but zero yield stress (Watanabe *et al.* 1982) (see Fig. 4.23). This was correlated to the disappearance with increasing temperature of Bragg peaks corresponding to a cubic micellar (microphase-separated) structure, and an increase in the width of the primary SAXS peak (Hashimoto *et al.* 1983*a*; Watanabe *et al.* 1982). Finally, at the highest temperatures, above the transition to a homogeneous solution, the flow behaviour became Newtonian (Fig. 4.23). For concentrated solutions ($\phi \gtrsim 0.2$), the yield stress and shear modulus were found to depend linearly on polymer concentration. This was accounted for in a calculation of the change in free energy resulting from changes in chain packing during deformation of the lattice under shear (Hashimoto *et al.* 1983*a*).

At higher shear rates, Watanabe and Kotaka (1983) observed thixotropy, i.e. stress decay increasing as a function of shear rate, in PS–PB diblocks in dibutyl phthalate (DBP), which is a selective solvent for PS. The fact that the flow crossed over from plastic to viscous non-Newtonian on increasing the shear rate indicated the breakdown of the micellar lattice structure, rather than of the individual micelles. This was confirmed by parallel measurements on a cross-linked PB–PS system, where stress decay and recovery were also observed. Thus the

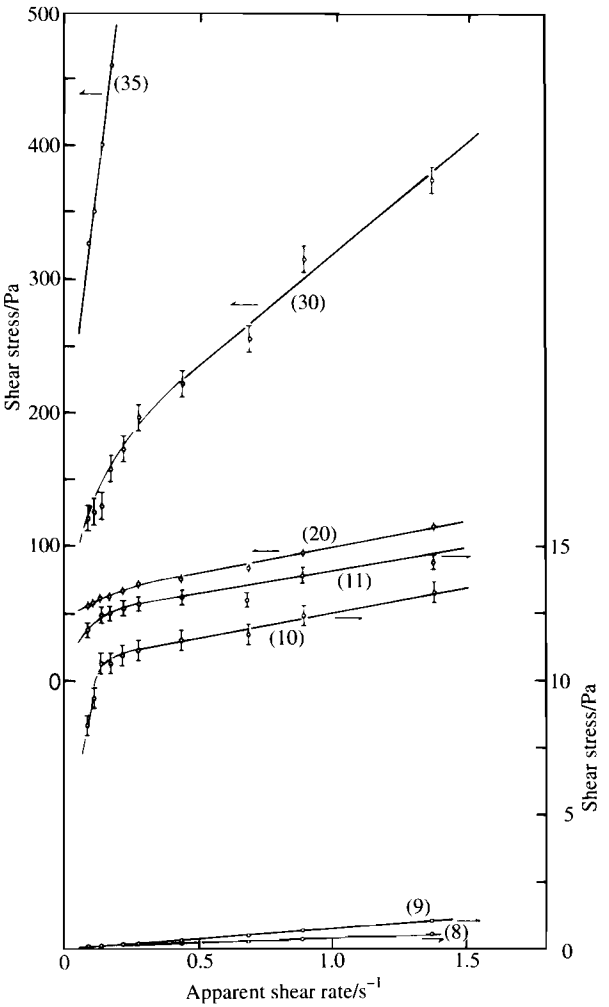

Fig. 4.22 Steady-state flow behaviour of solutions of a PS–PB diblock (M_n = 52 kg mol^{-1}, 29.5 wt% PS) in tetradecane at 25 °C at various concentrations (wt%, indicated) (Hashimoto *et al.* 1983*a*; Watanabe *et al.* 1982).

thixotropy must be due to the breakup of a micellar array, because the cross-linked micellar cores could not be broken (Watanabe and Kotaka 1983).

Gast and co-workers (Gast 1996; McConnell *et al.* 1993, 1995) have used SAXS to probe ordered micellar structures in PS–PI block copolymers dissolved in decane, which is a preferential solvent for PI. They determined the form factor of a range of diblocks by performing SAXS in dilute solution (McConnell *et al.* 1993). The same diblocks in more concentrated solutions were found to form cubic micellar structures, and the gelation (micellar disorder–order) transition on increasing concentration was determined. Remarkably, both BCC and FCC struc-

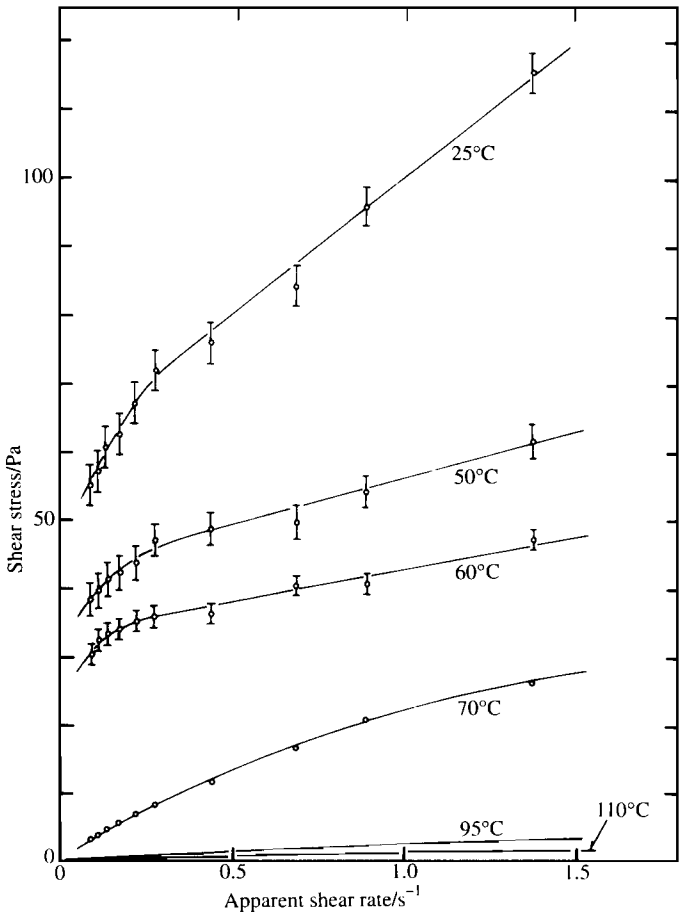

Fig. 4.23 Steady-state flow behaviour of solutions of a 20 wt% solution of a PS–PB diblock (M_n = 52 kg mol^{-1}, 29.5 wt% PS) in tetradecane at various temperatures (Hashimoto *et al.* 1983*a*; Watanabe *et al.* 1982).

tures were observed, depending on the PS core volume fraction and the thickness of the coronal layer relative to the core. The phase diagram constructed by McConnell *et al.* (1993) is shown in Fig. 4.24, which is parameterized in terms of the PS core volume fraction and the ratio of the coronal layer thickness to core size. By analogy with charged colloidal suspensions, the length-scale of the interparticle interactions is thought to control the ordered structure. As the repulsions become short range, an FCC structure is favoured over a BCC one. Repulsive interactions between micelles occur for thin coronal layers with a convex coronal density profile. In micelles with larger coronal layers, this profile is better described by a concave function leading to softer repulsions and a BCC lattice. Strikingly, no BCC to FCC phase transition was observed in these systems (McConnell *et al.* 1993), although as discussed in the previous section a thermally-

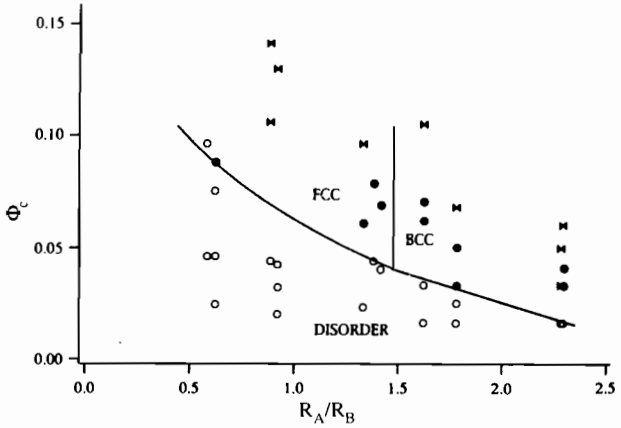

Fig. 4.24 Phase diagram for PS–PI diblocks in decane in terms of PS core volume fraction (Φ_c) as a function of the ratio of coronal layer thickness to core size (R_A/R_B). Unspecified structures are labelled (⋈) (McConnell *et al.* 1993).

induced transition between these structures has been observed for a poly(oxyethylene)/poly(oxybutylene) diblock in aqueous solution (Pople *et al.* 1997). The structures formed at high concentrations in the PS–PI diblocks in decane were determined using SAXS and a parallel-plate hand-shearing device (McConnell and Gast 1997). On increasing polymer concentration, a melting of FCC or BCC micellar crystals was observed before the development of two-fold anisotropy in the SAXS patterns, reflecting the symmetry of the melt phase at the highest concentrations (however, the melt morphology, e.g. lamellae, could not be confirmed unambiguously with the available diffraction data).

The effect of shear on creating long-range order in cubic gel phases was investigated using SANS by McConnell *et al.* (1995). They performed steady shear experiments in a Couette cell on two PS–PI diblocks in decane, one forming an FCC phase in decane and the other a BCC structure (McConnell *et al.* 1993). For the FCC structure, a transition from polycrystallinity to ⟨111⟩ sliding layers was observed on increasing the shear rate, as illustrated in Figs 4.25 and 4.26. As the shear rate increased, the layers did not hop perfectly from one registry site to the next, leading to sliding of layers. The BCC crystals were observed to gradually orient into a twinned BCC structure, with the ⟨110⟩ planes normal to the shear gradient. The BCC twins were observed to slip along the twinning planes, allowing the crystal to flow at moderate shear rates. At higher shear rates, a loss of long-range order associated with shear melting of the BCC structure was observed (McConnell *et al.* 1995). The diffraction patterns from ordered FCC and BCC crystals were modelled in detail using theory developed by Loose and Ackerson (1994) for layered structures in colloids. Figure 4.26 shows calculated diffraction patterns for the FCC structure, and should be compared with the experimental data in Fig. 4.25. The agreement is excellent. Similarities with the behaviour of colloidal crystals under shear were also highlighted by McConnell

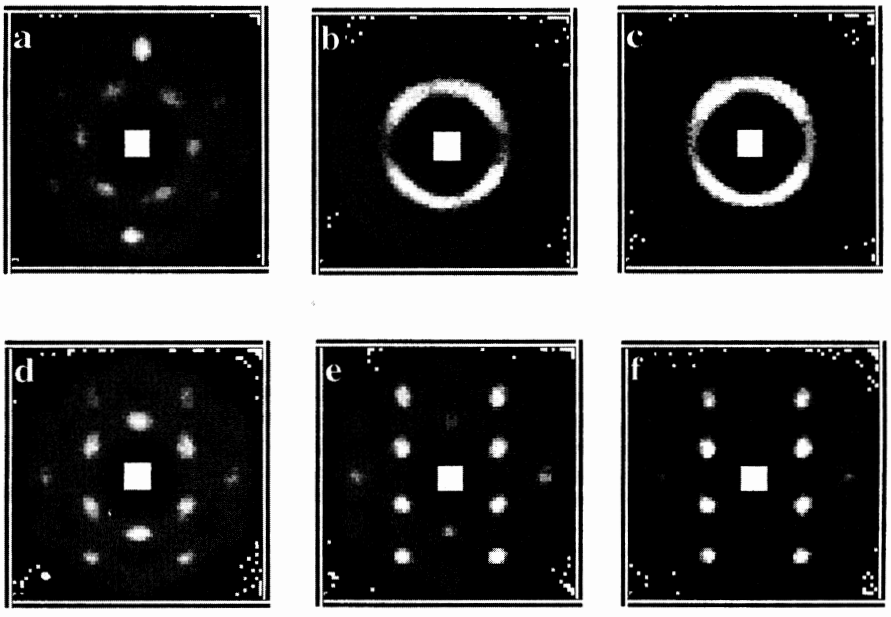

Fig. 4.25 Experimentally measured SANS patterns for an FCC micellar phase in a *d*PS-PI diblock ($M_w = 55\,kg\,mol^{-1}$, 60wt% PS) in core contrast-matched decane/*d*-decane mixtures (15wt% polymer) subject to steady shear in a Couette cell at different shear rates (McConnell *et al.* 1995): (a) $\dot{\gamma} = 0.01\,s^{-1}$; aligned by inserting the stator; (b) $\dot{\gamma} = 0.06\,s^{-1}$; (c) $\dot{\gamma} = 0.66\,s^{-1}$; (d) $\dot{\gamma} = 6.60\,s^{-1}$; (e) $\dot{\gamma} = 66.0\,s^{-1}$; (f) $\dot{\gamma} = 200.0\,s^{-1}$. The wavevectors q_v (horizontal) and q_e (vertical) for these patterns range from -0.028 to $0.028\ Å^{-1}$.

et al. (1995). They point out that Chen *et al.* (1992) first observed defect-mediated flow at low shear rates in FCC structures of essentially hard sphere colloids (charge-stabilized PS or PMMA spheres, radius $\approx 0.1\,\mu m$), leading to a polycrystalline structure. As the shear rate was increased, the polycrystalline structure transformed into sliding layers. Ackerson and co-workers have observed sliding layer structures for both FCC (Ackerson 1990) and BCC (Ackerson and Clark 1981, 1984) phases. At higher shear rates the crystals shear melt, forming an amorphous or a liquid-like structure. These microstructural transitions strongly affect the rheological properties of the suspensions (Chen *et al.* 1994). The sliding layer microstructure displays strong shear thinning, while the shear melting is associated with a discontinuous shear thickening.

The structure and dynamics of concentrated solutions of asymmetric block copolymers in a slightly selective solvent have recently been investigated (Hamley *et al.* 1998*a*; Lodge *et al.* 1996). Because the solvent was close to a theta solvent for one of the blocks, small changes in temperature could produce large changes in solution properties. Hamley *et al.* (1998*a*) and Lodge *et al.* (1996) studied a PS–PI diblock and matched triblock (with twice the molecular weight)

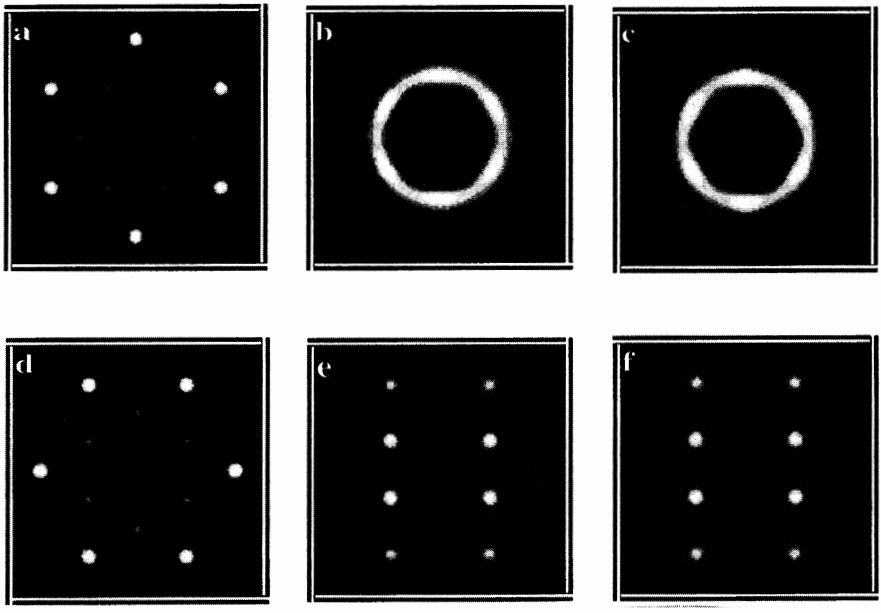

Fig. 4.26 Models for the SANS patterns for FCC micellar crystals in Fig. 4.27 (McConnell *et al.* 1995). (a) Faulted FCC crystal (with equal numbers of FCC and HCP sequences); (b) coexistence between ⟨111⟩ planes (20%) and polycrystalline phase (80%); (c) coexistence between ⟨111⟩ planes (25%) and polycrystalline phase (75%); (d), (e), (f) slipping planes hopping from registry sites with increasing shear-induced flow of layers of micelles. The wavevector range is the same as for Fig. 4.27.

with 17 wt% PS in solution in dibutylphthalate (DBP), which is a good solvent for PS, but a poor solvent for PI. In dilute solution, micelle characteristics were determined using dynamic light scattering and the critical micelle temperature was measured. In solutions with $\phi = 0.2$ (at the semidilute–concentrated regime boundary), SAXS and rheological measurements, together with SANS and oscillatory flow birefringence, were used to probe the micellar structure and interactions (Lodge *et al.* 1996). SAXS profiles at low temperatures provided the micellar form factor, as illustrated by the model fit in Fig. 4.27, which was consistent with elongated micelles, with a length to diameter ratio $\approx$ 5–7. As the solutions were heated, the dynamic shear moduli G' and G'' increased by up to two orders of magnitude over a 30 °C interval (Fig. 4.28). This was attributed to the swelling of the micelles as solvent penetrated the core, leading to steric interactions between micelles. Inter-micellar order was also evident in the development of a structure factor peak in the SAXS profiles, shown in Fig. 4.29. This, in the absence of higher order reflections, suggested the development of liquid-like order of the short rod-like micelles. At higher temperatures the micellar order was lost at a gel–sol transition (hereafter referred to as order–disorder transition (ODT), following the literature and the terminology for block copolymer melts) located via discontinuous changes in the SAXS peak intensity and position,

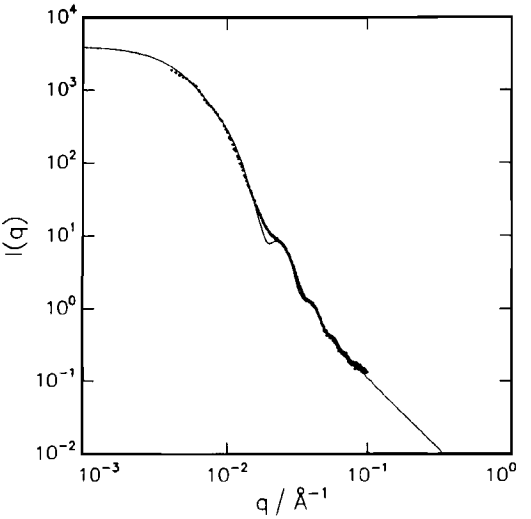

Fig. 4.27 SAXS intensity as a function of wavevector for a PS–PI diblock (M_w = 60 kg mol^{-1}, 17 wt% PS) (points) in dibutyl phthalate with a polymer volume fraction $\phi = 0.195$ (Lodge *et al.* 1996) at −35 °C. Also shown is a fit from a model for the form factor of an ellipsoidal micelle with a hard core and attached Gaussian chains (solid line).

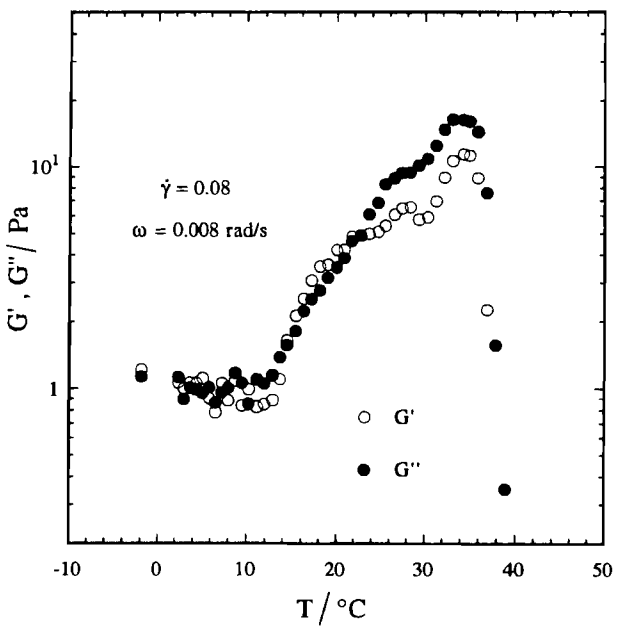

Fig. 4.28 Dynamic shear moduli as a function of temperature for a PS–PI diblock (M_w = 60 kg mol^{-1}, 17 wt% PS) (points) in dibutyl phthalate ($\phi = 0.195$) at the shear rate and amplitude indicated (Lodge *et al.* 1996).

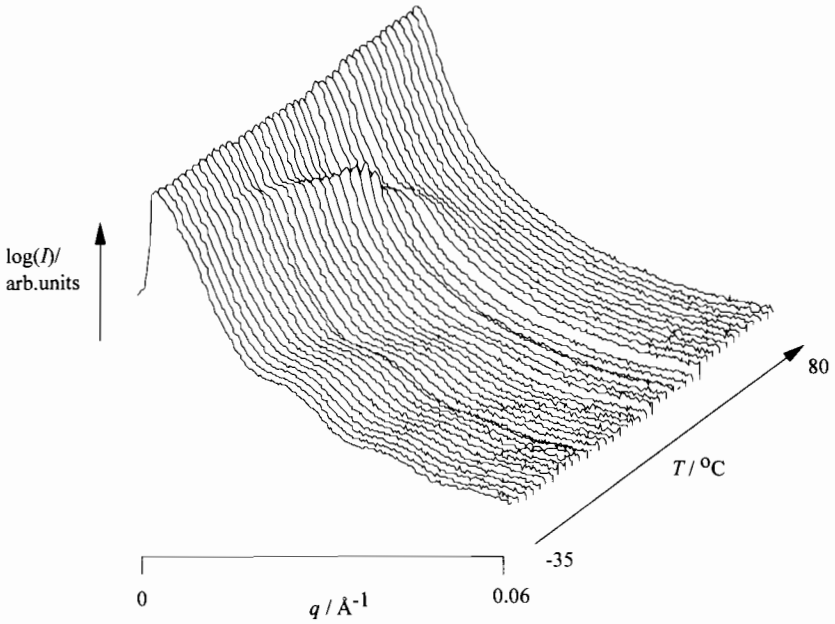

Fig. 4.29 SAXS intensity as a function of wavevector on varying temperature for a PS–PI diblock (M_w = 60 kg mol^{-1}, 17 wt% PS) (points) in dibutyl phthalate (ϕ = 0.195) (Lodge *et al.* 1996).

illustrated in Fig. 4.30. This transition occurred at the same temperature at which the dynamic shear moduli began to decrease sharply.

At temperatures above the ODT, the inverse peak intensity was found to depend non-linearly on inverse temperature. This is in contrast to mean field behaviour, and was ascribed to the effect of composition fluctuations in the disordered phase close to the transition. The behaviour of the structure factor for low-molecular-weight block copolymer above, but close to, the ODT, was shown in Section 2.2.1 to provide evidence for composition fluctuations (see Fig. 2.5 in particular). Upon further heating, dissolution of the micelles was inferred from the disappearance of the SAXS structure factor peak.Oscillatory flow birefringence measurements yielded the same ODT temperature, below the transition the solution being highly birefringent. This reflects the form birefringence of highly oriented anisotropic micelles (Lodge *et al.* 1996).

In subsequent work, ordering in solutions of the same matched diblock and triblock spanning a broader range of volume fractions, $0.1 \leq \phi \leq 0.4$, was explored (Hamley *et al.* 1997). For $\phi < 0.2$, the rheological response was found to be liquid-like and SAXS showed that there was no inter-micellar order in the liquid. Above a crossover concentration $\phi \approx 0.2$, ordering of micelles was shown by the presence of a structure factor peak. The ordered micellar structure, identified as hexagonal-packed cylinders for more concentrated solutions, persisted up to an order–disorder transition located from a discontinuity in the

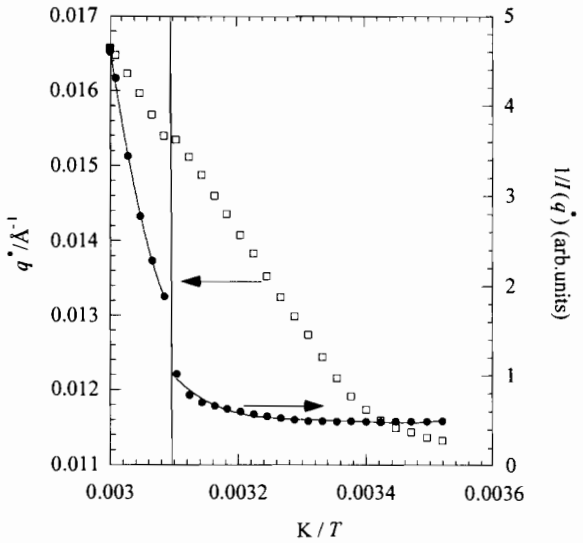

Fig. 4.30 SAXS peak position, q^*, and inverse peak intensity as a function of inverse temperature for a PS–PI–PS triblock (M_w = 120 kg mol^{-1}, 17 wt% PS) in dibutyl phthalate (ϕ = 0.201) (Lodge *et al.* 1996).

SAXS peak intensity as a function of temperature. The ODT temperature was essentially independent of concentration, indicating its origin in solvent selectivity rather than styrene–isoprene interactions. At higher temperatures, approximately 15 °C above the ODT for the $\phi = 0.2$ solutions, the micelles were found to break up as the polymer chains dissolved into solution. The concentration dependence of the domain spacing, d, in the ordered solutions obtained from the principal structure factor peak position, showed a crossover at $\phi \approx 0.2$ (as discussed in the next section) in agreement with rheology. Form factor oscillations in the SAXS data were again fitted with a model of ellipsoidal micelles with a homogeneous PI core and a corona of solvated PS chains. Detailed information on micellar size and shape was obtained by modelling the SAXS data for the $\phi = 0.20$ solutions as a function of temperature. At higher concentrations, $\phi \gtrsim 0.4$, there was evidence for a lamellar phase in these solutions (Hamley *et al.* 1996, 1997). This is not surprising, given that the structure must evolve with increasing concentration from rod-like micelles with a PI core formed due to solvent selectivity into the melt structure, which for these asymmetric copolymers is PS rods in a PI matrix at low temperatures. The formation of a zero mean curvature structure such as lamellae is reasonable as an intermediate between the hexagonal and 'inverse hexagonal' structures. A schematic phase diagram summarizing these findings is shown in Fig. 4.31.

Domain spacing scaling

For a *selective* solvent, a scaling relation for the domain spacing in the ordered lamellar phase $d \sim (1/T)^{1/3}$ was obtained from SAXS experiments on a PS–PB

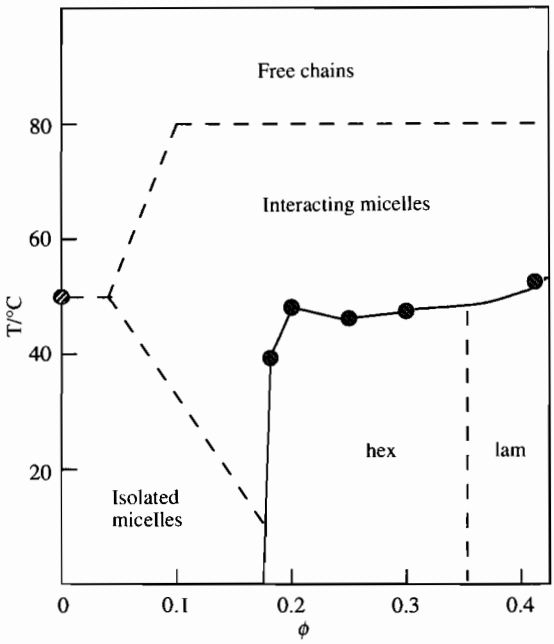

Fig. 4.31 Schematic phase diagram for the PS–PI diblock and PS–PI–PS triblock (details as Fig. 4.29 and Fig. 4.30) solutions in DBP (Hamley *et al.* 1998*a*).

diblock at a fixed concentration in tetradecane (Shibayama *et al.* 1983*a*). At low concentration, d was found to scale as $d \sim \phi^{-1/3}$ at a fixed T, while the micellar radius, R (obtained from the position of form factor oscillations), was found to be approximately independent of temperature. At higher concentrations, d was found to depend less strongly on concentration and R increased slowly (Shibayama *et al.* 1983*a*).

A systematic study of the domain spacing scaling in two nearly symmetric PS–PI diblocks in *neutral* solvents was also undertaken by Hashimoto *et al.* (1983*b*). Results of SAXS experiments on these polymers dissolved in toluene and dioctyl phthalate (DOP) were summarized in a scaling relationship for the domain spacing in the ordered phase in the semidilute and concentrated regimes ($0.15 \leq \phi \leq 0.6$)

$$d \sim N^{2/3}\left(\phi/T\right)^{1/3}, \tag{4.7}$$

where N is the copolymer degree of polymerization. This relationship is illustrated in Fig. 4.32. The scaling with N is the same as that for strongly segregated block copolymers (see Section 2.3.1). The scaling with temperature is the same as that observed for PS–PB copolymers in a selective solvent, while the concentration dependence is reversed, i.e. d decreases with ϕ for selective solvents, but increases for neutral ones. Hashimoto *et al.* (1983*b*) also observed that at high

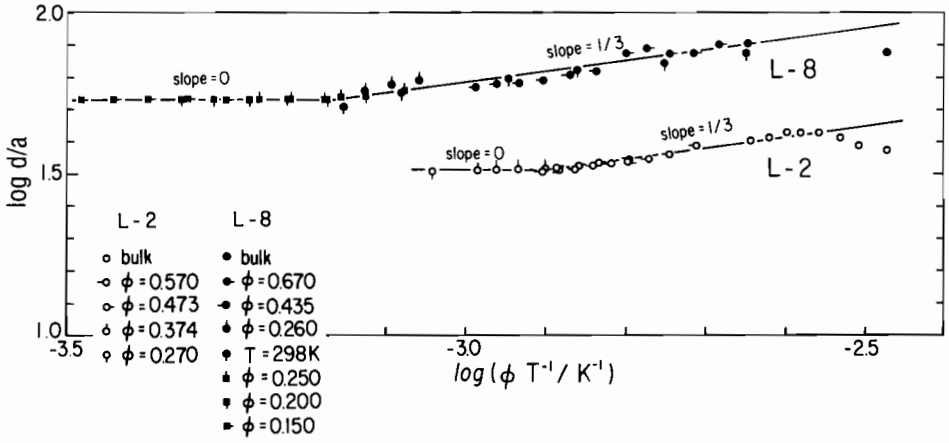

Fig. 4.32 'Master curve' of domain spacing, d (divided by segment length, a) versus ϕ/T for two PS–PI copolymers (L-2, $M_w = 31\,\mathrm{kg\,mol^{-1}}$, 40 wt% PS; L-8, $M_w = 94\,\mathrm{kg\,mol^{-1}}$, 50 wt% PS) in the neutral solvents toluene or dioctyl phthalate at the concentrations indicated (Hashimoto *et al.* 1993*b*).

temperatures and low concentrations, PS–PI in toluene solutions become homogeneous as the ordered lamellar domains dissolve. In the disordered phase, the domain spacing was found to be independent of temperature and polymer concentration, i.e. the scaling

$$d \sim N^{1/2+\beta}\left(\phi/T\right)^{0} \tag{4.8}$$

was obtained. Here β is an excluded volume exponent, found to be close to zero for the solutions studied. The temperature dependence of the inverse scattered intensity was also investigated. In mean field theory, the inverse intensity is expected to scale linearly with temperature. This follows from the mean field equation for the inverse intensity in the Random phase approximation (Leibler 1980). For block copolymer solutions in a non-selective good solvent the inverse structure factor is given in mean field theory by (Fredrickson and Leibler 1989; Olvera de la Cruz 1989)

$$S(q)^{-1} = \left(2\phi/a^3N\right)\left\{F(q) - 2\chi^*N\right\}. \tag{4.9}$$

Here $F(q)$ is a function of radius of gyration and composition of the block copolymer. This equation should be compared with eqn 2.11 for block copolymer melts. The effective chi parameter in semidilute solution is $\chi^*N = \chi_{AB}N\phi^{(1+z)/(3\nu-1)}$, where χ_{AB} is the chi parameter for the block copolymer, ν is the Flory exponent ($\nu = 0.588$ in good solvents) and $z = 0.22$ (Fredrickson and Leibler 1989; Olvera de la Cruz 1989). The function $F(q)$ has a minimum, and hence $S(q)^{-1}$ has a maximum, at $q = q^*$, which is independent of χ and thus temperature. Empirically, χ is found to be inversely proportional to temperature

($\chi = A + B/T$, where A and B are constants). Thus $S(q^*)^{-1}$ should change linearly with $1/T$. This was indeed observed by Hashimoto *et al.* (1983*b*) at high temperatures; however, at a temperature associated with the transition from the homogeneous disordered phase to the ordered phase, a deviation from linear behaviour was found. Such deviations are now ascribed to the effects of composition fluctuations (Bates *et al.* 1988; Lodge *et al.* 1996), and the crossover from linear to non-linear dependence of $S(q^*)^{-1}$ on $1/T$ does not correspond to the order–disorder transition, rather the mean-field to non-mean-field transition (see Section 2.2.1 for block copolymer melts).

The scaling (eqn 4.7) was also obtained for the lamellar phase formed by a symmetric PS–PI diblock in toluene, where the concentration was increased continuously by solvent evaporation (Shibayama *et al.* 1983*b*). However, above $\phi = 0.7$ it was suggested that microphase separation became kinetically controlled rather than thermodynamically limited due to the lower rate of solvent loss, leading to a deviation from the $d \sim \phi^{1/3}$ relationship (Hashimoto *et al.* 1983*b*; Shibayama *et al.* 1983*b*). Non-equilibrium effects for a symmetric and an asymmetric PS–PI diblock and an asymmetric PS–PB polymer in dioctyl phthalate were investigated in detail using SAXS by Shibayama *et al.* (1983*c*). They proposed that in the kinetically controlled regime, the interfacial area per block at the A–B interface cannot maintain the equilibrium value but is fixed at an approximately constant value. Then the domain spacing decreases with increasing ϕ and decreasing temperature due to deswelling and thermal contraction respectively. It was found that the crossover to non-equilibrium behaviour occurs at a lower concentration for the spherical micellar phase than the lamellar phase, which was explained on the basis of distinct thermodynamic barriers for growth of different ordered phases (Shibayama *et al.* 1983*c*). These results were later extended, following further SAXS experiments on a series of PS–PI diblocks in toluene (Mori *et al.* 1990). For spheres, non-equilibrium effects were proposed to result from 'suppressed mutual diffusivity' of the block chains between spheres with increasing ϕ. For other morphologies, non-equilibrium effects may results from 'grain boundary effects' and/or vitrification of one component. These effects illustrate the problems observed with kinetically trapped non-equilibrium structures in concentrated block copolymer solutions. Such studies also suggest a cautionary approach to assessing equilibrium structures for melt samples prepared by solvent casting.

Using SAXS, Hamley *et al.* (1998*a*) have investigated the dependence of domain spacing on copolymer volume fraction for a PS–PI diblock and a PI–PS–PI triblock in the slightly selective solvent dibutyl phthalate. At high concentrations it was shown that d scales as $d \sim \phi^{1/3}$ (see Fig. 4.33) showing three-dimensional shrinkage of micelles of finite length (i.e. short rod-like micelles). This concentration dependence is the same as that obtained earlier by Shibayama *et al.* (1983*a*) for a PS–PB diblock in a selective solvent, although it differs from the results from the same group for diblocks in neutral solvents (Hashimoto *et al.* 1983*b*).

The swelling of semidilute solutions of a PS–PMMA or a PMMA–*d*PMMA diblock in the neutral solvent toluene was investigated using SANS by Mayes

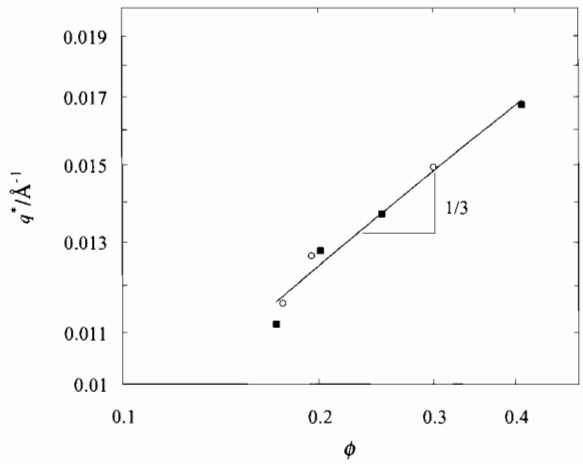

Fig. 4.33 SAXS peak position at a reference temperature of 35 °C for PS–PI diblock (M_w = 60 kg mol^{-1}, 17 wt% PS) solutions in dibutyl phthalate (○) and solutions of a matched triblock (M_w = 120 kg mol^{-1}, 17 wt% PS) copolymer (■) (Hamley *et al.* 1997).

et al. (1994). The peak position in the disordered phase was found to scale as $q^* \sim \phi^{0.05}$. This is illustrated in Fig. 4.34, which shows $q^*\phi^{-0.125}$ versus ϕ. This rescaling was chosen because it is consistent with that predicted for semidilute block copolymer solutions in a good solvent (eqn 4.14). Clearly, the data do not agree with this prediction. This differs from the results of Hashimoto *et al.* (1983*b*) for PS–PI copolymers in toluene (see above), which showed that q^* was independent of concentration in the disordered phase.

Dynamics

The effect of composition fluctuations on the rheological response was investigated in detail for three symmetric PS–PI diblocks in the neutral solvent dioctyl phthalate (Jin and Lodge 1997). The concentration range extended from disordered, dilute solutions to the (lamellar) ordered state, with the emphasis on the intermediate regime, where large-amplitude composition fluctuations were clearly evident. The dynamic shear moduli and apparent relaxation times, all normalized to their respective values in the absence of fluctuations, increased markedly as the disorder–order transition was approached by increasing concentration. This effect was most evident when the rheological data were plotted as phase angle versus frequency (reduced with respect to the longest relaxation time in the system, τ_1), as illustrated in Fig. 4.35. The ODT for this system was reached for a 24.7 wt% solution, occurring near 55 °C. The rate of increase of dynamic shear moduli and relaxation times was found to be consistent with recent theoretical predictions by Fredrickson and co-workers (Fredrickson and Helfand 1988; Fredrickson and Larson 1987), although the magnitude of the effect is larger than anticipated by theory, as for block copolymer melts (Bates

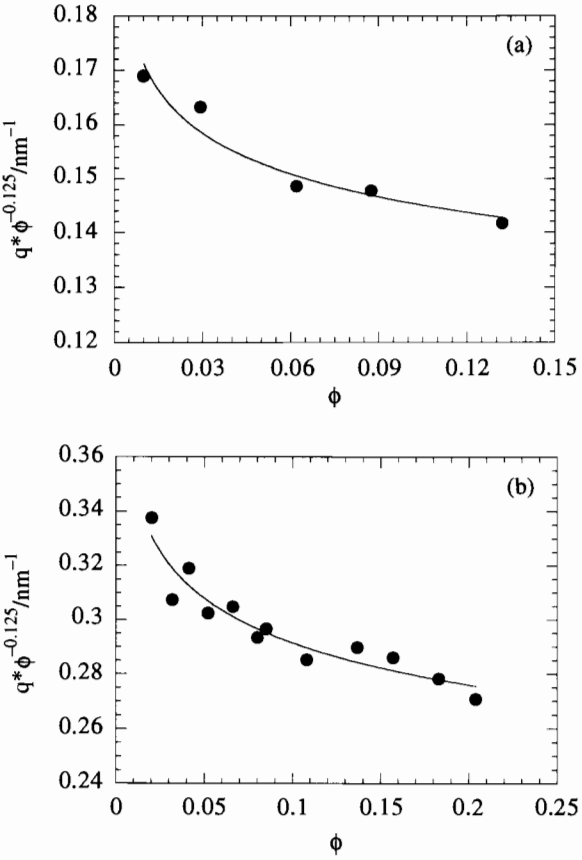

Fig. 4.34 SANS peak position, q^*, rescaled by $\phi^{0.125}$ as a function of polymer volume fraction in mixtures of normal and deuterated toluene and toluene at room temperature (Mayes *et al.* 1994): (a) *d*PS–PMMA diblock ($M_w = 301\,kg\,mol^{-1}$, $f_{PMMA} = 0.43$); (b) PMMA–*d*PS–PMMA triblock ($M_w = 93\,kg\,mol^{-1}$, $f_{PMMA} = 0.5$). The solid lines indicate the best fit scaling relation $q^* \sim \phi^{0.05}$.

1984; Bates *et al.* 1990; Rosedale and Bates 1990). It was pointed out that the onset of measurable fluctuation effects depends on molecular weight in a manner that suggests that entanglements play an important role in coupling fluctuations to the viscoelastic properties (Jin and Lodge 1997). This is consistent with earlier measurements of translational diffusion in a lamellar block copolymer melt, which demonstrated that entanglements severely diminish the mobility of lamellar block copolymers along the interface between microdomains (Lodge and Dalvi 1995). Thus, block copolymer composition fluctuations are manifested in the structure and rheology for solutions as well as block copolymer melts.

Dynamic light scattering has also been used to locate the order–disorder transition in a PS–PI solution in a neutral solvent (toluene). Balsara *et al.* (1991)

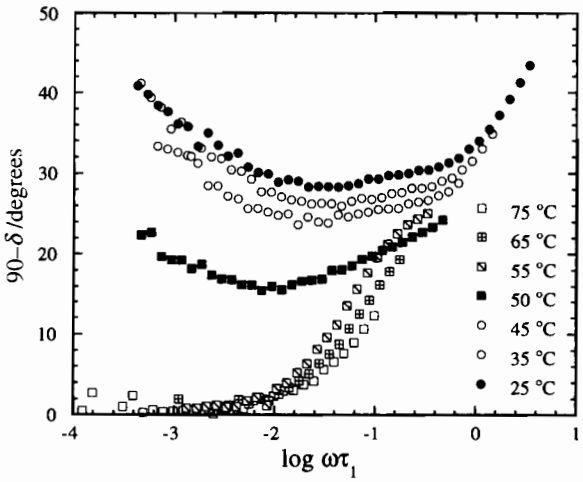

Fig. 4.35 Phase angle as a function of reduced frequency, determined from parallel plate rheology experiments, for a PS–PI diblock ($M_w = 130\,kg\,mol^{-1}$, 50 wt% PS) in dioctyl phthalate at a concentration 24.7 wt% polymer (Jin and Lodge 1997).

observed two distinct modes in the scattered intensity autocorrelation function. The faster one was diffusive and decreased in rate approximately exponentially with increasing concentration. The magnitude of the diffusivity suggested that it reflects the translational diffusion of the block copolymers. The slower mode was attributed to cooperative rearrangements of microdomains. This slower mode was also found to undergo a sharp decrease in rate over a narrow range of composition, corresponding to the ODT.

Effect of shear on concentrated solutions

The effects of shear on the lamellar phase of a concentrated block copolymer solution have been investigated using SANS on samples in a Couette cell (Balsara and Hammouda 1994; Balsara *et al.* 1994*a*). A solution of a PS–PI diblock in dioctyl phthalate (DOP) was investigated and the lamellar orientation was monitored below and above the order–disorder transition temperature with the neutron beam incident either radially or tangentially to the plane of the shear cell walls. It was found that below the quiescent ODT, oscillatory shear produces lamellae that are parallel to the plane of the shear cell walls. However, steady shear results in a reorientation of the lamellae into the perpendicular orientation (i.e. lamellar normals in the neutral direction) (Balsara *et al.* 1994*a*). These results were compared with those of Koppi *et al.* (1992, 1993) for block copolymer melts (see Section 2.4.3). Above the quiescent order–disorder transition, the alignment induced by steady shear above a critical rate, quantified by the anisotropy of the scattering ring, was found to follow a master curve as a function of reduced shear rate (with respect to the shear rate for onset of orientation) for all temperatures (Balsara and Hammouda 1994; Balsara *et al.*

1994*a*). The critical shear rate was found to increase exponentially with temperature (Balsara *et al.* 1994*a*).

Balsara and Dai (1996) have recently reported a transition from shear-induced order to shear-induced disorder at higher shear rates, above the quiescent ODT in a concentrated PS–PI solution. A 75 wt% solution in DOP of an asymmetric PS–PI diblock, forming a cylindrical phase of PS rods below the ODT (Balsara *et al.* 1994*b*), was investigated using SANS on samples sheared *in situ* in a Couette cell. The anisotropy of the SANS pattern (defined as ϱ = peak intensity in the q_e direction/peak intensity in the q_v direction in the (q_v,q_e) plane) as a function of shear rate shows shear-induced order, then disorder at higher shear rates (Fig. 4.36). It was pointed out that current theories for the effects of shear on block copolymers only predict shear-induced ordering due to the suppression of composition fluctuations (Cates and Milner 1989; Marques and Cates 1990), and the experimental observations of Balsara and Dai also differ from earlier results on block copolymer melts (Koppi *et al.* 1992, 1993) and solutions (Balsara and Hammouda 1994; Balsara *et al.* 1994*a*). Balsara and Dai (1996) proposed that fluctuations of the cylinders, if characterized by a lifetime larger than the inverse shear rate, lead to the disordering observed at high shear rates. In prior work, Balsara *et al.* (1994*b*) observed a large difference in the ordering transition of this system for shear oriented 'single crystals' (T_{ODT} = 62 °C) and polydomain samples prepared under quiescent conditions (T_{ODT} = 49 °C). In sheared polydomain samples where the imperfections were partially removed, coexistence of ordered and disordered regions was observed at temperatures between these limits. However, these observations have not been satisfactorily accounted for, and are still controversial.

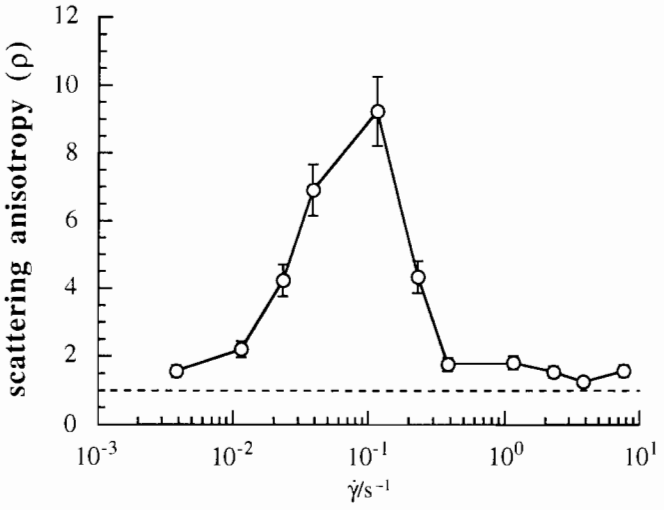

Fig. 4.36 Anisotropy of SANS intensity versus shear rate for a 75 wt% solution of a PS–PI diblock (M_w = 30 kg mol^{-1}, 27 wt% PS) in dioctyl phthalate at 58 °C (Balsara and Dai 1996).

4.4.2 Polystyrene–poly(ethylene-*co*-propylene) copolymers

As early as 1979, researchers at Shell provided evidence for the association of micelles of poly(styrene)–poly(ethylene-*co*-propylene) (PS–P(E/P)) (PS–hydrogenated PI) in decane (Mandema *et al.* 1979). These materials are known commercially as Kraton G copolymers. Mandema *et al.* performed viscosity and static and dynamic light scattering and found evidence of large structures with dimensions of the order of the wavelength of light. These in fact may be grains of ordered micellar phase.

The formation of ordered structures of micelles of Kraton-type diblocks in dodecane (selective for P(E/P)) was investigated using SANS by Higgins and co-workers (Higgins *et al.* 1986, 1988; Phoon *et al.* 1993). They observed ordered crystalline structures for polymer concentrations above 3 wt% (Higgins *et al.* 1988; Phoon *et al.* 1993). The effect of shear, applied using a Couette cell, on the orientation of the ordered structure was probed using SANS. Long-range order was found to be induced by very low shear rates, whereas shear melting was noted at high shear rates. An illustrative SANS pattern from an ordered micellar phase following shear at $\dot{\gamma} = 70\,s^{-1}$ is shown in Fig. 4.37. The data were interpreted using a model of a hexagonal structure, with an ABCABC layer stacking but distorted from a close-packed arrangement due to normal stresses (Phoon *et al.* 1993), illustrated in Fig. 4.38. The transition to an ordered structure was also evident in the rheology of the solution, with a change from a liquid-like to a soft solid dynamic response at 3–4 wt% polymer (Higgins *et al.* 1988). This rheological change was consistent with the overlap of micellar coronas when the interparticle separation was close to the sphere radius, as estimated from the hydrodynamic radius from light scattering and from modelling of the SAXS form factor. The structure factors observed at high concentrations were fitted using a model based on a

Fig. 4.37 SANS pattern for a 6 wt% solution of a PS–P(E/P) diblock ($M_w = 129\,kg\,mol^{-1}$, 38.5 wt% PS) in deuterated dodecane, following shear at $\dot{\gamma} = 66.0\,s^{-1}$ in a Couette cell (Phoon *et al.* 1993). The arrow indicates the direction of flow. The wavevector ranges from -0.01 to $0.01\ Å^{-1}$.

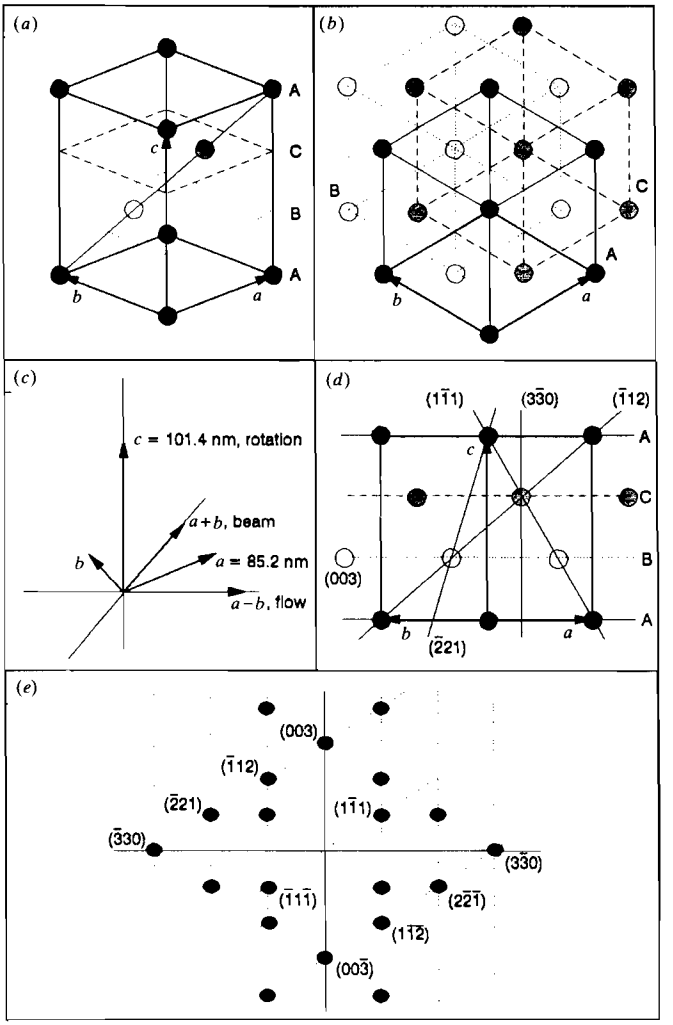

Fig. 4.38 Model for a structure giving rise to the diffraction pattern in Fig. 4.39 (Phoon *et al.* 1993). (a) Hexagonal ABC structure (not close-packed); (b) top view; (d) front view, showing lattice vectors and some of the lattice planes; (c) orientation of unit cell vectors (*a*,*b*,*c*) with respect to the flow direction, rotation axis and the direction of the neutron beam; (e) the Bragg diffraction pattern from a twinned structure.

screened Coulombic potential (i.e. hard core and soft tail), which yielded a core radius in good agreement with that extracted by modelling the form factor (Higgins *et al.* 1988). The model structure factor was found to fit the data best at higher shear rates as the structure became more disordered (liquid-like). Both SANS and rheological data consistently showed that long-range order was quickly restored after flow stopped, but long-range organization was very slow

to appear (Higgins *et al.* 1988). Schouten *et al.* (1989) have also used SANS to investigate micellar ordering in a PS–P(E/P) copolymer in dodecane. They found that for solution concentrations as low as 0.5%, micelles interact strongly, resulting in an ordered liquid micellar phase. However, at high temperatures, the degree of intermicellar interaction was found to diminish dramatically, accompanied by a decrease in micellar size. This was correlated to the sharp viscosity drop observed at high temperatures in the solutions studied.

Work by Pleštil *et al.* (1990) showed that a strong increase in viscosity occurred for poly(styrene)–poly(ethylene-*co*-propylene)–poly(styrene) triblocks in heptane for $c \geqslant 0.01\,\mathrm{g\,cm^{-3}}$. This indicated micelle–micelle interactions, but there was no evidence from SAXS of an ordered lattice (Pleštil *et al.* 1990). The Prague group (Hlavatá *et al.* 1996; Stejskal *et al.* 1992) also investigated the effects of selective solvents on the dissolution of a Kraton G (PS–PE/P) diblock copolymer using SAXS, SLS and DLS. They found that the solid-state morphology may be preserved to some extent even in solution, especially when the insoluble blocks were glassy. Dissolution at room temperature led to metastable solution structures in either decane (selective for P(E/P)) or dioxane (selective for PS). At room temperature, dissolution of PS–P(E/P) in decane led to aggregation of micelles. At higher temperatures, the aggregated particles were found to break up, leading to equilibrium micelles with a reduced molar mass (Hlavatá *et al.* 1996). The unaggregated micelles in dioxane were also found to be much smaller at higher temperatures. In other words, it was found that metastable structures formed upon dissolution may convert to classical equilibrium micelles only after heating. This again emphasizes the problem of non-equilibrium trapped structures in block copolymer solutions. These metastable micellar structures were termed frozen micelles, being unable to exchange unimers, and exist when the insoluble block is trapped in an unswollen or glassy micellar core. Upon cooling, the high-temperature equilibrium micellar solution is frozen and this was speculated to be the explanation for several observations of immeasurably low cmcs (Hlavatá *et al.* 1996). Similar observations of a substantial decrease in micellar association numbers after heating and cooling compared to solutions as prepared at room temperature were reported by other groups (Higgins *et al.* 1988; Schouten *et al.* 1989; Stacy and Kraus 1977). This may also be related to the change from cloudy to clear opalescent solutions following a heat–cool cycle reported for a number of systems (Price *et al.* 1986, Tsunashima *et al.* 1990).

The structure of gels formed by Kraton G copolymers in extender oil was elucidated by the Leuven group using SAXS and SANS (Mischenko *et al.* 1994, 1995). The triblock copolymers studied had PS end-blocks and a rubber midblock, consisting of either poly(ethylene/propylene) or poly(ethylene/butylene). For both types of polymer, the PS end-blocks formed the core of spherical micelles with a small polydispersity in the radius. The micelles were observed to have liquid-like order, with average interdomain distance two to three times larger than the mean diameter of the spheres (Mischenko *et al.* 1995). This was accounted for using two models for the SAXS profiles. The first was based on a liquid of dense PS cores interacting as hard spheres, which yielded volume fractions below $\phi = 0.45$, i.e. below the critical value for hard sphere crystallization,

consistent with the observation of liquid-like order. The second was a coordination model starting from short-range crystalline order of hypothetical rubber + oil domains with 'interstitial' PS spheres and involving distortions of the inter-domain distances (Mischenko *et al.* 1994, 1995). The structure of the same gels during stretching was investigated using SANS (Reynders *et al.* 1995). At low elongations for the most concentrated PS–P(E/B)–PS gels (18 and 20 wt% copolymer), the gel was found to deform affinely as shown by the development of the circularly symmetric broad scattering peak from the isotropic gel into an elliptical ring (Fig. 4.39). For lower concentration PS–P(E/B)–PS gels and all PS–P(E/P)–PS gels studied, the ellipticity in the SANS ring was smaller than that corresponding to an affine deformation. For gels with a 50% extension or greater, the development of azimuthal peaks in the SANS pattern was noted, as apparent in Fig. 4.39. The development of the azimuthal Bragg peaks was accounted for using a model hexagonal lattice, which was assumed to become oriented and distorted upon stretching, leading to correlations between layer planes, and hence diffraction peaks. At much higher deformations, tensile deformation of gels formed from the same copolymers was observed to lead to 'butterfly'-like SANS patterns with a region in the SANS pattern with no scattering perpendicular to

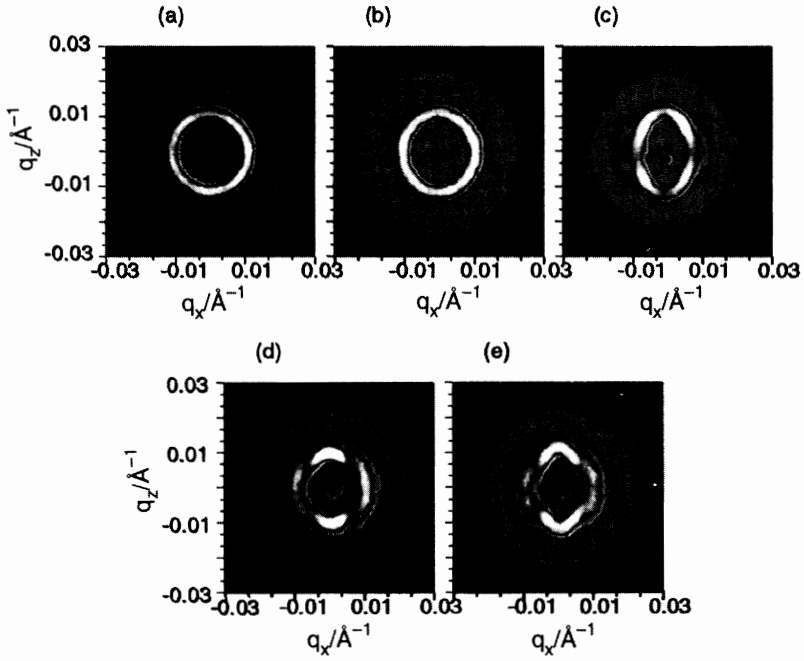

Fig. 4.39 SANS patterns from a stretched gel of a PS–P(E/P)–PS (M_n = 200 kg mol^{-1}, 50 wt% PS) gel in a 12 wt% solution in an aliphatic hydrocarbon mixture (Reynders *et al.* 1995): (a) original state; (b) 25% deformation; (c) 50% deformation; (d) 100% deformation; (e) 100% deformation for 2 days.

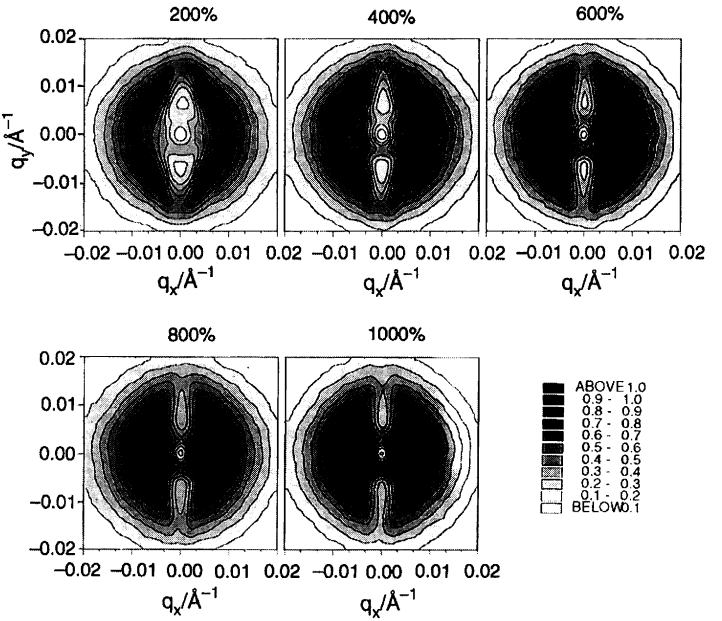

Fig. 4.40 SANS patterns for a gel (18 wt%) of the copolymer with details as Fig. 4.39 at high deformations (Mischenko *et al.* 1996).

the stretching direction (Mischenko *et al.* 1996), as shown in Fig. 4.40. This observation was attributed to formation of clusters of an ordered network (Mischenko *et al.* 1996).

4.5 Theories for ordered block copolymer solutions

4.5.1 Theories for semidilute solutions in a good solvent

Theory for concentrated block copolymer solutions in a neutral good solvent has been developed by Noolandi and co-workers (Hong and Noolandi 1983; Whitmore and Noolandi 1990), Fredrickson and Leibler (1989) and Olvera de la Cruz (1989). Hong and Noolandi (1983) applied self-consistent field theory (SCFT) to block copolymers in a non-selective solvent. They also presented phase diagrams for block copolymers in neutral good solvents. For block copolymer concentrations $\phi \gtrsim 0.6$, in a poor neutral solvent, they found that the ODT between homogeneous and microphase-separated phases can be described using the 'dilution' approximation (Helfand and Tagami 1972):

$$(\phi\chi N)_{\mathrm{ODT}} = \frac{F(f)}{2}, \tag{4.10}$$

where, for a symmetric diblock $F(f)/2 = 10.5$ is predicted using Leibler's mean field theory (Leibler 1980) (Section 2.3.2). In the dilution approximation it is assumed that the primary role of added solvent is to reduce the number of

unfavourable monomer–monomer contacts in a spatially uniform manner. Fredrickson and Leibler (1989) provide a justification for eqn 4.10 for neutral good solvents, whilst pointing out that even as $\phi \to 1$, the solvent will not be homogeneously distributed, rather it will segregate in the interfacial regions to screen monomer–monomer interactions. It was observed that inhomogeneities in solvent concentration exist whenever the solution is microphase separated (Fredrickson and Leibler 1989), a result not obtained by Hong and Noolandi (1983). This discrepancy was ascribed to an incorrect description of the solvent concentration field which was assumed to have the same period as the A–B composition profile, whereas it is actually has half this period, and is out of phase (Fredrickson and Leibler 1989).

Whitmore and Noolandi (1990) later developed this approach to consider the lamellar phase of diblocks in a neutral solvent. They found a slight tendency for solvent segregation to the lamellar interphase with an initial increase in excess solvent (ψ_s) with increasing copolymer concentration, followed by a decrease in the semidilute and concentrated regimes. This decrease necessarily results as ϕ approaches unity and the volume fraction of solvent, $1 - \phi$, approaches zero. The resulting maximum in ψ_s is enhanced with increasing degree of A–B segregation in the copolymer, ψ_s being approximately proportional to χ_{AB}. Competing with this trend is the approximate inverse dependence of ψ_s on N, which was noted by Fredrickson and Leibler (1989) for the weak segregation limit. Whitmore and Noolandi (1990) also obtained approximate scaling relationships for the domain spacing:

$$d/a = \left[\chi_{AB}\right]^p N^q \phi^r. \tag{4.11}$$

The strongest dependence occurs in the weak segregation limit, with $p \approx 1/3$, $q \approx 0.8$, $r \approx 0.4$, whereas in the strong segregation limit $p \approx 0.2$, $q \approx 2/3$, $r \approx 0.22$. This compares with the values $p = 0.14$ and $q = 0.64$ obtained by Helfand and Wasserman (1976, 1982) for strongly segregated block copolymer melts (Section 2.3.1). Whitmore and Noolandi (1990) also presented volume fraction profiles for the real system PS–PI in the nearly neutral solvent toluene. An example of their calculations for a solution with $\phi = 0.4$ is presented in Fig. 4.41. The scaling predictions of the theory were compared with the experimental results of Hashimoto and co-workers (Hashimoto *et al.* 1983*b*; Shibayama *et al.* 1983*b*). For a series of PS–PI copolymers in toluene or dioctyl phthalate (selective for PS) experimental domain spacings followed the scaling (eqn 4.7), where no distinction was made between the weak and strong segregation limits. The scaling with r observed experimentally was intermediate between the weak and strong segregation limit theory values, whilst that for N was close to the strong segregation limit theory prediction. The third exponent, p, was compared indirectly (Whitmore and Noolandi 1990) by assuming that $\chi \propto 1/T$, where χ is the most important interaction term (in this case χ_{PS-PI}), which is not strictly legitimate since it neglects the nor-zero B in $\chi = A/T + B$. Nevertheless, the experimental exponent was then found to be within the range of theoretical values.

The theories of Fredrickson and Leibler (1989) and Olvera de la Cruz (1989) concern microphase separation in semidilute block copolymer solutions in a non-

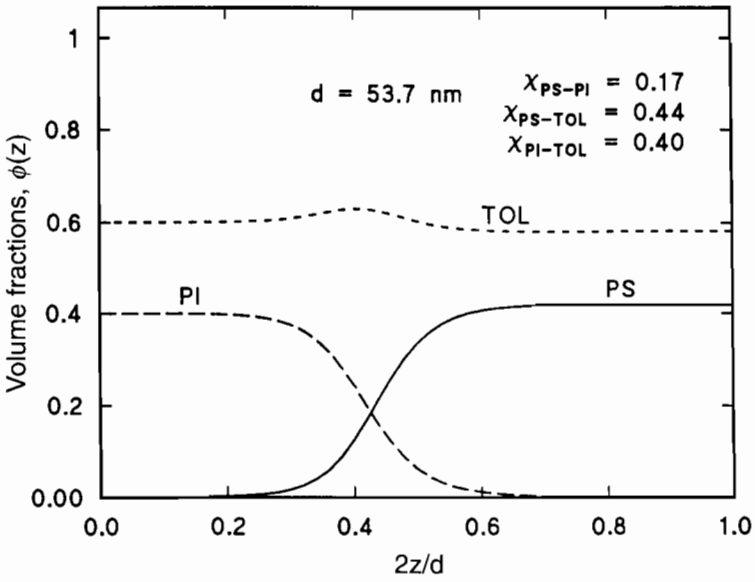

Fig. 4.41 Density profiles calculated using mean-field self-consistent field theory for a $PS_{587}PI_{647}$ diblock in toluene at room temperature with a polymer volume fraction $\phi = 0.4$ (Whitmore and Noolandi 1990). The profiles are plotted for one unit cell dimension (period d).

selective good solvent, analysed using the random phase approximation and the 'blob' model where monomers are grouped in blobs the size of the correlation length. These authors used Leibler's formulation of the RPA (Leibler 1980) for weakly segregated block copolymers. Whereas Olvera de la Cruz (1989) only considered the mean field limit, Fredrickson and Leibler (1989) also allowed for composition fluctuations, via the method of Brazovskii as applied to block copolymer melts (Section 2.3.2). Composition fluctuations are important close to the order–disorder transition in block copolymer melts, and there is evidence for their existence in semidilute solutions, as discussed in Section 4.4.1 (Lodge *et al.* 1996). In the semidilute region, excluded volume interactions are important on length-scales smaller than the 'blob' size ξ, but are screened out at distances larger than ξ. As the polymer concentration is increased, the screening becomes more important and the correlation length decreases as $\phi^{-\nu/(\nu+1)} \sim \phi^{-0.77}$ (de Gennes 1979), where $\nu = 0.588$ is the excluded volume exponent for good solvents. Because of these excluded volume effects at short distances, the probability of contacts between unlike segments is reduced by a factor of $\phi^{(2\nu-1)/(3\nu-1)} \sim \phi^{0.23}$. Renormalization group studies (Joanny *et al.* 1984; Kosmas 1984; Schafer and Kappeler 1985) indicate that the contact probability is even further reduced by an additional factor of $\phi^{\chi_{SD}}$, where $\chi_{SD} \approx 0.29$ is a crossover exponent given by $\chi_{SD} = \chi_S/(3\nu - 1)$, with $\chi_S \approx 0.22$ (Fredrickson and Leibler 1989). In the limit that contributions to the free energy from solvent inhomogeneities are negligible

(which is valid for long copolymer chains), mean field theory for semidilute solutions predicts that $\phi\chi N$ in eqn 4.10 can be replaced by $\phi^{\delta}\chi N$, where $\delta = (\chi_S + 1)/(3\nu - 1) \approx 1.6$ (the same substitution can be used to relabel the ordinate for phase diagrams within composition fluctuation theory (Fredrickson 1986)). This result is valid in the limit that $N^{-0.22} \ll 1$, i.e. very long copolymer chains. Then, at the order–disorder transition (Fredrickson and Leibler 1989; Olvera de la Cruz 1989)

$$\left(\phi^{1.6}\chi N\right)_{\mathrm{ODT}} = \frac{\tilde{F}(f)}{2}, \tag{4.12}$$

where $\tilde{F}$ differs by a multiplicative constant of order unity from F in eqn 4.10. At the transition, the concentration of copolymer scales as (Fredrickson and Leibler 1989; Olvera de la Cruz 1989)

$$\phi_{\mathrm{ODT}} \sim N^{-0.62}. \tag{4.13}$$

An exponent -0.626, close to the theoretical value, was obtained by Lodge *et al.* (1995) for the ordered lamellar–disordered phase transition concentration (determined from birefringence experiments) for a series of nearly symmetric PS–PI copolymers in toluene, dioctyl phthalate and in the melt. This is illustrated in Fig. 4.42 which shows data at a fixed temperature. The scaling (eqn 4.13) was obtained from the experimental data by determination of χ from a straight-line plot of $F/2N\phi^{1.6}$ versus $1/T_{\mathrm{ODT}}$ (eqn 4.12). However, in contrast to the theoretical predictions, the scalings (eqns 4.12 and 4.13) were observed for copolymer concentrations spanning the concentrated regime (up to the melt limit) as well as

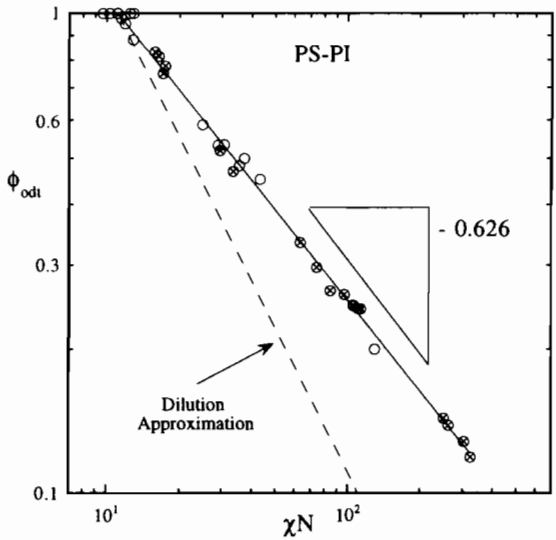

Fig. 4.42 Volume fraction at the ODT versus χN for a range of nearly symmetric PS–PI diblocks in toluene near 36 °C (Lodge *et al.* 1995).

the semidilute region. Thus, no region of validity of the 'dilution approximation' (which predicts $\phi_{ODT} \sim N^{-1}$) expected for concentrated solutions was observed. Allowance for composition fluctuations would add a correction term proportional to $(N\phi^{1.3})^{-0.33}$ to eqn 4.12, but this would not modify the scaling of ϕ_{ODT} with N appreciably (Lodge *et al.* 1995). For a different system, poly(ethylene-propylene)–poly(ethylethylene) diblocks in squalene, a scaling $\phi_{ODT} \sim N^{-0.81}$ was found (see Fig. 4.43), intermediate between the scalings for concentrated and semidilute solutions (Lodge *et al.* 1995). This suggests that the ϕ_{ODT} scaling may be non-universal. The fact that PEP–PEE solutions were closer to the dilution approximation predictions may be due to the fact that squalene is a nearly athermal solvent, whereas toluene is not a completely athermal solvent for PS–PI. Other factors that could account for the observed differences between the two systems include the difference in χ, which is much smaller for PEP–PEE than PS–PI, thus requiring considerably larger values of N for PEP–PEE for the same degree of segregation. Thus weaker chain stretching and diminished composition fluctuations (Lodge *et al.* 1995) were expected for the PEP–PEE solutions. Finally, excluded volume effects may be important, these decreasing with molar volume of the solvent, squalene being a relatively large diluent (Lodge *et al.* 1995).

The position of the structure factor peak, q^*, for semidilute block copolymer solutions is predicted to scale as (Fredrickson and Leibler 1989; Olvera de la Cruz 1989)

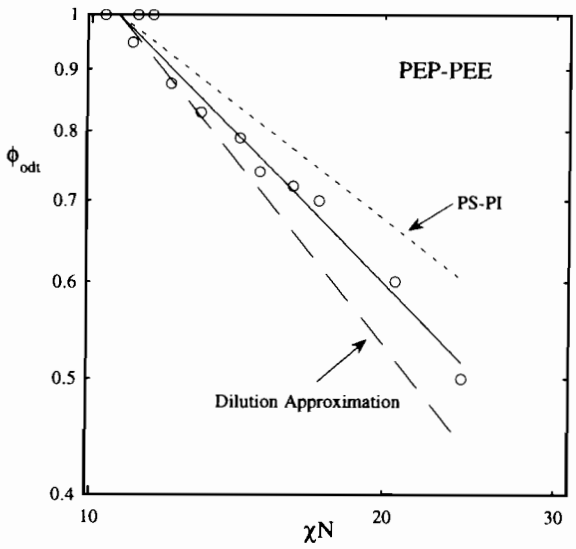

Fig. 4.43 Volume fraction at the ODT versus χN for a range of PEP–PEE diblocks in squalene (Lodge *et al.* 1995). The best fit to the data (solid line) gives a slope of −0.81, compared to −1 for the dilution approximation and −0.626 observed for PS–PI diblocks in toluene (Fig. 4.42).

$$q^* \sim \phi^{0.125} N^{-0.5}. \tag{4.14}$$

Mayes *et al.* (1994) tested this prediction using SANS on PS–PMMA and PMMA–*d*PMMA diblocks in contrast-matched toluene/*d*-toluene mixtures in the disordered phase. They did not obtain the scaling (eqn 4.14), instead a best fit to the data yielded $q^* \approx \phi^{0.05}$ (Fig. 4.34). This slower than expected scaling is presently unexplained. However, the expected concentration dependence of the blob size (Mayes *et al.* 1994)

$$\xi \cong a\phi^{-\nu/(\nu+1)} \sim \phi^{-0.75} \tag{4.15}$$

was confirmed. This scaling was reported earlier for homopolymer solutions in the semidilute regime (Brown *et al.* 1992; Daoud *et al.* 1975; Hamada *et al.* 1985; King *et al.* 1985). Experimental results for the scaling of q^* with ϕ yield different exponents. Duplessix *et al.* (1979) found an exponent 0.087 for PS–*d*PS–PS triblocks in CS_2. Daoud *et al.* (1975) obtained the predicted scaling $q^* \sim \phi^{0.125}$ for PS solutions in CS_2 containing small amounts of *d*PS. Similar experiments by King *et al.* (1985) on solutions of *d*PS in *d*-toluene containing unlabelled PS produced an exponent 0.078. Thus non-universal exponents are obtained for homopolymer solutions as well as block copolymers.

The Polymer Reference Interaction Site Model (PRISM) theory is currently the most advanced theory for block copolymer solutions. Guenza and Schweizer (1997) have applied the simplest Gaussian thread version of PRISM theory to study the equilibrium properties of diblock copolymer solutions under neutral solvent conditions. Analytical predictions were obtained for the influence of local and microdomain scale concentration fluctuations on the relationship between temperature, degree of polymerization and polymer concentration at the ODT. In the semidilute regime, PRISM predictions were found to agree with blob scaling and fluctuation-corrected mean field analyses. However, in concentrated solutions and the melt, strong disagreements were found, and the mean field dilution approximation was found to fail. Apparent scaling laws for the concentration at the ODT with copolymer degree of polymerization were found for concentrated solutions, with effective exponents which depend on solvent quality, melt screening length, chain aspect ratio, and other non-universal structural features. The primary reason for failure of the dilution approximation was found to be interchain non-random mixing, which is concentration dependent and driven by local entropic packing effects. Composition fluctuations on the microdomain length-scale were shown to yield corrections of secondary importance which vanish in the long-chain limit. For good solvents, the predicted apparent exponent for the scaling of ϕ_{ODT} with N is accidentally in close agreement with semidilute blob scaling results, and agrees with the experiments by Lodge *et al.* (1995) on PS–PI diblocks. Smaller effective exponents were found under theta solvent conditions. Detailed PRISM calculations for the small-angle scattering intensity and local physical clustering (via contact interchain pair correlation functions) were also presented by Guenza and Schweizer (1997). Distinctive dependences of these quantities on the degree of polymerization, copolymer concentration,

solvent quality and polymer screening length were established. In qualitative agreement with TEM experiments on PS–PI solutions in neutral solvents (Liu *et al.* 1997), significant local clustering of the copolymer was anticipated in asymmetric diblocks even very far from the ODT.

4.5.2 Theories for ordered micellar phases

Self-consistent field theory (SCFT, see Sections 2.3.3 and 3.4.2) has recently been applied to the phase behaviour of ordered micellar solutions. Noolandi *et al.* (1996) compared continuum SCFT to the lattice version of this theory for triblock copolymers such as the Pluronics in aqueous solution. From a different viewpoint, this work represents an extension of the SCFT employed by Hong and Noolandi (1981, 1983) and Matsen and Schick (1994) for the phase behaviour of block copolymer melts to block copolymers in solution. The approximations introduced by the adoption of a lattice model are found to lead to some significant differences in the solution phase behaviour compared with the continuum theory, as illustrated by Fig. 4.44. For example, the continuum theory predicts ordered phases for Pluronic L64 ($PEO_{13}PPO_{30}PEO_{13}$), whereas the lattice theory (neglecting polydispersity) predicts none.

Gast and co-workers (Gast 1996; McConnell *et al.* 1994) used SCFT to study interactions between spherical diblock copolymer micelles in solution. The theory was used to calculate intermicellar pair potentials and combined with liquid-state

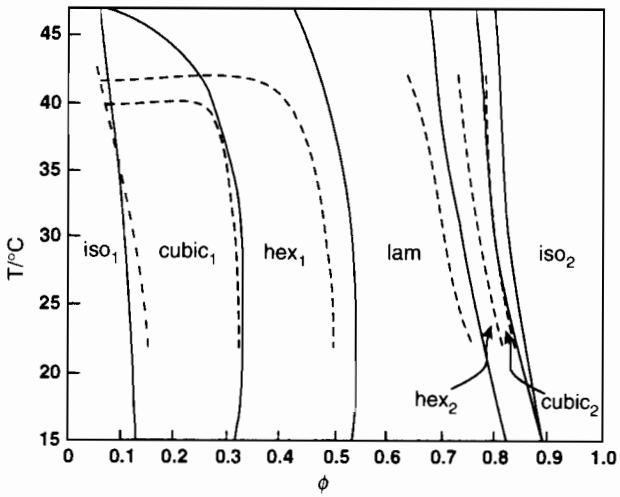

Fig. 4.44 Phase diagram for aqueous solutions of Pluronic P104 ($PEO_{27}PPO_{56}PEO_{27}$) (Noolandi *et al.* 1996). Notation: iso_1, isotropic (polymer poor) solution; $cubic_1$, cubic phase; hex_1, hexagonal phase; lam, lamellar phase, hex_2, inverse hexagonal phase, $cubic_2$, inverse cubic phase, iso_2, isotropic (polymer rich) solution. The solid and dashed lines are calculated from the continuum and lattice versions of self-consistent field theory respectively.

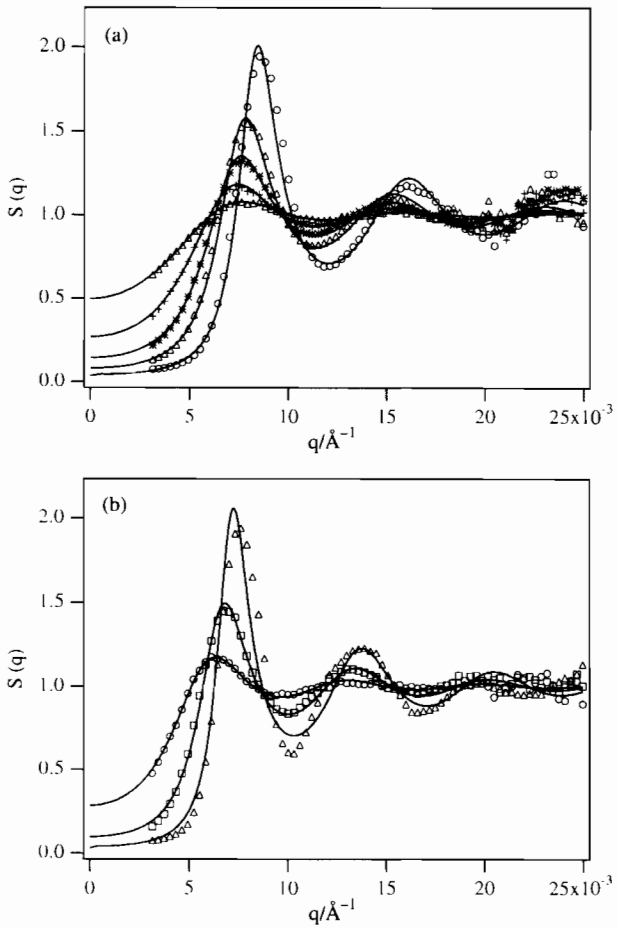

Fig. 4.45 Structure factors versus wavevector for *d*PS–PI diblocks in core–contrast matched decane solutions (Gast 1996; McConnell *et al.* 1994): (a) $d\text{PS}_{393}\text{PI}_{206}$ at core volume fractions of 0.012 (△), 0.02(+), 0.03(*), 0.04 (△) and 0.05 (○); (b) $d\text{PS}_{402}\text{PI}_{422}$ at core volume fractions of 0.006 (○), 0.013 (□) and 0.019 (△). The lines are theoretical fits from the self-consistent field interaction potentials and the Rogers–Young closure to the Ornstein–Zernike equation.

theory (specifically, the Rogers–Young closure to the Ornstein–Zernike equation) this enabled a comparison with the static structure factor determined from SANS experiments on PS–PI diblocks in decane, a selective solvent for PI (McConnell *et al.* 1994). Good agreement was obtained between the experimental and theoretical $S(q)$, with comparisons made for a range of core volume fractions for a system with short-ranged interactions (which lead to an FCC lattice) and one with longer-range interactions (which lead to a BCC lattice). This is illustrated in Fig. 4.45 which shows data for a diblock which forms an FCC phase at higher concentrations (a), and for a diblock which forms a BCC phase at higher

concentrations (b). McConnell and Gast (1996) later extended this work by using the homogeneous liquid-state theory as a basis for density functional theory (DFT) for an ordered lattice. A modified weighted density approximation was used to estimate the free energy of each solid structure and to predict the liquid–solid phase transition. The DFT theory only predicted a simple liquid–FCC transition, although the experimental phase diagram for PS–PI diblocks in decane indicates transitions from the liquid state to FCC or BCC phases (Fig. 4.24). Despite the failure of the theory to predict a BCC phase, it does provide a reasonable estimate of coexistence curves between the liquid and solid (McConnell and Gast 1996).

References

Ackerson, B. J. (1990). *Journal of Rheology*, **34**, 553.

Ackerson, B. J. and Clark, N. A. (1981). *Physical Review Letters*, **46**, 123

Ackerson, B. J. and Clark, N. A. (1984). *Physical Review A*, **30**, 906.

Alexandridis, P. and Hatton, T. A. (1995). *Colloids and Surfaces A*, **96**, 1.

Almgren, M., Stam, J., Lindblad, C., Li, P., Stilbs, P. and Bahadur, P. (1991). *Journal of Physical Chemistry*, **95**, 5677.

Almgren, M., Brown, W. and Hvidt, S. (1995). *Colloid and Polymer Science*, **273**, 2.

Bahadur, P., Pandya, K., Almgren, M., Li, P. and Stilbs, P. (1993). *Colloid and Polymer Science*, **271**, 657.

Balsara, N. P. and Dai, H. J. (1996). *Journal of Chemical Physics*, **105**, 2942.

Balsara, N. P. and Hammouda, B. (1994). *Physical Review Letters*, **72**, 360.

Balsara, N. P., Stepanek, P., Lodge, T. P. and Tirrell, M. (1991). *Macromolecules*, **24**, 6227.

Balsara, N. P., Hammouda, B., Kesani, P. K., Jonnalagadda, S. V. and Straty, G. C. (1994*a*). *Macromolecules*, **27**, 2566.

Balsara, N. P., Dai, H. J., Kesani, P. K., Garetz, B. A. and Hammouda, B. (1994*b*). *Macromolecules*, **27**, 7406.

Bates, F. S. (1984). *Macromolecules*, **17**, 2607.

Bates, F. S., Rosedale, J. H., Fredrickson, G. H. and Glinka, C. J. (1988). *Physical Review Letters*, **61**, 2229.

Bates, F. S., Rosedale, J. H. and Fredrickson, G. H. (1990). *Journal of Chemical Physics*, **92**, 6255.

Berret, J.-F., Molino, F., Porte, G., Diat, O. and Lindner, P. (1996). *Journal of Physics, Condensed Matter*, **8**, 9513.

Booth, C., Yu, C.-E. and Nace, V. M. (1997). Block copolymers of ethylene oxide and 1,2-butylene oxide. In *Amphiphilic block copolymers: self-assembly and applications*, (ed. P. Alexandridis and B. Lindman). Elsevier, Amsterdam.

Brown, W., Mortensen, K. and Floudas, G. (1992). *Macromolecules*, **25**, 6904.

Cates, M. E. and Milner, S. T. (1989). *Physical Review Letters*, **62**, 1856.

Chen, L. B., Zukoski, C. F., Ackerson, B. J., Hanley, H. J. M., Straty, G. C., Barker, J. *et al.* (1992). *Physical Review Letters*, **69**, 688.

Chen, L. B., Ackerson, B. J. and Zukoski, C. F. (1994). *Journal of Rheology*, **38**, 193.

Chu, B. and Zhou, Z. (1996). Physical chemistry of polyoxyalkylene block copolymer surfactants. In *Nonionic surfactants. Polyoxyalkylene block copolymers*, Vol. 60, (ed. V. N. Nace). Marcel Dekker, New York.

Daoud, M., Cotton, J. P., Farnoux, B., Jannink, B., Benoit, H., Duplessix, R. *et al.* (1975). *Macromolecules*, **8**, 804.
de Gennes, P. G. (1979). *Scaling concepts in polymer physics*. Cornell University Press, Ithaca.
Deng, N.-J., Luo, Y.-Z., Tanodekaew, S., Bingham, N., Attwood, D. and Booth, C. (1995). *Journal of Polymer Science B: Polymer Physics*, **33**, 1085.
Diat, O., Porte, G. and Berret, J.-F. (1996). *Physical Review B*, **54**, 14869.
Duplessix, R., Cotton, J. P., Benoit, H. and Picot, C. (1979). *Polymer*, **20**, 1181.
Fairclough, J. P. A., Ryan, A. J., Hamley, I. W., Pople, J. A. and Booth, C. (1998). Unpublished results.
Fredrickson, G. H. (1986). *Journal of Chemical Physics*, **85**, 5306.
Fredrickson, G. H. and Helfand, E. (1988). *Journal of Chemical Physics*, **89**, 5890.
Fredrickson, G. H. and Larson, R. G. (1987). *Journal of Chemical Physics*, **86**, 1553.
Fredrickson, G. H. and Leibler, L. (1989). *Macromolecules*, **22**, 1238.
Gast, A. P. (1996). *Langmuir*, **12**, 4060.
Glatter, O., Scherf, G., Schillén, K. and Brown, W. (1994). *Macromolecules*, **27**, 6046.
Guenza, M. and Schweizer, K. S. (1997). *Macromolecules*, **30**, 4205.
Hamada, F., Kinugasa, S., Hayashi, H. and Nakajima, A. (1985). *Macromolecules*, **18**, 2290.
Hamley, I. W., Fairclough, J. P. A., Ryan, A. J., Ryu, C. Y., Lodge, T. P., Gleeson, A. J. *et al.* (1998*a*). *Macromolecules*, **31**, 1188.
Hamley, I. W., Pople, J. A., Fairclough, J. P. A., Terrill, N. J., Ryan, A. J., Booth, C. *et al.* (1998*b*). *Journal of Chemical Physics*, **108**, 6929.
Hashimoto, T., Shibayama, M., Kawai, H., Watanabe, H. and Kotaka, H. (1983*a*). *Macromolecules*, **16**, 361.
Hashimoto, T., Shibayama, M. and Kawai, H. (1983*b*). *Macromolecules*, **16**, 1093.
Hecht, E. and Hoffmann, H. (1994). *Langmuir*, **10**, 86.
Hecht, E. and Hoffmann, H. (1995). *Colloids and Surfaces A*, **96**, 181.
Hecht, E., Mortensen, K., Gradzielski, M. and Hoffmann, H. (1995). *Journal of Physical Chemistry*, **99**, 4866.
Helfand, E. and Tagami, Y. (1972). *Journal of Chemical Physics*, **56**, 3592.
Helfand, E. and Wasserman, Z. R. (1976). *Macromolecules*, **9**, 879.
Helfand, E. and Wasserman, Z. R. (1982). Microdomain structure and the interface in block copolymers. In *Developments in block copolymers*, Vol. 1, (ed. I. Goodman), p. 99. Applied Science, London.
Higgins, J. S., Dawkins, J. V., Maghami, G. G. and Shakir, S. A. (1986). *Polymer*, **27**, 931.
Higgins, J. S., Blake, S., Tomlins, P. E., Ross-Murphy, S. B., Staples, E., Penfold, J. *et al.* (1988). *Polymer*, **29**, 1968.
Hlavatá, D., Stejskal, J., Plestil, J., Konák, C., Kratochvíl, P., Helmstedt, M. *et al.* (1996). *Polymer*, **37**, 799.
Hong, K. M. and Noolandi, J. (1981). *Macromolecules*, **14**, 727.
Hong, K. M. and Noolandi, J. (1983). *Macromolecules*, **16**, 1083.
Hoover, W. G. and Ree, F. H. (1968). *Journal of Chemical Physics*, **49**, 3609.
Hvidt, S., Jørgensen, E. B., Schillén, K. and Brown, W. (1994). *Journal of Physical Chemistry*, **98**, 12320.
Jin, X. and Lodge, T. P. (1997). *Rheologica Acta*, **36**, 229.
Joanny, J. F., Leibler, L. and Ball, R. (1984). *Journal of Chemical Physics*, **81**, 4640.
Jørgensen, E. B., Hvidt, S., Brown, W. and Schillén, K. (1997). *Macromolecules*, **30**, 2355.
Karlström, G. (1985). *Journal of Physical Chemistry*, **89**, 4962.

King, J. S., Boyer, W., Wignall, G. D. and Ullman, R. (1985). *Macromolecules*, **18**, 709.
Kjellander, R. and Florin, E. (1981). *Journal of the Chemical Society, Faraday Transactions 1*, **77**, 2053.
Koppi, K. A., Tirrell, M., Bates, F. S., Almdal, K. and Colby, R. H. (1992). *Journal de Physique II*, **2**, 1941.
Koppi, K. A., Tirrell, M. and Bates, F. S. (1993). *Physical Review Letters*, **70**, 1449.
Kosmas, M. K. (1984). *Journal de Physique Lettres*, **45**, 889.
Leibler, L. (1980). *Macromolecules*, **13**, 1602.
Li, H., Yu, G.-E., Price, C., Booth, C., Hecht, E. and Hoffmann, H. (1997). *Macromolecules*, **30**, 1347.
Linse, P. (1993). *Journal of Physical Chemistry*, **97**, 13896.
Linse, P. and Björling, M. (1991). *Macromolecules*, **24**, 6700.
Liu, Z., Kobayashi, K. and Lodge, T. P. (1997). Preprint.
Lodge, T. P. and Dalvi, M. C. (1995). *Physical Review Letters*, **75**, 657.
Lodge, T. P., Pan, C., Jin, X., Liu, Z., Zhao, J., Maurer, W. W. *et al.* (1995). *Journal of Polymer Science: Polymer Physics*, **33**, 2289.
Lodge, T. P., Xu, X., Ryu, C. Y., Hamley, I. W., Fairclough, J. P. A., Ryan, A. J. *et al.* (1996). *Macromolecules*, **29**, 5955.
Loose, W. and Ackerson, B. J. (1994). *Journal of Chemical Physics*, **101**, 7211.
Luo, Y. Z., Nicholas, C. V., Attwood, D., Collett, J. H., Price, C. and Booth, C. (1992). *Colloid and Polymer Science*, **270**, 1094.
Malmsten, M. and Lindman, B. (1992). *Macromolecules*, **25**, 5440.
Malmsten, M. and Lindman, B. (1993). *Macromolecules*, **26**, 1282.
Mandema, W., Zeldenrust, H. and Emeis, C. A. (1979). *Makromoleculaire Chemie*, **180**, 1521.
Marques, C. M. and Cates, M. E. (1990). *Journal de Physique*, **51**, 1733.
Matsen, M. W. and Schick, M. (1994). *Physical Review Letters*, **72**, 2660.
Mayes, A., Barker, J. G. and Russell, T. P. (1994). *Journal of Chemical Physics*, **101**, 5213.
McConnell, G. A. and Gast, A. P. (1996). *Physical Review E*, **54**, 5447.
McConnell, G. A. and Gast, A. P. (1997). *Macromolecules*, **30**, 435.
McConnell, G. A., Gast, A. P., Huang, J. S. and Smith, S. D. (1993). *Physical Review Letters*, **71**, 2102.
McConnell, G. A., Lin, E. K., Gast, A. P., Huang, J. S., Lin, M. Y. and Smith, S. D. (1994). *Faraday Discussions of the Chemical Society*, **98**, 121.
McConnell, G. A., Lin, M. Y. and Gast, A. P. (1995). *Macromolecules*, **28**, 6754.
Mischenko, N., Reynders, K., Mortensen, K., Scherrenberg, R., Fontaine, F., Graulus, R. *et al.* (1994). *Macromolecules*, **27**, 2345.
Mischenko, N., Reynders, K., Koch, M. H. J., Mortensen, K., Pedersen, J. S., Fontaine, F. *et al.* (1995). *Macromolecules*, **28**, 2054.
Mischenko, N., Reynders, K., Mortensen, K., Overberg, N. and Reynaers, H. (1996). *Journal of Polymer Science B: Polymer Physics*, **34**, 2739.
Mitchell, D. J., Tiddy, G. J. T., Waring, L., Bostock, T. and McDonald, M. P. (1983). *Transactions of the Faraday Society*, **79**, 975.
Mori, K., Hasegawa, H. and Hashimoto, T. (1990). *Polymer*, **31**, 2368.
Mortensen, K. (1992). *Europhysics Letters*, **19**, 599.
Mortensen, K. (1993*a*). *Progress in Colloid and Polymer Science*, **93**, 72.
Mortensen, K. (1993*b*). *Progress in Colloid and Polymer Science*, **91**, 69.
Mortensen, K. (1996). *Journal of Physics, Condensed Matter*, **8**, 103.
Mortensen, K. (1997). *Macromolecules*, **30**, 503.

Mortensen, K. and Brown, W. (1993). *Macromolecules*, **26**, 4128.
Mortensen, K. and Pedersen, J. S. (1993). *Macromolecules*, **26**, 805.
Mortensen, K., Brown, W. and Nordén, B. (1992). *Physical Review Letters*, **68**, 2340.
Mortensen, K., Brown, W. and Jørgensen, E. (1994). *Macromolecules*, **27**, 5654.
Noolandi, J., Shi, A.-C. and Linse, P. (1996). *Macromolecules*, **29**, 5907.
Olvera de la Cruz, M. (1989). *Journal of Chemical Physics*, **90**, 1995.
Phoon, C. L., Higgins, J. S., Allegra, G., van Leeuwen, P. and Staples, E. (1993). *Proceedings of the Royal Society of London, Series A*, **442**, 221.
Pleštil, J., Hlavatá, D., Hrouz, J. and Tuzar, Z. (1990). *Polymer*, **31**, 2112.
Pople, J. A., Hamley, I. W., Fairclough, J. P. A., Ryan, A. J., Komanschek, B. U., Gleeson, A. J. *et al.* (1997). *Macromolecules*, **30**, 5721.
Price, C., Chan, E. K. M., Hudd, A. L. and Stubbersfield, R. B. (1986). *Polymer Communications*, **27**, 196.
Prud'homme, R. K., Wu, G. and Schneider, D. K. (1996). *Langmuir*, **12**, 4651.
Reynders, K., Mischenko, N., Mortensen, K., Overbergh, N. and Reynaers, H. (1995). *Macromolecules*, **28**, 8699.
Rosedale, J. H. and Bates, F. S. (1990). *Macromolecules*, **23**, 2329.
Schafer, L. and Kappeler, C. (1985). *Journal de Physique*, **46**, 1853.
Schillén, K., Brown, W. and Konák, C. (1993). *Macromolecules*, **26**, 3611.
Schillén, K., Brown, W. and Johnsen, R. M. (1994). *Macromolecules*, **27**, 4825.
Schouten, M., Dorrepaal, J., Stassen, W. J. M., Vlak, W. A. H. M. and Mortensen, K. (1989). *Polymer*, **30**, 2038.
Scordari, F. (1992). Ionic crystals. In *Fundamentals of crystallography* (ed. C. Giacovazzo), p. 429. Oxford University Press, Oxford.
Shibayama, M., Hashimoto, T. and Kawai, H. (1983*a*). *Macromolecules*, **16**, 16.
Shibayama, M., Hashimoto, T., Hasegawa, H. and Kawai, H. (1983*b*). *Macromolecules*, **16**, 1427.
Shibayama, M., Hashimoto, T. and Kawai, H. (1983*c*). *Macromolecules*, **16**, 1434.
Stacy, C. J. and Kraus, G. (1977). *Polymer Engineering and Science*, **17**, 627.
Stejskal, J., Hlavatá, D., Sikora, A., Konák, C., Plestil, J. and Kratochvíl, P. (1992). *Polymer*, **33**, 3675.
Tanodekaew, S., Godward, J., Heatley, F. and Booth, C. (1997). *Macromolecular Chemistry and Physics*, **198**, 3385.
Tsunashima, Y., Hirata, M. and Kawamata, Y. (1990). *Macromolecules*, **23**, 1089.
Vadnere, M., Amidon, G., Lindenbaum, S. and Haslam, J. L. (1984). *International Journal of Pharmaceutics*, **22**, 207.
Wanka, G., Hoffmann, H. and Ulbricht, W. (1994). *Macromolecules*, **27**, 4145.
Watanabe, H. and Kotaka, T. (1982). *Polymer Journal*, **14**, 739.
Watanabe, H. and Kotaka, T. (1983). *Polymer Journal*, **15**, 337.
Watanabe, H. and Kotaka, T. (1984). *Polymer Engineering Reviews*, **4**, 73.
Watanabe, H., Kotaka, T., Hashimoto, T., Shibayama, M. and Kawai, H. (1982). *Journal of Rheology*, **26**, 153.
Whitmore, M. D. and Noolandi, J. (1990). *Journal of Chemical Physics*, **93**, 2946.
Yamakawa, H. (1971). *Modern theory of polymer solutions*. Harper and Row, New York.
Yang, Y.-W. (1996). Ph.D. thesis. Department of Chemistry. University of Manchester, Manchester.
Yang, Y.-W., Yang, Z., Zhou, Z.-K., Attwood, D. and Booth, C. (1996*a*). *Macromolecules*, **29**, 670.
Yang, Z., Yang, Y.-W., Zhao, Z.-K., Attwood, D. and Booth, C. (1996*b*). *Journal of the Chemical Society, Faraday Transactions*, **92**, 257.

Yang, Y.-W., Ali-Adib, Z., McKeown, N. B., Ryan, A. J., Attwood, D. and Booth, C. (1997). *Langmuir*, **13**, 1860.
Zhang, K. (1994). Ph.D. thesis. University of Lund, Lund.
Zhang, K., Lindman, B. and Coppola, L. (1995). *Langmuir*, **11**, 538.
Zhou, Z., Yang, Y.-W., Booth, C. and Chu, B. (1996). *Macromolecules*, **29**, 8357.

5 Solid state structure of block copolymers

5.1 Introduction

The term 'solid state structure' in this chapter refers largely to the morphology of semicrystalline block copolymers below the melting temperature of the crystallizable block. Mention is also briefly made of the structure below the glass transition temperature of block copolymers containing a glassy component. However, vitrification generally leads to trapping of the melt morphology and therefore there is little distinct thermodynamics in the phase behaviour of block copolymers in the glassy state compared to the melt. Because the work on semicrystalline diblocks is rather sparse it has not yet been reviewed. This chapter is thus a summary of work to date in an area in which there is a continued high level of activity.

Crystallization in polymers is accompanied by the adoption of an extended conformation, or often by chain folding. Folding of the crystalline block in semicrystalline block copolymers has been studied for diblocks containing poly(ethylene) and poly(oxyethylene), also known as poly(ethylene oxide) (PEO). Poly(ethylene) (PE) in block copolymers is prepared by anionic polymerization of poly(1,4-butadiene) (1,4-PB) followed by hydrogenation and has a melting point in the range 100–110 °C. This synthesis method leads to ethyl branches in the copolymer, with, on average, 2–3 branches per 100 repeats. These branches induce lengths for folded chains which are set by the branch density and not by the thermodynamics of crystallization.

The melting temperature of PEO in block copolymers is generally lower than that of PEO homopolymers (melting temperature $T_m = 76\,^{\circ}C$ for high molecular weight samples). In contrast to PE, prepared by hydrogenation of 1,4-PB, there is no chain branching in these copolymers and the fold length depends on the crystallization procedure. Molecules with 1,2,3, . . . folds can be obtained by varying the crystallization protocol (quench depth, annealing time, etc). It is important to distinguish between crystallization in homopolymers and in block copolymers. In homopolymers, chain folding leads to metastable structures introduced by the crystallization kinetics. In contrast, equilibrium chain folding in diblocks can be achieved, the equilibrium number of folds being controlled by the size of the second, non-crystallizable block.

Crystallization has been investigated for other block copolymers, in particular those containing poly(ε-caprolactone) (T_m = 57 °C). Experimental results for these materials are also summarized here. A study of morphology in block copolymers where both blocks are crystallizable is also discussed.

The structure of crystalline diblocks at the nanoscale level is usually probed using X-ray scattering. Small-angle X-ray scattering (SAXS) provides information on the (usually lamellar) crystalline domain spacing and a more detailed analysis can provide the crystal and amorphous layer thicknesses. The structure of the crystalline unit cell can be identified using wide-angle X-ray scattering (WAXS). The morphology of polymer crystals can be elucidated using scanning electron microscopy (SEM), in tandem with etching or shadowing techniques. At a larger, micrometre, length-scale, optical microscopy is used to identify spherulitic structures from the macroscopic stacks of crystalline lamellae. Spherulitic structures can also be identified indirectly via small-angle light scattering (SALS). The degree of crystallinity of crystallizable polymers can be determined using differential scanning calorimetry (DSC) or SAXS or WAXS, as described below. Dilatometry, which measures the specific volume change on crystallization, can also provide the degree of crystallinity.

In this chapter, structure formation in semicrystalline diblocks containing PE, PEO and other crystalline blocks is discussed in Section 5.2. Section 5.3 is concerned with theories for the equilibrium crystallization of block copolymers, whilst Section 5.4 summarizes recent experimental work on the kinetics of crystallization. There have been few studies of crystallization in thin block copolymer films, and consequently Section 5.5 is correspondingly short. Finally, structure formation in glassy diblocks is considered in Section 5.6.

5.2 Structure formation in semicrystalline diblocks

5.2.1 Poly(ethylene)-containing diblocks

Thermodynamics of crystallization

Structural changes in block copolymers containing a crystallizable component, in particular chain-folding, resulting from crystallization compete with those occurring due to microphase separation. Experiments suggest that the final morphology on crystallization depends on whether the sample is cooled from a microphase-separated melt or crystallizes from a homogeneous melt or solution. Furthermore, if crystallization occurs from an ordered phase, the degree of segregation influences the crystalline structure.

The mechanical and thermal properties of a range of poly(ethylene)/poly(ethylene-propylene) (PE/PEP) copolymers have been examined by Mohajer *et al.* (1982). They studied the effect of variation of composition and copolymer architecture on the polymer properties by synthesizing a range of PE–PEP–PE and PEP–PE–PEP triblocks and PE–PEP diblocks with high molecular weights ($M \approx 200\,\mathrm{kg\,mol^{-1}}$). The crystallinity, density and melting enthalpy for all copolymers were found to be linearly dependent on the PE content, indicating microphase separation of PE and rubbery PEP in the solid state. The

WAXS patterns were similar to those for the PE homopolymer, and spherulitic structures were inferred from small-angle light scattering patterns which revealed the 'four-leaf clover' structure characteristic of spherulites, for copolymers with high PE content (cast from solution). A small-angle light scattering pattern from a PE–PEP–PE triblock is shown in Fig. 5.1, together with a representative optical micrograph of a spherulitic structure in a semicrystalline copolymer. The tensile stress-strain properties of PE–PEP–PE and PEP–PE–PEP triblocks and a

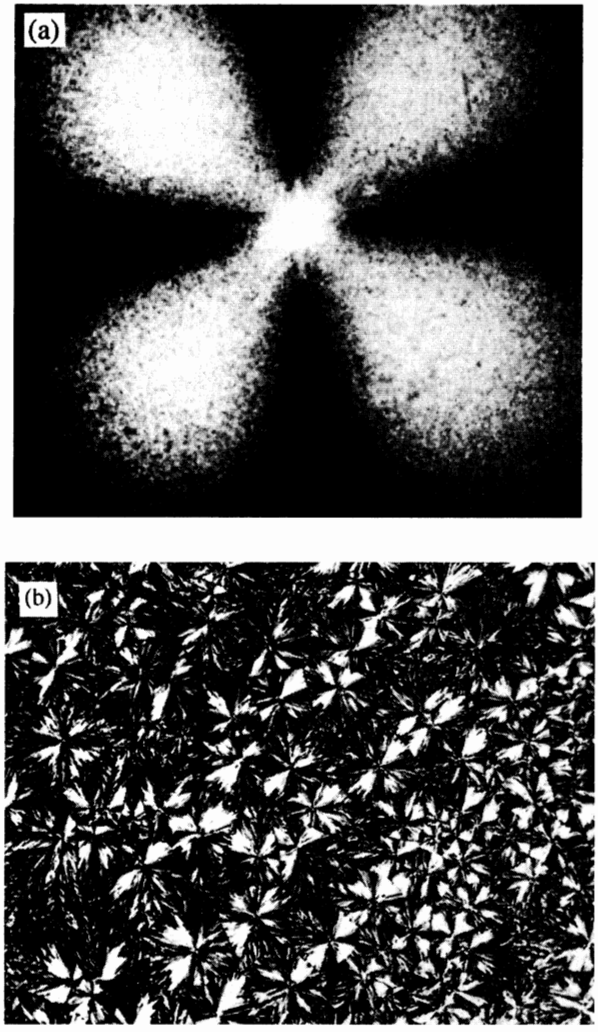

Fig. 5.1 (a) 'Clover leaf' pattern in the small-angle light scattering pattern from a PE–PEP–PE triblock ($M \approx 200\,\text{kg mol}^{-1}$, 86 wt% PE) (Mohajer *et al.* 1982). (b) Polarized optical micrograph of a PCL–PDMS–PCL triblock ($M \approx 7\,\text{kg mol}^{-1}$, 57 wt% PCL) showing spherulitic structure (Lovinger *et al.* 1993).

PE–PEP diblock were similar to each other at high PE content (50–90%). This was because the mechanical properties were determined predominantly by the behaviour of the more continuous PE phase. For lower PE contents (7–29%) there were major differences in the mechanical properties of polymers with different architectures, all of which formed a cubic-packed sphere phase. PE–PEP–PE triblocks were found to be thermoplastic elastomers, whereas PEP–PE–PEP triblocks behaved like particulate filled rubber. The difference was proposed to result from bridging of PE domains across spheres in PE–PEP–PE triblocks, which acted as physical cross-links due to anchorage of the PE blocks in the semicrystalline domains. No such arrangement is possible for the PEP–PE–PEP or PE–PEP copolymers (Mohajer *et al.* 1982).

Séguéla and Prud'homme (1989) investigated a PE–PEP–PE triblock copolymer containing 27 wt% poly(ethylene) cast from a neutral solvent close to the T_m of PE and well below it. The samples cast above T_m crystallized within the assumed hexagonal-packed cylinder microphase-separated structure. However, SAXS experiments performed on the samples cast at room temperature suggested that crystallization occurred without prior microphase separation in the melt. This path dependence is a general feature of crystallization in block copolymers.

Cohen *et al.* (1990) studied a poly(styrene)–poly(ethylene) (PS–PE) diblock that was solvent cast from toluene. Crystallization within microphase-separated PE spheres occurred when solvent-casting was done above the PE block melting temperature, T_m (see Fig. 5.2). When solvent was removed below T_m crystallization did not occur within spherical microdomains, instead TEM and SANS experiments suggested an irregular structure. Nojima *et al.* (1994) suggest that crystallization from the melt in this sample occurred within the microphase-separated block in the former case due to the high molecular weight of the

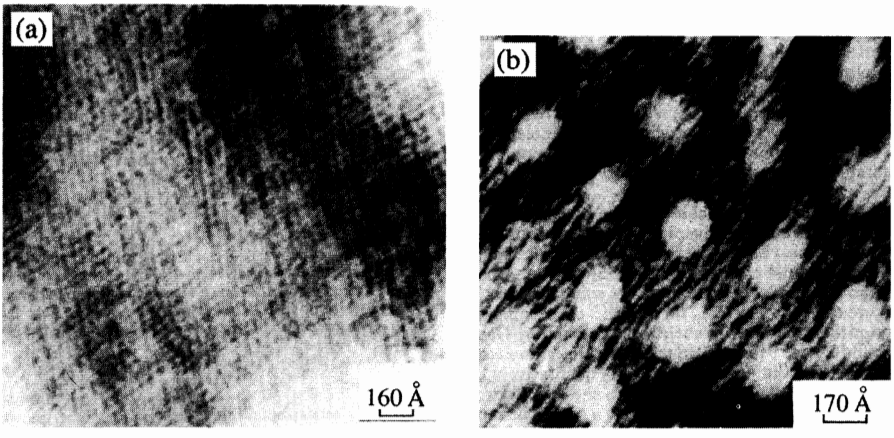

Fig. 5.2 Transmission electron micrographs of a PS–PE diblock (M = 101 kg mol^{-1}, 11 wt% PE): (a) cast at 65 °C and annealed at 140 °C for 3 h; (b) cast from toluene at 65 °C (Cohen *et al.* 1990). The sample is stained with RuO_4, which selectively stains PS.

copolymer, which increases the energy barrier between the microphase-separated and equilibrium crystal structures.

Crystallization in poly(ethylene)–poly(ethylethylene) (PE–PEE) semicrystalline diblock copolymers has been investigated using SAXS and WAXS on oriented specimens. Microphase separation was found to precede crystallization for all samples, with 37–90 wt% PE (Douzinas and Cohen 1992). The scaling of the lamellar domain spacing in the crystalline phase for the same samples was determined from measurements of the principal SAXS peak position (Douzinas *et al.* 1991). It was found that the domain spacing scales in agreement with the predictions of the theory of Whitmore and Noolandi (1988) (Section 5.3.5), i.e.

$$d \sim NN_a^{-5/12} \tag{5.1}$$

where N is the total degree of polymerization and N_a is the degree of polymerization of the amorphous block.

The structure of PE–PEP diblocks upon crystallization from the disordered melt has been investigated using simultaneous SAXS, WAXS and DSC together with SALS by Rangarajan *et al.* (1993, 1995*a*). For all compositions (12–56 wt% PE), a lamellar phase with a spherulitic superstructure crystallized from the homogeneous melt, as characterized using SAXS and SALS respectively. The scaling of domain spacing with N_a was also investigated, and Rangarajan *et al.* (1993) reported $d \sim NN_a^{-0.45}$, in good agreement with the predictions of the Whitmore–Noolandi model (Whitmore and Noolandi 1988). However, the theory did not account for the absolute values of d, because it only considers uniformly folded chains, which is unrealistic due to irregular folds induced by the presence of ethyl branches in these PE-containing diblocks.

The structure of PE–PEE, PE–PEP and PE–PVCH (here PVCH denotes poly(vinyl cyclohexane)) diblocks upon crystallization from the ordered melt has been elucidated using simultaneous SAXS, WAXS and DSC (Hamley *et al.* 1997*a*; Ryan *et al.* 1995). Here PEE and PEP are rubbery, whereas PVCH is glassy below $T_g \approx 140\,°C$. It was observed that the melt morphologies were destroyed due to PE chain folding upon crystallization. Whether the initial structure was a weakly segregated lamellar or a hexagonal-packed cylinder melt phase, on crystallization a lamellar phase distinct from the melt was always formed. This is illustrated in Fig. 5.3 which shows SAXS profiles for symmetric and asymmetric PE–PEE diblocks. However, it has been reported that crystallization from the strongly segregated cylindrical melt of PE–poly(3-methyl-1-butene) diblocks occurs within the pre-existing cylindrical structure (Quiram *et al.* 1997). For a more weakly segregated diblock of the same type, crystallization within cylinders occurred upon fast cooling from the ordered melt, whereas slower cooling led to a lamellar structure. These observations suggest that the structure with crystalline rods is metastable.

The domain spacing obtained by Hamley *et al.* (1997*a*) and Ryan *et al.* (1995) increased discontinuously upon crystallization, as indicated by the shift of the principal peak position, q^*, to lower q, as apparent in Fig. 5.3. Here $q = 4\pi \sin\theta/\lambda$ where 2θ is the scattering angle and λ is the X-ray wavelength. The SAXS profiles from the crystallized diblocks were shown to correspond to the sum of scattering from block copolymer lamellae, with up to four orders of reflection, plus a broad

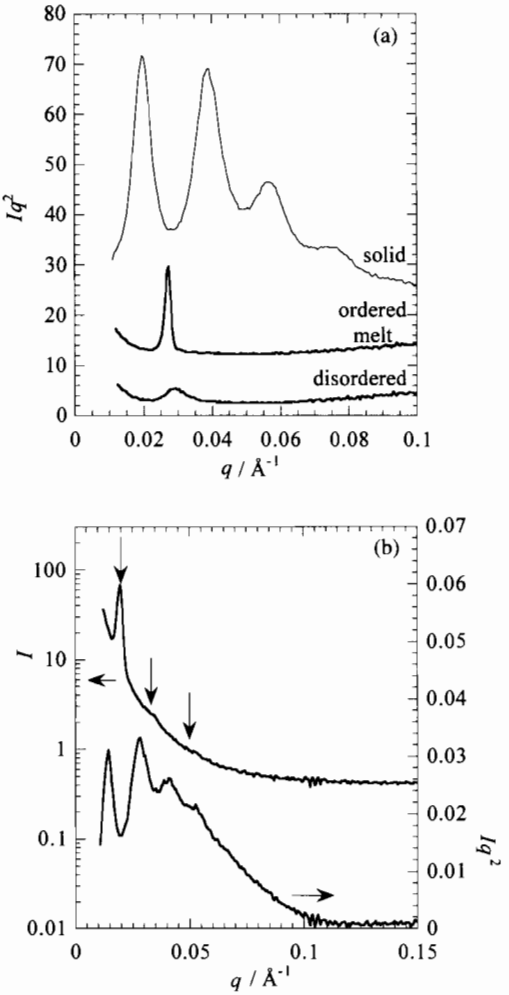

Fig. 5.3 SAXS intensity versus scattering vector magnitude for PE–PEE diblocks with: (a) $M_n = 120\,\text{kg mol}^{-1}$, $f_{PE} = 0.50$ (top two profiles at 100 °C, bottom profile at 140 °C), (b) $M_n = 47\,\text{kg mol}^{-1}$, $f_{PE} = 0.25$ (Ryan *et al.* 1995) (top, 140 °C; bottom, 100 °C).

peak arising from semicrystalline PE, as shown in Fig. 5.4. Scattering density correlation functions were extracted from the SAXS data and the thickness of the crystalline PE region was determined from the extrapolated linear region of the scattering density correlation function, which was computed using (Vonk 1973)

$$\gamma_1(r) = \frac{\int_0^\infty I(q) q^2 \cos(qr)\,\mathrm{d}q}{\int_0^\infty I(q) q^2\,\mathrm{d}q}, \tag{5.2}$$

which is normalized such that $\gamma_1(r = 0) = 1$. The data were extrapolated to large q using a damped Porod function. It was found from analysis of correlation

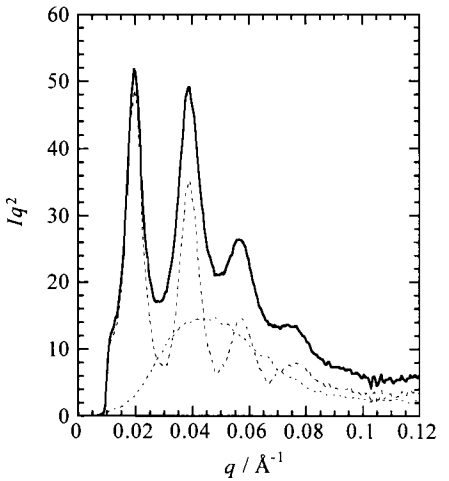

Fig. 5.4 Plot showing that the SAXS intensity from a PE–PEE diblock (M_n = 23 kg mol^{-1}, f_{PE} = 0.49) at a temperature below the PE crystallization temperature can be represented as the sum of a broad peak from amorphous and crystalline PE (dashed curve with one peak) plus the multiple Bragg peak scattering from a lamellar structure (dashed curve with four peaks) (Ryan *et al.* 1995).

functions that the PE lamellar thickness in the PE–PEE and PE–PEP copolymer was 45 ± 10 Å (Hamley *et al.* 1997*a*; Ryan *et al.* 1995). An example of a correlation function calculated for a PE–PEE diblock, together with its interpretation in terms of amorphous and crystalline layer thicknesses is shown in Fig. 5.5. The PE crystal thickness in these polymers is set by the density of ethyl branches in the PE, which was synthesized by hydrogenation of poly(1,4-butadiene). The equilibrium melting temperature of a PE homopolymer prepared by hydrogenating 1,4-PB is lower than that for linear PE due to chain folding induced by the short chain branches (Hamley *et al.* 1997*a*). In contrast to the constant PE crystal thickness, the lamellar domain spacing of PE homopolymers and PE-containing diblocks was found to decrease with increasing quench depth below T_m(PE), reflecting an increased degree of crystallinity. This is clear from Fig. 5.6 which shows the SAXS invariant (eqn 5.3), the total domain spacing, and the PE crystal thickness from correlation function analysis of SAXS data for a PE–PEE diblock quenched to different temperatures.

Wide-angle X-ray scattering shows (Fig. 5.7) that PE in these copolymers crystallizes in the orthorhombic form (Fig. 5.8) that is also the crystalline structure of homopolymer PE at normal densities. The PE degree of crystallinity, X_{PE}, was determined using DSC to be 0.4 ± 0.1. This value was obtained from $X_{PE} = \Delta H_{cxp}/\Delta H^0_{fus} w_{PE}$, where ΔH_{cxp} is the experimental melting enthalpy, w_{PE} is the weight fraction of PE, and $\Delta H^0_{fus} = 277\,J\,g^{-1}$ is the theoretical heat of fusion for 100% crystalline PE (Brandrup and Immergut 1989). The degree of crystallinity can also be obtained from the SAXS data as l_c/d', where l_c is the

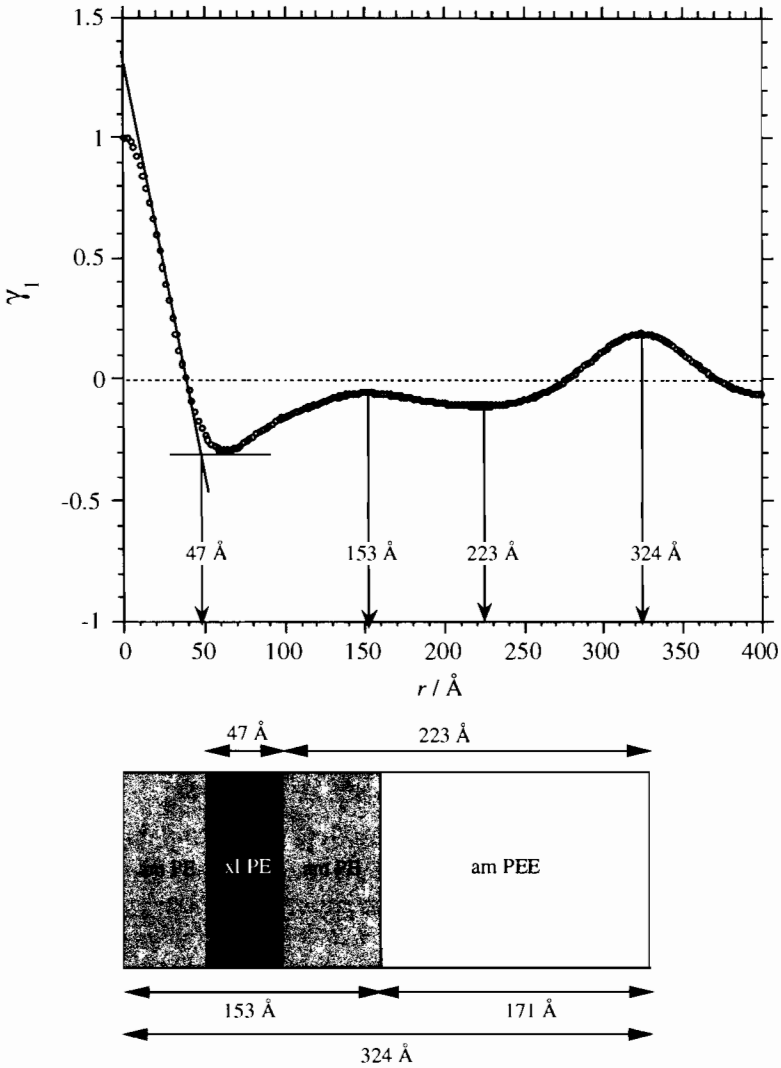

Fig. 5.5 Cosine-transform correlation function computed from the SAXS data for a PE–PEE diblock diblock ($M_n = 23\,\mathrm{kg\,mol^{-1}}$, $f_{PE} = 0.49$), with an interpretation of the distances based on extrapolation of the small r slope and subsequent maxima and minima (Ryan *et al.* 1995). Here am = amorphous (rubbery) and xl = crystalline.

crystalline region thickness and d' is the total PE domain thickness ($d' = df_{PE}$, where f_{PE} is the volume fraction of PE), both extracted from a correlation function analysis. The relative degree of crystallinity can additionally be tracked using the small-angle scattering invariant. The small-angle scattering invariant is a measure of the total small-angle scattering from a material, independent of the size or shape of structural inhomogeneities (Balta-Calleja and Vonk 1989)

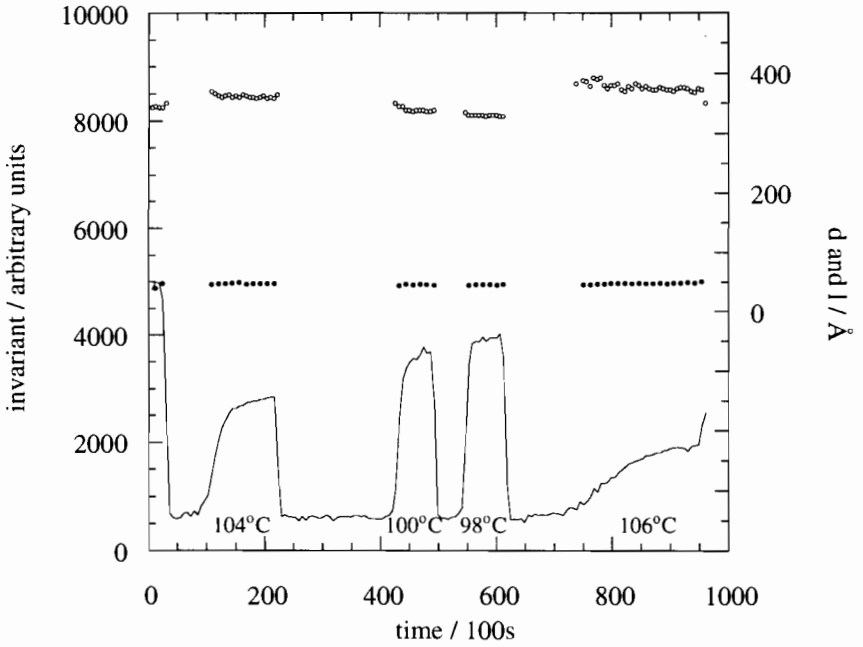

Fig. 5.6 Small-angle scattering invariant (line), domain spacing (d, open circles) and PE lamellar thickness (l, filled circles) versus time during a series of quenches for a PE–PEE diblock ($M_n = 20\,kg\,mol^{-1}$, $f_{PE} = 0.55$) (Hamley *et al.* 1997*a*). The sample was successively quenched from 140 °C to 104 °C, 100 °C, 98 °C, 106 °C. (T_m (PE) ≈ 108 °C for this sample.)

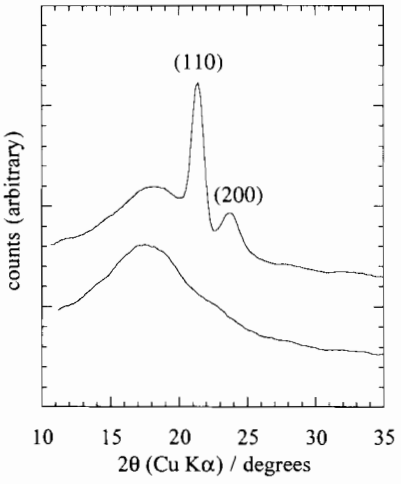

Fig. 5.7 Representative WAXS patterns for PE-containing diblocks. Data for a PE–PEE diblock with $M_n = 44\,kg\,mol^{-1}$, $f_{PE} = 0.75$ (Ryan *et al.* 1995). *Top*, 100 °C; *bottom*, 140 °C.

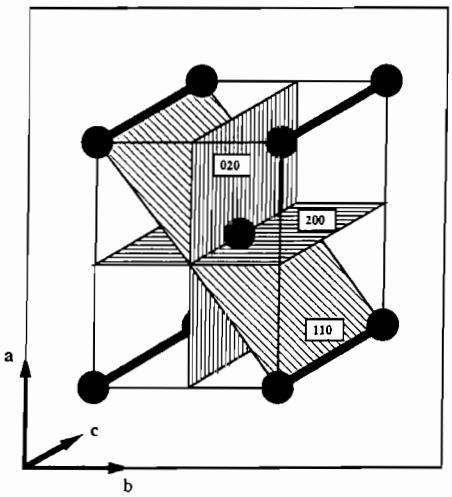

Fig. 5.8 Body-centred orthorhombic unit cell for PE (Douzinas and Cohen 1992). The chain stems lie along the *c* axis.

$$Q = \frac{1}{2\pi i_e} \int_0^\infty I(q) q^2 \, dq, \tag{5.3}$$

where i_e is the Thompson scattering factor. For an ideal two-phase model it can be written as (Ryan *et al.* 1994)

$$Q = \phi(1 - \phi)\langle \eta^2 \rangle, \tag{5.4}$$

where ϕ is the volume fraction of crystals and η is the electron density difference between crystalline and amorphous phases. The absolute value of the invariant requires absolute intensity measurements, thermal background subtraction and extrapolation to $q = 0$ and $q = \infty$. For the symmetric PE–PEE diblocks and PE–PVCH diblock studied by Hamley *et al.* (1997*a*), the $\phi(1 - \phi)$ term was relatively insensitive to the small change in volume fraction on crystallization. The SAXS invariant is then sensitive to the degree of crystallinity because formation of PE crystals causes the average electron density of the PE microphase to increase. The densities of the blocks in these polymers are in the order PVCH > crystalline PE > amorphous PE > PEE. Therefore, crystallization causes η to increase for the PE–PEE polymers, but to decrease for PE–PVCH, which is reflected in the invariant, dominated by η^2 (Hamley *et al.* 1997*a*).

The relative degree of crystallinity can also be estimated from the WAXS pattern from the ratio of the integrated intensity of the crystal peak to that of the total amorphous and crystalline scattering (Balta-Calleja and Vonk 1989). For PE, the amorphous scattering below the (110) peak (Fig. 5.7) is relatively insensitive to the degree of crystallinity, so the integrated area of the (110) reflection compared to the broad amorphous halo is directly proportional to X_{PE}. However, the absolute degree of crystallinity cannot be determined in this way (Ryan *et al.* 1995).

Crystallization from the ordered melt was observed for a PE/head-to-head poly(propylene) (PE–hhPP) sample by Rangarajan *et al.* (1995*b*) using simultaneous SAXS and WAXS. Higher order reflections in the SAXS profiles were found to grow concurrently with WAXS peaks during isothermal crystallization, indicating that the change in microdomain structure induced by crystallization occurs at the same time as the development of crystallinity. During crystallization, the first-order SAXS peak moved continuously to lower q with a concurrent increase in peak width. The peak shape and position during crystallization could be adequately approximately by a linear combination of the peaks observed before and after crystallization, consistent with a nucleation and growth process where melt is simply converted to crystallized material with no subsequent change in morphology. The position of the first-order SAXS peak after crystallization was found to be sensitive to even minor changes in the thermal history of the sample. As the cooling rate from the melt decreased, the change in domain periodicity between the molten and crystallized diblock increased. Such path dependence was not observed for PE–PEP diblocks crystallizing from the disordered melt (Rangarajan *et al.* 1995*a*), and indicated that in the PE–hhPP system microphase separation led to a substantial barrier to the large-scale structural reorganization which occurs on crystallization. Also in contrast to PE–PEP diblocks no change in domain spacing was observed after the primary crystallization process (Rangarajan *et al.* 1995*b*).

Orientation of chain-folded poly(ethylene)

The orientation of crystalline stems with respect to the lamellar interface in block copolymers is a subject of ongoing interest and controversy. In contrast to homopolymers, where folding of chains occurs such that stems are perpendicular to the lamellar interface, the parallel orientation has been observed for block copolymers crystallized from the heterogeneous melt. It is not yet clear whether this is always the preferred orientation, or whether chains can crystallize perpendicular to the lamellar plane, for example when crystallization occurs from the homogeneous melt or from solution.

The orientation of PE stems with respect to the lamellar microstructure was determined for an asymmetric PE–PEP–PE triblock prepared by solvent casting by Séguéla and Prud'homme (1989). They performed combined SAXS and WAXS on samples oriented by drawing. Two samples were studied: one cast from a solvent close to T_m(PE) and one from a solvent well below it. The samples cast above T_m crystallized within the assumed hexagonal-packed cylinder microphase-separated structure, whereas those cast from solution at room temperature did not microphase separate, but formed a weakly ordered lamellar crystalline structure directly. For the melt-crystallized sample, it was observed that at relatively low draw ratios (α = 1.8–3.5) four-point SAXS patterns developed (see Fig. 5.9). These are often observed for the hexagonal phase of triblocks subject to large uniaxial strains (Honeker and Thomas 1996). At a higher draw ratio (α = 6.5), the four-point pattern evolved into a pair of Bragg peaks normal to the draw direction, characteristic of a layered structure. At this draw ratio it was observed that the (110) and (200) WAXS reflections from PE oriented in the

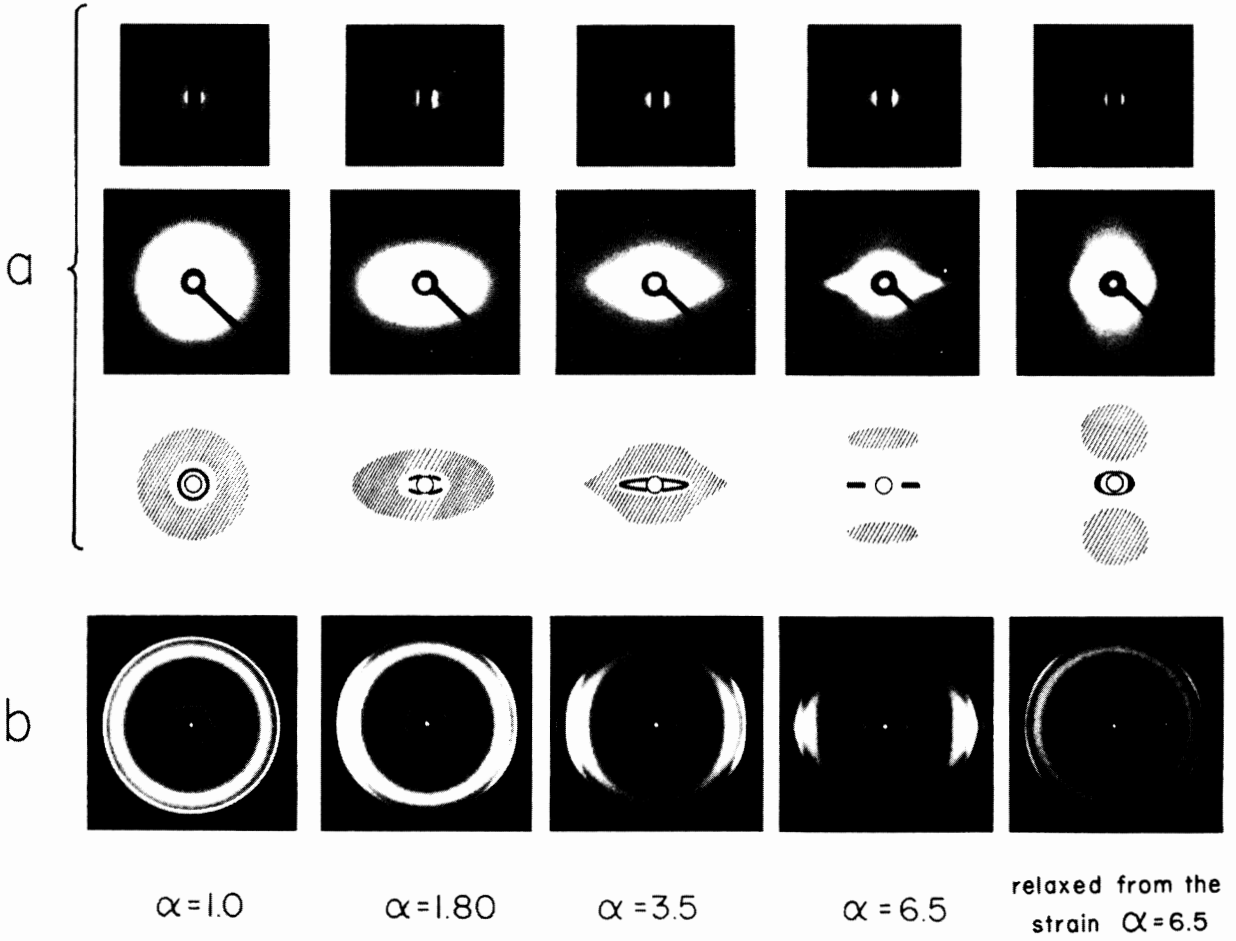

Fig. 5.9 Evolution with draw ratio, α, of (a) SAXS and (b) WAXS patterns of a melt-crystallized PE–PEE–PE triblock (M_n = 1.57 kg mol^{-1}, 27 wt% PE) deformed at room temperature (Séguéla and Prud'homme 1989). The draw direction was vertical. The SAXS patterns in (a) were obtained at two exposures, to reveal both strong Bragg scattering and weak diffuse scattering.

same direction as the peaks in the SAXS arising from the lamellar structure (Fig. 5.9). Following relaxation, the (110) peaks shift away from the normal to the draw direction to an azimuthal angle $\phi = 56°$, to give a pattern characteristic of the projection along the *a* axis of oriented body-centred orthorhombic PE. Thus the PE stems (which lie along the *c* axis, Fig. 5.8) were found to be oriented parallel to the lamellae (Fig. 5.10). In contrast, for the solution-crystallized sample a WAXS pattern characteristic of orientation of the PE unit cell *b* axis along the draw direction was observed, although most of the anisotropy in the WAXS was lost following relaxation. The corresponding SAXS patterns did not contain sharp peaks characteristic of highly ordered samples, only diffuse scattering features. At very high draw ratios ($\alpha = 20$) the WAXS patterns contained reflections from monoclinic PE as well as the usual orthorhombic form (Séguéla and Prud'homme 1989).

Chain folding in PE–PEE semicrystalline diblock copolymers has been investigated using SAXS and WAXS on specimens oriented by applying oscillatory shear or uniaxial compression above the melting temperature (Douzinas and Cohen 1992). Microphase separation preceded crystallization for all samples, with 37–90 wt% PE. From an analysis of pole figures for the (200) and (020) wide-angle reflections in two lamellar samples, the crystalline unit cell orientation was deduced, and it was found that the PE chains are oriented parallel to the layers, in agreement with the results of Séguéla and Prud'homme (1989). In subsequent work, the effect of reduction of the ethyl branch density in PE to essentially zero on the chain orientation in a PE–PS diblock was investigated (Cohen *et al.* 1994). Again using SAXS together with WAXS pole figure analysis, the orientation of

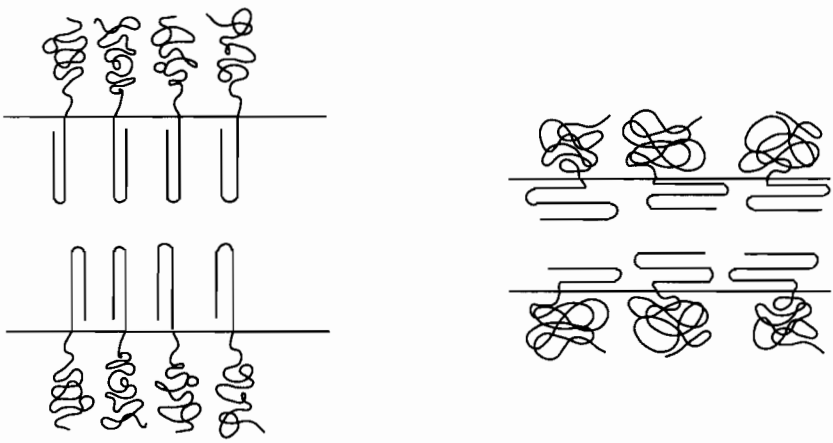

Fig. 5.10 Schematic of perpendicular and parallel chain folding in semicrystalline block copolymers.

the unit cell with respect to the lamellae was investigated for samples oriented in the lamellar melt in a channel die device, which applies a planar compression. It was found (Cohen *et al.* 1994) that the *a* axis of the unit cell was oriented normal to the lamellae, with the *b* and *c* axes (and thus stems) lying with random orientation in the lamellar plane, as for the PE–PEE samples studied earlier by Douzinas and Cohen (1992). Orientation in a series of PE–PEP diblocks oriented using a channel die has also been studied using SAXS/WAXS (Kofinas and Cohen 1994). The samples were subject to compression during a quench to room temperature. It was found that when the diblocks were oriented above the PE melting block (at temperatures below but close to the ODT) at various compression ratios, the lamellae oriented perpendicular to the plane of shear. In other words, the PE crystallized in the pre-existing perpendicular orientation formed in the melt close to the ODT (the observation of this orientation close to the ODT was first discussed by Koppi *et al.* (1992), see Section 2.4.3). In contrast, compression below T_m caused the lamellae to orient parallel to the plane of shear. However, the PE chains crystallized parallel to the lamellae (Fig. 5.10) in either orientation, as shown by analysis of WAXS pole figures (Kofinas and Cohen 1994), and in agreement with results from other samples investigated by the Cohen group.

Although Rangarajan *et al.* (1993) did not study oriented samples, they suggest a model for their PE–P(E/P) diblocks (12–56 wt% PE), crystallized from the homogeneous melt in which the PE domain consists of crystallites with chains folded perpendicular to the interface alternating with amorphous regions. This is in contrast to the X-ray scattering results of Cohen and co-workers (Cohen *et al.* 1994; Douzinas and Cohen 1992; Kofinas and Cohen 1994) and Séguéla and Prud'homme (1989) on oriented diblocks crystallized from the heterogeneous melt. For a strongly segregated PE–poly(3-methyl-1-butene) cooled from the cylindrical melt, Register and co-workers reported crystallization of PE within rods, with a tilted perpendicular orientation (Quiram *et al.* 1997). The stems were found to be oriented at $18 \pm 4°$ with respect to the cylinder axis, on the basis of SAXS and WAXS patterns obtained from samples oriented by flow.

Crystallization in oriented PE–PEE, PE–PEP and PE–PVCH diblock copolymers has been investigated using simultaneous SAXS and WAXS (Hamley *et al.* 1996*a*,*b*). Oriented semicrystalline samples were prepared by shearing in the ordered melt and quenching to room temperature. For a PE–PVCH sample this led to crystallization within a lamellar phase with glassy PVCH lamellae, because the PVCH glass transition temperature is greater than the T_m of PE. For symmetric diblocks containing PE and either a rubbery or glassy amorphous block, the orientation of the crystallized PE stems was deduced to be parallel to the lamellar interface. The (200) WAXS reflections were observed to be oriented in the same direction as the SAXS Bragg peaks from the lamellar structure, with four oriented (110) reflections at $\phi = 53°$ with respect to the normal to the shear direction. This is illustrated in Fig. 5.11 which shows X-ray scattering patterns for the nearly symmetric PE–PVCH sample. These results are consistent with orientation of the *c* axis (and thus PE stems) parallel to the lamellae, as noted earlier by Séguéla and Prud'homme (1989) and Cohen and co-workers (Cohen *et al.*

1994: Douzinas and Cohen 1992; Kofinas and Cohen 1994). For the PE–PVCH diblock, diffuse scattering was observed normal to the shear direction in the SAXS pattern (vertical bands centred on $|q| = 0.05\text{Å}^{-1}$ in Fig. 5.11) that was consistent with lateral correlations between PE crystallites within the layers of semicrystalline PE. This is sketched schematically in Fig. 5.12. In contrast, in all the samples containing an amorphous component, PE crystallization occurred with no lateral positional correlations of crystallites. The diffuse scattering resulting from lateral positional correlations of crystallites for the PE–PVCH diblock were modelled using a Markov lattice. In particular, a lattice was constructed from a stack of one-dimensional Markov sequences where the probability of a site crystallizing depends only on the state (crystalline or not) of the previous site in that sequence. This is equivalent to a one-dimensional Ising model with nearest-neighbour pair interactions. An example of a lattice generated in this fashion is shown in Fig. 5.13, whilst a scattering pattern computed using this model is presented in Fig. 5.14. This may be qualitatively compared to the SAXS pattern in

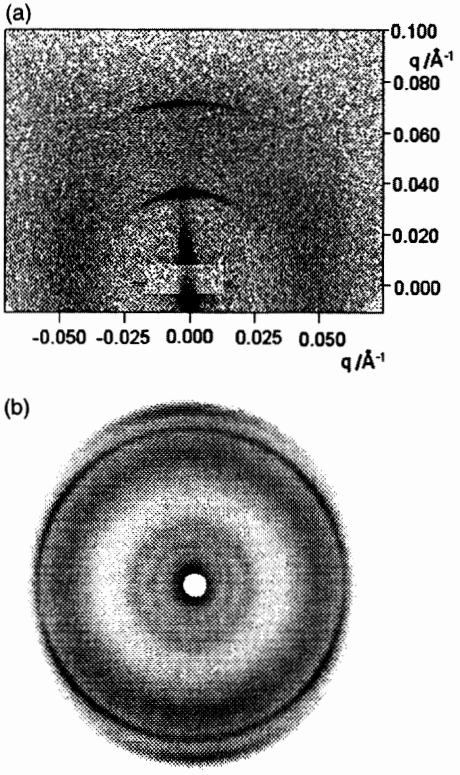

Fig. 5.11 Scattering patterns obtained for a PE–PVCH diblock ($M_n = 15\,\text{kg mol}^{-1}$, $f_{PE} = 0.52$) at room temperature (Hamley *et al.* 1996*b*): (a) SAXS pattern; (b) WAXS pattern. The X-ray beam was incident perpendicular to the shear direction and to the lamellar normal (perpendicular orientation in Fig. 5.12).

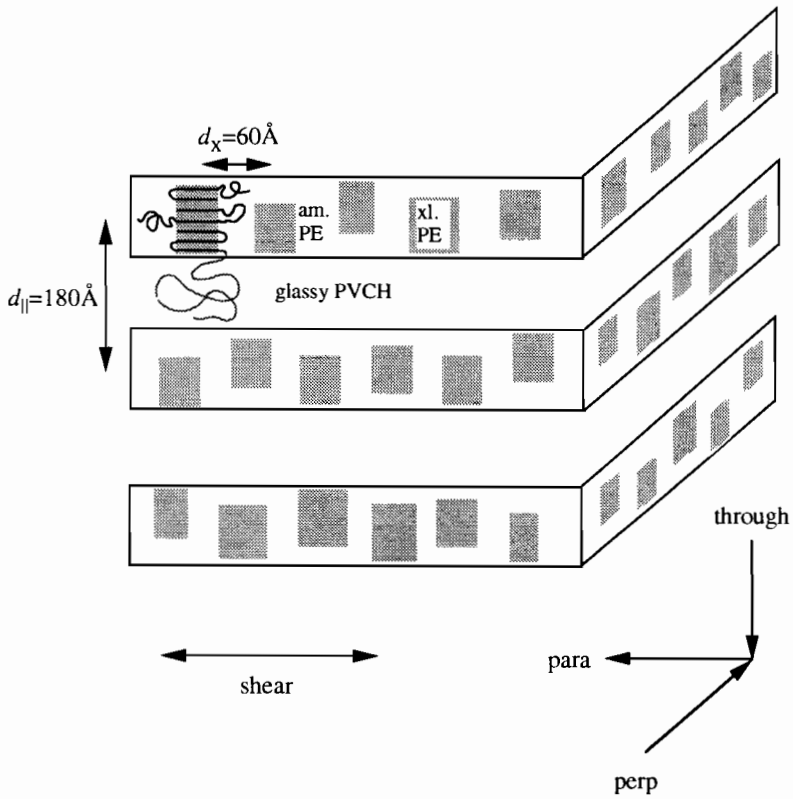

Fig. 5.12 Model for the lamellar organization in semicrystalline PE-PVCH diblocks crystallized from the ordered melt (Hamley *et al.* 1996*b*). The PE chains are folded with stems parallel to the lamellar interface. The convention for labelling of the axis system with respect to the shear direction is also indicated.

Fig. 5.11(a). The agreement is good, although the calculation does not allow for the spread of lamellar orientations that leads to the arcing of the Bragg peaks apparent in Fig. 5.11(a). Diffuse scattering bars normal to the deformation axis were observed earlier by Séguéla and Prud'homme (1989) in SAXS patterns obtained by drawing a melt-crystallized PE–PEP–PE triblock, as evident in Fig. 5.9.

Crystallization in asymmetric diblocks with compositions f_{PE} = 0.35 and 0.46 was also investigated by Hamley *et al.* (1996*b*). It was found that a lamellar structure melted epitaxially (i.e. the domain spacing and orientation were maintained across the transition) to a hexagonal-packed cylinder structure in the f_{PE} = 0.35 sample. This is illustrated in Fig. 5.15, which shows SAXS patterns in the solid and melt states, with a schematic of the epitaxial melting process (Hamley *et al.* 1996*a*,*b*). The same epitaxial transition has been observed for a poly(ethylene oxide)–poly(butylene oxide) diblock (Ryan *et al.* 1997) (*vide infra*).

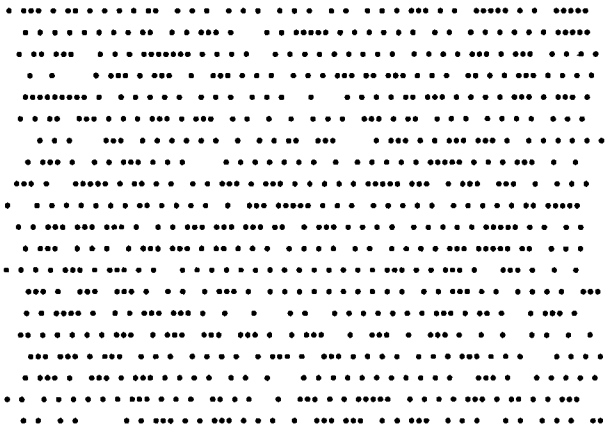

Fig. 5.13 Typical Markov lattice used to model the SAXS patterns for the PE–PVCH diblock in Fig. 5.11 (Hamley *et al.* 1996*b*). The disorder within and between stacks of linear arrangements of crystallites (represented as points) leads to diffuse scattering.

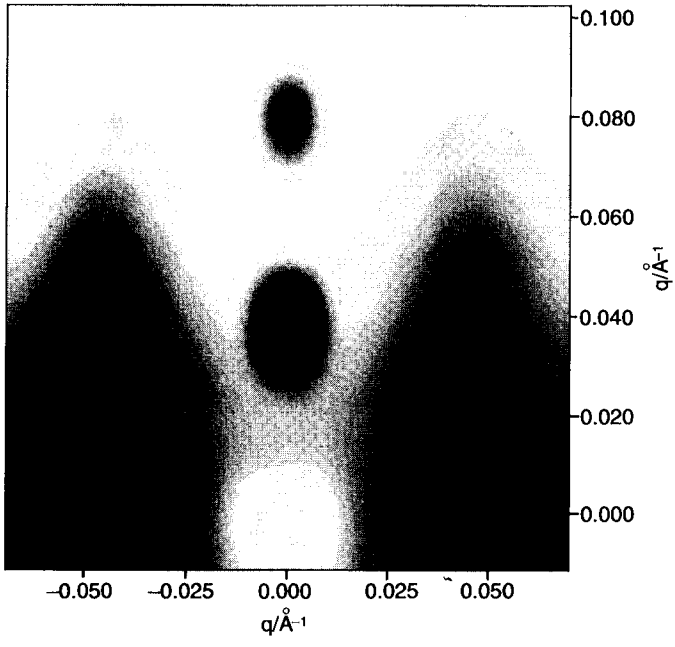

Fig. 5.14 Scattering pattern computed for the model based on stacked Markov chains using $d = 180$ Å and an average in-plane intercrystalline separation $d_{\perp} = 0.35d$ (Hamley *et al.* 1996*b*).

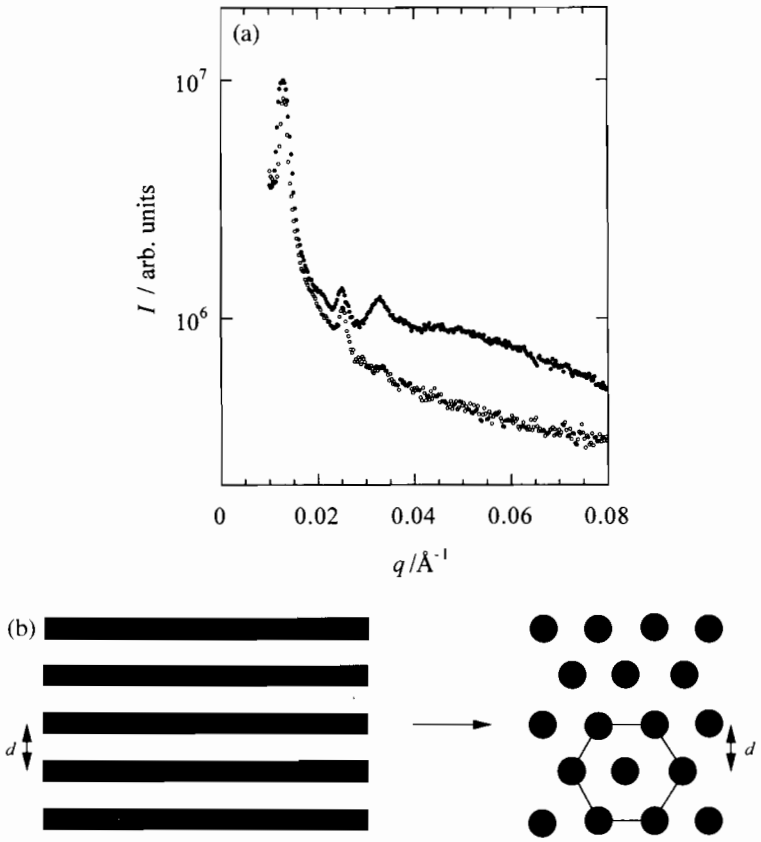

Fig. 5.15 (a) SAXS intensity profiles along the lamellar normal for a PE–PEE diblock (M_n = 81 kg mol^{-1}, f_{PE} = 0.35) (Hamley *et al.* 1996*b*). (b) Schematic of the epitaxial growth of a hexagonal-packed cylinder melt structure from a lamellar solid structure. The direction of incidence of X-rays is along the direction of the arrow.

5.2.2 Poly(ethylene oxide)-containing block copolymers

Poly(ethylene oxide)/poly(propylene oxide) copolymers

PEO homopolymer crystallizes in a monoclinic form, with alternating right- and left-hand distorted 7/2 helices (Takahashi and Tadokoro 1973). The crystallization of PEO in a PEO–PS–PEO triblock, a PEO–PPO–PEO triblock and a (PPO–PEO)$_4$ four-arm starblock in preferential solvents was investigated by Skoulios *et al.* as early as 1963. Here PPO denotes poly(oxypropylene) or poly(propylene oxide). They performed polarized light microscopy and SAXS experiments on the PS–PEO–PS triblock, the Pluronic triblock and the Tetronic starblock in selective solvents for the PS, PPO and PEO blocks and observed birefringent gels. However, in dry copolymers and in a poor solvent for PEO they observed crystallization of the PEO blocks. Above a certain PEO block length,

the PEO chains were found to be folded. The solvent was found to be located in the PEO layers in aqueous solution, whereas in selective solvents for PS and PPO it was located in the corresponding layers. The PEO chains were found to be increasingly tilted with increasing concentration of a solvent selective for PPO in the Pluronic and Tetronic copolymers (Skoulios *et al.* 1963).

Crystallization in PEO_mPPO_n diblocks with a fixed PEO block length $m = 40$ and a varying PPO block length $n = 0$–11 was studied by Ashman and Booth (1975). Lamellar spacings were determined using SAXS, and melting points were measured using dilatometry, whilst picnometry provided specific volumes of the polymers. This technique allows the determination of the specific volume at any temperature, the study of isothermal crystallization at a given temperature and the determination of the degree of crystallinity. Predominantly extended chain crystals were found. The specific volume in the crystalline solid was found to be greater than in the amorphous melt. The melting points of the block copolymers, $T_m = 47$–$51\,°C$, were low compared to perfectly crystalline PEO ($T_m = 76\,°C$). This was ascribed to the positive free energy of formation for the block copolymers of the amorphous layer from the melt, and of the crystalline/amorphous interface. The end interfacial theory was discussed in terms of the theories of Flory (1949) and Flory and Vrij (1963) for melting points of low-molecular-weight polymers (Section 5.3.2). The Flory–Vrij theory allows for partial melting of the crystalline lamellae with the formation of an amorphous layer containing chain ends (i.e. less than perfect crystallinity) which is not included in the Flory theory. The Flory–Vrij theory was extended to block copolymers by Ashman and Booth (1975). The end interfacial energy was found to be $\sigma_e \approx \sigma_a + \sigma_0$, where σ_a is the free energy of formation of the amorphous layer from the melt ($\sigma_a \approx 3.5\ kJ\,mol^{-1}$) and σ_0 is the free energy of formation of the crystalline/amorphous interface ($\sigma_0 \approx 3\,kJ\,mol^{-1}$).

In a companion paper (Ashman *et al.* 1975), lamellar spacings, specific volumes and melting points for a series of PPO–PEO–PPO triblocks were reported. These properties were compared for $PPO_nPEO_mPPO_n$ triblocks with $m = 48$ and different values of n in the range 0 to 7. The properties were interpreted using the Flory–Vrij model. For copolymers with $n \leq 2$, extended chain crystals were observed whereas longer chains were once and/or twice folded, the melting point decreasing for crystals containing more highly folded chains. This folding led to melting points significantly lower than that for perfectly crystalline PEO, as for PEO–PPO diblocks. The melting points and lamellar thicknesses of PPO_n-PEO_mPPO_n triblocks with $m = 70$–100 and $n = 0$–30 were investigated using dilatometry and SAXS by Booth and Pickles (1973). The melting points of the block copolymers were found to be lower than those of PEO homopolymer by an amount (up to 15 °C) which increased as the PPO block length increased. Most samples had more than one melting transition, and these were assigned to crystals with different numbers of folds, this being determined from SAXS measurements of the lamellar spacing. The higher melting transition corresponded to that of the least folded crystal (i.e. extended or once folded chain). End interfacial free energies, σ_e, for various crystals were estimated using Flory's theory (the Flory–Vrij theory would have led to similar results). For a given crystal type

(e.g. once-folded chain), σ_e was higher for longer end-blocks. For a given copolymer σ_e was lower for more highly folded PEO chains (Booth and Pickles 1973). The melting points of a range of PEO–PPO–PEO triblocks from the Pluronic range were measured by Booth and Dodgson (1973), and found to be lower than that of PEO homopolymer by up to 4 °C. Thus the melting point depressions were much smaller than those observed for comparable PPO–PEO–PPO triblocks.

The crystal structures of $PPO_nPEO_mPEO_n$ triblocks with $m = 39$ or 75 and end-block lengths in the range $n = 1$–13 have been investigating using SAXS and DSC and low-frequency Raman spectroscopy (LFRS) (Viras *et al.* 1988). Low-frequency Raman transitions were assigned to longitudinal acoustic modes (LAMs) of either unfolded or once-folded chains, a typical spectrum being shown in Fig. 5.16. Short chains (chain length $L < 20$ Å) were in an extended conformation, whereas longer chains were folded. The crystal structure comprised lamellae in which chains with $n > 1$ were tilted with respect to the lamellar plane by up to 40–50°, whether the PEO blocks were folded or not.

Poly(ethylene oxide)/poly(butylene oxide) copolymers

In poly(ethylene oxide)–poly(butylene oxide) (PEO–PBO) diblocks with short blocks, unfolded PEO blocks crystallize into lamellar crystals, and the PBO

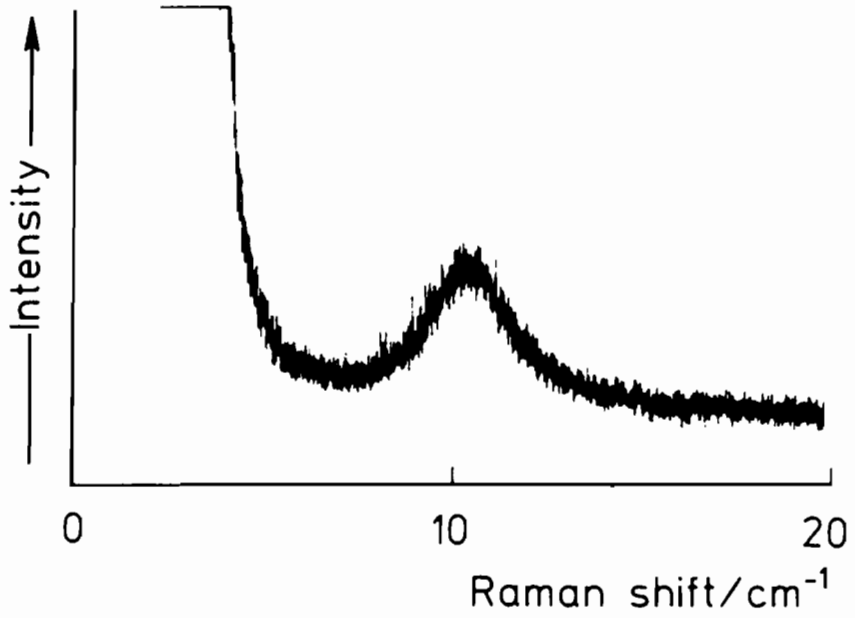

Fig. 5.16 Low-frequency Raman spectrum of a $PPO_7PEO_{75}PPO_7$ triblock at −10 °C (Viras *et al.* 1988). The band between 8 and 12 cm^{-1} is assigned to the longitudinal acoustic mode (LAM) of the copolymer.

blocks are also constrained to an unfolded conformation. This was demonstrated experimentally by a combination of SAXS and LFRS used to study the series of block copolymers PEO_mPBO_n, with m approximately constant (m = 26–32 units) and n in the range 3–30 units (Yang *et al.* 1995). WAXS showed that the PEO crystallized in its usual monoclinic form. Copolymers with $n \leq 20$ formed lamellae in which the whole chain was in extended conformation, i.e. the PEO blocks crystallized in the helical conformation and the extended PBO blocks formed a trans-planar conformation. As the PBO block length increased it was shown (via DSC) that the lamellae became increasingly disordered. For copolymers with $n < 13$, the excess volume of the PBO blocks caused an increase in lamellar thickness with increasing PBO block length. In the range n = 13–20 the relative lamellar spacing (d/L, where L is the calculated molecular length) decreased from its maximum value. However, if the PBO block length was increased to 30 units, it was shown that the unfolded conformation of the PEO_mPBO_n copolymers became unstable with respect to a folded conformation (Yang *et al.* 1995). Folding was judged to be a direct result of the difference in interfacial areas of the two chains coupled with the need to fill space at approximately normal density. The fractional PEO degrees of crystallinity for these copolymers determined from DSC and WAXS measurements at the melting point (35–44 °C) ranged between X_{PEO} = 0.62 and 0.82.

The crystallization of PEO–PBO diblock copolymers with PEO block lengths of 70 or more has been studied using simultaneous SAXS and WAXS (Ryan *et al.* 1997). The copolymers crystallized from their melts (disordered, lamellar or hexagonal) with folded PEO blocks. Rapid crystallization of lamellar melts was accompanied by a change of length-scale and led to kinetically-determined multiply folded PEO blocks and to slight stretching of the PBO blocks from their melt conformation. This is apparent in Fig. 5.17 which shows SAXS profiles for a PEO–PBO diblock crystallized under different conditions. Quenching the polymers forming a hexagonal phase in the melt into the solid state resulted in no change in length-scale and led to structures with multiply folded PEO blocks and PBO blocks unstretched from their melt conformation, as illustrated in Fig. 5.18. That no change of length-scale was associated with the crystallization process suggests an epitaxial relationship between the melt and crystalline structure. Epitaxy between the hexagonal melt and lamellar crystalline phase was previously observed on melting a PE–PEE diblock (Hamley *et al.* 1996*b*), as discussed in Section 5.2.1. The metastable folded structures that were formed during rapid crystallization did not unfold on heating but could be self-seeded to grow equilibrium structures with fewer folds. It was pointed out that the folded states are controlled by a balance of contributions to the Gibbs energy from PEO block folding (positive contribution) and PBO block relaxation (negative contribution). The kinetically-induced folded structures of PEO homopolymer have much larger stem lengths than those of the equilibrium folded structures of the diblocks. This emphasizes the importance of the competition between the two low Gibbs energy conformations in the block copolymers, i.e. unfolded PEO blocks and unstretched PBO blocks (Ryan *et al.* 1997).

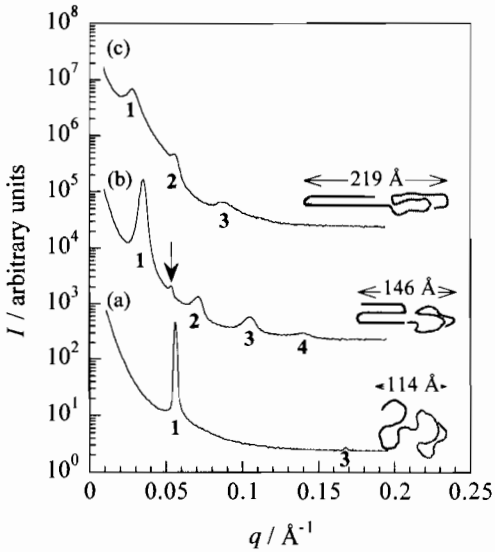

Fig. 5.17 SAXS patterns for $PEO_{76}PBO_{38}$ showing: (a) the ordered melt structure (T = 90 °C); (b) a metastable structure at T = 42 °C; (c) the equilibrium once-folded structure grown at T = 50 °C by a self-seeding process (Ryan *et al.* 1997). Numbers indicate the order of reflection from a lamellar structure and the arrow indicates the position of the peak in the ordered melt. The calculated repeat lengths for possible molecular conformations are indicated.

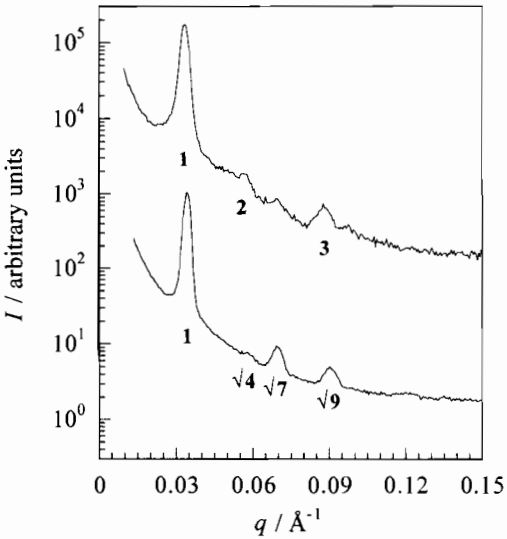

Fig. 5.18 SAXS patterns for copolymer $PEO_{115}PBO_{103}$ showing that q^* is the same for the ordered melt and the metastable crystalline structure, suggesting an epitaxial relationship between these phases (Ryan *et al.* 1997).

A more extensive study of crystallization in PEO–PBO diblocks with both ordered (hexagonal, lamellar and $Ia\bar{3}d$) and disordered melts has been published (Mai *et al.* 1997). SAXS and WAXS were combined with LFRS and DSC. The enthalpy of fusion was determined using DSC to be in the range ΔH^0_{fus} = 44–138 J g^{-1}; these values were used to calculate the degrees of crystallinity X_{PEO} = 0.70–0.83 using the known enthalpy of fusion of perfectly crystalline PEO. The effect of crystallization under different conditions on the melting point and lamellar spacings was investigated using DSC and SAXS respectively. Samples were cooled or quenched from above the melt temperature, or annealed at temperatures below T_m or were examined as removed from storage without further treatment. Finally, self-seeding was achieved by heating to the melting point, holding for 30–60 s, quenching to $T_m - 5$ °C, holding for 12–24 h and finally quenching to 20 °C. It was found that the lamellae in all crystals formed by quenching could be thickened by annealing. This is illustrated by the increase in d during annealing at 51 °C evident on the right-hand side of Fig. 5.19. However, the d spacings obtained from SAXS experiments after a period of annealing did not match the larger spacings obtained by self-seeded crystallization at high temperature. A model of helical PEO chains and oriented PBO chains was best able to account for the folding of both blocks. In this model the orientation of PBO chains emerging from the crystal end surface is maintained, so as to form an array of PBO blocks similar to a smectic liquid crystal. In contrast, in a 'normal density' model both blocks would have their normal densities, but this is inappropriate for short (extended) PBO blocks. Both PEO and PBO blocks can fold; however, due to the smaller cross-section of PEO, only conformations with more folds in the PEO block are usually accessed. Denoting the number of folds by (f,g), where

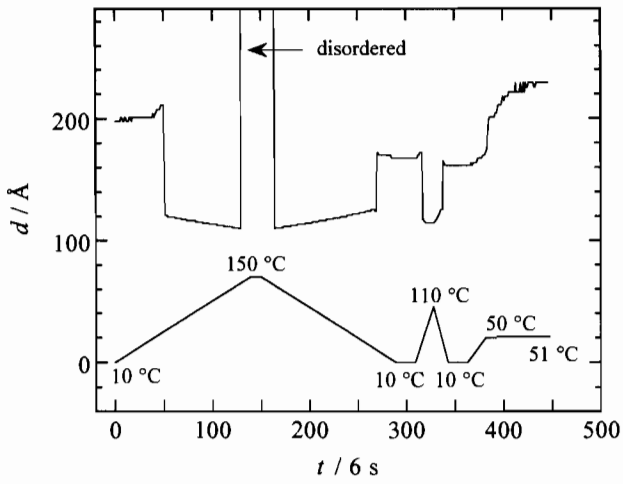

Fig. 5.19 Domain spacing (top line) obtained from SAXS for copolymer $PEO_{75}PBO_{54}$ as a function of time during the melting and crystallization programme indicated by the lower line (Mai *et al.* 1997). The melt has a gyroid structure.

f is the number of folds in the PEO block and g is the number of PBO folds, it was found that conformations with $f = g$ are disfavoured due to the mismatch in block cross-sectional areas and densities, as evident from an inspection of Fig. 5.20. These results were summarized in a diagram relating the extent of folding in the PEO block in the equilibrium state to the PEO and PBO block lengths in the copolymer, illustrated in Fig. 5.21 (Mai *et al.* 1997).

End-capped poly(ethylene oxide)

Crystallization in poly(ethylene oxide) capped with alkoxy end-groups, i.e. in highly asymmetric block copolymers, has been studied by Booth and co-workers (Al Kafaji and Booth 1981; Booth *et al.* 1979; Cooper *et al.* 1978; Domszy *et al.* 1979*a*,*b*). SAXS, WAXS, Raman scattering, picnometry and DSC were used to investigate α,ω-alkoxy-poly(ethylene oxide) copolymers with PEO inner blocks with 70 to 150 chain atoms and end-blocks ranging from $n_c = 1$ to 18, where n_c is the number of methylene carbons (Cooper *et al.* 1978). Crystallization occurred from the homogeneous melt into the usual crystalline structure, with alternating layers of crystalline PEO and non-crystalline methylene chains together with a significant fraction of the amorphous PEO. The PEO in polymers with longer methylene chains was found to be folded (with an average of 1.7 crystalline sequences per molecule, i.e. in molecules were not fully once-folded), whereas

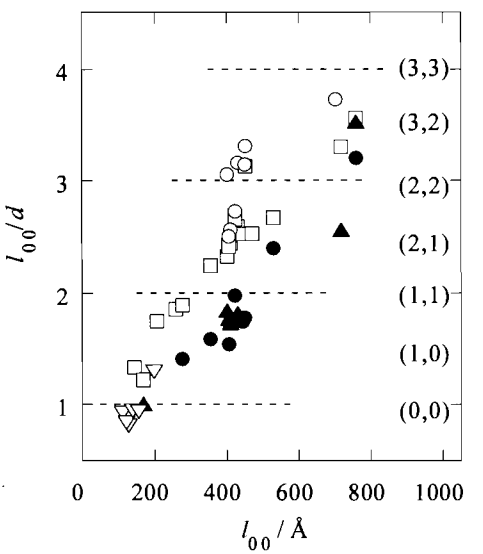

Fig. 5.20 Calculated lamellar spacings for copolymers with (f,g)-folded PEO and PBO blocks (l_{00}) divided by measured lamellar spacings (d) and plotted against l_{00} (Mai *et al.* 1997). Crystallization conditions are indicated by: (□) cooled at 10 °C min^{-1}; (○) quenched; (▲) annealed; (●) self-seeded. The symbol (▽) denotes results from Yang *et al.* (1995). The dashed lines indicate the integral values of l_{00}/d expected for the conformations with $f = g$.

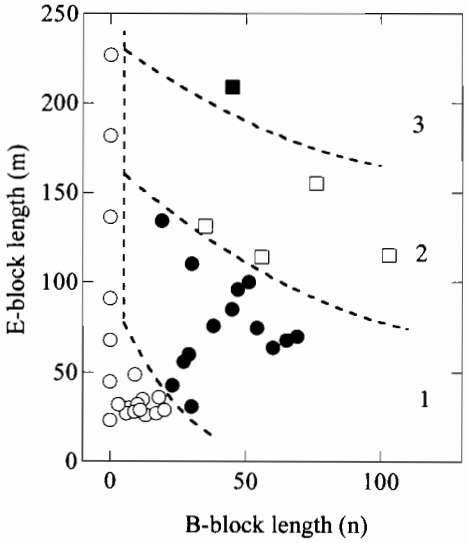

Fig. 5.21 The effect of PEO and PBO block lengths on the extent of chain folding of the PEO block in the equilibrium states of crystalline PEO_mPBO_n copolymers: (○) unfolded, (●) one fold, (□) two folds, (■) three folds (Mai *et al.* 1997). The dashed curves approximately delineate the four regions. The data points at $m = 0$ indicate the equilibrium state (unfolded) of low-molar-mass poly(oxyethylene)s.

those containing short terminal units were fully extended. The melting points were found to be independent of methylene chain lengths for extended crystals or to increase with methylene chain length for folded-chain crystals. The degree of crystallinity was determined from a number of models including that developed by Ashman and Booth (1975) (i.e. modified Flory–Vrij theory) and that of Buckley and Kovacs (1975, 1976) developed for crystallization of low-molecular-weight PEO.

Crystallization in the same type of copolymer, but with a shorter PEO block (45 units) and longer methylene chains ($n_c = 18, 21, 26, 30$), was investigated by Domszy *et al.* (1979*a*,*b*). The PEO chains were found to chain fold in all samples, and in addition the $n_c = 26$ and $n_c = 30$ methylene chains folded at low crystallization temperatures. The degree of crystallinity was found to be low in solids in which both chains crystallized, which was speculated to be due to crystallization of one component reducing crystallization of the other within the same molecule. The melting points of the PEO lamellae increased markedly as the methylene chain length was increased. This was explained by the high free-energy change on mixing ethylene oxide and methylene chains on melting the solid to a homogeneous melt, which is increased by segregation of longer methylene segments in the lamellar solid. Melting temperatures and lamellar spacings in end-capped PEO with a molecular weight of $2\,kg\,mol^{-1}$ were meas-

ured by Booth *et al.* (1979). Chain folding and melting thermodynamics were determined for polymers with a range of benzyloxy or alkoxy end-groups. Completely folded crystals were not observed; the average number of folds per stem for folded chains ranging between 1.27 and 1.72. The enthalpy of fusion was found to depend on whether the chain was folded or not, taking values $\Delta H^0_{fus} = 170 \pm 5\,J\,g^{-1}$ for the extended chain crystal and $\Delta H^0_{fus} = 145 \pm 5\,J\,g^{-1}$ for folded chain crystals, irrespective of the end-group. The melting point, being sensitive to the end surface free energy, was less useful as an indicator of chain folding (Booth *et al.* 1979).

Qualitatively similar findings were reported for α-methyl-ω-alkoxypoly(oxyethylene) polymers, which (neglecting the methyl group) can be considered as highly asymmetric diblocks of PEO and poly(methylene) (Al Kafaji and Booth 1981). All the polymers studied (from methoxy to octadecyloxy) could be obtained in extended chain conformation by annealing above a critical temperature for chain unfolding (T_x) following crystallization at a lower temperature. In contrast, for folded polymers, annealing at low temperatures enhanced the stability of lamellar crystals without promoting unfolding. Short copolymers (with $n_c = 4$ or 5) were not observed to fold, and T_x was found to be higher for copolymers with longer alkoxy chains. For all copolymers, fully once-folded crystals were not observed, the value of L/d ranging between 1.4 and 1.8 for the partly folded copolymers (Fig. 5.22). Evidence for a critical unfolding temperature is provided by Fig. 5.23 which shows DSC curves for α-methyl-ω-octadecyloxypoly(oxyethylene) crystallized at 35 °C and annealed at 35 °C and 43.5 °C. In the former case, a substantial fraction of the folded chain lamellar crystals does not unfold (even at a slower heating rate than that corresponding

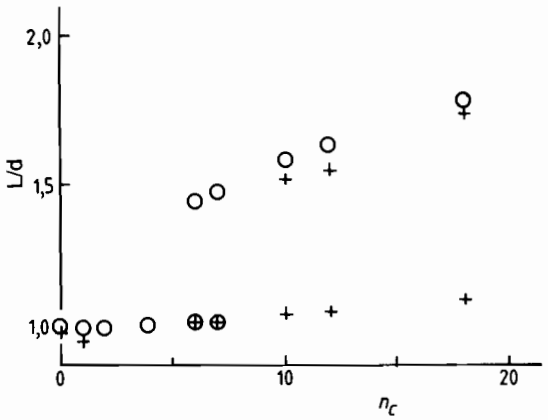

Fig. 5.22 Ratio of molecular length to lamellar thickness plotted against the number of alkyl chain atoms (n_c) for α-methyl-ω-alkoxypoly(oxyethylene) polymers (Al Kafaji and Booth 1981). The number of EO repeats was 53. Crystallization was at $T_c = 20$ °C (○) and $T_c = 35$ °C (+) for a time $t_c = 30$ min.

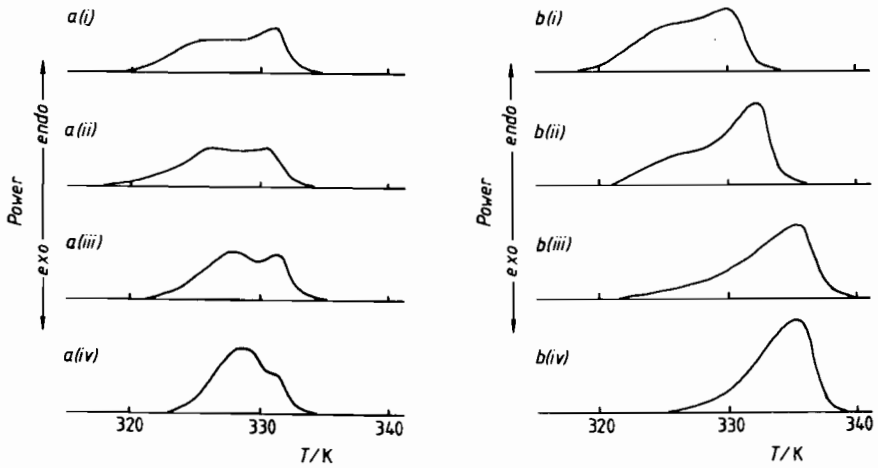

Fig. 5.23 DSC curves of α-methyl-ω-octadecylpoly(oxyethylene) crystallized at T_c = 35 °C for 30 min, at a heating rate of 16 °C min^{-1} (Al Kafaji and Booth 1981). (a) Annealing temperature T_A = 35 °C; (i) annealing time t_A = 0, (ii) t_A = 1140 min, (iii) t_A = 4200 min, (iv) t_A = 6000 min. (b) T_A = 43.5 °C; (i) annealing time t_A = 0, (ii) t_A = 20 min, (iii) t_A = 60 min, (iv) t_A = 900 min.

to Fig. 5.23), whereas at the higher temperature annealing unfolds chains into an extended conformation, leading to a well-defined melting endotherm at a higher temperature than for the folded crystal (Al Kafaji and Booth 1981).

Poly(ethylene oxide)/poly(styrene) block copolymers

A comprehensive study of crystallization from solution in PS–PEO diblocks was performed in the late 1960s and early 1970s (Gervais and Gallot 1973*a*,*b*; Lotz and Kovacs 1966; Lotz *et al.* 1966).

Single crystals of PS–PEO diblocks were prepared by crystallization from dilute solution and characterized using optical microscopy by Lotz and Kovacs (1966). The principal crystal habits and their morphological variations were described and related to the unit cell of PEO. Transitions between different crystal habits and their dependence on crystallization conditions were discussed in some detail. TEM was also used to probe crystal morphology in these diblocks (Lotz *et al.* 1966). Crystallization occurred in square tablets or long strips of layers, the latter breaking up into square-shaped multilayer crystals, often consisting of twisted spiral terraces. Crystals of a PS–PEO diblock prepared by crystallization from solution are shown in Fig. 5.24. Poly(ethylene oxide) can also form square tablet single crystals when crystallized from solution (and also hexagonal single crystals). Layer thickness measurements from electron micrographs and SAXS supported a model of chain-folded crystalline PEO lamellae sandwiched between amorphous PS (Lotz *et al.* 1966).

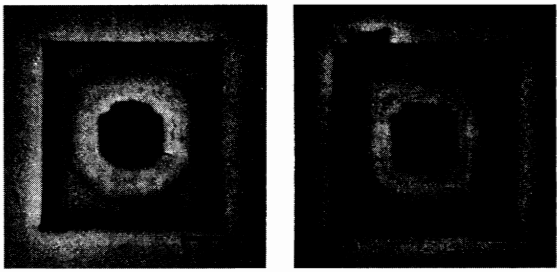

Fig. 5.24 Transmission electron micrograph of crystals (etched with ethanol) formed by a PS–PEO diblock (M_n = 34.1 kg mol^{-1}, 66 wt% PS) crystallized from solution in xylene (Lotz *et al.* 1996).

Gervais and Gallot (1973*a*) used SAXS and DSC to investigate the degree of crystallinity and chain folding in neat PS–PEO copolymers with 32–71 wt% PEO, and as a function of concentration of diethyl phthalate, which is a selective solvent for PS. Considering copolymers at a fixed concentration, the PEO melting temperature was found to decrease with decreasing PEO content in the copolymer, as might be expected. At low temperatures a lamellar crystal structure was observed using SAXS whether the high-temperatures mesophase (i.e. dry or swollen melt) structure was lamellar or hexagonal-packed cylinders. Representative phase diagrams are shown in Fig. 5.25. The PEO was shown to be crystalline using WAXS and formed spherulitic structures. It was found (via SAXS measurements of the PEO layer thickness) to be highly folded, with up to 28 folds at 25 °C for one diblock! Folding with stems perpendicular to the lamellar interface was assumed. The number of folds and the interfacial area per PS block were found to increase with increasing molar mass of the PS block. For copolymers with more than 59 wt% PEO, the number of folds also increased with the PEO molar mass, but the influence of PS was still dominant. For a copolymer with M_n = 9 kg mol^{-1} and 61% PEO, a step decrease in the number of folds from 8 to 7 to 6 to 5 was observed on increasing the crystallization temperature from 10 to 46 °C. The degree of crystallinity of the PEO was found to increase with the crystallization temperature and for this representative copolymer, the degree of crystallinity, X_{PEO}, was 0.58 at 25 °C and 0.66 at 35 °C.

The effect of concentration of the selective solvent for PS on the PEO crystallization was also explored by Gervais and Gallot (1973*a*). As expected, increasing the solvent concentration reduced the melting temperature of the PEO. It was found that for a given copolymer at a fixed temperature the number of folds increased (thus the PEO layer thickness decreased) as the solvent concentration increased. This is illustrated in Fig. 5.26 which shows regions of stability of structures with different number of PEO folds in the temperature–concentration plane. The PS layer was observed to swell (and the PS interfacial area to increase)

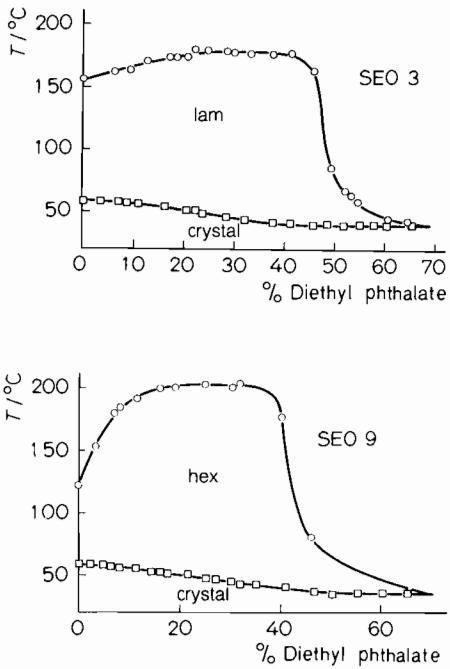

Fig. 5.25 Phase diagrams for PS–PEO diblocks in diethyl phthalate (Gervais and Gallot 1973*a*), a selective solvent for PS. SEO-3: $M_n = 34.7\,\text{kg mol}^{-1}$, 59% PEO. This sample forms a non-crystalline lamellar phase (lam) and a lamellar crystalline phase (crystal). SEO-9: $M_n = 75\,\text{kg mol}^{-1}$, 70.5% PEO. This sample forms a non-crystalline hexagonal-packed cylinder phase (hex) and a crystal phase.

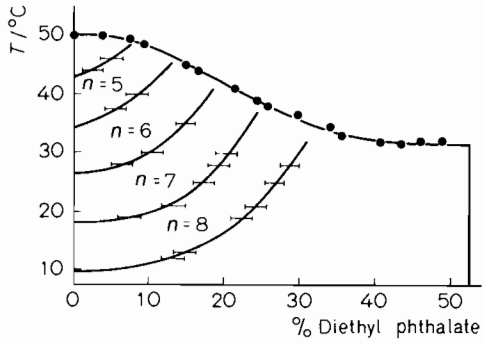

Fig. 5.26 Showing regions of stability of crystals with different numbers of folds n in the crystallization temperature–concentration plane for a PS–PEO diblock ($M_n = 9\,\text{kg mol}^{-1}$, 61% PEO) in diethyl phthalate (Gervais and Gallot 1973*a*).

with increasing solvent concentration, as demonstrated by Fig. 5.27, and this enables the PEO to adopt a more highly folded conformation.

Crystallization of PS–PEO diblocks in a selective solvent for the PEO block was investigated by Gervais and Gallot (1973*b*). A lamellar crystal structure was found below about 45 °C for solvent concentrations ranging from zero to a value characteristic of the copolymer. It was shown that the PEO crystallized in two layers separated by solvent. As the solvent concentration increased, the thickness of the solvent layer increased, separating the PEO layers but without dissolving them. It was found that above a critical PEO layer thickness (50 Å), increasing solvent concentration led to discontinuous decrements in the PEO layer thickness due to an increase in the number of chain folds by one, as shown in Fig. 5.28. At the same time, the degree of crystallinity decreased. As for PS–PEO diblocks, a lamellar crystal structure was found in PB–PEO diblocks in solvents selective for one of the blocks below about 45 °C (Gervais and Gallot 1977). The crystal structure was stable up to lower solvent concentrations for systems with thinner PEO layers. Similar results were reported to those for PS–PEO diblocks in regard to the stability of chain-folded structures in solvents selective for PB and PEO. Thus, replacing glassy, amorphous PS by rubbery amorphous PB has little effect in this context.

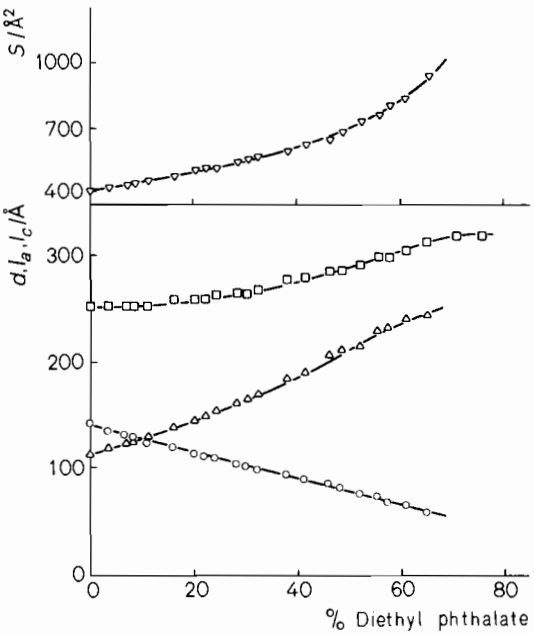

Fig. 5.27 Variation of length-scales and interfacial area (S) determined from SAXS with diethyl phthalate concentration for a PS–PEO diblock (SEO-3: details as Fig. 5.25) (Gervais and Gallot 1973*a*). (□) d, (△) l_a, (○) l_c, (▽) S.

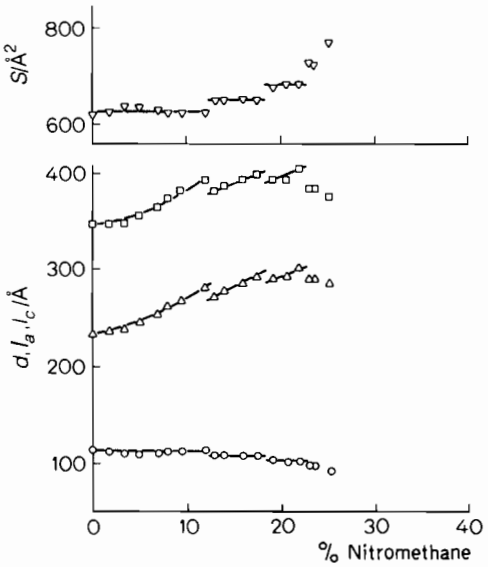

Fig. 5.28 Variation of length-scales and interfacial area (S) determined from SAXS with nitromethane concentration for a PS–PEO diblock (SEO-9: details as Fig. 5.25) (Gervais and Gallot 1973*b*). (□) d, (△) l_a, (○) l_c, (▽) S.

Other poly(ethylene oxide)-containing copolymers

The crystallization of PEO–poly(α-methyl styrene)–PEO triblocks from dilute solutions in selective solvents was investigated using electron microscopy by Kawai *et al.* (1969). Electron micrographs showed that the mid-block chains were excluded from the crystalline lamellae and were confined to the surface of the crystals during crystallization via chain folding of PEO. Later, Hirata *et al.* (1975) performed SAXS, TEM, optical microscopy and TEM experiments on a number of poly(ethylene oxide)–poly(isoprene) (PEO–PI) diblocks and PEO–PI–PEO triblocks cast from a selective and a non-selective solvent. A crystalline lamellar structure was observed when the PEO–PI samples were cast from ethyl benzene, which is a selective solvent for PI, so that microphase separation did not precede crystallization. A lamellar crystal structure was observed for a diblock with as little as 23% PEO when cast from this selective solvent. When cast from the non-selective solvent benzene, however, PEO crystallization was found to occur within microphase-separated morphologies. These morphologies might not have been in equilibrium because the crystallizable block could precipitate from solution, causing the amorphous domains to adopt non-equilibrium structures. For the lamellar crystals a model with chains perpendicular to the interface was presented on the basis of SAXS and WAXS data (Hirata *et al.* 1975).

Crystallization in a range of PDMS–PEO–PDMS triblocks was investigated using dilatometry, DSC and SAXS by Galin and Mathis (1981). They found that depending on the composition of the copolymer the PEO crystallized within

lamellar (for copolymers with $0.4 < w_{PEO} < 0.7$, where w_{PEO} is the weight fraction of PEO) or hexagonal structures (for copolymers with $w_{PEO} > 0.7$). This suggested that crystallization occurred within the pre-existing melt morphology. The degree of crystallinity and the melting point were observed to be lower than for PEO homopolymers. A feature of this work was the use of dilatometry to follow the crystallization process. The dilatometric curves showed the classical sigmoidal curves (another example is shown in Fig. 5.29) during crystallization. The initial induction period which is a complex function of the degree of supercooling and the copolymer structure is followed by a fast primary crystallization and a slower secondary crystallization process which is characterized by a slow monotonic increase in the degree of crystallinity. In most cases the secondary crystallization process was found to remain moderate, changing the degree of crystallinity in the range 5–10%. At 25–40 °C, the degree of crystallinity (X_{PEO}) ranged between 0.55 and 0.7, compared to approximately 0.8 for PEO homopolymers with $M_w \approx 10\,kg\,mol^{-1}$. The degrees of crystallinity determined from dilatometry were in good agreement with values obtained from DSC. The melting temperatures (50–59 °C) measured by DSC, dilatometry and gas chromatography were also in good agreement (Galin and Mathis 1981).

The scaling of the lamellar thickness with degree of polymerization of the crystalline and amorphous blocks was investigated for PEO–poly(*tert*-butyl methacrylate) (PEO–PtBMA) diblocks using DSC and SAXS by Unger *et al.* (1991). The non-equilibrium exponents obtained immediately after bulk crystallization were found to be different to those from equilibrium results extrapolated

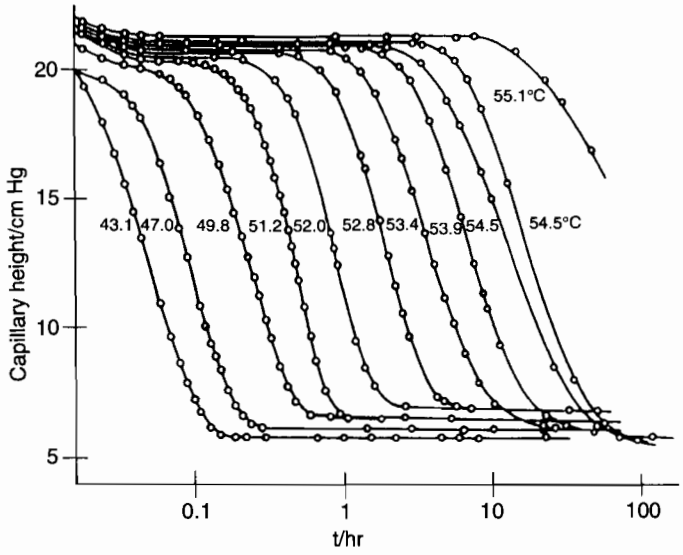

Fig. 5.29 Dilatometer capillary height during isothermal crystallization at the temperatures indicated of an α,ω-octadecyloxypoly(oxyethylene) triblock (M_w(PEO) = 11.4 kg mol^{-1}) following quenching from the melt (Thierry and Skoulios 1977).

to the equilibrium T_m. The experimental data for the scaling of the crystal layer thickness with degree of polymerization of the amorphous block were in agreement within the experimental errors with the theories of DiMarzio *et al.* (1980) and Whitmore and Noolandi (1988) (eqn 5.28), being closer to the latter. However, the scaling with total degree of polymerization was not assessed; instead the scaling with degree of polymerization of the crystalline block was determined, which cannot be directly compared to the Whitmore–Noolandi theory.

The isothermal crystallization of PEO in a PEO–PMMA diblock was monitored by observation of the increase in radius of spherulites or the enthalpy of fusion as a function of time by Richardson *et al.* (1995). Comparative experiments were also made on blends of the two homopolymers. The block copolymer was observed to have a lower melting point and lower spherulitic growth rate compared to the blend with the same composition. The growth rates extracted from optical microscopy were interpreted in terms of the kinetic nucleation theory of Hoffman and co-workers (Hoffman and Miller 1989; Lauritzen and Hoffman 1960) (Section 5.3.3). The fold surface free energy obtained using this model ($\sigma_e \approx 2.5$–$3\,kJ\,mol^{-1}$) was close to that obtained for PEO/PPO copolymers by Booth and co-workers (Ashman and Booth 1975; Ashman *et al.* 1975) using the Flory–Vrij theory.

5.2.3 Crystallization in other block copolymers

Early work

The morphology of block copolymers of poly(thiacyclobutane)–poly(isoprene)–poly(thiacyclobutane) (PTCB–PI–PTCB) with crystalline PTCB endblocks was studied using optical microscopy, electron microscopy and SAXS by Kuo and McIntyre (1975). A sample with 42 wt% PTCB solvent-cast above the melting temperature of PTCB ($T_m = 55\,°C$) but investigated at room temperature was shown to form a hexagonal structure, showing that crystallization had presumably occurred within a microphase-separated structure under these preparation conditions (Kuo and McIntyre 1975).

Poly(ε-caprolactone)-containing block copolymers

Time-resolved SAXS was employed by Nojima *et al.* (1992*a*) to examine the crystallization of poly(ε-caprolactone) in poly(ε-caprolactone)–poly(butadiene) (PCL–PB) diblock copolymers. PCL crystallizes in an essentially planar zigzag structure. The melting temperature of PCL homopolymer is $T_m = 57\,°C$, although the melting point of the PCL in the diblocks was up to 15 °C lower. A sample with an order–disorder temperature $T_{ODT} < T_m$ quenched directly from the disordered melt did not show the sharp diffraction peaks characterizing a microphase-separated phase, i.e. crystallization proceeded directly from the homogeneous state. However, for two samples with $T_{ODT} \approx T_m$ quenched from the homogeneous melt, microphase separation preceded crystallization, as evidenced by the appearance of transient sharp diffraction peaks in the SAXS

curves. The ordered melt morphology was destroyed by crystallization. An important factor in these observations was the proximity of T_m to T_{ODT} (Nojima *et al.* 1994). It was suggested that if crystallization occurs just below T_{ODT}, the energy barrier to disrupting the microphase-separated morphology can readily be overcome. An additional factor highlighted by Nojima *et al.* (1994) is the incompatibility of the diblock. The energy barrier between microphase-separated structure and crystal is expected to become larger with increasing molecular weight, N, and/or interaction parameter χ.

In subsequent work, the structure of a series of PCL–PB diblocks with fixed composition was studied as a function of copolymer molecular weight using SAXS (Nojima *et al.* 1995). It was again found that the melt morphology, disordered for several samples but ordered for others, was destroyed on crystallization, as shown by discontinuous changes in the position and intensity of SAXS peaks and directly in TEM images in samples cooled from the melt and solid states. It was found that the lamellar thickness for the amorphous layer increases more slowly with N than that for melt phases. The overall domain spacing was found to scale as $d \sim NN_a^{-\beta}$, the exponent $\beta = 0.54 \pm 0.04$ being in close agreement with the predictions of the Whitmore–Noolandi theory ($\beta = \frac{5}{12}$), and in agreement with earlier experimental results (Lovinger *et al.* 1993; Rangarajan *et al.* 1993). Results from these studies are collected together in Fig. 5.30. The scaling illustrated in this figure corresponds to a stronger dependence of domain spacing on N (although a weaker dependence for N_a) than the $\frac{2}{3}$ law found for strongly segregated block copolymer melts (Section 2.3.1). The PCL crystal thickness evaluated from a combination of SAXS and DSC measurements was found to

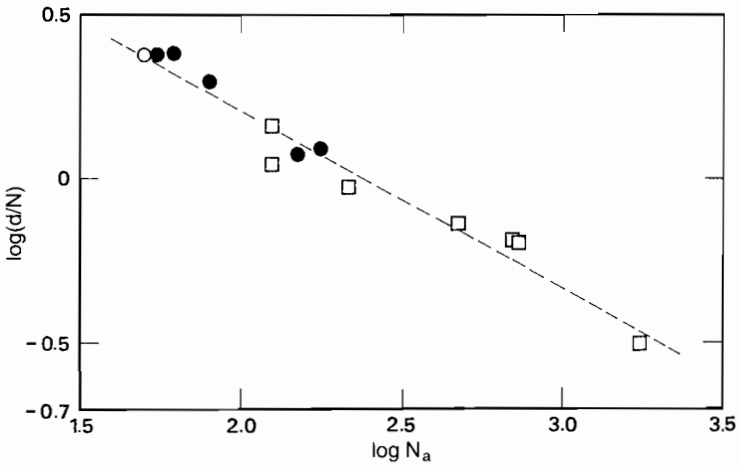

Fig. 5.30 Scaling of lamellar domain spacing (reduced by N) with the degree of polymerization of the amorphous block, N_a, for various semicrystalline diblocks (Nojima *et al.* 1995). (□) Data for PE–PEP diblocks from Rangarajan *et al.* (1993); (○) data for a PCL–PDMS–PCL triblock from Lovinger *et al.* (1993); (●) data for PCL–PB diblocks from Nojima *et al.* (1995).

be significantly reduced compared to PCL homopolymer, showing that the lamellar morphology is strongly affected by the PB blocks. The number of folds in the PCL block was calculated assuming that the crystal stems were normal to the lamellar interface; however, this assumption was not supported by experimental evidence.

The intriguing question of what happens upon crystallization in a block copolymer with two crystallizable blocks was addressed by Nojima *et al.* (1992*b*). They investigated poly(ε-caprolactone)–poly(ethylene glycol)–poly(ε-caprolactone) (PCL–PEG–PCL) triblocks using SAXS, WAXS and DSC (PEG is hydroxy-terminated PEO). Both components in these copolymers melt around 40–50 °C. The domain spacing was found to increase linearly with the length of the PCL blocks. The melting temperature showed a maximum depression for the copolymer with an equal proportion of PEG and PCL. The WAXS results revealed that the crystals of the PEG and PCL coexisted independently and that there were no eutectic or mixed crystals containing both PEG and PCL. The degree of crystallinity, extracted from the WAXS data, of one of the blocks decreased to zero when it comprised less than 25% of the block copolymer. In contrast, in a PCL/PEG binary blend, the two components were found to crystallize independently even with less than 25% of the minor component. Furthermore, in the blend, the lamellar domain spacings and melting temperatures did not change with the mixture composition and corresponded to those of the coexisting homopolymers. These results were interpreted on the basis of a model of independent crystallites of PEG and PCL in the homopolymer blend, segregated due to crystallization (as observed for other crystalline/crystalline polymer blends) (Fig. 5.31(a)). In contrast, in the block copolymer, chain connectivity was proposed to lead to crystalline PEG and PCL lamellae within individual crystallites when comparable fractions of each are present (Fig. 5.31(b)). This leads to the large reduction of lamellar thickness and the imperfectness of crystals (as evidenced by the melting temperature depression) and to the WAXS patterns corresponding to coexisting crystalline components (Nojima *et al.* 1992*b*).

The solid-state structure and thermal properties of two PCL–PDMS–PCL triblocks were probed using WAXS, optical microscopy, TEM and electron diffraction by Lovinger *et al.* (1993). Both copolymers (which differed only in the lengths of the PCL end-blocks) were found to crystallize in a lamellar structure. SAXS and electron diffraction indicated that the PCL blocks were folded once in the longer copolymer and adopted an extended conformation in the shorter one. As a result of the differing PCL content, the former crystallized as regular PCL spherulites, whereas the latter yielded only defective, immature axialites of low overall crystallinity. Electron diffraction indicated that the spherulites grew preferentially along the *b* axis of the PCL unit cell, and thus that the PCL stems were arranged perpendicular to the lamellar plane.

Other block copolymers

The morphology of two crystalline–amorphous diblocks of Nylon-6–PDMS was studied using TEM and WAXS by Veith *et al.* (1991). Each polymer (with 3 or 25 wt% PDMS) formed a spherical morphology in the melt. However, casting from

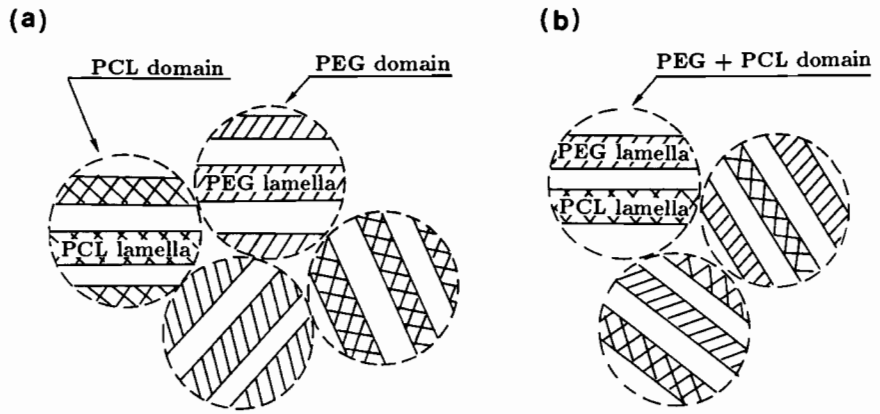

Fig. 5.31 Schematic illustration of the morphology formed by blends and copolymers of two crystallizable polymers (Nojima *et al.* 1992*b*): (a) a PEG/PCL blend, (b) a PCL–PEG–PCL triblock. In the blend, PEG and PCL are phase-separated into domains in which each homopolymer crystallizes in a lamellar texture. In the copolymer, PEG and PCL blocks cyrstallize in the same domain due to chain connectivity.

solutions in trifluorethanol (selective for Nylon-6) for the diblock with a lower PDMS content led to spherulitic structures, indicative of a lamellar crystalline phase. In contrast, in the copolymer with 25 wt% PDMS, crystallization occurred within the microphase-separated structure consisting of PDMS spheres even when cast from solution. This was suggested to be due to the onset of micellization before crystallization in the copolymers with the longer (less soluble) PDMS block. It was pointed out that solvents which are selective for the amorphous block can lead to non-equilibrium morphologies because the crystallizable block can precipitate from solution and crystallize, as observed for example by Hirata *et al.* (1975) (Section 5.2.2). Veith *et al.* (1991) also presented a useful table of solid-phase morphologies from the literature on solvent-cast semicrystalline diblocks. They suggest that the lamellar structure is not always the equilibrium one for semicrystalline diblocks but is sometimes trapped due to solvent casting. This is not accord with the findings of Ryan *et al.* (1995) and Hamley *et al.* (1996*b*), who found crystallization in a lamellar phase for a range of PE-containing diblocks including a number forming a hexagonal-packed cylinder phase in the melt. It is important to note that solvent casting was avoided in this work, thus reducing problems associated with trapped non-equilibrium morphologies.

The melting of a crystalline–amorphous block copolymer of poly(tetrahydrofuran)–poly(isoprene) (PTHF–PI) was investigated using DSC by Ishikawa *et al.* (1991). They found a double melting peak, which was proposed to result from the semicrystalline structure of the crystalline PTHF layer, with less-ordered crystallites melting before those with well-ordered domains of chain-folded PTHF. Alternative explanations include fractionation of the polydisperse block copolymer or melting of crystals with different fold lengths.

5.3 Theories for crystallization in block copolymers

5.3.1 The Thompson–Gibbs equation

The equilibrium melting temperature, T_m^0, can be obtained from data for crystals of finite thickness using the Thompson–Gibbs equation. The melting point of crystalline polymers with a well-defined crystal thickness (l_c) can be measured and the data extrapolated to $l_c^{-1} = 0$ using the Thompson–Gibbs equation (Gedde 1995):

$$T_m = T_m^0\left(1 - \frac{2\sigma}{\Delta H_{fus}^0 \varrho_c l_c}\right), \tag{5.5}$$

where ϱ_c is the crystal density, ΔH_{fus}^0 is the heat of fusion (per unit mass) and σ is the specific surface free energy. This equation is modified for a crystal which has thickened by a factor $\beta = l_c/l_c^* > 1$, where l_c^* is the initial crystal thickness:

$$T_m = T_m^0\left(1 - \frac{2\sigma}{\Delta H_{fus}^0 \varrho_c \beta l_c^*}\right). \tag{5.6}$$

The melting point of the crystal is equal to the crystallization temperature (T_c) under the assumption that $\beta = 1$. Making this substitution in eqn 5.6 and rearranging gives

$$l_c^* = \frac{2\sigma T_m^0}{\Delta H_{fus}^0 \varrho_c \left(T_m^0 - T_c\right)} \tag{5.7}$$

Thus the initial crystal thickness can be determined if the equilibrium melting temperature (obtained from extrapolation of T_m versus l_c via eqn 5.5) is known.

5.3.2 The Flory–Vrij theory

The Flory–Vrij theory (Flory and Vrij 1963) was originally developed for crystallization in homopolymers. Its application to semicrystalline block copolymers was first described by Ashman and Booth (1975). In this model, the probability that a segment chosen at random is a crystalline one is denoted f_c, which is the volume fraction of semicrystalline component. The parameter I accounts for the state of order of the chains in the crystal and is, effectively, the probability that a sequence of chain units sl_c long, where s is a positive integer (the polymer being folded if $s > 1$) does not contain a chain end. Given that the probability that the first segment is crystalline is f_c, the probability that the rest of the sequence does not contain a crystalline segment can be written for a polydisperse polymer as (Ashman and Booth 1975).

$$I = \sum_{s=1}^{\infty} \int_{sl_c}^{(s+1)l_c} w(y)\left[\left(y - sl_c + 1\right)/y\right] dy, \tag{5.8}$$

where $w(y)$ is the weight distribution of crystalline block lengths (y), which can be represented by a Schulz–Zimm distribution. The number of times the polymer chains traverse the crystalline lamellae is given by

$$t = \sum_{s=1}^{\infty} \left[\int_{sl_c}^{(s+1)l_c} s \frac{w(y)}{y} \, dy \Big/ \int_{0}^{\infty} \frac{w(y)}{y} \, dy \right]. \tag{5.9}$$

The number of folds $n = t - 1$. The melting point in the Flory–Vrij theory, as applied to block copolymers, is (Ashman and Booth 1975):

$$T_m = T_m^0 \left(\frac{1 - 2\sigma_e / \Delta H_{fus}^0 l_c}{1 - RT_m^0 \ln(f_c I) / \Delta H_{fus}^0 t l_c} \right). \tag{5.10}$$

This equation can be used to determine σ_e using the experimentally determined T_m if the other parameters are known. In the Flory–Vrij model, σ_e is the sum of the free energy of formation from the melt of the amorphous/crystalline interface, σ_0, and the free energy of formation from the melt of the amorphous layer, σ_d: (Ashman and Booth 1975; Cooper *et al.* 1978)

$$\sigma_e = \sigma_0 + \sigma_d. \tag{5.11}$$

The latter contribution can itself be written

$$\sigma_d = \sigma_m + \sigma_a, \tag{5.12}$$

where σ_m is the free energy change (enthalpy and non-combinatorial entropy changes) due to concentration changes of chain ends relative to the melt in the amorphous layer and σ_a is the free energy increase due to conformational restictions, relative to the melt, of the chains in the amorphous layer.

Assuming random mixing in the amorphous lamellae and the melt, the non-combinatorial free energy change per mole of segments on mixing can be written

$$\Delta G_m = RT\chi f_c f_a \tag{5.13}$$

where χ is the Flory–Huggins interaction parameter. Denoting the volume fractions of crystalline and amorphous components in the melt by f_c, f_a and those in the amorphous layer by f_c' and f_a', σ_m for a semicrystalline diblock can be written (Ashman and Booth 1975)

$$\sigma_m l_a = \Delta G_m = RT\chi \left[f_c' f_a' - \frac{f_c f_a}{\phi_a} \right] \tag{5.14}$$

where $\phi_a = l_a/d$. Here ΔG_m is expressed in J per mol of chain segments so that l_a is given in numbers of segments. σ_m is found to be significantly smaller than σ_a or σ_0 (Ashman and Booth 1975; Ashman *et al.* 1975), and can often be neglected.

The term σ_0 can be estimated via a simple calculation of the difference in entropy between a free chain and a chain tied at one end to an impenetrable surface. In one dimension, and for a chain with zero excluded volume, this leads to (Ashman and Booth 1975; DiMarzio 1965)

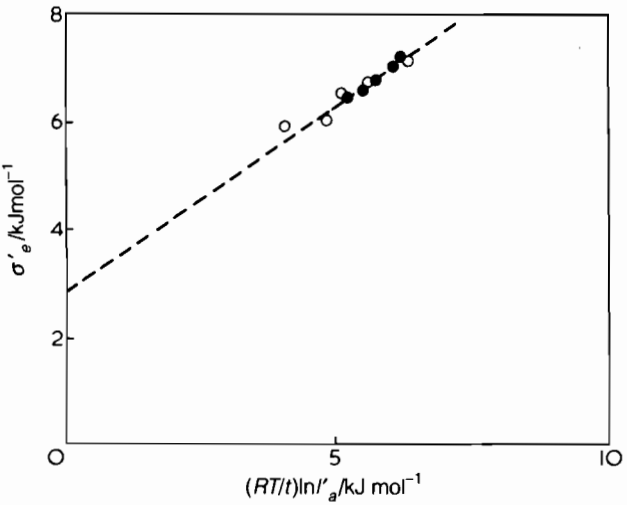

Fig. 5.32 Plot of σ'_e versus $(RT/t)\ln l'_a$, following eqn 5.17 and 5.18 (Ashman and Booth 1975). The broken line has a slope of 2/3. (●) PPO–PEO diblocks; (○) PEO homopolymers.

$$\sigma_a = RT\ln\left(l'_a\right)^{1/2} \tag{5.15}$$

where l'_a is the length of the tied chain. If allowance is made for excluded volume this equation is modified to (Bellemans 1972)

$$\sigma_a = RT\ln\left(l'_a\right)^{2/3} \tag{5.16}$$

For a crystal with $(t-1)$ folds this becomes

$$\sigma_a = \left(RT/t\right)\ln\left(l'_a\right)^{2/3} \tag{5.17}$$

where $l'_a = (tl_a/2) + 1$.

A quantity defined as (Ashman and Booth 1975)

$$\sigma'_e = \sigma_e - \sigma_m = \sigma_a + \sigma_0, \tag{5.18}$$

should be independent of mixing enthalpy terms and a plot of σ'_e versus $(RT/t)\ln l'_a$ yields σ_0 as the intercept. The plot of σ'_e versus $(RT/t)\ln l'_a$ in Fig. 5.32 for PEO–PPO diblocks and PEP homopolymers confirms the scaling 5.17. Here σ_e can be determined from eqn 5.10 and σ_m can be calculated from eqn 5.14 (or neglected to a good approximation). For PEO–PPO diblocks and PPO–PEO–PPO triblocks, σ_0 for extended chain crystals is $\approx 3\,\mathrm{kJ\,mol^{-1}}$, which compares to $\sigma_a \approx 3.5\,\mathrm{kJ\,mol^{-1}}$ and $\sigma_m < 0.5\,\mathrm{kJ\,mol^{-1}}$ (Ashman and Booth 1975; Ashman *et al.* 1975).

5.3.3 Kinetic nucleation theory

Although the kinetic nucleation theory of Hoffman and co-workers was developed for homopolymers, it has been applied to the crystallization of block copoly-

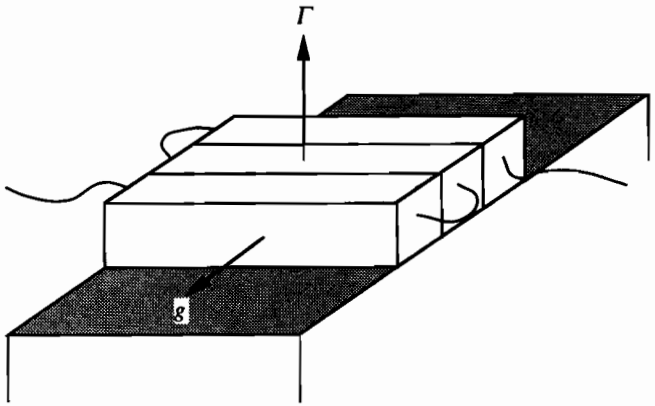

Fig. 5.33 Growth of a lamellar crystal according to the Lauritzen–Hoffmann (Lauritzen and Hoffmann 1960) theory. The lateral growth rate is denoted g and the linear growth rate Γ.

mers (Richardson *et al.* 1995). Because it has not been widely used to interpret crystallization of block copolymers, only a brief outline is presented here. In addition, there has been criticism of the theory even for homopolymers, as discussed by Gedde (1995).

In its original formulation, the Lauritzen–Hoffman theory (Lauritzen and Hoffman 1960) provides expressions for the linear growth rate (Γ), i.e. the rate at which spherulites or axialites grow, as a function of the degree of supercooling ($T_m^0 - T_c$), where T_m^0 is the equilibrium melting point and T_c is the crystallization temperature. In the model, crystal lamellae at the growth front grow at the same rate as the macroscopic linear growth rate (see Fig. 5.33). Nucleation, being either secondary or tertiary, controls the growth together with the short-range diffusion of the crystallizing units. A homopolymer of high molar mass is considered in this summary, with no allowance for fluctuations in fold lengths, i.e. the original theory (Lauritzen and Hoffman 1960) is considered. Modifications to the theory have been presented (Hoffman 1983; Hoffman and Miller 1988, 1989; Hoffman *et al.* 1976, 1979), but these do not change the essential features.

Three regimes of growth are predicted. In regime I, lateral growth of crystallites occurs with stems in a monolayer on the substrate. The lateral growth rate (g) is significantly greater than the rate of formation of secondary nuclei. Monolayers are added one by one according to the linear growth rate. In regime II, growth occurs by multiple nucleation, no longer within a monolayer, i.e. the secondary nucleation rate is faster than in regime I. Finally, in regime III, growth occurs by prolific multiple nucleation.

The growth rate in the three regimes, at a crystallization temperature T_c can be written as (Gedde 1995; Lauritzen and Hoffman 1960)

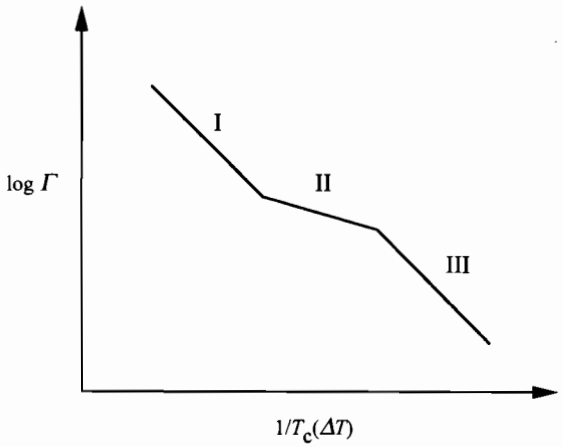

Fig. 5.34 Schematic of the growth rate in the three regimes of the Lauritzen–Hoffman theory. Here $\Delta T = T_m^0 - T_c$, where T_m^0 is the equilibrium melting point and T_c is the crystallization temperature.

$$\Gamma_i = \Gamma_{0,i} \exp\left(-\frac{U^*}{R(T_c - T_\infty)}\right) \exp\left(-\frac{2jb\sigma\sigma_L}{\Delta G k T_c}\right). \tag{5.19}$$

Here U^* is an activation energy, T_∞ is the temperature at which diffusion is stopped and $j = 2$ in regimes I and III, whereas $j = 1$ in regime II. The specific free energy of the surface is denoted σ and σ_L is the lateral surface free energy, and ΔG is the specific change in free energy on crystallization. The prefactors in eqn 5.19 depend on the growth regime:

$$\Gamma_{0,I} = b\left(\frac{kT_c}{h}\right) J_1 \exp\left(\frac{2ab\sigma\psi}{kT_c}\right), \tag{5.20}$$

$$\Gamma_{0,II} = b\left(\frac{kT_c}{h}\right) \exp\left(\frac{(2\psi - 1)ab\sigma}{kT_c}\right), \tag{5.21}$$

$$\Gamma_{0,III} \approx \frac{3\Gamma_{0,I}}{n_s}. \tag{5.22}$$

Here h is Planck's constant, b is the monolayer thickness, a is the stem length, J_1 is a constant and ψ is a fraction that parameterizes the reduction of the free energy of crystallization upon deposition of the first stem (Gedde 1995). The parameter n_s is the number of stems in a length of the growth substrate, and is approximately 240 for PE (Hoffman 1983).

The growth rates in the three regimes are illustrated schematically in Fig. 5.34.

5.3.4 The theory of DiMarzio *et al.*

A theory for crystallization in block copolymers was presented by DiMarzio *et al.* (1980). They considered lamellar structures with alternating layers of amorphous and crystalline blocks, with crystalline chains folded perpendicular to the interface. It was emphasized that the tendency for chains to be extended in the crystalline region is opposed by the preference for coiled chains in the amorphous block, and that these opposing tendencies lead to an equilibrium degree of chain folding in the crystalline layer (DiMarzio *et al.* 1980). Their model allows for the stretching of polymer chains, the change in packing entropy arising from changes in orientation of bonds, and the space-filling properties of the chains. It is purely an entropic model, with no allowance for the enthalpic mixing terms considered in the Flory–Vrij theory. Expressions were given for the thickness of the amorphous and crystalline lamellae, l_a and l_c, as functions of the lengths of the blocks, N_a and N_c, the surface and fold free energies, σ_s and σ_f, the amount of solvent in the amorphous phase $v_0 = 1 - v_x$, (v_x is the volume fraction of polymer) and the densities ϱ_a and ϱ_c ($\varrho_a = v_x\varrho_0$, where ϱ_0 is the density of pure amorphous polymer). DiMarzio *et al.* found that the amorphous lamellar thickness is

$$l_a = \frac{N_a^{2/3}\left(\sigma_s + \sigma_f \varrho_c\right)^{1/3}}{\left(3kT\varrho_a\right)^{1/3}}, \tag{5.23}$$

whereas the crystalline lamellar thickness is

$$l_c = \frac{N_c \varrho_c^{2/3}\left(\sigma_s + \sigma_f \varrho_c\right)^{1/3}}{\varrho_c\left(3kT\right)^{1/3} N_a^{1/3}}. \tag{5.24}$$

Measurements of the lamellar domain spacing by a number of groups (Douzinas *et al.* 1991; Nojima *et al.* 1995; Rangarajan *et al.* 1993; Unger *et al.* 1991) as a function of N_c yielded exponents consistent with eqn 5.24. However, this comparison assumes that $d = l_c$ which is not usually even a good approximation, thus the agreement seems fortuitous.

5.3.5 The theory of Whitmore and Noolandi

A more comprehensive theory for the thermodynamics of semicrystalline diblocks was developed by Whitmore and Noolandi (1988). The self-consistent mean field theory was applied to diblocks with one amorphous block and one crystallizable block. The amorphous regions were modelled as flexible chains, and the crystalline regions as folded chains. Both monolayers and bilayers of once-folded chains were considered. We do not give details of the self-consistent field equations here. Those for the amorphous block are the same as those for block copolymer melts (see the Appendix), whilst the free energy associated with the crystallizable block was simply a constant fold energy, chosen to be that for PS–PEO diblocks, for which comparison was made with experimental results from the literature (Gervais and Gallot 1973*a*,*b*, 1977).

Whitmore and Noolandi obtained scaling relationships for a number of quantities. For the number of times the polymer chains traverse the lamellae, at equilibrium,

$$t \propto W^{2/3}\left(\frac{k_B T}{E_{fold}}\right)^{1/3} N_a^{5/12} \tag{5.25}$$

where E_{fold} is the fold energy ($\approx 1.6 \times 10^{-20}$ J (Hoffmann *et al.* 1976)) and $W = 1$ or 2 for the single- or double-layer models respectively. A parameter $\alpha = (3/N_a)^{1/2}(d_A/a_A)$ was introduced by Whitmore and Noolandi as a measure of the thickness of the amorphous region relative to unstreched blocks (here a_A is a segment length). It was found to scale as

$$\alpha \propto W^{1/3}\left(\frac{E_{fold}}{k_B T}\right)^{1/3} N_a^{1/12}. \tag{5.26}$$

Finally the total domain spacing was found to scale as

$$d \propto W^{1/3}\left(\frac{E_{fold}}{k_B T}\right)^{1/3} N N_a^{-5/12}. \tag{5.27}$$

This leads to individual lamellar thicknesses

$$l_c \propto N_c N_a^{-5/12} \tag{5.28}$$

and

$$l_a \propto N_a^{7/12}. \tag{5.29}$$

The only difference between single and double layer models is in the prefactors of eqns 5.25–5.29. Experiments by several groups support the scaling (eqn 5.27) (Douzinas *et al.* 1991; Nojima *et al.* 1995; Rangarajan *et al.* 1993) (see Fig. 5.30) whilst Unger *et al.* (1991) reported SAXS results in agreement with eqn 5.28.

5.4 Crystallization kinetics in semicrystalline block copolymers

Poly(ethylene)-containing block copolymers

The kinetics of crystallization in PE-containing diblocks have been studied using simultaneous synchrotron SAXS and WAXS (Hamley *et al.* 1997*a*; Ryan *et al.* 1995). Using synchrotron radiation it proved possible to obtain diffraction patterns in 6 s, sufficient to ensure that the development of crystallinity could be followed with high temporal resolution. The development of PE crystallites (with an enhanced scattering contrast compared to the initial melt state) was followed via the SAXS invariant (eqn 5.3) using an Avrami equation (Avrami 1939). The Avrami theory is based on the nucleation and growth of crystallites, and is not specific to polymers. For athermal crystallization it is assumed that all crystal nuclei are formed and start to grow at time $t = 0$, the crystallites then grow at a constant rate until their boundaries meet leading to the formation of spherulites (Gedde 1995). In thermal crystallization, crystallites are nucleated at a constant

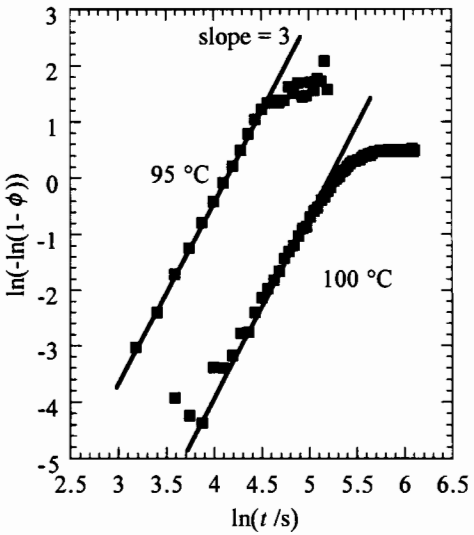

Fig. 5.35 Avrami plots showing the growth of the relative degree of crystallinity (ϕ) for a PE–PEE diblock ($M_n = 23\,\text{kg mol}^{-1}$, $f_{PE} = 0.49$) at 95 °C and 100 °C (Ryan *et al.* 1995). The double logarithm of the relative degree of crystallinity determined from the SAXS invariant is plotted against the logarithm of the time.

rate in space and time. For athermal and thermal crystallization, the initial radial growth of spherulites occurs during primary crystallization. This is followed by the slower process of secondary crystallization, where crystal thickening behind the crystal front occurs, together with the formation of subsidiary crystal lamellae and an increase in crystal perfection (Gedde 1995). Nucleation and growth via different mechanisms can be described using the Avrami equation

$$1 - \phi = \exp\left(-kt^n\right) \tag{5.30}$$

where ϕ is the relative degree of crystallinity, k and n are constants which depend on the nucleation and growth mechanism. For the PE–PEE diblocks (and PE homopolymers) studied by them, Ryan *et al.* (1995) and Hamley *et al.* (1997*a*) observed $n = 3$ (see Fig. 5.35). This is consistent with the athermal growth of spherulites in three-dimensional space, as usually observed for the growth of lamellae in crystallizing polymers. However, it was found that this exponent does not describe the secondary crystallization process.

The crystallization kinetics of PE-containing diblocks as a function of quench temperature below the PE melting temperature have been analysed using the Avrami equation (Hamley *et al.* 1997*a*). For a glassy PVCH-containing polymer $n = 3$ was found in the initial growth regime block, in agreement with the Avrami exponent for symmetric diblocks containing a rubbery amorphous block (e.g. PEE). However, the onset of crystallization was suppressed to lower temperatures in the PVCH-containing sample, indicating that grafting the PE chains to glassy

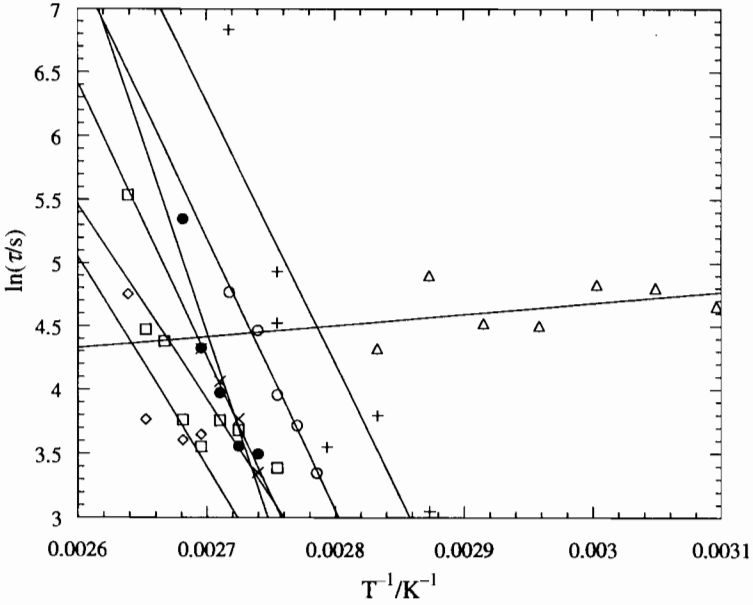

Fig. 5.36 Arrhenius plots of characteristic times $\tau = k^{-1}$ versus inverse temperature for (□) PE homopolymer (M_n = 23 kg mol^{-1}), (○) PE homopolymer (M_n = 180 kg mol^{-1}), (◇) PE–PEE diblock (M_n = 20 kg mol^{-1}, f_{PE} = 0.55), (x) PE–PEE diblock (M_n = 44 kg mol^{-1}, f_{PE} = 0.75), (+) PE–PEE diblock (M_n = 8.1 × 10^4 g mol^{-1}, f_{PE} = 0.50), (●) PE–PEE diblock (M_n = 23 kg mol^{-1}, f_{PE} = 0.49), (△) PE–PVCH diblock (M_n = 15 kg mol^{-1}, f_{PE} = 0.52). The lines are fits to Arrhenius equations.

walls significantly changes the crystallization process. The PE lamellar thickness l_c = 35 Å was smaller for this sample than for the diblocks containing an amorphous block (Section 5.2.1), also due to the constraint imposed by the glassy lamellae. Comparisons of crystallization rates and growth mechanisms were made by Hamley *et al.* (1997*a*) with high- and low-molecular-weight PE homopolymers (prepared by hydrogenation of 1,4-PB). The semicrystalline diblocks containing a rubbery block generally exhibited similar behaviour to the homopolymers. For diblocks and homopolymers, the characteristic time for crystallization, extracted from the Avrami fits, was shown to follow Arrhenius behaviour as a function of temperature. The activation energy was obtained from a plot of $\log(\tau)$ versus $1/T$, where $\tau = 1/k$ is a characteristic time, as illustrated in Fig. 5.36. Such plots for the two PE homopolymers and a number of PE–PEE diblocks yielded $E_a = 2.5 \pm 0.7$ kJ mol^{-1}, where as for PE–PVCH the activation energy was much lower, $E_a \approx 0$ kJ mol^{-1}, even though crystallization only occurred at much lower temperatures than for other samples. Interpretation of these activation energies is complicated because the overall crystallization rate in polymers is a function of segmental flexibility, the rate of short-range transport of the crystallizing segments and of the nucleation rate, as discussed in Section 5.3.3. However, it was

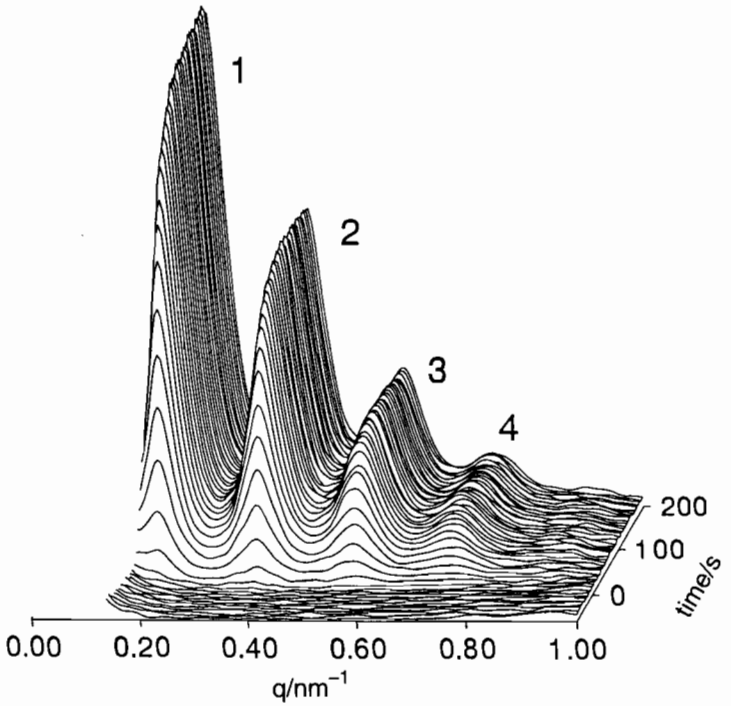

Fig. 5.37 Development of SAXS intensity profiles during isothermal crystallization at 98 °C of a PE–PEP diblock (M_w = 19.6 kg mol^{-1}, f_{PE} = 0.56) (Rangarajan *et al.* 1995*a*). Each data set is the q^2-corrected intensity integrated over 6 s.

noted (Hamley *et al.* 1997*a*) that the experimental activation energies are comparable to the heat of fusion of crystalline polymers, and were compared with a value ΔH^0_{fus} = 4.11 kJ mol^{-1} for PE homopolymer (Gedde 1995). The PE–PVCH diblock differed from the other samples due to the glassy component and the kinetics of crystallization were found to be quite different to the other samples. It was surmised that the presence of a glassy component inhibits nucleation and growth of spherulites, but instead leads to heterogeneously nucleated two-dimensional growth (Hamley *et al.* 1997*a*), which is also characterized by n = 3.

The dynamics of crystallization in PE–PEP and PE–PEE diblocks have been studied using time-resolved simultaneous SAXS, WAXS and DSC (Rangarajan *et al.* 1995*a*). It was observed that up to four orders of reflections in the SAXS profiles developed rapidly and simultaneously during isothermal crystallization following cooling from the homogeneous melt, as evident in Fig. 5.37. This showed that a domain structure with sharp interfaces, corresponding to a strongly segregated structure, developed even for small undercoolings. During the rapid primary stage of crystallization, the diblock SAXS patterns developed with constant peak positions, suggesting that the crystalline structures nucleate and grow to fill the sample, without any internal rearrangement. This contrasted with a PE

homopolymer which showed substantial changes in the crystallite size distribution over the same period. The simultaneous evolution of SAXS and WAXS data for the diblocks showed that microstructure and crystallinity developed with identical growth kinetics. At longer times, following primary crystallization, the SAXS and WAXS intensities continued to grow in parallel but at a much reduced rate. The parallel growth of SAXS and WAXS intensities indicated that the development of regions of crystalline material occurred in tandem with the creation of new lamellar stacks in regions that were previously homogeneous melts (Rangarajan *et al.* 1995*a*).

Other block copolymers

The kinetics of crystallization of a number of low-molecular-weight poly(ε-caprolactone)–poly(butadiene) (PCL–PB) diblocks were studied using synchrotron SAXS by Nojima *et al.* (1993, 1994), and compared to the crystallization kinetics of PCL homopolymers. The T_{ODT} for one sample was estimated to be below room temperature, whilst two other samples had T_{ODT} near T_m. The former thus crystallized directly from the homogeneous melt, whilst for the latter transient microphase-separated structures were observed following a quench, so that crystallization occurred from a heterogeneous structure. Other samples had $T_{ODT} > T_m$ and crystallized from a heterogeneous melt, one from a lamellar melt and two from a spherical melt. For the samples crystallizing from the ordered melt, it was found that the increase in the crystalline morphology was accompanied by a simultaneous decrease in the microphase-separated structure throughout the phase transformation, as illustrated in Fig. 5.38. This suggests that the PCL block does not crystallize within the pre-existing microphase-separated structure, but indicates that the decay of the microphase-separated structure occurs cooperatively with crystallization from the beginning of the phase transformation (Nojima *et al.* 1993, 1994). This finding was supported by the results of Rangarajan *et al.* (1995*a*) on PE-containing diblocks. Nojima *et al.* (1993, 1994) found that the initial stage of crystallization proceeded in the same way for both diblocks and homopolymer, with an Avrami exponent, n, ranging between 2 and 3 irrespective of the crystallization temperature. Indeed, Avrami curves for crystallizations at different temperatures were found to superimpose when plotted against reduced time $t/t_{1/2}$, where $t_{1/2}$ is the crystallization half time. The values for n were comparable to those obtained for PCL and other crystalline homopolymers. This indicated that crystallization of the PCL block drives the crystal structure formation, irrespective of the microphase-separated structure. When crystallization occurred from an ordered melt, the crystallization of the diblocks was found to be significantly retarded in the late state with respect to the homopolymer, with a more gradual increase in crystallinity compared to the latter (Nojima *et al.* 1993, 1994).

5.5 Crystallization in thin films

There has been very little work in this area to date. The structure of thin crystallized films of a diblock or a triblock copolymer deposited on silicon has been

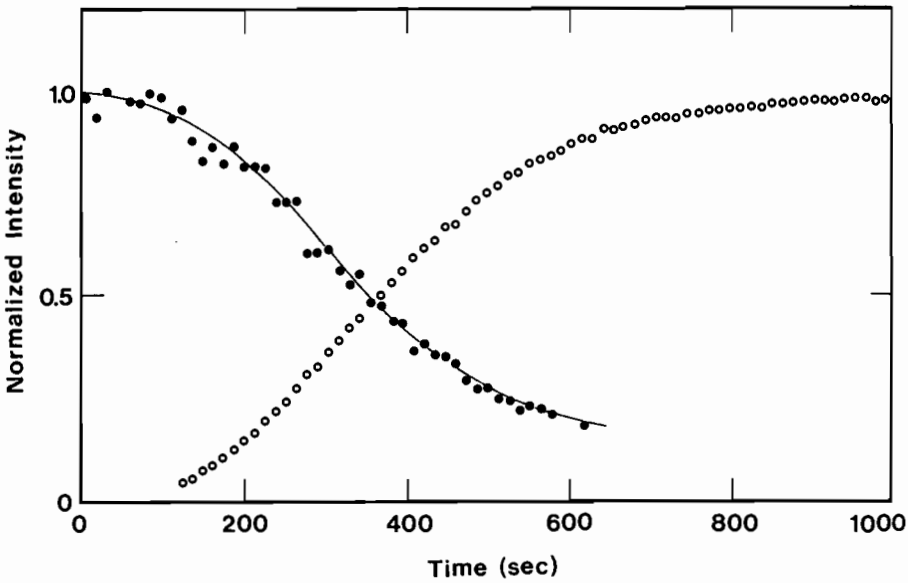

Fig. 5.38 Normalized intensities obtained from SAXS data for the isothermal crystallization of a PCL–PB diblock ($M_w = 12.5\,kg\,mol^{-1}$, 45% PCL) following a quench from the homogeneous melt to 26.5 °C (T_{ODT} is close to T_m for this polymer) (Nojima *et al.* 1992*a*): (•) melt peak; (○) crystal peak. The peak position was found not to change on crystallization.

investigated using atomic force microscopy (AFM) (Hamley *et al.* 1998). Non-contact mode AFM was used to investigate the topography of crystallites of PEO–PBO block copolymers at room temperature. The crystal thicknesses determined from AFM were compared to bulk layer spacings determined using SAXS. Two models were adopted to calculate d spacings for comparison with AFM domain heights and bulk measurements from SAXS. In both cases it was assumed that the PEO blocks were in an unfolded helical conformation (Yang *et al.* 1995). In the first model it was assumed that the PBO block had its normal liquid density. In the second model it was assumed that the PBO block was unfolded and in a trans-planar conformation, which essentially corresponds to a liquid crystal state. This liquid crystal model with a physically justified tilting of the blocks was able to account for the crystal thicknesses observed using AFM. It was shown that a triblock ($PEO_{41}PBO_{22}PEO_{41}$) largely crystallized in a monolayer as illustrated in Fig. 5.39. The model consistent with the measured crystal thickness consisted of unfolded PEO blocks at the substrate and folded (looped) PBO blocks at the polymer–air interface, and with the PEO blocks tilted at an angle of about 60° relative to the substrate plane (Fig. 5.40). Multiple layers with a common step height were observed for the diblock $PEO_{27}PBO_6$ crystallites, which were largely comprised of unfolded chains, also with chains tilted at an angle of about 60° with respect to the substrate plane (Fig. 5.40). These tilt angles

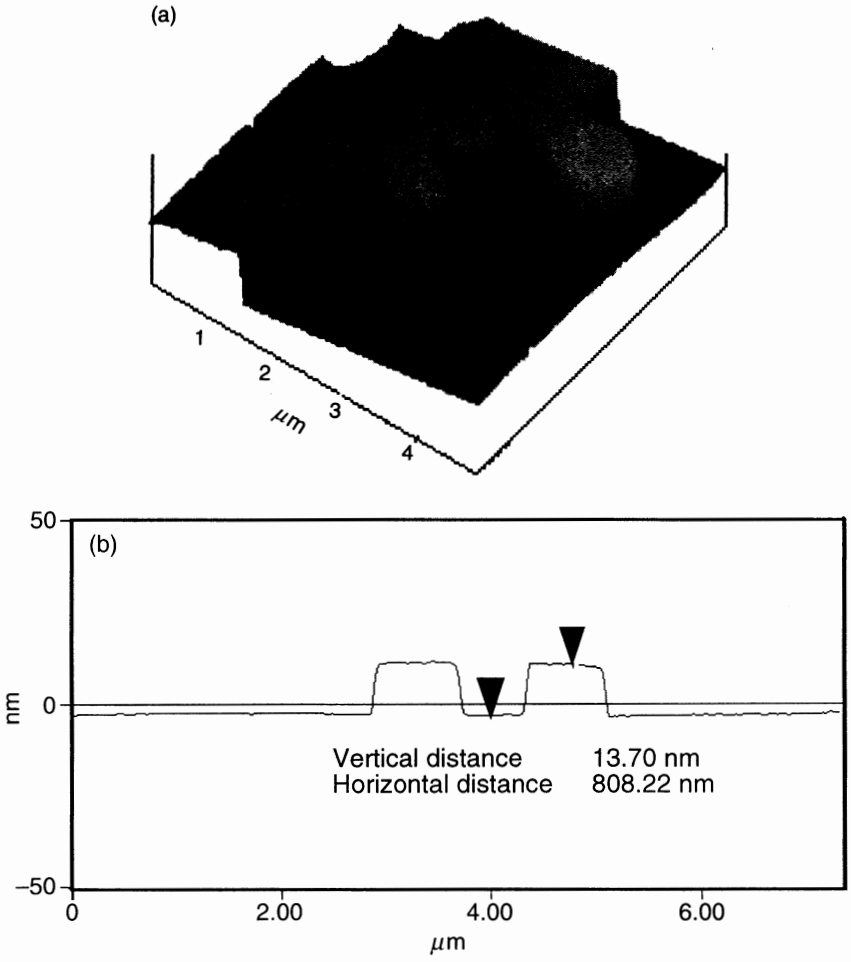

Fig. 5.39 Atomic force microscopy profiles of a crystal of $PEO_{41}PBO_{22}PEO_{41}$ on silicon (Hamley *et al.* 1998). (a) Surface plot showing the edge of a monolayer crystal. (b) Topography of steps, showing typical heights.

are consistent with tilting resulting from the displacement of a PEO chain by one repeat unit in its monoclinic unit cell (Hamley *et al.* 1998).

5.6 Structure formation in glassy block copolymers

The physics of the glass transition in block copolymers are essentially the same as those of homopolymers, and little experimental attention has been devoted to this aspect. Ordered phases in block copolymer melts can be vitrified by cooling below the glass transition temperature of a glassy block, and indeed this is often the method for preparing samples for transmission electron

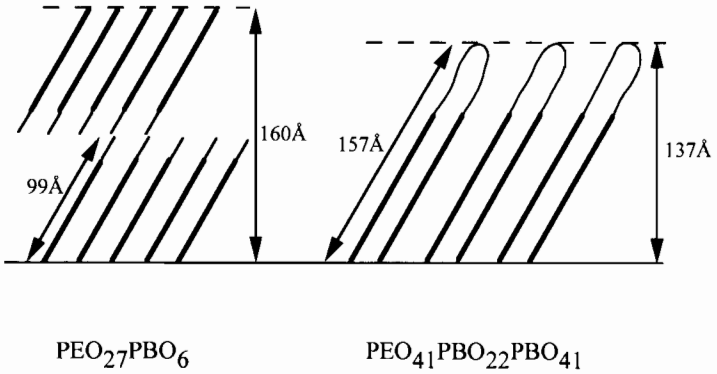

Fig. 5.40 Schematic of tilt models for thin films of copolymers $PEO_{27}PBO_6$ and $PEO_{41}PBO_{22}PEO_{41}$, consistent with AFM results (Hamley *et al.* 1998). The PEO block is shown as a thick line and the PBO block as a thin line.

microscopy. Crystallization within a pre-existing glassy lamellar structure formed by PE–PVCH diblocks has been investigated by (Hamley *et al.* 1996*a*,*b*) and is discussed in Sections 5.2.1 and 5.4.

A phenomenological theory for the glass transition in diblock copolymers was recently presented by Dobrynin (1995). It was shown that the interaction between composition flucturations, due to the loss of mobility of monomers in the glassy block, results in the elimination of microphase separation. Instead, there is predicted to be a third-order phase transition from the disordered phase into a glassy disordered phase. The calculated phase diagram also contains a narrow region of a glassy lamellar phase, between the microphase-separated lamellar and glassy disordered phases (Dobrynin 1995).

Work by Cohen and co-workers on the toughness of glassy block copolymers and crazing in these materials has been reviewed by Argon and Cohen (1990) and Spiegelberg and Cohen (1996). Glassy polymers are deformable under loading close to their glass transition temperature, but many exhibit brittle behaviour in tension. An important element in the brittleness of glassy polymers is their crazing response, because crazing almost always precedes ultimate fracture. Crazing is a form of cavitational localization of deformation, and involves the formation of a fine fibrillar polymer/void microstructure upon plastic deformation, followed by failure of the craze fibrils. Tensile experiments and craze growth rate experiments were performed on a series of PS–PB diblocks that form a PB sphere structure to elucidate the plastic behaviour due to crazing (DiCorleto and Cohen 1988; Schwier *et al.* 1985*a*). Crazing was induced from indentations using a microhardness tester. TEM indicated that crazes grow by cavitation of the PB domains. The growth rate of such crazes was modelled satisfactorily by the advance of a cavitation front in a planar layer of a thickness equal to the PB domain diameter. Crazing in PS–PB diblocks containing cylindrical PB domains was investaged via TEM and tensile experiments by Schwier *et al.* (1985*b*). TEM

revealed that crazing occurred via cavitation in the PB domains followed by necking and drawing of the continuous glassy PS matrix.

References

Al Kafaji, J. K. H. and Booth, C. (1981). *Makromoleculaire Chemie*, **182**, 3671.

Argon, A. S. and Cohen, R. E. (1990). *Advances in Polymer Science*, **91/92**, 301.

Ashman, P. C. and Booth, C. (1975). *Polymer*, **16**, 889.

Ashman, P. C., Booth, C., Cooper, D. R. and Price, C. (1975). *Polymer*, **16**, 897.

Avrami, M. (1939). *Journal of Chemical Physics*, **7**, 1103.

Balta-Calleja, F. J. and Vonk, C. G. (1989). *X-ray scattering of synthetic polymers*. Elsevier, London.

Bellemans, A. (1972). *Journal of Polymer Science C*, **39**, 305.

Booth, C. and Dodgson, D. V. (1973). *Journal of Polymer Science: Polymer Physics*, **11**, 265.

Booth, C., Domszy, R. C. and Leung, Y.-K. (1979). *Makromoleculaire Chemie*, **180**, 2765.

Booth, C. and Pickles, C. J. (1973). *Journal of Polymer Science: Polymer Physics*, **11**, 259.

Brandrup, J. and Immergut, E. H. (ed.) (1989). *Polymer handbook*. Wiley, New York.

Buckley, C. P. and Kovasc, A. J. (1975). *Progress in Colloid and Polymer Science*, **58**, 44.

Buckley, C. P. and Kovacs, A. J. (1976). *Colloid and Polymer Science*, **254**, 695.

Cohen, R. E., Bellare, A. and Drzewinski, M. A. (1994). *Macromolecules*, **27**, 2321.

Cohen, R. E., Cheng, P.-L., Douzinas, K., Kofinas, P. and Berney, C. V. (1990). *Macromolecules*, **23**, 324.

Cooper, D. R., Leung, Y.-K., Heatley, F. and Booth, C. (1978). *Polymer*, **19**, 309.

DiCorleto, J. A. and Cohen, R. E. (1988). *Polymer*, **29**, 1240.

DiMarzio, E. A. (1965). *Journal of Chemical Physics*, **42**, 2101.

DiMarzio, E. A., Guttman, C. M. and Hoffmann, J. D. (1980). *Macromolecules*, **13**, 1194.

Dobrynin, A. V. (1995). *Journal de Physique I*, **5**, 657.

Domszy, R. C., Mobbs, R. H., Leung, Y.-K., Heatley, F. and Booth, C. (1979*a*). *Polymer*, **20**, 1204.

Domszy, R. C., Mobbs, R. H., Leung, Y.-K., Heatley, F. and Booth, C. (1979*b*). *Polymer*, **21**, 588.

Douzinas, K. C. and Cohen, R. E. (1992). *Macromolecules*, **25**, 5030.

Douzinas, K. C., Cohen, R. E. and Halasa, A. F. (1991). *Macromolecules*, **24**, 4457.

Flory, P. J. (1949). *Journal of Chemical Physics*, **17**, 273.

Flory, P. J. and Vrij, S. (1963). *Journal of the American Chemical Society*, **85**, 3548.

Galin, M. and Mathis, A. (1981). *Macromolecules*, **14**, 677.

Gedde, U. W. (1995). *Polymer physics*. Chapman and Hall, London.

Gervais, M. and Gallot, B. (1973*a*). *Makromoleculaire Chemie*, **171**, 157.

Gervais, M. and Gallot, B. (1973*b*). *Makromoleculaire Chemie*, **174**, 193.

Gervais, M. and Gallot, B. (1977). *Makromoleculaire Chemie*, **178**, 1577.

Hamley, I. W., Fairclough, J. P. A., Ryan, A. J., Bates, F. S. and Towns-Andrews, E. (1996*a*). *Polymer*, **37**, 4425.

Hamley, I. W., Fairclough, J. P. A., Terrill, N. J., Ryan, A. J., Lipic, P. M., Bates, F. S. *et al.* (1996*b*). *Macromolecules*, **29**, 8835.

Hamley, I. W., Fairclough, J. P. A., Bates, F. S. and Ryan, A. J. (1997). *Polymer*, **39**, 1429.

Hamley, I. W., Wallwork, M. L., Smith, D. A. M., Fairclough, J. P. A., Ryan, A. J., Mai, S.-M. *et al.* (1998). *Polymer*, **39**, 3321.

Hirata, E., Ijitsu, T., Soen, T., Hashimoto, T. and Kawai, H. (1975). *Polymer*, **16**, 249.
Hoffman, J. D. (1983). *Polymer*, **24**, 3.
Hoffman, J. D., Davis, G. T. and Lauritzen, J. I. (1976). In *Treatise on solid state chemistry*, Vol. 3, (ed. N. B. Hannay). Plenum, New York.
Hoffman, J. D., Guttman, C. M. and DiMarzio, E. A. (1979). *Discussions of the Faraday Society*, **68**, 177.
Hoffman, J. D. and Miller, R. L. (1988). *Macromolecules*, **21**, 3038.
Hoffman, J. D. and Miller, R. L. (1989). *Macromolecules*, **22**, 3502.
Honeker, C. C. and Thomas, E. L. (1996). *Chemistry of Materials*, **8**, 1702.
Ishikawa, S., Ishizu, K. and Fukotomi, T. (1991). *Polymer Communications*, **32**, 374.
Kawai, T., Shiozaki, S., Sonoda, S., Nakagawa, H., Matsumoto, T. and Maeda, H. (1969). *Makromoleculaire Chemie*, **128**, 252.
Kofinas, P. and Cohen, R. E. (1994). *Macromolecules*, **27**, 3002.
Koppi, K. A., Tirrell, M., Bates, F. S., Almdal, K. and Colby, R. H. (1992). *Journal de Physique II*, **2**, 1941.
Kuo, C. and McIntyre, D. (1975). *Journal of Polymer Science: Polymer Physics*, **13**, 1543.
Lauritzen, E. A. and Hoffman, J. D. (1960). *Journal of Research of the National Bureau of Standards*, **64A**, 73.
Lotz, B., Kovacs, A. J., Bassett, G. A. and Keller, A. (1966). *Kolloid-Zeitschrift und Zeitschrift für Polymere*, **209**, 115.
Lotz, B. and Kovasc, B. (1966). *Kolloid-Zeitschrift und Zeitschrift für Polymere*, **209**, 97.
Lovinger, A. J., Han, B. J., Padden, F. J. and Mirau, P. A. (1993). *Journal of Polymer Science B: Polymer Physics*, **31**, 115.
Mai, S.-M., Fairclough, J. P. A., Viras, K., Gorry, P. A., Hamley, I. W., Ryan, A. J. *et al.* (1997). *Macromolecules*, **30**, 8392.
Mohajer, Y., Wilkes, G. L., Wang, I. C. and McGrath, J. E. (1982). *Polymer*, **23**, 1523.
Nojima, S., Kato, K., Yamamoto, S. and Ashida, T. (1992*a*). *Macromolecules*, **25**, 2237.
Nojima, S., Ono, M. and Ashida, T. (1992*b*). *Polymer Journal*, **24**, 1271.
Nojima, S., Nakano, H. and Ashida, T. (1993). *Polymer*, **34**, 4168.
Nojima, S., Nakano, H., Takahashi, Y. and Ashida, T. (1994). *Polymer*, **35**, 3479.
Nojima, S., Yamamoto, S. and Ashida, T. (1995). *Polymer Journal*, **27**, 673.
Quiram, D. J., Register, R. A. and Marchand, G. R. (1997). *Macromolecules*, **30**, 4551.
Rangarajan, P., Register, R. A. and Fetters, L. J. (1993). *Macromolecules*, **26**, 4640.
Rangarajan, P., Register, R. A., Adamson, D. H., Fetters, L. J., Bras, W., Naylor, S. *et al.* (1995*a*). *Macromolecules*, **28**, 1422.
Rangarajan, P., Register, R. A., Fetters, L. J., Bras, W., Naylor, S. and Ryan, A. J. (1995*b*). *Macromolecules*, **28**, 4932.
Richardson, P. H., Richards, R. W., Blundell, D. J., MacDonald, W. A. and Mills, P. (1995). *Polymer*, **36**, 3059.
Ryan, A. J., Naylor, S., Komanschek, B., Bras, W., Mant, G. R. and Derbyshire, G. R. (1994). *American Chemical Society Symposia Series*, **581**, 162.
Ryan, A. J., Hamley, I. W., Bras, W. and Bates, F. S. (1995). *Macromolecules*, **28**, 3860.
Ryan, A. J., Fairclough, J. P. A., Hamley, I. W., Mai, S.-M. and Booth, C. (1997). *Macromolecules*, **30**, 1723.
Schwier, C. E., Argon, A. S. and Cohen, R. E. (1985*a*). *Philosophical Magazine*, **52**, 581.
Schwier, C. E., Argon, A. S. and Cohen, R. E. (1985*b*). *Polymer*, **26**, 1985.
Séguéla, R. and Prud'homme, J. (1989). *Polymer*, **30**, 1446.
Skoulios, A. E., Tsouladze, G. and Franta, E. (1963). *Journal of Polymer Science C*, **4**, 507.

Spiegelberg, S. H. and Cohen, R. E. (1996). In *Polymeric materials encyclopedia*, Vol. 4, (ed. J. C. Salamone). CRC Press, Boca Raton.
Takahashi, Y. and Tadokoro, H. (1973). *Macromolecules*, **6**, 881.
Thierry, A. and Skoulios, A. (1977). *Colloid and Polymer Science*, **255**, 334.
Unger, R., Beyer, D. and Donth, E. (1991). *Polymer*, **32**, 3305.
Veith, C. A., Cohen, R. E. and Argon, A. S. (1991). *Polymer*, **32**, 1545.
Viras, F., Luo, Y.-Z., Viras, K., Mobbs, R. H., King, T. A. and Booth, C. (1988). *Makromoleculaire Chemie*, **189**, 459.
Vonk, C. G. (1973). *Journal of Applied Crystallography*, **6**, 81.
Whitmore, M. D. and Noolandi, J. (1988). *Macromolecules*, **21**, 1482.
Yang, Y.-W., Tanodekaew, S., Mai, S.-M., Booth, C., Ryan, A. J., Bras, W. *et al.* (1995). *Macromolecules*, **28**, 6029.

6 Polymer blends containing block copolymers

6.1 Introduction

In blends of two or more homopolymers with block copolymer, there is an interplay between macrophase separation of the homopolymers and microphase separation of the block copolymer. Which effect predominates depends on the relative lengths of the polymers, and on the composition of the blend.

Macrophase separation can be detected using turbidity measurements of the cloud point which generally indicates macrophase separation, i.e. this process leads to structures with a period ($\approx$ 0.1–10μm) on the order of the wavelength of light. Regions of macrophase and microphase separation can be delineated using transmission electron microscopy (TEM) and small-angle scattering techniques, microphase separation being characterized by a peak in the small-angle neutron or X-ray scattering region at non-zero q, whereas macrophase separation is characterized by $q = 0$. The segregation of block copolymers to the interface in ternary blends with two homopolymers and in other blends containing block copolymers can be determined in bulk from small-angle scattering techniques, or TEM. In thin films, neutron reflectivity, forward recoil spectroscopy and nuclear reaction analysis have been used to obtain volume fraction profiles, which quantify the selective segregation of block copolymers to interfaces.

One of the most important applications of block copolymers is as compatibilizers of otherwise immiscible homopolymers. This compatibilization results from the reduction of interfacial tension due to segregation of copolymer to the interface between homopolymers. Experiments and theory concerned with the understanding of the thermodynamics of these ternary blends are discussed in this chapter.

In binary blends, low-molecular-weight homopolymer is solubilized within a microphase-separated block copolymer structure at low concentrations. Increasing the molecular weight of the homopolymer such that it approaches that of the corresponding block in the copolymer leads to an increasing tendency for segregation of the homopolymer to the middle of the microdomain. Finally, if the molecular weight of the homopolymer is greater than that of the block copolymer, macrophase separation tends to predominate.

Binary blends of block copolymers can also macrophase separate if the mismatch in molecular weights is sufficient. In the other limit, blends of diblocks of

similar compositions and molecular weights have been used to map out phase behaviour, assuming that the blend can be approximated as a one-component system. The validity of this 'one-component' approximation has been examined using self-consistent field theory.

In this chapter, the emphasis is on the physics underlying the phase behaviour of blends containing block copolymers. The materials science of such blends has been covered in the thorough reviews of Fayt *et al.* (1989*a*) and Jiang and Xie (1991). Also homopolymer blends compatibilized by random copolymers are not considered; this subject is reviewed by Roe and Rigby (1987). The work of Hashimoto and co-workers on blends containing block copolymers is discussed in the review article by Hasegawa and Hashimoto (1996). Matsen and Schick (1996) have briefly reviewed theoretical approaches for the phase behaviour of block copolymers in blends.

This chapter is organized as follows. Section 6.2 is concerned with experiments on binary block copolymer/homopolymer blends, Section 6.3 deals with experiments on ternary blends containing a block copolymer and in Section 6.4 experiments on binary blends of block copolymers are reviewed. Theory for the corresponding type of blend is discussed successively in Sections 6.5 to 6.7. Finally, experiments on thin films are discussed in Section 6.8, separately from the work on bulk blends, in keeping with earlier chapters.

6.2 Experiments on binary block copolymer/homopolymer blends

6.2.1 General

Representative experimental work on blends of a block copolymer with a homopolymer is listed in Table 6.1.

The phase behaviour of a binary blend of a block copolymer and a homopolymer is primarily governed by the length of the homopolymer chain compared to the copolymer. Experiments by the groups of Hashimoto and Winey have led to the identification of three regimes, depending on the degree of polymerization of the homopolymer A, N_{Ah}, and that of the same component of the copolymer, N_{Ac}.

(i) If $N_{Ah} < N_{Ac}$, the homopolymer A tends to be selectively solubilized in the A domain of the microphase-separated copolymer, and is weakly segregated towards the domain centre. This leads to a swelling of the A blocks and hence also to an increase in interfacial area per block. This in turn can lead to changes in morphology. This regime has been termed 'wet brush', because copolymer chains in the strong segregation limit can be considered to be polymeric brushes, and in this case they are 'wetted' by the penetration of homopolymer chains.

(ii) If $N_{Ah} \approx N_{Ac}$, the homopolymer is still selectively solubilized in the A microdomains. However, it does not significantly swell the A block chains and tends to be more localized in the middle of the A microdomains. Hence the interfacial area is not significantly affected, and the conformations of the B chains are not significantly perturbed. This is the 'dry brush' regime.

Table 6.1 Experimental studies of binary block copolymer/homopolymer blends. Adapted and extended from Roe and Rigby (1987)

Copolymer	Homopolymer	Reference
PS–PI	PI	(Hashimoto *et al.* 1981; Inoue *et al.* 1970)
PS–PDMS	PS	(Gaines 1979; Gaines and Bender 1972; Lu *et al.* 1982)
PS–PB	PB	(Cheng *et al.* 1989; Rameau *et al.* 1982; Selb *et al.* 1983; Watanabe and Kotaka 1983)
PS–PB	PS	(Bates *et al.* 1983*a*,*b*; Berney *et al.* 1988; Disko *et al.* 1993; Jeon and Roe 1994; Kinning *et al.* 1988, 1989, 1991; Nojima and Roe 1987; Nojima *et al.* 1990; Rameau *et al.* 1982; Rigby and Roe 1984, 1986; Roe and Zin 1980, 1984; Schaefer *et al.* 1981; Winey 1992; Winey *et al.* 1992*a*; Zin and Roe 1984)
PS–PI	PS	(Hashimoto *et al.* 1981; Hashimoto *et al.* 1990; Inoue *et al.* 1970; Koizumi *et al.* 1994*a*; Tanaka *et al.* 1991; Tanaka and Hashimoto 1991*a*; Winey 1992; Winey *et al.* 1991*a*,*b*; 1992*a*)
1,4-PB–1,4PI	1,4-PB or 1,4-PI	(Cohen and Ramos 1979)
1,4-PB–1,2PB	1,2-PB or 1,4-PB	(Cohen and Torradas 1984)
Poly(α-methyl styrene) (PAMS)–PI	PAMS or PI	(Hsuie and Shih 1985)
PS–PMMA	Poly(2,6-dimethyl-1,4-phenylene oxide) (PDMPO)	(Kressler *et al.* 1990)
PS–PMMA	PS or PMMA	(Mayes *et al.* 1992)
PS–PMMA	PMMA	(Löwenhaupt and Hellmann 1991; Löwenhaupt *et al.* 1994)
PS–PMMA	Poly(styrene-*co*-acrylonitrile), PS, PMMA, poly(cyclohexyl methacrylate), polycarbonate or poly(tetramethyl carbonate)	(Löwenhaupt *et al.* 1994)
PS–poly(methyl styrene)	PVME	(Ha *et al.* 1993)
PS–PEE–PS	PEE	(Lee *et al.* 1994; Quan *et al.* 1987)
PS–PEE	PS or PEE	(Owens *et al.* 1989)
PS–PB–PS	PS	(Diamant *et al.* 1982; Flosenzier *et al.* 1990; Han *et al.* 1992; Hsuie and Ma 1984; Kimishima *et al.* 1995)
PS–PB–PS	PB	(Choi *et al.* 1973; Hsuie and Ma 1984; Toy *et al.* 1975)
PS–PB–PS	PAMS	(Han *et al.* 1992; Kimishima *et al.* 1995)
PS–PI–PS	PDMPO	(Meyer and Tritscher 1978)
PS–PAMS–PS	PS or PAMS	(Hansen and Shen 1975)
PDMS–PS–PDMS	PS	(Bajaj *et al.* 1985)
PS–poly(ethylene/butene)–PS (PS–P(E/B)–PS)	Polypropylene (PP)	(Gupta and Purwar 1985*a*,*b*)

(iii) If $N_{Ah} > N_{Ac}$, macrophase separation occurs, with domains of microphase-separated copolymer in the homopolymer matrix.

In the following, each of these regimes will be considered by discussing representative experimental results. We use the notation $\alpha = M_{Ah}/M_{Ac} = N_{Ah}/N_{Ac}$ for the ratio between molecular weights (or equivalently degrees of polymerization) of the homopolymer and the corresponding block in the copolymer.

6.2.2 The solubility limit

Most early work on blends of diblock with homopolymer was concerned with locating the regions of microphase separation and macrophase separation, i.e. the limit of solubility of the homopolymer in a microphase. This was primarily achieved using cloud point measurements, which are generally a good indicator of macrophase separation. However, caution must be exercised in some cases where large vesicles might form because solutions of large vesicles can exhibit turbidity, as noted by Kinning *et al.* (1988) who observed turbidity in systems containing elongated vesicles, as revealed by TEM.

The miscibility of a number of diblock/homopolymer systems has often been determined via cloud point measurements in tandem with other techniques. For example, Zin and Roe (1984) and Roe and Zin (1984) used SAXS and cloud point measurements to investigate the phase behaviour of blends of a PS–PB diblock or PS–PB–PS triblock with low-molecular-weight PS or PB homopolymer (forming spherical micellar phases). This work is reviewed by Roe (1985). The presence of a peak in small-angle scattering data at $q^* \neq 0$ is indicative of microphase separation, whereas strong scattering near the forward direction ($q = 0$) indicates macrophase separation. In an early study of macro- versus microphase separation, Ptaszynski *et al.* (1975) used SAXS and cloud point measurements to study mixtures of a PS–PI diblock with PS homopolymers of differing molecular weights. They found that at a fixed homopolymer molecular weight, the mixtures were transparent until a molecular weight ratio of $\alpha = 1.5$ was reached, and thereafter were visibly cloudy, consistent with the rule-of-thumb for relative molecular weights of homopolymer and copolymer. At the same time, the SAXS profiles indicated a lamellar structure for the transparent blends, and in the cloudy blends the SAXS peak positions were close to those of the pure copolymer, consistent with phase separation into copolymer-rich domains.

Löwenhaupt and Hellmann (1991) have determined whether microphase separation or macrophase separation occurs in blends of a PS–PMMA diblock with PMMA homopolymer with $\alpha < 1$ and $\alpha > 1$ using TEM. They found that the transition between purely microphase separation and macrophase separation occurs for a lower diblock content for blends with a smaller α, as supported by calculations of the instability limit using the random phase approximation. Blends with $\alpha < 1.4$ were always initially microphase separated, although in a blend with $\alpha = 1.4$ this was followed by macrophase separation. However, the macrophase-separated structure took the form of aggregates of micelles (see Fig. 6.1), suggesting a nucleation and growth mechanism for the secondary

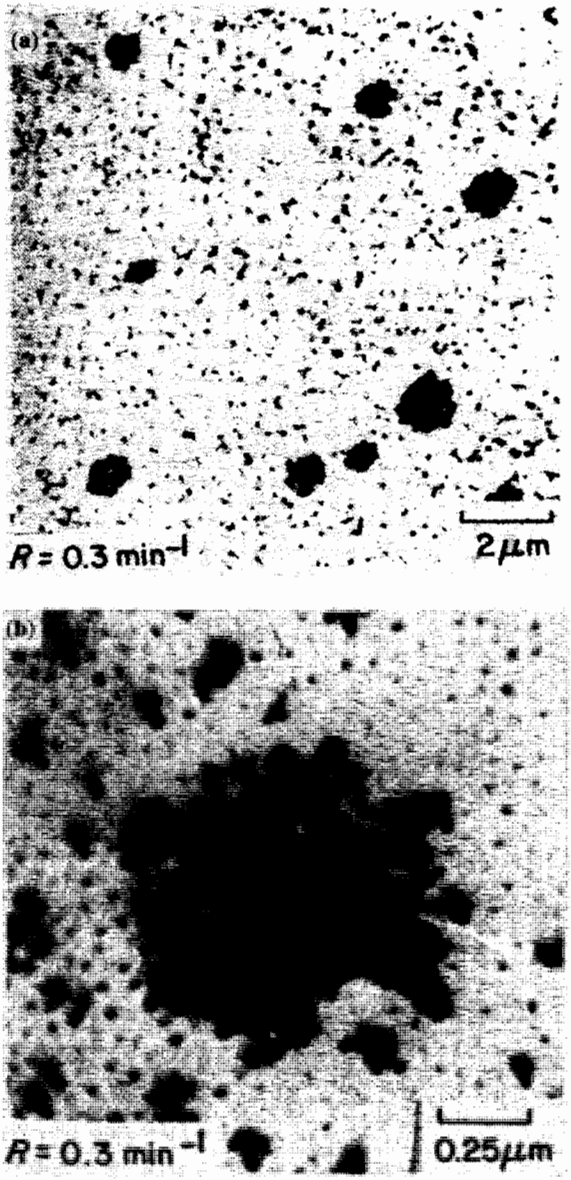

Fig. 6.1 (a) Electron micrograph showing micellar aggregates in a blend of a PS–PMMA diblock ($M_w = 175\,kg\,mol^{-1}$, $f_{PS} = 0.53$) in a blend with PS homopolymer ($M_w = 95\,kg\,mol^{-1}$) with a copolymer volume fraction $\phi_c = 0.3$, at room temperature (Löwenhaupt and Hellmann 1991). (b) Enlargement of a micellar aggregate. R denotes the solvent evaporation rate.

macrophase separation. In contrast, macrophase separation was observed to dominate the phase separation process for blends with $\alpha > 2.0$. Morphologies resembling those of typical polymer blends (see Fig. 6.2) were observed in this case. Structures similar to those for blends separating via spinodal decomposition or nucleation and growth were observed (Fig. 6.2) depending on the quench depth into the two-phase region. Jeon and Roe (1994) observed complete solubilization of PS homopolymer in a PS–PB diblock for $\alpha < 1$, whereas partial solubility was noted for homopolymers with molecular weights higher than that of the corresponding block. This confirms the rule-of-thumb value of $\alpha = 1$ for the crossover between complete miscibility and partial/complete immiscibility of the blends.

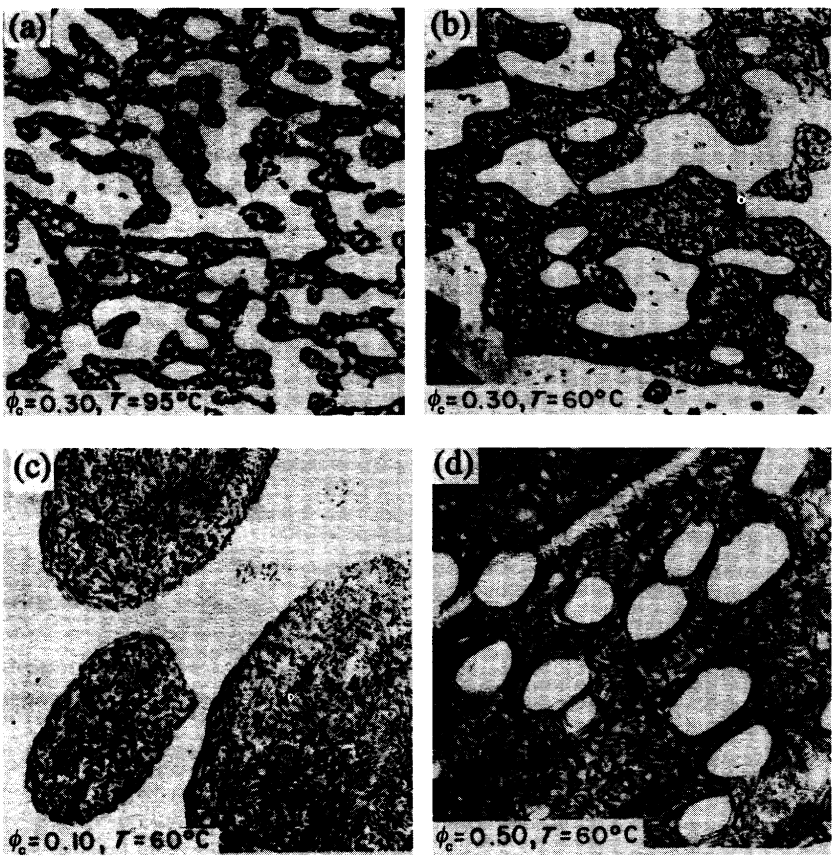

Fig. 6.2 Representative micrographs showing macrophase separation (Löwenhaupt and Hellmann 1991): (a) and (b) are bicontinuous structure, typical of those for spinodal decomposition; (c) and (d) show discrete domains, consistent with a nucleation and growth process of macrophase separation. The diblock details are as Fig. 6.1, the homopolymer has $M_w = 161\,\mathrm{kg\,mol^{-1}}$. Temperatures and volume fraction of copolymer are indicated.

6.2.3 Homopolymers with $N_{Ah} < N_{Ac}$

Disordered phase

The effect of addition of homopolymer to the χ parameter in blends of PS homopolymer and PS–PI diblocks has been studied via SAXS experiments in the disordered state (Tanaka and Hashimoto 1991*b*). The effective χ parameter was obtained from the temperature dependence of the SAXS intensity in concentrated solutions in the neutral solvent dioctyl phthalate. It was found that χ increases on addition of homopolymer, and with the degree of polymerization of the homopolymer. As usual, χ was observed to decrease with increasing temperature. Ordered structures in the same quaternary system were later probed using SAXS by Tanaka and Hashimoto (1991*a*), and the dependence of domain spacing on a reduced χ parameter was determined. A systematic study of the χ parameter in binary blends of poly(ethylene–propylene) (PEP) and poly(ethylene–butylene) (PEB) homopolymers was carried out and compared to χ for ternary blends of diblock with homopolymers (Balsara *et al.* 1993) and binary blends of diblocks (Lin *et al.* 1996). In each case, SANS was used to determine the interaction parameter in the disordered phase using the random phase approximation. At a fixed temperature, it was found to be independent of blend composition, molecular weight and blend type. Thus, within error, the χ parameter was the same as for the binary homopolymer blend. These results are evidently in conflict with those of Tanaka and Hashimoto (1991*a*), although in the latter case there is the additional complication of a fourth component, solvent, in the blend.

Jeon and Roe (1994) studied blends of a symmetric PS–PB diblock in PS using SAXS, light scattering and TEM. A representative phase diagram for this system is shown in Fig. 6.3. This includes regions of homogeneous disordered phase (transparent, region I_1) regions of macrophase separation (turbid, I_2), and the order–disorder transition (at A in the pure diblock) observed in blends with low PS content. On increasing homopolymer concentration, the ordered mesophase changed from lamellae (L) to worm-like micelles (M), as confirmed by TEM.

The order–disorder transition in binary blends of a PS–PB diblock (with 77 wt% PS) was determined using SAXS by Nojima and Roe (1987). Microphase separation was observed for blends with $\alpha < 3$, only a blend with $\alpha = 7$ was observed to be turbid, indicative of macrophase separation. It was found that the ODT in the former blends is depressed by addition of PS homopolymer. This decrease was found to be larger for larger amounts of low-molecular-weight copolymer. Similar results were reported for blends of a nearly symmetric PS–PEE diblock with PS or PEE homopolymer, studied using SAXS by Owens *et al.* (1989). They found that below a critical homopolymer molecular weight, the ODT is depressed, while for higher molecular weight the ODT is increased on increasing homopolymer content. Theory (Whitmore and Noolandi 1985*a*) predicts that this crossover occurs at $\alpha = \frac{1}{2}$ (as discussed in Section 6.5.3). However, the experimental value was found to be significantly lower (Owens *et al.* 1989).

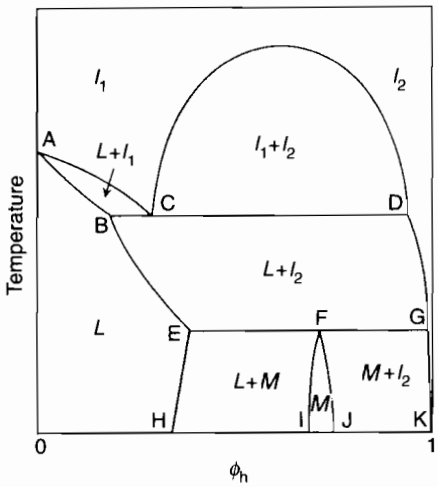

Fig. 6.3 Schematic phase diagram for lamellar PS–PB diblocks in PS homopolymer (volume fraction ϕ_h), where the homopolymer M_w is comparable to that of the PS block (Jeon and Roe 1994). L is a lamellar phase, I_1 and I_2 are disordered phases, M may correspond to microphase-separated copolymer micelles in a homopolymer matrix. Point A is the order–disorder transition. The horizontal lines BCD and EFG are lines where three phases coexist at a fixed temperature and are lines of peritectic points. The lines BE and EH denote the limit of solubility of the PS in the copolymer as a function of temperature.

Lamellar phase

The swelling of a lamellar PS–PI diblock with PS homopolymer was quantified using SAXS by Winey *et al.* (1991*b*). In general, blends with $\alpha < 1$ were investigated, although a series with $\alpha = 1.4$ was also examined. TEM was used to confirm the lamellar morphology, and the observation of a constant glass transition of PI established the presence of pure microdomains formed by strongly segregated copolymer. It was found that, for the blends with $\alpha < 1$, addition of homopolymer led to an increase in PS domain thickness, with a concomitant increase in interfacial area per block, and the PI layer thickness decreased. Jeon and Roe (1994) also observed a swelling of PS layer in PS–PB/PS blends with $\alpha < 1$, but the PB layer thickness was constant. Swelling of the PS domain was also observed (Winey *et al.* 1991*b*) for the blends with $\alpha = 1.4$, although in this case the PI domains did not contract significantly, consistent with solubilization of the homopolymer in the centre of the domain. The overall domain spacing in the blends was generally greater than that of the pure diblock, although blends with low concentrations of low-molecular-weight homopolymer were observed to have a smaller domain spacing. Increasing the homopolymer molecular weight at a fixed concentration was observed to increase the thickness of PS and PI layers and to decrease the interfacial area per block junction. The relative extent of axial and lateral expansion of the PS layer was ascertained. It was found that the PS layer swelled highly asymmetrically as the homopolymer molecular weight

increased and/or as the homopolymer concentration increased, favouring axial extension. The decrease in lateral extension on addition of homopolymer was ascribed to a reduced penetration of the PS blocks (or 'wetting of the brush') by the homopolymer, in other words an increasing tendency for segregation in the centre of lamellae with increasing α.

Lee *et al.* (1994) have also reported segregation of short homopolymers ($\alpha \ll 1$) to the centre of lamellar microdomains using SANS on a PS–PEE–PS in blends with PEE with deuterium labelling to vary contrast. However, the interpretation of these data was hampered by the qualitative nature of the model used to model the limited experimental data.

Transition from a cylindrical phase to a lamellar phase induced by addition of homopolymer

The viscoelastic behaviour of blends of an asymmetric ($f_{PS} = 0.24$) PS–PB–PS (Kraton) copolymer with PS or poly(α-methylstyrene) (PAMS) was used to map phase diagrams by Han *et al.* (1992). The neat triblock formed a cylindrical phase. Addition of PAMS of sufficient molecular weight led to the formation of a lamellar phase (Han *et al.* 1992; Kimishima *et al.* 1995). However, addition of lower-molecular-weight PAMS simply swelled the cylindrical phase (Han *et al.* 1992). Boundaries between ordered mesophases (lamellar or cylindrical) and the disordered phase were located from dynamic mechanical measurements, via the sharp decrease in dynamic moduli at the ODT. The morphologies of ordered structures were identified using SAXS and TEM, and turbidity measurements were used to locate the cloud points corresponding to macrophase separation. Addition of end-block-associating homopolymer to the triblock was found to increase the dynamic storage modulus (and plateau modulus) of the block copolymer and the solubility limits for added homopolymer depended on its molecular weight. Surprisingly, the homopolymer dissimilar to the end-block (PAMS) was found to have higher solubility limits in the triblock than homopolymer PS, which implies a lower effective interaction parameter for the former. The experimental phase diagrams were compared to those calculated using the theory of Hong and Noolandi (1983) (see Section 6.5.3). Some qualitative features were found to be similar, but as pointed out by Han *et al.* (1992), the calculated phase diagram is very sensitive to the value of χ used, which was not known accurately.

The spatial distribution of homopolymer within lamellar domains formed by the same PS–PB–PS triblock blended with homopolymer has been determined (Kimishima *et al.* 1995). Blends with PS or PAMS with molecular weights lower than that of the PS in the diblock were investigated using SAXS and TEM. It was found that both PS and PAMS were solubilized in the PS microdomains; however, the PAMS was not uniformly distributed, tending to be localized at the domain centres. This localization was diminished on increasing the temperature. In contrast, the PS homopolymer was uniformly distributed. The localization of the PAMS was ascribed to repulsive interactions between PS chains and the PAMS homopolymer, this effect decreasing with increasing temperature.

Transition from a spherical phase induced by addition of homopolymer

Cheng *et al.* (1989) investigated the spatial distribution of short labelled *d*PB chains in a blend with a PS–PB diblock containing 11 wt% PB that forms a spherical structure in the pure melt. It was shown that up to 15 mol% homopolymer could be solubilized in the spherical microdomains. For higher homopolymer contents, additional homopolymer was expelled from the spheres and formed macrophase separated domains, leading to substantial scattering near $q = 0$ in the SANS experiments, and producing notable domains of homopolymer in TEM images. The same effect was noted earlier for a PS–PB diblock blended with *d*PS (Berney *et al.* 1988). However, this was not thought to be an equilibrium event, reflecting the nature of the solvent-casting process. Experiments on blends containing longer homopolymers showed that the maximum concentration for complete solubilization of homopolymer was reduced.

Morphological transitions upon addition of PS homopolymer to PS–PB diblocks were studied by Kinning *et al.* (1988). Using TEM, they observed that transitions between ordered structures can be driven by changing the molecular weight of the homopolymer or copolymer or by varying the composition of the blend. For example, a transition from spherical micelles (liquid-like ordering) to worm-like cylindrical micelles was observed on increasing homopolymer molecular weight in a blend with a fixed copolymer content, or by increasing the copolymer content in a blend with a fixed homopolymer molecular weight. A vesicular morphology was also observed for a blend with $N_{Ah} \approx N_{Ac}$, with ellipsoidal shells of PB–PS bilayers in the PS matrix. The formation of vesicular structures was examined in more detail for the case $\alpha \approx 1$ by Koizumi *et al.* (1992) (see Section 6.2.4). Lamellar structures and multilayer lamellar structures were also observed by Kinning *et al.* (1988), although an insufficient number of samples was examined to determine rules for the circumstances under which particular morphologies are observed.

Kinning *et al.* (1989) analysed in detail micelle formation in blends of PS–PB diblocks with PS homopolymer using SAXS and TEM at low copolymer contents. The critical micelle concentration (cmc) was determined for a range of blends of symmetric and asymmetric PS–PB diblocks, all with $\alpha < 1$. A transition from isolated micelles (liquid-like arrangement) to an ordered cubic lattice (and ultimately rods) was observed on increasing the concentration of diblock, as illustrated in Fig. 6.4. This is in agreement with the earlier results of Hashimoto *et al.* (1981) and Bates *et al.* (1983*a*,*b*), who showed that addition of homopolymers to diblocks leads to a reduction of long-range structural order of PB spheres. Kinning *et al.* (1989) analysed SAXS data using the Percus–Yevick hard sphere model to obtain the structure factor. Together with TEM and analysis of the SAXS invariant (eqn 5.3), which depends on the width of the core–corona interphase, the structure of the micelles (core radius, volume fraction of PS in the core) was characterized in detail. In a subsequent paper (Kinning *et al.* 1991) these results were compared to the theory of Leibler *et al.* (1983) (Section 3.4.2) for micelle formation in block copolymer/homopolymer blends, generalized by Roe (1986) to consider asymmetric copolymers and the possibility of homopoly-

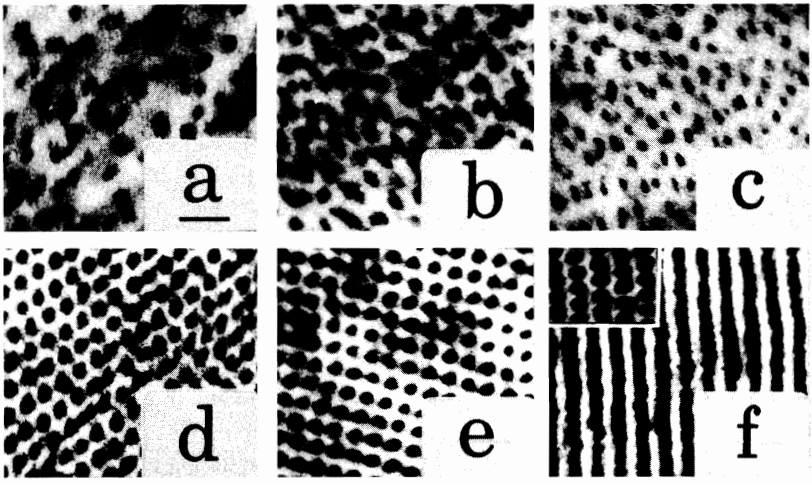

Fig. 6.4 TEM images of blends of a PS–PB diblock ($M_n = 41\,kg\,mol^{-1}, f_{PS} = 0.47$) blended with PS homopolymer ($M_n = 3.9\,kg\,mol^{-1}$) annealed at 115 °C (Kinning *et al.* 1989). Copolymer concentration: (a) 5.6 wt%; (b) 11.7 wt%; (c) 17.9 wt%; (d) 24.9 wt%; (e) 30.3 wt%; (f) 49.4 wt%. The scale bar in (a) denotes 100 nm.

mer residing in the micelle core, in the light of the experimental observation of swelling of the cores of PS–PB diblocks with PB with increasing temperature (Rigby and Roe 1986). Kinning *et al.* (1991) reported semiquantitative agreement with the theoretical predictions for the dimensions of the micelle core and corona. The trend for the cmc to decrease with increasing molecular weight of the homopolymer was reproduced. The tendency for the cmc to increase with either decreasing copolymer molecular weight (for constant copolymer concentration) or decreasing PS block length was also reproduced. However, the theory predicted cmcs of one to two orders of magnitude less than those obtained from experiments. In addition, the theory was found to underestimate the amount of free copolymer (not associated in micelles) above the cmc. It was suggested that these discrepancies could be attributed, at least in part, to the use of interaction energies in the calculations that were too large.

Roe and co-workers (Nojima *et al.* 1990; Rigby and Roe 1984, 1986; Roe 1986) have used SAXS to characterize micelles formed by PS–PB diblocks at low concentrations in blends with low-molecular-weight PB. Micellar dimensions and association numbers were determined for symmetric and asymmetric diblocks (Rigby and Roe 1984, 1986). The effective hard sphere radius, the core radius and volume fraction of hard spheres were determined using the Percus–Yevick model (Rigby and Roe 1986). These results were compared (Roe 1986) to the predictions of the theory of Leibler *et al.* (1983). The theory qualitatively reproduced the observed trend for the cmc to increase with temperature for blends containing a particular diblock. The cmc was found to decrease at a fixed temperature

on decreasing the PS content of the copolymer. Both these features were captured by the theory. SAXS was combined with SANS to elucidate the structure of PB micelles formed in blends of an asymmetric (77wt% PS) PS–PB diblock with PB by Nojima *et al.* (1990). In this work, the core–corona interface width was obtained from an analysis of the scattering data in the Porod regime (Section 1.4.11) in addition to the effective hard sphere parameters from fits using the Percus–Yevick model. Hashimoto *et al.* (1981) and Bates *et al.* (1983*a*,*b*) noted that long-range order of spherical micelles is lost on addition of homopolymer. The former observed a cubic-packed spherical structure in neat PS–PI diblocks, which transformed to a disordered phase of dispersed spheres on addition of PS, as confirmed by SAXS (see Fig. 6.5) and TEM. Bates *et al.* (1983*a*,*b*) noted the same effect using SANS and TEM on PS–PI/PS blends.

Complex phases

The formation of a bicontinuous cubic structure, identified as ordered bicontinuous double diamond (OBDD), in binary diblock/homopolymer blends was studied by Winey *et al.* (1992*a*). The OBDD structure (space group $Pn\bar{3}m$) was identified on the basis of TEM images of projections of the structure. However, as noted in Section 2.2.2, the structure identified as OBDD in block copolymer melts has subsequently been reassigned as gyroid (space group $Ia\bar{3}d$), on the basis of SAXS patterns, and this is likely to be the structure of the bicontinuous cubic phase observed by Winey *et al.* (1992*a*). The structure was observed in blends of PS–PI or PS–PB diblocks in PS homopolymer for total PS contents $f_{PS} = 0.64$–0.67. This compares well to the composition window where this structure is observed for pure PS-rich PS–PI diblocks, i.e. approximately $f_{PS} = 0.62$–0.66 (Bates and Fredrickson 1990; Hasegawa *et al.* 1987; Khandpur *et al.* 1995). If homopolymer was added to a lamellar structure to form a bicontinuous cubic structure, it was localized in the matrix of the structure. Addition of small amounts of PB or PI homopolymer to a cylindrical phase (with PB or PI rods) led to the formation of a cubic structure with homopolymer in the minority channels of the bicontinuous labyrinth. However, if large amounts of either of these homopolymers were added to a cylindrical structure in an attempt to prepare a bicontinuous phase with homopolymer in the matrix, phase separation was observed instead. In fact, the OBDD structure was not observed in blends on the low-f_{PS} side of the phase diagram, where it is observed in the melt for $f_{PS} \approx 0.28$–0.34 (Bates and Fredrickson 1990; Hasegawa *et al.* 1987; Khandpur *et al.* 1995).

'Complex' phases, induced by addition of homopolymer to a diblock forming a classical structure, have also been observed by other groups. A transition from lamellae to 'mesh' or 'strut' structures, resembling perforated layers, was reported by Hashimoto *et al.* (1992) on addition of PS homopolymer to a copolymer resin that contained four-arm star PS–PB copolymer. Disko *et al.* (1993) observed a perforated layer structure in blends of a PS–PB diblock with PS homopolymer where each block and the homopolymer had approximately the same molecular weight. The structure (shown in two projections in Fig. 6.6) was observed using TEM for blend compositions $f_{PS} = 0.65$ and 0.67. This is in good agreement with

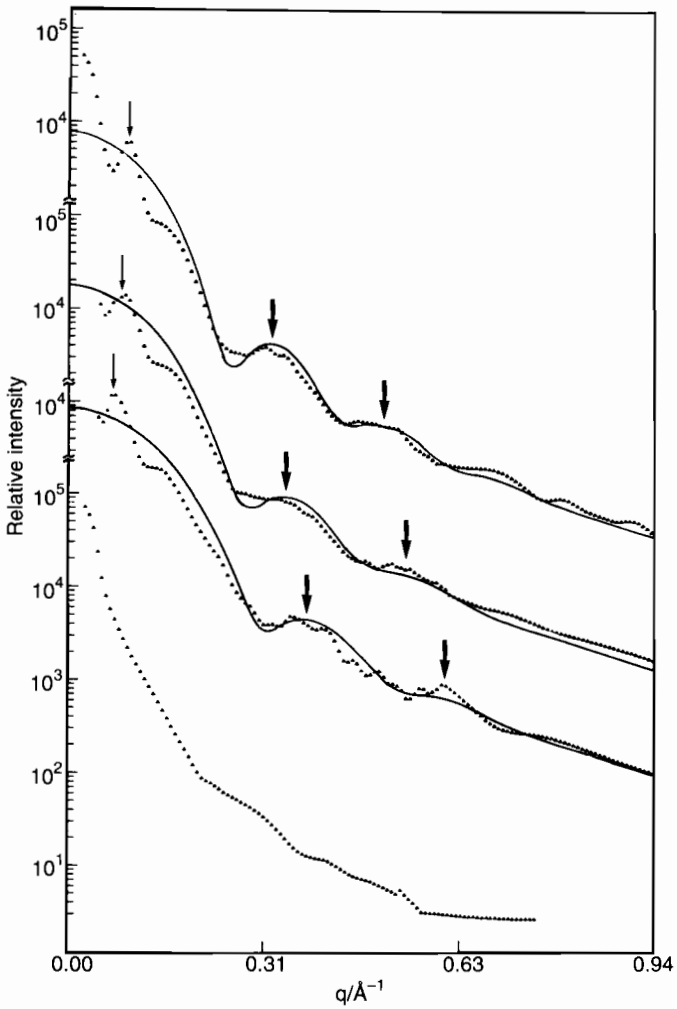

Fig. 6.5 Small-angle X-ray scattering profiles for blends of a PS–PI diblock (M_n = 200 kg mol^{-1}, 13 wt% PI) with PS homopolymer (M_n = 81 kg mol^{-1}) for (*top–bottom*) the pure diblock, a blend with 30 wt% PS, 60 wt% PS and 90 wt% PS (Hashimoto *et al.* 1981).

the composition range over which the hexagonal perforated layer (HPL) structure has been observed in diblock melts (see Section 2.2.2).

Comprehensive studies of phase behaviour

The domain spacing and interfacial area per block were determined for blends of PS–PI diblocks in PS for $\alpha \leq 1$ using SAXS by Hashimoto *et al.* (1990). The domain spacing was found to increase with increasing homopolymer volume fraction, as depicted in Fig. 6.7 for blends of a diblock forming a lamellar phase in the melt. Addition of homopolymer leads to transitions to other morphologies

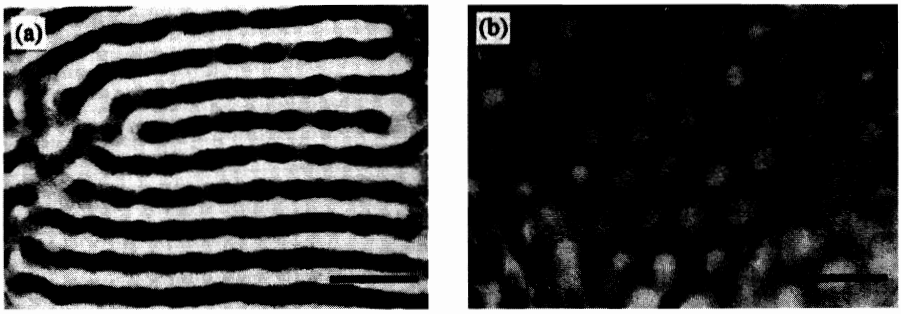

Fig. 6.6 TEM images of a 'catenoid lamellar' hexagonal perforated layer (HPL) structure in a blend of a PS–PB diblock (M = 49.9 kg mol^{-1}, 51 wt% PS) and PS homopolymer (M = 26 kg mol^{-1}) and a total PS volume fraction f_{PS} = 0.67 (Disko *et al.* 1993). The sample was annealed at 130 °C prior to microtoming: (a) view parallel to the lamellae; (b) view normal to the lamellae, showing hexagonal perforations in a PI lamella.

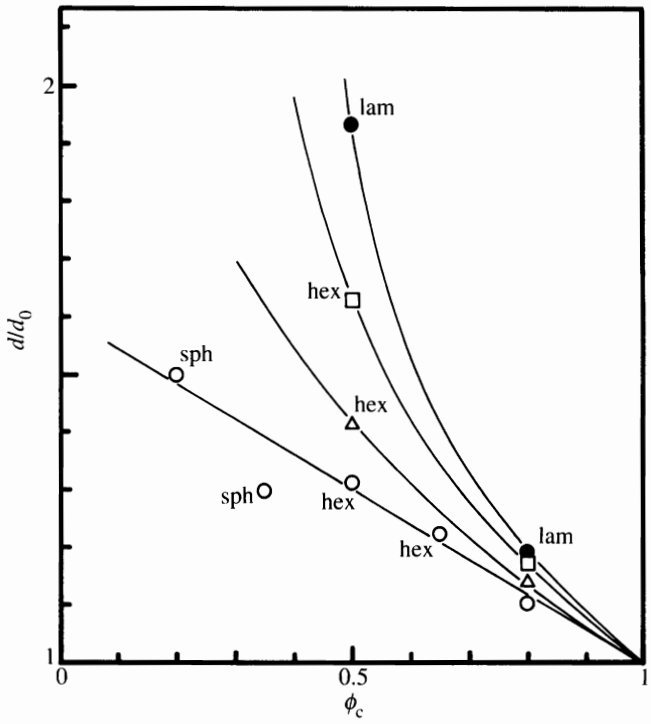

Fig. 6.7 Domain spacing of blends of a PS–PI diblock with PS homopolymer relative to that for the pure diblock (d_0 = 26.7 nm) (Hashimoto *et al.* 1990). The diblock has M_n = 31.6 kg mol^{-1}, and 48 wt% PS, the homopolymers have (○) M_n = 2.3 kg mol^{-1}, (△) M_n = 4.4 kg mol^{-1}, (□) M_n = 10.2 kg mol^{-1}, (●) M_n = 16.7 kg mol^{-1}. Experiments were performed at room temperature. The symbols L, C and S denote lamellar, cylindrical and spherical microstructures.

for $\alpha < 1$, as indicated in the figure. The increase in domain spacing is consistent with swelling of the PS domain resulting from solubilization of the homopolymer. It is also apparent from Fig. 6.7 that for a given volume fraction of homopolymer, $\phi_h = 1 - \phi_c$, the domain spacing increases with increasing α. It is interesting to note that for $\phi_h = 0.5$, a transition from cylinders to lamellae occurs with increasing α as the lamellar morphology of the pure diblock is recovered. The variation of average distance between block junctions, a (with respect to that of the pure diblock, a_0), with ϕ_h is shown in Fig. 6.8. The interfacial area per block evidently increases with increasing ϕ_h for a given α, consistent with selective solubilization of the homopolymer which causes lateral swelling of the PS block. For a given ϕ_h, this swelling is reduced with increasing α.

These results imply that homopolymer PS is not always miscible with the PS blocks of the copolymer, i.e. confinement of PS to an interface in a block copolymer can lead to immiscibility with homopolymer PS (Hashimoto *et al.* 1990). This has been interpreted in terms of the enthalpic and entropic contributions to the free energy (Hasegawa and Hashimoto 1996). For $\alpha < 1$ uniform solubilization increases the translational entropy of the homopolymer, but chain stretching in the homopolymer and in the PS chain of the diblock leads to a decrease in conformational entropy. At the same time, the lateral swelling of microdomains leads

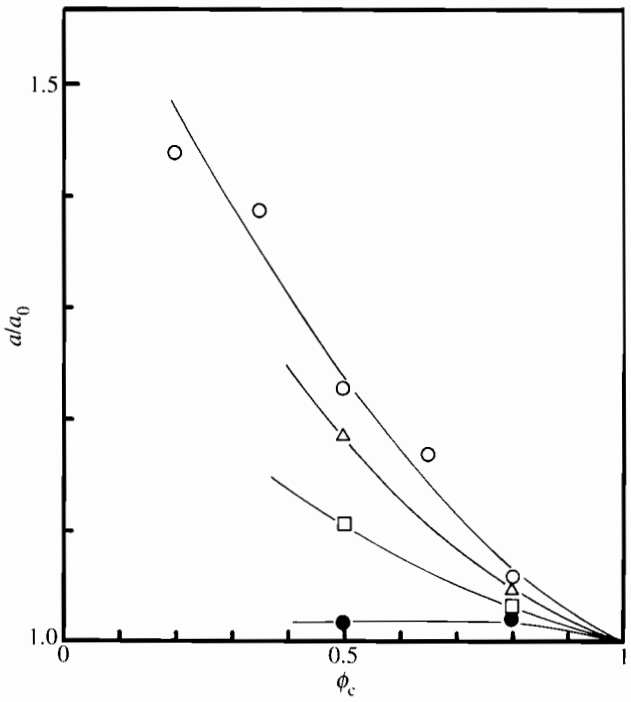

Fig. 6.8 Average distance between junctions along the interface for blends of a PS–PI diblock with PS homopolymer with respect to that of the pure diblock ($a_0 = 2\,\text{nm}$) (Hashimoto *et al.* 1990). Details as Fig. 6.7.

to an increase in interfacial energy. For $\alpha \approx 1$, the situation changes. Localization of the homopolymer chains in the middle of PS domains lowers the translational entropy, but the interfacial energy is simultaneously reduced because the lateral swelling of chains is suppressed. The conformational entropy is generally increased due to the relaxation of stretched chain configurations.

Transitions from the lamellar phase of a neat diblock to cylindrical and then spherical structures were observed using SAXS on addition of PS to PS–PI diblocks by Hashimoto *et al.* (1990) and Tanaka *et al.* (1991). This change in morphology has been explained on the basis of changes in interfacial curvature and packing density, as illustrated in Fig. 6.9. On addition of homopolymer PS, the PS chains of the block copolymer are swollen. However, the PI chains are not swollen, and this leads to a difference in the segmental volumes of PS and PI. In order to retain normal liquid-state densities, the PS block must stretch and/or the PI block contract, as shown in Fig. 6.9(b). However, an alternative is for the interface to curve as shown in Fig. 6.9(c). This situation predominates when the conformational entropy loss caused by stretching is outweighed by the interfacial curvature penalty. This can drive a transition from a lamellar phase to a phase where the minority PI component is on the concave side of a curved interface (e.g. in cylinders or spheres).

The phase behaviour of blends of PS–PI or PS–PB diblocks with PS homopolymer was summarized by Winey *et al.* (1992*b*). Regions of stability of lamellar, bicontinuous cubic, hexagonal-packed cylindrical and cubic-packed spherical structures were mapped out as a function of homopolymer molecular weight, copolymer composition and homopolymer concentration. All blends were

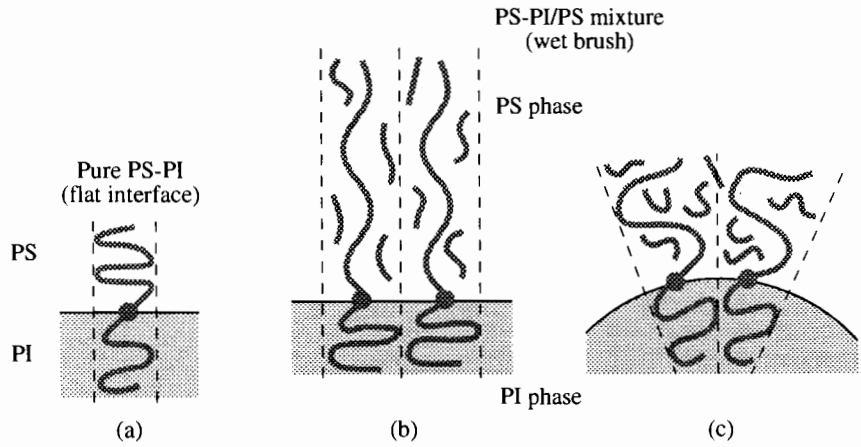

Fig. 6.9 Schematic showing the effect of addition of low-molecular-weight homopolymer on block copolymer chain configuration (Hasegawa and Hashimoto 1996). (a) A symmetric diblock forms a lamellar phase. (b) On addition of homopolymer, swelling induced by solubilized homopolymer causes stretching of the corresponding block chain/and or contraction of the other block, resulting in a decrease in conformational entropy. (c) Alternatively, a curved interface is formed to attain a uniform packing density.

solvent cast from a neutral solvent (toluene) and annealed at the same temperature (125 °C). Constant molecular weight isothermal phase diagrams for blends of three different homopolymers with a number of PS–PI diblocks with an average $M_n = 54\,\mathrm{kg\,mol^{-1}}$ are shown in Fig. 6.10 (Winey *et al.* 1992*b*). An example of TEM images showing the sequence of morphologies for a PS–PI diblock upon addition of increasing amounts of low-molecular-weight PS is shown in Fig. 6.11 (Winey *et al.* 1991*c*). The critical concentration above which micelles do not exist in these blends was estimated to be above 98 wt% PS homopolymer. The main effect of increasing homopolymer molecular weight is to reduce the regions of stability of ordered lamellar, cylindrical, bicontinuous cubic, and spherical microstructures, at the expense of a disordered micellar structure. Biphasic regions were not observed in all cases for these blends. For the blends with low PS-content diblock copolymers, limited PS solubility is the dominant effect, leading to macrophase separation, even when $N_{Ah} \ll N_{Ah}$.

A phase diagram for blends with PS–PI and PS–PB diblocks of approximately constant composition ($f_{PS} =$ 0.44–0.51, i.e. lamellar-forming diblocks) is shown in Fig. 6.12, based on experimental data for a large number of blends (Winey 1992). If the dependence of morphology on homopolymer molecular weight for blends with an overall PS content near $\phi_{PS} = 0.65$ is neglected, vertical lines drawn between the ordered structures are in good agreement with the phase boundaries for pure PS–PI diblock melts. These indicate the following sequence of phases: lamellae $f_{PS} = 0.34$–0.62, bicontinuous cubic $f_{PS} = 0.62$–0.66, cylinders $f_{PS} =$ 0.66–0.77, BCC spheres $f_{PS} > 0.77$. In the phase diagram in Fig. 6.12 (Winey *et al.* 1992*b*), different disordered micellar regions are not delineated. For example, at $\phi_{PS} = 0.93$, disordered spherical micelles were observed at a homopolymer/PS block molecular weight ratio $\alpha = 0.18$ and 0.41, disordered cylindrical micelles were noted at $\alpha = 0.71$, and disordered 'lamellar micelles' at $\alpha = 0.87$. Constant copolymer composition phase diagrams for blends with diblocks which form hexagonal-packed cylinder phases in the neat melt are shown in Fig. 6.13. These indicate that where an ordered phase is formed it is generally that of the neat copolymer, and that, especially when homopolymer is blended with the minority component of a diblock, substantial two-phase regions exist.

Taken together, these results (Winey *et al.* 1992*b*) have been interpreted, in general, as the result of increasing mean curvature and interfacial area per block with increasing homopolymer content and/or decreasing homopolymer molecular weight (Winey 1992; Winey *et al.* 1991*a*). When temperature is considered as an additional (in this case, unexplored) parameter it becomes apparent that there is considerable scope for tuning the morphology of block copolymers by blending with low-molecular-weight homopolymers.

6.2.4 Homopolymers with $N_{Ah} \approx N_{Ac}$

Cohen and Torradas (1984) investigated blends of a 1,2-PB–1,4-PB diblock with 1,2-PB or 1,4-PB with molecular weight equal to that of the corresponding block in the diblock. It was shown using rheology and SAXS that addition of the 1,2-PB homopolymer led to microphase separation, whereas the neat diblock formed

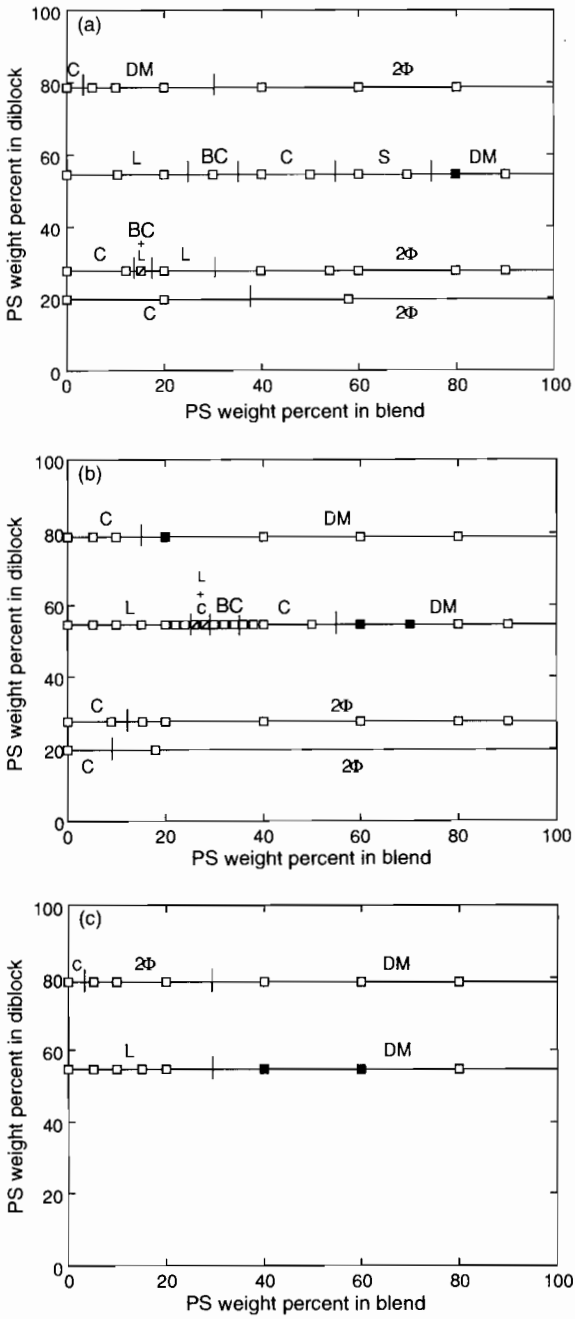

Fig. 6.10 Phase diagrams for blends of PS homopolymers with PS–PI diblocks of approximately constant molecular weight (average $M_n = 54.3\,\mathrm{kg\,mol^{-1}}$), annealed at 125 °C (Winey *et al.* 1992*b*). (a) M_n (PS) = $5.9\,\mathrm{kg\,mol^{-1}}$, (b) M_n (PS) = $14\,\mathrm{kg\,mol^{-1}}$, (c) M_n (PS) = $37\,\mathrm{kg\,mol^{-1}}$. Here L, C and S denote lamellar, cylindrical and spherical microstructures respectively, DM indicates disordered micelles, BC a bicontinuous cubic structure and 2Φ a two-phase macrophase-separated structure. Filled symbols indicate blends with partial order.

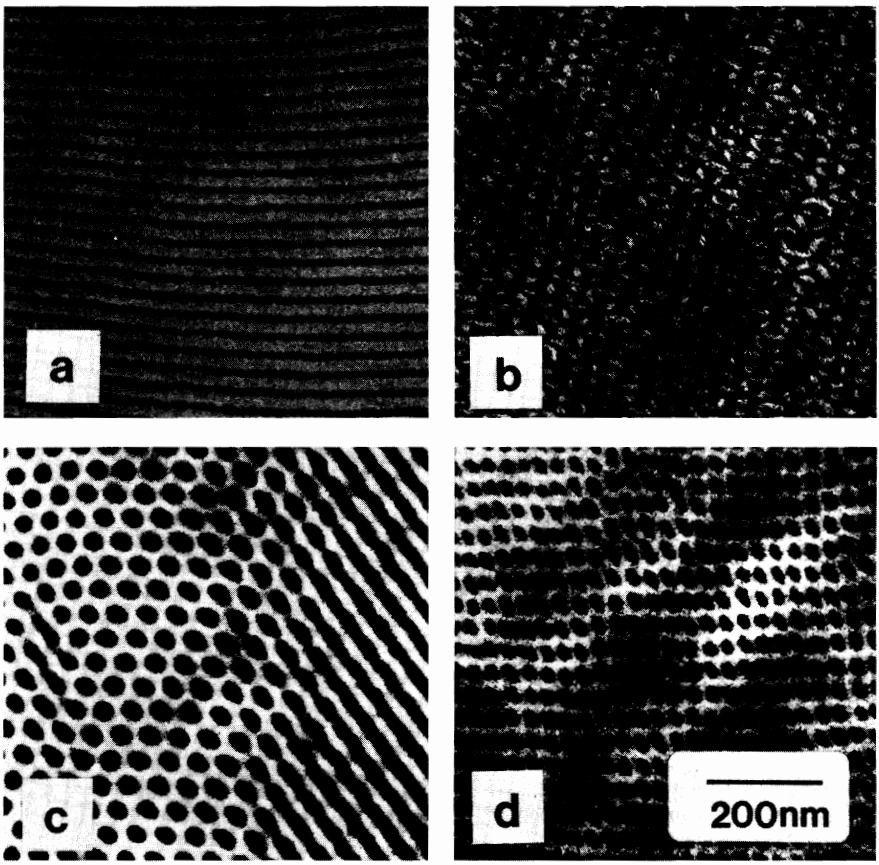

Fig. 6.11 TEM images showing a sequence of morphologies on increasing PS homopolymer (M_n = 5.9 kg mol^{-1}) concentration (wt%) in blends with a PS–PI diblock (M_n = 48.7 kg mol^{-1}, f_{PS} = 0.51) (Winey *et al.* 1991*c*). The blends were annealed at 125 °C. (a) 10% PS, lamellae, (b) 30% PS, bicontinuous cubic, (c) 50% PS, hexagonal-packed cylinders, (d) 70% PS, cubic-packed spheres.

a homogeneous phase, as expected for a copolymer where the two blocks only differ in microstructure. In contrast, addition of the 1,4-PB did not induce microphase separation. The formation of an ordered microphase from a homogeneous one on addition of homopolymer to a diblock was anticipated by Hong and Noolandi (1983); however, it is not clear why this effect was only noted on addition of one of the homopolymers.

The phase behaviour of a blend of a PS–PI diblock and a PS homopolymer with $\alpha = 1.2$ was investigated as a function of blend composition by Koizumi *et al.* (1992). The neat, symmetric, diblock formed a lamellar phase, as shown by the TEM image in Fig. 6.14. Upon increasing the concentration of homopolymer the domain spacing increases, and the distribution of domain spacings becomes broader as apparent from the TEM images in Fig. 6.14. At the same time, the thickness of the PI lamellae remains approximately constant and uniform. The

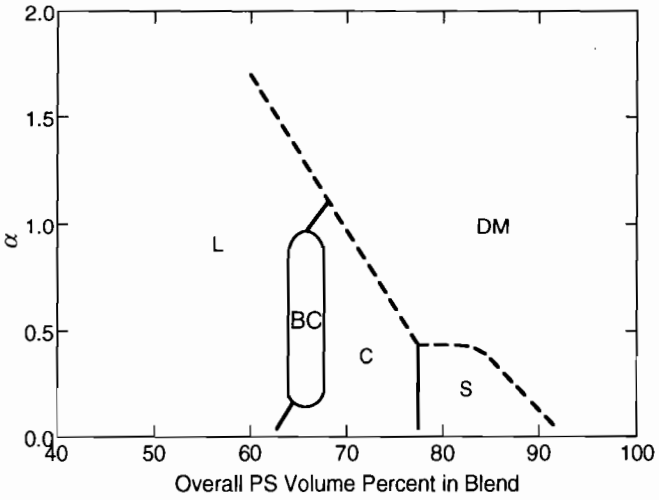

Fig. 6.12 Phase diagram for blends of various PS homopolymers with nearly symmetric PS–PI and PS–PB diblocks, with approximately constant copolymer composition (f_{PS} = 0.44–0.55) (Winey *et al.* 1992*b*). Symbols and annealing conditions as for Fig. 6.10.

result is the vesicular structures apparent in this figure, the vesicles tending to become isolated at high homopolymer contents. Such vesicular structures were first observed (in the $N_{Ah} < N_{Ac}$ regime) for mixtures of PS–PB diblocks with PS homopolymer (Kinning *et al.* 1988). These authors observed lamellar and spherical vesicles for blends of diblocks with total PS contents of 11 and 20 wt% respectively. At the corresponding compositions, spherical and cylindrical structures are expected for pure copolymers.

The spatial distribution of homopolymers in the lamellar structure of a diblock was studied using SANS, together with SAXS, by Koizumi *et al.* (1994*a*). A nearly symmetric PS–PI diblock was mixed with either normal or deuterated PS in a blend with $\alpha = 1.2$. The SAXS results indicated that the homopolymer PS was solubilized in the PS microdomains with a concomitant increase in domain spacing, and that the PI lamellae had a thickness independent of the PS content, but with an increasing distribution of thickness with increasing PS content, in agreement with the evidence from TEM (Fig. 6.14). The interface thickness between PS and PI was also found to increase with increasing homopolymer content. This implies that the PS was localized in the PS domains of the microstructure. This was confirmed by SANS using deuterium-labelled PS homopolymer in the PS–PI matrix. Detailed modelling of the SANS data together with the SAXS data using a one-dimensional paracrystal model (Hosemann and Bagchi 1962) indicated that the characteristic interface thickness between *d*PS and the PS brush in the copolymer was substantial ($\approx$ 11 nm). This is the same order of magnitude as the radius of gyration for the PS chains (homopolymer and diblock), consistent with theory (Shull and Winey 1992).

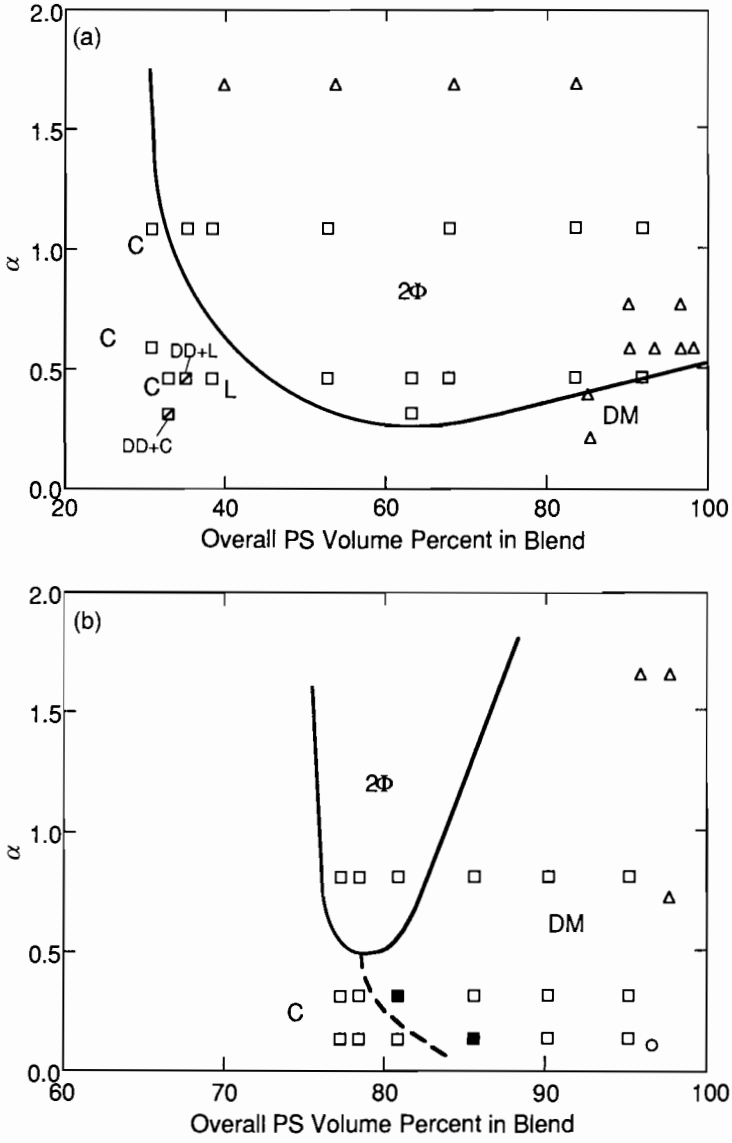

Fig. 6.13 Phase diagrams for blends of various PS homopolymers with asymmetric PS–PI and PS–PB diblocks, with approximately constant copolymer composition (Winey *et al.* 1992*b*). (a) $f_{PS} = 0.44$–0.55, (□) PS–PI $M_n = 46.6\,\mathrm{kg\,mol^{-1}}$, $f_{PS} = 0.25$, (△) PS–PB $M_n = 33.9\,\mathrm{kg\,mol^{-1}}$, $f_{PS} = 0.27$. (b) $f_{PS} = 0.68$–0.77, (□) PS–PI $M_n = 57.5\,\mathrm{kg\,mol^{-1}}$, $f_{PS} = 0.76$, (△) PS–PB $M_n = 52.3\,\mathrm{kg\,mol^{-1}}$, $f_{PS} = 0.77$, (○) PS–PB $M_n = 31.2\,\mathrm{kg\,mol^{-1}}$, $f_{PS} = 0.67$. Symbols and annealing conditions as for Fig. 6.10.

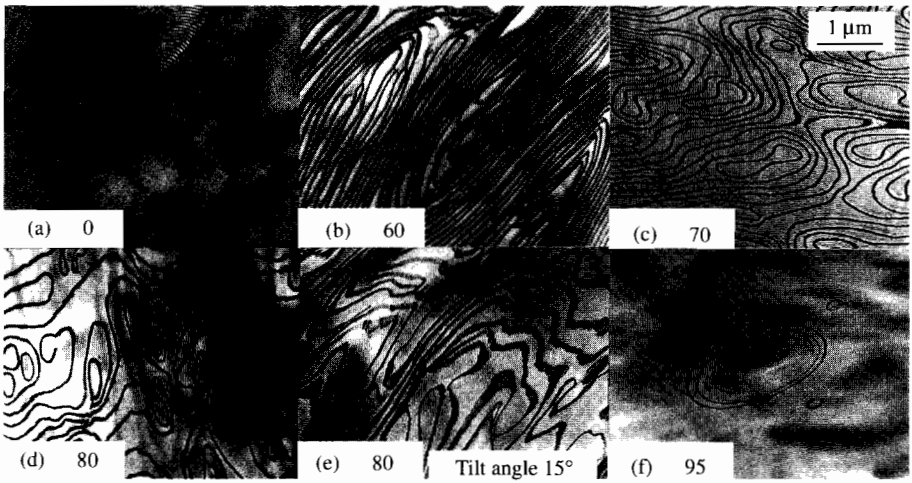

Fig. 6.14 Electron micrographs of PS–PI/PS blends with different composition (Koizumi *et al.* 1992). The diblock has $M_n = 100\,\text{kg mol}^{-1}$, $f_{PS} = 0.46$ and the homopolymer $M_n = 62\,\text{kg mol}^{-1}$. The mixture compositions are indicated as homopolymer wt%.

6.2.5 Homopolymers with $N_{Ah} > N_{Ac}$

In the limit $\alpha > 1$ there is an interplay between macrophase and microphase separation, and this was investigated using mixtures of PS–PI diblocks and PS homopolymer by Koizumi *et al.* (1992, 1994*b*). Figure 6.15 shows macrophase and microphase separation lines for a series of blends with increasing α, calculated using the random phase approximation. On increasing χN, it is evident that the microphase separation transition is encountered first over a wider range of blend compositions for the system with the smallest α. In other words, the point where microphase separation and macrophase separation lines meet, termed the Lifshitz point, ϕ_L, increases with α. For block copolymer content greater than ϕ_L, microphase separation occurs first and the PS homopolymer is solubilized in the PS domain of the microstructure. The phase behaviour of mixtures of a symmetric PS–PI diblock with PS homopolymer with $\alpha = 12.6$ was investigated using TEM by Koizumi *et al.* (1994*b*). They examined blends with 40% and 20% copolymer, which on the basis of Fig. 6.15 are expected to macrophase separate. Slow casting from good solvents led to the onion-like domain structure shown in Fig. 6.16. During macrophase separation, droplets of solution rich in PS–PI are formed in the PS-rich matrix. Microphase separation of the PS–PI then occurs within the PS–PI droplets. On preparing a blend containing 20% diblock by rapid evaporation, the structure shown in Fig. 6.17 was obtained. This shows domains with an 'onion' structure similar to that for the slow-cast 40% blend, although the microdomains are smaller. Also, the domains have a less pronounced ellipsoidal shape than that shown in Fig. 6.16. At low magnification, the size and shape of

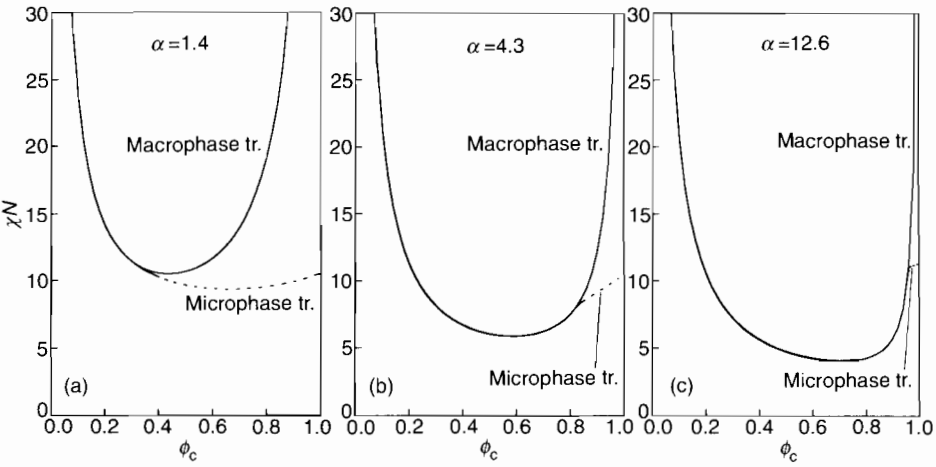

Fig. 6.15 Spinodal lines calculated using the random phase approximation for macrophase separation (solid lines) and microphase separation (dashed lines) for blends of a PS–PI diblock (M_n = 100 kg mol^{-1}, f_{PS} = 0.46) with homopolymers with M_n/kg mol^{-1} = (a) 62, (b) 200, (c) 580 (Koizumi *et al.* 1992). For the blends with $\alpha >> 1$, macrophase separation occurs first on lowering the temperature (increasing χN) for most compositions.

these domains was quite regular, suggesting phase separation by spinodal decomposition. Indeed, a spinodal ring was observed in the light scattering pattern from this specimen.

Koizumi *et al.* (1994*b*) also investigated blends of an asymmetric diblock (83 wt% PS, forming a hexagonal-packed cylinder phase in the pure melt) with a PS homopolymer. The structure of blends with α = 8.3 was examined for different casting conditions. Rapid evaporation favoured the formation of spherical microdomains of PI, which were found to be clustered within the PS matrix (Fig. 6.18). In contrast, blends prepared by slow evaporation of solvent exhibited lens-like (oblate ellipsoidal) macrodomains, in which cylinders are arranged hexagonally with their axes parallel to the axis of revolution of the ellipsoid (see Fig. 6.19). Clearly, the final morphology is strongly dependent on the casting method, although macrophase separation is observed to occur for both these blends.

6.2.6 Blend of AB diblocks with homopolymer C

Macrophase separation after microphase separation has been observed in an AB block copolymer/homopolymer C blend (Hashimoto *et al.* 1995). Blends of a PS–PB starblock copolymer (75 wt% PS) and PVME homopolymer were prepared by solvent casting. Binary blends of PS and PVME exhibit a lower critical solution temperature (LCST), i.e. they demix at high temperatures. The initial structure of a 50% mixture of a PS–PB diblock and PVME shown in Fig. 6.20(a) consists of worm-like micelles. Heating led to macrophase separation as evident

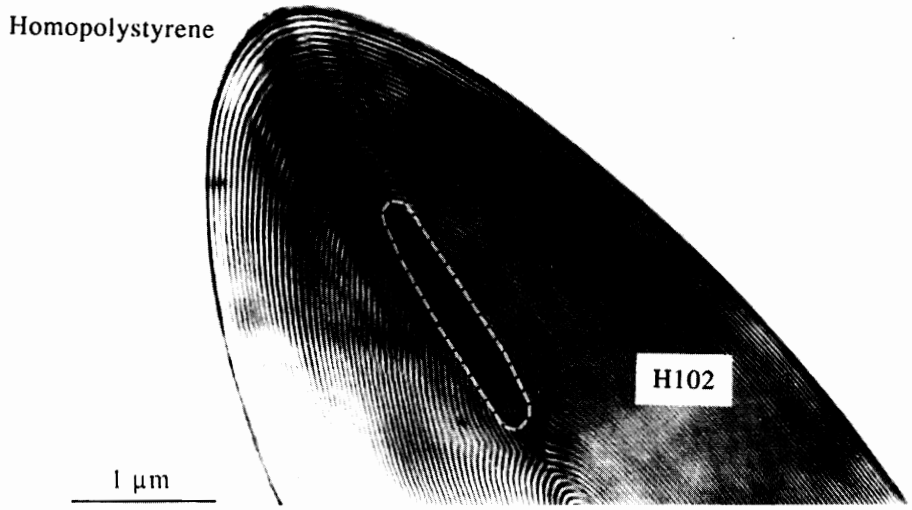

Fig. 6.16 Electron micrograph of a macrodomain, within which microphase separation has occurred in a blend of a PS–PI diblock termed H102 ($M_n = 100\,\text{kg mol}^{-1}$, $f_{PS} = 0.46$) with 60 wt% PS homopolymer ($M_n = 580\,\text{kg mol}^{-1}$) (Koizumi *et al.* 1994*b*). The blend was cast from a 5 wt% solution in toluene with a slow rate of solvent evaporation under normal pressure.

from Fig. 6.20(b), and a spinodal peak in the light scattering pattern. The macrophase-separated structure appears to consist of PVME regions dispersed within a matrix formed by PS–PB lamellae. This macrophase separation on heating is consistent with the LCST of PS/PVME binary blends.

The phase behaviour of blends of an AB diblock with a homopolymer C, where the interactions between A and C were attractive, was compared to that of AB diblocks in homopolymer A by Löwenhaupt *et al.* (1994). Here AB was a PS–PMMA diblock, and conventional blends with PMMA were studied, where the interactions of homopolymer with the diblock are repulsive ($\chi_{AB} > 0$). In contrast, A/C blends of PS/PCHMA (PCHMA = poly(cyclohexyl methacrylate)), PS/TMPC (TMPC = tetramethyl polycarbonate) or PS/SAN (SAN = poly(styrene-*ran*-acrylonitrile) are always homogeneous, thus C homopolymer interacts favourably with the A block in the AB diblock, and the corresponding interaction parameter $\chi_{AC} < 0$. In the conventional blends, both microphase and macrophase separation were observed, as usual. For blends with short PMMA homopolymers ($N_{Ah} < N_{Ac}$), microphase separation predominated, and a micellar microphase was observed using TEM in the blends at high PMMA content or a lamellar microstructure at low PMMA contents, as in the pure diblock. Macrophase separation was observed for blends with higher-molecular-weight PMMA. Microphase-separated structures within macrophase-separated domains were observed in this limit, in agreement with the findings of Koizumi *et al.* (1992,

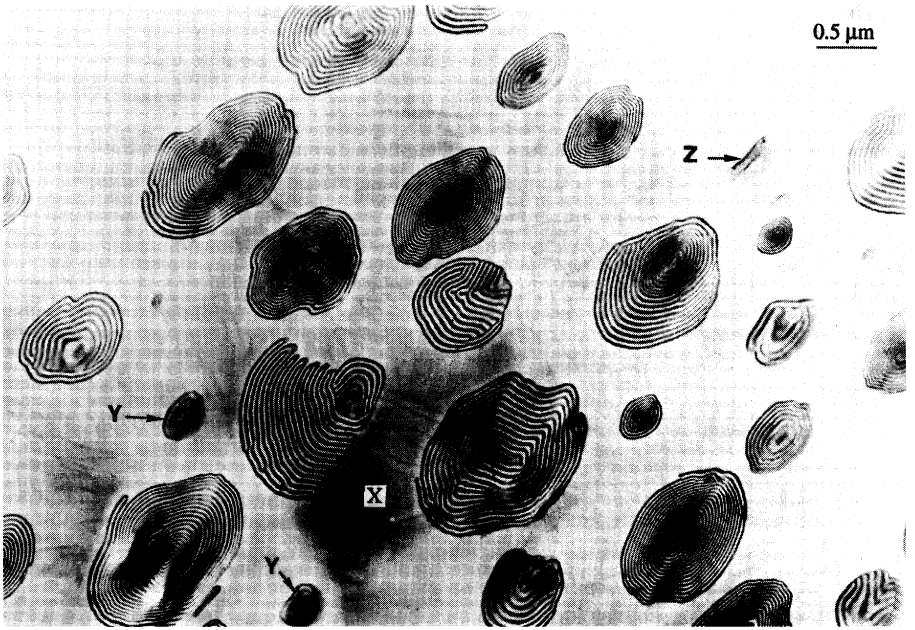

Fig. 6.17 Electron micrograph from the same binary mixture as Fig. 6.16, but cast from a 5 wt% toluene solution by rapid evaporation under reduced pressure (Koizumi *et al.* 1994*b*). The onion-like domains are smaller (and less anisotropic) than the one in Fig. 6.16.

1994*b*). In contrast, for the AB/C blends with $\chi_{AC} < 0$, microphase-separated structures were always observed. Even in a blend with a small $\chi_{AC} > 0$ (PS/PC where PC is polycarbonate), mostly microphases were observed. These results illustrate that in addition to control of phase separation through molecular weight of the homopolymer (as in conventional blends), mixing can be enhanced by selecting blends where the homopolymer has attractive interactions with one of the components of the block copolymer. Furthermore, these interactions can be controlled by the choice of homopolymer.

6.3 Experiments on blends of block copolymers with two homopolymers

6.3.1 General

There is an extensive literature on studies on ternary blends of a block copolymer with two homopolymers, largely focussed on the compatibilization of homopolymers by block copolymers. A cross-section of the literature is listed in Table 6.2.

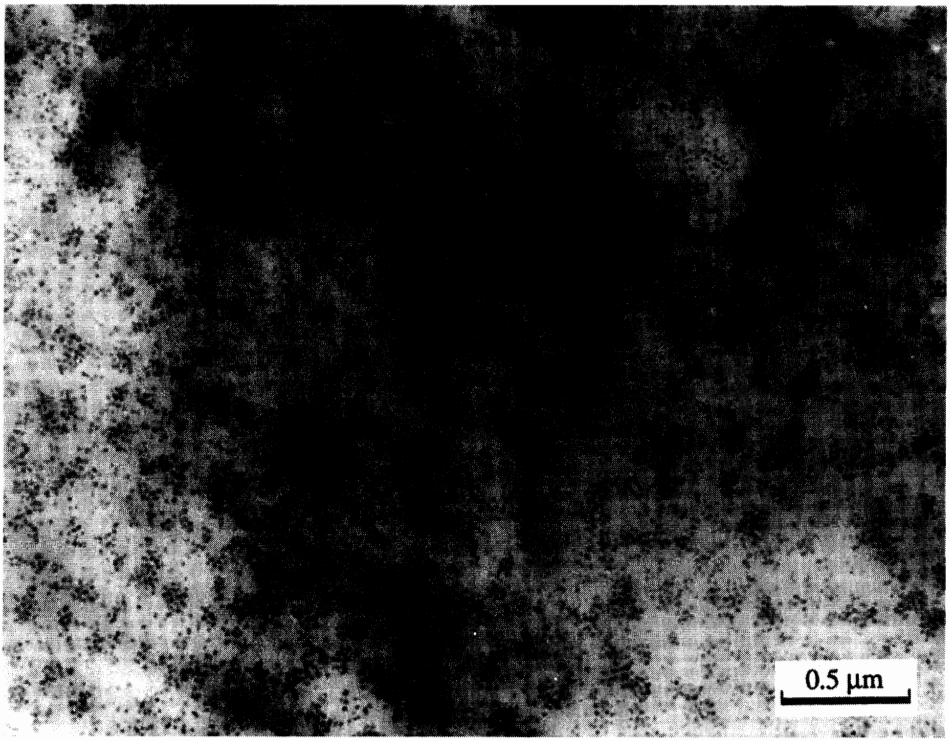

Fig. 6.18 TEM image from a mixture of a PS–PI diblock (M_n = 82 kg mol^{-1}, f_{PS} = 0.81) with 80% PS homopolymer (M_n = 580 kg mol^{-1}) (Koizumi *et al.* 1994*b*). The film was cast from a good solvent for both blocks under low pressure (rapid evaporation). Clustering of PI micelles is evident.

6.3.2 Compatibilization of homopolymers

One of the most important applications of block copolymers is as compatibilizers of incompatible homopolymer blends, and as strengthening agents of polymer/polymer interfaces. Macrophase separation of homopolymer can be suppressed by addition of block copolymer, and fracture toughness of an interface increased. This is due to the reduction of interfacial tension as block copolymer segregates to the interface. Addition of block copolymer also leads to a smaller domain size, i.e. enhanced microscopic mixing. Numerous studies (especially on random copolymers, reviewed by Roe and Rigby (1987)) have demonstrated the suppression of phase separation via cloud point measurements. One of the first such systematic studies was that of von Riess *et al.* (1967) on compatibilization of PS/PMMA and PS/PI blends by the respective diblocks. A large body of literature exists on characterization of the emulsified blend morphology using TEM and determination of dynamic mechanical properties through rheological or tensile deformation experiments. A representative selection of the literature is referenced in Table 6.2. It is not the purpose of the present chapter to discuss the

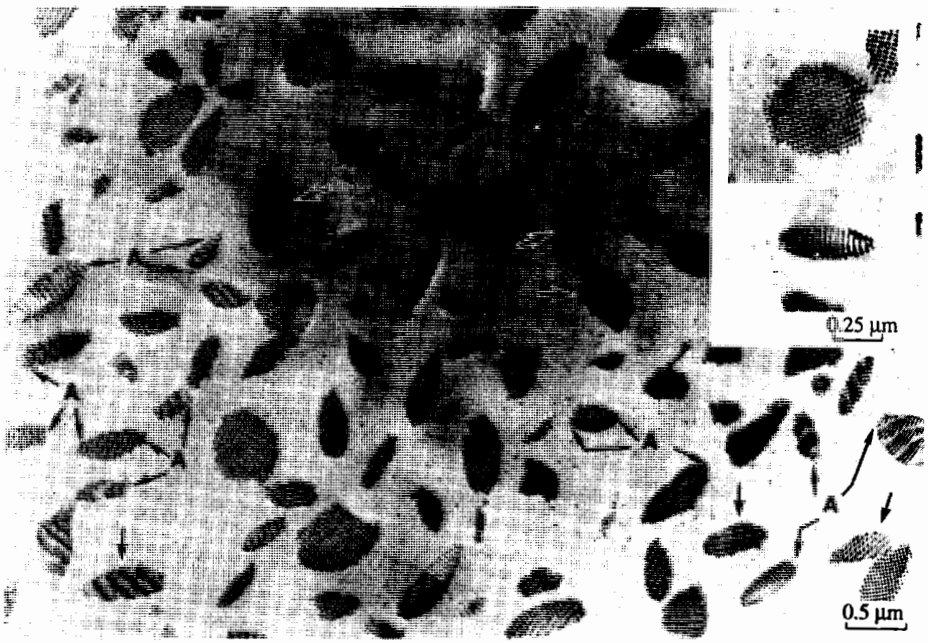

Fig. 6.19 TEM image from a blend of the same polymers and composition as Fig. 6.18 but slow cast (under normal pressure) (Koizumi *et al.* 1994*b*). Oblate ellipsoidal macrodomains rich in the diblock are apparent. The inset confirms that these contain PI cylinders which are packed hexagonally. Lens-like domains where the cylinders are viewed normal to their axis are arrowed, and/or labelled A.

materials science of specific blends. Excellent reviews on this subject are provided by Roe and Rigby (1987), Fayt *et al.* (1989*a*) and Jiang and Xie (1991). Here we outline the essential physics of compatibilization. The compatibilization of homopolymer blends on addition of block copolymer has also been demonstrated nicely in thin films using neutron reflectivity to determine the density profile across an interface between homopolymers (see Section 6.8).

The strengthening of homopolymer interfaces by addition of block copolymer has been studied by measuring the fracture toughness. This is achieved using an asymmetric double cantilever method where a razor blade of known thickness is driven into the homopolymer interface at a constant speed. Steady-state crack propagation, in particular the length of the crack ahead of the razor blade, is then monitored using a video camera. The interfacial fracture toughness, G_c (also known as the critical energy release rate) is thus determined. Kramer and coworkers have examined the toughening effects of diblock and triblock additives (and random copolymers) based on PS and P2VP at the interface between the corresponding homopolymers (Creton *et al.* 1992; Dai *et al.* 1996, 1997; Kramer *et al.* 1994; Washiyama *et al.* 1993*a*,*b*, 1994). The interfacial toughening of PS–glass and PS–silicon interfaces modified by PS–P2VP or PS–PMMA diblocks have also

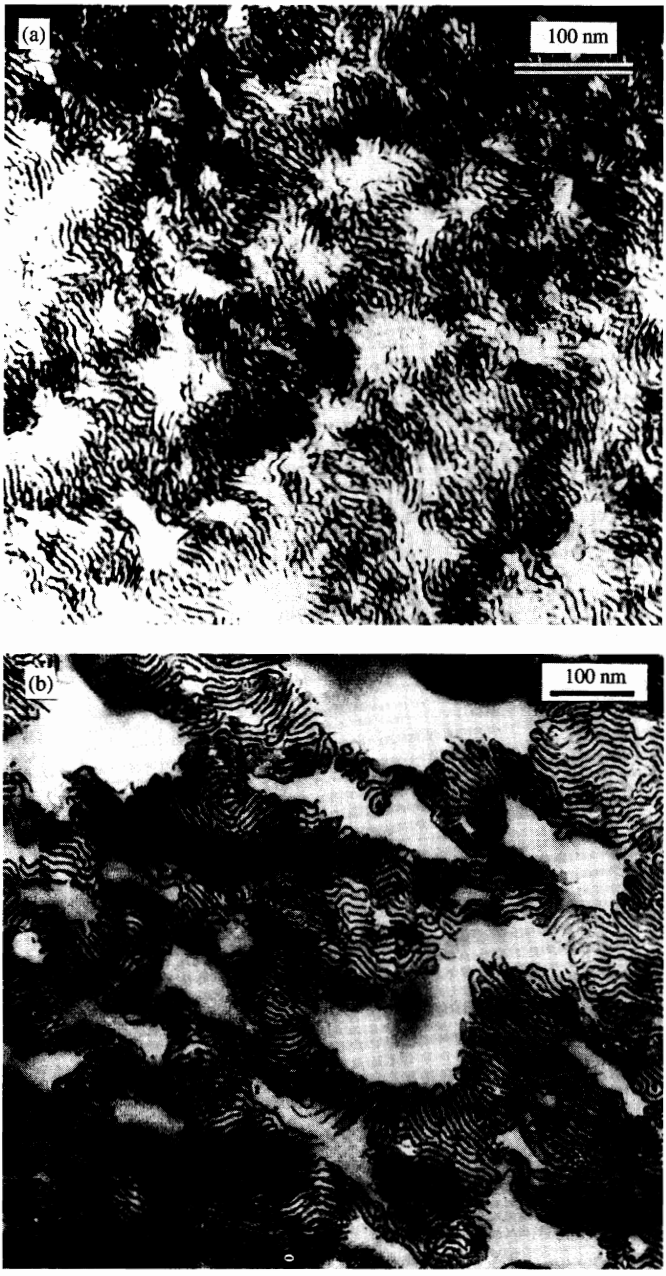

Fig. 6.20 (a) Electron micrographs obtained from a 50 wt% binary mixture of starblock copolymer and poly(vinyl methyl ether) (PVME) (PS/PB starblock $M_n = 14.5\,\mathrm{kg\,mol^{-1}}$, 24 wt% PB, PVME, $M_n = 2.6\,\mathrm{kg\,mol^{-1}}$) annealed at 111 °C for 20 min. This shows a worm-like micellar structure (Hasegawa and Hashimoto 1996; Hashimoto *et al.* 1995). (b) The same mixture after 180 min. Macrophase separation has progressed and a superlattice structure with copolymer lamellae separated by regions of homopolymer is apparent.

Table 6.2 Experimental studies of ternary block copolymer/homopolymer blends. Adapted and extended from Roe and Rigby (1987)

Copolymer	Homopolymer	Homopolymer	Reference
PS–PMMA	PS	PMMA	(Russell *et al.* 1991; von Riess *et al.* 1967)
PS–PI	PS	PI	(Hashimoto *et al.* 1981; Inoue *et al.* 1970; Tanaka *et al.* 1991; von Riess *et al.* 1967)
1,4-PB–1,4-PI	1,4-PB	1,4-PI	(Cohen and Ramos 1979; Ramos and Cohen 1977)
PS–PE	PS	PE or PP	(Heikens *et al.* 1978)
PS–PE	PS	PE	(Brahimi *et al.* 1991*a*,*b*; Fayt *et al.* 1981, 1982, 1985, 1989*b*; Harrats *et al.* 1995)
PEP–PMMA	Poly (vinylidene fluoride)	PE or PP	(Ouhadi *et al.* 1986)
PE–PMMA	PE	ABS (poly(acrylonitrile–butadiene–styrene))	(Fayt and Teyssié 1989)
PS–PMMA	PS	Poly(vinyl chloride) (PVC)	(Fayt *et al.* 1989*c*)
PS–PCL	PS	PVC	(Fayt *et al.* 1989*c*)
PS–PB	PS	PB	(Anastasiadis *et al.* 1989; Hasegawa *et al.* 1991; Park and Roe 1991; Rameau *et al.* 1982; Rigby *et al.* 1985; Roe and Kuo 1990)
PS–PAMS	PS	PAMS	(Hsuie and Shih 1985)
PS–P2VP	PS	P2VP	(Creton *et al.* 1992; Dai and Toprakcioglu 1992; Dai *et al.* 1996; Kramer *et al.* 1994; Shull *et al.* 1990, 1991; Washiyama *et al.* 1993*a*,*b*, 1994)
PEP–poly(ethylene–butylene) (PEP–PEB)	PEP	PEB	(Balsara *et al.* 1993)
PS–PMMA	PS-*ran*-poly (acrylonitrile)	PDMPO	(Auschra *et al.* 1993)
PE–PEP	PE	PEP	(Bates *et al.* 1995)
PS–PDMS	PS	PDMS	(Hu *et al.* 1995)
PS–PE	PS	PEP	(Cigana *et al.* 1996)
PE–PP	PE	PP	(Jeon *et al.* 1997)
PS–poly(ethylene/butylene)–PS (PS–P(E/B)–PS)	PS	PE	(Lindsey *et al.* 1981)
PE–PP–PE	PE	PP	(Dumoulin *et al.* 1984)
PS–P(E/B)–PS	PP	PE or PS	(Gupta and Purwar 1985*a*,*b*)
P2VP–PS–P2VP	PS	P2VP	(Dai *et al.* 1994, 1997)

been examined (Smith *et al.* 1993). Failure mechanisms were investigated by TEM and forward recoil spectroscopy (Washiyama *et al.* 1993*a*,*b*; Dai *et al.* 1997) and X-ray photoelectron spectoscopy and Rutherford backscattering spectrometry (Creton *et al.* 1992). PS and P2VP have approximately the same glass transition temperature ($T_g \approx 105\,°C$) and both deform in the glassy state primarily by crazing, although PS has a smaller crazing stress than P2VP (≈ 55 MPa for PS and ≈ 75 MPa for P2VP). Three mechanisms for failure of the homopolymer interface are observed depending on the areal density of copolymer chains (i.e. number per unit area) and the molecular weight of the homopolymer: chain pull-out, chain scission or crazing. At low areal densities, $\Sigma < \Sigma^*$, chain scission occurs if both blocks are entangled (M_{Ac}, $M_{Bc} \gg M_e$, where M_e is the entanglement molecular weight). The chain scission stress is given by (Creton *et al.* 1992; Dai *et al.* 1997)

$$\sigma_{\text{scission}} = f_b \Sigma, \tag{6.1}$$

where f_b is the force to break a single carbon–carbon bond. Thus, the bond-breaking stress of block copolymer chains is a linear function of the areal density. In the chain scission regime, G_c is independent of the homopolymer molecular weight (Dai *et al.* 1996).

On the other hand, if either or both of the copolymer blocks are unentangled (M_{Ac} or $M_{Bc} < M_e$), chain pull-out may be preferred (Creton *et al.* 1992; Dai *et al.* 1996, 1997). The stress required to cause chain pull-out is dependent on the frictional forces between the homopolymer and the copolymer block being pulled out and is also linearly dependent on the copolymer areal density. It is given by (Dai *et al.* 1997; Kramer *et al.* 1994)

$$\sigma_{\text{pull-out}} = f_{\text{mono}} N \Sigma, \tag{6.2}$$

where f_{mono} denotes a static friction coefficient per monomer.

For unentangled blocks, a transition from chain pull-out to crazing occurs for $\Sigma > \Sigma^0$. When $\Sigma = \Sigma^*$ for entangled chains a transition from chain scission to crazing occurs. Crazing occurs via chain disentanglement and/or chain scission. A crossover in areal density occurs at $\Sigma = \Sigma_{\text{sat}}$, such that at high densities the copolymer can no longer organize as a brush at the interface but forms other phases such as micelles or lamellae near the interface (Washiyama *et al.* 1993*b*). Micelles formed by asymmetric diblocks were found to have no effect on G_c; however, for symmetric diblocks, lamellar structures were formed which changed G_c. After exhibiting a maximum at Σ_{sat}, G_c decreased and reached a constant value when the interface was fully covered with one additional block copolymer lamella. This indicates that there are limits to the interface toughening that can be produced by adding symmetric block copolymers, the interface actually weakening if excess is added.

In the crazing regime, with $\Sigma \leq \Sigma_{\text{sat}}$, experiments using a symmetric PS–P2VP diblock showed a strong dependence of G_c on the molecular weight (specifically M_n) of a monodisperse PS homopolymer. In this case, G_c was found to increase sharply around $M_n = 100\,\text{kg mol}^{-1}$ and then level off at higher M_n values (Dai *et al.* 1996). In contrast, for $\Sigma \gg \Sigma_{\text{sat}}$, G_c is independent of the M_n of monodisperse

homopolymer. Polydisperse homopolymer PS was found to swell the lamellar microstructure leading to a decrease in G_c compared to that for the blend with monodisperse PS homopolymer (Dai *et al.* 1996). Triblocks P2VP–*d*PS–P2VP with long, entangled P2VP blocks were found to have a better toughening effect than diblock copolymers of similar molecular weight due to entanglements between *d*PS loops in the triblock and homopolymer PS (Dai *et al.* 1997). The areal density at the transition from chain scission to crazing was $\Sigma^* = 0.015$ chains nm^{-2} for the triblocks and 0.03 chains nm^{-2} for the diblocks examined by Dai *et al.* (1997). This implies that most of the triblocks are looped and thus the triblock 'staples' the homopolymers together. For entangled P2VP chains in these triblocks and $\Sigma \geq \Sigma_{sat}$, the G_c values at the PS/P2VP interface were shown (Dai *et al.* 1997) to approach those for PS homopolymer ($G_c = 400$–$500\,J\,m^{-2}$).

A model for craze failure at a crack tip has been proposed by Brown (1991) and Hui *et al.* (1992). These authors allowed for the fact that cross fibrils can support stress between the main fibrils. This load-transferring mechanism allows the stress at the crack tip to reach the breaking stress of the polymer chains. By treating the craze as an anisotropic continuum with independent longitudinal and shear elastic constants they derived an expression for the average stress on the fibril structure, which depends on the entanglement density of the crazed material. de Gennes (1991) has considered chain disentanglement. It was proposed that a craze fails at the craze–bulk interface where all the polymer chains are drawn into fibrils. Sha *et al.* (1995) have shown that for a thin craze, the asymptotic stress field used by Brown (1991) and Hui *et al.* (1992) underestimates the stress field at the crack tip fibril. They derived an expression for G_c using a discrete model and the full stress field ahead of the crack tip.

6.3.3 Reduction in interfacial tension of a homopolymer blend by addition of block copolymer

The reduction in interfacial tension of a bulk blend on addition of diblock has been measured by Gaillard *et al.* (1980), who investigated blends of PS and PB with the corresponding diblock in the presence of styrene monomer. However, they only observed a levelling off of interfacial tension beyond 5–10% of added copolymer, whereas Noolandi and Hong (1982) predict that its should fall to zero for concentrations in excess of about 0.01% (Section 6.6.3). The discrepancy was ascribed (Noolandi and Hong 1982) to non-equilibrium effects, for example due to spinning of the solution in the spinning-drop method used to measure the interfacial tension. Anastasiadis *et al.* (1989) determined the interfacial tension as a function of PS–PB diblock content in a blend with PS and PB. An initial sharp decrease was observed, followed by a levelling off at a concentration identified by them as the cmc; however, the interfacial tension was still substantial even at this transition.

A reduction in interfacial tension on addition of a PS–PB diblock to a blend of the corresponding homopolymers (low molecular weights) was determined by Park and Roe (1991). In contrast to the results of Anastasiadis *et al.* (1989), the interfacial tension was found to decrease to vanishingly small values on addition

of sufficient copolymer, which was ascribed to a cmc. They measured the radius, R, of droplets of a macrophase-separated PS-rich phase in a PB-rich matrix as a function of time. Using the Lifshitz–Slyozov theory (Lifshitz and Slyozov 1961), the interfacial tension was determined from plots of R^3 versus time. This theory assumes that domain coarsening in the phase separation process occurs through growth of large particles (radius above a critical radius R_c) at the expense of particles with a radius smaller than R_c. The larger particles grow by diffusion of the minority component through the matrix. The radius of the particles is predicted to grow with time, t, as (Lifshitz and Slyozov 1961)

$$R^3 = \frac{4}{9} D\varepsilon t \tag{6.3}$$

where D is the diffusion coefficient and ε is given by

$$\varepsilon = \frac{2\gamma}{(\Delta c)^2 (\mathrm{d}\mu/\mathrm{d}c)_{\mathrm{bin}}} \tag{6.4}$$

where γ is the interfacial tension, Δc is the concentration difference between the two phases, and $(\mathrm{d}\mu/\mathrm{d}c)_{\mathrm{bin}}$ is the chemical potential gradient evaluated at the binodal point (limit of stability of the two-phase region). The Lifshitz–Slyozov mechanism is expected to predominate where the collision and coalescence mechanism for droplet growth is hindered by the high viscosity of the matrix. The interfacial tensions determined by Park and Roe (1991) were compared to the predictions of the theory of Leibler (1988) (Section 6.6.1) in the wet brush limit, which accounted qualitatively for the observed reduction with increasing copolymer content.

The reduction of interfacial tension on addition of a PS–PDMS diblock to PS/PDMS blends was measured directly (using a pendant drop tensiometer) by Hu *et al.* (1995). They found that a maximum interfacial tension reduction of 82% is achieved for diblock copolymer concentrations as low as 0.002%, with saturation at higher concentrations, as illustrated in Fig. 6.21. This was compared to the theory of Leibler (Section 6.6.1) for the blends with high-molecular-weight homopolymer (dry brush regime). Theory predicted a saturation concentration (cmc) of 0.003%, in close agreement with the experimental result. However, for a lower-molecular-weight homopolymer, the experimental saturation limit (0.03%) was much higher than the theoretical prediction for a dry brush, suggesting that this blend was in the wet brush regime, where saturation of interfacial tension is predicted not to occur (Section 6.6.2) because the homopolymer chains can penetrate the copolymer brush. This penetration increases unfavourable contacts between PDMS and PS, thus increasing the interfacial tension compared to the non-penetration case.

6.3.4 Spatial distribution of block copolymers in ternary blends

The reduction in interfacial tension in homopolymer blends effected by addition of block copolymer is due to the segregation of copolymer to the interface. The

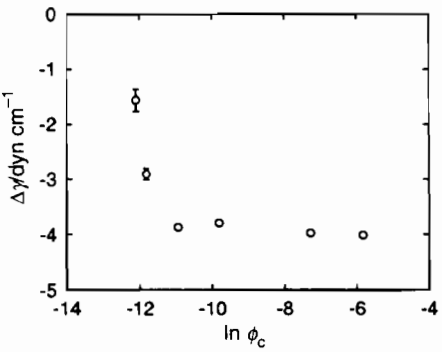

Fig. 6.21 Reduction of interfacial tension of a PS/PDMS blend (PS, $M_n = 4.0\,kg\,mol^{-1}$; PDMS, $M_n = 4.5\,kg\,mol^{-1}$) upon addition of a PS–PDMS diblock ($M_n = 13\,kg\,mol^{-1}$, 50wt% PS) (Hu *et al.* 1995). The interfacial tension of the blend without diblock is $\gamma_0 = 4.85 \pm 0.05\,dyn\,cm^{-1}$. All measurements were performed at 140°C.

spatial distribution of copolymer in the bulk has been investigated using SAXS and SANS. Results using neutron reflectivity on thin films (see Section 6.8) show that block copolymer tends to segregate to the interface as in binary homopolymer/copolymer blends. Hashimoto *et al.* (1981) observed that the interface thickness in ternary blends of sphere-forming PS/PI diblocks and the respective homopolymers was essentially independent of the homopolymer content in the blend. They analysed SAXS data in the Porod region to determine interfacial widths in the blends studied, which were close to the isopleth (line of eqaul homopolymer concentrations). Their results indicated selective solubilization, with copolymer segregating to the homopolymer interface. In contrast, Hasegawa *et al.* (1991) observed that low-molecular-weight PS and PB homopolymers tend to be solubilized essentially uniformly within their corresponding microdomains in the lamellar structure formed by a blend with a nearly symmetric diblock. The addition of a second homopolymer can stabilize the formation of an ordered phase for a very low copolymer content compared to a binary blend (as subsequently confirmed by theory (Banaszak and Whitmore 1992)). Tanaka *et al.* (1991) noted that long-range order of microdomains was observed for copolymer contents as low as 10%, confirming the strong solubilization effect of block copolymers in homopolymer blends.

The dimensions of a PS–PB chain in blends with PS and PB homopolymers (of much lower molecular weight) were studied using SANS and SAXS by Hasegawa *et al.* (1991). Contrast matching using mixtures of normal PS and deuterated PS was used to isolate neutron scattering from homopolymer chains within the lamellar-forming block copolymer blend. The conformation of the neat diblock chains was also probed using mixtures of labelled chains. These results suggested that homopolymer and block copolymer chains are stretched normal to the lamellar interface, and contracted parallel to it. On addition of homopolymer, the block copolymer chains were found to undergo an affine deformation with the extension of the chains perpendicular to the lamellae accompanied by

a corresponding contraction of the chains parallel to the interface, maintaining the overall radius of gyration.

6.3.5 Experimental observation of a Lifshitz point

Ordering in a blend of a symmetric diblock and with two homopolymers of equal molecular weight was studied by Bates *et al.* (1995). They studied a blend of a PE–PEP diblock in PE and PEP homopolymers with $\beta = N_h/N_c = 0.208$. Here N_h and N_c are the total degrees of polymerization of the two equal length homopolymers and copolymer respectively. Regions of macrophase and microphase separation were identified using SANS and rheology. Macrophase separation is characterized by an instability in the disordered state at $q^* = 0$, where q^* is the critical wavenumber, whereas microphase separation occurs with $q^* = q_0$, where q_0 is the finite wavenumber associated with the ordered microphase. The point along the line of critical transitions at which the $q^* = 0$ and $q^* \neq 0$ branches meet is termed the Lifshitz point (see Section 6.6.3 for a fuller discussion). The phase diagram for the system studied by Bates *et al.* (1995) is shown in Fig. 6.22, including experimental points and lines calculated using self-consistent field theory. Mean field theory suggests that adding homopolymer leads to the separation of the lamellar microphase into two phases at an unbinding transition, as indicated (although not observed experimentally). Mean field behaviour in the disordered phase within 1 K of the Lifshitz point was confirmed from plots of the correlation length, ξ, and the zero-angle scattering intensity $I(0)$ as a function of reduced temperature $\tau = (T - T_{LP})/T_{LP}$, where T_{LP} is the Lifshitz temperature for the blend at the Lifshitz point. Mean field theory predicts scalings $\xi \sim \tau^{1/4}$ and $I(0) \sim \tau$, and these scalings were confirmed within experimental errors, as shown in Fig. 6.23.

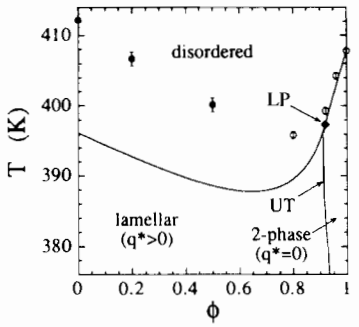

Fig. 6.22 Phase diagram for blends of PE and PEP homopolymers ($N_h = 392$ and 409 respectively) with a PE–PEP diblock ($N_c = 1925$) (Bates *et al.* 1995). Open and filled circles denote experimental phase transitions between ordered and disordered states measured by SANS and rheology respectively. Phase boundaries obtained from self-consistent field calculations are shown as solid lines. The diamond indicates the Lifshitz point (LP), below which an unbinding transition (UT) separates lamellar and two-phase regions in mean field theory.

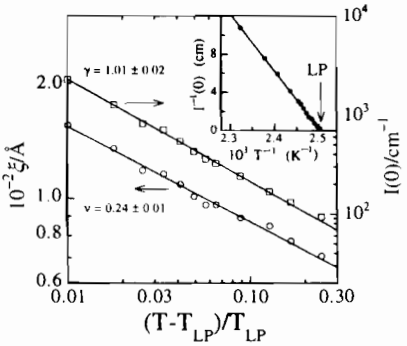

Fig. 6.23 Logarithmic plots of the correlation length (ξ) and zero-angle scattering intensity ($I(0)$) as a function of temperature reduced with respect to the Lifshitz temperature (T_{LP}) for a blend of PE and PEP homopolymers with a PE–PEP diblock (details as Fig. 6.22) at a copolymer volume fraction $\phi_c = 0.916$ (Bates *et al.* 1995). The slopes yield the exponents indicated. The theroretical mean-field Lifshitz point exponents are $\gamma = 1$ and $\nu = \frac{1}{4}$.

6.3.6 Effect of block copolymer on the kinetics of phase separation

The effect of added PS–PB diblock on the phase separation kinetics of blends of low-molecular-weight PS and PB (with an upper critical solution temperature, UCST) was investigated using light scattering by Roe and Kuo (1990). Addition of block copolymer was found to retard the phase separation process for block copolymers of sufficiently high molecular weight so as to be microphase separated under the conditions of the experiment. This was ascribed to the reduction in interfacial tension between the demixed phases due to the segregation of block copolymer to the interface. However, addition of a low-molecular-weight diblock which was not microphase separated did not slow down the phase separation, as determined in subsequent optical microscopy experiments on the growth of disordered domains during the phase separation process (Park and Roe 1991). In this paper, it was noted that the droplets of phase-separated PS homopolymer were not the thermodynamically stable aggregates anticipated by Leibler (1988) (Section 6.6.1), where copolymer adsorbed to the interface stabilizes a vesicular structure. The density of copolymer chains at the interface was too low for this structure, and the droplet formation was kinetically controlled.

These results were confirmed by Sung and Han (1995). They observed that addition of a PS–PB diblock copolymer to a blend of the corresponding homopolymers (of lower molecular weight than the diblock) leads to a retardation of phase separation in both early and late stages. Using time-resolved light scattering they determined the spinodal peak position and intensity as a function of time. Addition of copolymer was found to reduce the critical temperature of the blend.

In contrast to these studies, Lin *et al.* (1995) found no evidence for the retardation of spinodal decomposition in blends of poly(ethylene–propylene) and poly(ethylene–butylene) with the corresponding diblock where the homopolymers had higher molecular weights than those of the block copolymers. They performed time-resolved light scattering experiments during the late stages of decomposition and used small-angle neutron scattering to measure the onset of phase separation in the initial stage. They found that the block copolymer was not preferentially located at the homopolymer interface, in contrast to the usual situation; however, the uniform solubilization of copolymer did lead to a finer structure compared to blends without added diblock. The kinetics for the ternary blend were analysed using the standard Cahn theory (Cahn 1965) for the early stage of spinodal decomposition, as applied to polymer blends. The late stage of coarsening was described by power laws for the peak intensity and position similar to those observed for homopolymer pairs.

6.4 Experiments on blends of two block copolymers

6.4.1 General

Until recently, very little quantitative information was available on blends of block copolymers. The literature is summarized in Table 6.3. Hoffman *et al.* (1970) reported microscopic demixing of blends of PS–PB diblocks, with two maxima in the domain size distribution, but with no evidence for macrophase separation. These findings must be treated with caution in the light of more recent results. Hadziioannou and Skoulios (1982) used SAXS and SANS to investigate the morphology of binary blends of PS–PI diblocks, and binary PS–PI/PS–PI–PS or PS–PI/PI–PS–PI blends or blends of the two types of triblock. They found that the blends were microphase separated, and that the sharpness of the interface was not reduced in blends compared to neat copolymers. The transition between a lamellar and a cylindrical structure was shown to depend primarily on blend composition. In contrast, the transition from a lamellar to a disordered phase at

Table 6.3 Experimental studies of binary block copolymer/homopolymer blends. Adapted and extended from Roe and Rigby (1987)

Copolymer 1	Copolymer 2	Reference
PS–PB	PS–PB	(Hoffman *et al.* 1970)
PS–PB–PS	PS–PB	(Cohen and Tschoegl 1972, 1973)
PS–PI or PS–PI–PS or PI–PS–PI	PS–PI or PS–PI–PS or PI–PS–PI	(Hadziioannou and Skoulios 1982)
PS–PB star	PS–PB star	(Jiang *et al.* 1982)
PS–PB–PS	PS/PB random copolymer	(Diamant *et al.* 1982)
PS–PI	PS–PI	(Hashimoto *et al.* 1993, 1994; Koizumi *et al.* 1994c; Spontak *et al.* 1996)
PS–PB	PS–PB	(Vilesov *et al.* 1994)
PS–PMMA	PS–PMMA	(Mayes *et al.* 1994)
PE–PEE	PE–PEE	(Zhao *et al.* 1996)

a fixed temperature depended mainly on the overall molecular weight of the mixture. Jiang *et al.* (1982) used TEM to investigate the morphology of blends of PS–PB star copolymers, and observed distinct morphologies in the blend from those in the neat copolymers.

6.4.2 Mixtures of lamellar block copolymers

The dependence of domain spacing and interfacial area per molecule on blend composition was investigated by Hadziioannou and Skoulios (1982) for a series of PS/PI diblocks and triblocks. These data were analysed by Hashimoto (1982) and it was shown that the usual scaling of $d \sim M^{2/3}$ for strongly segregated block copolymers (Section 2.3.1) was followed, but with M (in this case M_n) for the blend given by $M_n = x_1 M_{n,1} + x_2 M_{n,2}$ where x_1 and x_2 are the mole fractions of the two components. A similar scaling was observed by Hashimoto *et al.* (1993). They performed TEM and SAXS on a range of nearly symmetric PS–PI diblocks, covering a wider range of molecular weights than those studied by Hadziioannou and Skoulios (1982). In blends of more asymmetric copolymers, macrophase separation into coexisting lamellar phases was observed and the $\frac{2}{3}$ scaling law for the domain period was followed. Examples of the domain spacings for a blend of diblocks with a molecular weight ratio $\delta = N_1/N_2 = 9.6$ (here N_1 and N_2 are the degrees of polymerization of the two diblocks) and different compositions are shown in Fig. 6.24.

Hashimoto *et al.* (1993) also probed the effect of varying the ratio of molecular weights of the two diblocks, δ. The blend morphology was determined using TEM. For $\delta < 5$, the diblocks were found to be miscible at all compositions, forming a single microdomain structure. This limiting value of δ was subsequently confirmed using self-consistent field theory by Matsen (1995*a*) (see Section 6.7.2). For $\delta > 10$, the mixtures were found to be only partially miscible, forming macrophase-separated lamellar microdomains with different periods, a representative example of which is illustrated in Fig. 6.25. In the partially miscible pairs, the copolymer with the larger molecular weight was found to solubilize the copolymer with the smaller molecular weight up to about 30 wt%, but the copolymer with the smaller molecular weight was found to hardly solubilize the copolymer with a larger molecular weight. It was shown that blending of a lamellar-forming diblock with $f_{PS} = 0.32$ and one with $f_{PS} = 0.60$ can induce the formation of a bicontinuous cubic structure in certain ranges of composition. In contrast, blending of a diblock forming a lamellar phase with $f_{PS} = 0.44$ with a diblock forming a bicontinuous cubic structure with $f_{PS} = 0.66$ resulted in the formation of a lamellar phase with a distinct period for blend compositions ranging from 20 to 80 wt%. Even when the overall blend composition was $f_{PS} = 0.62$, a lamellar phase was formed, although for a pure diblock of this composition, a bicontinuous cubic structure is stable (Section 2.2.1). These results indicate that caution is necessary when adopting a single-phase approximation for blends of block copolymers of different molecular weights. The morphology of a blend does not necessarily correspond to that of a pure copolymer with the same composition. A change in morphology can be driven by changes in interfacial

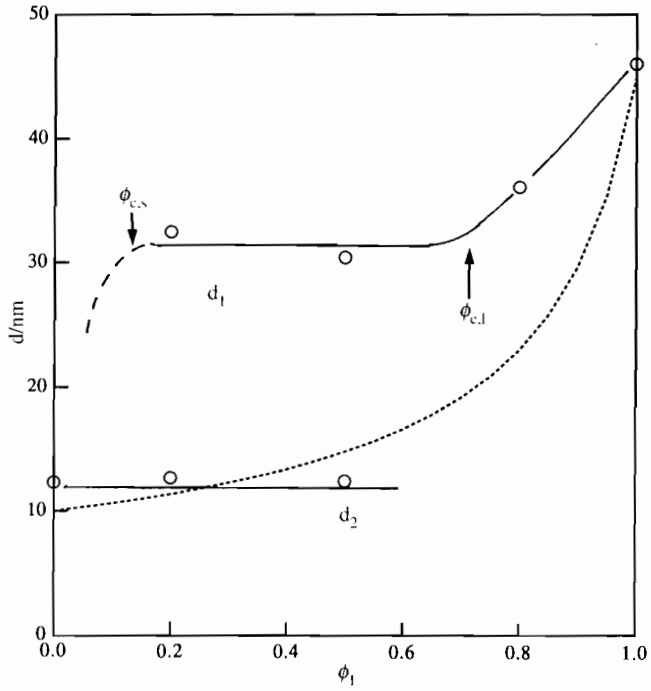

Fig. 6.24 Plots of the domain spacings against the weight fraction of the diblock with the larger molecular weight (solid lines) for a binary blend of PS–PI diblocks ($M_{n,1}$ = 81.4 kg mol^{-1}, $f_{PS,1} = 0.6$, $M_{n,2}$ = 8.5 kg mol^{-1}, $f_{PS,2} = 0.46$) (Hashimoto *et al.* 1993). The mixtures show partial miscibility between two coexisting macrophases of lamellae with large and small spacing d_1 and d_2 in the composition range between $\phi_{c,s}$ and $\phi_{c,l}$. Domain spacings were obtained from SAXS on samples pre-annealed at 120 °C. The dotted curve indicates the $\frac{2}{3}$ power law for the domain spacing as a function of the average M_n of the blend.

curvature and packing density, as illustrated in Fig. 6.26. This depicts packing frustration in a binary blend of asymmetric copolymers in a curved geometry. In Fig. 6.26(b) there is clearly a region X in which the copolymer is depleted, leading to packing frustration. This can be largely relieved by a transformation to a planar geometry, as sketched in Fig. 6.26(c).

For the nearly symmetric copolymers studied by Hashimoto *et al.* (1994), the mismatch in composition was small. Thus, the approximate effective Flory–Huggins interaction parameter

$$\chi_{\text{eff}} = \left(f_1 - f_2\right)^2 \chi \tag{6.5}$$

(where f_1 and f_2 denote, say, the A content of each diblock) was much lower than the critical interaction parameter for macrophase separation,

$$\chi_{\text{s,macro}} = \frac{1}{N_1\phi_1} + \frac{1}{N_2\phi_2}. \tag{6.6}$$

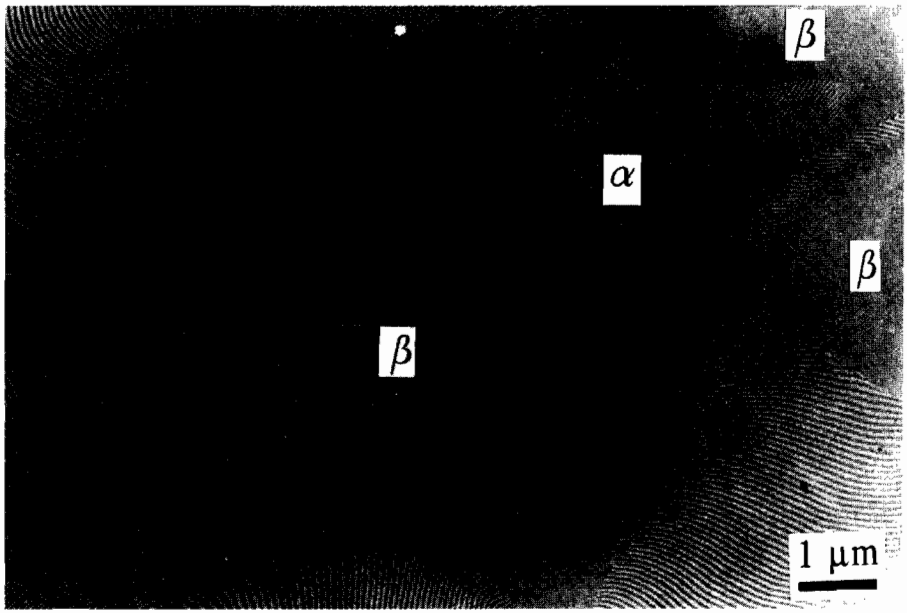

Fig. 6.25 TEM image for a 50:50 blend of PS–PI diblocks with different molecular weights but nearly identical composition ($M_n = 524\,\text{kg mol}^{-1}$, $f_{PS} = 0.46$, $M_n = 31.6\,\text{kg mol}^{-1}$, $f_{PS} = 0.45$) (Hashimoto *et al.* 1994). Different domains are labelled α and β.

Here $\phi_1 + \phi_2 = 1$, where ϕ_1 and ϕ_2 are the volume fractions of the two diblocks. Therefore, macrophase separation between disordered copolymers was not anticipated even for blends with $\delta > 10$. Nevertheless, it was observed for a blend containing equal proportions of long and short diblocks (Hashimoto *et al.* 1994). It was argued that macrophase separation is induced by initial microphase separation. Hashimoto *et al.* (1994) suggested that composition fluctuations of the long copolymer dominate those of the short copolymer because microphase separation occurs first for the long copolymer. These fluctuations cause segregation of the short diblocks to the interface which leads to macrophase separation of initially disordered domains of the short diblock if the asymmetry in chain length is sufficiently large. Within the small domains, microphase separation eventually occurs at a lower temperature or upon further loss of solvent. This process is sketched in Fig. 6.27. The segregation of short diblocks to the interface was confirmed by Shi and Noolandi (1994) in their self-consistent field theory calculations. An alternative explanation of these observations is that macrophase separation is a non-equilibrium effect resulting from the formation of a bimodal distribution of micelles in the solution from which the blend was cast.

The period of the lamellar phase observed in blends of two symmetric PS–PI diblocks was measured using SAXS and TEM by Kane *et al.* (1996). They observed that copolymers with $\delta = 5$ or less were microscopically mixed, whereas phase separation was observed in a blend with $\delta = 10$, in agreement with the

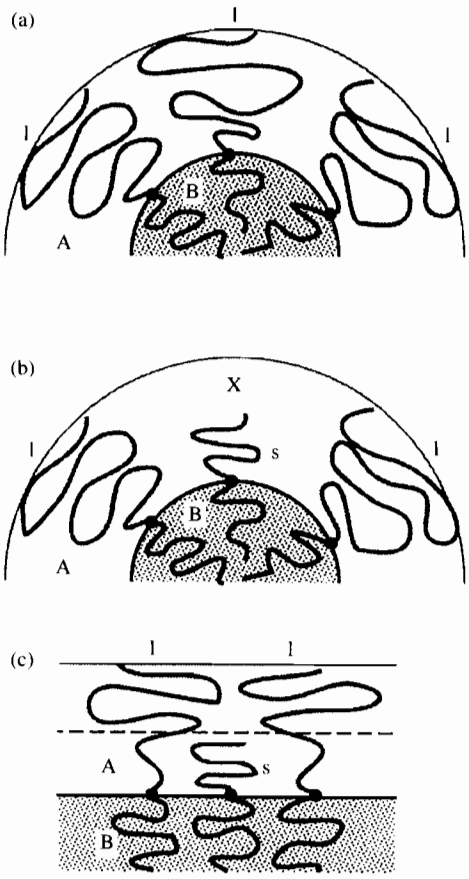

Fig. 6.26 Schematic illustrating packing frustration induced by addition of a short diblock (s) to a microphase of a long diblock (l) (Hasegawa and Hashimoto 1996). If the long diblock forms a spherical or cylindrical domain, for example, (a) segregation of the short diblock to the interface leads to regions of low packing density (region X in (b)). This frustration can be relieved if the interface adopts a planar geometry, driving a transition to a lamellar phase (with a bimodal copolymer brush at the interface) (c).

results of Hashimoto *et al.* (1993). A monotonic increase in domain spacings upon increase of high-molecular-weight copolymer content was observed. These results were compared to calculations using a model for strongly segregated diblock blends due to Spontak (1994) (see Section 6.7.1).

6.4.3 Mixtures of non-lamellar block copolymers

The morphology of blends of asymmetric PS–PI diblocks that do not form lamellar phases has been investigated using transmission electron microscopy by Koizumi *et al.* (1994*c*). They considered three cases: (i) approximately equal

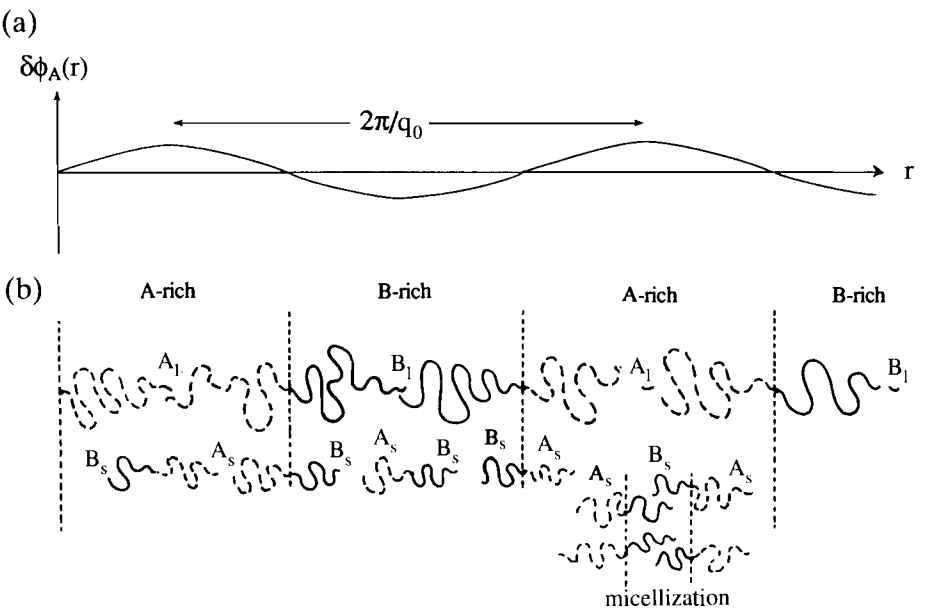

Fig. 6.27 Schematic illustrating the mechanism of macrophase separation of domains of a short diblock (s) in a binary diblock blend caused by the initial fluctuation-induced microphase separation of the long diblock (l) at a wavelength $d = 2\pi/q_0$ (a). This macrophase separation induced by microphase-separation mechanism was proposed by Hashimoto *et al.* (1994). The macrophase separation of the short diblocks is followed by microphase separation within their domains.

copolymer compositions (i.e. $\chi_{eff} \ll \chi_{s,macro}$) and a small value of δ so that macrophase separation was not expected; (ii) approximately equal copolymer compositions, but a sufficiently large δ to cause macrophase separation induced by microphase separation; (iii) a large difference in composition such that $\chi_{eff} > \chi_{s,macro}$ and macrophase separation occurs before microphase separation.

Using TEM to identify blend morphology, two diblocks with $f_{PS} \approx 0.8$ that form cubic-packed spherical phases and cylindrical phases respectively in the pure copolymer were found not to macrophase separate in a blend with $\delta = 2.2$, but to form single domain structures (cylinders or spheres) in the blend (Koizumi *et al.* 1994*c*). Similarly, blending a diblock with $f_{PS} = 0.26$ with one with $f_{PS} = 0.64$ ($\delta = 1.2$) led to uniform microphase-separated structures, with a lamellar phase induced in the 50:50 blend. Vilesov *et al.* (1994) also observed that blending two PS–PB diblocks with approximately inverse compositions (i.e. 22wt% PS and 72 wt% PS) induces a lamellar phase in the 50:50 blend. These examples all correspond to case (i).

In the case of two diblocks with $f_{PS} \approx 0.8$ forming spherical morphologies and a large molecular weight ratio $\delta = 7.4$ (case (ii)), the copolymers were found to be partly miscible (Koizumi *et al.* 1994*c*). The blend phase separated into large

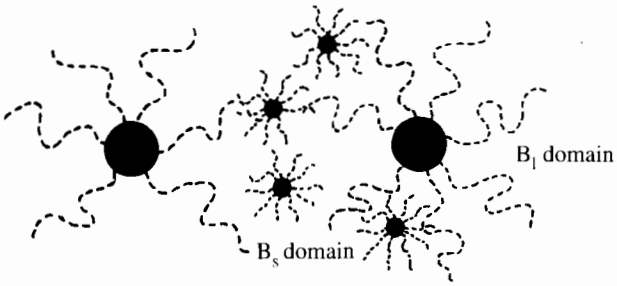

Fig. 6.28 Schematic showing segregation, in a binary diblock blend, of micelles formed by small diblocks induced by microphase separation of a large diblock into micelles (Koizumi *et al.* 1994*c*).

PI spheres rich in the longer copolymer l and small spheres of copolymer s for compositions $\phi_l \lesssim 0.8$, as depicted in Fig. 6.28. In other words, the long copolymer could solubilize up to about 20% of the small diblock. In the opposite case, it was found that the small copolymer could solubilize a lower fraction (less than 10%) of the long diblock. Since the inequality $\chi_{eff} << \chi_{s,macro}$ was satisfied because the composition difference between copolymers was small, the macrophase separation was assumed to result from the fluctuation-induced segregation of short copolymers to the interface similar to the mechanism discussed in the preceding section for lamellar-forming samples. In a sphere-forming blend, Koizumi *et al.* (1994*c*) propose that fluctuations lead to the initial formation of micelles of the long copolymer in the blend. The short diblocks are then constrained to self-assemble into small spheres in the corona of the pre-formed large spherical micelles.

In case (iii), a blend with $f_{PS,l} = 1 - f_{PS,2} = 0.8$ and $\delta = 1.2$ was examined (Koizumi *et al.* 1994*c*). For this asymmetric blend macrophase separation precedes microphase separation. A TEM image from a 30:70 blend is shown in Fig. 6.29. The continuous macrodomains consist of PI spheres in a matrix of PS, whereas the isolated domains contain PS cylinders dispersed in a matrix of PI. This was termed a superlattice structure, since two types of microphase-separated lattices coexist.

The phase behaviour of blends of a symmetric PS–PI diblock with an asymmetric PS–PI diblock (85 wt% PS) has recently been investigated using SAXS and TEM by Spontak *et al.* (1996). They report that, in general, the blends exhibit the same microstructure as a pure diblock with the equivalent composition. However, they noted coexisting morphologies in some of the blends. Addition of the asymmetric copolymer was initially observed to cause swelling of the lamellar domains of the symmetric diblock, and this was modelled using a simple strong segregation limit theory. On increasing the concentration of asymmetric copolymer further, coexistence of a cylindrical phase with the lamellar structure was observed. On further addition of the asymmetric copolymer, a bicontinuous morphology was observed (and imaged using three-dimensional images from

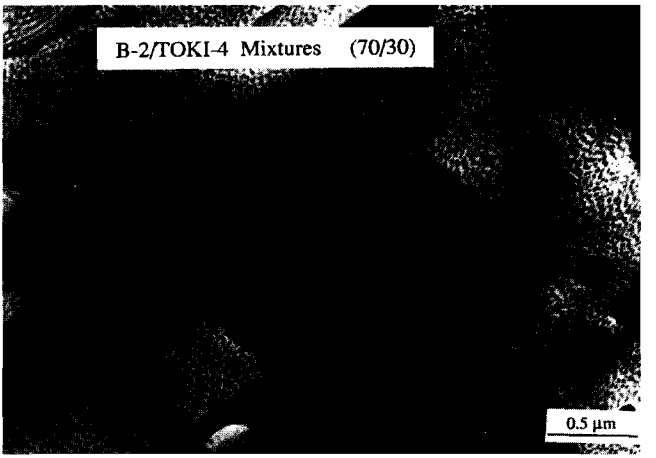

Fig. 6.29 TEM image of a 30:70 mixture of a diblock with $f_{PS} < 0.5$ ($M_n = 94\,kg\,mol^{-1}$, $f_{PS} = 0.83$) and a longer one with $f_{PS} > 0.5$ ($M_n = 176\,kg\,mol^{-1}$, $f_{PS} = 0.81$) (Koizumi *et al.* 1994*c*). The solvent-cast film was annealed at 150 °C. Domains rich in the diblock with $f_{PS} < 0.5$ (consisting of PS cylinders) are dispersed in the matrix of the diblock with $f_{PS} > 0.5$, which forms a microstructure of PI spheres. TOKI4 and B2 are notations of the authors for the diblocks.

electron tomographic analysis), then a hexagonal structure consisting of elliptical (and sometimes connected) cylinders.

Blends of diblocks have been used in the 'single component' approximation to map the phase behaviour of PE–PEE diblocks by Zhao *et al.* (1996). Here it is assumed that blends of diblocks with similar compositions satisfying $\chi_{eff} << \chi_{s,macro}$ exhibit the same morphology as diblocks with the same overall composition. The validity of this approximation has been tested using SCFT by Matsen and Bates (1995).

6.5 Theories for binary block copolymer/homopolymer blends

6.5.1 Theories for micellization

Micelle formation in solutions of an AB diblock in low-molecular-weight A homopolymer has been considered by Leibler *et al.* (1983), using Flory–Huggins theory to determine the free energy of mixing of micelles. This model is discussed in detail in Section 3.4.2.

The ordering of block copolymer micelles onto a lattice was considered by Leibler and Pincus (1984). They considered the interaction between a pair of micelles in homopolymer solvent and determined the repulsive interaction energy that arises from the change in homopolymer concentration in the micellar corona and related entropic effects. Using the estimated volume fraction for

ordering of hard spheres, the copolymer volume fraction for formation of an ordered phase, ϕ', was estimated. It was found to depend crucially on the length of the coronal block with respect to the homopolymer. When this ratio is large, ϕ' was found to be small. As noted by Leibler and Pincus (1984), the determination of the ordered phase is complicated by the nature of the intermicellar interactions, and they only considered repulsive interactions. Hard spheres with purely repulsive interactions crystallize in a close-packed (FCC) cubic structure, whereas for softer interaction potentials, a body-centred cubic lattice may result, as for neat block copolymers.

6.5.2 Strong segregation limit theory

A mean field approach was applied to determine homopolymer distributions in the lamellar phase of a blend of AB diblock and A homopolymer by Shull and Winey (1992). In the strong segregation limit, complete segregation of the A homopolymer into the A microdomain was predicted. Furthermore, in this limit, the diblocks were treated as 'brushes', wetted by homopolymer in the A domain. Composition profiles showing the distribution of homopolymer and copolymer were determined by numerical solution of the self-consistent field equations.

Theory for phase behaviour of such binary blends in the strong segregation limit was developed by Semenov (1993). He analysed the effect of varying homopolymer molecular weight. It was found that sufficiently long homopolymer A chains are incompatible with stretched A blocks in the copolymer, leading to macrophase separation. In other words, the solubility of a homopolymer in a microphase-separated block copolymer decreases sharply with increasing homopolymer molecular weight, in agreement with the earlier results of Whitmore and Noolandi (1985*b*) (Section 6.5.3). The formation of micelles with coronae containing long A blocks of copolymers (type IV in the Zhulina–Birshtein classification, see Fig. 3.18) and cores containing stretched B blocks was considered. The homopolymers were assumed to be sufficiently long such that penetration into the core (or inner part of the shell) did not occur. The interaction between micelles in this system was found to depend crucially on the homopolymer molecular weight. A critical degree of polymerization of the homopolymers, N_A^*, was found to be associated with the crossover from a regime where the interaction between micelles is purely repulsive to a regime where intermicellar attraction occurs. The critical degree of polymerization was found to be a function of copolymer molecular weight (here denoted N_{AB}), composition and the χ parameter. Attractive interactions for the $N_A > N_A^* \sim N_{AB}(\chi N_{AB})^{-1/9}$ regime were found to lead to macrophase separation of the system into homopolymer- and block copolymer-rich phases.

Addition of A homopolymer to type IV micelles was found to lead to a shift in the regions of stability of cylindrical and spherical morphologies towards more symmetric compositions compared to the neat copolymer. For sufficiently long homopolymers, the structure formed by asymmetric copolymer chains was anticipated to be copolymer micelles in a matrix of unstretched homopolymer chains. In contrast to the experimental results of Winey *et al.* (1991*c*) (who observed

transitions between lamellar, bicontinuous cubic, hexagonal cylindrical and spherical structures), Semenov (1993) found that in the limit of large ϕ_h, addition of homopolymer to a copolymer with a long A block does not induce morphological transitions.

Addition of A homopolymer to diblocks with short A blocks, however, was found to induce transitions from lamellae to cylinders to spheres. Indeed, it was observed that a spherical morphology can be stable even if the volume fraction of the minority component approaches 50% (Semenov 1993).

The stabilization of bicontinuous phases by addition of homopolymer to diblocks was studied in the strong segregation limit by Xi and Milner (1996). They found that a bicontinuous cubic structure (presumably the gyroid phase) is stable for $0.56 < f < 0.68$, with corresponding optimal volume fractions of homopolymer ranging from 0.18 to 1.00 for this range of f.

6.5.3 Self-consistent field theory

Self-consistent field theory was first applied to binary blends of diblock copolymer with homopolymer by Whitmore and Noolandi (1985*a*). The SCF method is outlined (for the case of block copolymer melts) in the Appendix. To simplify the calculations, they adopted the limiting Landau–Ginzburg perturbation approach (Section 2.3.2) to compute the free energy and polymer distribution functions near the order–disorder transition. A lamellar ordered structure formed by a symmetric diblock was considered, thus simplifying the expression for the free energy further, as there are then no cubic terms in the expansion in terms of the amplitudes of composition profiles. It was found that close to the ODT (occurring at $\chi N = 10.5$ in the pure diblock), addition of small amounts of homopolymer of high molecular weight to the homogeneous disordered phase can induce microphase separation. This was predicted to occur for $N_{Ah} \gtrsim N_{Ac}/2$ ($\alpha = \frac{1}{2}$), as illustrated in Fig. 6.30. Microphase separation induced by addition of homopolymer to the disordered phase of a diblock was observed experimentally by Owens *et al.* (1989) and Cohen and Torradas (1984). Whitmore and Noolandi (1985*a*) computed a large number of phase diagrams for the system PS–PB in PB at different temperatures and molecular weights of the components, for comparison with the experimental studies of Roe and Zin (1984) and Zin and Roe (1984). It was found that for blends with $\alpha \lesssim 1$, up to about 30% of homopolymer can be dissolved in the microstructure, depending on temperature. Increasing the degree of polymerization of the homopolymer led to a sharp decrease in solubility.

That new morphologies can be stabilized by blending a homopolymer with a diblock was shown by Matsen (1995*b*,*c*). He considered weakly segregated blends of AB diblock copolymer and A homopolymer using self-consistent field theory. It was found that, in general, minority component regions of a microstructure can accommodate a limited amount of homopolymer before macrophase separation occurs, whereas regions rich in the majority component can swell indefinitely leading to an unbinding transition. It was anticipated that the unbinding transitions in mean field theory would be replaced by transitions to micellar phases, when composition fluctuations are accounted for.

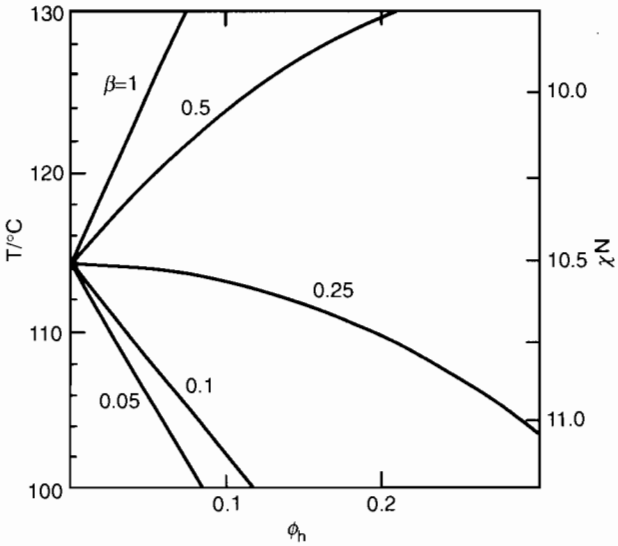

Fig. 6.30 Order–disorder transition in a binary homopolymer/diblock blend as a function of volume fraction of homopolymer computed using SCFT (Whitmore and Noolandi 1985*a*). The symmetric diblock has $N = 100$. Curves are shown for different values of $\beta = N_h/N_c$. The temperature scale on the left-hand side was calculated for PS–PB/PB blends.

Matsen (1995*b*) illustrated the applicability of the SCF method by performing calculations for blends of a diblock with $f = 0.45$ that forms an ordered lamellar phase, with homopolymers with different degrees of polymerization. The degree of polymerization of the copolymer was N, and that of the homopolymer βN. Considering blends of diblock and homopolymer with $\beta = \frac{2}{3}$, 1 and $\frac{3}{2}$, phase diagrams were computed as a function of χN and ϕ_h. The binodal lines separating one-phase and two-phase regions were determined by calculating the Helmholtz free energy as a function of ϕ_h, and performing a double tangent construction (Fig. 6.31(a)). For small values of χN, the copolymer and homopolymer are completely miscible and a single homogeneous disordered phase is stable. In Fig. 6.31, corresponding to the case of a homopolymer with a polymerization index greater than that of the copolymer, macrophase separation only occurs above the critical point at $\chi N = 5.45$. At higher χN, the system can separate into homopolymer- and copolymer-rich disordered phases, but only for $\chi N > 10.38$ does the diblock-rich phase order into a lamellar structure (in this calculation the hexagonal and BCC phases that are likely to be more stable than the lamellar phase close to the transition line were not considered). Decreasing the molecular weight of the homopolymer to $\beta = 1$ simply reduces the size of the two-phase region (Fig. 6.32). A further reduction can lead to the disappearance of a direct transition between the disordered phase and the two-phase region, as illustrated by the calculation for $\beta = \frac{2}{3}$ in Fig. 6.33. The structure of the two-phase region was investigated under these conditions. As ϕ_h increases from zero, the microstructure was found

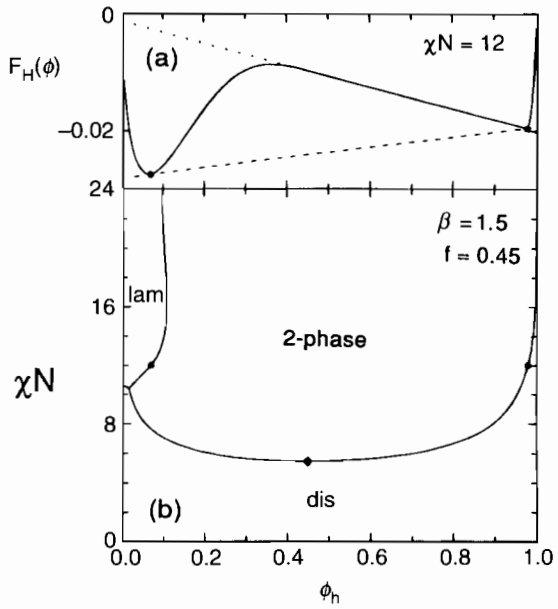

Fig. 6.31 Results from SCFT calculations for diblock/homopolymer blends (Matsen 1995*b*). (a) The dimensionless Helmholtz free energy $F_H(\phi)$ as a function of homopolymer volume fraction at $\chi N = 12$, $f = 0.45$ and $\beta = \frac{3}{2}$. The dashed line shows the double tangent construction used to locate the binodal points denoted with dots. The dotted line is the free energy of non-interacting bilayers. (b) Phase diagram obtained by repeating this construction over a range of χN. The dots are the binodal points obtained in (a), and the diamond indicates a critical point below which two-phase coexistence does not occur. The disordered homopolymer phase is labelled dis, and the lamellar phase lam.

to absorb homopolymer within the A-rich lamellae causing them to swell. At $\phi_h \approx 0.4$, the diblocks form bilayers, well separated by homopolymer. The exceptionally small interaction between bilayers is reflected in the nearly linear dependence of the free energy on ϕ_h. Additional homopolymer was found to further separate the bilayers, leading to a continuous unbinding transition where the domain spacing diverges to infinity, leaving a homopolymer-rich disordered phase.

The effect of adding homopolymer to ordered block copolymer melts was interpreted by considering how homopolymer is distributed within the microstructure (Matsen 1995*b*). Within the A-rich domains of a microstructure, the A blocks tend to segregate to the interfaces, whereas homopolymer A is preferentially located in the domain centre due to tension in the A blocks. This is countered by the entropy of mixing which favours a more uniform distribution of homopolymer. To allow homopolymer near the interface, a phase transition may occur to a microstructure where the interface is less curved towards the A-rich domains (this is the reverse of the process shown in Fig. 6.9). Even without such a phase transition, increasing homopolymer content leads to an increasing

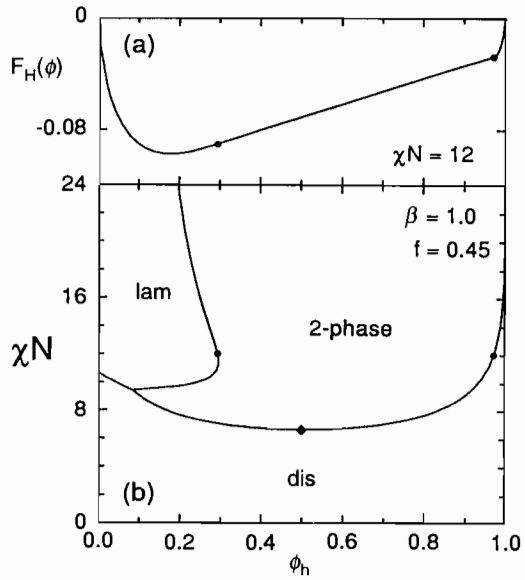

Fig. 6.32 Similar to Fig. 6.31, but for $\beta = 1$ (Matsen 1995*b*).

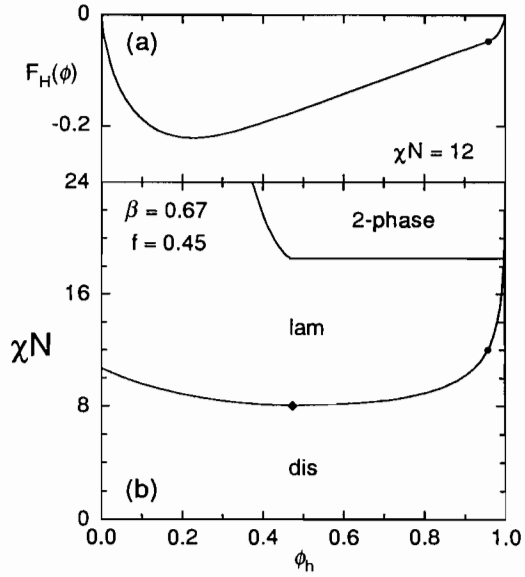

Fig. 6.33 Similar to Fig. 6.31, but for $\beta = \frac{2}{3}$ (Matsen 1995*b*). In this case the Helmholtz free energy curve indicates that macrophase separation does not occur, and so an unbinding transition occurs at the composition indicated by the dot. In the phase diagram, the diamond shows where the stability line for microphase separation meets the unbinding transition (Lifshitz point).

tendency for homopolymer to penetrate towards the interface. This in turn increases the interfacial area per block and increases the A domain thickness. This allows the B blocks to contract, and hence reduce the thickness of the B-rich domains (Matsen 1995*b*). These findings are in agreement with the experimental results of Winey *et al.* (1991*b*) discussed in Section 6.2.3. These domain spacing changes are illustrated in Fig. 6.34, which shows dimensionless lamellar spacings for a diblock with $f = 0.45$ as a function of concentration of homopolymers with $\beta \leq 1$. Addition of homopolymer generally causes the total lamellar spacing to increase, although it can decrease on addition of homopolymer of a sufficiently low molecular weight, as apparent in Fig. 6.34(a).

Matsen (1995*b*) also calculated sections through the phase diagram in the weak segregation limit for a fixed χN value for blends with given values of β. Because asymmetric copolymers were considered, ordered phases other than lamellae

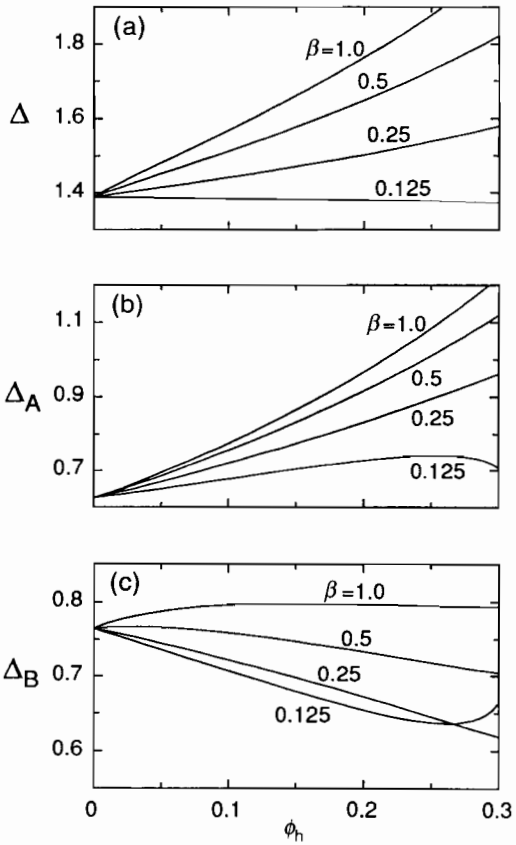

Fig. 6.34 Dimensionless lamellar spacing $\Delta = d/aN^{1/2}$ for an $f = 0.45$ diblock at $\chi N = 12$ as four different homopolymers are added (with degrees of polymerization βN) (Matsen 1995*b*). Dimensionless widths of the A- and B-rich lamellae are shown in (b) and (c) respectively.

were included in the calculations. A phase diagram computed for a blend of diblock and homopolymer with $\beta = 1$ at $\chi N = 12$ as a function of ϕ_h and f is illustrated in Fig. 6.35. Biphasic regions are generally narrow and were omitted from the phase diagram. However, biphasic regions separating lamellar and $Ia\bar{3}d$ (gyroid) and hexagonal and $Ia\bar{3}d$ phases are sufficiently wide to be noticeable. It was found that addition of homopolymer to the BCC micelle phase ($Im\bar{3}m$ symmetry) leads to the reordering of spheres into a close-packed spherical phase (CPS). Similarly, the $Ia\bar{3}d$ phase transforms to a hexagonal perforated lamellar (HPL) phase on addition of homopolymer to the matrix phase. In contrast, addition of homopolymer to the minority component of the $Ia\bar{3}d$ phase can lead instead to a transition to the $Pn\bar{3}m$ ('ordered bicontinuous double diamond') phase, provided that the homopolymer has a sufficiently low molecular weight, as found in a phase diagram for $\beta = \frac{2}{3}$ (not shown). These phase transitions on addition of homopolymer were attributed to the relief of packing frustration by the homopolymer. In order to accommodate homopolymer in the A block of the copolymer microstructure, a transition occurs to a structure in which the interface is more curved towards the B-rich domains. This is the same trend that occurs as f increases.

Self-consistent field theory has recently been employed by Janert and Schick (1996, 1997*a*) to analyse the swelling of diblock lamellar phases with homopolymer. It was shown that a complete unbinding transition, where added homopolymer swells the lamellae, finally leading to a transition to a disordered phase, is predicted by mean field theory. The swelling does not continue without limit.

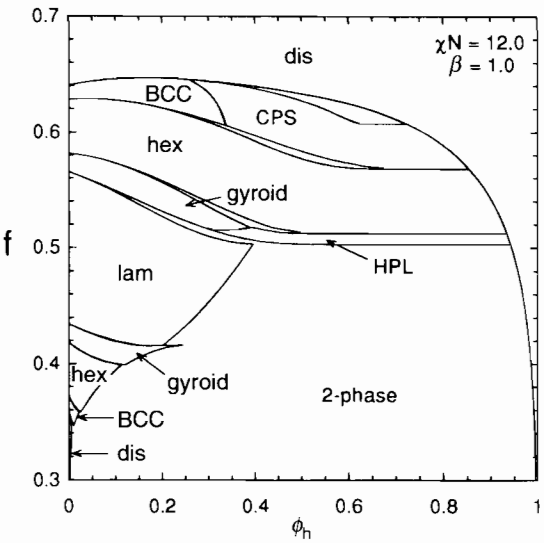

Fig. 6.35 Calculated constant χN (=12) phase diagram for a binary blend of a diblock and homopolymer with equal degree of polymerization ($\beta = 1$) as a function of the volume fraction of homopolymer, ϕ_h, and the composition of the diblock (f) (Matsen 1995*b*). For clarity, only the largest biphasic regions are indicated.

Instead, coexistence between a lamellar phase of finite wavelength and the disordered phase develops on increasing χ. This change of behaviour with increasing χ can be either continuous or first-order. Janert and Schick showed that for a symmetric system ($f = \frac{1}{2}$, $\alpha = 1$) the unbinding transition is first order, with an associated pre-unbinding transition line at lower χN, separating a region of coexistence of lamellar phases with different periods. The phase diagram for this system is shown in Fig. 6.36. The strongly segregated lamellar phase can only be swollen to a certain extent by homopolymer before phase separation occurs into an almost pure disordered homopolymer phase, A. However, below the unbinding transition, i.e. $\chi N < \chi_U N = 11.766$, the lamellar phase can be swollen indefinitely. At the unbinding line (dashed), the separation between lamellae diverges. The unbinding transition at $\chi_u N$ along the lamellar–disorder phase boundary is a first-order one. The pre-unbinding line extends to a critical point at $\chi_{pre} N = 11.344$, indicated in Fig. 6.36 by a dot. Along the pre-unbinding line, two lamellar phases coexist, one of unswollen lamellae L and one of layers

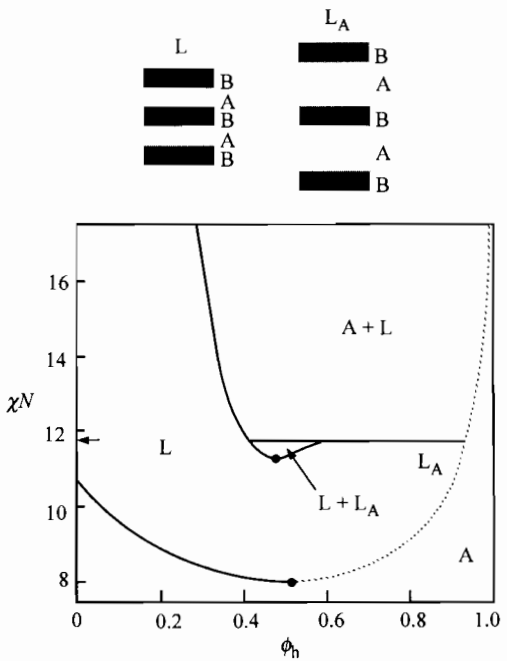

Fig. 6.36 Phase diagram calculated using SCFT for a blend of a symmetric diblock with a homopolymer with $\beta = 1$ (see Fig. 6.32 for a blend with a diblock with $f = 0.45$) as a function of the copolymer volume fraction ϕ_h (Janert and Schick 1997*a*). The lamellar phase is denoted L, L_A denotes a swollen lamellar bilayer phase and A is the disordered homopolymer phase. The pre-unbinding critical point and the Lifshitz point are shown with dots. The unbinding line is dotted, while the solid line is the line of continuous order–disorder transitions. The short arrow indicates the location of the first-order unbinding transition, $\chi_U N$.

strongly swollen by A homopolymer, L_A. The line of complete unbinding transitions extends to a Lifshitz critical point at $\chi_L N = 8.0$. Here it meets the line of continuous transitions from the disordered phase to the lamellar phase L (Janert and Schick 1996).

6.6 Theories for blends of block copolymers with two homopolymers

6.6.1 Brush theory

Polymer brush theory was applied to the compatibilization of homopolymers A and B by an AB diblock by Leibler (1988). The reduction in interfacial tension due to the segregation of copolymers to the interface was calculated. Considering a film of block copolymers at the homopolymer–homopolymer interface, the free energy was found to be

$$F_{\text{film}} = \gamma_0 A + Q\left[g_A(\sigma) + g_B(\sigma)\right], \tag{6.7}$$

where γ_0 is the interfacial tension of the homopolymer interface in the absence of copolymer, A is the interfacial area, $\sigma = A/Q$, where Q is the number of copolymer chains, and the g_i are free energies per chain of A and B brushes. Expressions for these were obtained accounting for elastic entropic contributions of stretching blocks, the entropy of mixing of the blocks with the homopolymers and the translational entropy of the homopolymers in a two-dimensional film. The interfacial tension is obtained from eqn 6.7 as

$$\gamma = \left(\frac{\partial F_{\text{film}}}{\partial A}\right)_Q = \gamma_0 - \pi_A - \pi_B, \tag{6.8}$$

where

$$\pi_i = -\partial g_i / \partial \sigma \tag{6.9}$$

is the film (Langmuir) pressure. Expressions for g_i were derived by Leibler for 'wet' and 'dry' brushes. For the case of long copolymer chains ($N_c > N_h^{3/2}$) with relatively large interfacial area, where homopolymer can still penetrate the copolymer brushes, the term wet brush was applied. In the dry brush, long homopolymer chains only penetrate the copolymer layer partially.

However, Noolandi (1991) has noted that eqn 6.7 only contains elastic contributions to the reduction in interfacial tension, and not the major contribution from enthalpic terms which are included in the expression derived by Noolandi and Hong (eqn 6.10). Noolandi (1991) argues that the major reduction in interfacial tension arises from the energetically favoured orientation of the copolymer blocks in their compatible homopolymers.

Leibler (1988) also noted that the very low interfacial tension resulting from the addition of copolymer could lead to a thermodynamically controlled vesicle phase containing minority homopolymer particles surrounded by a copolymer film and suspended in the majority homopolymer matrix. The size distribution of the droplets was found to depend on the rigidity and spontaneous

curvature of the interfacial film which is controlled by molecular parameters of the copolymer.

Wang and Safran (1990) considered the emulsification of polymer blends by diblocks using expressions for the stretching and bending free energy of a grafted polymer layer (i.e. brush). Expressions for the curvature elastic moduli and the radius of curvature were obtained. A phase diagram was constructed as a function of ratio of the volume fraction of block copolymer to homopolymer and the asymmetry of the copolymer, ε. For $\varepsilon \neq 0$, a spherical microstructure was found to always be the first emulsion phase to occur on increasing the diblock content in the blend. On further increasing the diblock content, successive regions of spheres + cylinders, cylinders, cylinders + lamellae were predicted.

6.6.2 Self-consistent field theory

Theory for blends of two homopolymers with block copolymers was developed by Noolandi and Hong (1982) using the SCF method. They considered a quaternary system with a diblock in a good solvent for two incompatible homopolymers. Calculation of density profiles revealed that the block copolymer tends to be selectively located at the interface, and that the homopolymer tends to be excluded from the interphase. This is illustrated by the representative density profiles in Fig. 6.37. The exclusion of homopolymer from the interphase was found to be enhanced by increasing the molecular weight of the block

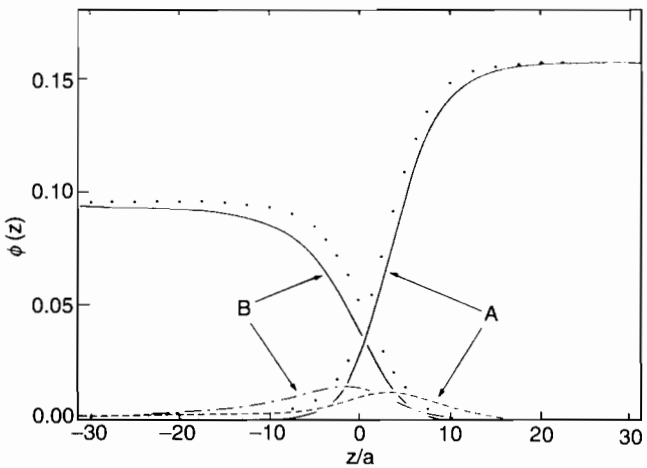

Fig. 6.37 Interfacial volume fraction profiles calculated for a ternary blend of a PS–PB block copolymer with PS and PB homopolymers in a good solvent (Noolandi and Hong 1982). The diblock has $N = 600$ and $f = \frac{2}{3}$. The homopolymers have infinite molecular weight. The solid lines are the volume fractions of homopolymer (A = PS) (B = PB), the dashed lines indicate the volume fractions of PS and PB blocks of the diblock. The dots correspond to the total volume fractions of the A and B components and the position is measured in units of a segment length $a = 6.95$ Å.

copolymer. The reduction of interfacial tension with increasing block copolymer concentration was calculated. The results were compared with the experimental results of Gaillard *et al.* (1980) on PS–PB diblocks in a blend with PS and PB homopolymers and styrene monomer. The presence of solvent dilutes the monomeric interactions and leads to a reduction in interfacial tension, as noted by Leibler (1988). The mechanism for reduction of the interfacial tension is then different to that for the ternary blend without solvent. Noolandi and Hong (1982) also estimated the critical concentration of block copolymer required for micellization in the bulk of the homopolymer. It was found that the cmc decreases with increasing copolymer molecular weight. Other theories for micellization of block copolymers (often developed for the case of homopolymer solvents) are discussed in Section 3.4.

Subsequently, Noolandi and Hong (1984) developed the SCF theory to model the reduction in interfacial tension due to addition of copolymer to a homopolymer blend. The reduction in interfacial tension with increasing copolymer molecular weight and concentration was found to arise mainly from the energetically preferred orientation of the blocks normal to the interface with their respective homopolymers. This is counterbalanced by the entropy loss resulting from localization of the copolymer at the interface. For a blend with equal concentrations of homopolymers with equal degrees of polymerization and a long symmetric diblock, the interfacial tension upon addition of homopolymer was shown to be reduced by an amount (Noolandi and Hong 1984)

$$\Delta\gamma = \gamma - \gamma_0 = \frac{1}{\varrho_0}\int \mathrm{d}z \left(\frac{\phi_c(z)}{N_c} \ln\left[\phi_c(z)/\phi_c\right] \right) - \frac{1}{N_c}\left[\phi_c(z) - \phi_c\right] - \frac{1}{2}\chi\phi_h\left[\phi_c(z) - \phi_c\right]. \tag{6.10}$$

Here $\Delta\gamma$ is in units of $k_B T$, ϱ_0 is the number density of pure components (assumed equal), $\phi_c(z)$ is the local volume fraction of block copolymer at the interface and ϕ_c is the overall volume fraction of block copolymer. For $N_c\chi\phi_h \ll 1$ this can be approximated as (Noolandi and Hong 1984)

$$\Delta\gamma \approx \frac{\phi_c \varrho_0 a}{N_c} \exp\left(\frac{1}{2}\chi N_c \phi_h \right) \tag{6.11}$$

This exponential dependence leads to the dramatic compatibilization effect of block copolymers in immiscible polymer blends. Leibler (1988) noted that for strongly incompatible systems, the exponential increase of $\Delta\gamma$ with ϕ_h only occurs for small ϕ_c. At larger copolymer content, the reduction in interfacial area per block causes a slower increase in $\Delta\gamma$ (i.e. reduction in γ).

Whitmore and Noolandi (1985*b*) developed the self-consistent field theory to examine micellization in AB diblocks in a blend of AB diblock and A homopolymer 'solvent'. The model was applied specifically to the case of PS–PB diblocks in PB homopolymer for comparison with the results of small-angle neutron scattering (SANS) experiment by Selb *et al.* (1983). This model is discussed in more detail in Section 3.4.2.

The Hong–Noolandi theory was later extended by Banaszak and Whitmore (1992), who calculated phase diagrams for blends undergoing macrophase separation as well as microphase separation. Only a lamellar microphase was considered for simplicity. Phase diagrams were computed for a model symmetric system, consisting of a symmetric diblock (with equal segment lengths) in a blend with two homopolymers of equal degrees of polymerization. It was found that along the isopleth the microphase is stabilized by a much lower concentration of diblock than that for either binary homopolymer/copolymer blend. For example, a microphase was stable in a blend with 15% diblock along the isopleth and 40% diblock in the binary blends at $\chi N = 16.4$. This is consistent with the experimental results of Tanaka *et al.* (1991), who found long-range order in PS/PI/PS–PI blends for copolymer volume fractions as low as $\phi_c = 0.1$. With a further increase in χ (e.g. to $\chi N = 17.2$) the regions of microphase and macrophase separation overlapped. At this point the ternary phase diagram became quite complex, exhibiting single-phase regions M and D (where M denotes microphase and D denotes homogeneous disordered phase), a two-phase DD region at the base of the triangle, two-phase MD 'fingers' and a very small three-phase region. On increasing χ further, macrophase separation of binary homopolymer/copolymer blends was observed.

Phase diagrams were also computed by Banaszak and Whitmore (1992) for asymmetric model systems, with symmetric diblocks in a blend with homopolymers of different degrees of polymerization or asymmetric copolymers in a blend of equal length homopolymers. Finally, they considered the PS–PI system, computing a phase diagram using model parameters for comparison with the experimental results of Hashimoto and co-workers (Hashimoto *et al.* 1981, 1990; Inoue *et al.* 1970; Tanaka *et al.* 1991). The calculations revealed that the pure copolymer (at $\chi N = 11.2$) is microphase separated. Addition of either homopolymer PI or PS dissolves the microphase, but more PS (50%) than PI (about 15%) is needed. This is consistent with the fact that as the PS homopolymer is initially added to the copolymer, the overall composition of the system changes from 45% PS towards 50% PS, leading to an increased stabilization of the ordered phase with respect to the homogeneous state. Competing against this is the lower molecular weight of the PS, which would tend to destabilize the ordered microphase. The binary homopolymer blend was predicted to macrophase separate, but not the binary copolymer/homopolymer blends. The ordered microphase was found to be most stable near the isopleth.

Self-consistent mean field theory was applied to study interfacial properties of ternary blends of A and B homopolymers and AB diblocks by Shull *et al.* (1990). It was found that a copolymer can compatibilize the homopolymers, with the surface tension disappearing depending on the copolymer molecular weight. The ability of a copolymer to reduce the interfacial tension was found to be highest for smaller block copolymers and smaller values of χ. In the strong segregation limit, the effects of copolymer on the interfacial properties were found to be dominated by the length of the longer copolymer block. The confinement of copolymer joints to the centre of the interphase was found to lead to a significant broadening of the A–B interface. The width of the profile is primarily determined

by χ. Under certain conditions, an attractive interaction between segregated polymer layers in a high-molecular-weight homopolymer matrix was predicted, due to a positive contribution to the interfacial tension (Shull *et al.* 1990).

The effect of AB diblock size relative to the homopolymers on the compatibilization of A/B homopolymer blends was examined using numerical self-consistent field theory (in two dimensions) by Israels *et al.* (1995). They found that the interfacial tension between homopolymers can only be reduced to zero if the blocks in the diblock are longer than the corresponding homopolymer. Short diblocks were observed to form multilamellar structures in the blend, whereas a microemulsion was formed when relatively long copolymers were added to the homopolymer mixture. These observations were compared to experiments on blends of PS/PMMA and symmetric PS–PMMA diblocks reported in the same paper. AFM was used to measure the contact angle of dewetted PS droplets on PMMA, and the reduction in the interfacial tension caused by addition of PS–PMMA diblocks was thereby determined. The experiments revealed that the interfacial tension was reduced to a very small value by addition of long diblocks, due to emulsification of the homopolymer by the diblock, in agreement with the theoretical expectation (Israels *et al.* 1995).

Janert and Schick (1997*b*) have applied SCF theory to study the phase behaviour of ternary blends of A and B homopolymers and AB diblocks. Considering first symmetric or nearly symmetric diblocks in blends with homopolymers of differing degrees of polymerization, they obtained phase diagrams containing all the classical ordered phases, and regions of two- and three-phase coexistence. In general, it was found that homopolymers longer than the diblocks are expelled from the microstructure. This is due to the loss of configurational entropy due to confinement in the microstructure. Large regions of coexistence between an A-rich ordered phase and a B-rich disordered phase are observed. Representative phase diagrams are shown in Fig. 6.38 for the case $N_{h,1} = N_{h,2} = 1.5N_c$ and $N_{h,1} = N_c$, $N_{h,2} = 1.5N_c$. In the former system, biphasic regions for low homopolymer contents are separated by a broad region of three-phase coexistence. Along the isopleth, there is a direct transition from the lamellar phase to three-phase coexistence. In contrast, for the system with $\beta_1 = 1$ and $\beta_2 = 1.5$, there is a wide two-phase coexistence region, and an unbinding transition (shown as a dashed line) from the lamellar phase into an almost B-free disordered phase. Janert and Schick (1997*b*) found that homopolymers shorter than the diblock are dissolved in the diblock microstructure, leading to phases characterized by increasing mean curvature of the internal interfaces. Homopolymers with $0.5 \leq \beta \leq 1.0$ can swell the microstructure indefinitely, leading to a complete unbinding transition within mean field theory, indicated by the dashed line in Fig. 6.38(b). It was anticipated that thermal fluctuations would destroy such a strongly swollen phase and bring about a weak, first-order transition to a disordered phase instead. Shorter homopolymers ($0.25 \leq \beta \leq 0.5$) were found to swell the microstructure, but due to the substantial entropy gain due to their random distribution, they cause the unbinding transition to be pre-empted by discontinuous transitions to a disordered phase. A phase diagram in this limit is shown in Fig. 6.39. Addition of a short homopolymer has a strong disordering effect on

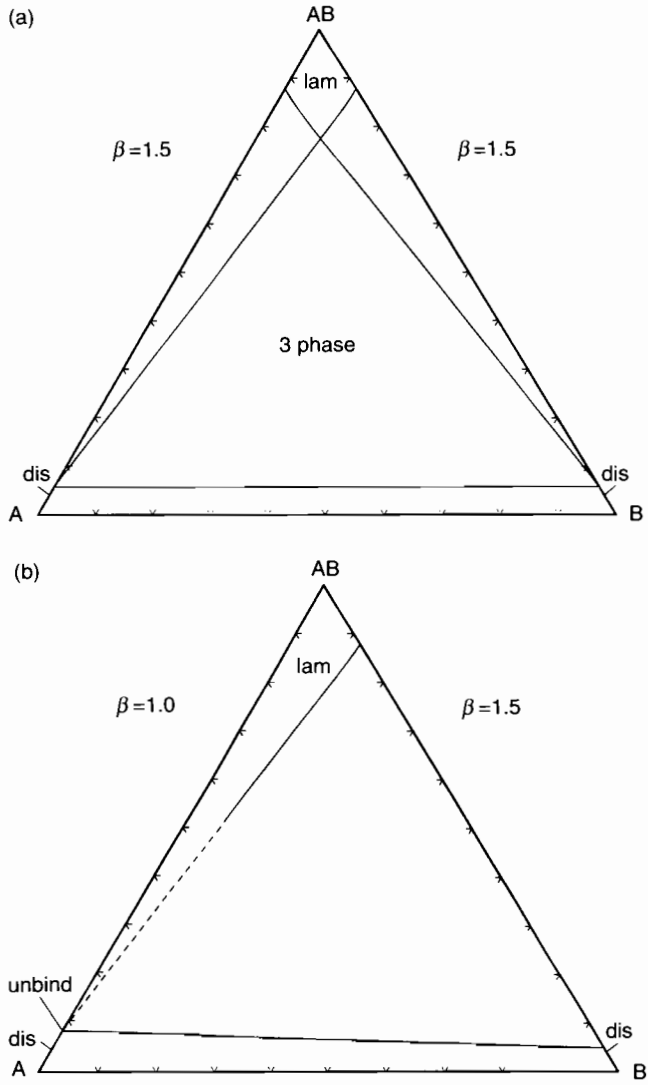

Fig. 6.38 Calculated constant χN (= 11) phase diagram for a symmetric diblock blended with high-molecular-weight homopolymers (Janert and Schick 1997*b*). Biphasic regions are unlabelled. Note the large region of three-phase coexistence between the lamellar and the A-rich and B-rich disordered phases. (a) Both homopolymers have $\beta = 1.5$; (b) $\beta_1 = 1.0, \beta_2 = 1.5$.

the ternary blend. The asymmetry in the phase diagram in Fig. 6.39 results from the fact that ordered phases in binary blends with the longer homopolymer can solubilize a lower volume fraction of the homopolymer than in the converse situation on the right-hand side. Addition of very short homopolymers ($\beta \leq 0.25$) leads to the disordering of the microstructure as the translational entropy of

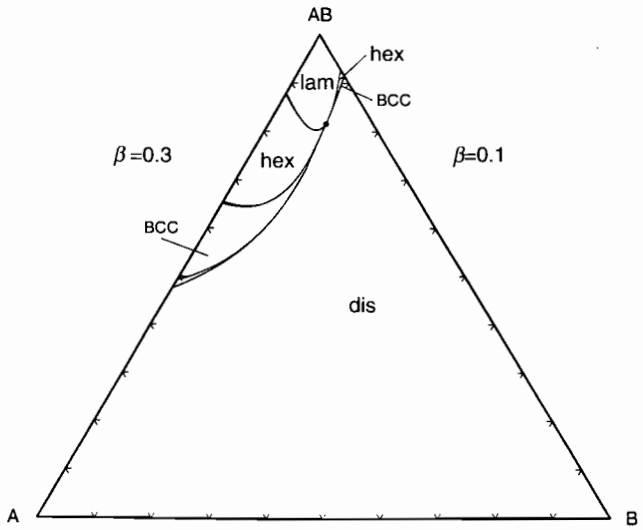

Fig. 6.39 Calculated constant χN (= 11) phase diagram for a symmetric diblock blended with low-molecular-weight homopolymers (Janert and Schick 1997*b*). Ordered and disordered phases are indicated. The homopolymers have $\beta = 0.1$ and $\beta = 0.3$.

mixing exceeds the enthalpic penalty due to the increased number of A, B contacts. The disordering effect below this value of β was noted earlier by Broseta and Fredrickson (1990). Finally, Janert and Schick (1997*b*) observed that for f close to 0.5 and β not very different from 1, increasing f and decreasing $N_{h,1}/N_{h,2}$ have similar effects on the overall topology of the phase diagram.

The case of a symmetric diblock blended with A and B homopolymers, all having equal chain length, was examined in depth by Janert and Schick (1997*a*). They found no hexagonal or cubic phases for any composition within mean field theory. Instead, up to three distinct lamellar phases were found to be able to coexist. One is symmetric and the other two are asymmetrically swollen by A or B homopolymer. For strong incompatibility, added homopolymer was found to eventually phase separate from the microstructure. In the weak segregation limit, the symmetric lamellar phase at moderate dilution was predicted to break up into two coexisting swollen lamellar phases. These phases can be swollen indefinitely, leading to an unbinding transition to the disordered phase. As a result, lamellar order can be found at much lower diblock concentrations towards the binary sides of the phase diagram than on the isopleth. The phase diagram for the isopleth (equal amounts of A and B homopolymer) is remarkably rich, as illustrated in Fig. 6.40. In this phase diagram, for large χN ($\chi N \geq \chi_U N = 11.222$), the symmetric lamellar phase can only be swollen to a certain extent before additional homopolymer phase separates from the microstructure. Since the homopolymers are immiscible for values of χN greater than 2.0, a three-phase region results with coexisting A-rich and B-rich disordered phases and the symmetric lamellar phase. For $\chi N < \chi_U N$, three-phase coexistence between ordered

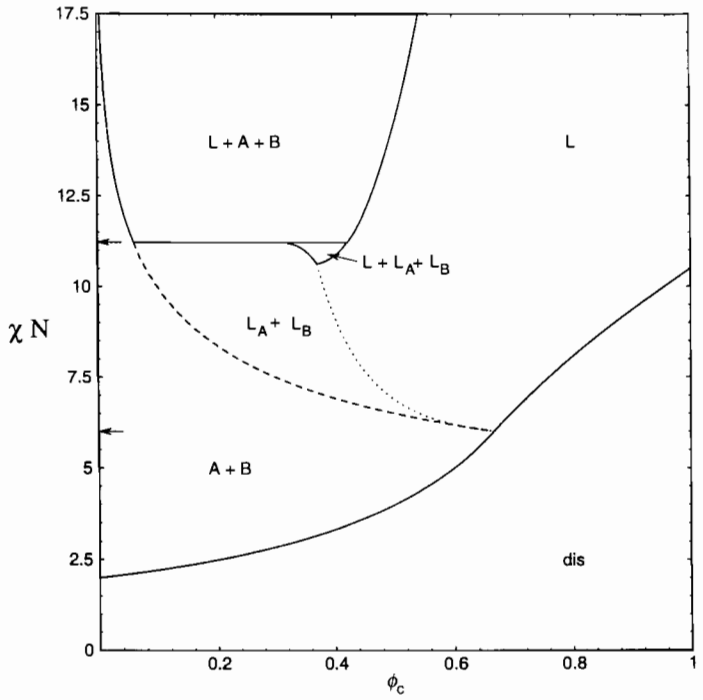

Fig. 6.40 A phase diagram calculated using SCFT for a mixture containing equal amounts of two homopolymers and a symmetric diblock, all with equal chain length (Janert and Schick 1997*a*). A-rich and B-rich swollen lamellar bilayer phases are denoted L_A and L_B respectively whilst the corresponding disordered phases are denoted A and B. The consolute line of asymmetric bilayer phases L_A and L_B, shown dotted, is schematic. The dashed line is the unbinding line. The arrows indicate the locations of the unbinding transition $\chi_U N$ and multicritical Lifshitz point, $\chi_M N = 6.0$.

and disordered phases is replaced by three ordered lamellar phases. These are the symmetric lamellar phase L, the A-rich lamellar phase L_A and the B-rich lamellar phase L_B. In the L_A phase, lamellae containing component A at a composition close to that of the disordered phase alternate with bilayers rich in B chains. At the unbinding line (denoted in Fig. 6.40 with dashes), the period of this structure diverges and the L_A phase undergoes complete unbinding into the A-rich disordered phase. Similarly the B-rich phase unbinds into the B-rich disordered phase. The three-phase region between lamellar phases L_A, L_B and L persists for $\chi_U N < \chi N < \chi_T N$. It ends at a tricritical point, $\chi_T N = 10.627$. At lower values of χN, the two asymmetric lamellar phases merge along a line of critical points (shown dotted in Fig. 6.40) at which they form the symmetric lamellar phase. This consolute line was presumed to end at the multicritical Lifshitz point, $\chi_M N = 6.0$. In a multidimensional phase diagram, this point represents the meeting of the consolute line of lamellar phases, the consolute line of disordered phases, two lines of Lifshitz points on the binary side of the diagram, and two

lines of critical end-points. The lines of Lifshitz points separate the sheets of microphase separation transitions from the sheets of complete unbinding transitions and the lines of critical end-points correspond to the intersection of sheets of unbinding transitions with the first-order sheet of transitions to A-rich and B-rich phases.

The stability of swollen lamellar phases was interpreted on the basis of interactions between isolated lamellae. The cost of creating an interface increases with the magnitude of the density difference across it. In a lamellar phase, there is an overall attraction between neighbouring layers, since the presence of the adjacent interfaces prevents the density difference across each one from achieving the value across an isolated interface. As the density difference across the interface increases with the degree of segregation, the attraction between lamellae grows with χN. At short distances, an elastic repulsion due to compression of copolymers stabilizes the lamellae at a non-zero separation. For large values of χN, the attraction is outweighed by the entropic penalty for phase separation. It then becomes more favourable for added homopolyer to phase separate from a dense lamellar phase than to swell it. The same mechanism prevents the formation of a symmetrically swollen phase for $\chi N \leq \chi_U N$ in Fig. 6.40. In a symmetrically swollen lamellar phase, each pair of interfaces is well separated, whereas in the bilayer phases L_A and L_B, only every second pair of interfaces is well separated. The binding energy thus gained compensates the entropy loss accompanying phase separation. Fig. 6.41 illustrates the instability of the symmetric

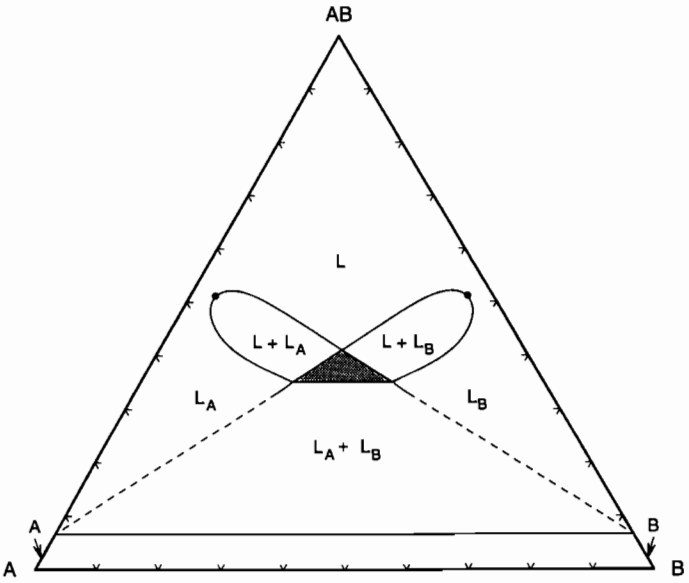

Fig. 6.41 Calculated constant χN (= 11.0) phase diagram for a blend containing equal amounts of two homopolymers and a symmetric diblock, all with equal chain length (Janert and Schick 1997*a*). The region of three-phase coexistence between ordered lamellar phases is shaded. Extrapolated phase boundaries are shown with dashes.

lamellar phase with respect to asymmetric ones. Going beyond mean field theory, composition fluctuations could stabilize a microemulsion phase instead of metastable ordered phases (Janert and Schick 1997*a*).

6.6.3 Flory–Huggins and Landau mean field theories

The emulsifying effects of diblock copolymer added to blends of homopolymer were first considered using Flory–Huggins theory and the random phase approximation by Leibler (1981, 1982). In the Flory–Huggins theory the combinatorial entropy and enthalpy for mixing polymer chains are computed using a mean field model for chain segments on a lattice, as discussed by, for example, Gedde (1995) and Young and Lovell (1991). For ternary blends containing block copolymer in the homogeneous state, the Flory–Huggins free energy per monomer can be approximated by (Leibler 1981; Scott 1952)

$$F_0/k_BT = \frac{1}{N}\sum_{i=1}^{3}\phi_i \ln\phi_i - \frac{1}{4}\chi(\phi_1 - \phi_2)^2. \tag{6.12}$$

Here ϕ_1, ϕ_2, ϕ_3 are the volume fractions of monomers of the two homopolymers and the AB diblock (of equal N) respectively and χ is the interaction parameter between A and B monomers.

Considering nearly compatible homopolymers (small χN), copolymer was found to promote mixing of the homopolymers with diblock present in both phases, but tending to segregate to the interface (Leibler 1982). In contrast, for nearly incompatible homopolymers, the copolymer chains were found to be more uniformly distributed in both domains. In highly incompatible blends, the tendency for segregation of the copolymer to the interface is enhanced. Leibler (1982) derived expressions for the structure factor, which are given below (eqns 6.16 and 6.17). He also calculated interfacial density profiles, and quantified the reduction in interfacial tension that accompanies increasing copolymer concentration.

Rigby *et al.* (1985) showed using a Flory–Huggins model that for symmetric blends, the spinodal and critical temperatures decrease linearly with increasing content of a symmetric diblock for blends with equal volume fractions of homopolymers (with the same molecular weight). The condition for a linear decrease of the binodal was less restrictive, not requiring equal concentrations of homopolymer in the blend.

The phase behaviour of blends of homopolymers containing block copolymers is governed by a competition between macrophase separation of the homopolymer and microphase separation of the block copolymers. The former occurs at a wavenumber $q^* = 0$, whereas the latter is characterized by $q^* \neq 0$. The locus of critical transitions at q^*, the so-called λ line, is divided into $q^* = 0$ and $q^* \neq 0$ branches by the (isotropic) Lifshitz point. The Lifshitz point can be described using a simple Landau–Ginzburg free-energy functional for a scalar order parameter $\psi(\boldsymbol{r})$, which for ternary blends containing block copolymers is the total volume fraction of, say, A monomers. The free energy density can be written (Selke 1992)

$$F\left[\psi(\boldsymbol{r})\right] = a_2\psi(\boldsymbol{r})^2 + a_4\psi(\boldsymbol{r})^4 + a_6\psi(\boldsymbol{r})^6 + \ldots + c_1\left(\nabla\psi(\boldsymbol{r})\right)^2 + c_2\left(\nabla^2\psi(\boldsymbol{r})\right)^2 + \ldots \tag{6.13}$$

where the phenomenological coefficients a_2, a_4, $a_6 \ldots c_1$, c_2 depend on the state of the system. At an ordinary critical point $a_2 = 0$, with all remaining coefficients positive. Such a critical point separates a disordered state from one that is phase separated with $q^* = 0$. A *Lifshitz point* is defined by the vanishing of both a_2 and c_1. Thus the Lifshitz point is a special type of critical point that connects three distinct phases: disordered ($a_2 > 0$), uniformly ordered ($a_2 < 0, c_1 > 0$) and periodically ordered ($a_2 < 0, c_1 < 0$). Lifshitz points in blends of two homopolymers with diblock copolymer were considered in detail by Holyst and Schick (1992), who computed structure factors, including allowance for composition fluctuations, in the vicinity of these points.

A line of ordinary critical points for macrophase separation is shown as the line C_{A-B} in Fig. 6.42 for a ternary blend of two homopolymers with equal degrees of polymerization and a diblock copolymer at high temperature. Four regimes have been identified by Broseta and Fredrickson (1990) and are indicated in

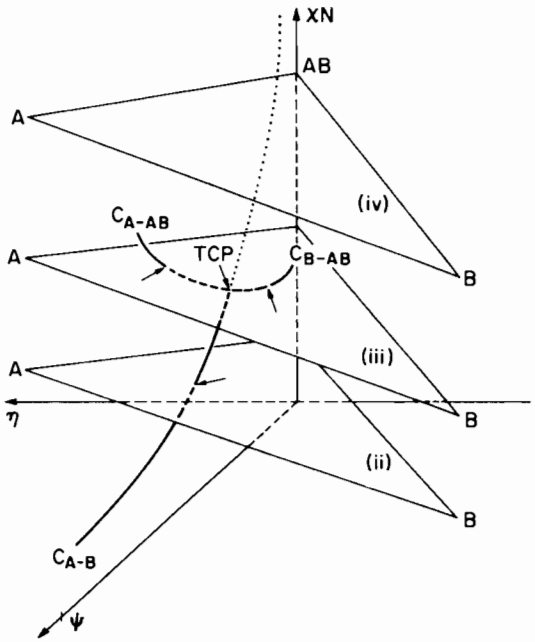

Fig. 6.42 Schematic of the critical line as a function of $\psi = \phi_A + \phi_B$, $\eta = \phi_A - \phi_B$ (where ϕ_A and ϕ_B are the volume fraction of A and B chains) and χN for a ternary blend of two homopolymers with $\beta = 2$ and a random or block copolymer (at high temperature) (Broseta and Fredrickson 1990). The three critical lines C_{A-B}, C_{A-AB} and C_{B-AB} meet at the tricritical point TCP. Beyond the TCP, Scott's branch is unstable (dotted line).

Fig. 6.42. For $\chi N < 2$, the system is homogeneous at all compositions (regime (i), not shown in Fig. 6.42). The general (multidimensional) phase diagram for $\chi N > 2$ is enriched by the presence of tricritical points and Lifshitz tricritical points under certain conditions. The critical line for homopolymer phase separation is given by $\phi_{h,crit} = 2/\chi N$, $\eta_{crit} = 0$ where $\phi_h = \psi_A + \psi_B$ and $\eta = \psi_A - \psi_B$ (Broseta and Fredrickson 1990) (the so-called Scott line (Scott 1949)). Here ψ_A and ψ_B are the volume fractions of A and B monomers. The point at which the Scott line meets the lines of critical points for phase separation (at $q^* = 0$) in the A–AB and B–AB systems is termed a *tricritical point.* This occurs at (Broseta and Fredrickson 1990)

$$\phi_{h,TCP} = 1/(2\beta + 1), \qquad \eta_{TCP} = 0, \qquad \chi N_{TCP} = 4\beta + 2. \tag{6.14}$$

The tricritical point separates regimes (ii) and (iii). Phase diagrams showing a tricritical point for a blend with $\beta = 2$ are shown in Fig. 6.42. For $\beta < \frac{5}{2}$, the tricritical point corresponds to the onset of separation into three phases with very similar compositions. This point was found to be unstable for $\beta > \frac{5}{2}$ and is replaced by a critical end-point temperature. For $\beta = 1$, the critical point corresponds to the confluence of three Lifshitz critical lines and is termed a *Lifshitz tricritical point.* The Lifshitz tricritical point signals a continuous segregation into three phases, a copolymer-rich lamellar phase and two other homopolymer-rich liquid phases. Regime (iii) extends from $(\chi N)_{TCP}$ to $\chi N = 2(1 + \sqrt{\beta})^2$ At higher incompatibilities, the ternary mixture eventually becomes triphasic (regime (iv) in Fig. 6.42). In addition to phases of A-rich and B-rich homopolymers, there is a phase with homopolymers in a more mixed state due to the presence of excess copolymer. This was termed the middle phase, because it has a density intermediate between that of the other phases, and by analogy with oil/water/surfactant systems.

The Lifshitz tricritical point corresponds to the point at which the Lifshitz line separating regions of A- and B-rich two-phase coexistence from the disordered phase meets the Lifshitz line separating the lamellar phase at high copolymer concentrations from the disordered phase and the *disorder line*, as shown in Fig. 6.43. The disorder line was analysed in detail by Holyst and Schick (1992). They describe it as being the locus of points at which a spatial correlation function $g(\boldsymbol{r})$ no longer decays monotonically but exhibits a long-wavelength oscillatory component. Thus on the copolymer-rich side of the disorder line, two lengths are needed to describe the disordered phase—the usual correlation length ξ and a wavelength λ. As the copolymer concentration decreases, λ increases and diverges at the disorder line. The Lifshitz tricritical point occurs at $\chi N = 6, \phi_h = \frac{2}{3}$ (Broseta and Fredrickson 1990; Holyst and Schick 1992).

Broseta and Fredrickson (1990) summarized their results in terms of the compatibilization of homopolymer pairs by copolymer. For small incompatibilities between homopolymer, e.g. at high temperatures, a homopolymer blend can be compatibilized by adding sufficient copolymer ($\phi_c > 1 - 2/\chi N$). When demixing occurs, the two homopolymers become increasingly segregated upon increasing incompatibility (e.g. lowering the temperature). At higher incompatibilites, a

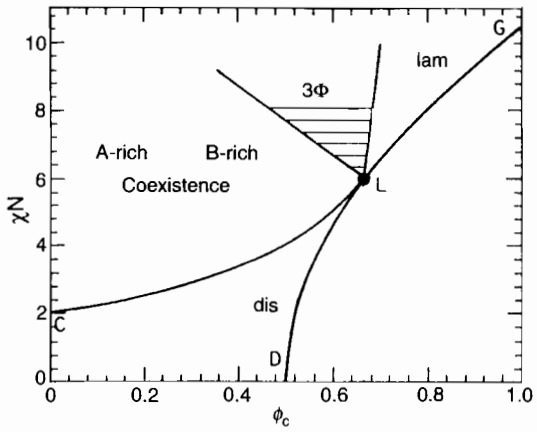

Fig. 6.43 Phase diagram for a ternary mixture of equal concentrations of A and B homopolymers and symmetric AB diblock (all with equal degrees of polymerization) computed by Holyst and Schick (1992). The Lifshitz tricritical point is shown at L, the line CL is that of continuous transitions from the disordered phase to coexisting A-rich and B-rich phases, and LG is the line of continuous transitions from the disordered to the lamellar phase. LD is the disorder line.

regime of three-phase coexistence develops, with A-rich, B-rich and copolymer-rich components.

The theory of Broseta and Fredrickson (1990) was primarily for blends containing AB random copolymer. However, they also found a region of validity of this approach for block copolymers at high temperatures. Using the random phase approximation (RPA), the structure factor associated with fluctuations of the total A monomer volume fraction was found to be (Broseta and Fredrickson 1990)

$$S_{\psi_A\psi_A} = \frac{S_A + S_{AA} - S_{AB}}{2\left[1 - \chi\left(S_A + S_{AA} - S_{AB}\right)\right]} \tag{6.15}$$

where the structure factors S_A etc. are defined by eqn 6.18a–d. The structure factors

$$S_{\eta\eta} = \frac{2S_A\left[1 - \chi\left(S_{AA} - S_{AB}\right)\right]}{\left[1 - \chi\left(S_A + S_{AA} - S_{AB}\right)\right]} \tag{6.16}$$

and

$$S_{\phi_c\phi_c} = 2\left(\frac{1}{S_A} + \frac{1}{S_{AA} + S_{AB}}\right)^{-1}, \tag{6.17}$$

were obtained by Leibler (1982). The notation for eqns 6.15–6.17 is that of Holyst and Schick (1992). Their expressions for the structure factors are:

$$S_A = \phi_{A,h} N g(1,x) \tag{6.18a}$$

$$S_B = \phi_{B,h} N g(1,x) \tag{6.18b}$$

$$S_{AA} = \phi_c N g\left(\frac{1}{2},x\right) \tag{6.18c}$$

$$S_{AB} = \frac{\phi_c}{2} N\left[g(1,x) - 2g\left(\frac{1}{2},x\right)\right] \tag{6.18d}$$

where the Debye function, $g(f,x)$, is defined in eqn 2.9 and $x = q^2Na^2/6 = q^2R_g^2$, where R_g is the radius of gyration of the copolymer.

6.7 Theories for blends of two block copolymers

6.7.1 Brush theory

Theory for blends of block copolymers in the strong segregation limit (SSL) was presented by Spontak (1994) and Zhulina and co-workers (Birshtein *et al.* 1990; Zhulina and Birshtein 1991). Zhulina and co-workers developed a theory for planar grafted layers formed by diblocks with two molecular weights. The free energy was computed using expressions from the theory of polymer brushes for the entropic contributions from elastic chain stretching and a contribution from steric interactions depending on the concentration of chains in the layer. Expressions for the height and free energy density of compressed layers were also developed. Detailed calculations of the distribution functions for both chain ends were presented for the equilibrium grafted layer and compressed layer (Birshtein *et al.* 1990). This theory was subsequently developed to calculate the stability of bulk lamellar phases formed by a binary mixture of block copolymers (Zhulina and Birshtein 1991). The narrow interphase approximation (Helfand and Wasserman 1976) was used to calculate the mean field free energy of the interface between grafted brushes. It was found that under certain conditions, a single lamellar phase was more stable than a system with two segregated coexisting lamellar phases. A phase diagram as a function of relative molecular weight for a blend with differing amounts of the two components was constructed. Regions of absolute stability of single lamellar phases were identified; unfortunately, outside these regions it was not determined whether single lamellar phases were stable or not.

Spontak (1994) developed expressions for the free energy and domain spacing of the lamellar phase also by considering the blend to be a bidisperse mixture of grafted polymer brushes. Repulsive monomer interactions localized at the interface were allowed for using the expression due to Helfand and Wasserman (1976). The elastic energy contributions were accounted for by modifying the SCF theory of Zhulina and Halperin (1992) for the conformation of triblock copolymers. Spontak noted that the SSL predicts a different scaling for blends than for neat block copolymers, the latter being $d \sim \chi^{1/6}N_n^{2/3}$. Here $N_n = q_lN_l + q_sN_s$ is the number-averaged degree of polymerization, (where the subscripts l and s refers to large and small diblocks respectively and q denotes a number frac-

tion). The Spontak model does not account correctly for the stretching energy of the large blocks in the region of the small blocks, as noted by Matsen (1995*a*). He found that the domain spacing of the lamellar phase in the strong segregation limit scales as

$$\frac{d}{aN_l^{1/2}} = 2\left(\frac{8\chi N_l}{3\pi^4}\right)^{1/6} \frac{\delta' + (1-\delta')q_l}{\left[\delta' + (1-\delta')q_l^3\right]^{1/3}}. \tag{6.19}$$

Here $\delta' = N_s/N_l$. The free energy per unit volume is then given by Matsen (1995*a*)

$$\frac{N_l F}{k_B T \varrho_0 V} = \frac{3}{4}\left(\frac{\pi^2 \chi N_l}{3}\right)^{1/3} \frac{\left[\delta' + (1-\delta')q_l^3\right]^{1/3}}{\delta' + (1-\delta')q_l} \tag{6.20}$$

where $1/\varrho_0$ is the volume of A and B segments.

6.7.2 Self-consistent field theory

Unequal length copolymers

Self-consistent field theory has been applied to analyse the phase behaviour of binary blends of diblocks by Shi and Noolandi (1994, 1995), Matsen (1995*a*) and Matsen and Bates (1995). Mixtures of long and short diblocks were considered by Shi and Noolandi (1994) and Matsen (1995*a*), whilst Shi and Noolandi (1995) and Matsen and Bates (1995) calculated phase diagrams for blends of diblocks with equal degrees of polymerization but different composition.

In mixtures containing a small amount of small diblock in a binary blend of short and long copolymers, a substantial fraction of short symmetric diblocks was found to segregate to the interface (Shi and Noolandi 1994). This results in a reduction of the interfacial free energy, and an increase of the packing free energy leading to a reduction of the equilibrium domain spacing. Segregation of short diblocks also generally leads to changes in the phase behaviour of the system, when the composition of short and long chains is varied. Experiments indicate that macrophase separation can occur for mixtures of diblocks of different compositions and a large asymmetry in molecular weights (Hashimoto *et al.* 1994). In the case of highly asymmetric short diblocks ($f_s \to 0$ or 1), the copolymers are localized in the centre of domains, and act as a filler, leading to an increase in the domain spacing. Volume fraction profiles that illustrate the localization of short chains and the changes in domain spacings are presented in Fig. 6.44. This also shows that the domain spacing reduction is greater on addition of a symmetric short diblock. Detailed calculations of the lamellar joint and end distributions were also reported by Shi and Noolandi (1994), and these confirmed that changes in phase behaviour are driven by localization of short diblocks, and changes in the packing density.

At certain points on the phase diagram, the increase in packing free energy due to addition of nearly symmetric short diblocks was found to cancel the reduction in the interfacial free energy density, and changing the concentration of the small diblock was observed to have no effect on the stability of the phases in the vicinity of so-called structural fixed points (Shi and Noolandi 1994). Elsewhere,

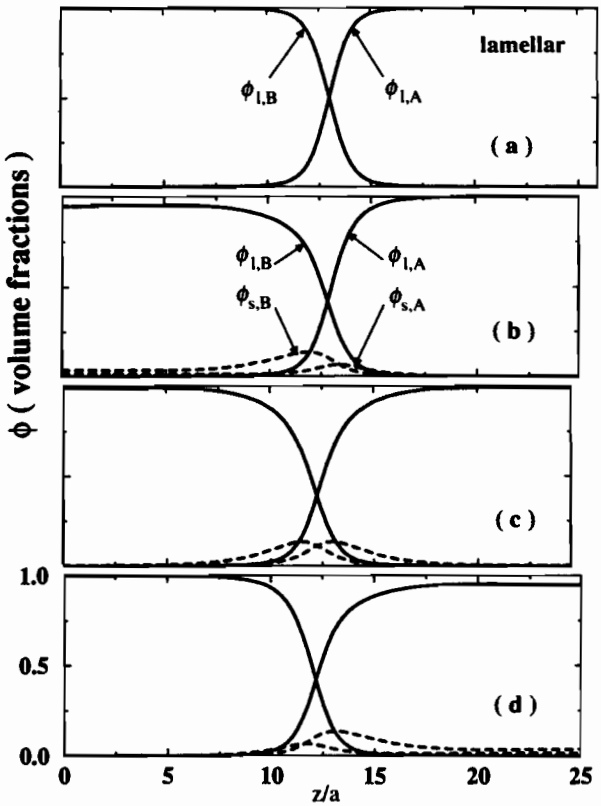

Fig. 6.44 Calculated lamellar volume fraction profiles for a blend of diblocks for $\chi = 0.2$ (Shi and Noolandi 1994). The long diblock has $N_l = 500$ and $f_l = 0.5$. The short diblock has $N_s = 50$. (a) Pure long diblock; (b)–(d) blends with a short diblock ($\phi_s = 0.05$). (b) $f_s = 0.3$, (c) $f_s = 0.5$ and (d) $f_s = 0.7$. The long chain profiles are shown as solid lines, and the short chain profiles are plotted as dashed lines. Changes in the lengths of the horizontal axes correspond to the changes in the domain size with added short chains.

large changes in the stabilities of different phases occur depending on the composition of the short and long diblocks. A phase diagram computed for a volume fraction of short diblocks $\phi = 0.05$ is shown in Fig. 6.45. Structural fixed points are indicated as solid circles. Also shown are the points for $N_s = N_l$, for which the fixed points obviously occur at $f_s = f_l$.

Matsen (1995*a*) analysed the phase behaviour of binary blends of symmetric diblocks using SCFT, also allowing for biphasic regions. It was found that when the ratio of degrees of polymerization exceeds about $\delta = 5$, the copolymers become immiscible producing a coexistence between long- and short-period lamellar phases. This behaviour is not anticipated by strong-segregation limit (SSL) theory (Spontak 1994; Zhulina and Birshtein 1991). Consistent with the experimental observations of Hashimoto *et al.* (1993, 1994) and Koizumi *et al.*

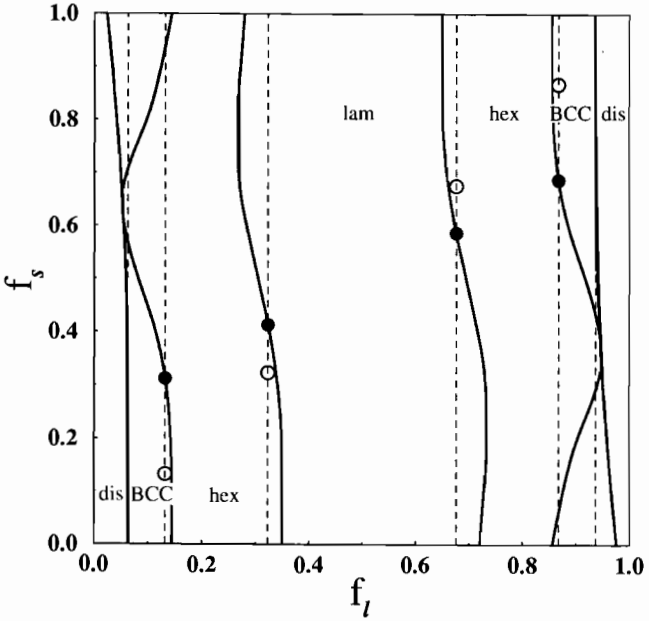

Fig. 6.45 Two-dimensional phase diagram as a function of chain composition for a blend of two diblocks ($\phi_s = 0.05$), calculated using SCFT (Shi and Noolandi 1994). The long diblock has $N_l = 500$ and the short diblock has $N_s = 50$ and the interaction parameter $\chi = 0.2$. Structural fixed points are shown as solid circles. The fixed points on the spherical–disordered boundaries are not shown as their vertical position was poorly defined. The open circles show the positions of the points for the case $N_s = N_l$, for which $f_s = f_l$, corresponding to the pure diblock melt.

(1994*c*), the short-period lamellar phase contains few large diblocks, but the long period one contains a substantial volume fraction of small diblocks. For highly asymmetric diblocks, $\delta = N_s/N_l \to 0$, it was found that the 'dilution approximation' becomes valid, and that the disordering of the short-period lamellar structure occurs via a second-order transition at $\chi N_l(1 - \phi_s)$, where ϕ_s is the volume fraction of the short diblock. The scaling of lamellar domain spacing with ϕ_s was compared to the strong segregation limit calculations of Spontak (1994). The SSL theory (corrected by Matsen (1995*a*), see previous section) was found to provide domain spacings in reasonable agreement with the SCFT result.

Equal length copolymers

The phase behaviour of binary blends of copolymers of equal length but differing composition was analysed using SCF theory by Shi and Noolandi (1995). Again, biphasic regions between ordered phases were not considered. Phase diagrams computed for a weakly segregated diblock blend are presented as a phase diagram 'cube' in Fig. 6.46. The relative stability of two-phase regions, disordered, lamellar, cylindrical and spherical micellar phases was evaluated, bicontinuous

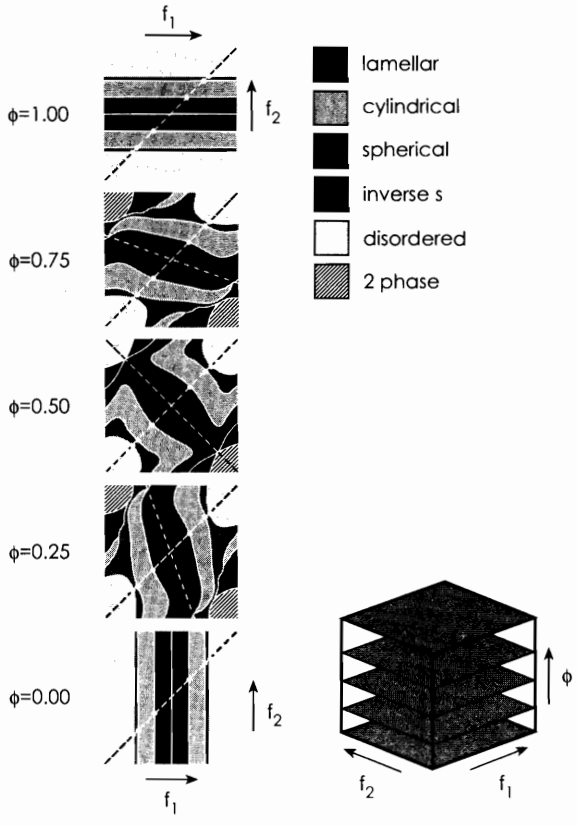

Fig. 6.46 Calculated phase diagram 'cube' for binary blends of symmetric diblocks (equal degrees of polymerization) with $\chi N = 20$ (Shi and Noolandi 1995). The diblock compositions are denoted f_1, f_2 and the blend composition as ϕ.

cubic structures not being considered. The centre of each plane ($f_1 = f_2$) is a point of inversion in the plane, due to the interchangeability of the blocks of equal segment length. Due to the equivalence of the two components ($N_1 = N_2$), the centre of the cube is also a point of inversion in the cube. This symmetry is broken for $N_1 \neq N_2$. The white dots indicate the intersections of the vertical plane defined by $f_1 = f_2$ and the phase boundaries in the horizontal planes. Since $f_1 = f_2$ in this vertical plane and $N_1 = N_2$ the system reduces to a one-component diblock. Details of the phase diagrams for $\phi = 0.25, 0.5$ and 0.75 are enlarged in Fig. 6.47. A schematic showing one quarter of the phase diagram in Fig. 6.47(b) is represented in Fig. 6.48, along with sketches of the polymer chains in different regions. The line $f_1 = f_2$ corresponds to a pure diblock copolymer melt, and the sequence of phases lamellar—hexagonal cylinders—spheres—disorder occurs on increasing volume fraction. For the case $f_1 + f_2 = 1$, the diblocks have inverse compositions. Due to the symmetry of the system shown in Fig. 6.48, a lamellar phase is formed, at least if f_1 is not too different to f_2. The asymmetry of the short and

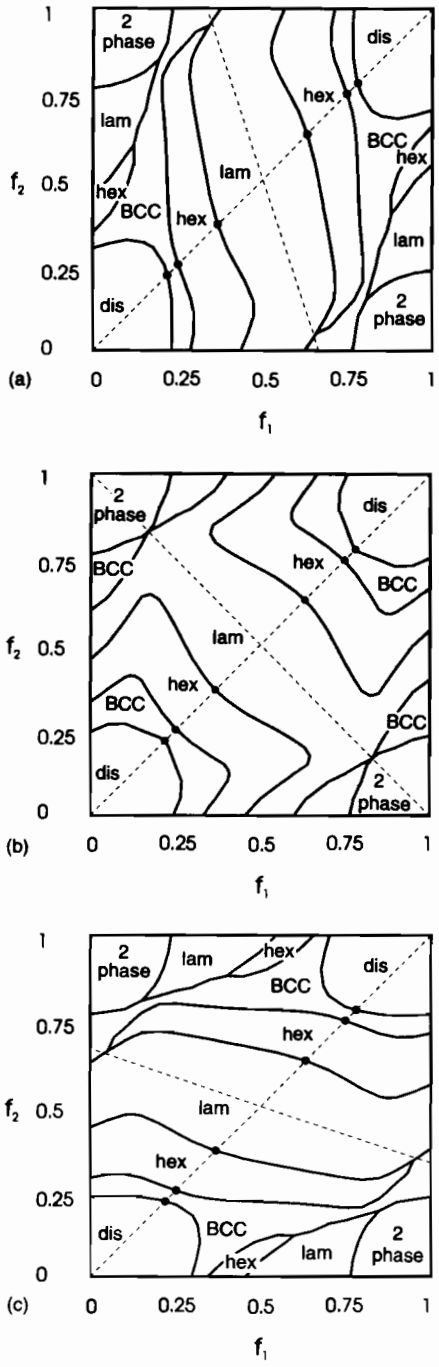

Fig. 6.47 Detail of the phase diagram shown in Fig. 6.46 for the horizontal plane corresponding to (a) $\phi = 0.25$, (b) $\phi = 0.5$, (c) $\phi = 0.75$ (Shi and Noolandi 1995).

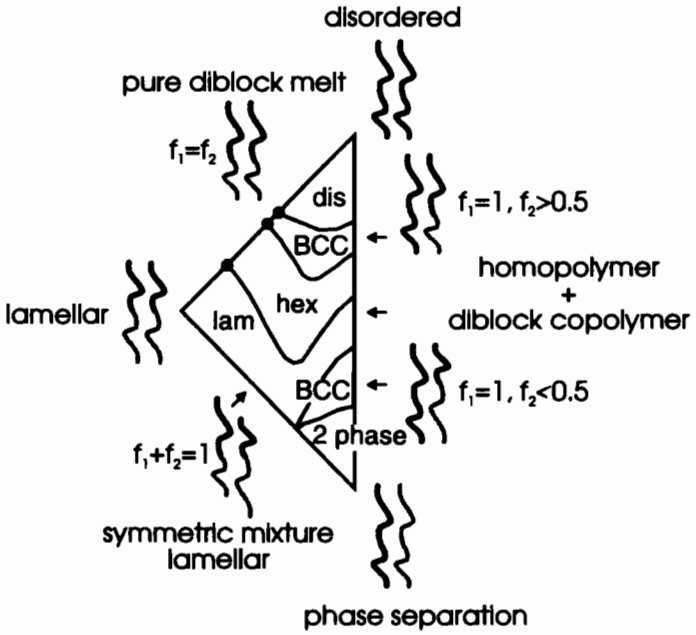

Fig. 6.48 Quarter of the phase diagram shown in Fig. 6.47(b) (Shi and Noolandi 1995) with sketches of the copolymers, indicating compositions.

long blocks is balanced in a uniform lamellar structure. This was confirmed by calculations of the volume fraction profiles. Increasing f_1 along the line $f_1 + f_2 = 1$ leads to increasing instability of the lamellar phase and finally separation into two disordered phases occurs, with two homopolymers at $f_1 = 1$. Along the line $f_1 = 1$, the system moves from being a homogeneous homopolymer A melt at $f_2 = 1$ to a phase-separated homopolymer mixture at $f_2 = 0$. In between, spherical, cylindrical, lamellar and inverse spherical microphase-separated structures are stable. The spherical phase is formed by B blocks in a matrix of A blocks and dispersed A homopolymer. The A and B blocks are similarly distributed in the cylindrical phase. In the lamellar phase, large domains of A homopolymers are separated by bilayers of diblock lamellae, as confirmed by density profile calculations. In the inverse spherical phase, homopolymer A is solubilized in the spherical A domains in the B matrix.

Similar calculations were also performed in the strong segregation limit. In this case, the two-phase and disordered homogeneous regions were found to be smaller, and the phase boundaries were more vertical (see Fig. 6.49) (Shi and Noolandi 1995). This phase diagram was interpreted on the basis of interfacial curvature. If the diblocks are completely segregated, the phase boundaries are determined by the total composition f $(=\phi_1 f_1 + \phi_2 f_2)$ only, and the phase boundaries are parallel to this line (dashed line sloping to the left in Fig. 6.49) ('one-component approximation'). This explains the approximately parallel

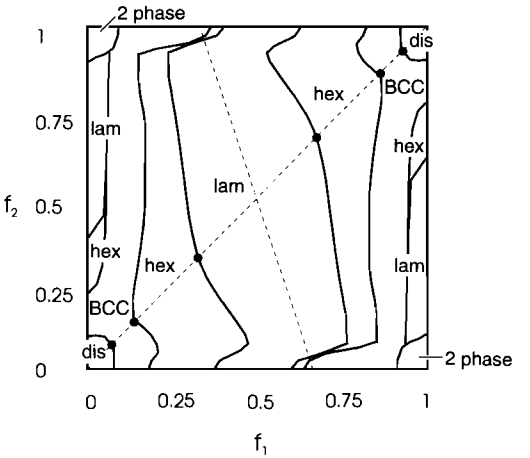

Fig. 6.49 Phase diagram calculated using SCFT for blends of strongly segregated diblocks (both symmetric, $N_1 = N_2 = 400$, $\chi N = 100$). The blend composition $\phi = 0.25$ (cf. Fig. 6.47(a)).

phase boundaries in the interior of $f_1 - f_2$ phase diagrams. When f_1 and f_2 are close to 0.5, the diblocks are segregated to the interfaces. On the other hand, when f_1 or f_2 are close to 0 or 1, the highly asymmetric diblocks are localized in the middle of the domains (confirmed by volume fraction profile calculations) and the interfacial curvature is no longer determined by f. For example when $f_1 \rightarrow 1$, the interfacial curvature is determined by f_2.

Matsen and Bates (1995) also considered blends of diblocks with equal degrees of polymerization using SCFT and presented phase diagrams in the intermediate segregation regime. In contrast to Shi and Noolandi (1995), they computed biphasic regions between ordered phases. These become wider away from points $f_1 = f_2$ in the f_1–f_2 planes, as shown in Fig. 6.50 which should be compared to Fig. 6.47(b). The 'one-component approximation' was explored by them. In common with Shi and Noolandi (1995), it was found that the phase boundaries at constant f map onto those of the corresponding pure diblock, at least if f_1 and f_2 do not differ too much. In the case that either f_1 or f_2 becomes close to 0 or 1 this approximation completely breaks down. It was pointed out that the one-component approximation is useful for locating phase transitions in diblocks. Instead of synthesizing new molecules, diblocks on either side of a transition can be blended, and the phase behaviour of the blends will be qualitatively similar to that of pure materials. However, the resultant phase diagram will contain biphasic regions. Matsen and Bates (1995) estimated that the one-component approximation is satisfactory for $0.3 < f_1 < 0.7$ (at least the sequence of phases is the same as that for the pure diblock, although separated by biphasic regions). For more asymmetric copolymers, e.g. $f_1 = 0.2$, they found that macrophase separation precedes microphase separation on increasing χN except for ϕ very close to 0 or 1.

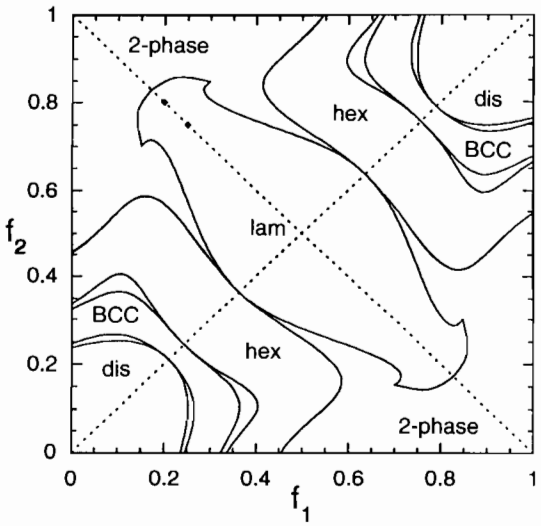

Fig. 6.50 Phase diagram for the same blend as Fig. 6.47(b) also calculated using SCFT, by Matsen and Bates (1995), but allowing for biphasic regions.

6.8 Thin films

6.8.1 Thin films of block copolymer/homopolymer blends

The distribution of (nearly symmetric) PS–PMMA diblocks in blends of PS or PMMA homopolymers has been investigated in thin films (Mayes *et al.* 1992). Using neutron reflectivity on mixtures of molecules selectively labelled with deuterium, they showed that low-molecular-weight homopolymer ($\beta < 1$) is confined within the corresponding copolymer domain, with a distribution peaked at the domain centre, as shown in Fig. 6.51(a), which shows volume fraction profiles determined by modelling neutron reflectivity profiles. These results are in good agreement with bulk experiments (Kimishima *et al.* 1995; Lee *et al.* 1994; Winey *et al.* 1991*b*) (Section 6.2.3). Increasing the molecular weight further to the limit $\beta > 1$ leads to a uniform density distribution of diblock. This is illustrated in Fig. 6.51(b), which shows volume fraction profiles for a blend of a symmetric PS–PMMA diblock and a very-high-molecular-weight *d*PS homopolymer. It is expected that this blend would be macrophase separated in the bulk. Volume fractions calculated using the theory of Shull and Winey (1992) were in good agreement with the experimental ones.

6.8.2 Thin films of blends of block copolymer with two homopolymers

Density distributions at the interface of nearly symmetric PS–PMMA diblocks between high-molecular-weight PS and PMMA homopolymers were investigated using neutron reflectivity by Russell *et al.* (1991). Thin films were

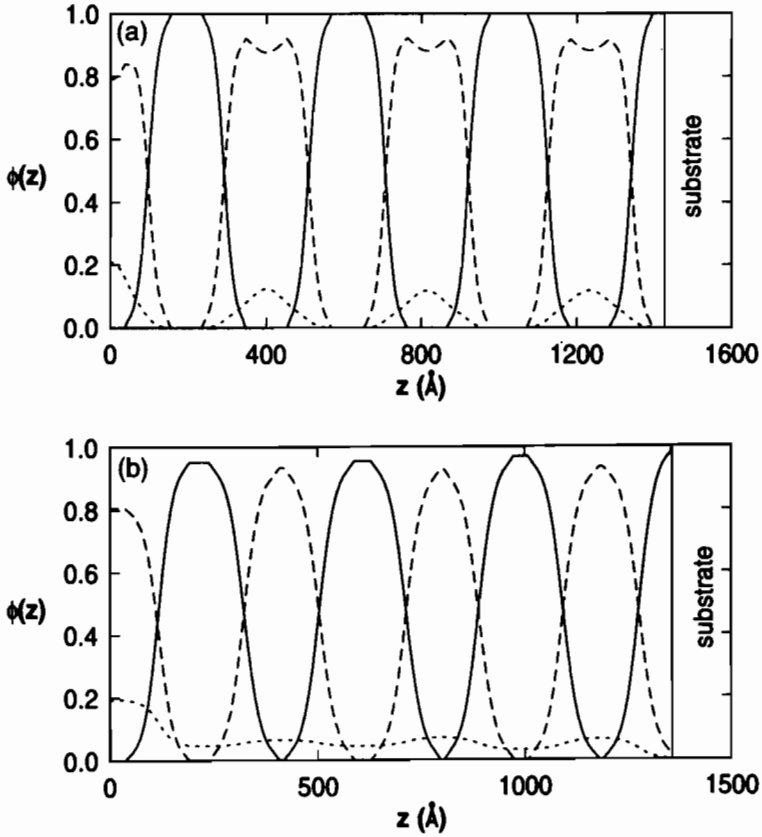

Fig. 6.51 Volume fraction profiles determined from modelling reflectivity profiles for blends of a PS–PMMA diblock ($M = 91.5\,\mathrm{kg\,mol^{-1}}$, $f_{PS} = 0.53$) with 5 wt% of *d*PS homopolymers with (a) $M = 500\,\mathrm{kg\,mol^{-1}}$, (b) $M = 50\,\mathrm{kg\,mol^{-1}}$ (Mayes *et al.* 1992). The solid line is the volume fraction of PMMA, the dashed line that of PS, and the dotted line that of the *d*PS homopolymer.

prepared by deposition of a PMMA homopolymer, onto which a diblock film (thickness approximately half a bulk layer spacing) was floated. PS homopolymer was then spin coated on the top and the film was annealed. By selective deuterium labelling of either block of the diblock or of the homopolymers contrast was provided to determine the density profiles of PS and PMMA segments at the interface. It was found that the interface width was 50% broader than that between the homopolymers in the absence of diblock. Furthermore, the area occupied by the copolymer at the interface was 30% larger than that of copolymers in the bulk lamellar structure. These results indicate significant penetration of the interfacial region by homopolymers, i.e. a wet copolymer brush.

The segregation of asymmetric *d*PS–PVP diblocks to the interface between high-molecular-weight PS and P2VP (where P2VP was the underlayer) has been

investigated using forward recoil spectroscopy (described in Section 1.4.18) (Shull *et al.* 1990). The results were compared to a mean field theory, using a simple Flory–Huggins-type approach, and this was able to quantitatively account for the excess amount of copolymer at the interface that was observed above a critical copolymer concentration. Above this critical concentration of copolymer micelles formed, which segregated to the film surface (i.e. this is the thin film analogue of the cmc), as directly confirmed by TEM experiments (Shull *et al.* 1991). It was suggested that the driving force for this segregation of micelles was enthalpic interactions between PS segments in the homopolymer and *d*PS segments in the copolymer and from entropic effects resulting from the reduction of interfacial area when micelles assemble at the surface, which increases the conformational entropy of chains. This leads to an attractive interaction between block copolymer micelles, and between the micelles and a free surface. In contrast, interactions between bulk micelles are usually dominated by repulsive interactions (Section 6.5.1). The equilibrium segregation of block copolymer to the interface was found to be a function of the copolymer chemical potential, i.e. concentration of copolymer. It was shown that the chemical potential can be obtained from the measured surface excess of copolymer.

Subsequent to these experiments on block copolymers at the interface of high-molecular-weight homopolymers, Dai *et al.* (1992) investigated the influence of homopolymer molecular weight. In contrast to the results of Russell *et al.* (1991), it was reported that for homopolymers with molecular weights greater than that of the copolymers, the interfacial area per block was not significantly affected by the presence of homopolymer, i.e. a dry brush was formed. However, in the case $N_{Ah} < N_{Ac}$, a lower interfacial areal density for the copolymer was observed. The variation of excess copolymer at the interface (z_i^*) as a function of copolymer concentration was compared to the predictions of Leibler (wet or dry brush as appropriate) (Leibler 1988), and to the self-consistent field theory of Shull and Kramer (1990), as illustrated for example in Fig. 6.52 for a copolymer forming a dry brush. The latter theory was found to be able to account quantitatively for the excess, without requiring a dependence of χ on N_{Ah}, whereas an adjustable χ parameter was necessary to get quantitative agreement from the Leibler theory. The cmc, determined from the onset of surface segregation of micelles, was found to decrease as the molecular weight of the homopolymer matrix increased.

The segregation of a P2VP–*d*PS–P2VP triblock to the interface of PS and P2VP homopolymers was compared to that of a diblock with the same P2VP content ($f_{PS} \approx 0.15$) and total molecular weight using forward recoil spectroscopy by Dai *et al.* (1994). The interfacial excess for the triblock was found to be approximately half that of the diblock. A mean field model based on the theory of Leibler (1988) for dry brushes was able to account for this difference, which originates in the different areal density of copolymer chains for the triblock which can adopt looped as well as bridged conformations. An increase in interfacial excess was observed above a saturation plateau (apparent on the right-hand side of Fig. 6.52, for example) which was ascribed to the segregation of micelles to the interface. The increase in interfacial area occurred for a higher copolymer volume fraction for the triblock than the diblock due to its higher cmc. In a companion

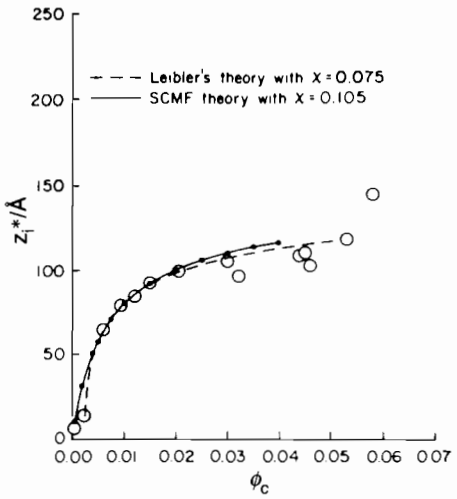

Fig. 6.52 Interfacial excess in thin films of blends of a *d*PS–P2VP diblock (N_{dPS} = 391, N_{P2VP} = 68) with PS homopolymer (N_{PS} = 6440) (Dai *et al.* 1992). Since the homopolymer is much longer than the diblock, the diblock forms a dry brush. The circles are the results from forward recoil spectrometry, the lines correspond to theoretical calculations. The dashed line was computed using the theory of Leibler (1988), and the solid line is from the self-consistent mean field calculation of Shull and Kramer (1990).

paper, blends of a *d*PS–P2VP diblock with the corresponding homopolymers were examined in the limit that $N_h \gg N_c$, and it was shown that the normalized interfacial excess (z_i^*/R_g) is a universal function of that part of the chemical potential due to chain stretching (Dai and Kramer 1994). This function was in good agreement with self-consistent mean field calculations, using the approach of Shull (1991), At low copolymer contents, the surface excess varies linearly with concentration, a conclusion confirmed by forward recoil spectroscopy experiments on PS–PMMA diblocks at the interface of the corresponding homopolymers (Green and Russell 1991). This dependence was accounted for using a modification of the theory of Leibler (1988) for wet copolymer brushes at a homopolymer interface, in the limit of low copolymer content.

6.8.3 Thin films of blends containing two block copolymers

Two symmetric diblocks

The distribution of chains in a lamellar film formed by a binary blend of symmetric PS–PMMA diblocks has been probed using neutron reflectivity by Mayes *et al.* (1994). The microphase self-assembled parallel to the substrate, giving a lamellar stack, as for pure diblocks (see Section 2.5.1). By blending mixtures of unlabelled and selectively labelled long and sort diblocks, it was determined that short diblock copolymer chains are localized at the PS–PMMA interface, while the longer chains are selectively located at the domain centres. These results

support the conclusions from bulk SAXS experiments on PS–PI diblocks by Hashimoto *et al.* (1994) and assumptions used in the development of the theories discussed in Section 6.7. The domain spacing in the thin film was shown to vary with the $\frac{2}{3}$ power of the number-average mass of the blend, in agreement with the bulk results of Hashimoto (1982), based on the SANS results of Hadzioannou and Skoulios (1982) (Section 6.4.2).

A symmetric and an asymmetric diblock in a blend with homopolymer

The competitive adsorption of a short symmetric PS–PI diblocks or a long asymmetric PS–PI diblock to the surface of a PS homopolymer was examined by Budkowski *et al.* (1995). They used nuclear reaction analysis (Section 1.4.18) with labelled diblocks to determine the concentration of deuterium atoms as a function of depth, and hence the volume fraction of labelled chains, It was thus found that the shorter diblock tends to adsorb preferentially to the interface. The surface excess of PS and its interfacial density were compared to a theory for bidisperse brushes, a generalization of the model due to Leibler (1988). Excellent quantitative agreement was found, with no adjustable parameters.

References

Anastasiadis, S. H., Gancarz, I. and Koberstein, J. T. (1989). *Macromolecules*, **22**, 1449.

Auschra, C., Stadler, R. and Voigt-Martin, I. G. (1993). *Polymer*, **34**, 2094.

Bajaj, P., Gupta, D. C. and Varshney, S. K. (1985). *Journal of Applied Polymer Science*, **23**, 820.

Balsara, N. P., Jonnalagadda, S. V., Lin, C. C., Han, C. C. and Krishnamoorti, R. (1993). *Journal of Chemical Physics*, **99**, 10011.

Banaszak, M. and Whitmore, M. D. (1992). *Macromolecules*, **25**, 249.

Bates, F. S. and Fredrickson, G. H. (1990). *Annual Reviews of Physical Chemistry*, **41**, 525.

Bates, F. S., Berney, C. V. and Cohen, R. E. (1983*a*). *Macromolecules*, **16**, 1101.

Bates, F. S., Cohen, R. E. and Argon, A. S. (1983*b*). *Macromolecules*, **16**, 1108.

Bates, F. S., Maurer, W., Lodge, T. P., Schulz, M. F., Matsen, M. W., Almdal, K. *et al.* (1995). *Physical Review Letters*, **75**, 4429.

Berney, C. V., Cheng, P.-L. and Cohen, R. E. (1988). *Macromolecules*, **21**, 2235.

Birshtein. T. M., Liatskaya, Y. V. and Zhulina, E. B. (1990). *Polymer*, **31**, 2185.

Brahimi, B., Aitkadi, A., Ajji, A. and Fayt, R. (1991*a*). *Journal of Polymer Science B: Polymer Physics*, **29**, 945.

Brahimi, B., Aitkadi, A., Ajji, A., Jérome, R. and Fayt, R. (1991*b*). *Journal of Rheology*, **35**, 1069.

Broseta, D. and Fredrickson, G. H. (1990). *Journal of Chemical Physics*, **93**, 2927.

Brown, H. R. (1991). *Macromolecules*, **24**, 2752.

Budkowski, A., Klein, J., Fetters, L. J. and Hashimoto, T. (1995). *Macromolecules*, **28**, 8579.

Cahn, J. W. (1965). *Journal of Chemical Physics*, **42**, 93.

Cheng, P.-L., Berney, C. V. and Cohen, R. E. (1989). *Makromoleculaire Chemie*, **190**, 589.

Choi, G., Kaya, A. and Shen, M. (1973). *Polymer Engineering and Science*, **13**, 231.

Cigana, P., Favis, B. D. and Jérome, R. (1996). *Journal of Polymer Science B: Polymer Physics*, **34**, 1691.
Cohen, R. E. and Ramos, A. R. (1979). *Macromolecules*, **12**, 131.
Cohen, R. E. and Torradas, J. M. (1984). *Macromolecules*, **17**, 1101.
Cohen, R. E. and Tschoegl, N. W. (1972). *International Journal of Polymeric Materials*, **2**, 49.
Cohen, R. E. and Tschoegl, N. W. (1973). *International Journal of Polymeric Materials*, **2**, 205.
Creton, C., Kramer, E. J., Hui, C.-Y. and Brown, H. R. (1992). *Macromolecules*, **25**, 3075.
Dai, K. H. and Kramer, E. J. (1994). *Journal of Polymer Science B: Polymer Physics*, **32**, 1943.
Dai, L. and Toprakcioglu, C. (1992). *Macromolecules*, **25**, 6000.
Dai, K. H., Kramer, E. J. and Shull, K. R. (1992). *Macromolecules*, **25**, 220.
Dai, K. H., Washiyama, J. and Kramer, E. J. (1994). *Macromolecules*, **27**, 4544.
Dai, C.-A., Kramer, E. J., Washiyama, J. and Hui, C.-Y. (1996). *Macromolecules*, **29**, 7536.
Dai, C.-A., Jandt, K. D., Iyengar, D. R., Slack, N. L., Dai, K. H., Davidson, W. B. *et al.* (1997). *Macromolecules*, **30**, 549.
de Gennes, P.-G. (1991). *Europhysics Letters*, **15**, 191.
Diamant, J., Soong, D. and Williams, M. C. (1982). *Polymer Engineering and Science*, 22, 673.
Disko, M. M., Liang, K. S., Behal, S. K., Roe, R. J. and Jeon, K. J. (1993). *Macromolecules*, **26**, 2983.
Dumoulin, M. M., Farha, C. and Utracki, L. A. (1984). *Polymer Engineering and Science*, **24**, 1319.
Fayt, R. and Teyssié, P. (1989). *Polymer Engineering and Science*, **29**, 538.
Fayt, R., Jérome, R. and Teyssié, P. (1981). *Journal of Polymer Science: Polymer Letters*, **19**, 79.
Fayt, R., Jérome, R. and Teyssié, P. (1982). *Journal of Polymer Science: Polymer Physics*, **20**, 2209.
Fayt, R., Hadjiandreou, P. and Teyssie, P. (1985). *Journal of Polymer Science: Polymer Chemistry*, **23**, 337.
Fayt, R., Jérome, R. and Teyssié, P. (1989*a*). *American Chemical Society Symposia Series*, **395**, 38.
Fayt, R., Jérome, R. and Teyssié, P. (1989*b*). *Journal of Polymer Science B: Polymer Physics*, **27**, 775.
Fayt, R., Jérome, R. and Teyssié, P. (1989*c*). *Journal of Polymer Science A: Polymer Chemistry*, **27**, 2823.
Flosenzier, L. S., Rohlfing, J. H., Schwark, A. M. and Torkelson, J. M. (1990). *Polymer Engineering and Science*, **30**, 49.
Gaillard, P., Ossenbach-Suater, M. and Riess, G. (1980). *Makromoleculaire Chemie, Rapid Communications*, **1**, 771.
Gaines, G. L. (1979). *Macromolecules*, **12**, 1011.
Gaines, G. L. and Bender, G. W. (1972). *Macromolecules*, **5**, 82.
Gedde, U. W. (1995). *Polymer Physics*. Chapman and Hall, London.
Green, P. F. and Russell, T. P. (1991). *Macromolecules*, **24**, 2931.
Gupta, A. K. and Purwar, S. N. (1985*a*). *Journal of Applied Polymer Science*, **30**, 1799.
Gupta, A. K. and Purwar, S. N. (1985*b*). *Journal of Applied Polymer Science*, **30**, 1777.
Ha, C.-S., Cho, W.-J., Ryou, J.-H. and Roe, R.-J. (1993). *Polymer*, **34**, 505.
Hadziioannou, G. and Skoulios, A. (1982). *Macromolecules*, **15**, 267.

Han, C. D., Baek, D. M., Kim, J., Kimishima, K. and Hashimoto, T. (1992). *Macromolecules*, **25**, 3052.
Hansen, D. R. and Shen, M. (1975). *Macromolecules*, **8**, 903.
Harrats, C., Blacher, S., Fayt, R., Jérome, R. and Teyssié, P. (1995). *Journal of Polymer Science B: Polymer Physics*, **33**, 801.
Hasegawa, H. and Hashimoto, T. (1996). Self-assembly and morphology of block copolymer systems. In *Comprehensive polymer science. Suppl.* 2, (ed. S. L. Aggarwal and S. Russo), p. 497. Pergamon, London.
Hasegawa, H., Tanaka, H., Yamasaki, K. and Hashimoto, T. (1987). *Macromolecules*, **20**, 1651.
Hasegawa, H., Tanaka, H., Hashimoto, T. and Han, C. C. (1991). *Journal of Applied Crystallography*, **24**, 672.
Hashimoto, T. (1982). *Macromolecules*, **15**, 1548.
Hashimoto, H., Fujimara, M., Hashimoto, T. and Kawai, H. (1981). *Macromolecules*, **14**, 844.
Hashimoto, T., Tanaka, H. and Hasegawa, H. (1990). *Macromolecules*, **23**, 4378.
Hashimoto, T., Koizumi, S., Hasegawa, H., Izumitani, T. and Hyde, S. T. (1992). *Macromolecules*, **25**, 1433.
Hashimoto, T., Yamasaki, K., Koizumi, S. and Hasegawa, H. (1993). *Macromolecules*, **26**, 2895.
Hashimoto, T., Koizumi, S. and Hasegawa, H. (1994). *Macromolecules*, **27**, 1562.
Hashimoto, T., Izumitani, T. and Ono, K. (1995). *Makromoleculaire Chemie, Macromolecular Symposia*, **98**, 925.
Heikens, D., Hoen, N., Barentsen, W., Piet, P. and Ladan, H. (1978). *Journal of Polymer Science: Polymer Symposia*, **62**, 309.
Helfand, E. and Wasserman, Z. R. (1976). *Macromolecules*, **9**, 879.
Hoffman, M., Kampf, G., Kromer, H. and Pampus, G. (1970). *Advances in Chemistry Series*, **99**, 351.
Holyst, R. and Schick, M. (1992). *Journal of Chemical Physics*, **96**, 7728.
Hong, K. M. and Noolandi, J. (1983). *Macromolecules*, **16**, 1083.
Hosemann, R. and Bagchi, S. N. (1962). *Direct analysis of diffraction by matter*. North-Holland, Amsterdam.
Hsuie, G. H. and Ma, M.-Y. M. (1984). *Polymer*, **25**, 882.
Hsuie, G. H. and Shih, S. W. F. (1985). *Journal of Applied Polymer Science*, **30**, 1659.
Hu, W., Koberstein, J. T., Lingelser, J. P. and Gallot, Y. (1995). *Macromolecules*, **28**, 5209.
Hui, C.-Y., Ruina, A., Creton, C., Kramer, E. J. (1992). *Macromolecules*, **25**, 3948.
Inoue, T., Soen, T., Hashimoto, T. and Kawai, H. (1970). *Macromolecules*, **3**, 87.
Israels, R., Jasnow, D., Balazs, A. C., Guo, L., Krausch, G., Sokolov, J. *et al.* (1995). *Journal of Chemical Physics*, **102**, 8149.
Janert, P. K. and Schick, M. (1996). *Physical Review E*, **54**, 33.
Janert, P. K. and Schick, M. (1997*a*). *Macromolecules*, **30**, 3916.
Janert, P. K. and Schick, M. (1997*b*). *Macromolecules*, **30**, 137.
Jeon, K.-J. and Roe, R.-J. (1994). *Macromolecules*, **27**, 2439.
Jeon, H. S., Lee, J. H., Balsara, N. P., Majumdar, B., Fetters, L. J. and Faldi, A. (1997). *Macromolecules*, **30**, 973.
Jiang, M. and Xie, H. K. (1991). *Progress in Polymer Science*, **16**, 977.
Jiang, M., Xie, J.-V. and Yu, T.-Y. (1982). *Polymer*, **23**, 1557.
Kane, L., Satkowski, M. M., Smith, S. D. and Spontak, R. J. (1996). *Macromolecules*, **29**, 8862.

Khandpur, A. K., Förster, S., Bates, F. S., Hamley, I. W., Ryan, A. J., Bras, W. *et al.* (1995). *Macromolecules*, **28**, 8796.
Kimishima, K., Hashimoto, T. and Han, C. D. (1995). *Macromolecules*, **28**, 3842.
Kinning, D. J., Winey, K. I. and Thomas, E. L. (1988). *Macromolecules*, **21**, 3502.
Kinning, D. J., Thomas, E. L. and Fetters, L. J. (1989). *Journal of Chemical Physics*, **90**, 5806.
Kinning, D. J., Thomas, E. L. and Fetters, L. J. (1991). *Macromolecules*, **24**, 3893.
Koizumi, S., Hasegawa, H. and Hashimoto, T. (1992). *Macromolecules Chemie, Makromolecular Symposia*, **62**, 75.
Koizumi, S., Hasegawa, H. and Hashimoto, T. (1994*a*). *Macromolecules*, **27**, 7893.
Koizumi, S., Hasegawa, H. and Hashimoto, T. (1994*b*). *Macromolecules*, **27**, 6532.
Koizumi, S., Hasegawa, H. and Hashimoto, T. (1994*c*). *Macromolecules*, **27**, 4371.
Kramer, E. J., Norton, L. J., Dai, C.-A., Sha, Y. and Hui, C.-Y. (1994). *Faraday Discussions*, **98**, 31.
Kressler, J., Kammer, H. W., Morgenstern, U., Litauski, B. and Berger, W. (1990). *Macromoleculaire Chemie*, **191**, 243.
Lee, S.-H., Koberstein, J. T., Quan, X., Gancarz, I., Wignall, G. D. and Wilson, F. C. (1994). *Macromolecules*, **27**, 3199.
Leibler, L. (1981). *Makromoleculaire Chemie, Rapid Communications*, **2**, 393.
Leibler, L. (1982). *Makromolecules*, **15**, 1283.
Leibler, L. (1988). *Makromoleculaire Chemie, Macromolecular Symposia*, **16**, 1.
Leibler, L. and Pincus, P. A. (1984). *Macromolecules*, **17**, 2922.
Leibler, L., Orland, H. and Wheeler, J. C. (1983). *Journal of Chemical Physics*, **79**, 3550.
Lifshitz, I. M. and Slyozov, V. V. (1961). *Journal of Physics and Chemistry of Solids*, **19**, 35.
Lin, C. C., Jeon, H. S., Balsara, N. P. and Hammouda, B. (1995). *Journal of Chemical Physics*, **103**, 1957.
Lin, C. C., Jonnalagadda, S. V., Balsara, N. P., Han, C. C. and Krishnamoorti, R. (1996). *Macromolecules*, **29**, 661.
Lindsey, C. R., Paul, D. R. and Barlow, J. W. (1981). *Journal of Applied Polymer Science*, **26**, 1.
Löwenhaupt, B. and Hellmann, G. P. (1991). *Polymer*, **32**, 1065.
Löwenhaupt, B., Steurer, A., Hellmann, G. P. and Gallot, Y. (1994). *Macromolecules*, **27**, 908.
Lu, Z.-H., Krause, S. and Iskandar, M. (1982). *Macromolecules*, **15**, 367.
Matsen, M. W. (1995*a*). *Journal of Chemical Physics*, **103**, 3268.
Matsen, M. W. (1995*b*). *Macromolecules*, **28**, 5765.
Matsen, M. W. (1995*c*). *Physical Review Letters*, **74**, 4225.
Matsen, M. W. and Bates, F. S. (1995). *Macromolecules*, **28**, 7298.
Matsen, M. W. and Schick, M. (1996). *Current Opinion in Colloid and Interface Science*, **1**, 329.
Mayes, A. M., Russell, T. P., Satija, S. K. and Majkrzak, C. F. (1992). *Macromolecules*, **25**, 6523.
Mayes, A. M., Russell, T. P., Deline, V. R., Satija, S. K. and Majkrzak, C. F. (1994). *Macromolecules*, **27**, 7447.
Meyer, G. C. and Tritscher, G. E. (1978). *Journal of Applied Polymer Science*, **22**, 719.
Nojima, S. and Roe, R.-J. (1987). *Macromolecules*, **20**, 1866.
Nojima, S., Roe, R.-J., Rigby, D. and Han, C. C. (1990). *Macromolecules*, **23**, 4305.
Noolandi, J. (1991). *Makromoleculaire Chemie, Rapid Communications*, **12**, 517.
Noolandi, J. and Hong, K. M. (1982). *Macromolecules*, **15**, 482.

Noolandi, J. and Hong, K. M. (1984). *Macromolecules*, **17**, 1531.
Ouhadi, T., Fayt, R., Jérome, R. and Teyssié, P. (1986). *Journal of Applied Polymer Science*, **31**, 5647.
Owens, J. N., Gancarz, I. S., Koberstein, J. T. and Russell, T. P. (1989). *Macromolecules*, **22**, 3388.
Park, D.-W. and Roe, R.-J. (1991). *Macromolecules*, **24**, 5324.
Ptaszynski, B., Terrisse, J. and Skoulios, A. (1975). *Makromoleculaire Chemie*, **176**, 3483.
Quan, X., Gancarz, I., Koberstein, J. T. and Wignall, G. D. (1987). *Macromolecules*, **20**, 1431.
Rameau, A., Lingelser, J. P. and Gallot, Y. (1982). *Makromoleculaire Chemie, Rapid Communications*, **3**, 413.
Ramos, A. R. and Cohen, R. E. (1977). *Polymer Engineering and Science*, **17**, 639.
Rigby, D and Roe, R.-J. (1984). *Macromolecules*, **17**, 1778.
Rigby, D and Roe, R.-J. (1986). *Macromolecules*, **19**, 721.
Rigby, D., Lin, J. L. and Roe, R.-J. (1985). *Macromolecules*, **18**, 2269.
Roe, R. J. (1985). *Polymer Engineering and Science*, **25**, 1103.
Roe, R. J. (1986). *Macromolecules*, **19**, 728.
Roe, R. J. and Kuo, C.-M. (1990). *Macromolecules*, **23**, 4635.
Roe, R.-J. and Rigby, D. (1987). *Advances in Polymer Science*, **82**, 103.
Roe, R.-J. and Zin, W.-C. (1980). *Macromolecules*, **13**, 1221.
Roe, R.-J. and Zin, W.-C. (1984). *Macromolecules*, **17**, 189.
Russell, T. P., Anastasiadis, S. H., Menelle, A., Felcher, G. P. and Satija, S. K. (1991). *Macromolecules*, **24**, 1575.
Schaefer, J., Sefcik, M. D., Stejskal, E.O. and McKay, R. A. (1981). *Macromolecules*, **14**, 188.
Scott, R. L. (1949). *Journal of Chemical Physics*, **17**, 279.
Scott, R. L. (1952). *Journal of Polymer Science*, **9**, 423.
Selb, J., Marie, P., Rameau, A., Duplessix, R. and Gallot, Y. (1983). *Polymer Bulletin*, **10**, 444.
Selke, W. (1992). Spatially modulated structures in systems with compeing interactions. In *Phase transtitions and critical phenomena*, (ed. C. Domb and J. L. Lebowitz), p. 1. Academic, London.
Semenov, A. N. (1993). *Macromolecules*, **26**, 2273.
Sha, Y., Hui, C.-Y., Ruina, A. and Kramer, E. J. (1995). *Macromolecules*, **28**, 2540.
Shi, A.-C. and Noolandi, J. (1994). *Macromolecules*, **27**, 2936.
Shi, A.-C. and Noolandi, J. (1995). *Macromolecules*, **28**, 3103.
Shull, K. R. (1991). *Journal of Chemical Physics*, **94**, 5723.
Shull, K. R. and Kramer, E. J. (1990). *Macromolecules*, **23**, 4769.
Shull, K. R. and Winey, K. I. (1992). *Macromolecules*, **25**, 2637.
Shull, K. R., Kramer, E. J., Hadziioannou, G. and Tang, W. (1990). *Macromolecules*, **23**, 4780.
Shull, K. R., Winey, K. I., Thomas, E. L. and Kramer, E. J. (1991). *Macromolecules*, **24**, 2748.
Smith, J. W., Kramer, E. J., Xiao, F., Hui, C.-Y., Reichert, W. and Brown, H. R. (1993). *Journal of Materials Science*, **28**, 4234.
Spontak, R. J. (1994). *Macromolecules*, **27**, 6363.
Spontak, R. J., Fung, J. C., Braufeld, M. B., Sedat, J. W., Agard, D. A., Kane, L. *et al.* (1996). *Macromolecules*, **29**, 4494.
Sung, L. P. and Han, C. C. (1995). *Journal of Polymer Science B: Polymer Physics*, **33**, 2405.

Tanaka, H. and Hashimoto, T. (1991*a*). *Macromolecules*, **24**, 5713.
Tanaka, H. and Hashimoto, T. (1991*b*). *Macromolecules*, **24**, 5398.
Tanaka, H., Hasegawa, H. and Hashimoto, T. (1991). *Macromolecules*, **24**, 240.
Toy, L., Niimomi, M. and Shen, M. (1975). *Journal of Macromolecular Science, Physics B*, **11**, 281.
Vilesov, A. D., Floudas, G., Pakula, T., Melenevskaya, E. Y., Birshtein, T. M. and Lyatskaya, Y. V. (1994). *Macromolecular Chemistry and Physics*, **195**, 2317.
von Riess, G., Kohler, J., Tournut, C. and Banderet, A. (1967). *Makromoleculaire Chemie*, **101**, 58.
Wang, Z.-G. and Safran, S. A. (1990). *Journal de Physique*, **51**, 185.
Washiyama, J., Kramer, E. J., Hui, C.-Y. (1993*a*). *Macromolecules*, **26**, 2928.
Washiyama, J., Creton, C., Kramer, E. J., Xiao, F. and Hui, C.-Y. (1993*b*). *Macromolecules*, **26**, 6011.
Washiyama, J., Kramer, E. J., Creton, C. F. and Hui, C. Y. (1994). *Macromolecules*, **27**, 2019.
Watanabe, H. and Kotaka, T. (1983). *Macromolecules*, **16**, 769.
Whitmore, M. D. and Noolandi, J. (1985*a*). *Macromolecules*, **18**, 2486.
Whitmore, M. D. and Noolandi, J. (1985*b*). *Macromolecules*, **18**, 657.
Winey, K. I. (1992). *Materials Research Society Symposium Proceedings*, **248**, 365.
Winey, K. I., Thomas, E. L. and Fetters, L. J. (1991*a*). *Journal of Chemical Physics*, **95**, 9367.
Winey, K. I., Thomas, E. L. and Fetters, L. J. (1991*b*). *Macromolecules*, **24**, 6182.
Winey, K. I., Thomas, E. L. and Fetters, L. J. (1991*c*). *Journal of Chemical Physics*, **95**, 9367.
Winey, K. I., Thomas, E. L. and Fetters, L. J. (1992*a*). *Macromolecules*, **25**, 422.
Winey, K. I., Thomas, E. L. and Fetters, L. J. (1992*b*). *Macromolecules*, **25**, 2645.
Xi, H. and Milner, S. T. (1996). *Macromolecules*, **29**, 2404.
Young, R. J. and Lovell, P. A. (1991). *Introduction to polymers*. Chapman and Hall, London.
Zhao, J., Majumdar, B., Schulz, M. F., Bates, F. S., Almdal, K., Mortensen, K. *et al.* (1996). *Macromolecules*, **29**, 1204.
Zhulina, E. B. and Birshtein, T. M. (1991). *Polymer*, **32**, 1299.
Zhulina, E. B. and Halperin, A. (1992). *Macromolecules*, **25**, 5730.
Zin, W.-C. and Roe, R.-J. (1984). *Macromolecules*, **17**, 183.

Appendix The self-consistent field theory for block copolymer melts

As mentioned in Section 2.3.3, because SCFT is the most general theory for the ordering of block copolymers to date, a brief outline is given here. The simplest case of a diblock copolymer melt is considered, following Matsen and Schick (1994). The extension to other melts of other architectures, solutions, blends or semicrystalline copolymers is discussed in the appropriate chapter.

A system of n AB diblock copolymers each with a degree of polymerization N and A-monomer fraction, f, is considered. The A and B monomers occupy a fixed volume, $1/\varrho_0$, and the system is incompressible with a total volume, V, equal to nN/ϱ_0. A variable s is used as a parameter than increases continuously along the length of a polymer. At the A monomer end, $s = 0$, at the junction point, $s = f$, and at the other end, $s = 1$. The functions $r_\alpha(s)$ define the space curve occupied by the copolymer α (Matsen and Schick 1994).

The partition function used for the system is

$$Z = \int \prod_{\alpha=1}^{n} \tilde{D}\boldsymbol{r}_\alpha \delta\left[1 - \hat{\phi}_A - \hat{\phi}_B\right] \exp\left\{ -\chi\varrho_0 \int d\boldsymbol{r} \hat{\phi}_A \hat{\phi}_B \right\}, \tag{A.1}$$

Where the functional integral over all configurations is weighted, $\tilde{D}\boldsymbol{r}_\alpha = D\boldsymbol{r}_\alpha P[r_\alpha;0,1]$, with the functionals

$$P\left[r_\alpha; s_1, s_2\right] \propto \exp\left\{ -\frac{3}{2Na^2} \int_{s_1}^{s_2} \left| \frac{d}{ds} r_\alpha(s) \right|^2 \right\}. \tag{A.2}$$

Here a is the Kuhn or segment length. The delta functional selects out only those configurations satisfying the incompressibility constraint. The Flory–Huggins parameter, χ, measures the incompatibility between A and B monomers. The dimensionless A monomer-density operator is given by

$$\hat{\phi}_A(\boldsymbol{r}) = \frac{N}{\varrho_0} \sum_{\alpha=1}^{n} \int_0^f ds \delta\left(\boldsymbol{r} - \boldsymbol{r}_\alpha(s)\right), \tag{A.3}$$

and $\hat{\phi}_B$ by a similar expression. Replacing the operator $\hat{\phi}_A$ by a function Φ_A using a functional integral, and inserting standard integral representations for the delta functionals, the partition function can be expressed as

$$Z = N\int D\Phi_A DW_A D\Phi_B DW_B \exp\{-F/k_BT\}, \tag{A.4}$$

where N is a normalization constant, the free energy

$$F/nk_BT \equiv -\ln Q + V^{-1}\int d\boldsymbol{r}\left[\chi N\Phi_A\Phi_B - W_A\Phi_A - W_B\Phi_B - \Xi\left(1-\Phi_A-\Phi_B\right)\right], \tag{A.5}$$

and

$$Q \equiv \int \tilde{D}\boldsymbol{r}_\alpha \exp\left\{-\int_0^f ds W_A\left(\boldsymbol{r}_\alpha\right) - \int_f^1 ds W_B\left(\boldsymbol{r}_\alpha\right)\right\}. \tag{A.6}$$

The functional $F[\Phi_A, W_A, \Phi_B, W_B, \Xi]$ can be evaluated exactly, but the functional integrals in eqn A.4 cannot. In the SCFT, this integral is approximated by the extremum of the integrand. Thus the free energy, $-k_BT\ln Z$, is given by $F[\phi_A, w_A, \phi_B, w_B, \xi]$, where ϕ_A, w_A, ϕ_B, w_B and ξ are the functions for which F attains its minimum. From the definition, eqn A.5, it can be shown that these functions satisfy the self-consistent equations

$$w_A(\boldsymbol{r}) = \chi N\phi_B(\boldsymbol{r}) + \xi(\boldsymbol{r}) \tag{A.7}$$

$$w_B(\boldsymbol{r}) = \chi N\phi_A(\boldsymbol{r}) + \xi(\boldsymbol{r}) \tag{A.8}$$

$$\phi_A(\boldsymbol{r}) + \phi_B(\boldsymbol{r}) = 1 \tag{A.9}$$

$$\phi_A = -\frac{V}{Q}\frac{DQ}{DW_A} \tag{A.10}$$

$$\phi_B = -\frac{V}{Q}\frac{DQ}{DW_B} \tag{A.11}$$

The last two equations identify $\phi_A(\boldsymbol{r})$ and $\phi_B(\boldsymbol{r})$ as the average densities of A and B monomers at $\boldsymbol{r}$, as calculated in an ensemble of non-interacting polymers subject to the fields $w_A(\boldsymbol{r})$ and $w_B(\boldsymbol{r})$, which act on A and B monomers, respectively. Once the partition function of this problem is known, eqns A.7–A.11 can be solved and the free energy obtained.

Often at this point additional approximations are made, such as expanding ln Q in cumulants and only keeping the first few terms. Such expressions are unnecessary because the exact expression for Q can be evaluated. The partition function is written as $Q = \int d\boldsymbol{r} q(\boldsymbol{r},1)$, where

$$q(\boldsymbol{r},s) = \int D\boldsymbol{r}_\alpha P[\boldsymbol{r}_\alpha;0,s]\delta\left(\boldsymbol{r}-\boldsymbol{r}_\alpha(s)\right)\exp\left\{-\int_0^s dt\left[\gamma(t)w_A\left(\boldsymbol{r}_\alpha(t)\right)\right.\right.$$
$$\left.\left.+\left(1-\gamma(t)\right)w_B\left(\boldsymbol{r}_\alpha(t)\right)\right]\right\}, \tag{A.12}$$

is the end-segment distribution function. The step function, $\gamma(s)$, is 1 for $s < f$ and 0 otherwise. This distribution function satisfies the modified diffusion equation

$$\frac{\partial q}{\partial s} \equiv \begin{cases} \frac{1}{6}Na^2\nabla^2 q - w_A(\mathbf{r})q, & \text{if } s < f \\ \frac{1}{6}Na^2\nabla^2 q - w_B(\mathbf{r})q, & \text{if } s > f \end{cases} \tag{A.13}$$

and the initial condition $q(r,0) = 1$ (Helfand 1975). Because the two ends of the copolymer are distinct, a second end-segment distribution function, $q^\dagger(\mathbf{r},s)$, is defined with an almost identical definition to eqn A.12, except that the functional integral over $\mathbf{r}_\alpha(t)$ is done for $t = s$ to 1. It satisfies $q^\dagger(\mathbf{r},1) = 1$, and eqn A.13 with the right-hand side multiplied by -1. In terms of these functions, the A-monomer density is

$$\phi_A(\mathbf{r}) = \frac{V}{Q}\int_0^f \mathrm{d}s\, q(\mathbf{r},s)q^\dagger(\mathbf{r},s) \tag{A.14}$$

with a similar expression for $\phi_B(\mathbf{r})$.

The SCF equations can be solved by expanding functions of position, $g(\mathbf{r})$, as $\Sigma_i g f_i(\mathbf{r})$, where $f_i(\mathbf{r})$, $i = 1,2,3,\ldots$, are orthonormal basis functions (i.e. $V^{-1}\int f_i(\mathbf{r})f_j(\mathbf{r})\,\mathrm{d}\mathbf{r} = \delta_{ij}$) each possessing the symmetry of the phase being considered. They are chosen to be eigenfunctions of the Laplacian operator; $\nabla^2 f_i(\mathbf{r}) = -\lambda_i D^{-2} f_i(\mathbf{r})$, where D is a length-scale for the phase. In this basis, the diffusion equation (A.13) for $q(\mathbf{r},s)$ becomes

$$\frac{\mathrm{d}q_i(s)}{\mathrm{d}s} = \begin{cases} \sum_j A_{ij} q_j(s), & \text{if } s < f, \\ \sum_j B_{ij} q_j(s), & \text{if } s > f, \end{cases} \tag{A.15}$$

$$A_{ij} = -\frac{1}{6}Na^2\lambda_i D^{-2}\delta_{ij} - \sum_k w_{A,k}\Gamma_{ijk}, \tag{A.16}$$

Where $\Gamma_{ijk} = V^{-1}\int f_i(\mathbf{r})f_j(\mathbf{r})f_k(\mathbf{r})\,\mathrm{d}\mathbf{r}$ and the matrix elements B_{ij} are given by a similar expression to eqn A.16. The initial condition is $q_i(0) = \delta_{i1}$. The solution to this set of linear differential equations is

$$q_i(s) = \begin{cases} T_{A,i1}(s), & \text{if } s < f, \\ \sum_j T_{B,ij}(s-f)T_{A,j1}(f), & \text{if } s > f, \end{cases} \tag{A.17}$$

where $T_A(s') \equiv \exp(As')$ and $T_B(s') \equiv \exp(Bs')$ are matrices that transfer $q_i(s)$ a distance s' along the A and B blocks of the copolymer respectively. These matrices are easily evaluated by performing an orthogonal transformation that diagonalizes either A or B. Similarly,

$$q_i^\dagger(s) = \begin{cases} \sum_j T_{A,ij}(f-s)T_{B,j1}(1-f), & \text{if } s < f, \\ T_{B,i1}(1-s), & \text{if } s > f, \end{cases} \tag{A.18}$$

Using the amplitudes of the end-segment distribution functions, Q is given by $Vq_1(1)$, and the amplitudes of $\phi_A(\mathbf{r})$ are

$$\phi_{A,i} = \frac{1}{q_i(1)} \int_0^f ds \sum_{jk} q_j(s) q_k^\dagger(s) \Gamma_{ijk}, \tag{A.19}$$

and the amplitudes $\phi_{B,i}$ are given by a similar expression. The amplitudes $w_{A,i}$ and $w_{B,i}$ of the fields are adjusted so that the densities calculated from them satisfy $\phi_{B,i} = -\phi_{A,i} = (w_{A,i} - w_{B,i})/2\chi N$ (eqns A.7 and A.8). For $i = 1$, ξ_1 is set to zero, so that $w_{A,1} = \chi N \phi_{B,1}$ and $w_{B,1} = \chi N f_{A,1}$. This completes the cycle of self-consistent equations. The free energy, eqn A.5, to within an additive constant can be written

$$F/nk_BT = -\ln\left[q_1(1)\right] - \chi N \sum_i \phi_{A,i} \phi_{B,i} \tag{A.20}$$

For the disordered phase, $F/nk_BT = \chi N f(1 - f)$. For an ordered periodic phase, the free energy is minimized with respect to the wavelength, D. By comparing the free energies for different phases, the phase diagram is obtained (see Fig. 2.44 for an example).

References

Helfand, E. (1975). *Journal of Chemical Physics*, **62**, 999.
Matsen, M. W. and Schick, M. (1994). *Physical Review Letters*, **72**, 2660.

Index

Here the abbreviation bcp is used for block copolymer.
HB denotes a homopolymer/block copolymer blend.
HHB denotes a blend of two homopolymers with a block copolymer.
BB denotes a binary blend of block copolymers.

This comprehensive and systematic text is the first of its kind to deal with the fundamental physics underlying the remarkable structural and dynamical properties of block copolymers. It provides the polymer scientist and technologist with a firm grounding in the principles underlying the wide applications of these important materials, highlighting the fascinating properties of block copolymers, such as nanoscale self-assembly in bulk and two-dimensions. The book discusses in depth experimental and theoretical advances during the last decade including: the thermodynamics and dynamics of block copolymer melts; block copolymers in dilute, semidilute and concentrated solutions; the structure of crystalline block copolymers; and block copolymers in blends with other polymers.

This informative book is essential to the polymer and materials science researcher in industry and academia, and postgraduates in related fields and is a useful reference text to final year undergraduate students in chemistry, physics, and materials science.

Ian W. Hamley is a Lecturer in Physical Chemistry, University of Leeds.

ISBN 0-19-850218-4

9 780198 502180

OXFORD
UNIVERSITY PRESS